

DTIC FILE COPY

①

AGARD-CP-444

AGARD-CP-444

AGARD

ADVISORY GROUP FOR AEROSPACE RESEARCH & DEVELOPMENT

7 RUE ANGELE - 92200 NANTERRE-CEDEX - FRANCE

AD-A215 832

AGARD CONFERENCE PROCEEDINGS No.444

New Light Alloys

DTIC
ELECTE
DEC 06 1988
S B D

NORTH ATLANTIC TREATY ORGANIZATION



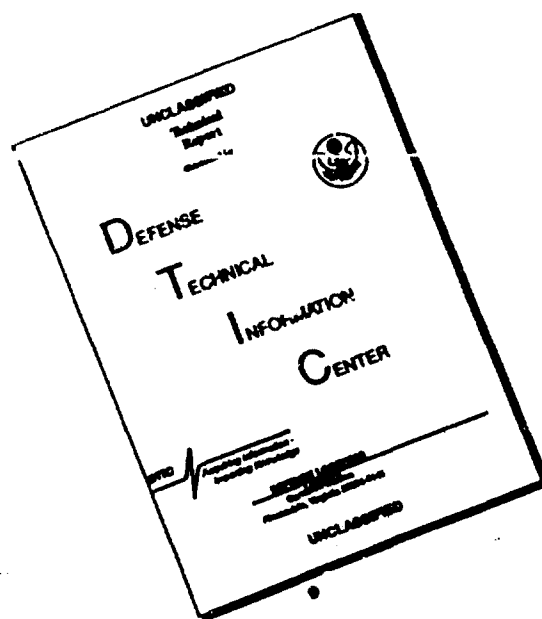
DISTRIBUTION AND AVAILABILITY
ON BACK COVER

DISTRIBUTION STATEMENT A

Approved for public release
Distribution Unlimited

89 12 05 255

DISCLAIMER NOTICE



**THIS DOCUMENT IS BEST
QUALITY AVAILABLE. THE COPY
FURNISHED TO DTIC CONTAINED
A SIGNIFICANT NUMBER OF
PAGES WHICH DO NOT
REPRODUCE LEGIBLY.**

AGARD-CP-444

NORTH ATLANTIC TREATY ORGANIZATION
ADVISORY GROUP FOR AEROSPACE RESEARCH AND DEVELOPMENT
(ORGANISATION DU TRAITE DE L'ATLANTIQUE NORD)

AGARD Conference Proceedings No.444
NEW LIGHT ALLOYS

Papers presented at the 67th Meeting of the Structures and Materials Panel of AGARD in Mierlo,
Netherlands, 3—5 October 1988

THE MISSION OF AGARD

According to its Charter, the mission of AGARD is to bring together the leading personalities of the NATO nations in the fields of science and technology relating to aerospace for the following purposes.

- Recommending effective ways for the member nations to use their research and development capabilities for the common benefit of the NATO community;
- Providing scientific and technical advice and assistance to the Military Committee in the field of aerospace research and development (with particular regard to its military application);
- Continuously stimulating advances in the aerospace sciences relevant to strengthening the common defence posture;
- Improving the co-operation among member nations in aerospace research and development;
- Exchange of scientific and technical information;
- Providing assistance to member nations for the purpose of increasing their scientific and technical potential;
- Rendering scientific and technical assistance, as requested, to other NATO bodies and to member nations in connection with research and development problems in the aerospace field.

The highest authority within AGARD is the National Delegates Board consisting of officially appointed senior representatives from each member nation. The mission of AGARD is carried out through the Panels which are composed of experts appointed by the National Delegates, the Consultant and Exchange Programme and the Aerospace Applications Studies Programme. The results of AGARD work are reported to the member nations and the NATO Authorities through the AGARD series of publications of which this is one.

Participation in AGARD activities is by invitation only and is normally limited to citizens of the NATO nations.

The content of this publication has been reproduced directly from material supplied by AGARD or the authors.

Published August 1989
Copyright © AGARD 1989
All Rights Reserved
ISBN 92-835-0519-0



*Printed by Specialised Printing Services Limited
40 Chigwell Lane, Loughton, Essex IG10 3TZ*

PREFACE

The last fifteen years have been marked by considerable changes in aeronautical materials. One of the main areas of change has been a notable lightening of the structures employed in aircraft design, thereby increasing specific thrust, of principal concern in military aeronautics, for both aircraft and helicopters. Reduction in weight has been achieved in a number of ways; mainly through the increasing use of polymer matrix composites, from the initial small-scale applications involving mechanical parts with a low critical value to the more extensive applications in wings, as demonstrated with current designs for combat aircraft.

Within the last few years, in response to the development of the polymer matrix materials, the main producers of aluminium alloys have once again taken up the development of aluminium-lithium alloys in order to exploit their advantages of low density and high elastic modulus. In fact, these alloys had been known about for some thirty years but major investment was required for their development, especially in production technology. Work in this field has been particularly dynamic and productive. In less than a decade, a fairly low level of understanding of the field has been transformed into the industrial production of new optimised alloys, (obtained using highly specialised casting techniques), the development of associated technologies such as superplastic forming and the adoption of these alloys for current aircraft design projects.

A great many meetings have been held on aluminium-lithium alloys over the last five years, but the AGARD Specialists' Meeting organised in Mierlo in October 1988 came at a particularly opportune moment. For the first time, it enabled a comparison to be made between existing alloys on the basis of research and characterization studies. These studies were mostly carried out on a cooperative basis by alloy manufacturers and the major research establishments and provided a picture of the industrial developments planned by the aircraft manufacturers.

At the same Meeting, one session (out of five) was devoted to other light alloys. A number of materials have emerged concurrently in recent years: firstly, the aluminium and magnesium base alloys produced by powder metallurgy, often involving rapid solidification routes; secondly, particulate composite alloys (often produced via powder metallurgy routes) and intended for similar applications to the first group, and finally long fibre composites for use in space-flight structures of high dimensional stability, but which may also find a use in certain aeroengine parts or for second generation supersonic (and hypersonic) transport aircraft.

Although these materials have not yet reached such an advanced stage as the aluminium-lithium alloys, the time seemed right to make a comparison of these developments in the form of a series of papers given by independent scientists, concluding with a round table discussion led by Doctors G. Waldman (USA), C.J. Peel (UK) and K. Schulte (GE).

Dr P. Costa
Chairman, Subcommittee on
New Light Alloys.

Accession For	
NTIS GRA&I	<input checked="" type="checkbox"/>
DTIC TAB	<input type="checkbox"/>
Unannounced	<input type="checkbox"/>
Justification	
By	
Distribution	
Availability Codes	
Dist	Avail and/or Special
A-1	



PREFACE

La période de quinze ans qui s'achève a été marquée par un renouvellement considérable des matériaux aéronautiques. L'une des lignes de force de cette modification est l'allègement des structures qui contribue à l'augmentation de la poussée spécifique, préoccupation centrale de l'aéronautique militaire, tant pour les avions que pour les hélicoptères. Diverses solutions sont apparues: application tout d'abord des composites à matrice polymère à des parties d'importance croissante, éléments peu critiques sur le plan mécanique tout d'abord, puis progressivement parties de la voilure, notamment dans les avions de combat actuellement en cours de conception.

A quelques années d'intervalle et en concurrence des matériaux précédents, les principaux producteurs d'alliages d'aluminium ont repris le développement des alliages aluminium-lithium, alliages de densité et de module d'élasticité très favorables. Ces alliages étaient connus depuis une trentaine d'années, mais leur mise au point et *plus encore leur production* exigeaient des investissements importants. Les études dans ce domaine ont été particulièrement actives et fructueuses, puisque l'on a su, en guère plus de dix ans, parcourir tout le trajet séparant un niveau initial de connaissances assez fruste, de la production industrielle d'alliages nouveaux optimisés, obtenus par des technologies de coulée très particulières, du développement de technologies connexes comme le formage superplastique, et de l'insertion dans les projets en cours de nouveaux avions.

De nombreuses réunions se sont tenues au cours des cinq dernières années sur ce thème. La Réunion de Spécialistes qui s'est tenu dans le cadre de l'AGARD à Mierlo en octobre 1988 est intervenu à un moment tout à fait opportun, dans la mesure où il a permis pour la première fois une comparaison entre les alliages existants, sur la base des recherches et des caractérisations, menées souvent sur le mode coopératif, par les industriels et les grands établissements de recherche, et de faire le bilan des développements industriels envisagés par les constructeurs aéronautiques.

Parallèlement, il a paru utile de consacrer une partie de la réunion — en fait une session sur cinq — à d'autres matériaux dérivant des alliages légers. Plusieurs autres familles sont en effet apparues concurremment au cours des dernières années: alliages d'aluminium ou de magnésium, produits par métallurgie des poudres, et relevant le plus souvent de techniques de refroidissement rapide, alliages composites particuliers, proches des précédents, tant par la technologie (métallurgie des poudres) que par les applications, composites à fibres longues, applicables aux structures spatiales de grande stabilité dimensionnelle, mais qui peuvent également trouver un emploi pour certains éléments de moteurs aéronautiques, ou des avions de transport supersoniques de seconde génération — voire hypersoniques.

Bien que ces matériaux n'aient pas atteint un stade aussi avancé, l'occasion paraissait bien venue de faire un bilan comparatif de ces développements par le biais d'une série de présentations effectuées par des scientifiques indépendants, et d'une table ronde finale, qui a été animée par les Docteurs G.Waldman (USA), C.Peel (UK) et K.Schulte (RFA).

Dr P.Costa
Chairman, Subcommittee on
New Light Alloys.

STRUCTURES AND MATERIALS PANEL

Chairman: Prof Dr-Ing Hans Förtsch
Direktor der DFVLR Institut
für Aeroelastik
Bunsenstrasse 10
D-3400 Göttingen
Germany

Deputy Chairman: Mr Samuel I. Vennert
Director, Materials & Structures
Division (Code RM)
Office of Aerodynamics & Space
Technology
NASA Hq
Washington DC 20546, USA

SUB-COMMITTEE MEMBERS

Chairman: Dr Paul Costa
Directeur Scientifique des Matériaux
ONERA
29 ave de la Division Leclerc
92320 Châtillon, France

SMP MEMBERS

J. Auvinet	Fr
H.J.G. Carvalhinhos	Po
D. Coutsouradis	Be
G.L. Denman	US
A. Deruytere	Be
M. Donik	Tu
M.H. Guler	Tu
R. Labourdette	Fr
J.S.L. Leach	UK
H.P. van Leeuwen	Ne
J.J. De Luccia	US
J.M. Pintado	Sp
M. Sclaris	It
O. Sensburg	Ge
M. Theofilou	Gr
W. Wallace	Ca

PANEL EXECUTIVE

Mr Murray C. McConnell — UK

AGARD-OTAN
7, rue Ancelle
92200 Neuilly sur Seine
France
Tel: (1) 4738 5790 & 5792
Telex: 610176F

From USA and CANADA
AGARD-NATO
Attn: SMP Executive
APO New York 09777

CONTENTS

	Page
PREFACE	iii
STRUCTURES AND MATERIALS PANEL	v
	Reference
 <u>SESSION I – PART 1 – PRODUCERS STATEMENTS</u>	
CURRENT STATUS OF ALCAN LITAL PROGRAMME by R. Grimes	1*
Al-Li ALLOYS DEVELOPED BY PECHINEY by M.Doudeau, P.Meyer and D.Constant	2
COMMERCIAL DEVELOPMENT OF Al-Li PRODUCTS by R.S.James	3*
 <u>SESSION I – PART 2 – PROPERTIES</u>	
THE MICROSTRUCTURE AND PROPERTIES OF ALUMINUM-LITHIUM ALLOYS by E.A. Starke, Jr and W.E. Quist	4
 <u>SESSION II – PART 2 – PROPERTIES</u>	
MECHANICAL PROPERTIES AND FRACTURE TOUGHNESS OF 8090-T651 PLATE AND 2091 AND 8090 SHEET by W.G.J. 't Hart, L.Schra, D.S.McDarmaid and M.Peters	5†
FATIGUE PROPERTIES OF Al-Li ALLOYS by M.Peters, K.Welpmann, D.S.McDarmaid and W.G.J. 't Hart	6†
CORROSION AND STRESS CORROSION OF ALUMINIUM-LITHIUM ALLOYS by C.J.E.Smith, et al	7†
PROPRIETES DES ALLIAGES Al-Li par Y.Barboux	8
INVESTIGATION ON SHEET MATERIAL OF 8090 AND 2091 ALUMINIUM-LITHIUM ALLOYS by W.Zink, J.Weilke, L.Schwarmann and K.H.Rendigs	9
ALUMINUM LITHIUM ALLOYS FOR NAVY AIRCRAFT by E.W.Lee and J.Waldman	10
 <u>SESSION III – PART 2 – PROPERTIES</u>	
FATIGUE, FRACTURE MECHANICS AND CORROSION PROPERTIES OF SOME ALUMINIUM-LITHIUM ALLOYS by G.Cavallini, et al	11
FATIGUE AND FRACTURE BEHAVIOUR OF A PM Al-Li ALLOY by R.Schäfer and B.Weiss	12

* Not available at time of printing

† Paper contributed by Group for Aeronautical Research & Technology – Europe (Garteur)

SESSION III – PART 3 – FABRICATION

FABRICATION OF TEST-ARTICLES FROM Al-Li 2091 FOR FOKKER 100 by G.J.H.Vaessen, C.van Tilborgh and H.W.van Rooijen	13
MISE EN OEUVRE DE L'ALLIAGE 2091 par J.Bevalot	14
FABRICATION CHARACTERISTICS OF 8090 ALLOY by V.H.Mould	15
SUPERPLASTIC FORMING AND JOINING OF Al-Li ALLOYS by A.K.Ghosh and C.Gandhi	16*
SUPERPLASTIC PERFORMANCE AND PROPERTIES OF THE LITAL ALLOYS by R.G.Butler and B.J.Dunwoody	17

SESSION IV – PART 4 – USERS STATEMENTS

POINT OF VIEW OF A CIVIL AIRCRAFT MANUFACTURER ON Al-Li ALLOY by J.Koshorst	18
USES AND PROPERTIES OF Al-Li ON THE NEW EH101 HELICOPTER by A.F.Smith	19
ALUMINUM-LITHIUM: APPLICATION OF PLATE AND SHEET TO FIGHTER AIRCRAFT by B.A.Davis	20
CURRENT STATUS OF THE APPLICATION OF CONVENTIONAL ALUMINIUM-LITHIUM ALLOYS AND THE POTENTIAL FOR FUTURE DEVELOPMENTS by C.J.Peel	21

SESSION IV – PART 5 – OTHER ALLOYS

HIGH PERFORMANCE POWDER METALLURGY ALUMINUM ALLOYS – AN OVERVIEW by M.J.Koczak and M.K.Premkumar	22
MICROSTRUCTURE/MECHANICAL PROPERTY RELATIONS IN A MECHANICALLY ALLOYED ALUMINUM by W.J.D.Shaw	23

SESSION V – PART 5 – OTHER ALLOYS

COMPOSITES A MATRICE METALLIQUE ET A FIBRES LONGUES INORGANIQUES par P.F.Gobin	24
SHORT FIBRE AND PARTICULATE REINFORCED METAL MATRIX COMPOSITES by S.J.Harris	25
METAL MATRIX COMPOSITES – A PROMISING ALTERNATIVE TO CONVENTIONAL ALLOYS ? by K.Schulte and W.Bunk	26
MAGNESIUM ALLOY TECHNOLOGY FOR AEROSPACE APPLICATIONS by D.J.Bray	27

* Not available at time of printing

AL-LI ALLOYS DEVELOPED BY PECHINEY

M. DOUDEAU	Research Engineer	B.P. 27, 38340 VOREPPE, France
P. MEYER	Research Engineer	B.P. 27, 38340 VOREPPE, France
D. CONSTANT	Development Engineer	B.P. 130, 63504 ISSOIRE, France

SUMMARY

This paper presents an up-to-date view of Al-Li development in terms of both properties and production readiness. Successes achieved to date, mostly where damage tolerance and medium strength targets are concerned, will be outlined. Design allowables, properties and product size capabilities will be presented for some alloy/product form combinations which are close to commercialization. As certification has started on some product forms, the introduction of Al-Li alloys on the aerospace market is under way.

1. INTRODUCTION

The major producers involved in the development of Al-Li alloys have been very active over the last 5 to 8 years, working on similar property targets and sometimes coming up with similar answers, although not always identical.

Despite generally optimistic prospects (the high potential of the Al-Li family has been confirmed on many product forms), this development work is taking longer than initially anticipated :

- few qualification programs have been launched,
- supply of commercial material has, here and there, overstepped delivery dates,
- the decisions to launch industrial casting facilities have been delayed.

Among possible explanations, one can quote :

- the extensive sampling over the past 5 years, with variants to meet different customers' specifications,
- the difficulty in meeting or exceeding each of the individual properties of the conventional alloys to be replaced (philosophy of direct substitution),
- the competition between producers, which has increased the choice but also the difficulty in choosing among the various candidate alloys.

The prospects nevertheless remain good since :

- qualification has started with at least some customers, while extensive field testing is still going on with the others,
- there is still time to scale up, as no major commitment (e.g. use of massive quantities of Al-Li semis with a given time-table) from aircraft makers has been announced. In particular, a massive need in 2 years time is unlikely, while it takes only from 16 months to 2 years to complete an industrial casting facility.

This paper intends to review the overall situation, both in terms of property combinations and engineering properties, and to reflect PECHINEY's strong commitment to the development of Al-Li alloys during the past 5 years.

2. PROCESSING OF AL-LI

2.1 CASTING

With an experience of several hundreds of castings in both slab and billet forms, and on a variety of alloys and ingot cross-sections, the casting technology of Al-Li is well mastered. The casting procedure is designed to provide adequate metal quality under safe conditions, in spite of the reactivity of lithium.

Regardless of the Aluminum-Lithium alloy used, current 3 ton ingots present a good surface condition, leading to the same amount of scalping as on conventional alloys. Their processing is performed solely in plant, under fully industrial conditions. We are now able to guarantee properties, including the short-transverse direction on thick products. This confirms the good quality control of the cast ingot, in terms of :

- homogeneity of composition,
- inclusion and impurity level,
- gas content, porosity,
- grain size.

The 3 ton casting unit is flexible enough, should the customers' requirements increase, to meet the demand for the next 2 to 3 years, with capacity left for early introduction of Al-Li semis on aircrafts. It enables the manufacture of the same semi-products (dimension-wise) as on conventional alloys with representative properties, which is the key point when supplying for qualification programs.

2.2 TRANSFORMATION

Sheets and plates are rolled from 3-ton ingots on the existing hot and cold rolling lines at Issoire. Sheets are produced by continuous rolling. The stretch applied after quenching is between 1.5 and 3 %. PECHINEY's experience is now based on the rolling of sheets from 1 mm to 88 mm thick, in widths from 1000 mm to 2000 mm. Cladding of sheets is possible, regardless of the cladding material (7072 or 7xxx).

Extrusions are produced in the Montreuil-Juigné plant. Profiles are directly extruded from machined or pre-extruded billets. The usual amount of stretching is applied to aluminum-lithium profiles, after quenching.

Forgings are carried out at FORGEAL (Issoire). Large hand forgings have been processed in order to evaluate the potential use of 2091 for thicker gauges, without any difficulty. Numerous shapes in precision and thin-walled forgings have been successfully produced out of 8090 and 2091 alloys.

3. METALLURGICAL GOALS AND ALLOYS REVIEW

PECHINEY has developed three main Al-Li alloys, covering the whole strength range of conventional alloys, with a density reduction of 8 to 10 % and a Young Modulus increase of about 11 %.

They belong to the Al-Li-Cu-Mg-Zr family, which turned out to be the most promising. The replacement of 2024 and 7075 guides the work on Al-Li alloy design.

Al-Li Alloy	Main Properties	Alloy to replace	Density Reduction	Young Modulus Increase
2091	damage tolerance	2024-T3	- 8 %	+ 7 %
	medium strength	2214-T6 7075-T73(*)		
8090	medium strength	2214-T6 7075-T73(*)	- 10 %	+ 11 %
	fatigue resistance	2024-T3		
CP 276	high strength	7075 7010 7050	- 8 %	+ 11 %
		T6 or T76		

(*) strength-wise = excluding
ST stress-corrosion resistance

Development is conducted on every possible product form, apart from a few combinations of semi-products and alloys which either do not correspond to a sizeable market, or were not selected initially, after discussion with customers. The overall status is as follows :

2091 is a good candidate for 2024-T3 replacement :

- rolled products are processed according to fixed procedures, under fully industrial conditions (quality assurance system), hence the existence of minimum guaranteed properties. Short-transverse properties of plates are also guaranteed.
- the same status has been reached on thin extrusions and thick forgings, although 8090 is also a good candidate for thin extrusion replacement.

For medium strength replacement, both 2091 and 8090 give promising results : extrusions, thicker sheets, thin-walled forgings. Guaranteed properties have been established only in the case of thin extrusions, due to a more limited experience.

CP 276 is PECHINEY's candidate for high strength replacement, with confirmed achievements in two cases : medium-thickness plates and thin extrusions. The extent to which CP 276 can replace 7075-T6 or -T76 in the other product forms is still being evaluated.

In the following chapters we will present properties of a selection of combination semi-products (sheets, plates, extrusions, forgings) and alloys (2091, 8090, CP 276).

4. PROPERTIES

4.1. PHYSICAL PROPERTIES

Comparison between the aluminum-Lithium alloys under industrial production at PECHINEY and the corresponding conventional alloys and testing procedures (mechanical properties, toughness, corrosion resistance) are given in Tables 1 and 2 at the end of this paper.

4.2. DAMAGE TOLERANCE ALLOY

The intrinsically good damage tolerance of 2091 and the successful industrial experience gained by PECHINEY on all product-forms make 2091 the favoured candidate for the replacement of 2024. Qualification programs have been launched. The statistical and thorough evaluation of industrial products confirms the hopes placed in 2091 for this type of application. 8090 is a good candidate for fatigue resistant structural parts such as tubes and thinner extrusions. It is currently produced for these applications.

4.2.1 2091-T8X Sheets

The highest damage tolerance and isotropy are obtained with the association of a recrystallised structure together with an underaged temper called T8X (Ref. 2 and 3). The overall set of properties meets the damage tolerance required for 2024 replacement (Table 3). Fatigue resistance is good (Table 4). Over 30 ingots have been processed into sheets. Minimum guaranteed properties have been derived and MIL HANDBOOK 5 types of guaranteed values are also available.

However, the recrystallised structure does not ensure the highest stress-corrosion cracking (S.C.C.) resistance. Where stress corrosion resistance is of importance, or for certain types of riveting, new versions (called CPH) have been developed to match the S.C.C. threshold of 2024.

4.2.2 2091 CPHK-T8X Sheets

The increase in stress corrosion resistance of 2091-T8X recrystallised sheets has been obtained thanks to metallurgical adjustments, "CPH". The ageing practice remains unchanged (same T8X temper), to maintain a higher damage tolerance. The CPHK version is that which favours the toughness (hence the "K" letter) within the possible range of CPH treatments. The CPH treatment leads to a three-fold increase in stress corrosion resistance for 2091 T8X sheets, at a slight expense of strength and toughness. (Table 5)

The overall set of properties remains within the range of damage tolerance requested for 2024 replacement. More than 20 ingots have been processed under CPH conditions. Statistical evaluation of 2091 CPHK-T8X sheets has started and minimum guaranteed properties have been established, leading to a real choice between this version and that of the previous page.

4.2.3 2091-T8X51 Sheets and Plates

As shown in Table 6, the yield strength exceeds that of 2024, while other properties (fatigue and crack propagation) meet the 2024 replacement goal. The large experience bearing on these intermediate thicknesses leads to minimum guaranteed properties which are significantly higher than those of 2024-T351.

The intrinsic damage tolerance potential of 2091 ensures good levels of toughness for the whole range of thickness, whatever the structure of the material (fibred or recrystallised). The good toughness, as measured by C.T. specimens on 12 mm thick plates, is confirmed when measuring the R curve on 5 mm-thick specimens machined within the plate. Thanks to an essentially unrecrystallised structure, the stress corrosion behaviour tested in the rolling plane is excellent.

4.3 MEDIUM STRENGTH

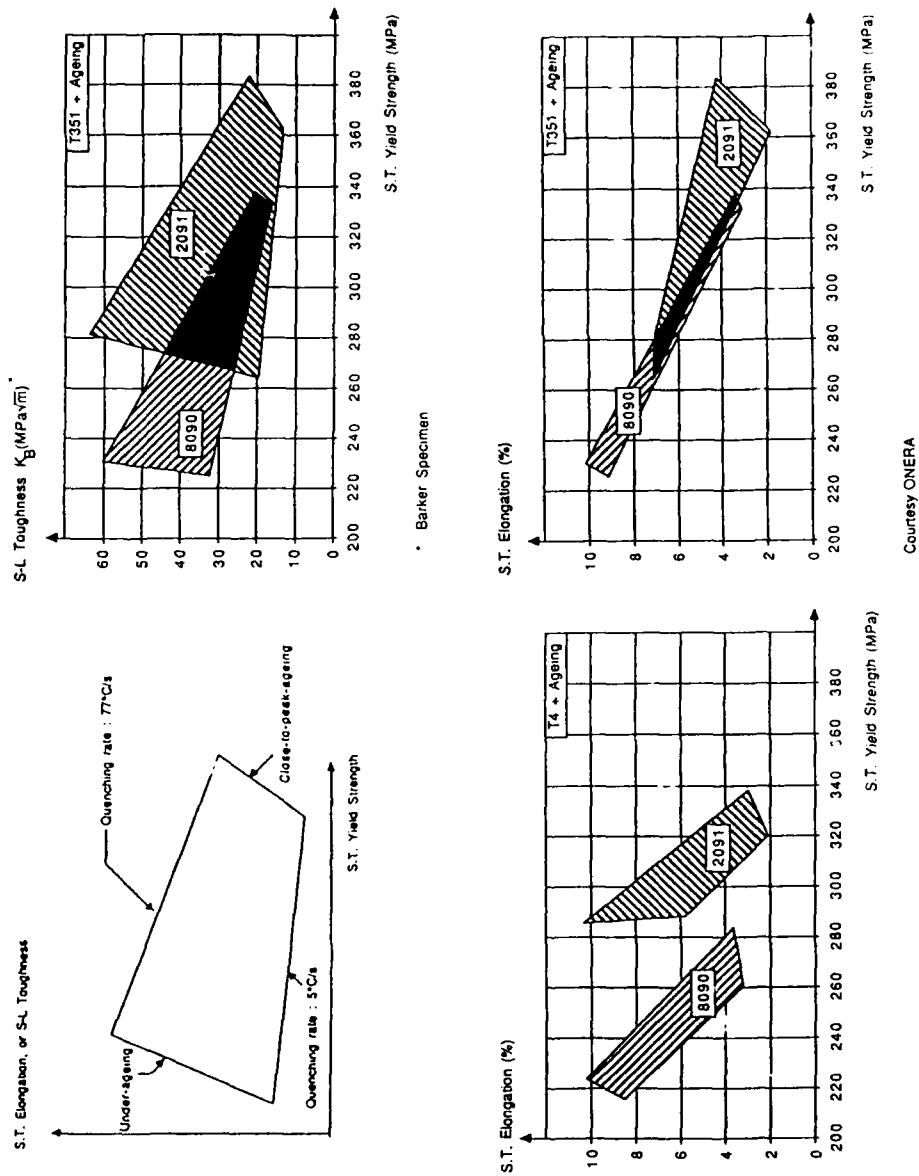
2091 and 8090 both possess the strengthening potential to meet this replacement goal. They are aged close-to-peak in order to reach the required strength level.

Their winning cards are, respectively, that 2091 offers a better strength-toughness combination, particularly in the short-transverse direction, either in the -T6, -T851 or -T852 condition, as indicated (Figure 1).

The short-transverse measurements are performed on 30 mm thick flat extrusions which provide a one-to-one comparison of both alloys : same extrusion process, same location for specimens (core). This advantage is maintained over the whole range of quenching rates tested : from 5 to 77°C/sec.

FIGURE 1

SHORT-TRANSVERSE COMBINATIONS OF PROPERTIES
FOR 2091 AND 8090
AS A FUNCTION OF QUENCHING RATE AND AGEING



The tendency towards exfoliation on 8090 is more easily reduced when using a close-to-peak or slightly overaged heat treatment. Its density and modulus are more attractive. Hence 2091 is recommended for applications where strength-toughness combination is of prime interest, especially for structural parts usually made out of 2214-T6 type of alloys : plates and thick forgings. 8090 is favoured for some 7075-T7351 replacements, where very high short-transverse stress corrosion resistance is not important : thinner plates and extrusions.

4.3.1 2091-T851 Plates

2091 can be easily brought to medium strength when using a close-to-peak ageing treatment. Short-transverse properties have now reached acceptable levels, although very thick sections still remain a technical challenge. The ageing practice has been chosen in order to offer the best balance between strength and toughness. Hence, at least up to about 40 mm thick, 2091 appears to be a good candidate for the replacement of 2214-T6 type alloys (Table 7).

4.3.2 8090-T851 Plates

8090 can be used as a medium strength and corrosion resistant alloy for thinner plates or extrusions when slightly overaged. The reduced sensitivity to texture and resistance against exfoliation have guided the choice of the ageing treatment. Except for parts where short-transverse properties (including stress corrosion resistance) are critical, 8090 is a good candidate for 7075-T73 replacement (Table 8).

4.3.3 8090-T851 Extrusions

The set of properties obtained meets not only the requirements for the replacement of 2024, but also the typical strength and corrosion resistance measured on 7075-T7351 extrusions (Table 9). Additional advantages result from the comparison of fatigue and crack-propagation data on both alloys.

8090 is hence a promising candidate for the replacement of 7075-T7351 extrusions, when stress-corrosion resistance in the short-transverse direction is not the key point. It offers a 10 % density reduction and a 24 % increase in specific modulus. 8090 extrusions are under current production and minimum guaranteed properties have been derived.

4.4 HIGH STRENGTH

Among the alloys of the Al-Li-Cu-Mg-Zr family, CP 276 is the promising candidate for high strength applications. It combines a high hardening potential together with an elevated modulus, a good resistance to exfoliation and a remarkable crack-propagation rate. Thinner extrusions are currently produced out of CP 276 and take full advantage of its anisotropy. In this case, we will only present the properties obtained on extrusions. An underaged temper has been chosen in order to combine higher strength and good toughness levels.

As for other aluminum lithium alloys, CP 276 extrusions are sensitive to texture and the highest properties are obtained within the axisymmetrical parts of the extrusion. Depending on the texture, the strength is comparable to that of 7075-T651 as measured on thicker extrusions (Table 10). Taking into account the lowest values (obtained in the flat parts of the extrusions), CP 276-T851 provides a strength level which is intermediate between that of 7075-T651 and that of 7075-T7651, with a good resistance against exfoliation.

5. ENGINEERING PROPERTIES

This chapter is concerned with the ease of manufacturing for the aircraft maker, as well as with performance in service for the end-user. The results given here are based on the experience conducted by customers and on the results of in-house programs. The engineering properties of Al-Li alloys are similar to those of conventional alloys, with improvements in certain cases. The manufacturing techniques therefore remain unchanged for the aircraft maker.

5.1 FORMING

As a general rule, the as-quenched condition provides the best forming ability for Aluminum-Lithium alloys. In this temper, the forming ability of 2091 recrystallised sheets exceeds that of 2024. The n and r (Lankford) coefficients, as measured by M.B.B., are respectively 0.33 and 1.0 for 2091 and 0.22 and 0.70 for 2024. This outstanding behavior facilitates forming operations : it authorizes a decrease in the number of forming steps as compared to 2024. This benefit has been checked in bending, drawing and rubber-forming tests by DASSAULT and FOKKER.

As-quenched and fibred 8090 sheets have been successfully submitted by DASSAULT to the usual forming sequences applied to thinner sheets or stiffeners. The forming ability of 2091 sheets in T3 or T8X is high enough for some forming operations. FOKKER has successfully manufactured stringers out of 2091 sheets in the final (T8X) condition. The solution-treatment holding time and quenching techniques applied to 2024 can be used for aluminum-lithium alloys on the whole, and in particular for 2091 and 8090. The natural ageing of aluminum-lithium alloys is significantly lower than that of 2024. This gives rise to an increased comfort in the workshops (Figure 2).

The influence of the cold working between quenching and ageing has been measured on 2091. This alloy is less sensitive to cold working than 2024. This leads to an improved homogeneity of properties within the formed part, as observed by AEROSPATIALE and by DASSAULT on 2091-(T8-T6)X sheets (Figure 3).

As measured by DASSAULT, the cold working has a minor influence on the crack-propagation rate of 2091-T8X sheets, which remains lower than that of 2024-T3 anyway. Increasing cold working tends to improve the stress-corrosion resistance of 2091 CPHK-T8X sheets. However, no significant effect of cold working on intercrystalline corrosion or on exfoliation has been observed.

Because of grain coarsening, the critical lower work hardening ϵ_c limits the maximum intermediate strain in the forming sequence before the last solution heat treatment. The same limitation exists on conventional alloys. To be precise, the actual values of ϵ_c are : 5 to 13 % for 2091, 6 % for 2091-CPHK and 6 % for 2024 sheets.

Aluminum-lithium semi-products display a lithium depleted zone (L.D.Z.) beneath their surface. Reducing the holding time to the minimum acceptable level is one possible way of limiting the depth of the L.D.Z. The use of salt baths is another efficient method : it divides the L.D.Z. depth by 3. So far, no harmful effect of the L.D.Z. has been detected, except for a reduction in strength for very thin products (below 1 mm thick).

5.2 CHEMICAL MILLING - MACHINING

Chemical milling can be successfully applied to aluminum-lithium alloys and in particular to 2091 and 8090. The surface quality naturally depends on the baths used by customers (additives, etc.). The chemical milling speed of 2091 is equivalent to that of 2024 when measured in a pure soda aqueous solution. The influence of the ageing temper is negligible. The presence of Lithium does not alter the stability of the baths, although more mud is generated during the chemical milling of Al-Li alloys. Machining can be performed on existing tools ; it is safe providing that a vacuum system is placed at the base of the tool, or a proper lubrication used to avoid dust formation.

5.3 SURFACE TREATMENTS

Acid etching is recommended to get rid of the Li_2CO_3 carbonate layer resulting from the solution heat treatment. Before anodizing, acid (e.g. sulfochromic) etching is preferable to caustic etching. As observed on 8090, the attack due to the sulfochromic etching is regular and slightly slower than on 2024.

Chromic anodizing creates an efficient barrier against corrosion in Al-Li alloys. The thickness of the oxide layer is equivalent for 2024 and 8090. Hard anodizing has been proved feasible on CP 276. Sulfuric anodizing has been tested on 8090, the thickness of the oxide increases continuously with time, resulting in a thicker layer than on 2024.

5.4 JOINING

Riveting performs well on Al-Li alloys, with a fatigue behavior usually close to that of 2024, or even better, as measured by AEROSPATIALE and DASSAULT. Spot welding is used by DASSAULT. It is easier than with conventional alloys due to the increased resistivity of Al-Li alloys. The resulting weld is also stronger. TIG welding has been tested, especially on 2091 and CP 276. A complete heat treatment is still needed (including the solution heat treatment) in order to reach an acceptable elongation in the weld.

5.5 DEPENDANCE OF PROPERTIES ON TIME AND TEMPERATURE

The T8X treatment has been chosen in order to ensure a stable damage tolerance during the service life of the airplane. A 7-days exposure at 100 °C has been applied to 2091 CPHK-T8X sheets ; the stability of the stress-corrosion resistance has been checked (simulation of 20 years service life).

Peak-aged forgings out of 2091 have been tested by HISPANO SUIZA after a long holding time (3000 hours) at 130 °C. The properties of 2091 are slightly improved. This temperature behavior is a new advantage for Al-Li alloys as compared to 7XXX-series alloys (Figure 4).

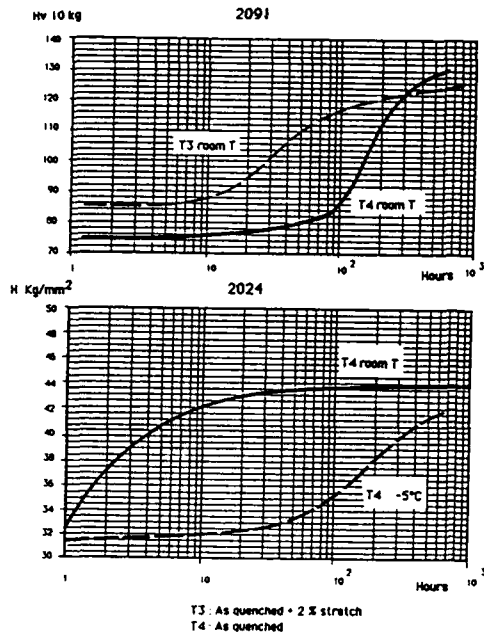


FIGURE 2

NATURAL AGING OF 2091 AND 2024 ALLOYS
AT ROOM TEMPERATURE (22°C) AND - 5°C (for 2024)

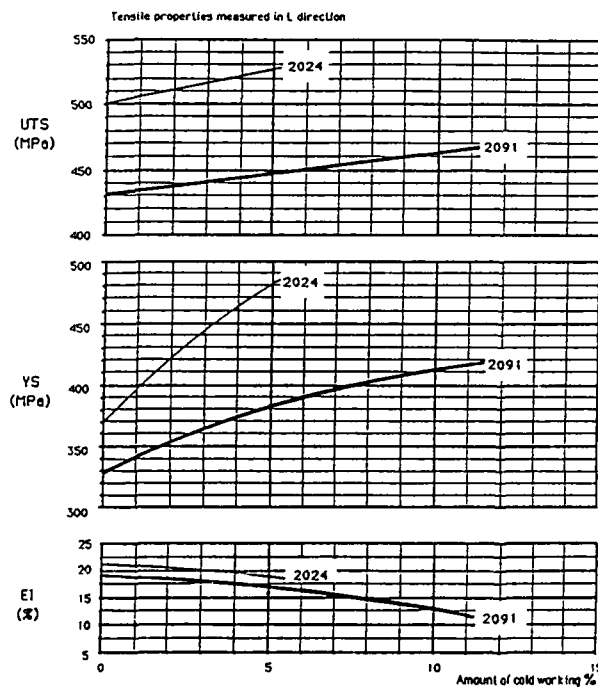


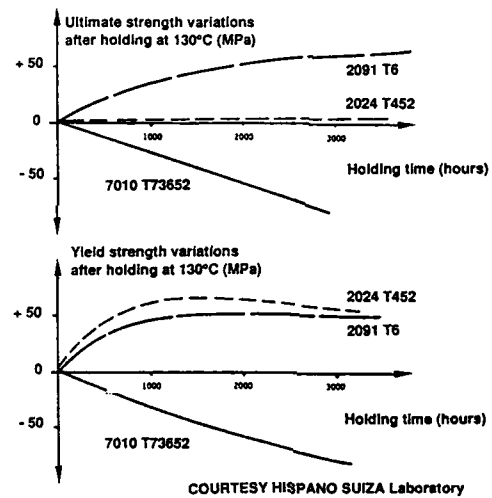
FIGURE 3

Both alloys are quenched and submitted to different levels of cold working.
2024 is naturally aged - 2091 is aged to T8X

Courtesy AEROSPATIALE

FIGURE 4

Influence of long holding time at 130°C
on the mechanical properties of various forgings



6. CONCLUSIONS

The results of five years intensive development on Al-Li alloys at PECHINEY have been reviewed in this paper. Among other achievements :

- 2091 appears capable of replacing 2024, the damage-tolerant alloy in use on major portions of aircrafts : sheets and thin extrusions (fuselage), plates and thick extrusions (lower wing). It can also be brought to medium strength (2214-T6 level), which widens its potential use.
- 8090 gives adequate properties on some product forms, with some possible applications (fatigue resistant structures) : stringers, tubes, thin forgings.
- CP 276 is a promising candidate for high strength applications: forgings, extrusions, plates (upper wing, structural parts) ; 7xxx-T6 or -T7G replacement.
- The physical and engineering properties remain similar to those of conventional aluminum alloys, so that aircraft design and manufacturing techniques are unchanged: same tools, same procedures. The only significant difference lies in scrap segregation.
- Airline maintenance practices remain unchanged.

The basic property combinations having been established, aircraft manufacturers can now launch extensive programs for the evaluation of service properties on a large scale, and for the qualification of the most advanced alloys. This is being done at present with some customers, using 2091 (sheets, plates and forgings) and 8090 alloys (extrusions). The qualification procedures would speed up if all producers agreed on a worldwide standardisation of alloys and tempers.

Taking all the above into consideration, prospects for the large-scale production of aluminum-lithium are high, especially in the fuselage and other vital components of high-performance aircraft.

REFERENCES

- (1) M. Reboul and P. Meyer
Intergranular and Exfoliation Corrosion Study on Al Li Cu Mg Zr Alloys
4th International Aluminium Conference
Journal de Physique, Col C3, 48, 9, Sept 87, 881-889
- (2) P. Meyer, Y. Cans, D. Fertou and M. Reboul
The Metallurgy of Industrial Al-Li Alloy
4th International Aluminium Conference
P C3, 131-138
- (3) G. Le Roy and P. Meyer
Aluminium Lithium Symposium
Westec - Los Angeles - March 86 and 87

TABLE 1

TESTING PROCEDURE

Tensile properties :

The specimens are taken in the core of the product, except where otherwise indicated.

Toughness :

Same location as for tensile specimens.

Kq : measured with C.T. specimens (minimum thickness : 12 mm).

Kc : measured on 405 mm wide CCT specimens with propagation of the crack and plastic zone correction.

Kapp : same specimen, but without crack-propagation, ($2a_0 = 100$ mm); no-plastic zone correction.

Bending radius :

The specimens are machined in the full thickness.

Fatigue, crack propagation :

The geometry of the specimens and the testing conditions are detailed for each figure.

Corrosion :

Stress corrosion :

The results refer to the alternate immersion/emersion test (10mm/50mm) performed in 3.5% NaCl aqueous solution (test duration : 30 days).

Exfoliation :

The results on Al-Li refer to the normalized EXCO procedure after 48 hours immersion, since this test turned out to give the best correlation with sea-coast exposure for Al-Li-Cu-Mg-Zr alloys (Ref 1). The test duration is 96 hours on conventional alloys (ASTM G34-80).

Intercrystalline corrosion :

This test performed in NaCl aqueous solutions +H₂O₂ (MILH 6088) is not correlated with stress-corrosion resistance. However, the sensitivity to intercrystalline corrosion may be observed in the case of sea-coast exposure, in addition to exfoliation. The results of this test must hence be used very carefully.

TABLE 2

Aluminum lithium alloys		Conventional alloys	
2091 T6 T8 T8X		2024 T3	
density (g/cm ³)	2.57	density (g/cm ³)	2.57
modulus (GPa)	78	modulus (GPa)	73
Coefficient of linear expansion (°C ⁻¹ × 10 ⁶) [20° to 100°C]	22	Coefficient of linear expansion (°C ⁻¹ × 10 ⁶) [20° to 100°C]	22.9
Thermal conductivity (W/m°C) [at 20°C/100°C]	76/88	Thermal conductivity (W/m°C) [at 20°C/100°C]	120
Specific heat (J/kg°C) [at 40°C]	980	Specific heat (J/kg°C) [at 40°C]	920
Resistivity (μΩcm) [at 20°C]	100 9.4	Resistivity (μΩcm) [at 20°C]	5.7
8090 T6 T8		2014 T6	
density (g/cm ³)	2.53	density (g/cm ³)	2.80
modulus (GPa)	81	modulus (GPa)	74
Coefficient of linear expansion (°C ⁻¹ × 10 ⁶) [20° to 100°C]	22	Coefficient of linear expansion (°C ⁻¹ × 10 ⁶) [20° to 100°C]	22.5
Thermal conductivity (W/m°C) [at 20°C/100°C]	78/88	Thermal conductivity (W/m°C) [at 20°C/100°C]	151
Specific heat (J/kg°C) [at 40°C]	987	Specific heat (J/kg°C) [at 40°C]	920
Resistivity (μΩcm) [at 20°C]	9.3	Resistivity (μΩcm) [at 20°C]	4.3
CP 276 T6 T8		7075 T6	
density (g/cm ³)	2.58	density (g/cm ³)	2.80
modulus (GPa)	80	modulus (GPa)	72
Coefficient of linear expansion (°C ⁻¹ × 10 ⁶) [20° to 100°C]	22	Coefficient of linear expansion (°C ⁻¹ × 10 ⁶) [20° to 100°C]	23.5
Thermal conductivity (W/m°C) [at 20°C/100°C]	75/83	Thermal conductivity (W/m°C) [at 20°C/100°C]	130
Specific heat (J/kg°C) [at 40°C]	980	Specific heat (J/kg°C) [at 40°C]	915
Resistivity (μΩcm) [at 20°C]	9.5	Resistivity (μΩcm) [at 20°C]	5.2

TABLE 3

DAMAGE TOLERANT SHEETS							
ALLOY		2091			2024		
TEMPER		T8X			T3		
THICKNESS		1.2 < t ≤ 3.5 mm			1.2 < t ≤ 3.5 mm		
TENSILE		YS (MPa)	UTS (MPa)	E1 (%)	YS (MPa)	UTS (MPa)	E1 (%)
L		348	441	18	369	498	20
LT		335	459	17	331	486	22
60°/L		298	429	23	330	479	24
TOUGHNESS		Kc Kapp (MPa√m)			Kc Kapp (MPa√m)		
LT		151 99			155		
TL		137 92			142 93.5		
BENDING		BENDING RADIUS r / t			BENDING RADIUS r / t		
L		< 3			≤ 1.5		
LT		< 3			≤ 1.5		
SURFACE		EXCO			EXCO		
CORE		N - EA P - EA			N - EA EA		
SURFACE		INTERCRYSTALLINE (μm) (%)			INTERCRYSTALLINE (μm) (%)		
CORE		250 25-50 150 100			0 - 150 0-75 0 - 75 0-75		
LT		SCR (Tensile) 30 d. 75 ≤ S < 100 MPa			SCR (Tensile) 30 d. 200 < S < 250 MPa		

* 1.6 mm sheets

TABLE 4

FATIGUE RESISTANCE OF 2091 T6X - T8X AND 2024 T3 SHEETS
 $R = 0.1$ $K_t = 3.6$

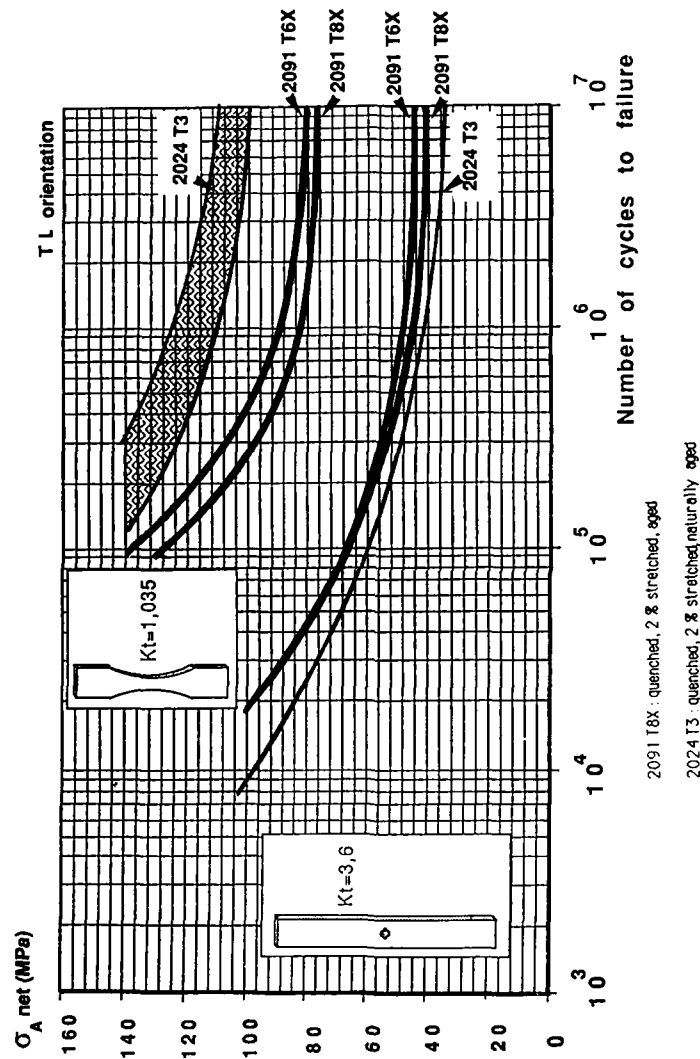


TABLE 5

DAMAGE TOLERANT SHEETS						
ALLOY	2091			2024		
TEMPER	CPH K T8X			T3		
THICKNESS	1.0 < t ≤ 3.5 mm			1.2 < t ≤ 3.5 mm		
TENSILE	YS	UTS	E1	YS	UTS	E1
	(MPa)	(MPa)	(%)	(MPa)	(MPa)	(%)
L	335	419	14	369	498	20
LT	326	435	13	331	486	22
60°/L	291	407	17	330	479	24
TOUGHNESS	K _c	K _{app}		K _c	K _{app}	
	(MPa√m)			(MPa√m)		
LT	128	89		155		
TL	124	86		142	93.5	
BENDING	BENDING RADIUS			BENDING RADIUS		
	r / t			r / t		
L	< 2.5			≤ 1.5		
LT	< 2.5			≤ 1.5		
SURFACE	EX00			EX00		
CORE	P - EA			N - EA		
	P - EA			EA		
	INTERCRYSTALLINE			INTERCRYSTALLINE		
	(μm)	(%)		(μm)	(%)	
SURFACE	0-150	0-25		0-150	0-75	
CORE	125	75		0-75	0-75	
	SCR (Tensile) 30 d.			SCR (Tensile) 30 d.		
	200 < S ≤ 250 MPa *			200 < S < 250 MPa *		
LT						

* : 1.6 mm thick sheets

TABLE 6

DAMAGE TOLERANT SHEETS and PLATES						
ALLOY	2091			2024		
TEMPER	T8X51			T351		
THICKNESS	$3.5 < t \leq 12.7$ mm			$3.5 < t \leq 12.7$ mm		
TENSILE	YS (MPa)	UTS (MPa)	E1 (%)	YS (MPa)	UTS (MPa)	E1 (%)
L	411	491	13	368	468	20
LT	363	486	15	334	484	16
60°/L	317	443	21	318	468	20
TOUGHNESS	KQ (MPa√m)			KQ (MPa√m)		
LT	44					
TL	41					
BENDING	BENDING RADIUS r/t			BENDING RADIUS r/t		
L	≤ 5					
LT	≤ 5					
SURFACE	EXCO			EXCO		
COPE	EA EA			P - EC EB - ED		
SURFACE	INTERCRYSTALLINE (μm) (%)			INTERCRYSTALLINE (μm) (%)		
COPE	75 local. 100 50			150 120		
LT	SCR (Tensile) 30 d. S > 200 MPa S > 250 MPa			SCR (Tensile) 30 d. S > 250 MPa		

* $t < 6$ mm** $t \geq 6$ mm

TABLE 7

MEDIUM STRENGTH SHEETS AND PLATES						
ALLOY	2091			2214		
TEMPER	T851			T651		
THICKNESS	3.5 < t ≤ 12.7 mm			12.7 mm		
TENSILE	YS	UTS	E1	YS	UTS	E1
	(MPa)	(MPa)	(%)	(MPa)	(MPa)	(%)
L	477	524	9	455	480	13
LT	453	513	9	455	505	10
60°/L	394	470	11	440	495	11
TOUGHNESS	KQ			KQ		
	(MPa√m)			(MPa√m)		
LT	35			40		
TL	25			36		
SURFACE	EX00			EX00		
CORE	P - EA EA - EB			EC EC		
SURFACE	INTERCRYSTALLINE			INTERCRYSTALLINE		
CORE	(μm) (%)			(μm) (%)		
	P					
	200	50		150	75	
LT	SCR (Tensile) 30 d.			SCR (Tensile) 30 d.		
	> 200 MPa			# 205 MPa		

TABLE 8

MEDIUM STRENGTH PLATES							
ALLOY TEMPER		8090 T851		7475 T7351			
THICKNESS		3.5 < t ≤ 12.7 mm		10.0 < t ≤ 25 mm			
TENSILE		YS (MPa)	UTS (MPa)	E1 (%)	YS (MPa)	UTS (MPa)	E1 (%)
L		455	500	7	475	540	12
LT		455	500	7			
60°/L		395	480	9	450	520	12
TOUGHNESS		Kc (MPa√m)		Kc (MPa√m)			
LT		33		30			
TL		30					
SURFACE		EXCO		EXCO			
CORE		P - EA P - EA		N - EA N - EA			

TABLE 9

MEDIUM STRENGTH EXTRUSIONS						
ALLOY TEMPER	8090 T851			7175 T7351		
THICKNESS	1.2 < t < 8 mm			1.1 < t < 2.5 mm		
TENSILE	YS (MPa)	UTS (MPa)	E1 (%)	YS (MPa)	UTS (MPa)	E1 (%)
L	440	513	6.8	418	503	13
LT	465	517	6.3			
SURFACE CORE	EXCO N - EA EA			EXCO N - EA N - EA		
L	SCR (Flexion) MPa. > 400 MPa			SCR (Tensile) 30 d. > 350 MPa		

* 13 mm thick extrusions

* * 3 to 5 mm thick extrusions (courtesy A.S.)

TABLE 10

HIGH STRENGTH EXTRUSIONS			
ALLOY	CP 276	7075	
TEMPER	T 851	T 651	
THICKNESS	8 < t ≤ 30 mm	13 mm	
TENSILE	YS UTS E1 (MPa) (MPa) (%)	YS UTS E1 (MPa) (MPa) (%)	
L (F)	532 604 7	562 613 11	
L (Ax)	662 681 3.5		
LT	446 549 7	525 587 14	
* specimen within a flat part of the extrusions			
** specimen within an axisymmetric part of the extrusions			
TOUGHNESS	KQ	KQ	
	(MPa√m)	(MPa√m)	
LT	41	31	
TL	34	25	
SURFACE	EXCO	EXCO	
CORE	N - EA	EB	
	EA - EB	EB	
SURFACE	INTERCRYSTALLINE	INTERCRYSTALLINE	
	(μm) (%)	(μm) (%)	
CORE	pitting	pitting	
	150 100	60 local.	
LT	SCR (Tensile) 30 d.	SCR (Tensile) 30 d.	
	MPa	MPa	
ALLOY	CP 276	7075	
TEMPER	T 851	T 651	
THICKNESS	2.0 < t ≤ 8 mm	< t ≤ mm	
TENSILE	YS UTS E1 (MPa) (MPa) (%)	YS UTS E1 (MPa) (MPa) (%)	
L (F)	493 588 8	562 620 12.5	
L (Ax)	415 524 3.5		

THE MICROSTRUCTURE AND PROPERTIES OF ALUMINUM-LITHIUM ALLOYS

Edgar A. Starke, Jr.
School of Engineering and Applied Science
University of Virginia
Charlottesville, Virginia 22901

William E. Quist
Boeing Commercial Airplane Company
P.O. Box 3707, M/S 73-43
Seattle, Washington 98124

ABSTRACT

The advantages to be gained by weight reduction of aerospace structures have encouraged the aluminum industry to develop a family of aluminum alloys which contain lithium as one of the alloying elements. When alloyed with aluminum, lithium can reduce the density by approximately three percent and increase the elastic modulus by six percent for every weight percent added. A new series of aluminum alloys, typified by 2090, 2091, 8090, and 8091, have been developed and are currently being produced in commercial quantities. These alloys have densities between 7% and 10% lower than the conventional alloy 7075 with correspondingly higher stiffness. Although a combined set of specific properties of the Al-Li-X alloys often exceeds those of the conventional aluminum materials used in aerospace, these properties seem to be much more sensitive to processing parameters. The strong processing-property relationship is associated with sharp crystallographic textures that are developed during primary processing and very complex precipitate microstructures whose distributions are sensitive to quench rates and degree of deformation prior to aging. This paper describes the processing-microstructure-property relationships of the new Al-Li-X alloys and focuses on strength, ductility, fracture toughness, fatigue and stress corrosion properties.

INTRODUCTION

The development of Al-base alloys containing lithium began in Germany in the 1920's and was primarily concerned at first with additions of very small amounts of lithium to Al-Zn-Cu alloys to increase their strength (1,2). However, the development of modern aluminum-lithium alloys can be traced to the discovery by LeBaron in 1942 that lithium could be a major strengthening element in aluminum-copper alloys (3). Subsequent work by Hardy and Silcock (4,5) identified the lithium-containing strengthening phases in Al-Cu-Li alloys and contributed significantly to the scientific understanding of these complex materials. In the 1950's metallurgists at Alcoa recognized that lithium also increased the elastic modulus of aluminum and developed the high strength Al-Cu-Li alloy 2020. Later, metallurgists in Russia (6) developed the Al-Mg-Li alloy 01420 which had a considerable density advantage over other medium strength aluminum alloys. However, production problems combined with marginal engineering properties inhibited the widespread use of these lithium-containing aluminum alloys.

In the early 1970's escalating fuel costs and the desire to develop more fuel-efficient and high-performance aircraft generated a major interest in materials that would reduce weight and thereby increase structural efficiency. Reducing the density, without compromising strength, toughness, and corrosion resistance, has been shown to be the most efficient way to accomplish this goal (7). Although carbon fiber and boron fiber non-metallic composites offer a considerable density advantage over all other structural materials used in aircraft, improvements in the properties of aluminum alloys seemed desirable due to their relatively low acquisition cost and the aircraft community's extensive design and manufacturing experience with these materials. Aluminum-lithium alloys appeared attractive since lithium can reduce the density of aluminum by three percent and increase the elastic modulus by six percent for every weight percent added (8). These advantages have encouraged every major aluminum alloy producer in the U.S. and abroad to develop alloys containing lithium, usually at levels of 2.0 weight percent and higher. Both ingot metallurgy (I/M) and powder metallurgy (P/M) approaches were used during the alloy development programs; however, most major advances were made using the former technique.

Alloy designations and compositions of the new lithium-containing aluminum alloys are listed in Table 1. Many of these alloys possess good combinations of strength, damage tolerance and durability and in general are quite weldable. In addition, several have demonstrated excellent cryogenic and elevated temperature properties. However, the properties of the new aluminum-lithium alloys appear particularly sensitive to small variations in composition and processing. This sensitivity seems to be associated with the difficulty in maintaining metal quality during casting, the presence of recrystallization inhibiting elements, and the complexity of the microstructure after primary processing and heat treatment. As with most aluminum alloys, microstructural features of importance for property control of Al-Li alloys include: (a) cast structure, (b) grain structure and crystallographic texture, (c) volume fraction, size and distribution of insoluble intermetallic particles and grain boundary precipitates and (d) coherency, volume fraction and distribution of strengthening precipitates.

TABLE 1. Current Al-Li Alloys and Compositions.

Alloy	2090	2091	8090	8090A	8091	X8092	X8192
Element*	Alcoa 8/6/84	C Pechiney 4/8/85	Alcan and C Pechiney May 1985	Alcoa (Late 1985)	Alcan 3/29/85	Alcoa May 1985	Alcoa Aug 1985
Si	0.10	0.20	0.20	0.10	0.30	0.10	0.10
Fe	0.12	0.30	0.30	0.15	0.50	0.15	0.15
Cu	2.4-3.0	1.8-2.5	1.0-1.6	1.1-1.6	1.8-2.2	0.5-0.8	0.4-0.7
Mn	0.05	0.10	0.10	0.05	0.10	0.05	0.05
Mg	0.25	1.1-1.9	0.6 to 1.3	0.8-1.4	0.5-1.2	0.9-1.4	0.9-1.4
Cr	0.05	0.10	0.10	0.05	0.10	0.05	0.05
Ni	—	—	—	—	—	—	—
Zn	0.10	0.25	0.25	0.10	0.25	0.10	0.10
Ti	0.15	0.10	0.10	0.15	0.10	0.15	0.15
Li	1.9-2.6	1.7-2.3	2.2-2.7	2.1-2.7	2.4-2.8	2.1-2.7	2.3-2.9
Zr	0.08-0.15	0.04-0.16	0.04-0.16	0.08-0.15	0.08-0.16	0.08-1.5	0.08-1.5
Other: Each	0.05	0.05	0.05	0.05	0.05	0.05	0.05
Total	0.15	0.15	0.15	0.15	0.15	0.15	0.15

*Numbers Shown Are Either Maximums or Ranges

MICROSTRUCTURE AND DEFORMATION BEHAVIOR

Cast Structure:

Casting problems have been associated with the development of Al-Li alloys since Alcoa's entry with alloy 2020. Some of these are related to the reactivity of lithium-containing aluminum alloys and associated safety problems which have necessitated the use of modified refractories and degassing procedures, protective inert cover gases and/or surface fluxes during melting and casting, and special ingot cooling techniques (some employing organic coolants in place of water). These techniques have minimized the hazards of casting Al-Li alloys and current work is focusing on improving the quality of the as-cast product. The "as-cast quality" of ingot depends on both the surface quality, which determines the amount of scalping prior to further processing, and the internal structure which determines the processing steps necessary to produce the desired microstructure-property relationship. There can be, of course, some casting defects which are impossible to remove during subsequent processing. In addition to having a high surface quality and a crack free ingot, the ingot should be free of spherical voids and blisters and have a medium-fine grain structure, a consistent composition throughout, a low inclusion and alkali impurity content, and a low gas content (9).

A fine cast grain structure reduces porosity and the tendency for ingot cracking. Aluminum-lithium alloys have been found to be more difficult to grain refine than conventional aluminum alloys (10). The difficulty has been partly associated with the presence of zirconium which is used to control the wrought grain structure, since zirconium enhances the formation of twinned columnar grains (TCG) (11). Zirconium has beneficial effects, of course, since it forms the coherent Al_3Zr during ingot preheat which is very efficient in inhibiting recrystallization without the adverse effects on fracture toughness that is sometimes associated with large $Al_{12}(Fe,Mn)_3Si$, Al_3Mn_3Si , and $Al_{20}Cu_2Mn_3$ particles present in many 2XXX alloys. During normal ingot breakdown, hot working and subsequent heat treatment, the Al_3Zr dispersoids inhibit recrystallization although the cast grains do elongate in the direction of metal flow. Consequently, in the final produce most Al-Li alloys are unrecrystallized, and the cast grain structure relates directly to the grain structure.

Typical grain refining problems include a non-uniform grain size and the formation of twinned columnar grains (TCG) which not only result in increased cracking during processing but also reduce the elongation of the final product as shown in Figure 1. The as-cast grain size correlates well with both the toughness and the stress corrosion resistance of the final product. A fine as-cast grain size reduces fracture toughness, Figure 2, and fatigue crack growth resistance, since it minimizes the beneficial crack branching and the tortuous crack path often observed in larger-grained aluminum alloys.

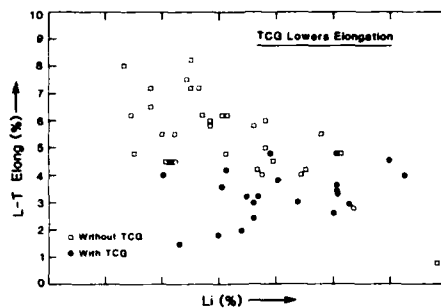


Figure 1. The effect of twin columnar grains and lithium content on the elongation of Al-Li alloys (From Labarre et al., reference 10).

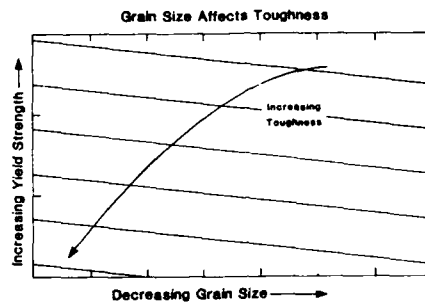


Figure 2. A schematic illustration of the increase in toughness with decreasing strength and increasing grain size (From Labarre et al., reference 10).

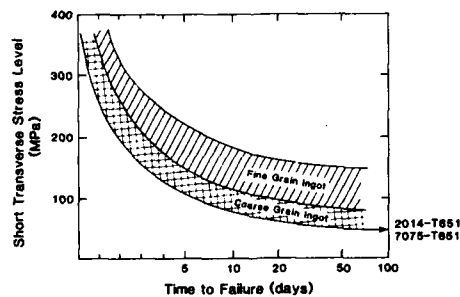


Figure 3. The effect of as-cast grain structure on the stress corrosion behavior of 8090-T851 plate. Base-line data of 2012-T651 and 7075-T651 is shown for comparison (Courtesy of A. Gray, Alcan International).

However, a fine as-cast grain size has been shown to have beneficial effects on the stress corrosion resistance of aluminum-lithium alloys, Figure 3. A reduction in grain size decreases the slip length and reduces the stress concentrations at grain boundaries thus reducing the mechanical component of stress corrosion cracking.

Inclusions may originate from the lining of the furnace, the flux, or from the presence of certain impurities, e.g., iron and silicon. The effect of iron content on the

strength/toughness of alloy 2020 aged to the T8 temper (12) is shown in Figure 4. Molten metal filtering, fluxless or inert gas casting, and high purity starter materials are common methods used to minimize inclusion problems. Besides the well-known relationship between inclusion content and fracture toughness, a high silicon content is believed to have a detrimental effect on the corrosion properties of Al-Li alloys (13). For compositions containing greater than 0.08 wt.% Si, the equilibrium AlLiSi phase forms upon solidification and is retained through all subsequent thermal mechanical treatments. This phase serves as an active nucleation site for surface pitting upon exposure to salt water, and greatly diminishes the material's resistance to stress corrosion cracking.

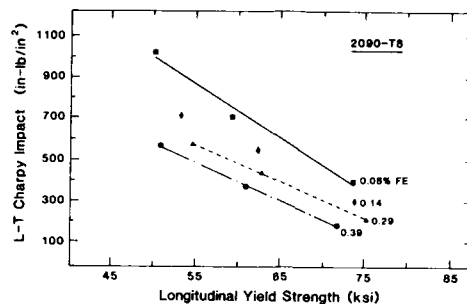


Figure 4. The effect of iron content on the strength/toughness relationship of 2090 (From Ashton et al., reference 12).

Precipitate Structure, Deformation Behavior and Fracture:

Al-Li: When binary Al-Li alloys containing more than 1 wt.% lithium are quenched from the single-phase field and aged at a temperature below the solvus, homogeneous precipitation of the metastable ordered phase δ' (Al_3Li) occurs. For alloys containing more than 1.7 wt.% Li it may be impossible to suppress δ' formation during quenching even when using ice water as the quenching medium (14). These precipitates have an L1_2 type superlattice structure, a spherical shape, and a cube/cube orientation with the aluminum matrix (15,16). Although they can be sheared by moving dislocations, they impede their motion and, consequently, greatly improve the strength over that of unalloyed aluminum. During artificial aging the δ' precipitates coarsen but retain their coherency and spherical morphology to relatively large sizes (>50 nm). A change in deformation mode from shearing to Orowan looping does not occur during practical heat-treatment times and temperatures.

In commercial Al-Li alloys that contain zirconium the small (≈ 50 nm) coherent, ordered Al_3Zr dispersoids that form during the ingot preheat are isostructural with Al_3Li and can act as nucleation sites for these precipitates. These composite precipitates are often observed coexisting with the homogeneously nucleated δ' . High temperatures and/or long aging times at normal aging temperatures result in the heterogeneous precipitation of the equilibrium δ (AlLi) phase at grain boundaries and other planar interfaces. These precipitates consume lithium from the surrounding region and produce a lithium-depleted precipitate-free-zone (PFZ) adjacent to the grain boundary. The microstructural features just described are shown in the transmission electron micrographs of Figure 5.

When the δ' precipitates are sheared by dislocations during deformation, their strengthening effect is reduced as both the degree of order and the precipitate size on the glide plane is reduced when the precipitate is sheared. Although dislocations move in pairs (superdislocations) in order to minimize the creation of antiphase domain boundaries in the δ' , their shearing results successively in a local decrease in resistance to further dislocation motion, a concentration of slip into intense shear bands and a reduction in ductility and fracture toughness. Sanders and Starke (14) have presented clear evidence of such inhomogeneous deformation, and Cassada et al. (17) have shown how the deformation can be homogenized and ductility improved by the addition of non-shearable precipitates. Since PFZ's are weaker than the precipitation-hardened matrix they can also lead to strain localization, thus further lowering the ductility and fracture toughness. This adverse effect is enhanced by the presence of the coarse grain boundary precipitates which may fracture or act as stress risers and preferential sites for microvoid nucleation and growth. Because of the severe strain localization effects associated with δ' and PFZ's, all aluminum alloys containing lithium that are being developed for commercial use contain other alloying elements in order to modify the precipitate types and sequences and thereby develop acceptable combinations of strength and toughness.

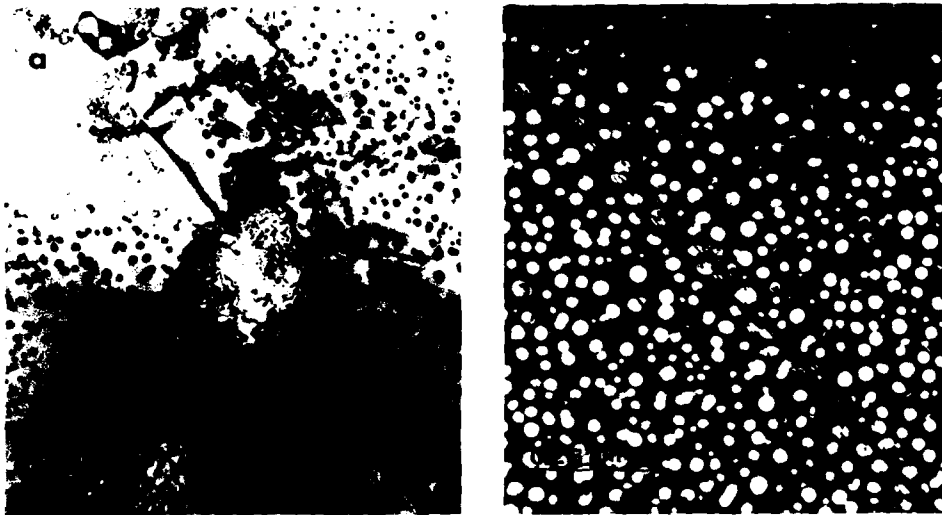
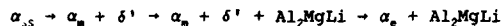


Figure 5. Transmission electron micrographs of an Al-Li alloy aged 24 h at 363K: (a) Bright-field image showing Al_3Li in the matrix, AlLi at grain boundaries and PFZ. (b) Dark field image showing the shearing of Al_3Li that occurs during deformation (Courtesy of W.A. Cassada).

Al-Li-Mg: The effect of magnesium additions on the phase equilibria of Al-Li alloys has been reported by a number of investigators (6,18,19). Magnesium decreases the solubility of lithium in aluminum at all temperatures below about 425°C (20). Similarly, the solubility of magnesium in aluminum is drastically reduced by the presence of lithium. Beyond the region of solid solution, in Al-Li-Mg ternary alloys with compositions close to the Al-Li binary, the decomposition of the supersaturated solid solution occurs via the δ' to δ precipitation sequence. However, as the composition of the ternary alloy is varied from the Al-Li binary towards the Al-Mg binary by increasing the magnesium to lithium ratio, the phase that is in equilibrium with the α solid solution changes from δ to Al_2MgLi . When supersaturated Al-Li-Mg alloys of practical interest are aged at temperatures below about 240°C, the precipitation sequence occurs as follows:



where α_{ss} , α_m , and α_e refer to the supersaturated, the metastable and the equilibrium α solid solutions, respectively.

The δ' phase that forms in Al-Mg-Li alloys is similar to that which occurs in the Al-Li binary. Al_2MgLi has a cubic α -Mn crystal structure and forms as rods along the $\langle 110 \rangle$ directions of the matrix (19). This phase is incoherent with the matrix, and nucleates predominately along the grain boundaries, dislocations and other structural inhomogeneities, Figure 6. Consequently, it does not contribute to precipitation hardening. Al_2Li is the only phase responsible for the strength of Al-Li-Mg alloys, with the magnesium contributing to some solid solution hardening (21). Therefore, the deformation behavior is coarse-planar, similar to that which occurs in Al-Li binary alloys, and the extensive strain localization that develops during deformation leads to premature failure. The lithium-rich Al_2MgLi phase that precipitates along grain and subgrain boundaries results in the formation of δ' PFZ's during prolonged artificial aging. As discussed previously, these zones, and their associated coarse grain boundary precipitates, have deleterious effects on ductility, fracture toughness, and possibly corrosion resistance (18).

Al-Li-Cu: The addition of copper decreases the maximum solid solubility of lithium in aluminum at all temperatures (5). Copper in solid solution does not influence the basic character of the δ' precipitation reaction (22), but it does introduce additional beneficial precipitation reactions that occur independent of the δ' reaction. The nature of the metastable and equilibrium phases that form within this alloy system have been shown to be dependent on the Cu:Li ratio and the aging temperature (5). For example, during aging at temperatures typical of commercial aging practices (120° to 200°C) the decomposition of the solid solution in a 2090 type alloy (Al-2.2Li-2.7Cu-0.12Zr) results in the formation of the metastable θ' (Al_2Cu -the primary strengthening phase in Al-Cu alloys) and the equilibrium T_1 phase (Al_2CuLi) (5,23,24). Al_2Cu has not been observed for Cu:Li ratios less than approximately 1.3. Al_2Cu has a tetragonal crystal structure and the

precipitates form as platelets parallel to the (100) planes of the matrix. T_1 has a hexagonal crystal structure with $a = 0.497$ and $c = 0.934$ nm and also forms as thin platelets but with a (111) habit plane. In commercial Al-Li-Cu alloys such as 2090, T_1 is the predominant copper bearing strengthening phase present after artificial aging to the near peak strength condition, although θ' may be present to a lesser degree. Figure 7 is a TEM of a 2090-type alloy showing the complex precipitate structure after aging to peak strength.

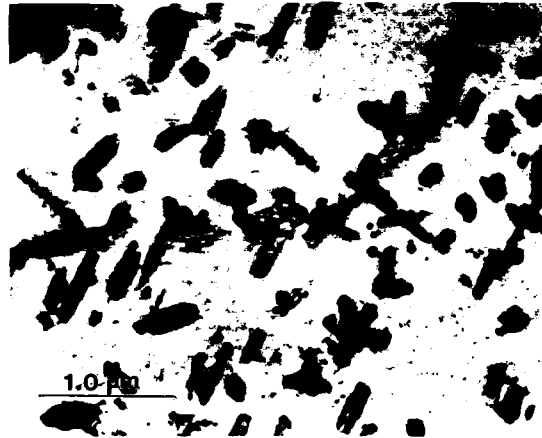


Figure 6. Bright-field micrograph showing the preferential nucleation of rod-like Al_2MgLi phase precipitates in a peak-aged Al-2Li-4Mg-0.12Zr alloy (Courtesy of G.H. Narayanan).

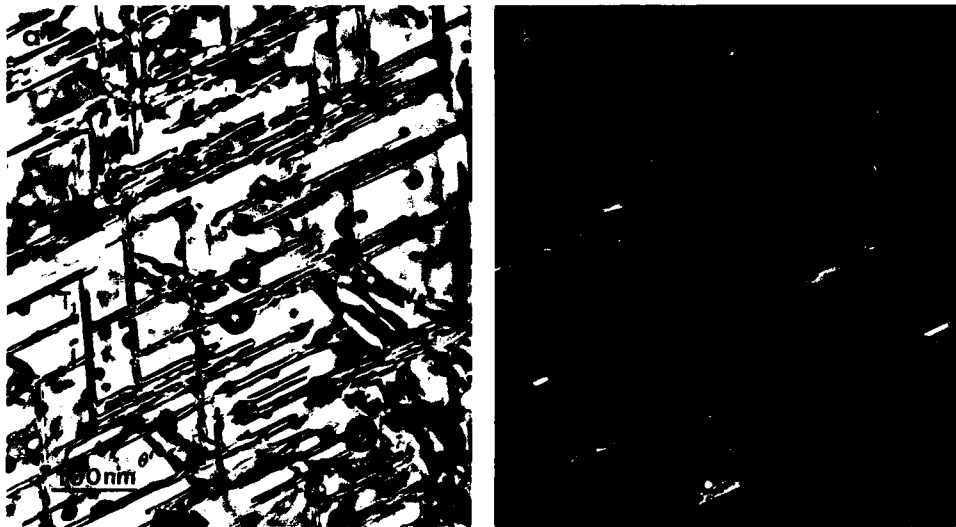


Figure 7. Transmission micrographs of Al-2.4Li-2.43Cu-0.18Zr alloy solution heat treated at 773K and aged 24h at 463K showing a complex precipitate structure that includes θ' , T_1 , δ' , and Al_3Zr (β'). (a) Bright field, (b) dark field of one variant of the T_1 precipitates (Courtesy of W.A. Cassada).

Both T_1 and θ' nucleate heterogeneously on dislocations and low angle grain boundaries, and other substructural features, Figure 8. Al_3Li normally is the first precipitate that forms during the aging of $Al-Li-Cu$ alloys having compositions of commercial interest. Subsequent precipitation of T_1 and θ' may reduce the volume fraction and alter the distribution of δ' since T_1 incorporates lithium and artificial aging may result in some reversion and reprecipitation of δ' . Although Noble and Thompson (23) and Gregson and Flower (25) have suggested that growth of the T_1 platelets is sustained by lithium from solid solution rather than dissolution of the δ' particles, Sanders (26) has clearly shown that during growth the T_1 precipitates cut through the δ' precipitates and may consume them, Figure 9. Reducing the volume fraction of δ' is beneficial in reducing the degree of strain localization (14).

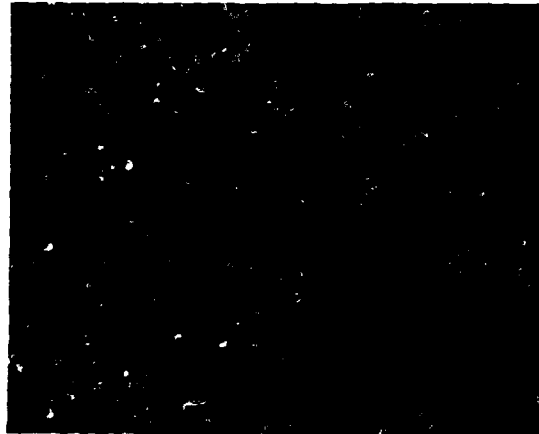


Figure 8. Weak beam dark field image showing the preferential nucleation of T_1 on matrix dislocations (Courtesy of G.H. Narayanan).

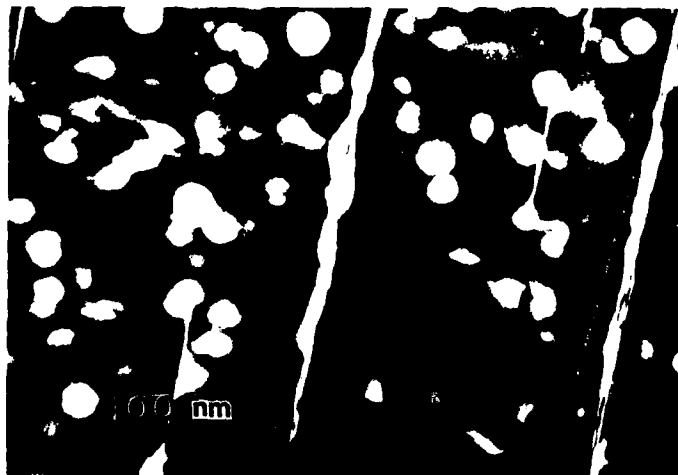


Figure 9. Dark-field micrograph showing T_1 precipitates cutting through and consuming Al_3Li precipitates (Courtesy of T.H. Sanders, Jr.).

Apart from the metastable θ' and equilibrium T_1 precipitates, the addition of copper also introduces another copper-containing phase, T_2 , having the stoichiometry of Al_4CuLi_5 (5) which nucleates predominately on high angle boundaries. Electron (27-30) and x-ray diffraction (29) analyses of this phase provide strong evidence that T_2 displays five fold icosahedral symmetry. The formation of the T_2 phase particles (which are richer in lithium than δ') along the grain boundaries lead to the development of δ' PFZ's adjacent to these boundaries, Figure 10, with concomitant reduction in ductility and fracture toughness. Cassada et al. (29) have shown that in 2090-type Al-Li alloys the T_2 phase is stable over the temperature range of 170°-520°C. Consequently, grain boundary precipitation of this phase should be anticipated in products that are slowly cooled or aged at temperatures above 170°C.

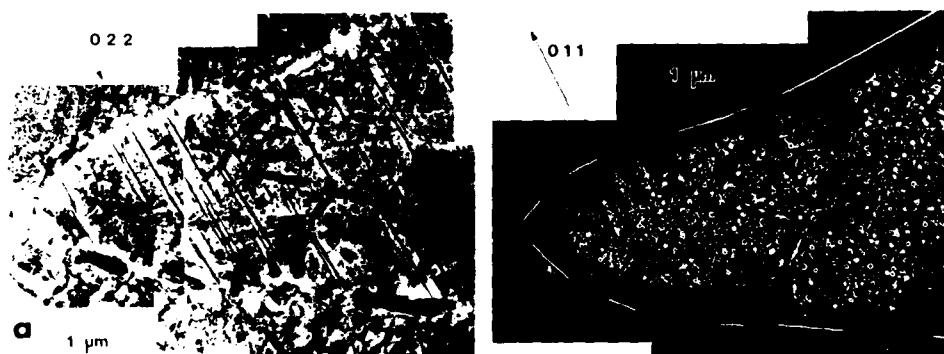


Figure 10. Micrographs illustrating grain boundary precipitates and associated PFZ: (a) Bright-field micrograph with T_2 grain boundary precipitates with five-fold diffraction symmetry arrowed. (b) Al-Li dark field showing the location of grain boundary and grain boundary precipitates (Courtesy of W.A. Cassada).

Early work by Price and Kelly (31) on Al-Cu single crystals aged to precipitate θ' indicated that θ' was not sheared but was looped and bypassed by moving dislocations in accordance with the Orowan model of strengthening. However, Starke and Lin (32) clearly showed that when the Al-Cu-Li alloy 2020 was aged to peak strength, where both θ' and δ' were present, deformation occurred by coarse planar slip. Huang and Ardell (33) obtained indirect evidence that T_1 is looped and bypassed by glissile dislocations, confirming an earlier suggestion by Sainfort and Guyot (34). The former authors aged an Al-Li-Cu alloy to produce δ' and T_1 , then applied a reversion treatment to eliminate δ' . However, Jata and Starke (35) showed direct evidence of T_1 shearing in an Al-Li-Cu alloy which also contained θ' and δ' precipitates. Shearing of T_1 and θ' when δ' is present may result from the superdislocations associated with δ' having a pileup force sufficient to shear these partially coherent precipitates.

Although both θ' and T_1 may be sheared in the presence of δ' , they do appear to decrease the extent of strain localization that occurs in binary Al-Li alloys. The resistance that a shearable strengthening precipitate offers to a glissile dislocation depends on a number of factors which include the coherency strain field, the interfacial energy, the internal structure of the precipitate, etc. For ordered precipitates, such as δ' , the strengthening mechanism associated with the internal structure is reduced by shearing. The small lattice misfit ($\sim 0.18\%$) (15) and the small interfacial energy (180 ergs/cm²) (36) between δ' and the matrix suggest that these strengthening mechanisms are not important for δ' . However, the much larger misfits and interfacial energies between θ' , T_1 , and the matrix suggest that these strengthening mechanisms do operate when these precipitates are present. Neither strengthening mechanism is as effectively destroyed by particle shearing as is order strengthening and, therefore, the tendency for strain localization by work softening on the glide plane is reduced when θ' and T_1 are present.

Al-Li-Cu-Mg: When magnesium is added to Al-Li alloys containing copper, matrix precipitation of S' (Al_3CuMg) occurs. The exact nature of the phase equilibria of the quaternary Al-Li-Cu-Mg alloys depends on the relative concentrations of all three alloying elements. For example, the addition of small amounts (0.5 to 1.0 wt.%) of magnesium to a high copper alloy such as 2090 suppresses the formation of θ' and introduces the S' phase (37). Since S' contains no lithium δ' precipitation is not markedly influenced by the magnesium addition and T_1 remains the dominant secondary phase in such an alloy. For alloys such as Al-3Cu-1.6Li-0.8Mg little or no δ' forms and there appears to be equal amounts of T_1 and S' (37). In higher lithium - lower copper alloys such as 8090, S' , which

precipitates with δ' and a small amount of T_1 , becomes the dominant Cu-bearing phase (25,38), Figure 11. As the magnesium to copper ratio is progressively increased, the precipitation of T_1 is fully suppressed and S' becomes the primary Cu-bearing strengthening phase. This is the case for 2091 which has a nominal composition of Al-2Li-2.2Cu-1.5Mg-0.8Zr (39,40). When the concentration of magnesium exceeds that of copper the Al_2MgLi phase may precipitate in addition to S' (41).

The S' phase has an orthorhombic crystal structure ($a = 0.405$ nm; $b = 0.905$ nm; $c = 0.72$ nm) and forms initially as rods or needles aligned along the $\langle 100 \rangle$ directions in the matrix. The precipitates are partially coherent with the matrix and show a strong tendency for heterogeneous nucleation along matrix dislocations, low angle grain boundaries and other structural inhomogeneities. However, unlike the case of T_1 precipitation, the heterogeneous precipitation of S' does not result in PFZ's along either low or high angle grain boundaries. A T_2 -type phase (possibly $Al_2Cu(LiMg)_2$) has been observed on grain boundaries of 8090-type alloys and, similar to such precipitation in Al-Li-Cu alloys, it does result in PFZ's. The combination of these microstructural features may lead to low ductility, fracture toughness, and corrosion resistance although the presence of S' in the matrix certainly minimizes these effects. Crooks et al. (42) and Crooks and Starke (37) have clearly shown that when S' is present in Al-Li-Cu-Mg alloys strain localization is suppressed indicating that the precipitate is not sheared by glissile dislocations. These observations were later confirmed by Gregson and Flower (25). The S' precipitates do not have densely packed slip planes parallel to the matrix slip planes and are, therefore, unlikely to be penetrated by dislocations (25).

A schematic representation of the various phases found in basic as well as the more complex Al-Li-X systems that encompass modern Al-Li alloys is shown in Figure 12.

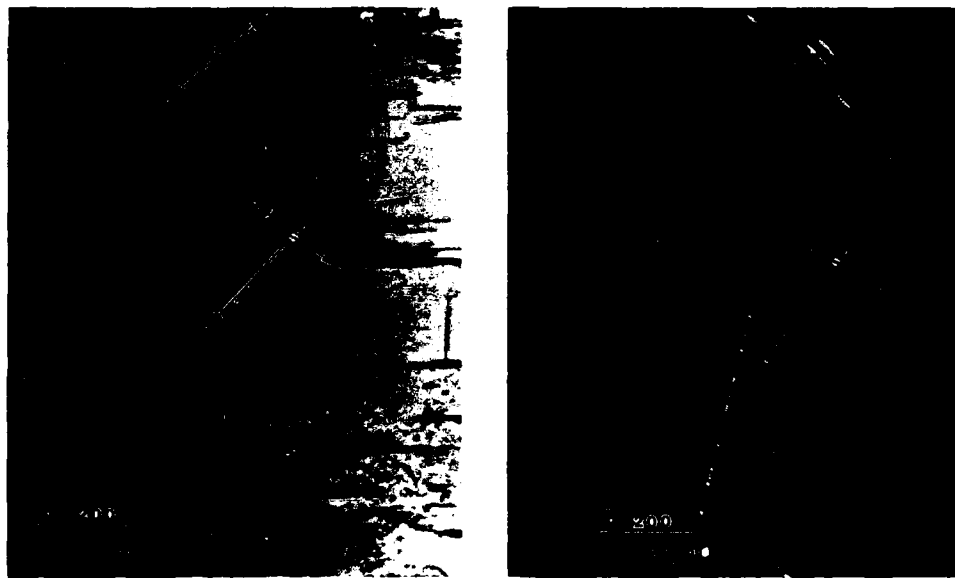


Figure 11. Micrographs of the S' and T_1 precipitates in an 8090 alloy: $B = 001$. (a) Bright field, (b) Dark field (Courtesy of R. Sinko).

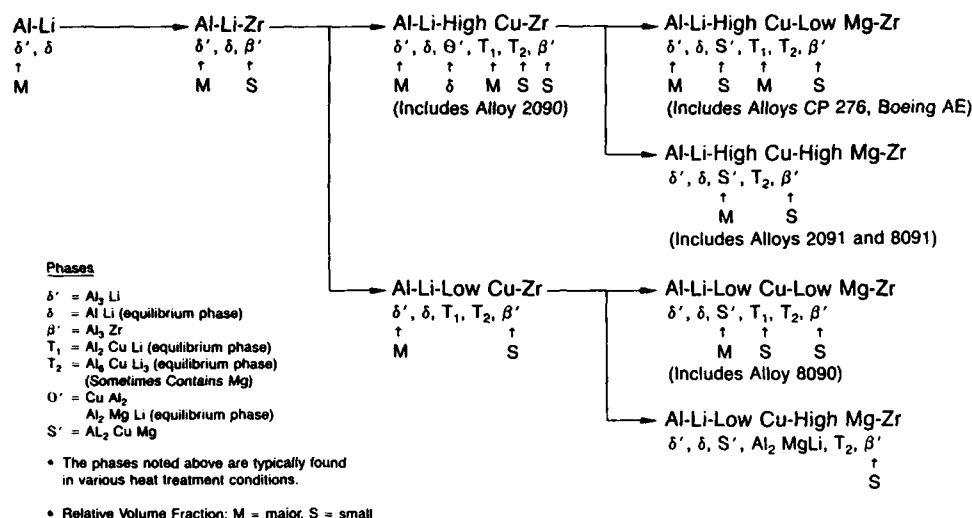


Figure 12. A schematic illustration of the precipitate phases that form in Al-Li-X alloys (from Narayanan and Quist).

EFFECT OF PROCESSING ON MICROSTRUCTURE DEVELOPMENT AND PROPERTIES

As mentioned previously, the first Al-Li-X alloys that were developed for commercialization suffered from low ductility and fracture toughness. These problems were primarily associated with strain localization and grain boundary precipitates, and alloying additions and processing methods were selected to minimize these problems. A variety of production methods, including rapid solidification and powder metallurgy consolidation, mechanical alloying, and ingot casting have been used for the development of the new Al-Li alloys. Rapid solidification and mechanical alloying were used as a means of reducing the grain size and extending solid solubility; however, ingot casting has proven to be the most feasible method for the production of large plate and extrusion products and is being used for the alloys that are currently in commercial production. However, powder metallurgy methods, including mechanical alloying, may offer advantages for certain product forms such as forgings.

Processing begins with homogenization to reduce segregation, remove the low-melting nonequilibrium phases, and thus improve workability. This thermal treatment also serves to precipitate the dispersoid-forming elements, such as those containing zirconium, so that they may perform their role of grain control during subsequent processing. One must be very careful in going to the final homogenization temperature to ensure that the low-melting phases are dissolved before their melting temperatures are reached. A heating rate of 10°C/hr from 315°C to the normal homogenization temperature of 543°C is frequently used. The atmosphere used in the homogenization treatment should be relatively dry in order to minimize oxidation and hydrogen pickup. One also needs to be concerned about lithium loss from the surface (43). The homogenization treatment is followed by hot working for ingot breakdown and shape change to the appropriate product form. The wrought product is then solution heat treated, quenched, possibly worked, and aged to develop the desired microstructure. The temperature, amount of deformation prior to aging, etc., depend on the alloy composition and the final microstructure and properties that are desired.

Density and Elastic Modulus:

Lithium is the lightest metallic element and, with the exception of beryllium, is the only metal that both increases the modulus and reduces the density when alloyed with aluminum. Although the presence of heavier elements such as copper will somewhat offset the density advantage afforded by lithium, the overall reduction in density achieved will still be dominated by the amount of lithium added (44), Figure 13. Several investigators have developed empirical equations to predict alloy densities from known composition. One such formula by Peel et al. (38) is as follows:

$$\text{Density (g/cc)} = 2.71 + 0.024\% \text{Cu} + 0.018\% \text{Zn} + 0.022\% \text{Mn} - 0.079\% \text{Li} - 0.01\% \text{Mg} - 0.004\% \text{Si}.$$

In this equation the elemental concentrations are expressed in weight percent.

The modulus enhancement of aluminum by lithium additions is due to both solid solution effects as well as to the precipitation of lithium bearing compounds, and will change relative to both the amount of lithium added and the prior thermal treatment (45,46). Copper has a slight beneficial effect and magnesium a slightly negative effect on the modulus of aluminum (47,48). Recent studies by O'Dowd et al. (49) for 2090-type alloys and Broussaud and Thomas (50) for Al-Li binary alloys have shown that a maximum in modulus occurs just prior to the peak strength condition, Figure 14. Using the law of mixtures and a modulus for aluminum of 80.7 GPa O'Dowd et al. calculated a modulus for δ' of 97 GPa and a modulus for T_1 of approximately 350 GPa. They observed a sharp drop in modulus with the precipitation of the icosahedral T_2 phase. Their data suggested that T_2 has an extremely low intrinsic modulus and is very detrimental to the elastic properties of Al-Li-Cu alloys. Figure 15 shows a comparison of the modulus of elasticity of several Al-Li-X and baseline aluminum alloys (51).

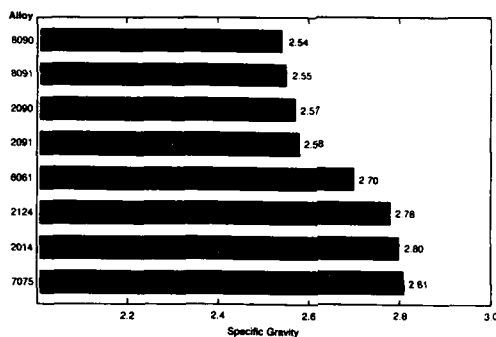


Figure 13. A comparison of densities for several Al-Li and conventional alloys (From Wakeling, reference 51).

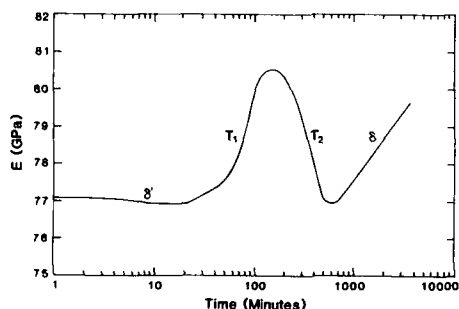


Figure 14. Young's modulus versus aging time at 190°C for an Al-2.31Li-2.24Cu-0.16Zr alloy. Precipitation occurs as indicated on the figure (From O'Dowd et al., reference 49).

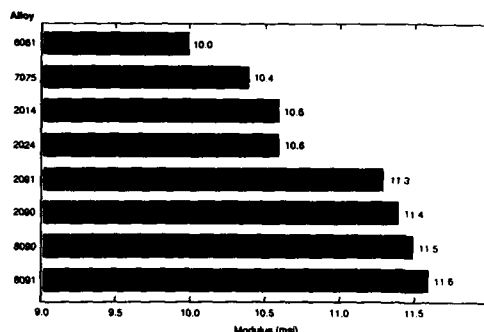


Figure 15. A comparison of Young's modulus for several Al-Li and conventional alloys (From Wakeling, reference 51).

Grain Structure and Crystallographic Texture:

Starke and Lin (32) showed that grain structure and texture can have a significant effect on the ductility of aluminum-lithium alloys. They related the poor ductility and fracture toughness of a 2020 alloy plate product to a partially recrystallized structure, very large recrystallized grains, and a high volume fraction of large inclusions. They were able to significantly improve the ductility of 2020 by thermomechanical treatments that produced either a completely recrystallized structure with small recrystallized grains or a completely unrecrystallized structure with a sharp deformation texture. Subsequently, Lin (52) showed that when PFZ's are present the grain aspect ratio of the recrystallized grains also has a major effect on the deformation behavior and fracture mode.

For alloys that deform by planar slip and/or have soft PFZ's, e.g., 2020, large recrystallized grains result in long slip lengths which produce large stress concentrations at grain boundaries and enhance low-energy intergranular fracture. Deformation is localized within the PFZ only when this region is favorably oriented for slip. This is always the case for equiaxed grains but occurs with less frequency for elongated grains when the stress axis is parallel to the long grain dimension. Grain boundary misorientation, i.e., texture, also plays a role in determining slip length and type of fracture. Grain boundaries can be a major barrier to slip if the misorientation is large, which is the usual case for recrystallized aluminum alloys. However, grain boundaries may not inhibit slip if the misorientation is small, e.g., for unrecrystallized materials with sharp deformation textures (53) (this is the situation for most Al-Li alloy products). The deformation process, i.e., the operative slip system(s), strongly depends on the crystal orientation. Shape accommodation, due to the constraint of material flow, varies with the crystal orientation and the misorientation between adjacent grains.

Small grains and large misorientations enhance multiple slip due to von Mises criterion, which may reduce stress concentrations at grain boundaries and the incidence of intergranular fracture. However, when the grain size is larger than some critical value, (which depends on the strength of the boundary, the degree of slip planarity, etc.) a large misorientation produces an effective barrier to slip, resulting in a stress concentration which may increase the incidence of intergranular fracture. A sharp deformation texture enhances slip continuity across grain boundaries and increases the probability of higher energy transgranular fracture. However, if slip is coarse-planar and strain localization extensive, the fracture toughness may be low even though the fracture mode is transgranular (25).

The desired grain structure may depend on the stress condition (54). Plane stress fracture toughness is believed to be controlled by the amount of plastic deformation occurring in a large plastic zone and a fine recrystallized grain structure aids in producing a maximum amount of plastic deformation. On the other hand, plane strain fracture toughness may be more influenced by grain boundary particles and increased toughness may result from a large grain boundary spacing. In Al-Li alloys these effects are particularly important, and it is found that sheet material with an unrecrystallized fine grain size often produce the highest plane stress toughness whereas unrecrystallized coarse grained thick section material is best for high plane strain fracture toughness (54).

In addition to its effect on deformation and fracture modes, texture may have a significant effect on strength as predicted by the Taylor relationship: $\sigma = M\tau$, where σ is the yield strength, τ the critical resolved shear strength on (111) planes and M an orientation factor which averages the distribution of grain orientations. When this distribution is isotropic, $M = 3$. The textures produced in aluminum alloys depend on a variety of parameters which include alloy content, precipitate structure and deformation mode, grain size and shape, starting texture, degree of recrystallization, directionality

of deformation, and temperature of deformation. The crystallographic texture usually cannot be simply described since it may consist of a number of deformation and recrystallization components.

Commercial aluminum-lithium alloys normally have very strongly developed textures with resultant anisotropic properties (55-64). Both Al-Li-Cu-Zr and Al-Li-Cu-Mg-Zr alloys exhibit pronounced yield stress and ductility anisotropy in sheet, plate, and extruded products. In sheet products the texture is normally uniform throughout the thickness and the mechanical properties only vary with angle of the stress axis to the rolling direction (64), Figure 16. However, in thicker products, e.g., plate and extrusions, the texture may vary throughout the thickness resulting in an additional anisotropy, Figure 17 (62). Some of the through-thickness texture variation is usually associated with a limited amount of recrystallization that normally occurs near the surface. In addition to anisotropic effects due to crystallographic texture, variation in properties throughout a product may be due to variations in volume fraction and distribution of the strengthening and grain boundary precipitates (13). Rapid heat-up rates during solution heat treatment, e.g., associated with salt baths, may decrease the degree of anisotropy, Figure 16 (64).

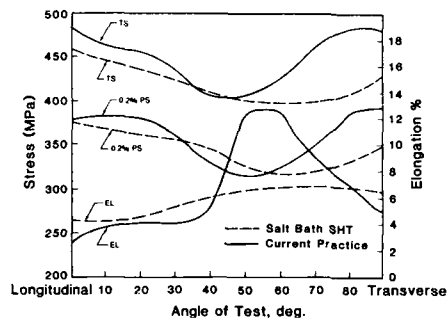


Figure 16. The mechanical properties of Al-Li alloy 8090 as a function of solution heat treatment practice and angle to the rolling direction (From Reynolds et al., reference 64).

The sharp textures that occur in Al-Li-X-Zr alloys are strongly associated with the use of zirconium as a grain refiner and recrystallization inhibitor. In addition, lithium probably has a contributory effect (65). Unless special procedures are applied no significant amount of recrystallization occurs in Al-Li-X-Zr alloys during ingot breakdown or subsequent thermomechanical processing, including intermediate anneals and solution heat treatments. This results in a very well defined deformation texture and the consequential effects mentioned previously. Cross rolling may spread the predominant poles and decrease the degree of anisotropy (12,58). As noted earlier, recrystallization textures normally lead to more isotropic properties and a very fine recrystallized grain size offers advantages under plane stress conditions (assuming grain boundary effects do not dominate). Sheet products of two alloys, 2091 and 8090, which are being marketed in the recrystallized condition to optimize their plane stress fracture toughness.

Alloying additions and/or microstructural features that homogenize deformation normally reduce the effect that a sharp texture has on property variations. Although Hirsch et al. (60) have shown that some control over texture may be obtained by controlling the initial texture, grain shape and aging, the anisotropy of properties associated with the texture of commercial Al-Li-X alloys is still a major problem and production methods need to be developed to produce the desired texture in all product forms.

Quench Sensitivity and Grain Boundary Precipitates:

The primary purpose of quenching age-hardenable aluminum alloys is to maintain a large degree of supersaturation of solute atoms homogeneously distributed in solid solution. This permits precipitation of an optimum concentration and distribution of hardening particles during the aging treatment. As quench rates decrease, more time is allowed for solute atoms to migrate to grain boundaries or precipitate as matrix phases. Grain boundaries act as heterogeneous nucleation sites by reducing the free energy barrier to nucleation (66). When thermodynamic and kinetic demands are satisfied, precipitation can occur along the grain boundary and enhance intergranular cracking, grain boundary decohesion and premature material failure (43).

Slow quench rates are unavoidable in very thick plate or heavy section forgings and under such conditions precipitation of grain boundary phases may occur. Lewis et al. (13) have shown that when 8090 is quenched from the solution treatment temperature at rates slower than 10°C/sec, precipitation of the icosahedral T_1 phase occurs at high angle grain boundaries. These brittle precipitates can lead to low fracture toughness by acting as stress risers and preferential sites for microvoid nucleation and growth (67).

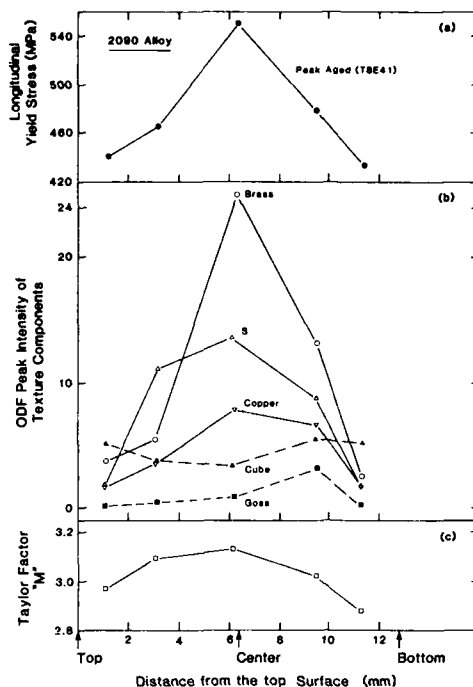


Figure 17. (a) Through thickness variation in longitudinal yield stress, (b) Through thickness variation in intensity of texture components, (c) Variation in the calculated Taylor factor (M) through the thickness (From Vasudevan et al., reference 62).

Colvin and Starke (68) have determined time-temperature-transformation diagrams for the precipitation of both the T_2 and S phases for two compositional variants of 8090, Figure 18. A solute-rich Al-2.58Li-1.36Cu-0.9Mg-0.13Zr alloy exhibited a greater sensitivity to quenching rates than did a solute-lean Al-2.28Li-0.86Cu-0.9Mg-0.13Zr alloy. Colvin and Starke related the precipitation of the T_2 and S phases with the fracture toughness of the alloy, Figure 19, and concluded that T_2 was the principal cause for the loss of mechanical properties in poorly quenched 8090. Staley (69) has recently determined TTT diagrams and related mechanical properties for 2090 and has found results similar to those obtained for 8090.

Strengthening Precipitates:

Engineering properties important in the design of Al-Li alloys for aerospace applications include a proper balance between strength, ductility, fracture toughness, fatigue resistance, formability, and corrosion resistance. The volume fraction, size, spacing, and distribution of the strengthening precipitates are important microstructural features that impact all of these properties. Processing of the wrought product to optimize the microstructure and properties begins with the proper selection of the solution heat-treatment temperature. This treatment should ensure that the maximum amount of solute has been put in solid solution and that the rate of heat-up and maximum temperature does not result in nonequilibrium eutectic melting (70). For most Al-Li-X alloys the maximum solution heat treatment temperature has been determined to be approximately 545°C (43). The solution heat treatment is followed by a quench which should be sufficiently rapid to prevent deleterious precipitation of grain boundary phases, as discussed previously, without causing quench residual stresses that will produce warping. The warping issue is more serious than with normal aluminum alloys due to the relatively high solution treatment temperatures and low thermal conductivity associated with Al-Li alloys.

Quenching is often followed by some type of cold work in order to redistribute the quenched in residual stresses. However, for Al-Li-Cu and Al-Li-Cu-Mg alloys that contain θ , T_1 , and S' strengthening precipitates, cold work prior to aging is used in conjunction with the aging temperature to control the distribution of the precipitates. Deformation prior to aging increases the dislocation density and thereby the number of nucleating sites for heterogeneous precipitation. Since the dislocations would also be in the vicinity of

the grain boundary, precipitation of the strengthening precipitates would be encouraged in this region, thus minimizing the probability of PFZ formation. Dislocations are most effective as nucleation sites for those precipitates that have large interfacial energies and/or strains, e.g., θ' , T_1 , and S' , but have no significant effect on the nucleation of δ' .

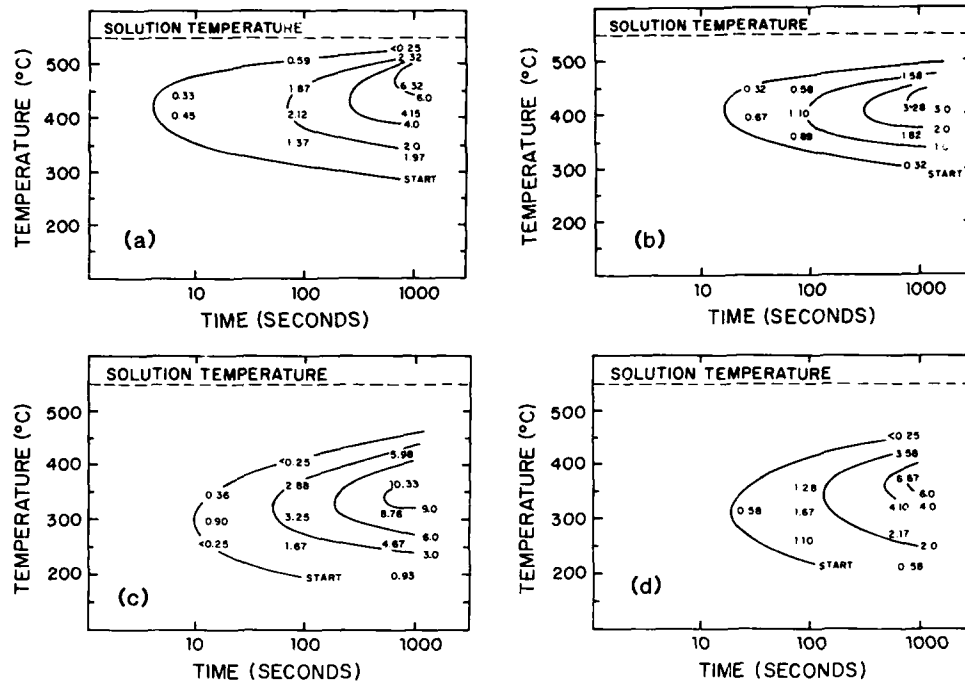


Figure 18. Time-temperature-transformation curves showing volume percents of T_2 and S phases. (a) T_2 for Al-2.58Li-1.36Cu-0.9Mg-0.13Zr (rich) alloy; (b) T_2 for Al-2.28Li-0.86Cu-0.9Mg-0.13Zr (lean) alloy; (c) S for the rich alloy and (d) S for the lean alloy (From Colvin and Starke, reference 68).

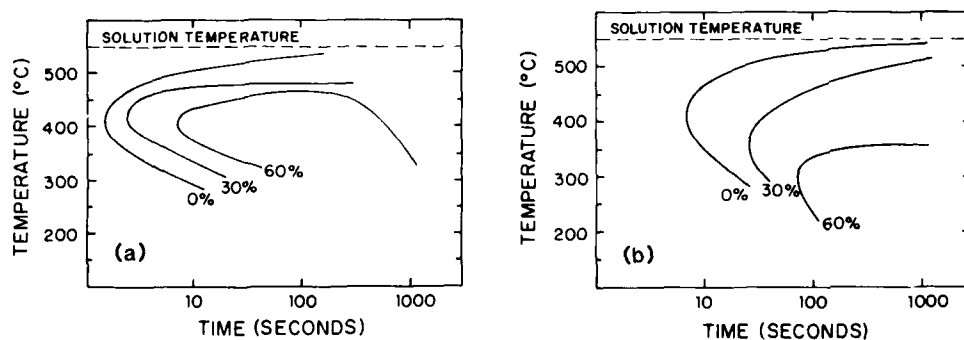


Figure 19. Iso mechanical lines showing the percent loss of Charpy energy values as a function of time at various temperatures (a) rich 8090 alloy and (b) lean 8090 alloy (From Colvin and Starke, reference 68).

Figure 20(a) shows the effects of different amounts of deformation prior to aging on the number density of the T_1 precipitates formed during aging for various times at 190°C (71). Since strength is related to the precipitate structure, there is a corresponding effect on strength, as shown in Figure 20(b). The significance of this data relates to commercial processing and different product forms, since a nonuniform distribution of deformation prior to aging can result to wide variances in strength within a product. Some product forms, such as complex forgings and those formed by superplastic deformation, are not easily conducive to cold deformation prior to aging. Consequently, there is interest in examining heat treatment procedures and/or alloying additions that may aid in the nucleation of the strengthening precipitates in a way that is similar to the effect of dislocations.

Lewis et al. (13) have improved the fracture toughness and stress corrosion resistance of 8090 by aging at 150°C instead of the commonly used 190°C. Pitcher (72) has recently shown that a slow heat-up rate to the aging temperature can lead to a better balance of tensile strength and toughness in 8091 than a rapid heat-up rate when deformation prior to aging is impossible. He relates the enhanced precipitation of S' to the release of vacancies, as the δ' precipitates grow during the slow heat up. These vacancies assist the formation of homogeneous S' . A slow heat-up rate has the same effect as a duplex age, i.e., at a low temperature followed by aging at a high temperature. Both a slow heat-up rate to the aging temperature and a low - high temperature duplex age are common practices for 7XXX alloys. Recent studies by Blackburn et al. (73) have demonstrated that small additions of indium to 2090 can aid in the nucleation of both T_1 and θ' . This has an effect similar to a 3 to 4% stretch, when compared with an indium-free alloy.

Ashton et al. (43) have established that a combination of cold work (up to 7%) prior to aging and a low aging temperature can significantly improve the strength-toughness relationship in both 2090 and 8091. The combined effect of stretch, aging time, and aging temperature on yield strength and toughness is shown in Figures 21 and 22. As mentioned, deformation increases the number of nucleation sites for θ' , T_1 , and S' . Lowering the aging temperature increases the degree of supersaturation and the driving force for nucleation of the strengthening precipitates. Consequently, higher strengths than realized at higher aging temperatures may be obtained. In addition, since diffusion rates are decreased, the size and volume fraction of the grain boundary precipitates are also decreased, which produces an improvement in the fracture toughness.

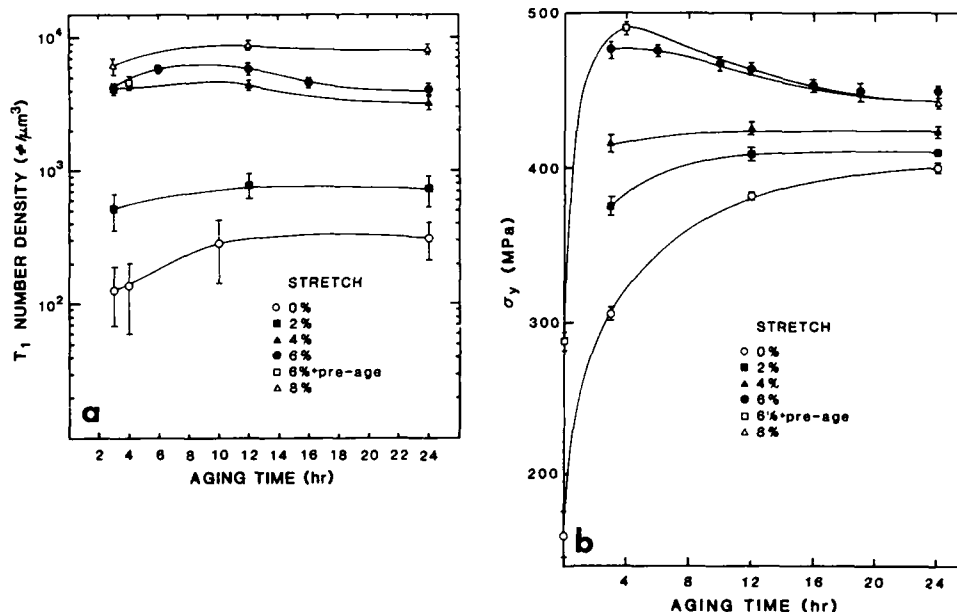


Figure 20. Effect of stretch on the precipitation and strength of an Al-2.4Li-2.4Cu-0.18Zr alloy. (a) Number density of T_1 as a function of aging time at 463K for various degrees of stretch prior to aging and (b) corresponding yield strength vs. aging time (From Cassada, Shiflet and Starke, reference 71).

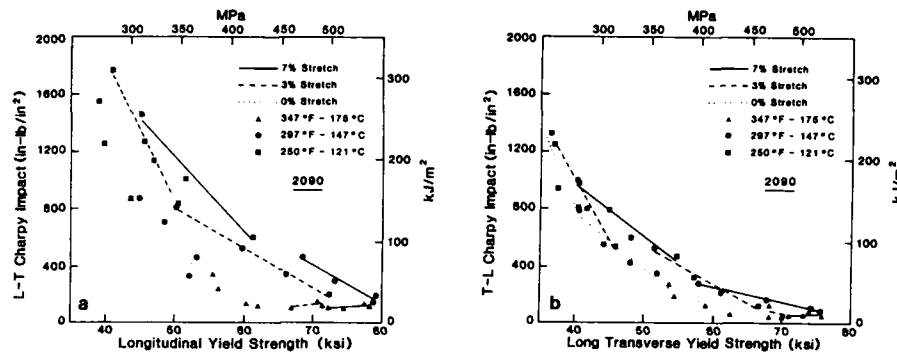


Figure 21. Effect of percent stretch and aging practice on the yield strength and Charpy impact energy of 2090 plate. (a) L orientation, (b) LT orientation (From Ashton et al., reference 43).

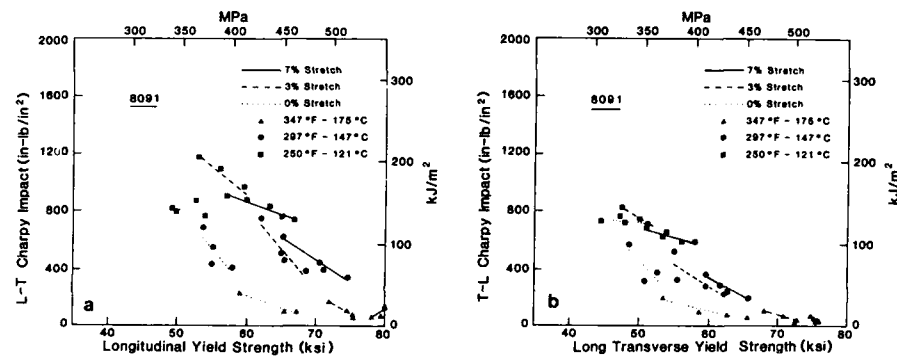


Figure 22. Effect of percent stretch and aging practice on the yield strength and Charpy impact energy of 8091 plate. (a) L orientation, (b) LT orientation (From Ashton et al., reference 43).

In general, for alloys that contain a low volume fraction of constituent phases and grain boundary precipitates, the fracture toughness is controlled by the deformation behavior, being maximized when deformation is homogeneous (35). Jata and Starke (35) showed that the fracture toughness variation with aging time can be quantitatively related to the changes in slip planarity, i.e., the fracture toughness decreases as the slip band width decreases and the slip band spacing increases. They also determined (75) that slip localization decreases with decreasing temperature, thus explaining the major reason for the large improvement in fracture toughness with decreasing temperature. The higher fracture toughness at cryogenic temperatures has also been attributed to: (a) low melting point grain boundary phases which solidify at low temperatures and remain liquid at room temperature (75,76), (b) a larger number of crack delaminations perpendicular to the short transverse direction or perpendicular to the fracture surface in an L-T oriented specimen (77,78) and in plane crack deflections (78) and (c) higher strain hardening capacity at low temperatures (79). The Jata and Starke model is consistent with the increase in strain hardening capacity at low temperatures.

The optimum microstructure for fatigue crack initiation resistance is consistent with that required for high fracture toughness (80). However, the situation is somewhat different for fatigue crack growth resistance (81). Lin and Starke (82) have shown that a tortuous crack path and crack branching, both of which are enhanced by coarse planar slip, are desirable for a high fatigue crack growth resistance in aluminum alloys. The tortuous crack path reduces the "crack driving force" due to extrinsic effects which include roughness-induced crack closure (83-85). The propensity of Al-Li alloys to deform by coarse planar slip results in a significant improvement in fatigue crack growth resistance under both constant amplitude (54,85-87) and variable amplitude loading (88) when compared with conventional high strength aluminum alloys. Figure 23, taken from the work of Ritchie and co-workers (89), compares the crack growth behavior of 2090-T8E41 (T-L orientation) with that for two different tempers of 2124 and 7150.

Aluminum-lithium alloys have not demonstrated the same significant advantages over baseline alloys for short crack growth resistance (90). This is partially the result of reduced crack tip shielding effects (85,91). However, even in this regime Al-Li should show some improvement considering that they normally have a modulus of between 10 to 15 percent larger than conventional aluminum alloys. Although the fatigue crack initiation resistance of Al-Li alloys may be somewhat poorer than that of conventional alloys (92,93) (most likely due to the extensive strain localization and sharp texture normally present) their overall fatigue performance under S-N type test conditions is generally equivalent to, or better than, that of standard aluminum alloys.

The precipitate structure also has a significant effect on the stress corrosion cracking behavior of Al-Li alloys (94). While Al-Li, Al-Li-Zr, and Al-Mg-Li-Zr alloy systems exhibit a high resistance to stress corrosion crack initiation (95,96) the Al-Li-Cu-Zr and Al-Li-Cu-Mg-Zr systems do not (95,97-101). This suggests that the presence of one of the copper containing precipitate phases, e.g., T_1 , S' , T_2 or $Al_2Cu(MgLi)$, may be responsible for promoting crack initiation rather than $AlLi$ or Al_2MgLi (94). Underaged tempers have been shown to be less susceptible than peak or overaged tempers to SCC initiation for Al-Cu-Li-Zr alloys (94) but overaging has been shown to decrease the susceptibility of Al-Li-Cu-Mg-Zr alloys, Figure 24. Although underaged tempers appear to offer the highest resistance to SCC propagation for both alloy systems, Figure 25, the propagation behavior is relatively insensitive to temper as well as being insensitive to alloy chemistry and test environment (94).

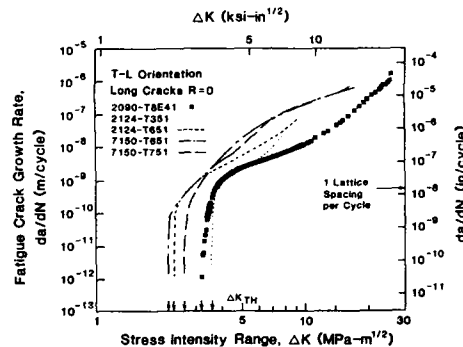


Figure 23. Crack propagation behavior of long fatigue cracks in 2090-T8E41 (T-L orientation), as a function of the nominal stress intensity range, compared to corresponding results in 2124 and 7150 alloys. Data for tests in moist air at $R = 0.1$ (From Ritchie and coworkers, reference 89).

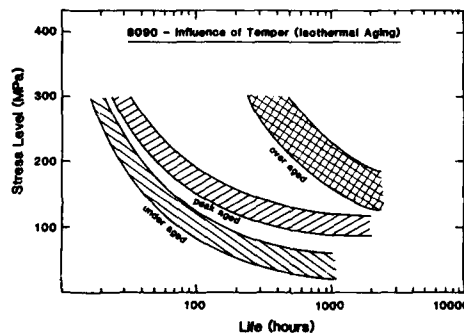


Figure 24. The influence of temper on the stress-life curve of 8090 plate (ST orientation). Underaged = 4 h at 190°C; Peak-aged = 16 h at 190°C; Overaged = 96 h at 190°C (From Gray et al., reference 94).

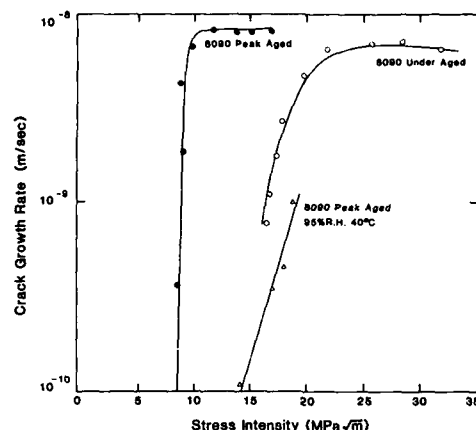


Figure 25. Crack growth velocity versus stress intensity curves for under- and peak-aged 8090 in artificial sea water and peak-aged 8090 in a 95 percent relative humidity atmosphere at 40°C (From Gray et al., reference 94).

Aluminum-lithium alloys, particularly 2090, have surprisingly different forming characteristics than the industry standard aircraft aluminum alloys such as 2024 and 7075 (102). These differences in formability reflect the unique deformation behavior and grain structure exhibited by Al-Li alloys, in particular, their propensity for localized planar slip. The formability of Al-Li alloys has also been shown to be more sensitive to grain direction and prior cold work than the standard aircraft aluminum alloys. Maximum formability has been observed when Al-Li alloys are in the "as-quenched" condition and the bend axis is parallel to the long grain direction (102). It was previously shown that cold work prior to aging is necessary to develop the optimum strength-fracture toughness in Al-Li-Cu-X alloys. However, this step often reduces formability, forcing a compromise between the most desirable part shape and the resulting properties. This has necessitated the development of procedures which utilize the cold work imparted during forming to bring the final product to the required strength level.

OTHER ENGINEERING PROPERTIES

In addition to those properties discussed above, there are certain other engineering properties of Al-Li alloys that are attractive in comparison to conventional baseline aluminum alloys. For example, most Al-Li alloys are amenable to superplastic forming (103,104), display moderate to good weldability (105,106), can be chemically milled, bonded, anodized, alclad, and painted. On the debit side, as noted previously, Al-Li alloys often display considerable anisotropy in strength and ductility. They are somewhat more susceptible to surface oxidation at moderate temperatures, and are prone to warping during quenching (mostly attributable to the relatively high quenching temperature). Diffusion of lithium can occur out to the surface during high temperature heat treatments which may lead to a lithium-depleted layer, and for sheet products a reduction in strength (107). In addition, all Al-Li-X alloys suffer from low ductility and fracture toughness in the short transverse direction. These problems are due to a combination of grain structure and segregation effects and should be minimized by improved processing. Most problems associated with Al-Li-X alloys appear to be solvable by the development of intelligent processing methods and the advantages in density and modulus that they offer over conventional aluminum alloys have already led to their usage in a number of aerospace systems.

REFERENCES

1. Reuleaux, O., J. Inst. Met., 33, 1925, p. 346.
2. Scheuer, E., Z. Metallkunde, 19, p. 16.
3. LeBaron, I. M., U.S. Patent No. 2,381,219, Application date 1942, Granted 1945.
4. Hardy, H.K. and J.M. Silcock, J. Inst. Met., 84, 1955-56, p. 423.
5. Silcock, J.M., J. Inst. Met., 88, 1959-60, p. 357.
6. Fridlyander, I.N., V.F. Shamray and N.V. Shirayera, Russian Metallurgy, No. 2, 1965, p. 83, Translated from Izvestiya Akademii nauk SSSR Metally, No. 2, p. 153.
7. Ekvall, J.S., J.E. Rhodes and G.G. Wald in Design of Fatigue and Fracture Resistant Structures, ASTM STP 671, 1982, p. 328.
8. Sankaran, K.K. and J.J. Grant, Aluminum-Lithium Alloys, ed. T.H. Sanders, Jr. and E.A. Starke, Jr., The Metall. Soc. AIME, 1981, p. 205.
9. Bretz, P.E., Aluminum-Lithium Alloys: Design, Development and Application Update, ed. Ramesh J. Kar, Suphal P. Agrawal and William E. Quist, ASM International, 1988, p. 1.
10. Labarre, L.C., R.S. James, J.J. Witters, R.J. O'Malley and M.R. Emptage, 4th International Aluminum Lithium Conference, ed. by G. Champier, B. Dubost, D. Miannay and L. Sabetay, J. de Physique, Colloque C3, 1987, p. C3-93.
11. Last, H.R., T.H. Sanders, Jr. and J. G. Gonsalves, "Stability of Twinned Columnar Grain Structures in Aluminum Alloy Castings," submitted to Metall. Trans. A.
12. Ashton, R.F., D. S. Thompson and F.W. Gayle, Aluminum Alloys - Physical and Mechanical Properties, ed. E.A. Starke, Jr. and T.H. Sanders, Jr., EMAS, Warley, West Midlands, U.K., 1986, p. 403.
13. Lewis, R.E., E.A. Starke, Jr., W.C. Coons, G.J. Shiflet, E. Willner, J.G. Bjeletich, C.H. Mills, R.M. Harrington, and D.N. Petrakis, 4th International Aluminum Lithium Conference, ed. by G. Champier, B. Dubost, D. Miannay, and L. Sabetay, J. de Physique, Colloque C3, 1987, p. C3-643.
14. Sanders, T.H., Jr., and E.A. Starke, Jr., Acta Met., 36, 1982, p. 927.
15. Noble, B., and G.E. Thompson, Met. Sci. J., 5, 1971, p. 114.
16. Williams, D.B., and J.W. Edington, Met. Sci., 9, 1975, p. 529.
17. Cassada, W.A., G.J. Shiflet and E.A. Starke, Jr., Acta Met., 34, 1986, p. 367.
18. Sanders, T.H., Jr., "Development of an Al-Mg-Li Alloy", Final Report, Naval Air Developmental Center Contract No. N622269-74-C-0328, 1976.
19. Thompson, G.E., and B. Noble, J. Inst. of Met., 101, 1973, p. 111.
20. Mondolfo, L.F., "Aluminum Alloys - Structure and Properties", Butterworths, London, 1976, p. 554.
21. Sanders, T.H., Jr., H.R. Last and S.C. Jha, "Microstructure and Properties of Al-Li-Mg Alloys," Proceedings of the International SAMPE Metals Conference, Cherry Hill, N.J., August 18-20, 1987, in press.
22. Bauman, S.F., and D.B. Williams, in Aluminum-Lithium Alloys II, ed. E.A. Starke, Jr. and T.H. Sanders, Jr., The Metallurgical Society of AIME, Warrendale, PA., 1983, p. 17.
23. Nobel, B., and G.E. Thompson, Met. Sci. J., 6, 1972, p. 167.
24. Rioja, R.J., and E.A. Ludwiczak, in Aluminum-Lithium Alloys III, ed. by C. Baker, P.J. Gregson, S.J. Harris, and C.J. Peel, The Institute of Metals, London, 1985, p. 471.
25. Gregson, P.J. and H. M. Flower, Acta Met., 33, 1985, p. 527.
26. Sanders, T.H., Jr., Unpublished Research Presented at "Aluminum-Lithium II", Monterey, CA, April 12-14, 1983.
27. Cassada, W.A., G.J. Shiflet, and E.A. Starke, Jr., Scripta Met., 20, 1986, p. 751.
28. Cassada, W.A., G.J. Shiflet, and S.J. Poon, Phys. Rev. Let., 56, 1986, p. 2276.
29. Cassada, W.A., G.J. Shiflet and E.A. Starke, Jr., in Aluminum Alloys. Their Physical and Mechanical Properties, Vol. II., ed. by E. A. Starke, Jr. and T.H. Sanders, Jr., EMAS, 1986, p. 695.

30. Barges, C., M.H. Tosten, P.R. Howell and E.R. Ryba, *J. Mat. Sci.*, **22**, 1987, p. 1663.
31. Price, R.J., and A. Kelly, *Acta Met.*, **12**, 1964, p. 159.
32. Starke, E.A., Jr., and F.S. Lin, *Metall. Trans. A.*, **13A**, 1982, p. 2259.
33. Huang, J.C., and A.J. Ardell, 4th International Aluminum-Lithium Conference, ed. by G. Champier, B. Dubost, D. Miannay, and L. Sabetay, *J. de Physique, Colloque C3*, 1987, p. C3-373.
34. Sainfort, P. and P. Guyot, in Aluminum-Lithium Alloys III, ed. by C. Baker, P.J. Gregson, S. J. Harris and C.J. Peel, *Inst. of Metals, London*, 1986, p. 420.
35. Jata, K.V., and E. A. Starke, Jr., *Metall. Trans. A.*, **17A**, p. 1011.
36. Tomura, M., T. Mori and T. Nakamura, *J. Japan Inst. Metals*, **34**, 1970, p. 919.
37. Crooks, R.E., and E.A. Starke, Jr., *Metall. Trans. A.*, **15A**, 1984, p. 1367.
38. Peel, C.J., B. Evans, C.A. Baker, D.A. Bennett, P.J. Gregson and H.M. Flower, in Aluminum-Lithium II, ed. by E.A. Starke, Jr. and T.H. Sanders, Jr., *The Metall. Society AIME, Warrendale, PA*, 1984, p. 363.
39. Sainfort, P., and B. Dubost, in 4th International Aluminum-Lithium Conference, ed. G. Champier, B. Dubost, D. Mainnay, L. Sabetay, *Journal De Physique, Colloque C3*, 1987, p. 407.
40. Hautefeuille, I., R. Rahouadj, Y. Barbaux and M. Clavel, *ibid*, p. 669.
41. Narayanan, G.H., B.L. Wilson, W.E. Quist, and A.L. Wingert, "Low Density Aluminum Alloy Development", Third Interim Technical Report; 1983, AFWAL Contract No. F33615-81-5053.
42. Crooks, R.E., E.A. Kenik and E.A. Starke, Jr., *Scripta Met.*, **17**, 1983, p. 643.
43. Ashton, R.F., D.S. Thompson, E.A. Starke, Jr., and F.S. Lin, in Aluminum-Lithium Alloys III, ed. by C. Baker, P.J. Gregson, S.J. Harris and C.J. Peel, *The Institute of Metals, London*, 1986, p. 66.
44. Dean, W.A., in Aluminum-Properties and Physical Metallurgy, ed. J.L. Hatach, *ASM, Metals Park, OH*, 1984, p. 200.
45. Muller, W., E. Bubeck and V. Gerold, in Aluminum-Lithium Alloys, III, ed. by C. Baker, P.J. Gregson, S.J. Harris, and C. Peel, *The Institute of Metals, London*, 1986, p. 435.
46. Agyekum, E., W. Ruch, E.A. Starke, Jr., S.C. Jha, and T.H. Sanders, Jr., *ibid*, p. 448.
47. Narayanan, G.H., W.E. Quist, B.L. Wilson, and A.L. Wingert, "Low Density Aluminum Alloy Development", First Interim Tech. Report, 1982, AFWAL Contract No. F33615-81-C-5053, p. 95.
48. Dudzinski, N., *J. Inst Met.*, **81**, 1952-53, p. 49.
49. O'Dowd, M.E., W. Ruch and E.A. Starke, Jr., in 4th International Aluminum-Lithium Conference, ed. G. Champier, B. Dubost, D. Miannay, L. Sabetay, *J. de Physique, Colloque C3*, 1987, p. 565.
50. Broussaud, F., and M. Thomas, in Aluminum-Lithium Alloys, III, C. Baker, P.J. Gregson, S.J. Harris, and C.J. Peel, *The Institute of Metals, London*, 1986, p. 442.
51. Wakeling, P.O., "ALCAN Developments in Al-Li Technology," *NASA Workshop, Langley, VA*, 1987.
52. Lin, F.S., *Scripta Met.*, **16**, 1982, p. 1295.
53. Kuo, Victor W.C., and E.A. Starke, Jr., *Metall. Trans. A.* **16A**, 1985, p. 1089.
54. Peel, C.J., D. McDermid, and B. Evans, "Considerations of Critical Factors for the Design of Aerospace Structures Using Current and Future Aluminum-Lithium Alloys", in Aluminum-Lithium Alloys: Design, Development and Application Update, ed. Ramesh J. Kar, Suphal P. Agrawal, and William E. Quist, *ASM International, Metals Park, Ohio*, 1987, p. 315.
55. Peters, M., K. Welpmann, and T.H. Sanders, Jr., Advanced Materials Research and Developments for Transport Light Metals, *RVII, Les Editions, Les Ulis, France*, 1985, p. 63.
56. Peters, M., J. Eschweiler and K. Welpmann, *Scripta Met.*, **20**, 1986, p. 259.

57. Fox, S., H.M. Flower and D.S. McDermid, Aluminum Alloys - Physical and Mechanical Properties, ed. E.A. Starke, Jr., and T.H. Sanders, EMAS, West Midlands, United Kingdom, 1986, p. 939.
58. Bull, M.J. and D.J. Lloyd, Aluminum Lithium Alloys III, ed. C. Baker, P.J. Gregson, S.J. Harris and C.J. Peel, The Institute of Metals, London, 1986, p. 402.
59. Broussaud F. and C. Diot, 4th International Aluminum Lithium Conference, ed. G. Champier, B. Dubost, D. Miannay and L. Sabetay, J. de Physique, Colloque C3, 48, 1987, p. C3-597.
60. Hirsch, J., O. Engler, K. Lucke, M. Peters and K. Welpmann, 4th International Aluminum Lithium Conference, ed. G. Champier, B. Dubost, D. Miannay and L. Sabetay, J. de Physique, Colloque C3, 48, 1987, p. C3-605.
61. Lipinski, P., M. Berveiller, A. Hihi, P. Sainfort and P. Meyer, 4th International Aluminum Lithium Conference, ed. G. Champier, B. Dubost, D. Miannay and L. Sabetay, J. de Physique, Colloque C3, 48, 1987, p. C3-613.
62. Vasudevan, A.K., W.G. Fricke, Jr., R.C. Malcolm, R.J. Bucci, M.A. Przystupa and F. Barlat, Metall. Trans. A, 19A, 1988, p. 731.
63. Sadananda, K., and K.V. Jata, Metall. Trans. A, 19A, 1988, p. 847.
64. Reynolds, M.A., A. Gray, E. Creed, R.M. Jordan and A.P. Titchener, in Aluminum-Lithium Alloys III, ed. by C. Baker, P.J. Gregson, S.J. Harris and C.J. Peel, The Institute of Metals, London, 1986, p. 57.
65. Makin, P.U. and W.M. Stobbs, *ibid*, 1986, p. 392.
66. Christian, J.W., The Theory of Transformations in Metals and Alloys, First Edition, Pergamon Press, Oxford, England (1965).
67. Starke, E.A., Jr., in Strength of Metals and Alloys, ICSMA 6, ed. by R.C. Gifkins, Vol. 3, Pergamon Press, 1982, p. 1025.
68. Colvin, G.N., and E.A. Starke, Jr., SAMPE Quarterly, 19, 1988, p. 10.
69. Staley, J.T., Alcoa Research Laboratory, Alcoa Center, PA, unpublished research, 1988.
70. Bourgasser, P., J.A. Wert and E.A. Starke, Jr., "Intergranular Fracture of an Al-Li-Cu-Mg Alloy as a Result of Non-equilibrium Eutectic Melting During Solution Treatment", submitted to Materials Science and Technology.
71. Cassada, W.A., G.J. Shiflet and E.A. Starke, Jr., in 4th International Aluminum Lithium Conference, ed. by G. Champier, B. Dubost, D. Miannay, and L. Sabetay, J. de Physique, Colloque C3, 1987, p. C3-397.
72. Pitcher, P.D., "Ageing of Forged Aluminum-Lithium 8091 Alloy", Scripta Met., in press.
73. Blackburn, L., W. Casada, G. Colvin, G. Shiflet, and E.A. Starke, Jr., Aluminum-Lithium Alloys: Design, Development and Application Update, ed. by Ramesh J. Kar, Suphal P. Agrawal, and William E. Quist, ASM International, Metals Park, Ohio, 1987, p. 187.
74. Jata, K.V., and E.A. Starke, Jr., Scripta Met., 22, 1988, p. 1553.
75. Webster, D., Aluminum Lithium Alloys III, ed. by C. Baker, P.J. Gregson, S.J. Harris and C.J. Peel, Institute of Metals, London, 1986, p. 602.
76. Webster, D., Met. Trans. A, 18A, 1987, p. 2181.
77. Dorward, R.C., Scripta Met., 20, 1986, p. 1379.
78. Venkateswara Rao, K.T., H.F. Hayashigatani, W. Yu and R. O. Ritchie, Scripta Met., 22, 1988, p. 93.
79. Glazer, J., S.L. Verzasconi, R.R. Sawtell and J.W. Morris, Met. Trans. A, 18A, 1987, p. 1695.
80. Starke, Edgar A., Jr., and Gerd Luetjering, "Cyclic Plastic Deformation and Microstructure", in Fatigue and Microstructure, ed. M. Meshii, ASM, Metals Park, Ohio, 1979, p. 205.
81. Starke, E.A., Jr., and J. C. Williams, "Microstructure and the Fracture Mechanics of Fatigue Crack Propagation", Proceedings of the 20th National Symposium on Fracture Mechanics, Bethlehem, PA, June 23-25, 1987, ASTM, Philadelphia, PA, in press.

82. Lin, F.S., and E.A. Starke, Jr., *Mater. Sci. and Engr.*, **43**, 1980, p. 65.
83. Jata, K.V., and E.A. Starke, Jr., in Aluminum-Lithium Alloys III, ed. by C. Baker, P.J. Gregson, S.J. Harris and C.J. Peel, The Institute of Metals, London, 1986, p. 247.
84. Petit, J., S. Suresh, A.K. Vasudevan and R.C. Malcolm, *ibid*, 1986, p. 257.
85. Venkateswara Rao, K.T., W. Yu and R.O. Ritchie, *Scripta Met.*, **20**, 1986, p. 1459.
86. Coyne, E.J., Jr., T.H. Sanders, Jr., and E.A. Starke, Jr., in Aluminum-Lithium Alloys, ed. by T.H. Sanders, Jr., and E.A. Starke, Jr., AIME, Warrendale, PA, 1981, p. 293.
87. Vasudevan, A.K., P.E. Bretz, A.C. Miller and S. Suresh, *Mat. Sci. and Engr.*, **64**, 1984, p. 113.
88. Scarich, G.V., K.M. Bresnahan, and P.E. Bretz, in "Fatigue Crack Growth Resistance of Aluminum Alloys Under Spectrum Loading", Vol. II, Aluminum-Lithium Alloys, Tech. Rep. No. NOR-85-141, NASC, Northrop Corporation, Hawthorne, CA.
89. Venkateswara Rao, K.T., W. Yu and R.O. Ritchie, *Met. Trans. A*, **19A**, 1988, p. 549.
90. Venkateswara Rao, K.T., W. Yu and R.O. Ritchie, *ibid*, 1988, p. 563.
91. James, M.R., *Scripta Met.*, **21**, 1987, p. 783.
92. Peters, M., K. Welpmann, W. Zink and T.H. Sanders, Jr., in Aluminum-Lithium Alloys III, ed. by C. Baker, P.J. Gregson, S.J. Harris and C.J. Peel, The Institute of Metals, London, 1986, p. 239.
93. Farcy, L., C. Carre, M. Clavel, Y. Barbaux and D. Aliaga, in 4th International Aluminum-Lithium Conference, ed. by G. Champier, B. Dubost, D. Miannay and L. Sabetay, J. de Physique, Colloque C3, 1987, p. 565.
94. Gray, A., N.J.H. Holroyd and W.S. Miller, "The Environmental Cracking Behaviour of Aluminum-Lithium Based Alloys", Proceedings of the International SAMPE Metals Conference, Cherry Hill, N.J., August 18-20, 1987, in press.
95. Holroyd, N.J.H., A. Gray, G.M. Scamans and R. Hermann, in Aluminum-Lithium Alloys III, ed. by C. Baker, P.J. Gregson, S.J. Harris and C.J. Peel, Institute of Metals, London, 1986, p. 310.
96. Christodoulou, L., L. Struble and J.R. Pickens, in Aluminum-Lithium Alloys II, ed. by E.A. Starke, Jr., and T.H. Sanders, Jr., The Met. Soc. AIME, 1984, p. 561.
97. Meletis, E.I., "Stress Corrosion Cracking Properties of 2090 Al-Li Alloy", Proceedings International Conference on Fatigue Corrosion Cracking, Salt Lake City, UT, 1985.
98. Rinker, J.G., M. Marek and T.H. Sanders, Jr., *Mat. Sci. Eng.*, **64**, 1984, p. 203.
99. Vasudevan, A.K., P.R. Ziman, S.C. Jha and T.H. Sanders, Jr., in Aluminum-Lithium Alloys III, ed. by C. Baker, P.J. Gregson, S.J. Harris and C.J. Peel, Institute of Metals, London, 1986, p. 303.
100. Colvin, E.L., S.J. Murtha and R.K. Wyss, in Aluminum Alloys: Physical and Mechanical Properties, ed. by E.A. Starke, Jr., and T.H. Sanders, Jr., EMAS, 1986, p. 1853.
101. Meletis, E.I., J.M. Sater and T.H. Sanders, Jr., *ibid*, 1986, p. 1157.
102. Yavari, P., D. Ward and J.J. Christiana, "Forming and Post-Formed Properties of 2090", presented at the Al-Li Conference, WESTEC, Los Angeles, CA, March, 1988, to be published in the Proceedings.
103. Agrawal, S.P. and R.J. Kar, eds., "Aluminum-Lithium Development, Application and Superplastic Forming", Proceedings, WESTEC '86, ASM, Metals Park, Ohio, 1986.
104. Wadsworth, J., C.A. Hensahall and T.E. Nieh, in Aluminum-Lithium III, ed. by C. Baker, P.J. Gregson, S.J. Harris and C.J. Peel, The Institute of Metals, London, 1986, p. 199.
105. Pickens, J.R., "A Review of the Weldability of Lithium-Containing Aluminum Alloys", Martin-Marietta Report MML TR 84-22.
106. Edwards, M.R. and V.E. Stoneham, in 4th International Aluminum-Lithium Conference, ed. by G. Champier, B. Dubost, D. Miannay and L. Sabetay, J. de Physique, Colloque C3, 1987, p. C3-293.
107. Papazian, J.M., G.G. Bott, and P. Shaw, in Proceedings of the 17th National SAMPE Conference, 1985, p. 688.

MECHANICAL PROPERTIES AND FRACTURE TOUGHNESS OF
8090-T651 PLATE AND 2091 AND 8090 SHEET

by
W.G.J. 't Hart*, L. Schra*, D.S. McDarmaid** and M. Peters***

* NLR - Nationaal Lucht- en Ruimtevaartlaboratorium
Structures and Materials Division
P.O. Box 153
8300 AD Emmeloord
The Netherlands

** RAE - Royal Aerospace Establishment
Materials and Structures Department
Farnborough, Hants, GU14 6TD
United Kingdom

*** DFVLR - Deutsche Forschungs- und Versuchsanstalt für Luft- und Raumfahrt
Institut für Werkstoff-Forschung
D-5000 Köln 90
Federal Republic of Germany

SUMMARY

The strength and toughness properties of the medium strength Al-Li plate alloy 8090-T651 were determined and compared to those of damage tolerant 2000 series plate alloys. For the LT and TL orientations similar K_{IC} values were obtained but 8090-T651 was inferior in terms of short transverse fracture toughness. Tensile tests through-the-thickness and with respect to rolling direction indicated considerable anisotropy. Residual strength tests were performed on centre cracked sheet panels of the Al-Li alloys 2091 and 8090 in different tempers and 2024-T3 reference material. Fracture modes and characteristics were analysed using fractography and resulted in a better understanding of the fracture behaviour of the Al-Li alloys.

Recrystallized Al-Li sheet in specific tempers achieved plane stress fracture toughness values similar to those of 2024-T3, but at somewhat lower yield strengths.

1. INTRODUCTION

The quest for advanced aircraft materials with higher specific strength and stiffness properties has led to the introduction of lithium as an alloying element in aluminium alloys. Development programmes by Alcoa in the US and by Alcan and Pechiney in Europe have resulted in a new generation of Al-Li alloys with a density reduction and stiffness increase of about 10 % as compared to conventional alloys. Different types of Al-Li alloys are being introduced for potential replacement of damage tolerant, medium strength and high strength conventional aluminium alloys.

Before these Al-Li alloys can be accepted for application in aerospace structures, extensive qualification programmes have to be performed by the manufacturers and potential users. To coordinate these activities in Europe a Garteurl action group (AG07) on Al-Li alloys was established in 1984. The members of the action group are the national research institutes RAE, DFVLR, ONERA and NLR, and the industrial participants British Aerospace, Alcan, Dassault, Cegedur Pechiney, ABB, Dornier and Fokker. The aluminium producers Alcan and Pechiney supply Al-Li alloys for investigation. The agreed evaluation programme covers engineering properties, fatigue, corrosion, microstructure and formability. The test programme concentrated initially on the medium strength plate alloy 8090-T651 from Alcan and was continued with investigation of damage tolerant Al-Li sheet alloys supplied by Alcan and Pechiney. Comparisons were made with conventional aluminium alloys.

In this paper, which is mainly based on Garteurl work-phase I (Ref. 1), the tensile properties and fracture toughness of the tested Al-Li alloys, as determined by the Garteurl members, are discussed. The observed fracture behaviour in 8090-T651 plate and in Al-Li sheets is explained with the aid of fractographic studies.

† Group for Aeronautical Research and Technology in Europe

2. MATERIALS AND EXPERIMENTAL PROGRAMME

The medium strength Al-Li alloy 8090-T651 was produced as pre-production quality and was supplied by Alcan to Garteur AG07 in the form of 25 mm thick plate. Samples of 8090 and 2091 1.6 mm thick sheet, mainly in a recrystallized condition, were supplied by Alcan and Pechiney respectively. Chemical compositions of all the materials investigated are shown in table 1. For the Al-Li sheet materials different artificial heat treatments were applied.

In the experimental programme the following topics were considered:

- Strength : Through the plate thickness and with respect to the rolling direction.
- K_{Ic} : Fracture toughness for LT, TL, SL and ST orientation by testing compact tension and chevron notched bar specimens taken from plate.
- K_{Ic} : Residual strength of 400, 500 and 760 mm wide centre cracked panels.
- Fractography

The strength and fracture toughness of 8090-T651 plate were compared to those of 2024-T351 and 2324-T39 plate materials, which are conventional damage tolerant alloys. The Al-Li sheet materials were basically compared to a 2024-T3 reference material of the same thickness, but also to 7075-T6 and 7475-T761 with respect to anisotropy.

3. TENSILE STRENGTH AND ANISOTROPY

3.1 Plate

Longitudinal and long transverse tensile properties for 8090-T651 plate in comparison with those of 2024-T351 and 2324-T39 are given in figure 1 (Ref. 2). The properties were determined for specimens from core and surface material.

Differences in tensile strength between surface and core material of 8090-T651 is evident. The variation in through-the-thickness properties is highest for the Al-Li plate and lowest for the 2324-T39 plate. The effect of test direction on UTS of the three alloys was small. 0.2 % TYS values were generally lower in the T direction than in the L direction. The most conspicuous difference in properties is the low elongation to fracture for 8090-T651.

Figure 2 gives the range of tensile properties for 8090-T651 as determined by the Garteur participants (Ref. 1). Reasonable consistency was achieved between the laboratories. The values for surface, 1/6 t and 1/4 t test-piece positions were combined since they were very similar. For comparison typical and minimum properties as given by the producer are indicated (Ref. 3).

It is seen that the UTS fulfils the minimum requirement irrespective of test orientation and test position. The 0.2 % TYS and elongation to fracture requirements are not fully met.

Tensile anisotropy for the 8090-T651 plate was investigated more extensively in reference 4, see figure 3. The most pronounced anisotropy occurs for the plate midplane where a maximum dip in 0.2 % TYS of 75 MPa was measured at an angle of about 67° with the rolling direction.

3.2 Sheet

To obtain damage tolerant properties in Al-Li sheets the 8090 and 2091 alloys are produced in a recrystallized condition. Adequate strength properties are obtained by artificial ageing, usually at 150 °C and 135 °C for 2091 sheet and 150 °C for 8090 sheet. Figure 4 shows the strength development trend lines for 2091 and 8090 sheet. Since the damage tolerant Al-Li sheet alloys are intended to replace 2024-T3, interest was focussed on achieving the minimum strength properties quoted for the latter alloy [i.e. $293/440/15 = 0.2 \% \text{ TYS/UTS}/\delta$].

Exploratory heat treatments of 48 hrs/150 °C and 12 hrs/150 °C were applied to 2091. The strength properties met the 2024-T3 minima but poor fracture toughness behaviour forced Pechiney to change the heat treatment to 12 hrs/135 °C (heat treat designation T8X). Alloy 8090 was also tested in different heat treatment conditions. The heat treatment 12 hrs/150 °C resulted in a strength level comparable to that of 2091-T8X.

Tensile anisotropy in recrystallized 2091 (100 hrs/150 °C) and unrecrystallized 8090 (48 hrs/150 °C) sheet was determined by the DFVLR and compared with that of 2024-T3, 7075-T6 and 7475-T761 sheet, figure 5. For the unrecrystallized 8090 a marked effect in terms of reduced 0.2 % TYS and an increased elongation to fracture was obtained at about 60° to the rolling direction. The recrystallized 2091 showed a less pronounced anisotropy more or less corresponding to that of 2024-T3 sheet.

The effect of recrystallization on tensile anisotropy was more extensively investigated by the RAE for 1.6 mm thick 8090 sheet (Ref. 5). Unrecrystallized, partially recrystallized and fully recrystallized sheets were heat treated to similar transverse 0.2 % TYS, after which the off-axis tensile properties were determined, figure 6. It is seen that increasing recrystallization reduces the tensile anisotropy considerably.

For recrystallized 2091 an increased ageing time did not further improve the isotropy, figure 7. This was established by the DFVLR (Ref. 1).

4. FRACTURE TOUGHNESS

4.1 K_{Ic} (K_Q) of 8090-T651 Plate

The plane strain fracture toughness for the LT and TL orientations in 8090-T651 and the reference materials 2024-T351 and 2324-T39 were determined using 24 mm thick compact tension specimens (Ref. 2). For these orientations consistent results were obtained by the DFVLR and NLR. For the short transverse direction some variation in test results was found. DFVLR obtained higher K_Q values with chevron-notched short bar specimens than the NLR with small compact tension specimens. Figure 8 gives the mean fracture toughness values for 8090-T651 and compares them to those of the damage tolerant reference materials.

Comparison with the 2000 series alloys indicates a broad equivalence for 8090-T651 in the LT and TL orientations. However, the short transverse fracture toughness is evidently inferior to typical values for 2024-T351. Subsequently Alcan has improved the short transverse fracture toughness by introducing the T8771 temper for plate. This improvement is illustrated in figure 9, where the obtained test results for 8090-T651 are compared with typical properties for 8090-T8771 as determined by Alcan. Improvement in fracture toughness was realized without sacrificing strength properties.

4.2 Fracture Toughness of Damage Tolerant Sheet

Residual strength tests

Plane stress fracture toughness (K_c) tests were performed by the RAE and NLR on centre cracked 2091 and 8090 1.6 mm thick panels. Anti-buckling guides were used to prevent local buckling. The RAE tested 400, 500 and 760 wide panels with a starter crack length ($2a_0$) of 0.3 W where W is the panel width. Starting crack lengths in the NLR tests on 500 mm wide panels were 0.2 W and 0.312 W. The residual strength tests were executed according to ASTM specification E 561-81 for R-curve determination. Load-Crack Opening Displacement (COD) records were made to derive the effective crack length. Both fracture toughness values and R-curves were derived from these records. The engineering fracture toughness K_c , based on maximum load and initial crack length, and the plane stress fracture toughness K_{c0} , based on maximum load and corresponding physical crack length, were calculated. In the RAE tests the physical crack length at maximum load was derived from the compliance crack length minus the Irwin plastic zone correction. In the NLR tests this crack length could be established visually.

The fracture toughness data (LT) for recrystallized 2091 and 8090 sheet are given in table 2 and plotted in figure 10 as a function of the 0.2 % TYS. Test results for 2024-T3 sheet are indicated for comparison.

Increased ageing time at 150 °C for 2091 sheet resulted in decreasing fracture toughness values. The original Pechiney-recommended ageing treatment of 48 hrs at 150 °C to obtain damage tolerant properties gave the lowest fracture toughness.

In the light of these results the ageing treatment was finally modified to 12 hrs at 135 °C, resulting in fracture toughness values more than twice as high. However, compared to the naturally aged sheet only a marginal increase in strength is obtained by this treatment.

Artificially ageing 8090 at 150 °C resulted in a considerable increase in tensile strength and fracture toughness. However, it has to be mentioned that the fracture toughness values for naturally aged sheet are invalid (too low) due to the occurrence of net section yielding. Table 2 shows that ageing for 8 - 24 hours resulted in a 0.2 % TYS of about 340 MPa and a K_{c0} of about 110 - 120 MPa \sqrt{m} .

The effect of test panel width on residual strength is evident. For low yield strength materials small test panels do not result in valid K_c values. For higher yield strength Al-Li sheets marginally valid K_c values were obtained with 500 mm wide panels, but RAE tests on 760 mm wide panels resulted in still higher K_c values. This indicates that the 500 mm wide panels were too narrow to obtain maximum K_c values. The same is true for the 2024-T3 residual strength tests.

If the residual strength test results are used to show trends, see figure 10, it can be concluded that 2091 and 8090 achieve fracture toughnesses similar to those of 2024-T3 at a 10 - 15 % lower 0.2 % TYS.

R-curve analysis

The crack growth resistance, K_R was calculated from

$$K_R = \sigma \sqrt{a_{eff}} \sec \left(\frac{\pi a_{eff}}{W} \right) \quad (\text{ASTM E 561-81})$$

where: σ = gross stress

a_{eff} = effective half crack length

= physical crack length + plastic zone correction

$\sqrt{\sec \left(\frac{\pi a_{eff}}{W} \right)}$ = finite width correction,

and a_{eff} was derived from the load-COD records using the compliance method described in ASTM E 561-81.

Typical R-curves for the LT and TL orientation of recrystallized 2091 and 8090 in different heat treatment conditions are shown in figure 11. The R-curves for 2024-T3 are also indicated. For a valid K analysis the net section stress based on the physical crack size must be less than the yield strength of the material. Therefore the points from which crack growth is governed by net section yield are indicated. K_R values at maximum load are also indicated. Figure 11 illustrates that improvement in the crack growth resistance of 2091 is obtained for the successive heat treatments 48 hrs/150 °C, 12 hrs/150 °C and

12 hrs/135 °C. The crack growth resistances of 2091 - 12 hrs/135 °C, 8090 - 12 hrs/150 °C and 2024-T3 loaded in the longitudinal direction were almost similar. However, this conclusion has to be made with some reservation since the occurrence of net section yield hinders direct comparison at longer crack lengths.

The effect of degree of recrystallization on the R-curve was investigated by the RAE for 1.6 mm thick 8090 sheet. Unrecrystallized, partially recrystallized and fully recrystallized sheets were heat treated to similar 0.2 % TYS before residual strength testing. Figure 12 shows that increasing crack growth resistance is obtained with increasing degree of recrystallization.

5. SELECTED TOPICS OF PARTICULAR INTEREST

5.1 Texture in Al-Li Plate and Sheet

Quantitative texture measurements (Refs. 4,6,7) established that 8090-T651 plate exhibited a much more pronounced anisotropy than e.g. 2024-T851 plate of the same thickness. Furthermore the texture of 8090-T651 plate was strongest in the core and weakest near the surfaces. Consequently the properties depend not only on the test direction but also on the location within the plate. The measurements revealed a close correlation between texture and tensile properties.

Recrystallization treatments diminish the texture and thereby improve the isotropy, as was demonstrated for Al-Li sheet. However, this is only possible for sheet since the required heating rate cannot be realized in the core of plate material. Even in nominally recrystallized 1.6 mm thick sheet of 2091 and 8090 an unrecrystallized central region is frequently present, figure 13. This shows that the recrystallization process is not yet optimized.

5.2 Brittle Fracture and Intergranular Delamination in 8090-T651 Plate

Brittle fracture and intergranular delamination in the LT plane was observed especially when testing tensile specimens in the short transverse direction and specimens of surface material, see figures 14 and 15. Possible explanations for the delamination behaviour are:

- (1) The presence of brittle grain boundary phases:
It has been observed (Ref. 8) that deformation of 8090-T651 results in void nucleation at Al₂(Fe,Cu) particles situated on high angle grain boundaries. This void formation was preceded both by particle/matrix decohesion and by particle cracking. NLR investigations revealed the forementioned particles but void nucleation at these particles was not observed, reference 9.
- (2) Impurity segregation:
Grain boundaries in aluminium-lithium alloys might contain Na and K impurities if high purity Li is not used in alloying. No indications for Na and/or K segregation were found in the present investigation.
- (3) Strain localization:
If deformation is concentrated in a few coarse slip bands and grain boundaries act as strong barriers to dislocation movement, the dislocations will pile up strongly against grain boundaries (see Fig. 16) This can open up the grain boundaries and the flaws thus created act as sinks in which the piled up dislocations disappear.

The last possibility can explain most observations (Ref. 9). For instance, the fact that tensile specimens taken from the surface of the 8090 plate exhibited delamination whereas specimens taken from the core did not is explained as follows: In the plate core a sharp texture was present (section 5.1). Thus the orientation differences between the grains were generally small and the grain boundaries did not present strong barriers to dislocation motion. This facilitated the concentration of deformation in a few coarse slip bands and ultimately gave rise to slip band cracking (Fig. 17).

However, a much weaker texture existed near the surfaces. Therefore, in the surface layers grain boundaries will have been stronger barriers and this explains why delamination instead of slip band cracking took place.

5.3 Fracture Modes and Characteristics of Residual Strength Tested Al-Li Sheet (Ref. 10)

Fracture surfaces of residual strength tested panels have been examined to determine relations between load-COD records and fracture modes. Scanning electron microscopy was performed for fracture surface characterization.

Examples of load-COD records and fractographic characteristics of stable and unstable crack growth are shown in figure 18 for 2091 - 48 hrs/150 °C and 2091 - 12 hrs/150 °C. The transition from stable to unstable crack growth was characterized by a change from fully ductile fracture to intergranular fracture. Also, crack jumping followed by crack arrest was characterized by intergranular fracture changing to fully ductile fracture. An overview of fracture modes and fracture surface characteristics for 2091 and 8090 in different heat treatment conditions is given in figure 19. Fractographic characteristics of stable and unstable crack growth are shown in figures 20 and 21. Considering these observations and the residual strength test results in section 4.2 the following aspects of concern can be mentioned:

- Although the crack resistance and fracture toughness of 2091 - 12 hrs/135 °C and 8090 - 24 hrs/150 °C were similar to those of the damage tolerant 2024-T3 alloy, signs of intergranular fracture are observed for the Al-Li sheet alloys during unstable crack growth (50 % for 2091 - 12 hrs/135 °C and 5 - 10 % for 8090 - 24 hrs/150 °C).

- The occurrence of intergranular fracture during unstable crack growth may indicate a strain rate dependent fracture process (Ref. 10).
- If the crack resistance and fracture toughness depend on strain rate the dynamic fracture toughness, K_d , could be much lower than the quasi-static fracture toughness K_C or K_E . This implies that the fail-safe crack arrest properties could be significantly inferior to those of 2024-T3. This aspect needs further investigation.

6. CONCLUDING REMARKS

The strength and fracture toughness properties of medium strength 25 mm thick 8090-T651 plate and 1.6 mm thick 2091 and 8090 sheet in different tempers were determined as part of a Garteur cooperative programme. Comparisons were made with conventional plate and sheet alloys.

The ultimate tensile strengths of 8090-T651, 2024-T351 and 2324-T39 plate materials were broadly equivalent. However, 8090-T651 was strongly anisotropic, which is related to texture. Also the consistently lower fracture strain and poor short transverse fracture toughness are of concern. Alcan demonstrated that the latter is improved by changing to the T8771 heat treatment. The overall anisotropy could be reduced by improving the rolling process, subject to mill width limitations on cross-rolling.

With respect to sheet materials, recrystallization is necessary to achieve damage tolerant properties for 2091 and 8090. Recrystallization decreases anisotropy and enables suitable heat treatments to provide plane stress fracture toughnesses and crack growth resistances similar to those of 2024-T3. However, there is a 10 - 15 % penalty in yield strength.

Fractographic investigation of the residual strength specimens showed that intergranular fracture, which occurs especially during unstable crack growth, is related to inferior fracture toughness; and it appears that Al-Li alloys can be sensitive to dynamic effects, i.e. the yield strength, crack growth resistance and fracture toughness can depend on strain rate (Ref. 10). This means that the fail-safe crack arrest properties could be significantly inferior to those of 2024-T3. In particular, the fail-safe crack arrest capability of 2091-T8X should be checked. And we recommend determining the fail-safe crack arrest capability of other candidate damage tolerant Al-Li sheet alloys if unstable crack growth is partly characterized by intergranular fracture, e.g. 8090 - 24 hrs/150 °C.

When considering Al-Li alloys for use in aerospace structures, it must be said that strength and fracture toughness are only two - albeit very important - aspects of material behaviour. An acceptable balance of properties has to include good resistances to fatigue crack growth and stress corrosion. Thus on the basis of the present results it is not possible to state definitely whether the tested Al-Li alloys are suitable replacements for conventional alloys. On the other hand, the various shortcomings (actual and potential) that have been indicated suggest that these Al-Li alloys are not yet fully developed.

7. REFERENCES

1. B. Evans, "Evaluation of aluminium-lithium based alloys produced by Alcan and Cegedur Pechiney - phase I". Garteur/TP-044, 1988.
2. W.G.J. 't Hart and L. Schra, "Properties of the Al-Li plate alloy DTD XXXA-T651 (AA 8090-T651) in comparison with two damage tolerant 2000 series plate alloys", NLR TR 86115 L, National Aerospace Laboratory, Amsterdam, 1985.
3. C.J. Peel, B. Evans, R. Grimes and W.S. Miller, "The application of improved aluminium-lithium alloys in aerospace structures". Ninth European Rotorcraft Forum, Paper No. 94, Stresa, Italy, September 1983.
4. S. Fox, D.S. McDermid and H.M. Flower, "Anisotropy of Mechanical Properties of Al-Li based Alloy Plate" in Aluminium Technology, Inst. of Metals, London, March 1986.
5. C.J. Peel and D.S. McDermid, "The present status of the development and application of 8090 and 8091 alloys" Presented at - ASM Aluminium-Lithium symposium Westec, Los Angeles, 1988.
6. M. Peters, J. Eschweiler and K. Welpmann, "Strength profile in Al-Li plate material", Scripta Met., Vol. 20, pp. 259-264 (1986).
7. J. Hirsch, O. Engler, K. Lücke, M. Peters and K. Welpmann, "The Rolling Texture Development in an 8090 Al-Li Alloy" in: Proc. 4th International Al-Li Conference, Paris, pp. 665-611, (1987).
8. N.J. Owen, D.J. Field and E.P. Butler, "Initiation of voiding at second-phase particles in a quaternary Al-Li alloy, Met. Sci. and Technology, Vol. 2, pp 1217-1222 (1986).
9. H.J. Kolkman, W.G.J. 't Hart and L. Schra, "Additional investigation on the Al-Li plate alloy DTD XXXA-T651 (AA 8090-T651)", NLR TR 87149, National Aerospace Laboratory, Amsterdam, 1987.
10. R.J.H. Wanhill, L. Schra and W.G.J. 't Hart, "Fracture and fatigue of damage tolerant Al-Li sheet alloys", NLR Technical Report in preparation, National Aerospace Laboratory, Amsterdam, 1988.

TABLE 1 Chemical compositions of the investigated plate and sheet materials:
 (1) Producers data for Al-Li alloys
 (2) Aluminium Association limits for 2024-T3 and -T351

Materials	Cu	Mg	Li	Mn	Zn	Cr	Ti	Zr	Fe	Si
8090 plate	1.24	0.60	2.42	0.00	0.00	0.00	0.05	0.12	0.12	0.05
2091 sheet	2.10	1.60	1.80	-	-	-	0.02	0.07	0.04	0.03
8090 sheet	1.20	0.71	2.38	0.001	0.02	0.001	0.02	0.11	0.03	0.03
2024-T3 sheet	3.8-4.9	1.2-1.8	-	0.3-0.9	0.25 max	0.1 max	-	-	0.50 max	0.50 max
2024-T351 plate										

TABLE 2 Fracture toughness of recrystallized 2091 and 8090 sheet (LT) RAE, NLR

Material	Ageing treatment	Panel width mm	Tensile data 0.2 % TYS MPa	UTS Mpa	$2a_o$ mm	$K_{e,c}^{3)}$ MPa \sqrt{m}	$K_c^{3)}$ MPa \sqrt{m}
2091	Natural age	400	326	425	133	100.1	110
		400	326	425	133	102.7	113
	12 hrs 150 °C	500 ¹⁾	375	463	156	85.0	86
	48 hrs 150 °C	500 ¹⁾	381	479	156	62.0	62
	48 hrs 150 °C	400	379	479	133	55.0	55.9
		400	379	479	133	58.0	57.3
	12 hrs 135 °C	400	328	439	133	94.6	115.0
		760	328	439	228	126.1	140.0
		500 ¹⁾	331	442	156	105.0	121.0
		500 ¹⁾	331	442	100	99.0	120.0
8090	Natural age	500 ¹⁾	381	502	156	111.0	131.0
					100	104.0	124.0
	Natural age	400	260	314	133	84.0	92.0 ²⁾
		500	236	305	167	87.0	93.0 ²⁾
		500	236	305	167	87.0	94.0 ²⁾
		500	242	304	167	87.0	91.0 ²⁾
	8 hrs 150 °C	400	342	448	133	98.0	112.0
		400	342	448	133	94.0	111.0
		500	337	435	167	103.4	125.0
		500	335	428	167	105.9	126.0
		500	334	435	167	106.6	120.0
		762	324	426	254	118.2	141.0
		400	324	426	133	94.4	114.0
	12 hrs 150 °C	500	351	448	167	105.1	126.0
		500	344	446	167	104.4	122.0
		500 ¹⁾	341	445	156	98.0	112.0
		500 ¹⁾	341	445	100	93.0	111.0
	16 hrs 150 °C	500	360	457	167	103.1	123.0
	24 hrs 150 °C	400	358	455	133	83.8	103.0
		400	358	455	133	89.5	105.0
		762	358	455	254	99.0	117.0
		760	340	438	253	108.0	139.0
		760	346	443	253	102.0	124.0
	48 hrs 150 °C	400	388	482	133	79.9	92.0

1) NLR test results

2) invalid - failed to meet plasticity requirements

$$3) K_{e,c} = \sigma_c \sqrt{a_{o,c} \sec \frac{\pi a_{o,c}}{W}}$$

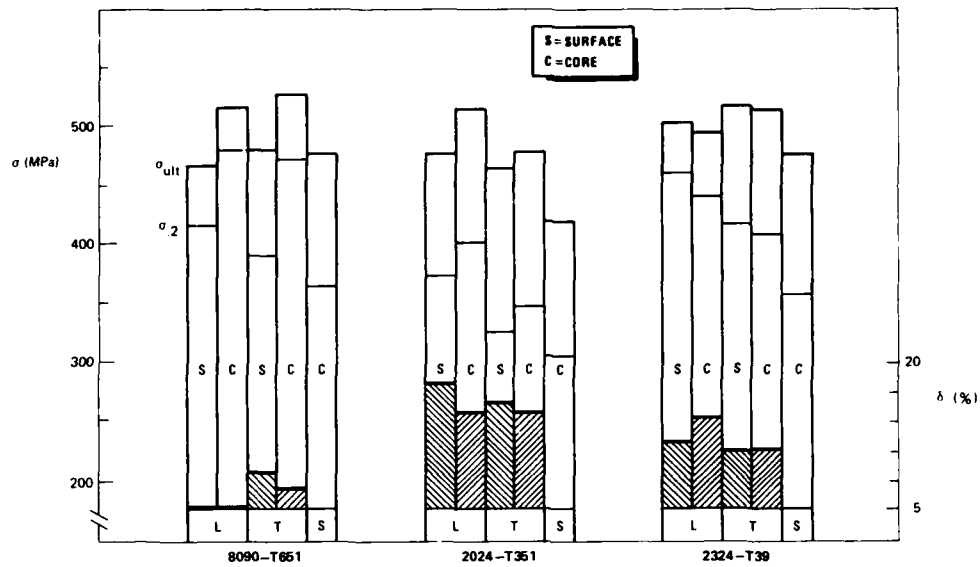


Fig. 1 Tensile properties of 8090-T651 plate in comparison with 2024-T351 and 2324-T39 plate (ref. 2)

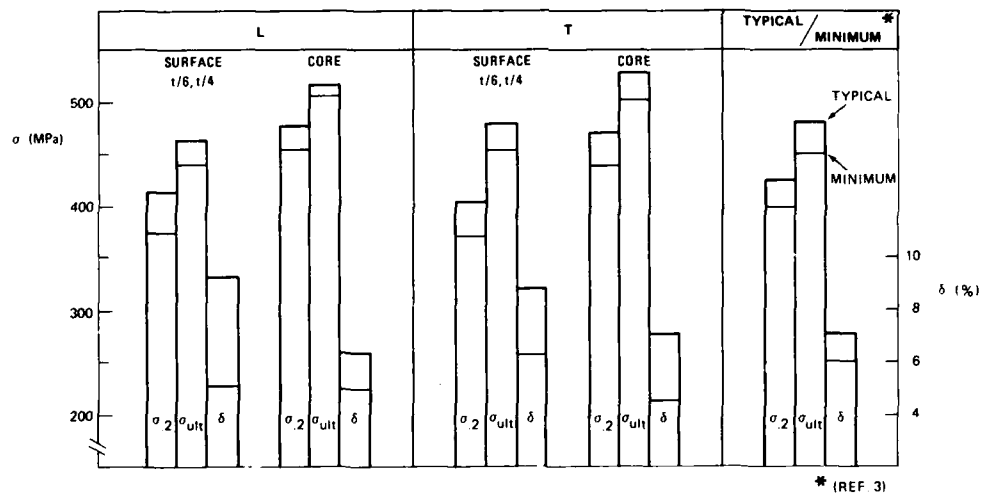


Fig. 2 Range of tensile properties for 8090-T651 plate as determined by Garteau members (ref. 1)

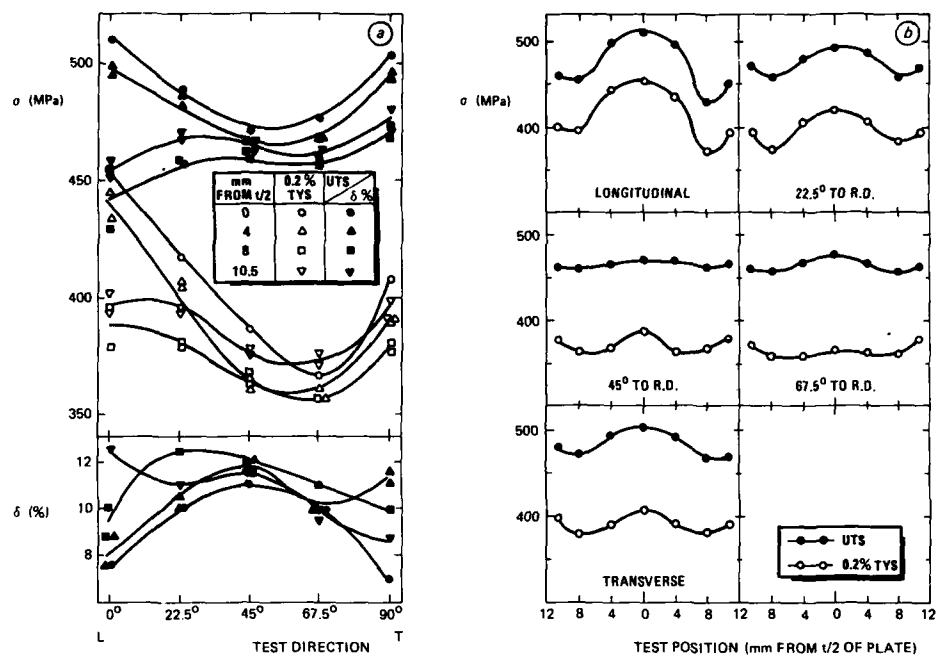


Fig. 3 Variation in tensile properties with test direction and position through the plate thickness for 8090-T651 (ref. 4)

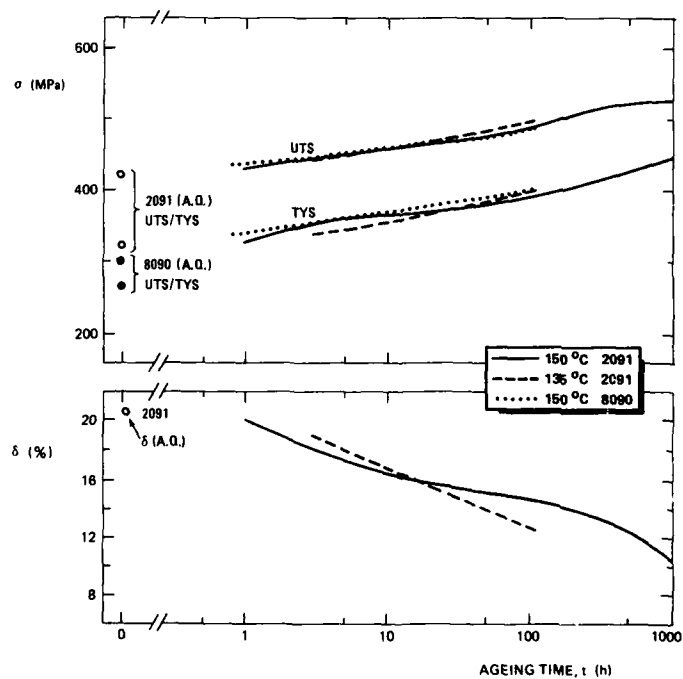


Fig. 4 Strength development in 2091 and 8090 sheet with artificial ageing

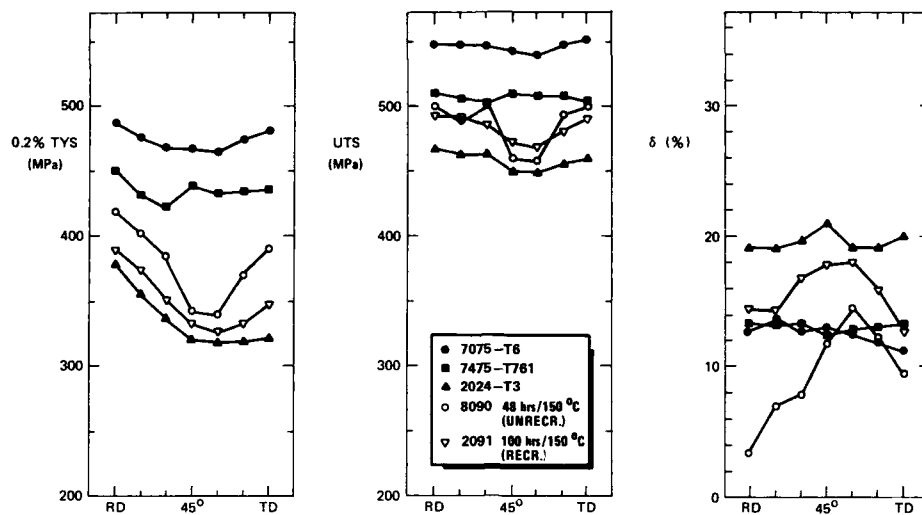


Fig. 5 Variation in tensile properties with test orientation for 1.6 mm thick sheet materials, DFVLR (ref. 1)

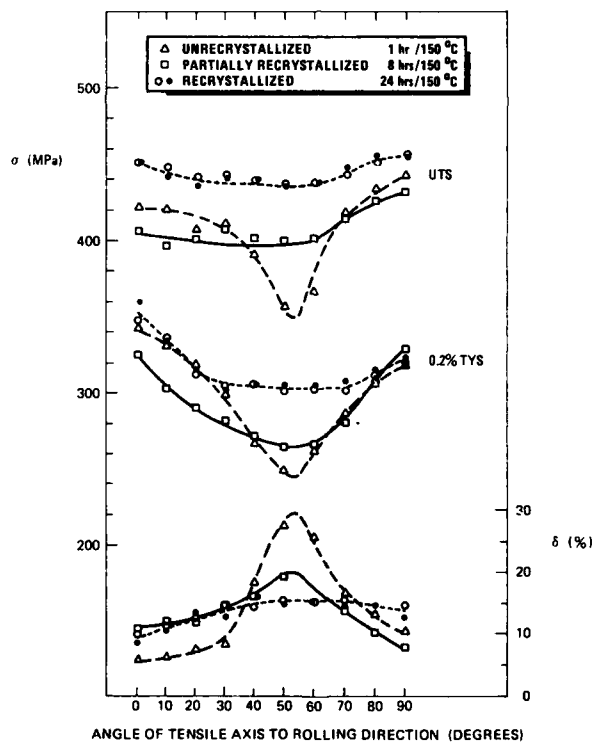


Fig. 6 Effect of microstructure on the tensile anisotropy in 1.6 mm thick sheet, RAE (ref. 5)

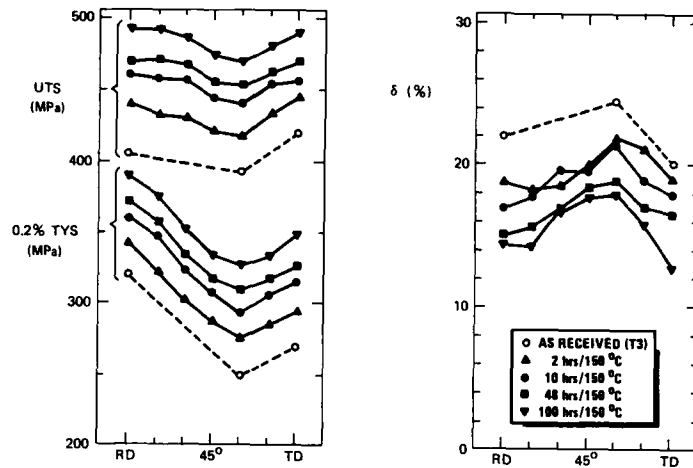


Fig. 7 Influence of ageing time on tensile anisotropy for 1.6 mm thick 2091 sheet, DFVLR (ref. 1)

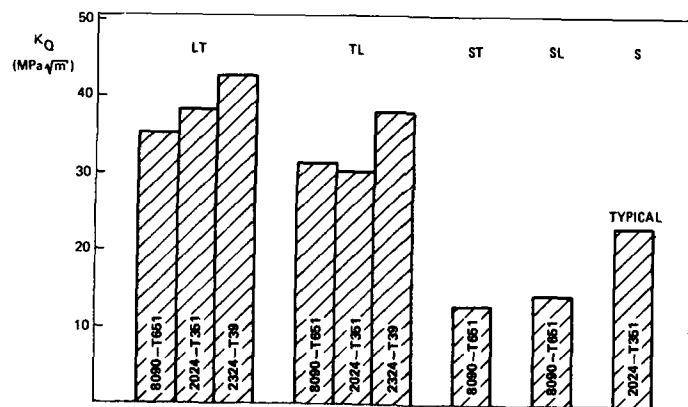


Fig. 8 Comparison of fracture toughness properties

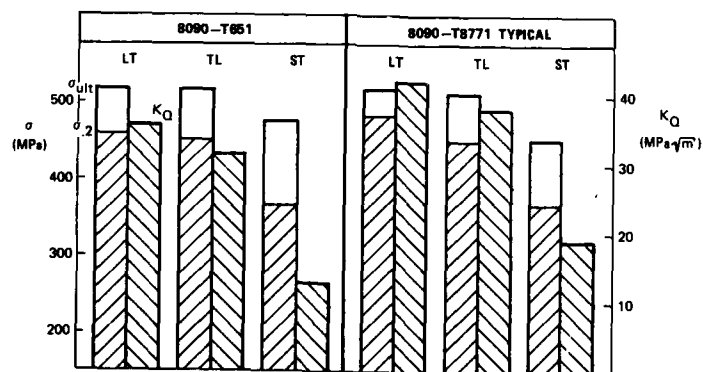


Fig. 9 Improvement of fracture toughness performance by the T8771 heat treatment: 8090-T8771 data supplied by Alcan

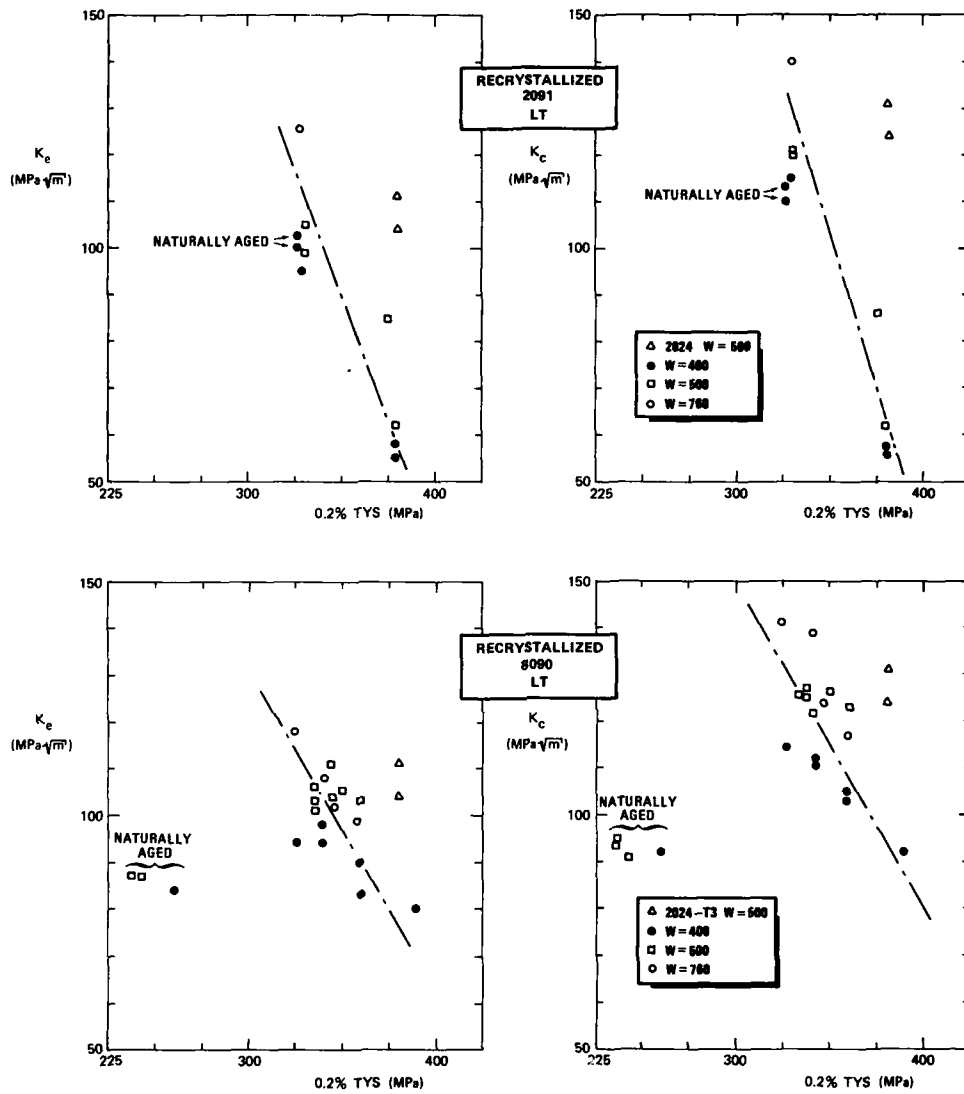


Fig. 10 Fracture toughness based on initial crack length and physical crack length at maximum load as function of TYS. (Test results for 400, 500 and 700 mm wide centre cracked panels)

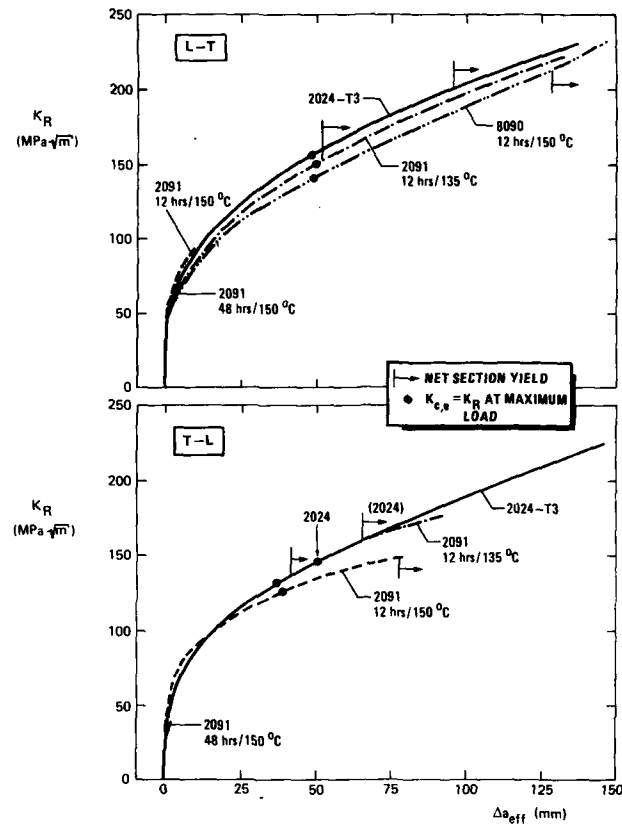


Fig. 11 Comparison of R curves for 2091, 8090 and 2024-T3 sheet, $W = 500$, NLR

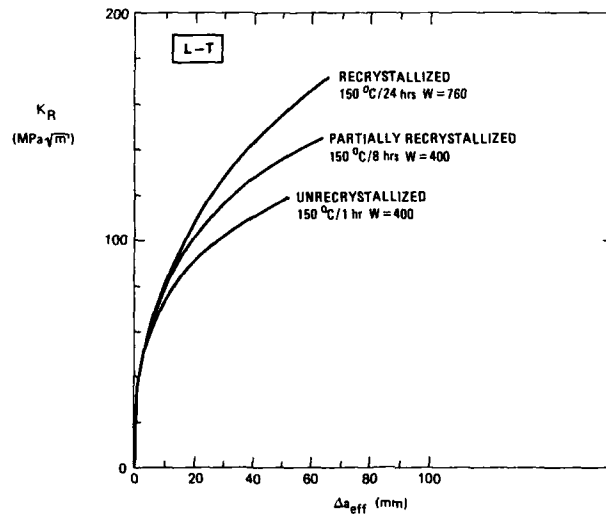


Fig. 12 Effect of microstructure on the R curve for 1.6 mm thick 8090 sheet aged at 150 °C to give 0.2% proof stress 325 MPa, RAE

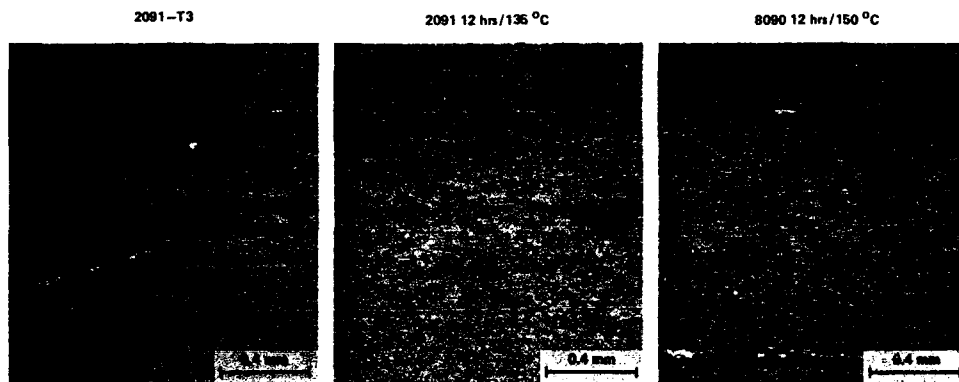


Fig. 13 The grain structures of damage tolerant recrystallized Al-Li sheets

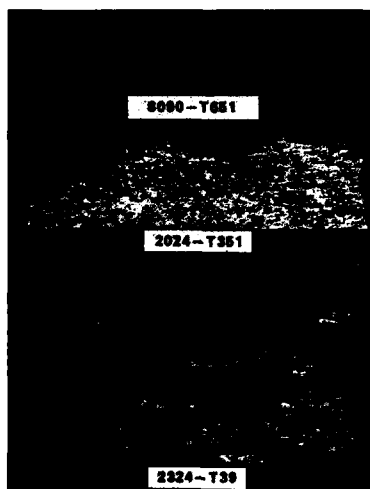
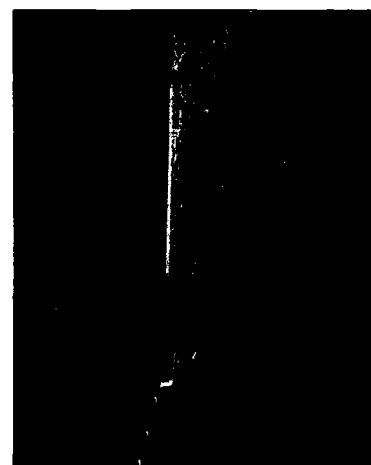


Fig. 14 Different fracture behaviour for short transverse tensile testing



Specimen of surface material tested in the L-direction

Fig. 15 Brittle fracture and delamination in tensile specimens of alloy 8090-T651

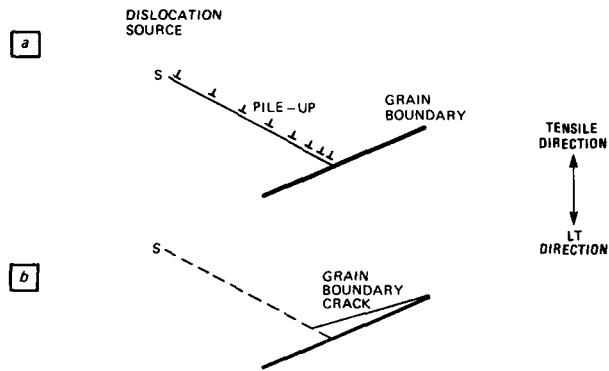
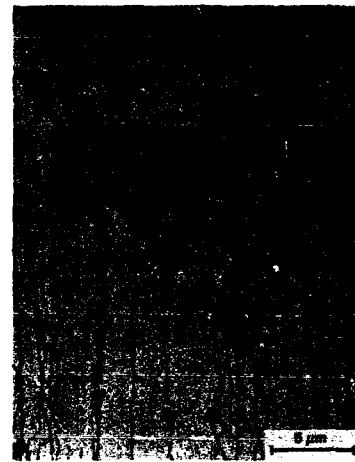


Fig. 16 Schematic of intercrystalline cracking by slip band impingement
 a) Dislocations pile-up against grain boundary
 b) Pile-up is released by the creation of an intercrystalline crack
 For the sake of clarity only one pile-up is shown but generally one grain can contain several pile-ups



SLIP BAND CRACKING

Fig. 17 Cross-section through an 8090-T651 tensile specimen taken from the plate core

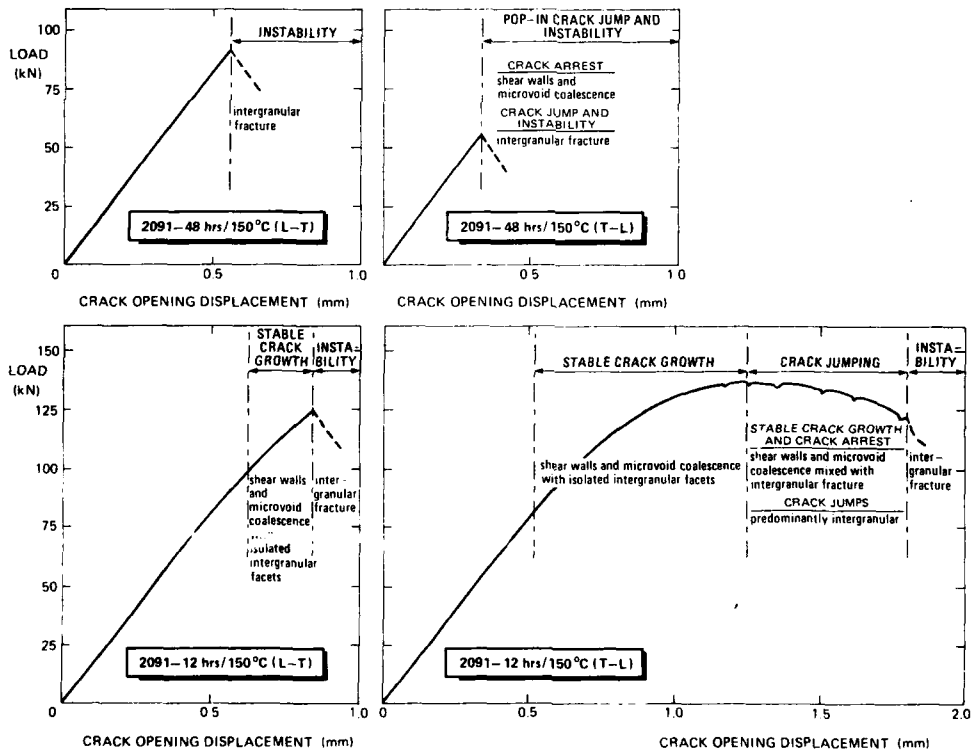















Fig. 18 Relations between residual static strength load-crack opening displacement records, stable and unstable crack growth, and fractographic characteristics for 2091-48 hrs/150°C and 2091-12 hrs/150°C (NLR, ref. 10)

MATERIALS	MACROSCOPIC FRACTURE MODES		FRACTOGRAPHIC CHARACTERISTICS	
	STABLE CRACK GROWTH	INSTABILITY	STABLE CRACK GROWTH	INSTABILITY
2091 48 hrs/150 °C	L-T - T-L *		POP-IN CRACK FRONT SHOWED INTERMITTENT SHEAR WALLS AND MICROVOID COALESCENCE	INTERGRANULAR WITH DELAMINATIONS ESPECIALLY AT ELONGATED GRAINS IN SHEET CORE
2091 12 hrs/150 °C			SHEAR WALLS AND MICROVOID COALESCENCE GRADUALLY BECOMING MIXED WITH INTERGRANULAR FRACTURE	INTERGRANULAR WITH DELAMINATIONS ESPECIALLY AT ELONGATED GRAINS IN SHEET CORE
2091 12 hrs/135 °C			SHEAR WALLS AND MICROVOID COALESCENCE	50% INTERGRANULAR AND 50% MICROVOID COALESCENCE WITH OCCASIONAL SHEAR WALLS
8090 ** 8 hrs/185 °C			NARROW SHEAR WALLS AND MICROVOID COALESCENCE: STRONGLY FIBERED APPEARANCE	MICROVOID COALESCENCE, INTERGRANULAR FRACTURE AND OCCASIONAL NARROW SHEAR WALLS
8090 12 hrs/150 °C			SHEAR WALLS AND MICROVOID COALESCENCE	SHEAR WALLS AND MICROVOID COALESCENCE
8090 24 hrs/150 °C			SHEAR WALLS AND MICROVOID COALESCENCE	SHEAR WALLS, MICROVOID COALESCENCE AND 5 - 10% INTERGRANULAR FRACTURE
2024-T3			MICROVOID COALESCENCE AND OCCASIONAL SHEAR WALLS	MICROVOID COALESCENCE AND OCCASIONAL SHEAR WALLS

* A "POP-IN" CRACK OCCURRED. THE CRACK WAS MACROSCOPICALLY FLAT EXCEPT FOR SLANT FRACTURE AROUND THE TEMPORARILY ARRESTED CRACK FRONT

** UNRECRYSTALLIZED

Fig. 19 Fracture modes and fractographic characteristics of fracture surfaces of tested centre cracked sheet panels

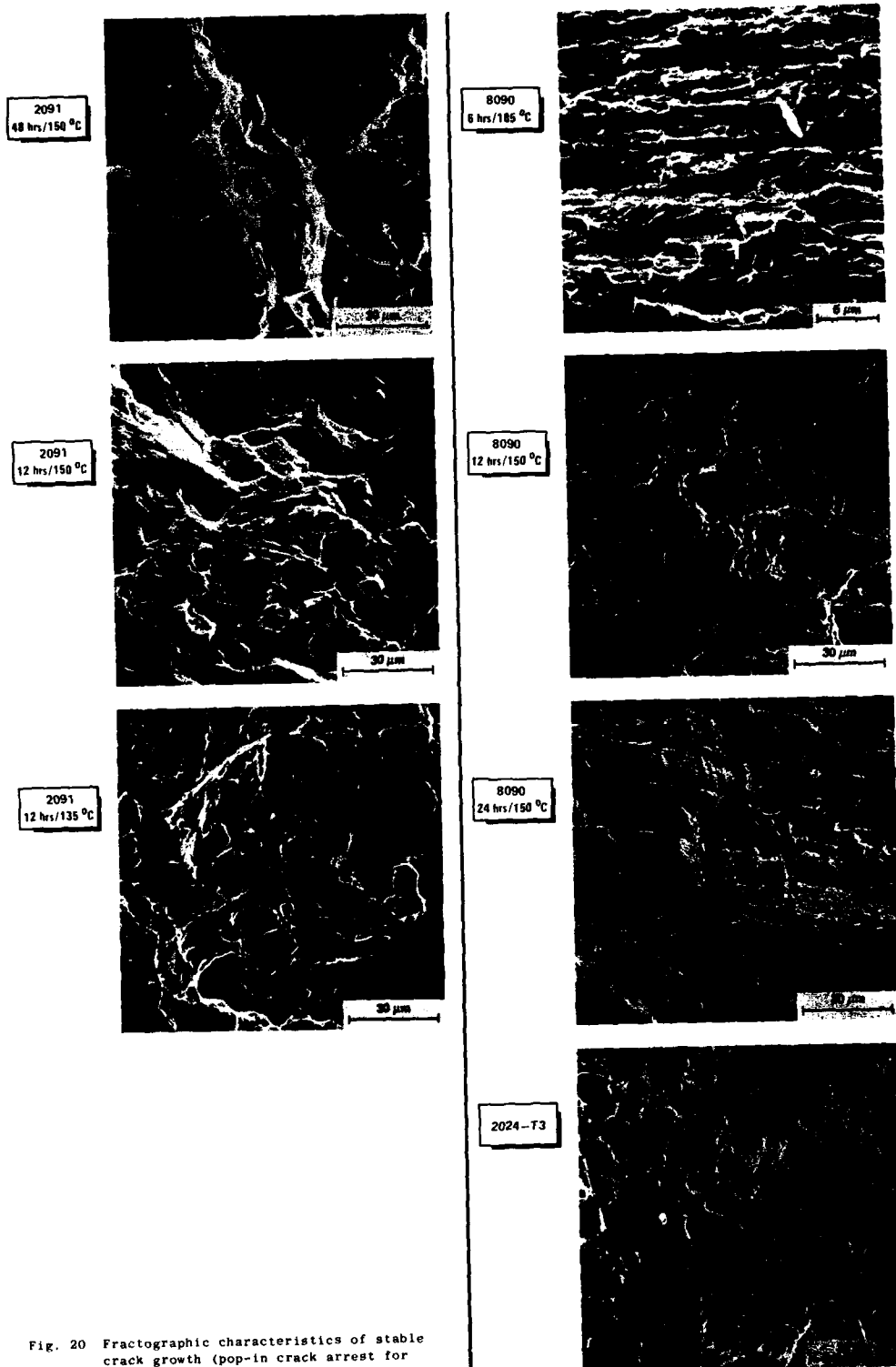


Fig. 20 Fractographic characteristics of stable crack growth (pop-in crack arrest for 2091 - 48 hrs/150 C)

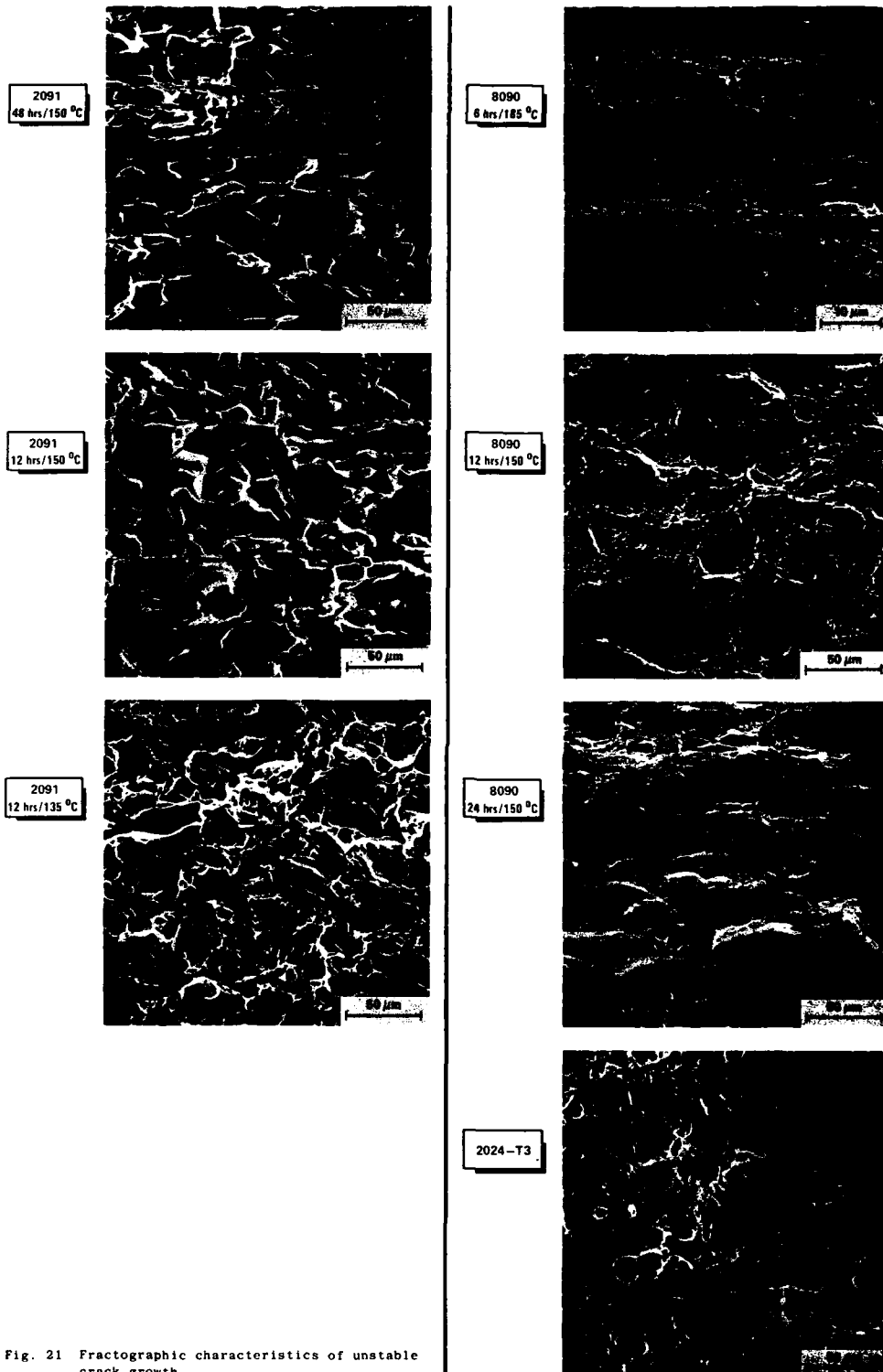


Fig. 21 Fractographic characteristics of unstable crack growth

FATIGUE PROPERTIES OF Al-Li ALLOYS

by

M. Peters*, K. Welpmann*, D.S. McDarmaid**, W.G.J. 't Hart***

* DFVLR -Deutsche Forschungs- und Versuchsanstalt für Luft- und Raumfahrt
 Institut für Werkstoff-Forschung
 D-5000 Köln 90
 Federal Republic of Germany

** RAE - Royal Aerospace Establishment
 Materials and Structures Department
 Farnborough, Hants, GU14 6TD
 United Kingdom

*** NLR - Nationaal Lucht- en Ruimtevaartlaboratorium
 Structures and Materials Division
 8300 AD Emmeloord
 The Netherlands

Summary

The paper presents results on fatigue properties of Al-Li 8090 plate material generated at DFVLR, NLR and RAE in the frame of a GARTEUR activity on Al-Li alloys. High cycle fatigue results are discussed as well as fatigue crack growth properties. Comparison is made to conventional high strength Al alloys. In most cases the Al-Li alloy showed at least equivalent high cycle fatigue properties and improved resistance to fatigue crack growth, primarily due to crack closure effects.

Introduction

The increased demand of the aerospace industry for new light-weight components has spurred the development of Li-containing Al alloys. Main efforts are concentrated in the United States and in Europe, here especially to mention Alcan International in England and Cégédur Pechiney in France. As a result of this growing interest a GARTEUR activity on Al-Li alloys was initiated in Europe in 1984. GARTEUR stands for "Group for Aeronautical Research and Technology in Europe" the members of which are from Aerospace industry and research laboratories of the four nations France, the United Kingdom, the Netherlands and the Federal Republic of Germany. The Al-Li Action Group was composed of four governmental research establishments - ONERA, RAE, NLR and DFVLR - six airframe manufacturers - Avions Marcel Dassault/Brequet Aviation, Aerospatiale, British Aerospace, Fokker Aircraft, Messerschmitt-Bölkow-Blohm and Dornier - and two metal producers - Alcan and Pechiney.

This paper is intended to report about one particular aspect covered in the Al-Li action group, i.e. the fatigue behaviour, a knowledge of which is essential since a significant proportion of these new alloys will be used for fatigue critical components.

Although work was done on both Alcan and Pechiney Al-Li alloys in sheet and plate form, the paper will essentially concentrate on results generated on 8090 plate material which proved, however, to be quite typical for Al-Li alloys in general.

It should be mentioned, that although the best available methods were used to produce the materials supplied to the GARTEUR group, it was inevitable that they were of a pre-production quality and were not representative of current industrial-scale output. Since 1984 considerable progress was made by both suppliers in improving the casting, rolling and heat treatment methods for the alloys and in understanding their physical metallurgy leading to consequent improvements in today's production Al-Li alloys.

Material and Experimental Procedure

Most of the investigations were performed on the Al-Li alloy 8090. This alloy was supplied by Alcan International in the form of 25 mm thick plate material which had been solution heat treated at 520°C, quenched, stretched 2.5 % and artificially aged for 16 h at 190°C, to a T651 condition. The alloy had a chemical composition (wt.%) of Al-2.42Li-1.24Cu-0.60Mg-0.12Zr-0.05Si-0.12Fe-0.05Ti. Comparison investigations were performed on a variety of high strength 2000 series Al alloys [1-7]. The microstructure of the Al-Li alloy was investigated by both light and transmission electron microscopy. Texture investigations were performed on a X-ray goniometer by employing the reflection technique. {111} pole figures were generated in the through-thickness direction, and compared to tensile properties determined on flat specimens. High cycle fatigue tests were performed on notched and unnotched specimens at R-ratios of -1 and 0.1 in laboratory air and aqueous 3.5 % sodium chloride solution. Constant amplitude fatigue crack propagation tests were performed on servohydraulic machines using Compact Tension (CT), Center Cracked Tension (CCT), and Single Side Cracked Hole (SSCH) specimens. R-ratios varied between 0.1 and 0.7; laboratory air and 3.5 % sodium chloride solution were used as test media. The test frequency was 13 and 30 Hz. To monitor crack growth, both a DC potential drop technique as well as optical measurements were applied. Load - Crack Opening Displacement (COD) measurements were made at regular crack length intervals. From the load - COD records, periodically made during K -decreasing tests, the crack opening load P_{op} was determined at the point of first deviation from the linear part of the curve. From P_{op} the opening stress S_{op} and hence the effective stress range $\Delta S_{eff} = S_{max} - S_{op}$ was calculated. Fractography was performed on a scanning electron microscope.

The experimental procedures performed differed from laboratory to laboratory. Therefore, for a more detailed information the reader is referred to references 1 to 7.

Results and Discussion

Microstructure

Fig. 1 is an optical micrograph showing a three dimensional view of the microstructure of the Al-Li alloy 8090 (Fig. 1a) and, for comparison, of the conventional Al alloy 2024 (Fig. 1b). Both alloys exhibit a pancake structure which is typical for high strength Al alloys. The Al-Li alloy, however, is unrecrystallized and reveals a finer subgrain structure with a subgrain size of about 2 to 10 μm . Furthermore, the volume fraction of big constituent particles is lower and in contrast to other high strength Al alloys, 8090 contains only one type of large constituent phase. These particles were often aligned along grain boundaries, and their dimensions were up to 10 μm . By energy dispersive X-ray analysis they were analysed as Fe/Cu rich, and can approximately be described by the formula $\text{Al}_6(\text{Fe}, \text{Cu}, \text{Mg})$. 8090 also contains very fine (10-30 nm) Al_3Zr particles, which are known to inhibit recrystallization.

Fig. 2 shows the matrix and grain boundary phases which precipitated during the artificial aging treatment. The three micrographs are taken from the same position. The typical high volume fraction of the spherical, homogeneously distributed δ' particles can most easily be recognized in the dark field (Fig. 2a), but are also visible in the two bright field images, which were taken under different tilting angles (Figs. 2b and c). Figure 2c also shows the plate-like S' precipitates. At grain boundaries the equilibrium δ phase has formed, along with a δ' precipitate-free zone (PFZ), which can be seen from Figs. 2b and c.

Fatigue Behaviour

To characterize the fatigue behaviour of a material it is essential to separate between fatigue initiation and fatigue crack propagation. In a high cycle fatigue test, initiation is a significant proportion of total life, whereas information about fatigue crack growth is generated in a fatigue crack propagation test. Since fatigue is a key issue for aerospace components a large portion of the GARTEUR work was devoted to the generation of S-N and da/dN - ΔK data.

High Cycle Fatigue Properties

In Fig. 3 the fatigue performance of smooth (Fig. 3a) and notched (Fig. 3b) 8090-T651 is compared with available data at $R = 0.1$ for currently used 2000 series aerospace aluminium alloys. In LT and L direction, 8090 shows improved fatigue performance in the high stress/low cycle regime whereas in the low stress/high cycle regime its performance is similar to that for the conventional 2000 series Al alloys. For the higher strength Al-Li alloy 8091-T651, similar findings are shown in Fig. 4a and b, where this alloy is compared to various conventional high strength 7000 series Al alloys. To investigate the influence of a corrosive environment on the fatigue behaviour of 8090 tests under push-pull loading ($R = -1$) were performed on smooth specimens of 8090-T651 and 2024-T851 which shows a similar strength level. The results in laboratory air indicated an advantage of 8090 compared to 2024 after 10^7 cycles of about 50 MPa for L and T specimens (Fig. 5a). However, in the presence of 3.5 % NaCl, the fatigue strength of the Al-Li alloy was reduced by about 100 MPa whereas the conventional Al alloy was hardly effected in the case of L specimens but suffered a reduction similar to 8090 in the T direction (Fig. 5b). This indicates that 8090 might be more susceptible to an aggressive environment than 2024, when both alloys are aged to about peak strength.

High cycle fatigue tests on notched specimens taken from the core and the surface of the 8090-T651 plate did not show any specific difference (Fig. 6a). This is in contrast to other mechanical properties which differ depending on the location of the specimen in the plate as will be shown later. Again the comparison to two 2000 series alloys showed that 8090 was equivalent or - in the high cycle fatigue regime - even better than the control alloys (Fig. 6b).

Light microscopy on the polished surface of smooth S-N specimens of 8090-T651 indicated that crack initiation takes place at constituent particles (Fig. 7). This means that the initiation mechanism is the same as for conventional high strength Al alloys. Therefore, a large portion of the higher fatigue strength of 8090 compared to conventional Al alloys can be attributed to the smaller size and lower volume fraction of constituents, since large particles lead to intensified local stress fields, i.e. early crack nucleation and thus reduced fatigue strength.

Fatigue Crack Propagation

Fatigue-life curves give a quick impression about the fatigue performance of materials. In Fig. 8 constant amplitude tests on 8090-T651 with $R = 0.1$ and $S_{max} = 70$ MPa are compared to two different 2000 series alloys in terms of plots of half crack lengths vs. number of fatigue cycles. 8090-T651 exhibited a fatigue crack growth life about five times as long.

More insight into the fatigue crack propagation behaviour can be obtained from $da/dN-\Delta K$ plots. Fig. 9 shows fatigue crack growth rate data for different 8090-T651 plates in T-L orientation at $R = 0.1$. It is evident that for the entire fatigue crack growth range measured the Al-Li alloy is superior to the two 2000 series control alloys. For low and intermediate ΔK values, cracks in the Li-containing alloy propagated more than an order of magnitude slower than for the conventional alloys. Furthermore, a distinct plateau in the $da/dN-\Delta K$ curve was observed at about 10^{-5} mm/cycle which is also evident in Fig. 10. Here, fatigue crack growth results under constant amplitude loading are shown for LT (Fig. 10a) and TL orientations (Fig. 10b) of 25 mm 8090-T651. Again, the comparison to two different 2024 tempers revealed the superior behaviour of the Li-containing alloy.

The investigation of fracture surfaces of fatigued specimens gave explanations for the retarded growth behaviour of 8090 especially in the plateau regime. Fig. 11 shows a macrograph of the fracture surface of a fatigued and fractured 8090 specimen in LT orientation tested at $R = 0.1$. Four different areas can be clearly distinguished: a light grey area of the threshold regime, a dark area corresponding to the plateau regime of the curve in Fig. 10a, a grey high growth rate area, and finally, the area of fast fracture. Higher magnification scanning electron microscopy revealed that the plateau area showed a much rougher appearance (Fig. 12b) than the threshold regime (Fig. 12a). Furthermore, large portions of the plateau area were densely covered with often spherical deposits (Fig. 12c) which are the reason for the dark appearance of this area of the fractured surface in Fig. 11. It is believed that these deposits originate from fretting of the fracture surfaces during crack propagation. In general the fracture surfaces of 8090 proved to be considerably rougher than those of the control alloys. This is evident from Fig. 13 where cross sections of fatigue fracture surfaces of 8090-T651 and 2024-T351 are compared. To quantify the surface roughness, a roughness factor, l_r/l_p , was introduced. This factor is defined as the ratio of the measured actual length of the surface profile and the projected length of the surface. Fig. 14a shows the quantified surface roughness as a function of ΔK . Compared to the 2000 series control alloys, the roughness factor for 8090 was substantially higher and increased with increasing ΔK . The much rougher fracture path in the Al-Li alloy is probably a result of the strong crystallographic texture for this material, as X-ray measurements on 8090 and 2024 plate material have shown /6/.

All these findings give strong indications that the superior fatigue growth behaviour of the Al-Li alloy is primarily due to crack closure effects resulting from surface roughness and fretting deposits. This assumption is supported by K_{op} measurements shown in Fig. 14b. Comparison of Figs. 14a and b shows that the surface roughness and the crack opening behaviour reveal similar tendencies. This indicates a direct relation between these parameters and proves that surface roughness is the main cause of high crack opening stress intensities which reduce the effective ΔK -values and can explain the overall superior fatigue crack growth behaviour of the Al-Li alloy. In addition the fretting deposits tend to further close the crack in the plateau regime, thus explaining the strong crack retardation of 8090-T651 at intermediate ΔK values (Figs. 9 and 10).

The above assumptions are further supported by high R-ratio fatigue crack growth tests, where crack closure is less dominant. It is evident that the differences in fatigue crack

growth behaviour between 8090 and 2024 become smaller once the R-ratio is raised from $R = 0.1$ to 0.5 (compare Figs. 9 and 15). Increasing the R-ratio further to 0.7 brings the curves for the various alloys even closer together with 8090-T651 partly matching 2024-T351 but still being superior to 2024-T851 (Fig. 16). Furthermore, the characteristic plateaus present for low R-ratio crack growth curves (Figs. 9, 10 and 16) become less pronounced or even disappear at high R-ratios (Figs. 15 and 16). The fact that even at high R-ratios the Al-Li alloy still shows partly a superior propagation behaviour in air over the conventional alloys, suggests that closure effects cannot account alone for their excellent fatigue crack propagation behaviour. For instance, the improved Young's modulus will contribute to their better fatigue crack propagation performance. Other possible factors include crack deflection and crack branching. Both lead to reduced stress intensities at the crack tip(s) thus decreasing the fatigue crack growth rate. A specifically impressive example for crack branching in the Al-Li alloy is shown in Fig. 17. Secondary cracks are longer than 10 mm.

Another interesting observation was made by performing fatigue crack growth measurements on specimens taken from the core of the plate and on near-surface specimens. In Fig. 18a crack growth curves are plotted for these two specimen locations and compared to 2000 series alloys. Apart from the fact that 8090 was superior over the conventional alloys, the core specimens showed much better behaviour than the surface material. In addition, both Al-Li specimens not only showed a pronounced plateau but also decreasing crack growth rates with increasing ΔK at about $8 - 12 \text{ MPa } \sqrt{\text{mm}}$ and 10^{-5} mm/cycle , where usually the plateau was determined (Figs. 9, 10 and 16). Such a decrease in growth rate with increasing stress intensity amplitude in the plateau regime was also observed during other fatigue crack growth tests on 8090 plate material /1, 3/. This somewhat abnormal behaviour can be explained by measurements of the crack opening stresses. From Fig. 18b it is evident that the crack opening load for 8090 increases dramatically at the lower end of the curve - contrary to the two conventional alloys. Therefore it is obvious that the strong increase of S_{op} drastically reduces the effective ΔK experienced at the crack tip. This effect overcompensates the increase in ΔK due to the increase in crack length and therefore can explain the negative slope in the $da/dN - \Delta K$ curves of Fig. 18a.

To better understand the difference in fatigue crack growth behaviour between core and surface material (Fig. 18a) it is essential to know that the core and the centre of the plate revealed severe differences in preferred crystallographic orientation. From the $\{111\}$ pole figures in Fig. 19 it is evident that the texture is much more pronounced in the centre of the plate ($t/2$) compared to the near surface location ($t/10$). A more pronounced crystallographic texture means that the differences in orientation between neighbouring grains are small. Since cracks propagate along crystallographic planes, grain boundaries in highly textured material represent less severe obstacles for propagating cracks. This increase in slip length will lead to rougher fracture surfaces for the highly textured core material as can be seen from Fig. 20 where core and surface roughness factors are plotted versus ΔK . Therefore, the difference in crystallographic texture between core and surface can explain the higher crack opening loads and therefore the slower crack growth rates for core material compared to near-surface material (Fig. 18).

To investigate the influence of an aggressive environment on the fatigue crack propagation behaviour of Al-Li alloys additional tests were performed in aqueous 3.5 % NaCl solution. Fig. 21 shows the results for 8090-T651 tested at two different R-ratios in LT and TL orientation. Compared to the two 2000 series tempers the Al-Li alloy showed mostly superior growth rates at the low R-ratio, while this superiority essentially disappeared at the high R-ratio. Nevertheless, 8090 still showed equivalent fatigue crack growth properties to the 2024 tempers at $R = 0.7$.

Another interesting observation made for 8090 is the fact that the threshold for fatigue crack growth at $R = 0.1$ is higher in the more aggressive 3.5 % NaCl solution than in air

(Fig. 22). It is believed that such a behaviour is due to another closure effect caused by corrosion debris on the fracture surface; especially since this effect disappears at the high R-ratio (Fig. 22). To get experimental evidence on this statement, a CT specimen of 8090-T651 was fatigued in air at $R = 0.1$ to near-threshold fatigue crack growth rates. Then the crack tip of the specimen was flooded with aqueous 3.5 % NaCl solution while the specimen was continuously cycled. As expected from the da/dN -curves, the crack growth rate decelerated and finally stopped in the sodium chloride solution. During the whole procedure the load/displacement of the specimen was continuously monitored. From Fig. 23 it is obvious that the crack tip opening stress intensity increased by about 10 % when the environment was changed from air to NaCl solution. Therefore, it is very likely that the fact that for the Al-Li alloy at low R-ratio the threshold in the corrosive environment is higher than in air is due to an additional closure effect caused by corrosion debris which deposits on the fracture surface. Similar observations were also made for 2024-T351 but not for 2024-T851 (compare Figs. 16 and 21).

Summary and Conclusions

- Compared to conventional high strength Al alloys 8090 plate material investigated in the frame of GARTEUR showed at least equivalent high cycle fatigue properties in air as well as in sodium chloride solution.
- Crack initiation takes place at large constituent particles for both Li-containing and Li-free alloys.
- In general, the constant amplitude fatigue crack propagation behaviour for 8090 is much superior compared to the control alloys.
- The main reason for the excellent fatigue crack propagation behaviour is crack closure due to fracture surface roughness and fretting debris.
- The pronounced roughness is probably a result of a strong crystallographic texture.
- The difference in fatigue crack propagation behaviour of core and surface material is caused by a texture gradient over the plate thickness.
- In aqueous 3.5 % NaCl solution 8090 showed equivalent or better fatigue crack propagation behaviour than 2000 series control alloys.
- At low growth rates cracks in 8090 propagated slower in NaCl solution than in air, which is attributed to an additional closure effect caused by corrosion debris.

Acknowledgements

Valuable discussions with B. Evans and C.J. Peel (RAE) are gratefully acknowledged.

References

- /1/ D.S. McDarmaid, "Fatigue and Fatigue Crack Growth Behaviour of Medium and High Strength Al-Li-Cu-Mg-Zr Alloy Plate", TR 85016, RAE, 1985.

- /2/ D.S. McDermald, S. Fox and H.M. Flower, "Fatigue of Medium and High Strength Al-Li-Cu-Mg-Zr Alloys in Plate and Sheet Form", in: "Advanced Materials Research and Developments for Transport, Light Metals", Eds. R.J.H. Wanhill, W.J.G. Bunk and J.G. Wurm, p. 93 - 100, Les Editions de Physique, Les Ulis Cedex, 1985.
- /3/ W.G.J. 't Hart and L. Schra, "Properties of the Al-Li Plate Alloy DTD XXXA-T651 (AA 8090-T651) in Comparison with two Damage Tolerant 2000 Series Plate Alloys", TR 86115 L, NLR, 1986.
- /4/ H.J. Kolkman, W.G.J. 't Hart and L. Schra, "Additional Investigation on the Al-Li Plate Alloy DTD XXXA-T651 (AA 8090-T651)", TR 87149 L, NLR, 1987.
- /5/ M. Peters, V. Bachmann, K. Welpmann, H. Bellingradt, J. Eschweiler and R. Braun, "Mechanical Properties of Al-Li DTD XXXA Plate Material", DFVLR-FB 86-40, DFVLR, 1986.
- /6/ M. Peters, J. Eschweiler and K. Welpmann, "Strength Profile in Al-Li Plate Material", Scripta Metallurgica 20, (1986), p. 259 -264.
- /7/ M. Peters, V. Bachmann and K. Welpmann, "Fatigue Behaviour of the Al-Li Alloy 8090 Compared to 2024", Zeitschrift für Werkstofftechnik 18 (1987), p. 277 - 283.

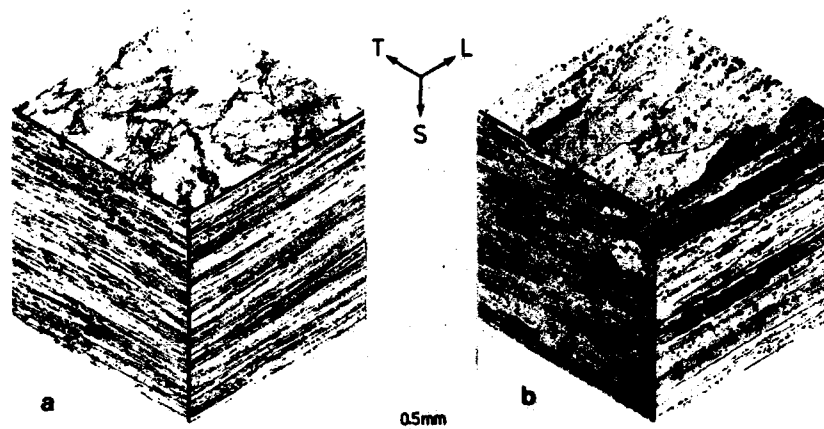


Fig. 1: Optical micrograph showing a three dimensional view of 8090 (a) and 2024 (b) (DFVLR).



Fig. 2: TEM dark field (a) and bright field (b and c) micrographs of 8090-T651 of the same area showing σ' (a and b), S' (b and c), PFZ (a to c) and grain boundary σ (b and c) (DFVLR).

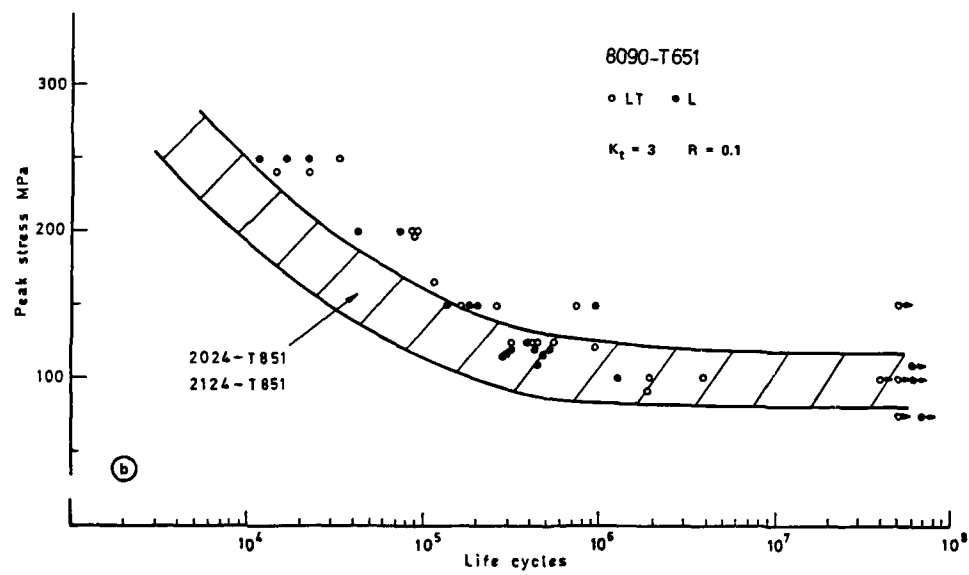
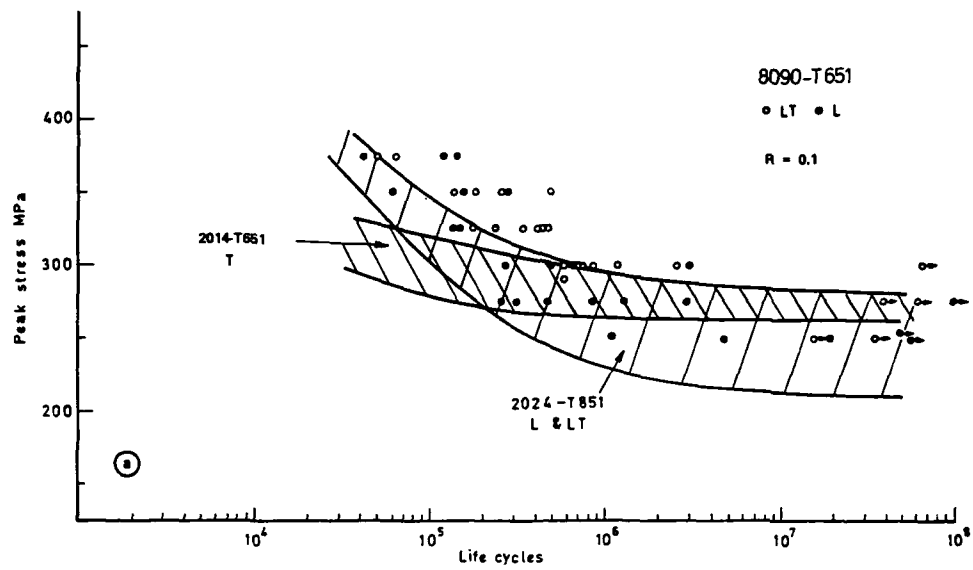


Fig. 3: S-N data at $R = 0.1$ for 8090-T651 compared to 2000 series alloys for smooth (a) and notched (b) specimens tested in laboratory air (RAE).

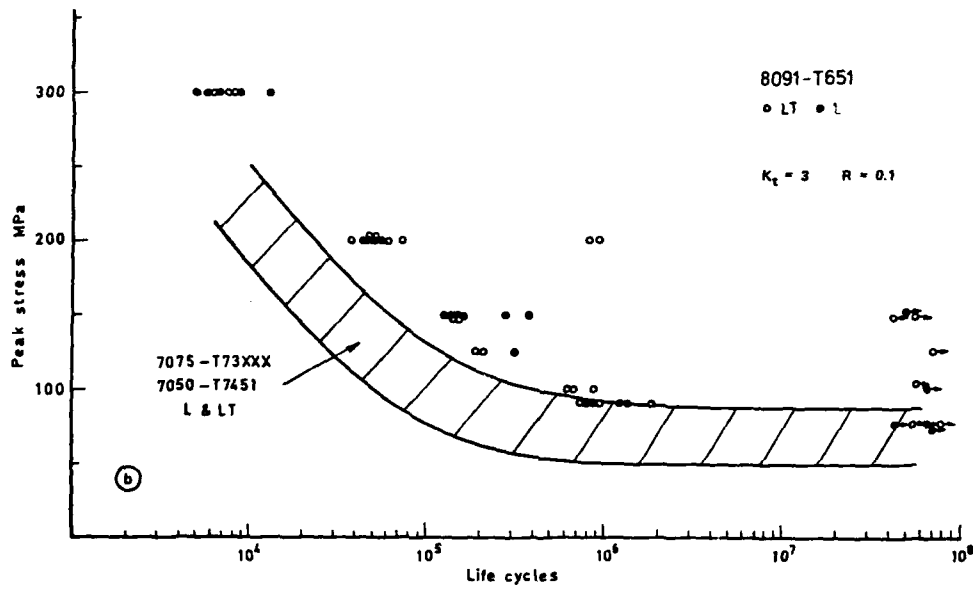
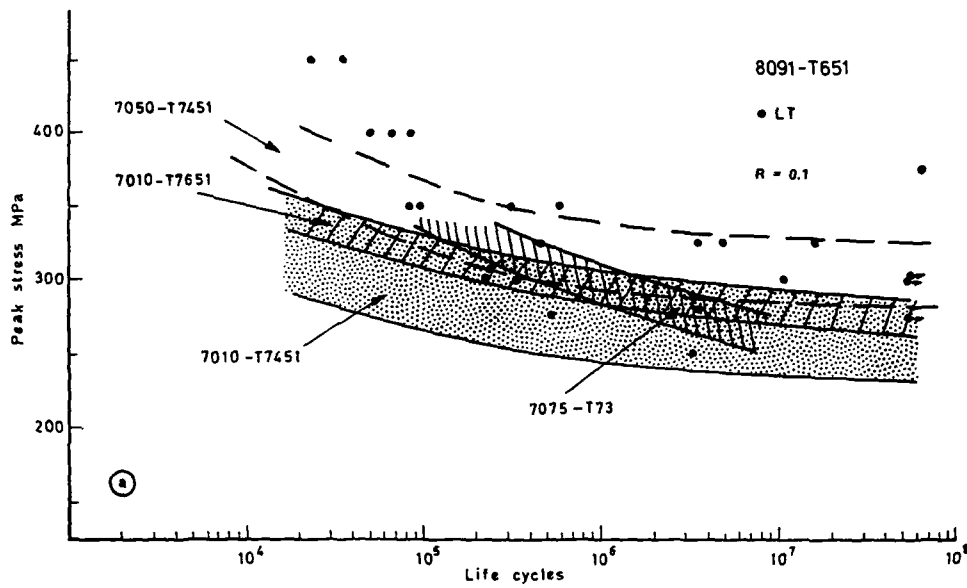


Fig. 4: S-N data at $R = 0.1$ for 8091-T651 compared to 7000 series alloys for smooth (a) and notched (b) specimens tested in laboratory air (RAE).

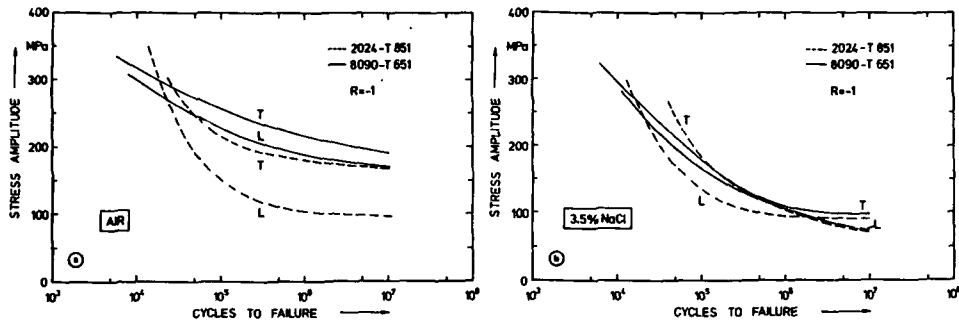


Fig. 5: S-N curves at $R = -1$ for 8090-T651 and 2024-T851 tested in laboratory air (a) and aqueous 3.5 % NaCl solution (b) (DFVLR).

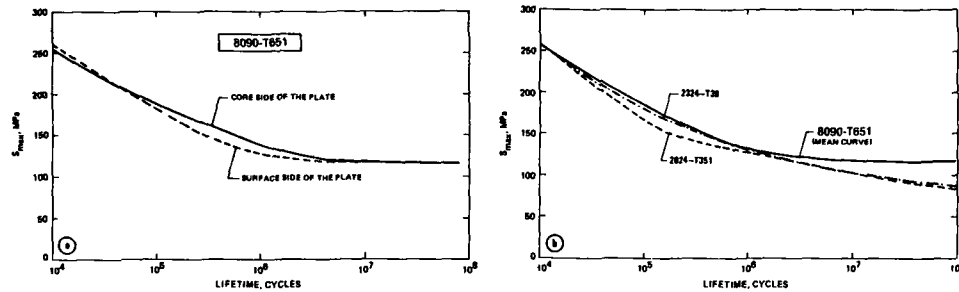


Fig. 6: S-N curves for notched specimens ($K_t = 3.1$) at $R = 0.1$ in L direction. 8090-T651, comparison of core and near-surface specimens (a), comparison of 8090-T651 and 2000 series alloys (b) (NLR).

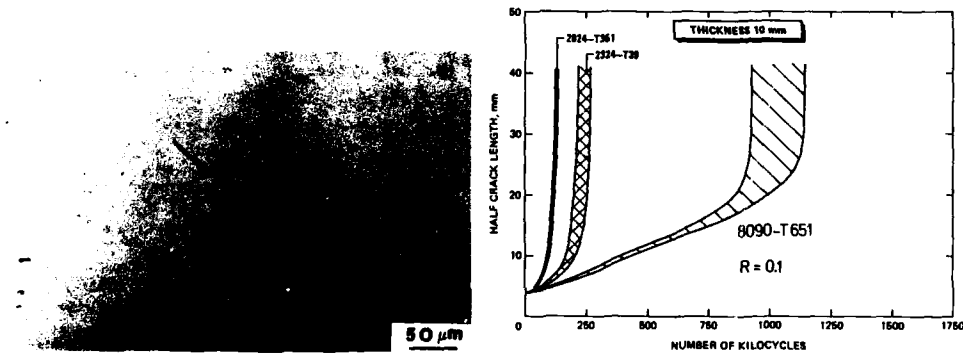


Fig. 7: Optical micrograph of the polished surface of a 8090-T651 specimen tested at $R = -1$ in L direction in laboratory air showing crack initiation at constituent particle (DFVLR).

Fig. 8: Fatigue life curves at $R = 0.1$ for two different 8090-T651 specimens in L direction compared to 2000 series alloys (NLR).

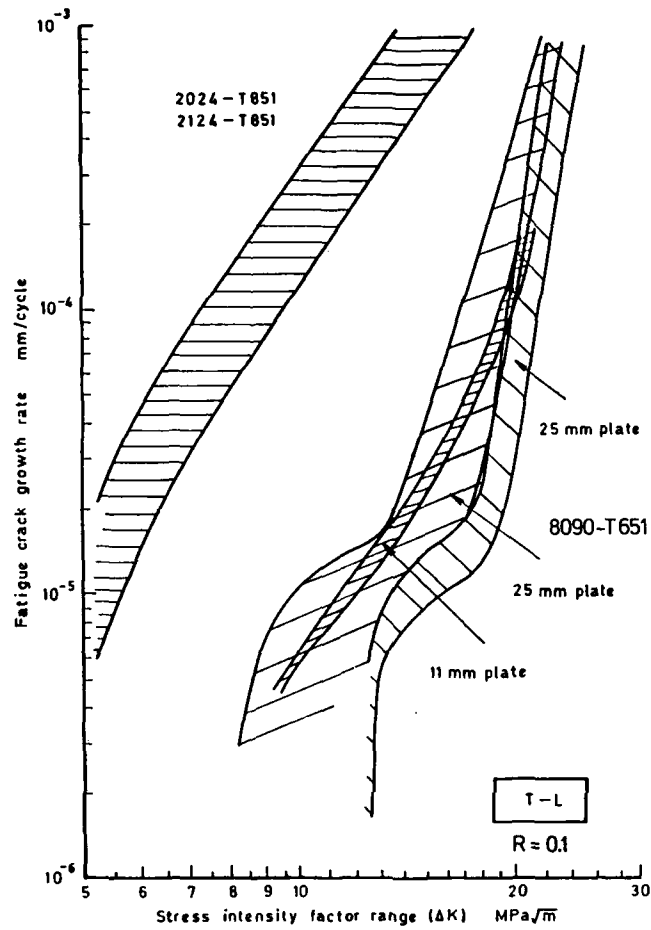


Fig. 9: Fatigue crack growth behaviour at $R = 0.1$ for 8090-T651 plates compared to 2000 series alloys (two scatterbands for two different 25 mm 8090 plates) (RAE).

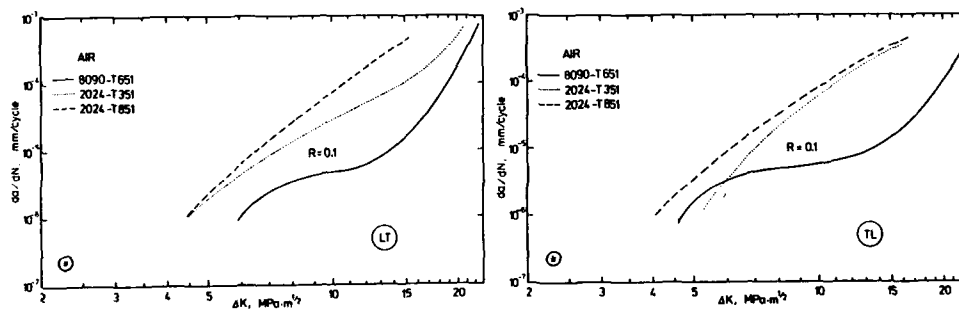


Fig. 10: Fatigue crack growth curves at $R = 0.1$ for 8090-T651 compared to two 2024 tempers for L-T (a) and T-L (b) specimens tested in laboratory air (DFVLR).

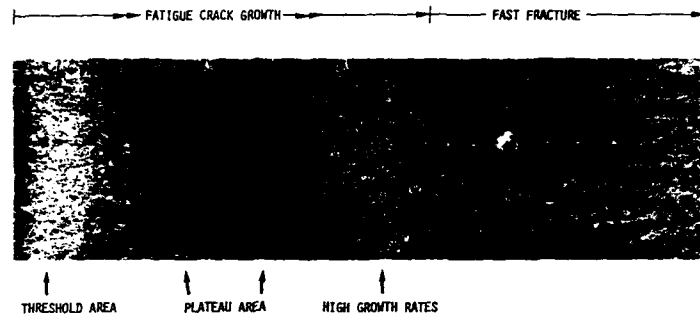


Fig. 11: Optical macrograph of the fracture surface of a fatigued and fractured 8090-T651 CT specimen in L-T orientation tested at $R = 0.1$ in laboratory air (DFVLR).

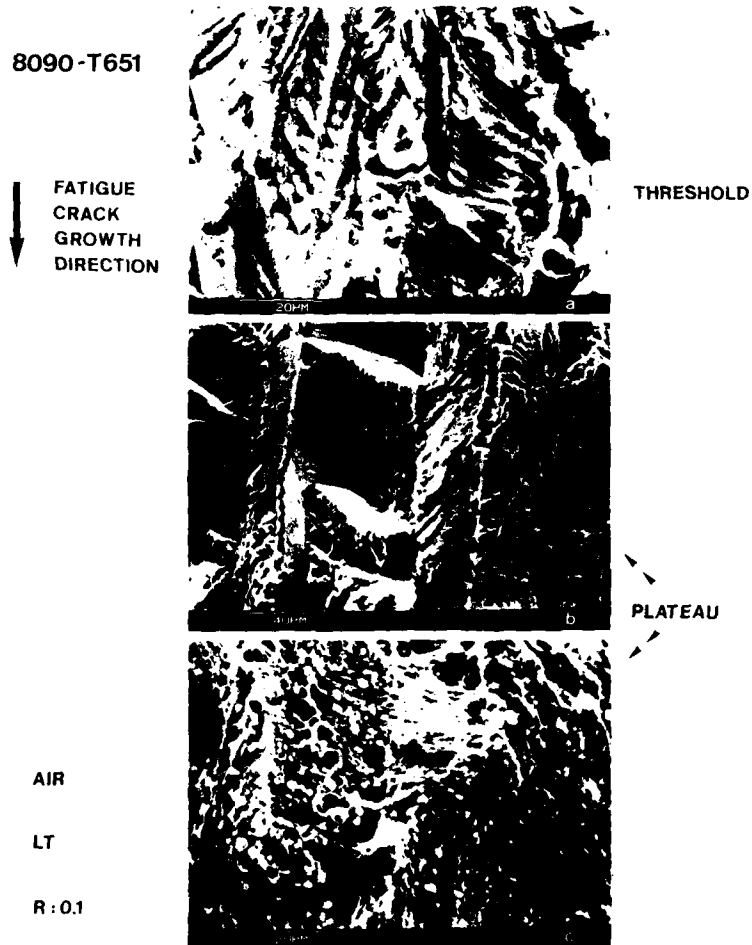


Fig. 12: SEM micrographs taken from different areas of the fracture surface given in figure 11 (DFVLR).

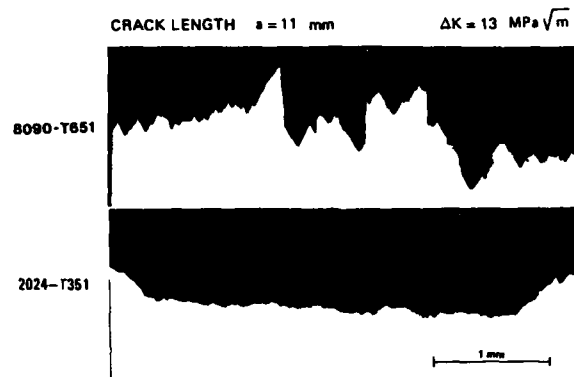


Fig. 13: Cross sections of fatigued crack growth specimens showing the fracture surface roughness of 8090-T651 and 2024-T351 (NLR).

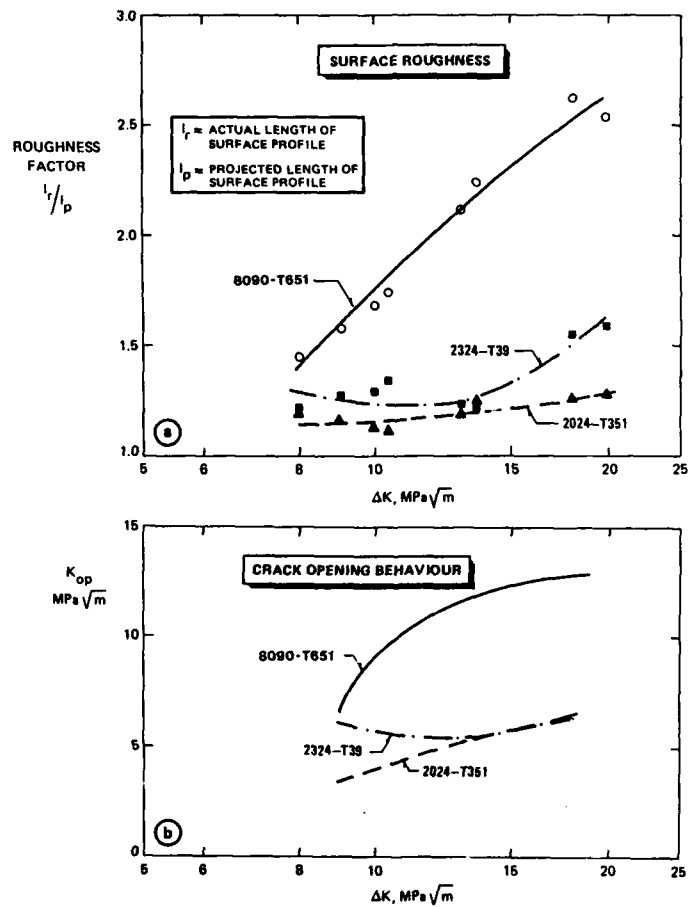


Fig. 14: Surface roughness (a) and crack opening behaviour (b) as a function of ΔK for 8090-T651 and 2000 series fatigue crack growth specimens tested at $R = 0.1$ (NLR).

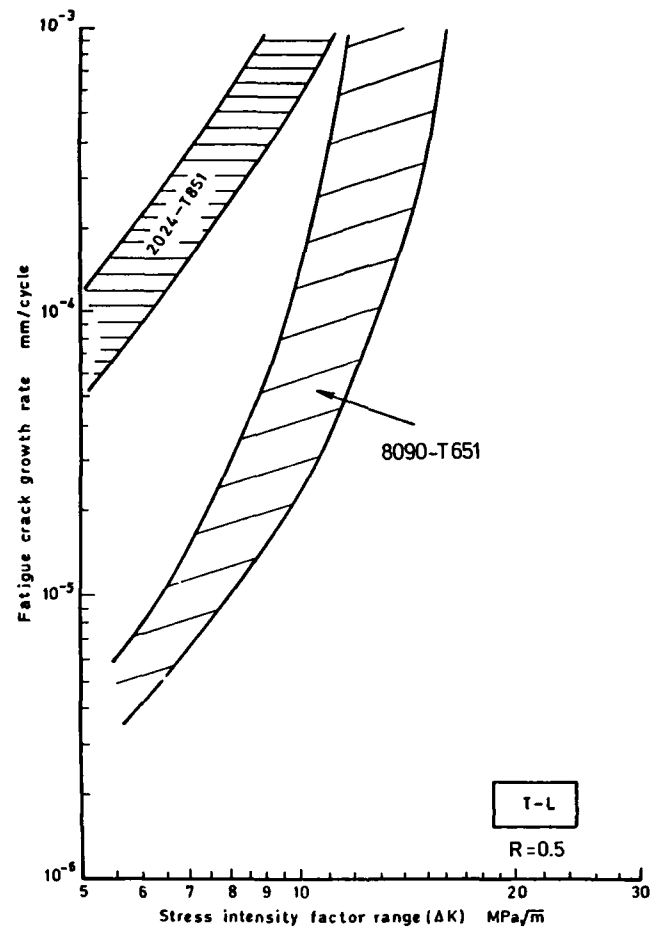


Fig. 15: Fatigue crack growth behaviour at $R = 0.5$ for 8090-T651 and 2024-T851 (RAE).

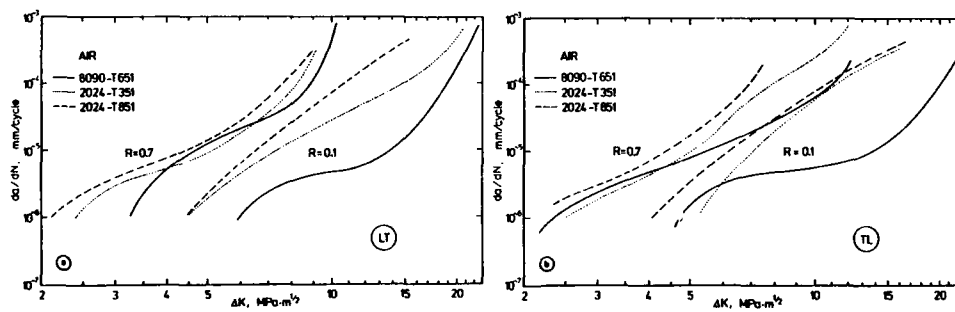


Fig. 16: Fatigue crack growth curves at $R = 0.1$ and $R = 0.7$ for 8090-T651 compared to two 2024 tempers for L-T (a) and T-L (b) specimens tested in laboratory air (DFVLR).

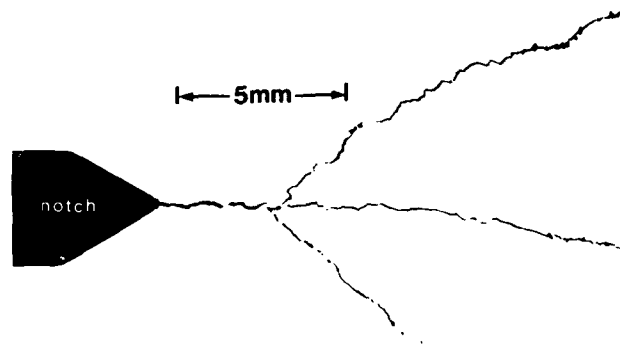


Fig. 17: Polished surface of a fatigued CT specimen of 8090-T651 in L-T orientation showing extensive crack branching (DFVLR).

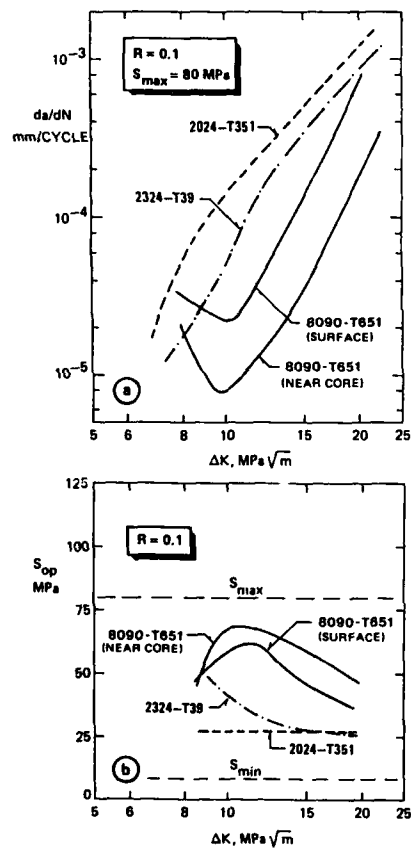


Fig. 18: Fatigue crack growth rate (a) and crack opening stress (b) as a function of ΔK for 8090-T651 near-surface and near-core specimens tested at $R = 0.1$ and compared to 2000 series alloys (NLR).

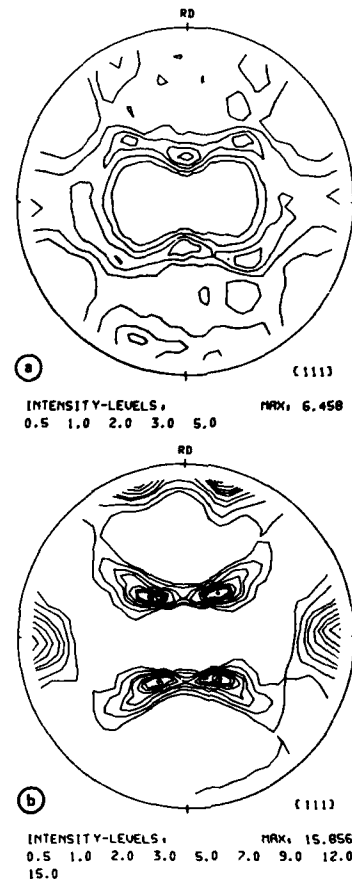


Fig. 19: $\{111\}$ pole figures of the 25 mm thick 8090 plate determined at $t/10$ (near surface) (a) and $t/2$ (core) (b) (DFVLR).

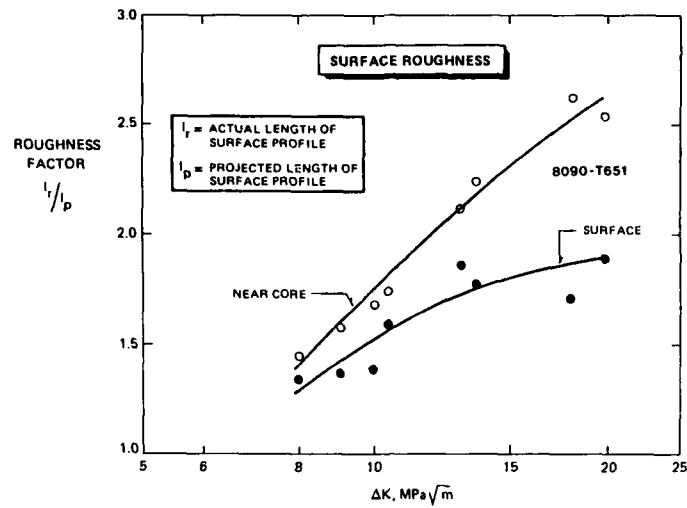


Fig. 20: Surface roughness as a function of ΔK for 8090-T651 near-surface and near-core specimens tested at $R = 0.1$ (NLR).

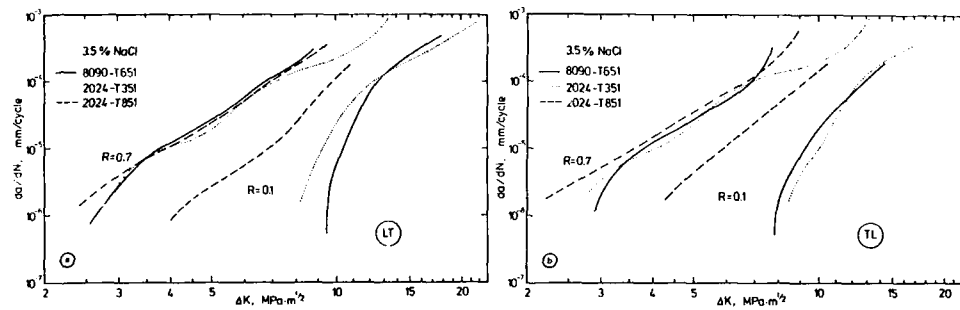


Fig. 21: Fatigue crack growth curves at $R = 0.1$ and $R = 0.7$ for 8090-T651 compared to two 2024 tempers for L-T (a) and T-L (b) specimens tested in aqueous 3.5 % NaCl solution (DFVLR).

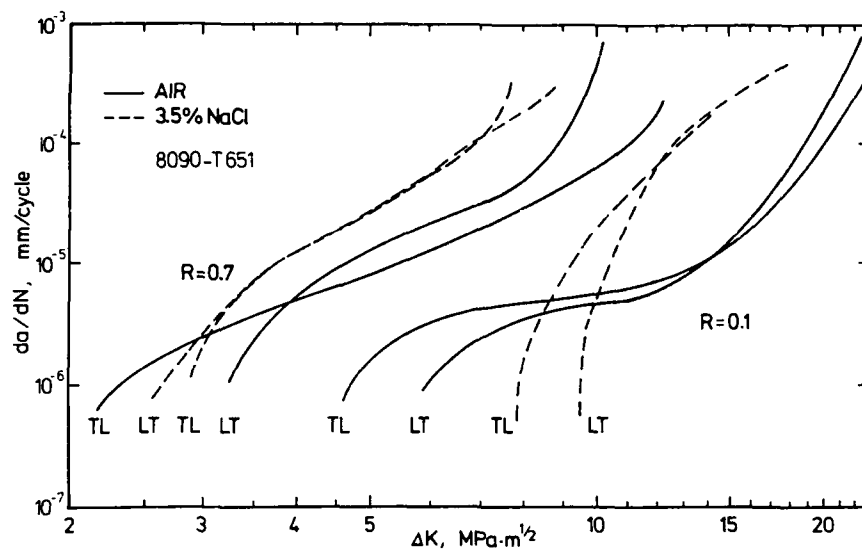


Fig. 22: Fatigue crack growth curves for 8090-T651 tested in air and in aqueous 3.5 % NaCl solution. Curves are given for two different R values and specimen orientations (DFVLR).

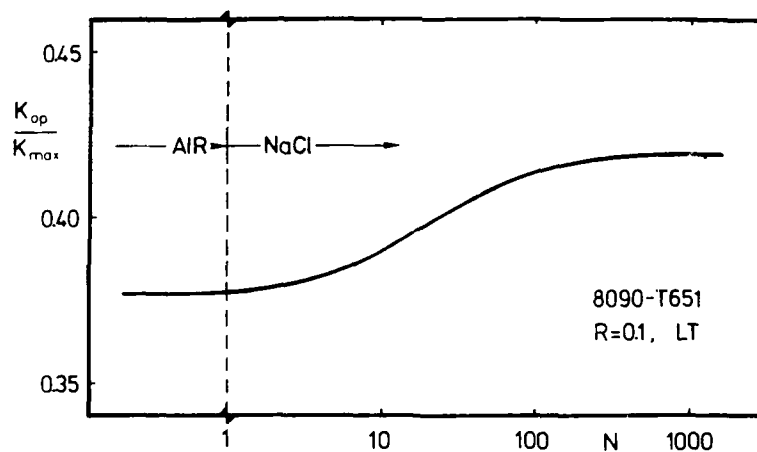


Fig. 23: Increase of crack tip opening load of 8090-T651 ($R = 0.1$, L-T orientation) at threshold growth rates during the change of environment from air to aqueous 3.5 % NaCl solution (DFVLR).

CORROSION AND STRESS CORROSION OF ALUMINIUM - LITHIUM ALLOYS

by

C J E Smith*, J A Gray*, L Schra**, J A M Boogers**,
R Braun***, H Buhl***, G Vaessen****

* Royal Aerospace Establishment (RAE)
Materials and Structures Department
Farnborough, Hants GU14 6TD
United Kingdom

** National Lucht- en Ruimtevaartlaboratorium (NLR)
Structures and Materials Division
P.O. Box 153
8300 AD Emmeloord
The Netherlands

*** Deutsche Forschungs- und Versuchsanstalt für Luft- und
Raumfahrt (DFVLR)
Institut für Werkstoff-Forschung
5000 Köln 90
Federal Republic of Germany

****Fokker Aircraft Engineering Laboratories
Fokker B.V.
P.O. Box 7600
1117 ZJ Schiphol
The Netherlands

SUMMARY

A programme of research to evaluate the corrosion and stress corrosion resistance of experimental, pre-production and production quality aluminium - lithium sheet and plate alloys is described. Accelerated laboratory tests and outdoor trials have been used to compare the corrosion behaviour of aluminium - lithium alloys with conventional aerospace alloys. The work was carried out at NLR, DFVLR, Fokker and RAE as part of the collaborative GARTEUR Group of Responsables for Structures and Materials AG07 activity on aluminium - lithium alloys.

1 INTRODUCTION

The last few years has seen the development of aluminium - lithium alloys in Europe and North America. The potential advantages of these materials compared with conventional aerospace aluminium alloys in terms of lightness and stiffness have been well documented (Ref 1). The aim has been to develop a family of alloys in the form of plate, sheet, forgings and extrusions which may be regarded as replacements for the current medium and high strength aluminium alloys and damage tolerant alloys. Most of the early research was naturally concentrated on achieving the desired mechanical properties but it was appreciated that the corrosion and stress corrosion resistance of any new alloy should be at least as good as the material it was intended to replace. Corrosion continues to be a major problem with both military and civil aircraft and although modern paint schemes are very effective, the inherent corrosion resistance of the substrate metal is important if the paint is damaged in service.

In 1983 a meeting was held to discuss the formation of a GARTEUR (Group for Aeronautical Research and Technology in Europe) action group to coordinate collaborative research on aluminium - lithium alloys. An important part of the GARTEUR programme was to evaluate the corrosion and stress corrosion behaviour of aluminium - lithium alloys. One of the main objectives has been to compare the aluminium - lithium alloys with existing alloys and to assess which of the accelerated tests gives the most accurate prediction in a real environment. This paper describes the research carried out at NLR, DFVLR, Fokker and RAE. A number of reports and papers have been published during the course of this programme which go into some depth about various aspects of the work. These are detailed in references 2-6.

2 MATERIALS

All research reported in this paper was carried out on either sheet or plate material. Details of the compositions and heat treatments of the sheet alloys studied are given in table 1. The sheets with one exception were all approximately 1.6mm thick. Of the early materials produced at RAE, alloy 96 aged for 1.5h at 170°C was intended as a low strength high toughness material. Alloy 98 was roughly equivalent to DTD XXXA and was considered as a possible replacement for 2014-T6. Alloy 88R was a high strength variation now replaced by 8091 and alloy C2M4 was similar in composition to Soviet produced material.

The other sheet materials examined were manufactured commercially. The 8090 alloys were supplied by Alcan whilst the 2091 alloys were provided by Cegedur Pechiney. The 8090 alloys evaluated included early materials produced from laboratory dc cast alloys as well as current production quality material. In the later stages of the programme

recrystallised material was available and is identified as B090C. The 2091 sheet was supplied as production quality material.

The plate alloys were supplied by Alcan and composition and heat treatment details are given in table 2. The 11mm (QRI-2), 25mm (RDV) and 50mm (RKT) alloys were early production materials. The remaining B090 plate alloys represent production grade materials.

3 TESTING PROCEDURES

3.1 Accelerated Corrosion Tests

Details of the various accelerated corrosion tests employed in the programme are given in table 3. Neutral salt fog (ASTM B117 ref 8) and alternate and total immersion tests in salt solution were used to compare with the medium strength aluminium - copper and high strength aluminium - zinc - magnesium alloys the resistance of aluminium - lithium alloys to general and pitting corrosion. Marine exposure trials on early sheet alloys indicated that aluminium - lithium alloys may be susceptible to intergranular and exfoliation corrosion. The MASTMAASIS (Intermittent acidified salt fog) test originally developed by Lifka and Sprowls (ref 9) and the EXCO test detailed in ASTM standard G34-79 (ref 10) were therefore extensively used to assess the susceptibility of sheet and plate aluminium - lithium alloys to exfoliation attack. Resistance to intergranular corrosion was evaluated using the corrosion test described in Mil-H-6088 (ref 11).

Standard electrochemical techniques have been employed to determine the open circuit and pitting potentials of aluminium - lithium and conventional aerospace aluminium alloys.

3.2 Outdoor Exposure

Marine exposure trials were conducted at the Fleet Maintenance and Repair Organisation, Exposure Trials Station, Eastney, England. Samples were fixed on wooden frames using ceramic bushes so that they faced due south. The frames were inclined at an angle of 45°.

Tests were also made at NLR, North East Polder, in The Netherlands. Specimens were mounted on a corrosion rack at an angle of 45° to the horizontal and faced south - west. The site is basically rural but is sometimes affected by industrial pollution. The acidity of the rainwater over a year varied from pH 4.3 to 6.9 the average being pH 5.3.

3.3 Stress Corrosion Tests

Smooth specimens were used to study the initiation of stress corrosion cracking and to enable the threshold stresses to be determined. For the sheet material both alternate immersion tests to ASTM specification G44-75 (ref 12) and slow strain rate tests were used. The specimens used in the alternate immersion test were of the bent beam type and consisted of 20mm wide by 200mm long strips. Testing was carried out in 3.5% salt solution and synthetic seawater prepared to ASTM D1147-75 (ref 13) but without the addition of heavy metals. Slow strain rate tests were made in 3.5% salt solution.

The stress corrosion behaviour of 25mm thick plate was evaluated using C-ring and tuning fork type specimens machined so that the ST direction was stressed. For the 44mm and 50mm plate tension bars were used and were stressed in a modified Alcoa rig. Testing was carried out using alternate immersion and marine exposure at the Eastney site. Some of the 25mm thick plate was also examined using the slow strain test. Details of this technique have been published elsewhere (ref 14). In these tests the performances in both the LT and ST directions were studied.

The resistance to stress corrosion crack growth in 25mm plate was determined using Double Cantilever Beam (DCB) type specimens machined in the longitudinal direction. After fatigue precracking specimens were either subjected to alternate immersion in synthetic seawater or were exposed at the NLR site in North East Polder.

4 RESULTS AND DISCUSSION

4.1 Corrosion Resistance

4.1.1 Sheet Alloys

The corrosion behaviour of a number of experimental sheet alloys cast and rolled at the Royal Aerospace Establishment were evaluated using both accelerated laboratory tests and exposure to a marine environment. The performances of the alloys were compared with four commercially produced sheet aerospace aluminium alloys. Table 4 summarises the appearances of the test coupons after exposure and fig. 1 gives the depths of attack.

Under marine exposure conditions, all the experimental sheet aluminium - lithium alloys investigated were found to undergo exfoliation attack. In contrast, the unclad control alloys were only pitted and sectioning confirmed that whilst intergranular attack had occurred in two of the alloys, no exfoliation had taken place. The EXCO and

MASTMAASIS tests succeeded in generating exfoliation corrosion in most of the aluminium - lithium alloys. Weightloss and pitting depth measurements made after total immersion, alternate immersion and neutral salt fog tests, indicated that the aluminium - lithium alloys were generally more resistant to pitting corrosion than the unclad aluminium alloys currently used in airframe construction. The copper free alloy, C2M4, was particularly resistant to pitting and compared with the Alclad 7475 - T761 alloy. The corrosion data obtained suggested that although the experimental sheet aluminium - lithium alloys were susceptible to exfoliation, the depth of attack was no greater than the depth of pitting which occurred in the control alloys.

The limited data obtained with alloy 96 further indicated that ageing may influence the susceptibility to exfoliation corrosion. This aspect was looked at further using early sheet aluminium - lithium alloy (RCO) manufactured by Alcan. Material was aged at 170°C and 185°C for various times upto 64h. Coupons were subjected to accelerated laboratory corrosion tests and exposure to a marine environment. The results obtained are summarised in table 5, and show that the susceptibility of the sheet material was strongly dependent on ageing treatment. Table 5 indicates that material was most susceptible to exfoliation corrosion when it was heat treated at 170°C for 8h or at 185°C for 1.5h. Heat treating for longer times at these temperatures considerably improved the resistance of the alloy to this type of corrosion. Confirmation that this was due to a reduction in susceptibility to intergranular corrosion is provided by the data presented in fig 2. This shows that the mean width of attack which is directly related to the susceptibility to intergranular corrosion decreases with extended ageing times at 170°C and 185°C.

The corrosion resistance of unrecrystallised 8090 aluminium - lithium alloy sheet has been evaluated in both a rural environment and when exposed to a marine atmosphere. Data obtained by NLR for material in the T6 and T8 tempers after 1 years exposure at the North East Polder test site is included in table 6. The alloy in both tempers showed the beginning of exfoliation blistering but an aluminium - copper alloy, 2024-T3, exposed over the same period showed no appreciable corrosion attack. In a marine environment the development of exfoliation corrosion is more rapid. Fig 3 shows the results of trials made on two 8090 type alloys (RDT and RGS). Both alloys showed extensive exfoliation attack after 1 years exposure. The degree of attack was greatest when the alloys were only lightly aged ie. 3h at 170°C. Extending the heat treatment to 64h significantly reduced the exfoliation. This is in keeping with results obtained on early sheet material.

Accelerated corrosion tests in the form of EXCO and MASTMAASIS have been used to evaluate the resistance to exfoliation. Results obtained by NLR for 8090 - T8 sheet using various immersion times in EXCO solution are reproduced in table 7 and DFVLR data for 8090 - T6 sheet are given in table 8. Both materials readily exfoliated in EXCO solution. In the MASTMAASIS, intermittent acidified salt fog test, the level of exfoliation attack developed was less severe as indicated by the data in tables 9 and 10. No difference in performance could be detected in the NLR tests between the T6 and T8 conditions.

A limited amount of 8090C recrystallised sheet became available during the later stages of the collaborative programme. Results obtained for material aged at 150°C for 1 hour are given in table 11. After 19 months marine exposure some evidence of exfoliation attack was detected. It was also possible to generate exfoliation in the laboratory tests.

2091 aluminium alloy sheet which had been produced commercially was evaluated in a number of temper conditions by DFVLR, NLR, Fokker and RAE. The results of natural exposure trials made in a rural environment and under marine conditions are given in tables 6 and 11 respectively. In the T3 temper the alloy showed only a slight tendency to exfoliate after 19 months marine exposure. In the other tempers examined early signs of exfoliation were detected in both environments.

Data obtained using the EXCO test is included in tables 7,8,11 and 12. Tests made by Fokker, NLR and RAE failed to develop exfoliation in material in the T3 temper. All the other ageing treatments examined promoted exfoliation attack. In the MASTMAASIS test exposure periods of upto 16 days failed to generate exfoliation corrosion although evidence of intergranular attack was found in material in the T_x and T8_x tempers examined by NLR. The work at DFVLR on material aged at 150°C for 12h and 100h and material aged at 135°C for 12h showed that all three alloys had a P/EA rating after 5 weeks exposure. Differences in weightloss were determined though as shown in fig. 4. Material aged at 135°C for 12h appears to have suffered less corrosion than material aged at 150°C. Sheet which had been aged at 150°C for 48h by RAE was found to give an EA/EB rating after 2 weeks exposure.

The intergranular corrosion test described in Mil-H-6088F was employed by Fokker to compare the depth of attack in 2091 in the T3 and T8 tempers with 2024-T3. It was found that 2091-T3 possesses an equal or better corrosion resistance than 2024-T3 unclad. In the T8 temper (48h at 150°C) the 2091 alloy shows greater depths of intergranular attack than 2024-T3. Tests made by DFVLR indicated that pitting and intergranular attack could occur to depths of upto 150µm.

The identification of a suitable test for the exfoliation of aluminium - lithium alloys has been one of the aims of the programme. The data in table 5 indicate that the

MASTMAASIS test gave reasonable correlation with exposure to a marine atmosphere. Subsequent work with the commercially produced 8090 and 2091 alloys has tended to support this. The data in tables 6, 7 and 9 show that the MASTMAASIS test gives a similar alloy ranking to that found in atmospheric exposure. The weightloss data in fig. 4 suggest that extending the period of testing for upto 5 weeks may be advantageous in detecting differences in performance between alloys which superficially show similar levels of exfoliation.

4.1.2 Plate Alloys

The corrosion behaviour of 11mm (QRI-2) and 25mm (RDV) thick 8090 plate materials produced in the early stages of the programme were evaluated. Each alloy was evaluated in the naturally aged condition and after artificially ageing. In the case of the 11mm plate ageing treatments of 1.5h at 170°C and 16h at 190°C were employed whilst the 25mm thick plates were aged at 190°C for 16 and 64 hours. The results of marine exposure, EXCO and MASTMAASIS tests are summarised in table 13. Exposure of the 25mm plate to a marine atmosphere for 415 days generated only slight exfoliation attack. The 11mm plate exhibited slightly more severe exfoliation after exposure for 630 days, which may be attributed to the longer exposure period or may be associated with a more elongated grain structure in the thinner section. The EXCO and MASTMAASIS tests generated severe exfoliation corrosion, more so than in the marine exposure trials. The 11mm plate was particularly susceptible to attack in the artificially aged conditions when the 1/2T plate was exposed to acidified salt fog. Artificially aged test coupons of the 25mm plates were less susceptible in this test.

The corrosion resistance of production quality 25mm 8090 plate in the T651 condition was evaluated by NLR and DFVLR. The EXCO test results given in tables 14 and 15 suggest that the alloy is very susceptible to exfoliation corrosion. In the NLR work three hours immersion was found to be sufficient to generate significant exfoliation attack. Comparisons were made with two aluminium - copper alloys 2024-T351 and 2324-T39 and whilst both materials showed a tendency to exfoliate, the level of attack was not as great as with the aluminium - lithium alloy. In the MASTMAASIS test, NLR found that the ranking of the alloys was reversed, with the control alloys showing greater weightloss than 8090 plate. This pattern of behaviour was closer to that found when samples were exposed at the rural test site. After one year, the control alloys were more corroded than 8090-T651 plate which showed only slight attack.

Research at DFVLR has looked at the behaviour of the 25mm plate in neutral and acidified salt spray. The results presented in figs. 5 and 6 indicate that the degree of attack is highest when tests are made in continuous acidified salt spray. Under these conditions considerable exfoliation occurs whilst in the neutral salt fog test the attack is mainly pitting. The MASTMAASIS test also generated exfoliation corrosion as well as pitting and intergranular attack. The intergranular corrosion test (MIL-H-6088) showed that there were differences in the level of attack between the centre and edge region of the plate. At the centre the intergranular attack extends more in the rolling plane and the maximum depth of attack is 80µm. At the edge the pitting attack is more pronounced and the maximum level of attack is 160µm.

The general conclusions from this work are that 25mm plate in the T651 temper is susceptible to exfoliation but the degree of attack is less severe than in alloys such as 2024-T351 and 2324-T39. The limited data available suggest that the MASTMAASIS test is probably a more reliable test for the aluminium - lithium alloys than the EXCO test.

4.2 Stress Corrosion Resistance

4.2.1 Sheet Alloys

The resistance of sheet aluminium-lithium alloy to stress corrosion cracking was evaluated by NLR and DFVLR using bent beam specimens. Additionally DFVLR carried out slow strain rate tests. The results obtained by NLR for 2091 and 8090 sheet materials in various tempers and a control alloy tested by alternate immersion in synthetic seawater are presented in fig 7. The 2091-T3, 8090C-T3 and 8090-T3 alloys all showed a high stress corrosion resistance but in the other alloys early crack initiation occurred.

In the DFVLR work bent beam specimens were used to compare the stress corrosion resistance of 2091 sheet in three tempers. The threshold stresses determined are given in table 16. The values were determined using two failure criteria, crack initiation and macroscopic fracture. The results obtained indicate that increased ageing in underaged tempers of 2091 leads to an increase in stress corrosion resistance. Tests made on using bent beam specimens cut from 8090-T6 sheet material showed no signs of crack initiation when tested by alternate immersion in 3.5% sodium chloride solution or by continuous immersion in 2% NaCl + 0.5% Na₂CrO₄ at pH3. Similarly slow strain tests on this material failed to detect a susceptibility to stress corrosion cracking.

Concerning the stress corrosion testing of 2091 sheet alloys it should be mentioned that with recrystallised aluminium - lithium alloys, i.e. 2091 and 8090-Lital C, the stress corrosion cracking behaviour determined by accelerated tests is strongly dependent upon environmental conditions. Bent beam specimens of 2091 sheet alloys (and also of 8090 Lital C) in underaged heat treatments are susceptible to stress corrosion cracking if they are alternately immersed in aqueous 3.5% NaCl solution. When continuously immersed in 3.5% NaCl solution these underaged recrystallized alloys show

no macroscopic fracture and no crack initiation (detection of a first crack at 20x magnification). This should be borne in mind when comparing the results of conventional corrosion tests with those of determined using the slow strain rate technique. More investigations on that topic are in progress. Reasons for this behaviour are discussed in the paper by Craig et al. (ref.15)

4.2.2 Plate Alloys

4.2.2.1 Initiation Studies

The stress corrosion resistance of 25mm thick early commercially produced 8090 type material (RDV) was evaluated by RAE using C-ring type specimens. These were tested using alternate immersion in 3.5% salt solution and marine exposure. The threshold stresses determined are given in table 17 together with values for three control alloys. The macro-threshold stress refers to the stress below which a loaded specimen did not fail after 84 days testing. However sectioning and microscopic examination of a number of C-rings which had apparently not failed revealed the presence of intergranular cracking perpendicular to the direction of application of stress. Thus although the threshold values given in table 17 give a ranking order for the alloys they cannot be regarded as threshold values in the sense that at stress below the threshold no stress corrosion cracking will develop. A second threshold value has been included in table 17 which corresponds to the stress below which no evidence of microcracking is found. If the 8090 plate alloys are compared on this basis it is clear that they approach 2014-T6 in performance and are rather better than 7075-T6. Tests in marine environment indicate that the macro-threshold stresses are likely to be less than 2024-T3 material.

More recently Alcan produced 8090-T651 25mm plate has been evaluated by NLR and DFVLR. Constant strain and constant load tests used by DFVLR have demonstrated that the plate material is not susceptible to stress corrosion cracking when tested in the LT direction. This was confirmed by slow strain rate tests which showed that in the LT direction testing in 3.5% sodium chloride solution does not effect the mechanical properties. In the ST direction however tests show that the alloy is susceptible to stress corrosion cracking. C-ring data obtained by DFVLR is presented in fig.8 and shows that the threshold stress is <50MPa and compares with 2014-T651 and 7075-T651 plate. However at a given stress level the time to failure of the 8090-T651 plate was found to be longer in comparison with the control alloys. Results of the constant load tests in the ST direction are given in fig.9 and indicate that some failures occurred at stresses below 70MPa. Metallographic analysis of unbroken specimens indicated that deep cracks had formed.

NLR work using tuning fork type specimens has established that the resistance to stress corrosion cracking of 8090-T651 is slightly better than that of 2024-T351 and 2324-T39. Results obtained are presented in fig.10.

44mm and 50mm thick plate has been evaluated by RAE. Tests were made using tension bars machined in the ST direction. Data obtained for the 50mm thick plate (RKT) using alternate immersion testing in 3.5% sodium chloride solution and exposure to a marine environment are given in fig.11 and show that extending the ageing time from 16 to 64 hours improves the stress corrosion resistance. Threshold stresses obtained using alternate immersion testing are similar to those determined under marine exposure conditions. For material aged at 190°C the threshold stresses are similar to those contained for 25mm thick plate.

The 44mm thick plate which is currently being evaluated was aged at 170°C for 32 hours to give the T8771 temper. First results indicate that much higher threshold stresses may be possible with material in this temper.

4.2.2.2 Crack Growth Measurements

Stress corrosion crack propagation in 25mm thick plate has been evaluated using double cantilever beam specimens machined from the core material in the longitudinal direction. Results comparing the crack growth with 2024-T251 and 2324-T39 are reproduced in figs.12 and 13. In the laboratory tests the two control alloys showed higher crack growth rates than the aluminium - lithium alloy but under rural exposure conditions the crack growth rate in the aluminium - lithium alloy was highest. It was found that corrosion product wedging had occurred in the laboratory tests and was probably the main driving force for stress corrosion cracking for 2024-T351 and 2324-T39.

4.3 Electrochemical Measurements

A limited amount of data has been obtained on the effects of ageing on the rest and pitting potentials of aluminium - lithium alloys. Pitting potential measurements made by DFVLR are summarised in table 18 and show that with increased ageing the pitting potential of 2091 sheet aluminium - lithium alloy becomes more electronegative approaching the values obtained for aluminium - zinc -magnesium 7010 alloy.

4.4 Effect of Marine Exposure on Mechanical Properties

The effect of exposure to a marine environment on the mechanical properties of two 8090 type sheet aluminium - lithium alloys (RGS and RDT) was examined. Both alloys were given ageing treatments of either 3 hours at 170°C, 64 hours at 170°C or 8 hours at

185°C before being machined into tensile test pieces. These were exposed together with specimens machined from 2000 and 7000 series clad and unclad aluminium alloy controls at the Eastney Test Site. Specimens were returned for testing at RAE after 6 months, 1 year and 2 years and the results obtained are given in fig.14. The loss in strength due to corrosion suffered by the aluminium - lithium sheets is greater than that suffered by all but one of the commercial alloys. The exception was L150 an artificially aged unclad 2014-T6 type aluminium - copper alloy which showed losses in strength similar to 8090. The results in fig.14 indicate that the performance of 8090 type alloys can be significantly improved by extending the ageing treatment. If comparison is made with 2014 - T6 the material it is designed to replace, the unrecrystallised 8090 alloy aged to the peak strength yields higher tensile strength after 2 years exposure and gives comparable ductility.

5 CONCLUSIONS

- 1) Lithium containing sheet aluminium alloys show varying degrees of susceptibility to exfoliation corrosion. In general the unrecrystallised medium strength 8090 material in the T6 and T8 tempers is more susceptible to exfoliation attack than the recrystallised 8090 and 2091 type alloys in various damage tolerant tempers. The 2091 alloy has in the naturally aged T3 condition an exfoliation susceptibility equal or better than that of the 2024-T3 control alloy. The exfoliation susceptibility of 2091 increases with increased ageing for underaged tempers. Control alloys tested under similar conditions are relatively resistant to exfoliation showing mainly pitting and intergranular attack.
- 2) Plate 8090 type aluminium - lithium alloys are susceptible to exfoliation corrosion. In the T651 temper, the level of attack was less than on 2024-T351 and 2324-T39 alloys.
- 3) The MASTMAASIS test gives a more reliable indication of exfoliation susceptibility than the EXCO test.
- 4) The recrystallised 2091 and 8090 sheet alloys have in the T3 temper a high resistance to stress corrosion cracking. Early crack initiation occurs when these alloys are slightly underaged. For 2091 it was found that the SCC resistance increases again with increased ageing.
- 5) 8090 type aluminium lithium alloy plate will suffer stress corrosion cracking when tested in the ST direction. Threshold stresses determined compare favourably with control alloys.
- 6) Exposure to a marine environment for two years produced substantial decreases in the tensile strength of 8090 type aluminium alloys. However when compared with 2014 - T6, the 8090 alloy aged to peak strength yields higher tensile strengths after two years exposure and comparable ductility.

REFERENCES

- 1 Peel C J, Evans B and McDermid D S. "Development of aluminium -lithium alloys in the UK", Metals and Materials (1987) 449
- 2 Weipmann K, Buhl H, Braun R and Peters M. "Mechanical properties and corrosion behaviour of 2091 sheet material", Proc. 4th Int. Aluminium-Lithium Conference, Paris, (1987)
- 3 Braun R and Buhl H. "Corrosion behaviour of the Al-Li-Cu-Mg-Alloy 8090-T651", Proc. 4th Int. Aluminium-Lithium Conference (1987)
- 4 Schra L and Boogers J A M. "Corrosion properties of Al-Li-Cu-Mg-Zr sheet materials", NLR TR 88047L (1988)
- 5 t'Hart W G J and Schra L. "Properties of the Al-Li plate alloy DTDXXXA-T651 (AA 8090-T651) in comparison with two damage tolerant 2000 series plate alloys", NLR TR 86115L (1986)
- 6 Koikman H J, t'Hart W G J and Schra L. "Additional investigation on the Al-Li plate alloy DTDXXXA-T651 (AA 8090-T651)", NLR TR 87149L (1987)
- 7 Lane P L, Gray J A and Smith C J E. "Comparison of corrosion behaviour of lithium - containing aluminium alloys and conventional aerospace alloys" Proc. 3rd Int. Aluminium - Lithium Conference, Oxford (1985) 273
- 8 American Society for Testing and Materials, "Salt Spray (Fog) Testing", ASTM B117-73
- 9 Lifka B W and Sprowls D O. "An improved exfoliation test for aluminium alloys", Corrosion, (1966) 22 7
- 10 American Society for Testing and Materials, "Exfoliation corrosion susceptibility in 2XXX and 7XXX aluminium alloys (EXCO TEST)", ASTM G34-79

- 11 Military Specification "Heat treatment of aluminium alloys" Mil-H-6088
- 12 American Society for Testing and Materials, "Alternate immersion stress corrosion testing in 3.5% sodium chloride solution", ASTM G44-75
- 13 American Society for Testing and Materials, ASTM D1147-75
- 14 Buhl H, "Validity of the slow straining test method in the stress corrosion cracking research compared with conventional testing techniques" in Stress corrosion cracking - The slow strain rate technique, ASTM STP 665 (1979) 333
- 15 Craig J G, Newman R C, Jarrett M R and Holroyd N J H. "Local chemistry of stress corrosion cracking in Al-Li-Cu-Mg alloys", Proc. 4th Int. Aluminium-Lithium Conference, Paris, (1987)

Table 1. Compositions and heat treatments of sheet aluminium - lithium alloys

Alloy	Composition w/o						Ageing/ Temper	Thickness mm
	Li	Cu	Mg	Zr	Fe	Si		
RAE Research Alloys								
96	2.33	1.26	0.49	0.08	0.15	0.04	1.5h 170C	1.6
							16h 170C	1.6
							64h 170C	1.6
98	2.44	1.18	0.57	0.13	0.11	0.04	8h 170C	1.6
C2M4	2.46		4.41	0.14			16h 170C	1.6
88R	2.78	1.26	1.32	0.14	0.23	0.15	9h 170C	1.6
Early Alcan 8090 ^o type alloys - Produced from laboratory dc castings								
RCD	2.48	1.28	0.60	0.12	0.09	0.04	various	1.6
RDT	2.36	1.20	0.69	0.12	0.10	0.05	various	1.6
RGS	2.36	1.19	0.67	0.13	0.08	0.03	various	1.6
Alcan Commercially Produced 8090								
unrecryst	2.36	1.17	0.55		0.09	0.04	nat. aged	1.6
unrecryst	2.31	1.18	0.64	0.12	0.03	0.04	T6	1.65
unrecryst	2.44	1.11	0.54	0.11	0.03	0.03	T8	4.30
recryst 8090C	2.38	1.2	0.71	0.11	0.03	0.03	T3 nat T81	1.58
Cegedur Pechiney Commercially Produced 2091								
recryst	2.0	2.0	1.4	0.07	0.04	0.03	T3	1.56
							48h 150C	
							12h 150C	
							12h 135C	
recryst	1.8	2.1	1.6	0.07	0.04	0.03	100h 150C	1.68
							12h 135C	

Table 2 Compositions and heat treatments of plate aluminium - lithium alloys

[illegible]

Table 3. Accelerated Corrosion Tests

Neutral Salt Fog (ASTM B117)

Continuous exposure to 5% salt fog
 Test temperature 35°C
 Position of specimens 70° to horizontal
 Exposure time 21 or 42 days

Acidified salt spray test (ASTM B287)

Continuous exposure to 5% NaCl solution
 at pH =3.2 acidified using acetic acid

Intermittent acidified salt spray test (MASTMAASIS) ref.9

5% NaCl solution at pH =3 acidified using acetic acid
 Test temperature 35°C
 Position of specimens 45° to horizontal
 Application of four 6 hour cycles per day consisting of
 - spray period 3/4 hours
 - purge period 2 hours
 - soak period at relatively high humidity

EXCO test (ASTM G34-79)

Continuous immersion in a solution of 4.0M NaCl,
 0.5 M KNO₃ and 0.1 HNO₃, pH=0.4
 Test temperature 25°C
 Position of specimens horizontal

Intergranular Corrosion Test (Mil-H-6088F)

Continuous immersion in 57g/l NaCl and 10ml/l H₂O₂

Table 4. Visual assessment of coupons after corrosion testing. Experimental aluminium - lithium alloys and controls. (RAE)

Test	Exposure period (days)	Experimental Al - Li alloys 96 aged at 170°C						Control alloys			
		1.5h	16h	64h	98	C2M4	BSR	7075 T6	2014 T6	7475 T761	2014 T3
Marine	43	N	N	N	N	N	N	N	N	N	N
	127	S	S	S	S	S	S	N	P	N	P
	192	S	S	S	B	B	B	N	P	N	P
	233	B	B	B	B	B	B	P	P	P	P
	300	B	B	B	B	B	B	P	P	P	P
	359	B	B	B	B	B	B	P	P	P	P
	414	B	B	B	B	B	B	P	P	P	P
	469	B	B	B	B	B	B	P	P	P	P
	558	B	B	B	B	B	B	P	P	P	P
Alternate immersion (ASTM G44)	15	P	P	E	P	N	P	P	P	N	P
	30	P	P	E	P	N	P	P	P	N	P
5% neutral salt fog (ASTM B117)	21	P	P	P	P	N	S	P	P	S	P
	42	P	P	P	P	N	S	P	P	S	P
MASTMAASIS Ref. 9	7	EA	EA	EB	EB	N	EB	P	P	P	P
	14	EB	EB	EC	EC	N	ED	P	P	P	P
EXCO total immersion (ASTM G34)	1	P	EB	EB	EA	N	EB				
	2	P	EC	EB	EA	N	ED	P	P	P	P
	4	P	ED	ED	ED	N	EC	EA	P	P	P
Total Immersion											
Distilled water	21	P	P	P	P	P	P	P	P	P	P
1mM NaCl	21	P	P	P	P	P	P	P	P	P	P
10mM NaCl	21	P	P	P	P	P	P	P	P	P	P
178mM NaCl	21	P	P	P	P	P	P	P	P	P	P
600mM NaCl	21	P	P	P	P	P	P	P	P	P	P

B - Blisters P - Pitting N - No attack S - Staining
E - Slight exfoliation; EA to ED - Exfoliation rating
As ASTM G34; EA - least; ED - most severe

Table 5. Visual assessment of exfoliation on aluminium - lithium coupons (RCO 8090 type sheet) exposed to various corrosion tests. (RAE)

Aged Condition	Marine Exposure (280 days)	Alternate Immersion (30 day)	MASTMAASIS (14 day)	EXCO (48 hours)	EXCO (96 hours)
Nat. Age	N	P	P	N	N
1.5 hours at 170°C	E	E	EA	EA	EA
4 hours at 170°C	EA	EB	EA	EA	EB
8 hours at 170°C	EB	EA	EC	EA	EC
16 hours at 170°C	EA	EA	EC	EA	ED
64 hours at 170°C	E	E/P	EA	EB	ED
1.5 hours at 185°C	EB	EB	EC	EA	EB
4 hours at 185°C	EA	EB	EC	EA	EB
8 hours at 185°C	EA	EA	EB	EA	EC
16 hours at 185°C	E	EA	EA	EA	ED
64 hours at 185°C	E	E/P	EA	EA	ED

Table 6. Survey of the corrosive attack after 1 year of outdoor exposure (NLR)

Alloy	front side	rear	Weight change, mg/cm ²	
			before cleaning	after cleaning
2091-T3	N	P	-0.12	-0.36
2091-Tx	N	E	+0.64	-0.44
2091-T8x	G	G/E	+0.12	-0.37
2024-T3	N	N	+0.30	-0.04
8090-T6	G+E	G+E	+0.12	-0.07
8090-T8	G+E	G+E	+0.12	-0.08

Table 7. Classification of corrosive attack after EXCO testing according to ASTM G34-79 (NLR)

Exposure time hours	Alloy				
	2091-T3	2091-Tx	2091-T8x	2024-T3	8090-T8
4	N	G	G	N	G
8	P	G/E	G	N	EA
24	P	EA	G/E	N/E	EB
24*	P/E		G/P		EB
48	P	EB	EA	E	EC

* Li-depleted zone removed

Table 8. Visual assessment of exfoliation corrosion according to ASTM G34-79 (DFVLR)

Material	Temper	24h	48h	72h	96h
2091-CP274	12h/135°C	P	P/EA	EA	EA/EB
	12h/150°C	P	EA	EA	EA/EB
	100h/150°C	N	P/EA	EA/EB	EA/EC
2024	T3, unclad	N/P	P	P	P/EA
8090	T6		P	P/EA	EC/ED

Table 9. Classification of corrosive attack after intermittent acidified salt spray testing (MASTMAASIS) (NLR)

Exposure time days	Alloy					
	2091-T3	2091-Tx	2091-T8x	2024-T3	8090-T6	8090-T8
2	N	(G)	(G)	(G)	E	E
4	N	G	(G)	(G)	E/EA	E/EA
8	(P)	G+1	G+(1)	G	EA	EA
16	P	G+1	G+(1)	G	EA	EA

Table 10. Classification of corrosive attack on 8090-T6 sheet alloy after intermittent acidified salt spray testing (MASTMAASIS) (DFVLR)

	Exposure time				
	1w	2w	3w	4w	5w
rating	N	P	P	P/EA	P/EA
weight-loss	0.11	0.20	0.36	1.02	0.81

Table 11. Classification of corrosive attack after EXCO, MASTMAASIS and marine exposure. (RAE)

Alloy		EXCO		MASTMAASIS		Marine
		48h	96h	7d	14d	
8090C	8h 150°C	E	EA ⁻	EA ⁺	EB	E
8090	1h 150°C	EA ⁻	E	EA	EA ⁺	P
2091	48h 150°C	EA ⁺	EB ⁻	EA	EA/EB	EA/EB
2091	T3	S	P	P	P	C ⁻
7075	T6					P
2014	T3					P
2014	T6					P

Table 12. Classification of corrosive attack according to ASTM G34-79 after EXCO testing. (Fokker)

	2024-T3	2091-T3	2091-T8
24h	N	N	EA
48h	N	P	EA
72h	P	P	EB
96h	P	P	EB-EC

Table 13. Visual assessment of exfoliation corrosion on 11mm (QRI-2) and 25mm (RDV) 8090 type plate alloys after EXCO, MASTMAASIS and marine exposure. (RAE)

Plate		EXCO 96h		14d MASTMAASIS		Marine	
		surf. 1/2T		surf. 1/2T		surf. 1/2T	
11mm	RT	EA	EA	E ⁻	EA	E ⁻	
QRI-2	1.5h 170°C	EB	EA/EB	EA	ED	E ⁻	EA
	16h 190°C	ED ⁺	ED	ED	EA ⁻	E/EA	EA ⁺
25mm	RT		EA	E	EA	E ⁻	
RDV	16h 190°C	EA	EB/EC	EB/EC	EB	E ⁻	E/EA
	64h 190°C	E ⁻	ED ⁺	E ⁻	E	E ⁻	

Table 14. Classification of corrosive attack on 25mm 8090-T651 after EXCO testing. (NLR)

Exposure time hours	Material			
	8090-T651 core	8090-T651 surface	2024-T351	2324-T39
3	EA	EA	E/EA	E
6	EA	EA	EA	E
24	EA/EB	EA/EB	EA	E/EA
48	EC	EC	EA	E/EA
96	ED	ED	EB/EC	EA

Table 15. Classification of corrosive attack on 25mm 8090-T651 plate after EXCO testing. (DFVLR)

exposure time	visual rating
3h	P
6h	P/EA
24h	EA
48h	ED

Table 16. Threshold stresses for 2091 in various tempers and for unclad 2024-T3. Bent - beam specimens tested by alternate immersion in 3.5% NaCl for 30 days. (DFVLR)

Material	Temper	Crack Initiation	Fracture
2091-CP274	12h/135°C	< 100	150
	12h/150°C	< 100	200
	100h/150°C	300	300
2024	T3, unclad	150	> 350

Table 17. Threshold stresses for 25mm 8090 type plate (RDV) tested by alternate immersion (ASTM G44-75) and by marine exposure. (RAE)

Plate		Threshold Stress MPa		
		Alternate Immersion Macro	Alternate Immersion Micro	Marine Macro
25mm	RT	88	88	125
RDV	16h 190°C	75	750	125
	64h 190°C	100	725	100
2014 -	T651	240	100	
7075 -	T651	110	33	

Table 18. Pitting potentials in aerated aqueous 3.5% NaCl solution (pH=6) potentiodynamically measured with a scan rate of 0.05mV/min. (DFVLR)

Material	Pitting Potential mV (SCE)
8090-T651	-742
2091-CP274 as received	-653
12h/135°C	-684
12h/150°C	-689
100h/150°C	-755
2014-T351	-603
2024-T351	-618
7010-T7351	-748
7010-T73651	-749

(In this electrolyte the difference between the free corrosion and pitting potential was about 3mV)

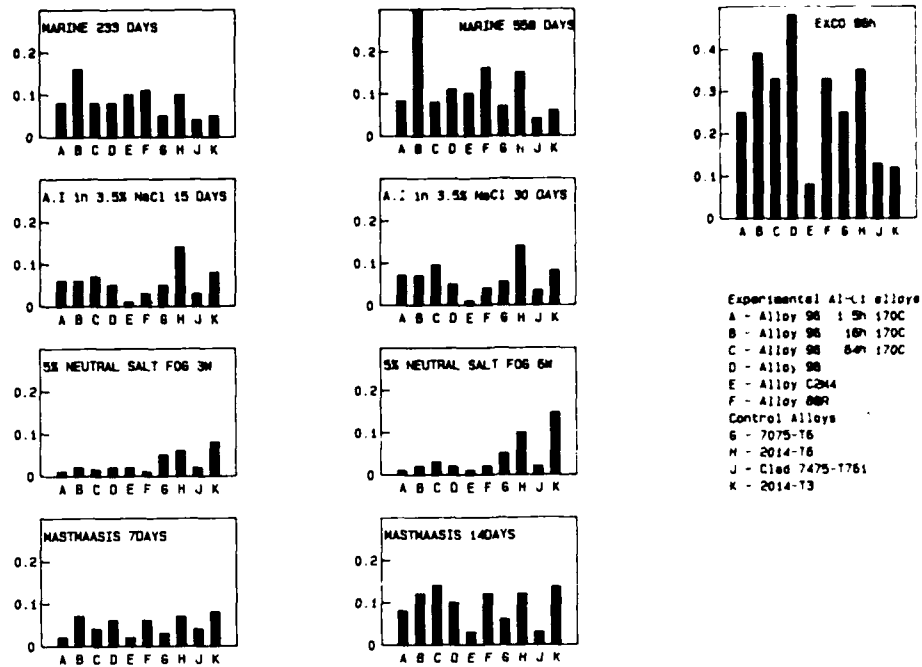


Fig.1 Mean depth of attack (mm) in experimental aluminium - lithium alloys following corrosion testing. (RAE)

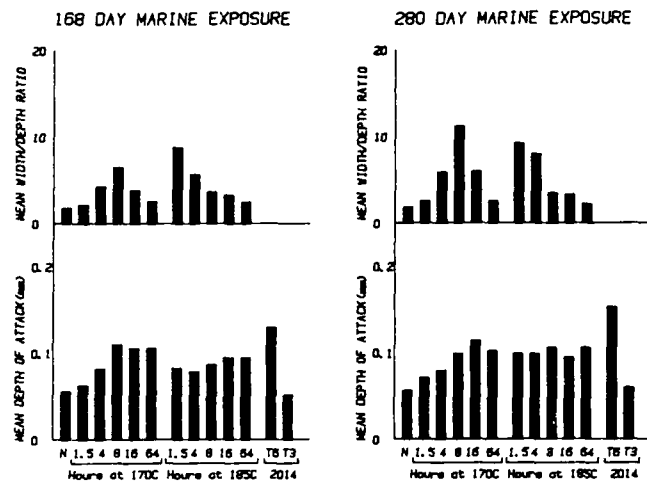


Fig. 2 Effect of ageing on the mean depths of attack and width/depth ratios in 8090 type aluminium - lithium sheet alloy (RCO) after 168 and 280 days marine exposure. (RAE)

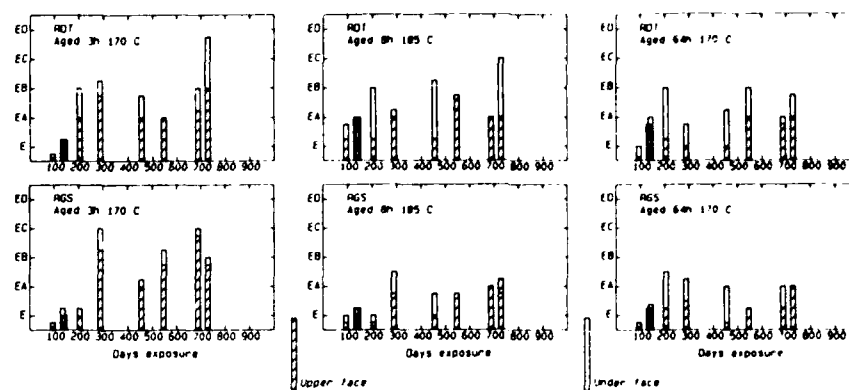


Fig. 3 Assessment of superficial exfoliation corrosion of sheet aluminum alloy coupons after marine exposure. RDT and RGS are 6061 type Al-Li alloys. (PAE)

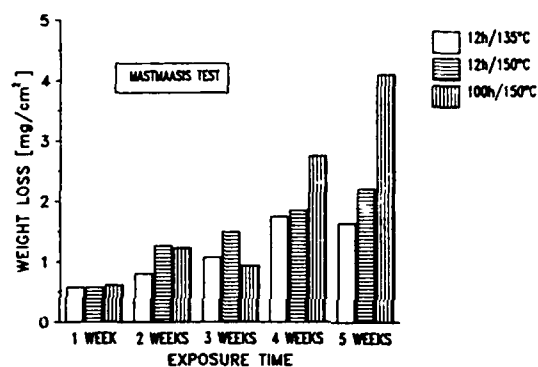


Fig. 4 Weight loss of 2091 specimens after various exposure time periods to MASTMAASIS. (DFVLR)

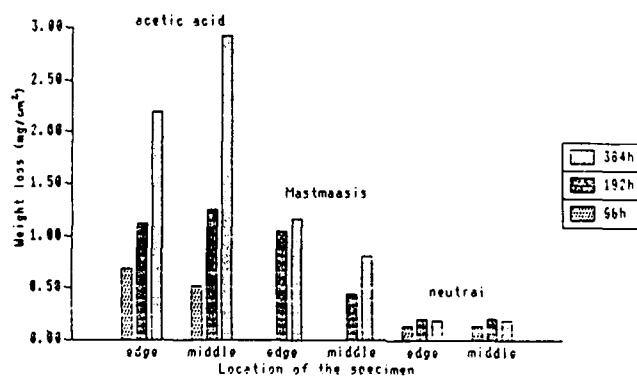


Fig. 5 Weight loss of 25mm 8090-1651 plate tested in different salt spray fog for various exposure periods and different positions in the plate. (DFVLR)

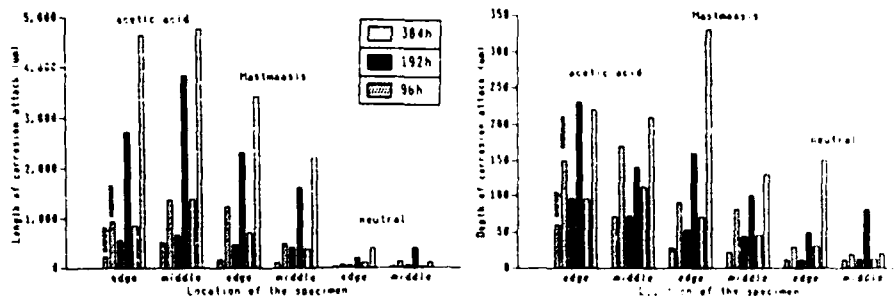


Fig. 6 Length and depth of the corrosion attack of 25mm B090-T651 plate tested in different salt spray fogs for various exposure periods and different positions in the plate. For identical conditions, the first and second columns represent average and maximum values respectively. (DFVLR)

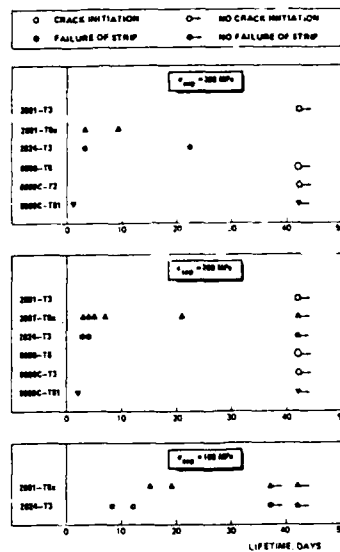


Fig.7 Results of stress corrosion testing bent beam sheet specimens by alternate immersion in synthetic seawater. (NLR)

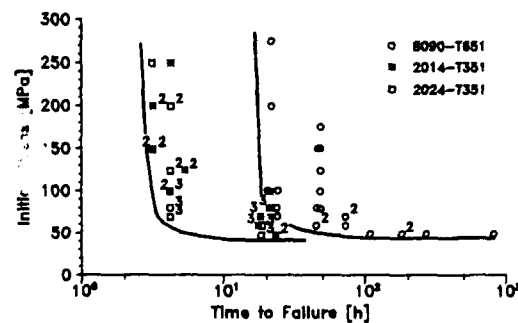


Fig. 8 Initial stress time to failure relationship of C-ring specimens of B090-T651, 2014-T351 and 2024-T351 tested by alternate immersion in 3.5% NaCl solution (ST-direction). (DFVLR)

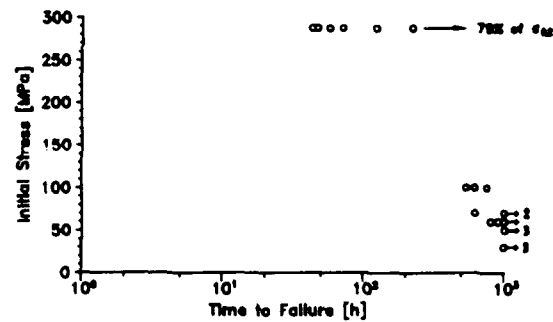


Fig. 9 Time to failure versus applied stress of tensile specimens of 8090 T651 tested in ST-direction according to German Spec. M6566. (DFVLR) (Constant load and continuous immersion in 2%NaCl + 0.5%Na₂CrO₄ at pH3)

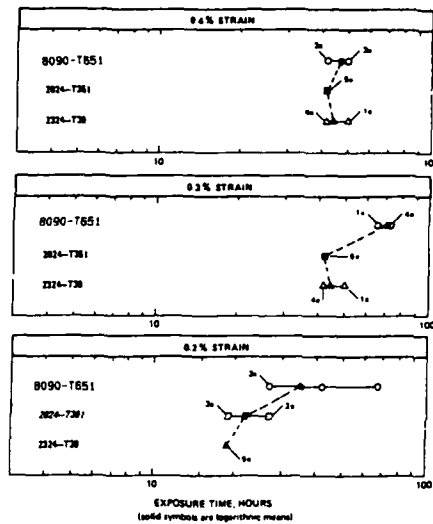


Fig. 10 A survey of stress corrosion lives for 8090-T651 25mm plate and control alloys tested by alternate immersion in synthetic seawater. (NLR)

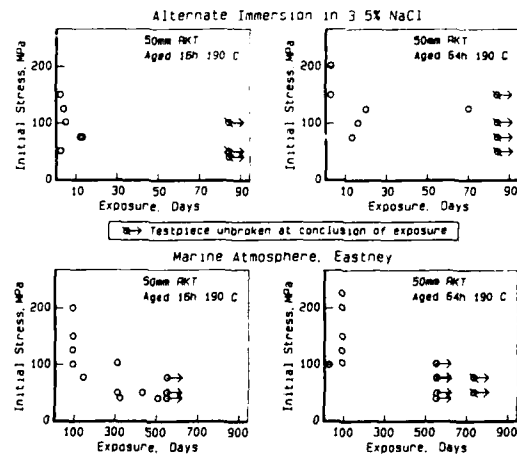


Fig. 11 Effect of ageing on the stress corrosion cracking of 50mm 8090 type plate (RKT). (RAE)

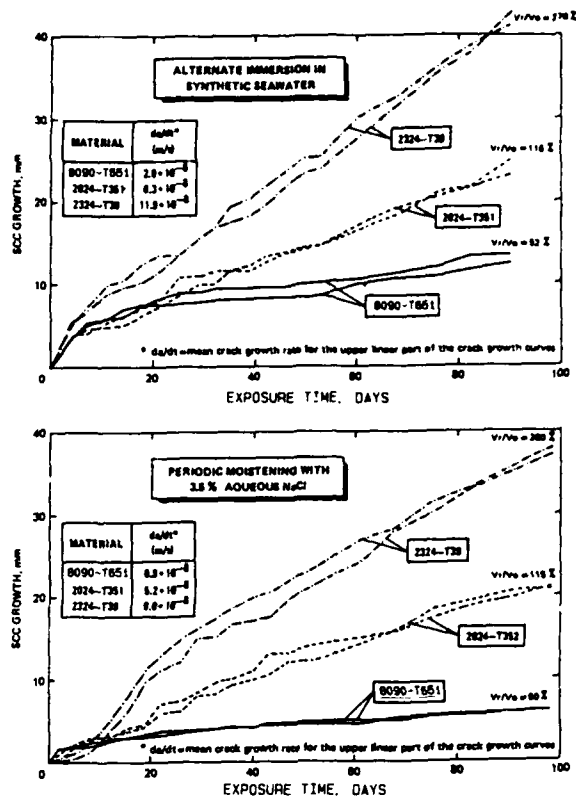


Fig. 12 Stress corrosion crack growth as a function of the exposure time for different environmental conditions. (NLR)
12 specimens per material tested $K_I = 9 \text{ MPa m}$

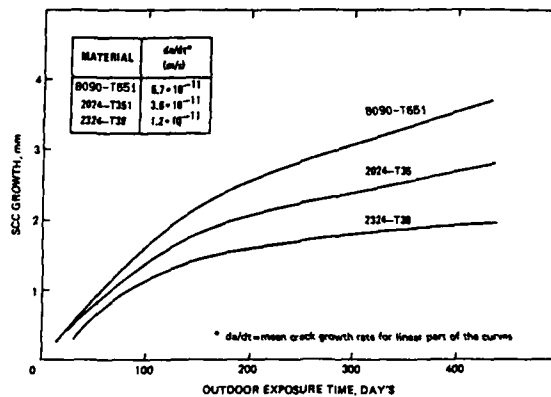


Fig. 13 Stress corrosion crack growth as a function of the exposure time. (NLR)
(mean curves for 2 specimens $K_I = 9 \text{ MPa m}$)

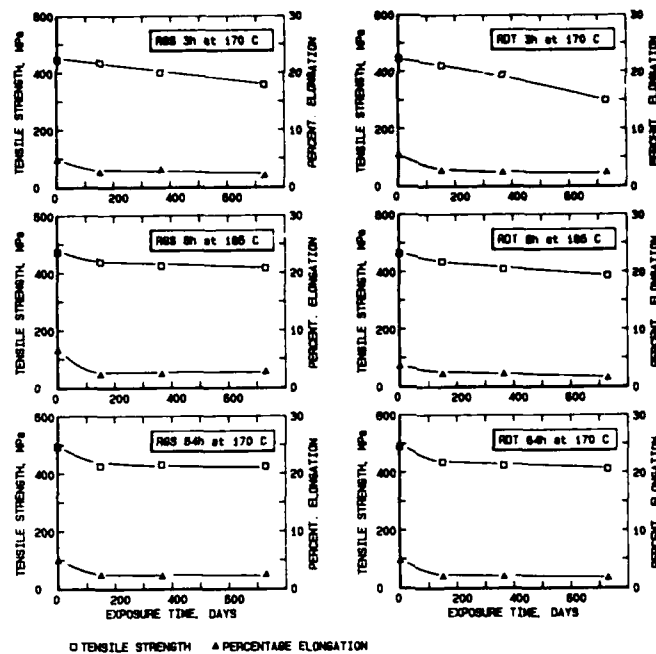


Fig. 14(a) Effect of marine atmosphere exposure on the tensile strength and elongation of two sheet 8090 type aluminium-lithium alloys (RDT and RGS). (RAE)

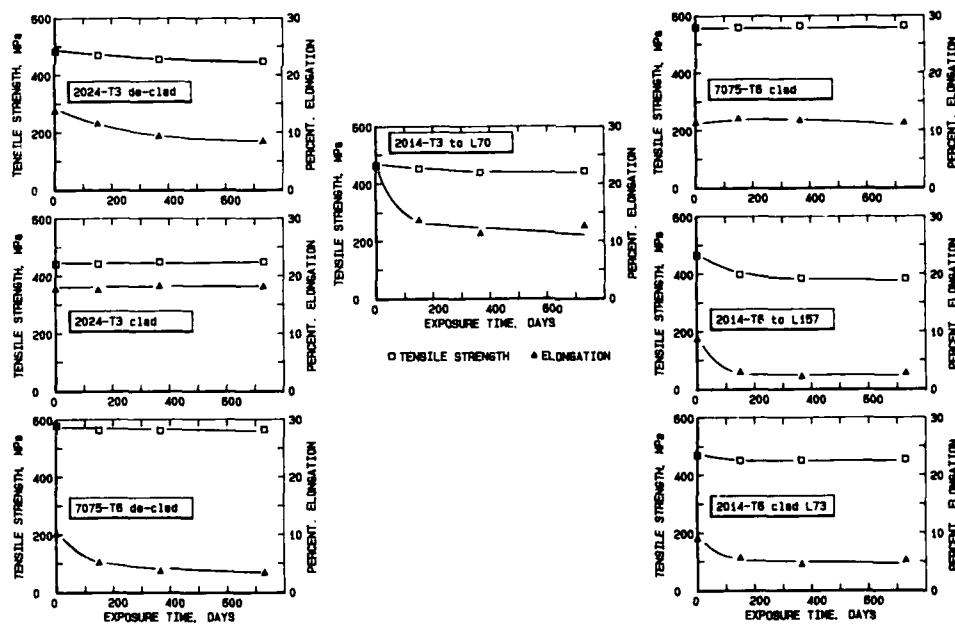


Fig. 14(b) Effect of marine atmosphere on the tensile strength and elongation of aerospace sheet aluminium alloys (RAE)

PROPRIETES DES ALLIAGES Al-Li

Y. BARBAUX - Chef de la Section Métallurgie
Laboratoire Central de l'AEROSPATIALE
Centre Commun de Recherches Louis BLERIOT
12, rue PASTEUR - 92152 SURESNES - FRANCE

RÉSUMÉ :

Les alliages Aluminium-Lithium présentent du fait de leur faible densité et de leur haut module un intérêt évident pour les applications sur aéronefs et en particulier sur les avions de transport civil qui représentent la part la plus importante et la plus stratégique de ce marché. Cependant le coût élevé de ces nouveaux matériaux les limite à des utilisations en produits minces à faible taux de chute (tôles minces, tôles moyennes et profilés).

La présente communication fait le point des études réalisées à l'AEROSPATIALE depuis 5 ans sur les produits commercialement disponibles :

- les tôles minces en 2091 CPH T8X,
- les tôles minces en 8090C T81,
- les tôles moyennes en 2091 T8x51,
- les profilés en 8090 et 2091 T8511.

et dégage parmi eux ceux qui sont retenus pour être utilisés éventuellement sur la partie AEROSPATIALE de l'AIRBUS A340.

Les alliages Aluminium-Lithium possèdent, grâce aux caractéristiques intrinsèques de l'atome Lithium (densité de 0,53 pour un volume dans la maille du réseau légèrement supérieur à celui de l'Aluminium auquel il se substitue), une densité et un module d'élasticité très intéressants pour des applications aéronautiques et spatiales.

Ainsi l'addition de 2 à 2,5 % en poids de Lithium dans un alliage d'Aluminium permet un gain en densité de 8 à 10 % et une amélioration du module d'Young de l'ordre de 10 %.

Sur une structure d'aéronef ces améliorations devraient permettre un gain de :

- 20 % en masse dans le cas d'un redimensionnement en rigidité prenant en compte intégralement l'augmentation du module d'élasticité,
- 8 à 10 % en masse dans le cas du remplacement d'alliages classiques sans redimensionnement.

Ces calculs supposent cependant que toutes les caractéristiques dimensionnantes sont identiques entre alliages Al-Li et alliages classiques.

Par ailleurs 2 facteurs économiques peuvent limiter l'emploi des alliages Al-Li :

- leur coût (2 à 4 fois celui des alliages classiques),
- le problème industriel du tri et de la récupération des chutes et copeaux qui peut nécessiter la création d'ateliers spécialisés et accroître par là même le coût industriel de l'introduction de ces nouveaux alliages.

APPLICATION DES ALLIAGES Al-Li SUR AVION CIVIL TYPE AIRBUS

Au début des années 80, quand les études de développement des alliages Aluminium-Lithium ont pris un nouvel essor (après l'échec commercial du 2020 dans les années 60), parmi les nouveaux produits à l'étude à l'AEROSPATIALE, seuls les avions civils de type AIRBUS ou ATR pouvaient justifier l'effort financier et industriel important correspondant à l'introduction d'Al-Li.

Les enquêtes faites alors ayant montré que :

- le gain de masse est plus intéressant, économiquement, sur un avion gros porteur long-courrier que sur un court-courrier ou un commuter type ATR,
- l'introduction d'un nouveau matériau en parties structurales en retrofit sur des appareils déjà certifiés est très difficile du fait du coût de la certification (cellules d'essais, essais de sous ensembles...),

- du fait du problème industriel lié aux particularités des Al-Li (ségrégation des chutes et copeaux, mais aussi formation des boues en usinage chimique) qui nécessite la mise en place d'outils voire d'ateliers spécialisés, seule une introduction massive sur appareil est économiquement viable et envisageable,

la décision fut prise de bâtir un programme cohérent de caractérisation et de qualification des alliages Aluminium-Lithium avec comme objectif la réalisation du fuselage A330/A340 en alliage Al-Li.

SELECTION DES 1/2 PRODUITS PAR LE COUT

De façon à limiter le champ d'investigation très vaste nécessaire à l'homologation des différentes parties constitutives du fuselage A330/A340 une réflexion a été portée sur l'aspect coût au kilo gagné, paramètre différent si l'on considère une tôle mince ou une pièce forgée épaisse.

Entrent dans ce coût au kilo gagné :

- d'une part, le prix du 1/2 produit ; pour les Al-Li il est respectivement de l'ordre de :

- . 120 F/Kg pour une tôle mince (x4 par rapport à l'alliage classique),
- . 175 F/Kg pour un profilé (x2,5),
- . 80 F/Kg pour une tôle épaisse (x3,2),
- . 400 F/Kg pour un matricé classique (x2),
- . 1950 F/Kg pour un matricé de précision (x1,3),

(il s'agit de prix typiques).

- d'autre part, le rapport "buy to fly" c'est à dire le rapport entre la masse de matière achetée pour réaliser les pièces et la masse de ces pièces sur avion ; ce rapport directement lié au taux de chute, varie également d'un 1/2 produit à l'autre en fonction des habitudes technologiques et de dessin de l'avionneur. C'est ainsi que s'il est typiquement compris entre 2 et 4 pour des tôles minces, il peut aller jusque 8 ou 10 pour des tôles épaisses ou des matricés épais, mais ne dépasse pas 1,5 pour des matricés minces ou de précision.

Le coût du kilogramme gagné sur la structure grâce à l'introduction de ces nouveaux alliages est donné par la relation suivante, dans l'hypothèse d'un remplacement des pièces à mêmes dimensions :

$$C = \frac{(d_{Al-Li} \times C_{Al-Li} - d_{Al} \times C_{Al})}{d_{Al} - d_{Al-Li}} \times b$$

C = coût du kilogramme gagné

b = buy to fly

d_{Al} , d_{Al-Li} = densité

C_{Al} , C_{Al-Li} = Coût d'un Kg de matière

En utilisant ce concept et les estimations de surcoûts admissibles communiquées par AIRBUS-industrie, nous avons très rapidement éliminé de notre programme d'évaluation :

- les matricés et forgés classiques (C 12 000 F/Kg),
- les tôles épaisses au-delà de 20 mm (C 4 000 F/Kg),

ne retenant que :

- les tôles minces et moyennes (20 mm),
- les profilés,
- certains matricés minces ou de précision.

STRUCTURE DU PROGRAMME DE QUALIFICATION

Dans le cas de l'introduction d'un matériau nouveau sur une structure d'aéronef nous devons répondre à 3 questions essentielles :

- quelles sont les caractéristiques sûres de ce matériau ?
- quelles gammes de mise en oeuvre pouvons-nous lui appliquer ?
- notre outil industriel est-il adapté ou doit-il être modifié ?

Le canevas adopté à l'AEROSPATIALE dans le cas des Al-Li pour répondre à ces questions reprend donc les principaux chapitres suivants :

- acquisition de données techniques,
- mise au point ou vérification des gammes de mise en oeuvre (usinage chimique, traitement de surface...),
- rédaction de documents normatifs,
- évaluation du système d'assurance qualité propre aux Al-Li chez les différents fournisseurs,
- réflexion économique sur les outils industriels nécessaires.

Par la suite nous nous consacrerons au premier de ces chapitres et aux résultats obtenus dans ce cadre.

Le programme d'acquisition de données techniques, toujours dans le but d'optimiser le coût de qualification des Al-Li, été scindé en quatre phases :

- une caractérisation métallurgique de base visant, à partir d'essais sur éprouvettes élémentaires, à obtenir les propriétés physiques ainsi que les caractéristiques typiques de traction, de fatigue, de tolérance aux dommages et de corrosion des produits disponibles. Cette phase permet également d'écarter très tôt, dans le processus d'évaluation, des alliages dont les caractéristiques ne seraient pas conformes à nos cahiers des charges,
- une caractérisation complémentaire visant, toujours à partir d'essais sur éprouvettes élémentaires et en se limitant aux produits sortis avec succès de la première phase, à obtenir les propriétés typiques spécifiques aux cas d'utilisation sur avion (fatigue sous spectre, compression, corrosion sur éprouvettes peintes avec défauts...),
- des essais d'applications réalisés sur des éprouvettes représentatives de parties avion ou intégrant des paramètres technologiques (assemblages, usinage chimique, grenaillage) visant à vérifier les cas de dimensionnement,
- une acquisition de données statistiques, par des essais sur éprouvettes élémentaires, pour obtenir des valeurs sûres de calcul pour les paramètres dimensionnants.

Notons également que, toujours dans le but de réduire les coûts de qualification, les 2 partenaires associés dans la réalisation du fuselage d'AIRBUS, à savoir MBB et AEROSPATIALE, se sont mis d'accord très tôt pour se partager les 2 premières phases de la caractérisation des alliages Al-Li.

RESULTATS OBTENUS

Parmi tous les alliages existants ou en développement, nous ne présentons ici les résultats que sur ceux dont nous estimons qu'ils peuvent être introduits sur AIRBUS A330/A340 à savoir :

- les tôles minces en 2091 CPHK T8X,
- les tôles minces en 8090C T81,
- les tôles moyennes (20 mm) en 2091 T8X51,
- les profilés en 2091 T8510/11,
- les profilés en 8090 T8510/11,
- les matricés de précisions en 8090 et 2091.

Notons que les propriétés annoncées ont été mesurées sur des produits à l'état d'utilisation.

Notons également qu'en fonction de l'objectif recherché, un fuselage d'avion civil, l'ensemble des produits cités répond à un cahier des charges où la tolérance aux dommages a une place importante si ce n'est primordiale.

a - Tôles minces de revêtement de fuselage

Pour cette application, 2 alliages sont actuellement disponibles :

- le 2091 développé par CEGEDUR et également produit par ALCOA,
- le 8090 C développé par ALCAN.

Si nous disposons actuellement d'une connaissance statistique du 2091 (plus de 50 lingots produits et testés par CEGEDUR, plus de 20 lingots par ALCOA), la mise au point de la version définitive du 8090 C est plus récente et les résultats partiels qui seront présentés ne concernant qu'une coulée.

Tôles minces en 2091 CPHK T8X

Jusqu'à une épaisseur de 3,5 mm, ces tôles ont une structure entièrement recristallisée équiaxe (comparable à celle du 2024 dans les mêmes épaisseurs) (page 8-6).

Le traitement thermo-mécanique CPHK (désignation CEGEDUR) ainsi que le sous-revenu 1^{er} (12h à 135°C) ont été mis au point pour se rapprocher du compromis caractéristiques mécaniques/ténacité/corrosion sous contrainte du 2024 T3.

Les caractéristiques de traction, de matage et de cisaillement obtenues sur 5 coulées sont reportées en page 8-6 où elles sont comparées aux valeurs typiques obtenues sur 2 coulées de 2024 T3 ainsi qu'aux valeurs A de la production de CEGEDUR pour ce même alliage.

On ne note pas pour ces paramètres de différence significative ou pouvant être pénalisante entre 2091 et 2024.

En ténacité les résultats reportés sous forme de courbe R à la page 8-7 mettent en évidence une perte de l'ordre de 30 % du 2091 par rapport au 2024 T3.

En fatigue endurance les 2 matériaux présentent un comportement semblable pour les durées de vie avion (jusqu'à 200 000 cycles - page 8-7) tandis qu'en fissuration le 2091 aurait un comportement globalement meilleur que le 2024 aussi bien en rapport $R_{0.1}$ qu'en spectre avec surcharges (page 8-8).

Enfin on peut estimer que les 2 matériaux sont identiques en corrosion (page 8-8).

Au vu de l'ensemble de ces résultats l'AEROSPATIALE estime possible d'utiliser les tôles minces en 2091 CPHK T8X en remplacement du 2024 T3, à iso-dimensionnement, sur les tronçons de fuselage de l'A330/A340 qui sont de sa responsabilité.

Par contre la perte de ténacité par rapport au 2024 T3 ne permet pas que l'on utilise le 2091 CPHK T8X dans ces conditions sur des tronçons plus chargés (tels que le fuselage arrière de responsabilité MBB).

Pour ces parties un alliage comme le 8090 C, de structure également entièrement recristallisée, qui possède une plus forte ténacité (page 8-9) pourrait convenir, sous réserve que les résultats statistiques sur les nouveaux lots produits viennent confirmer ceux obtenus sur la première coulée.

b - Tôles moyennes en 2091 T8X51 (revêtement de fuselage et intrados de caisson central de voilure).

Ces tôles ont une structure fibrée partiellement recristallisée (page 8-10).

Elles sont disponibles jusqu'à des épaisseurs de l'ordre de 40 mm et présentent dans cette gamme d'épaisseurs des caractéristiques similaires ou légèrement supérieures au 2024 T351, y compris une tenue à la corrosion sous contrainte en sens travers-court très modeste (50 MPa).

Jusqu'à 20 mm d'épaisseur (limite correspondant à la fois à nos applications sur A330/A340 et au surcoût admissible) le compromis de caractéristiques obtenu à l'état d'utilisation T8X51 (revenu de 12h à 135°C identique à celui des tôles minces) est très satisfaisant comparé à la référence 2024 T351 (voir pages 8-10 à 8-12).

Dans ces conditions le remplacement à isodimensionnement du 2024 T351 par du 2091 T8X51 pour les tôles moyennes de revêtement du fuselage et d'intrados de caisson central de voilure ne semble pas poser de problème.

Dans ce cas cependant, comme dans le cas des tôles minces, seuls les essais sur éprouvettes technologiques permettront de prendre la décision définitive.

c - Les profilés : 2091 T8510 ou 8090 T8510 ?

Les profilés en 2091 présentent pour les épaisseurs minces (typiquement en dessous de 2 mm) une structure entièrement recristallisée qui se traduit par une forte sensibilité à la corrosion sous contrainte (CSC) incompatible avec nos utilisations sur avion.

Pour les profilés minces de type lisses de fuselage, nous préférons donc l'alliage 8090 qui présente une excellente tenue en C.S.C. (350 MPa - 30 jours) (page 8-13).

Pour cette application le plus haut module et la plus basse densité du 8090 représentent par ailleurs deux attraits supplémentaires.

Pour les profilés plus épais le 2091, qui retrouve alors une structure fibrée (page 8-14) et le 8090 sont en concurrence aussi bien pour le remplacement du 7075 T73xx que du 2024 T3xx.

Cependant pour les applications tolérantes aux dommages telles que l'intrados de caisson central de voilure, le 2091, en dépit d'une tenue à la corrosion médiocre comparable à celle du 2024, sera préféré au 8090 moins bon en fissuration, en fatigue et en ténacité (page 8-15 et 8-16).

d - Les matricés de précision en 8090 et 2091

Les deux alliages présentent dans le cas des matricés minces des structures très polygonisées plus ou moins fortement recristallisées (page 8-17).

Les structures leur confèrent une forte sensibilité à la corrosion intercristalline (130 à 200 m) bien supérieure à celle de l'alliage de référence 7175 T73.

Ils présentent par contre une bonne tenue à la corrosion sous contrainte.

Leurs caractéristiques mécaniques sont nettement inférieures à celles du 7175 T73.

CONCLUSION

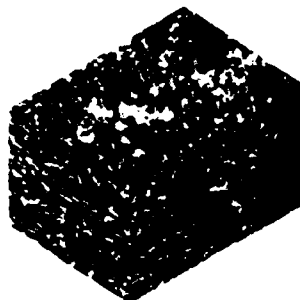
Les études réalisées à l'AEROSPATIALE depuis 5 ans sur les alliages Aluminium-Lithium commercialement disponibles ont permis de démontrer la possibilité de remplacement d'alliages classiques à isodimensionnement et pour un surcoût admissible sur A340 dans les cas suivants :

- Tôles minces de fuselage en 2091 CPHK T8X ou 8090C T81.
- Tôles moyennes de fuselage ou d'intrados de caisson central de voilure en 2091 T8x51.
- Profilés lisses de fuselage en 8090 T8510.
- Profilés type traverses de plancher en 8090 T8510 ou 2091 T8510.
- Profilés raidisseurs d'intrados de caisson central de voilure en 2091 T8510.

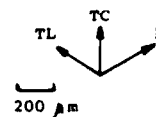
A ce jour les compromis de caractéristiques obtenus sur matricés minces en 2091 ou en 8090 sont insuffisants pour envisager le remplacement du 7175 T73.

Nous remercions le Service Technique des Programmes Aéronautiques pour le soutien apporté aux études sur les alliages Aluminium-Lithium.

TOILES MINCES EN 2091 CPHK T8X
MICROSTRUCTURE



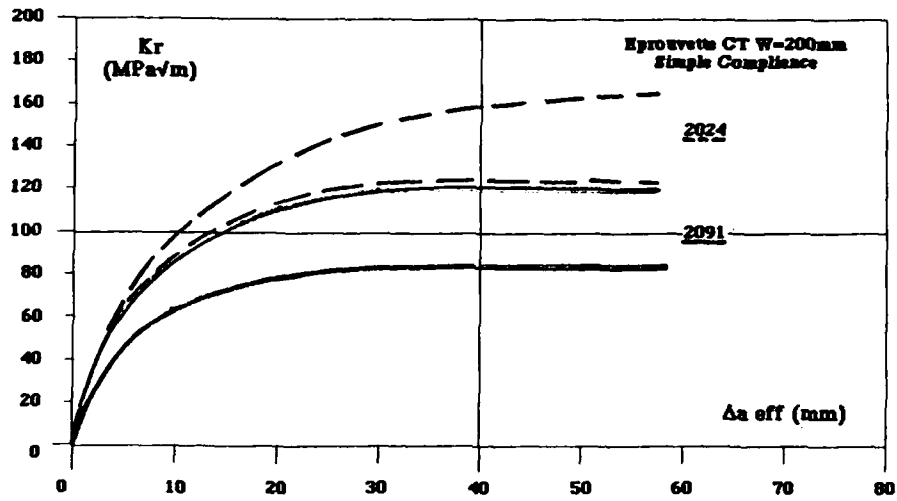
Cliché N° 55683



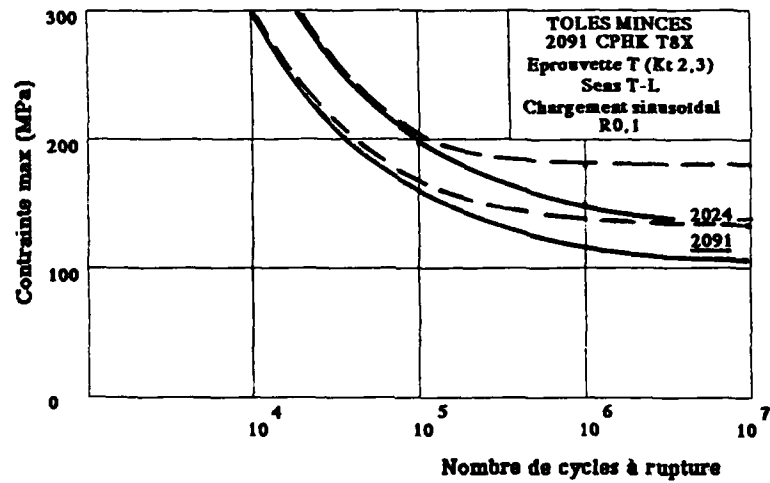
CARACTERISTIQUES MECANIQUES

Parametre	Sens	2091 CPHK T8x			2024 T3	
		Moyenne	Valeur A	Valeur B	Moyenne	Valeur A
R _{0,2} (MPa)	L	330	295	305	375	345
	TL	335	280	300	335	305
	60°	295	265	275	345	315
R (MPa)	L	425	400	405	510	485
	TL	440	415	420	495	470
	60°	410	390	400	495	470
A%	L	13	9,5	10,5	21	18,5
	TL	12,5	10	10,5	23,5	21
	60°	18,5	15	16	22,5	19,5
E (GPa)	L	78,4			73	
	TL	78			72,9	
	60°	77,2			71,1	
Métal	F _{br} (MPa)	L	605		625	
	TL	615				
Fibre	F _{br} (MPa)	L	840		948	
	TL	835				
Châssis	R _{0,2c} (MPa)	L	125		155	
	R _c (MPa)	L	240		290	
	G (GPa)	L	29,5		27,8	

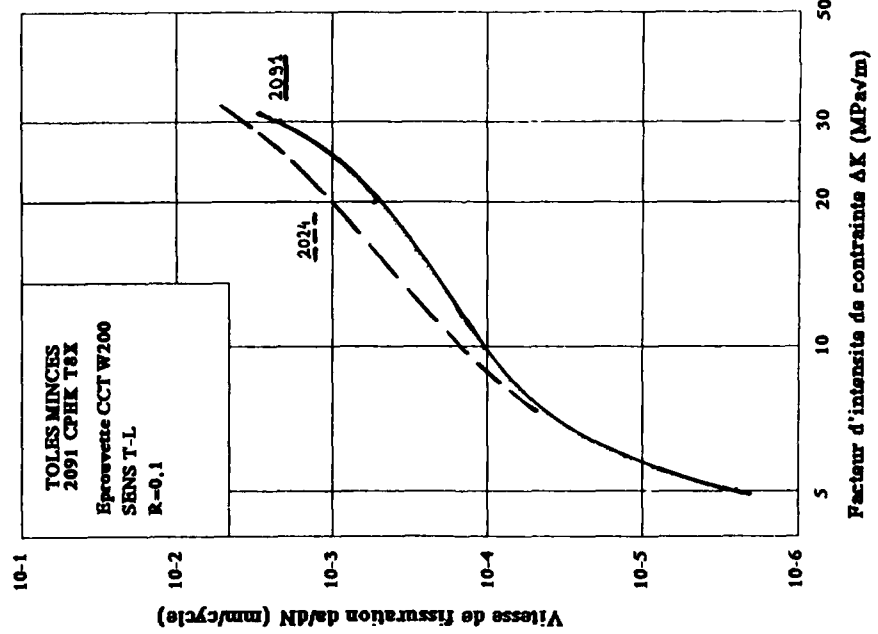
TENACITE - COURBE R



FATIGUE AMORCAGE - ENDURANCE



FISSURATION EN FATIGUE

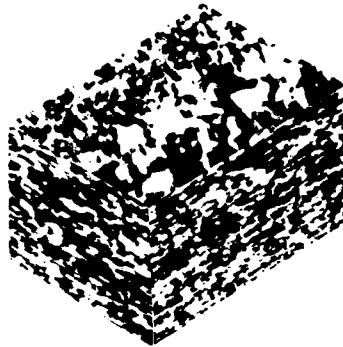


COMPORTEMENT EN CORROSION

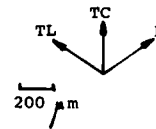
2091 CPHK T8x		2024 T3
CORROSION GENERALISEE	Atmosphère Marine 4 mois	12 / 14
	Corrosion Feuille d'essai ASTM G 34	96 h : P
	Corrosion Interstitielle	13
CORROSION SOUS CONTRAINTE Flexion Plaine sur Eproutettes Lisses	Contrainte (MPa)	250
	Ruptures / Essais	0 / 6
	Durée (jours)	> 70
PROTECTION + PEINTURE	Adhère 7 jours eau	100 %
	IEA 1200 h	G = 2
	Adhère 7 jours eau	100 %
	IEA 1200 h	G = 1

G : indice de gravité de corrosion sur éproutette peinte avec échantillon

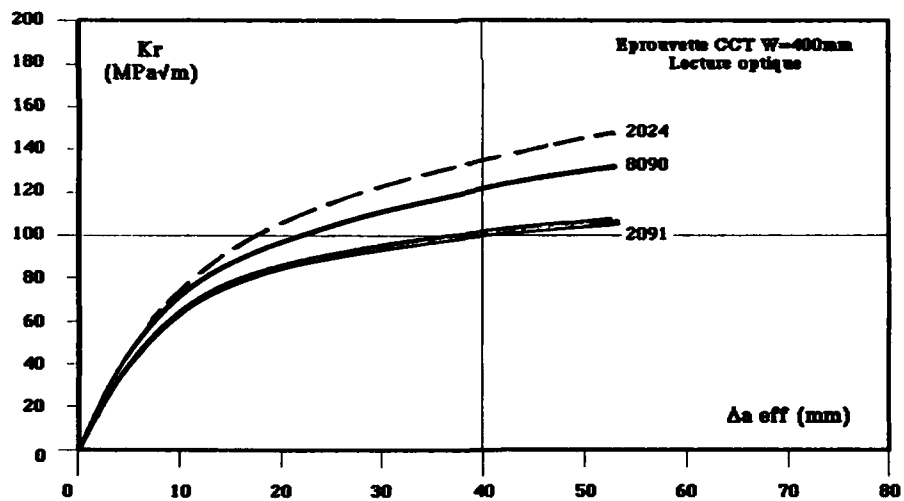
TOLES MINCES EN 8090C T81
MICROSTRUCTURE



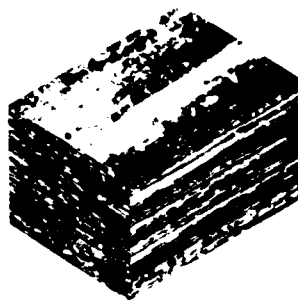
Cliché N° 58271



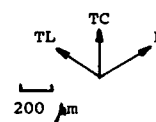
TENACITE - COURBE R



TOLES MOYENNES EN 2091 T8x51
MICROSTRUCTURE



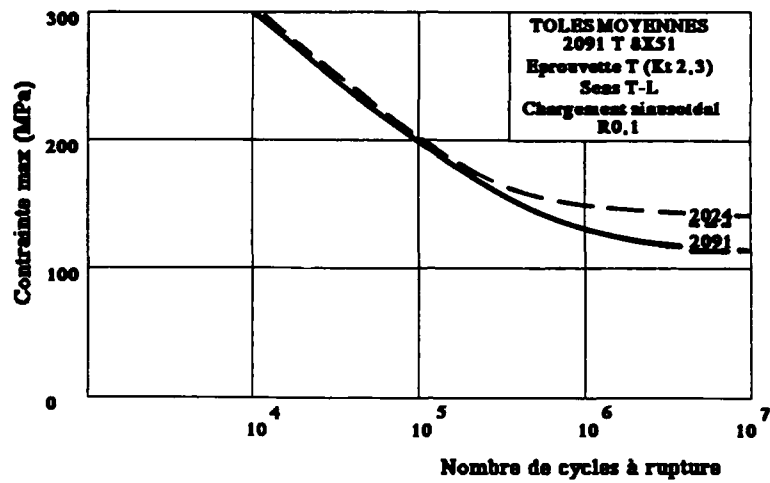
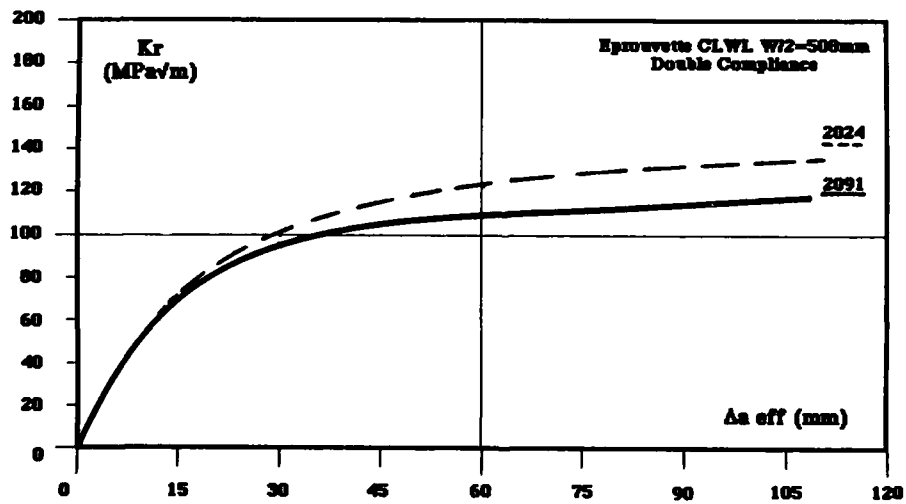
Cliché N° 55682



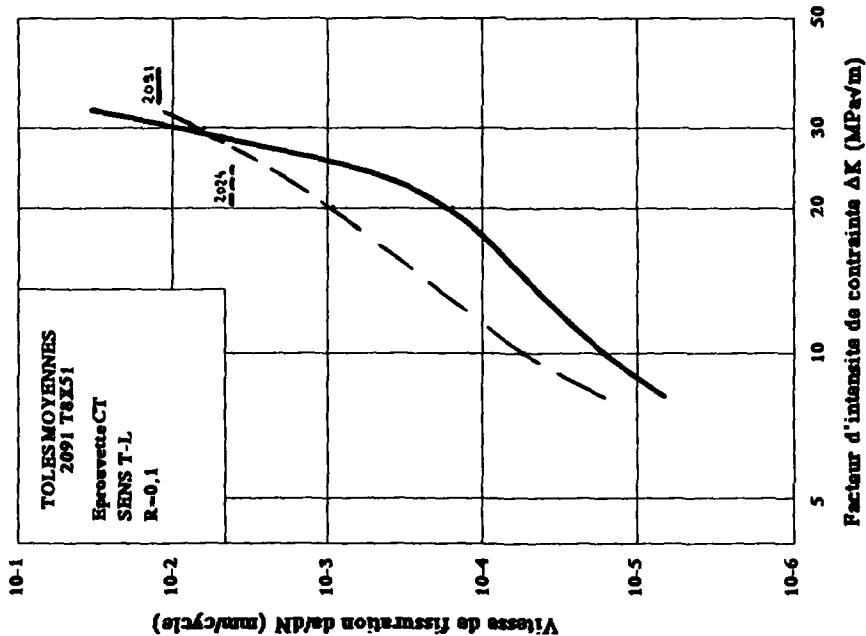
CARACTERISTIQUES MECANIKES STATIQUES

Paramètre		Sens	2091 T8X51			2024 T351	
			Moyenne	Valeur A	Valeur B	Moyenne	Valeur A (1)
R _{0,2} (MPa)	L		440	415	425	410	330
	TL		380	355	365	345	290
	60°		325	300	310	355	-
R(MPa)	L		510	485	495	495	440
	TL		505	480	490	490	440
	60°		460	435	445	490	-
A%	L		9,5	7	8	16,7	-
	TL		11,0	8,5	9,5	16,9	12
	60°		17,5	15	16	17,2	-
E(GPa)	L		79,3	78,5	78,9	70,8	-
	TL		79,8	78,1	78,8	70,3	-
	60°		79,5	78,3	78,8	69,6	-
Matage	F _{by} (MPa)	L	-			-	-
		TL	635			-	600
	F _{bru} (MPa)	L	-			-	-
		TL	845			-	820

(1) MILL HDBK5

FATIGUE AMORCAGE - ENDURANCETENACITE - COURBE R

FISSURATION EN FATIGUE

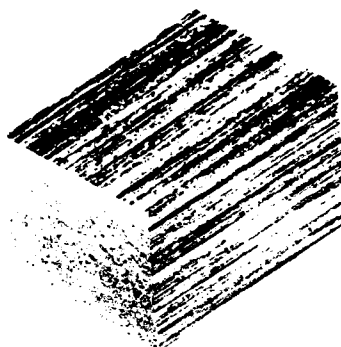


COMPORTEMENT EN CORROSION

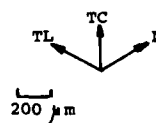
		2091 T 8X51	2024 T351
CORROSION GENERALISÉE	Atmosphère Marine 10 mois	I 2 / E 5 (1)	E 2 / E 3
	Corrosion Fertilisante ASTM G 34	96 h : HA	96 h : HB
	Corrosion Interstitielle	I 3	I 4
CORROSION SOUS CONTRAINTE Flexion Plane sur Eprovettes Lisses	Contrainte (MPa)	400	280
	Ruptures / Fissiles	0 / 6	0 / 3
	Durée (jours)	> 60	> 60
PROTECTION + PEINTURE	OAC non collant + peinture	Adhère 7 jours eau	100 %
		I E A 1200 h	G = 1
	Alodine 1200 + peinture	Adhère 7 jours eau	100 %
		I E A 1200 h	G = 1

G : indice de gravité de corrosion sur éprovette peinte avec défaut
(1) Dispersion importante d'une corloée à l'autre

PROFILES MINCES EN 8090 T8510/11
MICROSTRUCTURE



Cliché N° 58315



CARACTERISTIQUES MECANQUES SEN L

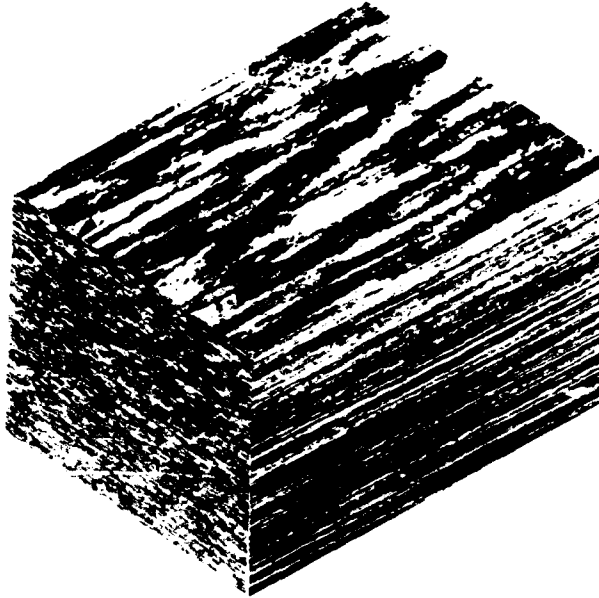
RO,2 (MPa)	Rm (MPa)	A %	E (GPa)
420	490	6,5	80,5

CORROSION SOUS CONTRAINTE

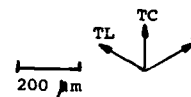
CONTRAINTES (MPa)	Nbre rupt/épr.	Temps (jours)
350	0/3	30

PROFILES MOYENS EN 2091 ET 8090 T8510/II
MICROSTRUCTURE

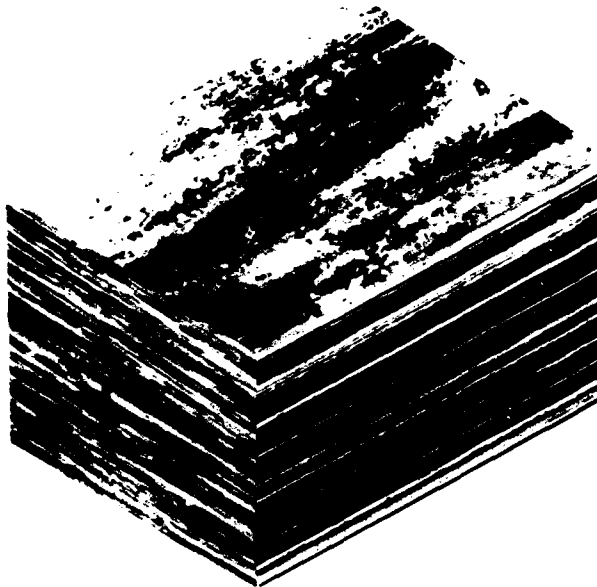
8090 T8510



Cliché N° 55615



2091 T8510



Cliché N° 55617

CARACTERISTIQUES MECANQUES STATIQUES
MOYENNES POUR $2 < e < 10$ mm

Parametre	Scas	2091 T8xx	8090 T8xx	2024 T3xx	7175 T7xx	
R _{0,2} (MPa)	L TL	460 430	490 460	430 -	450 445	
R _m (MPa)	L TL	535 515	550 520	535 -	525 520	
A%	L TL	6,9 9,1	6,1 6,1	11 -	9,9 14,3	
E (GPa)	L TL	79 77,5	81 80	72,4 -	72 -	
Compression	R _{0,2c} (MPa)	L	515	490	390	450
	E _c (GPa)	L	76,4	79,2	73,4	73
Mase	F _{br} (MPa)	L (e/D=2)	650	690	655	725
	F _{br} (GPa)	L (e/D=2)	845	845	925	980

COMPORTEMENT EN CORROSION

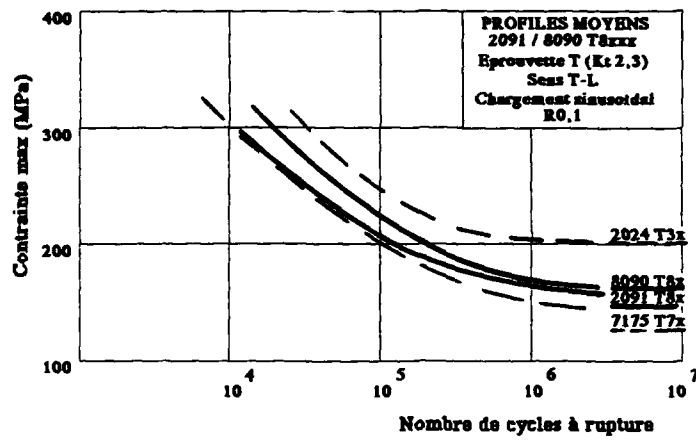
		2091 T8x	8090 T8x	2024 T3x	7175 T7x	
CORROSION GENERALISEE	Atmosphère Marine 10 mois	E 5	I 3 / I 5	E 5	P2 / P4 (1)	
	Corrosion Feuilletante ASTM G 34	96 h : EC	96 h : EC	96 h : ED	96 h : EB	
	Corrosion Intercristalline	I 3	I 3	-	I 2	
CORROSION SOUS CONTRAINTE Flexion Plane sur Eprouvetttes Lisses	Contrainte (MPa)	300	400	280	400	
	Ruptures / Essais	0 / 6	0 / 6	0 / 3	0 / 3	
	Durée (jours)	> 60	> 60	> 47	> 30	
PROTECTION + PEINTURE	OAC non calmatée + peinture	Adherence 7 jours eau	100 %	100 %	100 %	100 %
		I E A 1200 h	G = 0	G = 0	G = 0	G = 1
	Alodine 1200 + peinture	Adherence 7 jours eau	100 %	100 %	80 %	100 %
		I E A 1200 h	G = 1	G = 0	G = 0	G = 1

G : indice de gravité de corrosion sur éprouvette peinte avec défaut

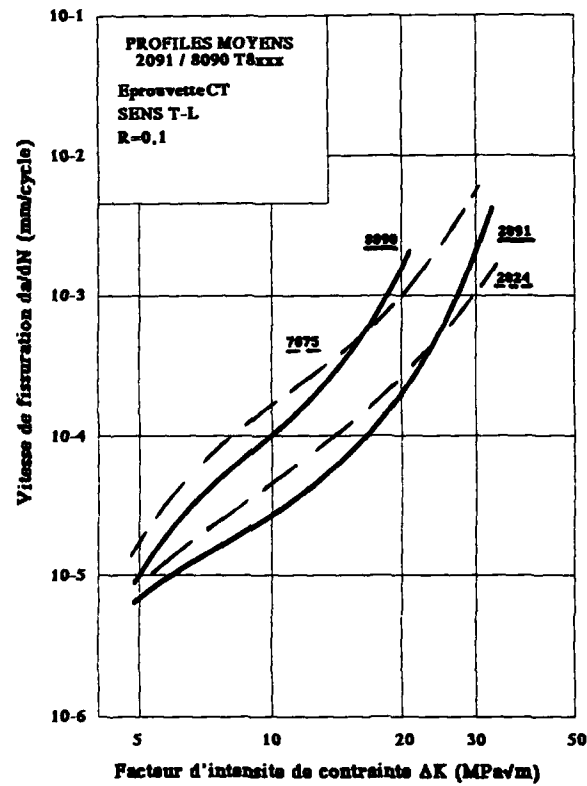
(1) Exposition de 4 mois

(2) Grande dispersion avec la géométrie

FATIGUE AMORCAGE - ENDURANCE

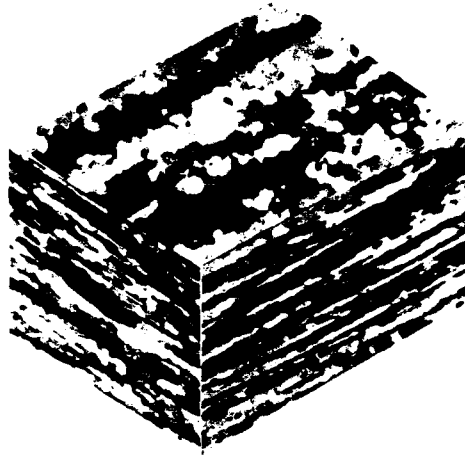


FISSURATION EN FATIGUE

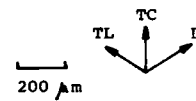


MATRICES DE PRECISION EN 2091 ET 8090
MICROSTRUCTURE

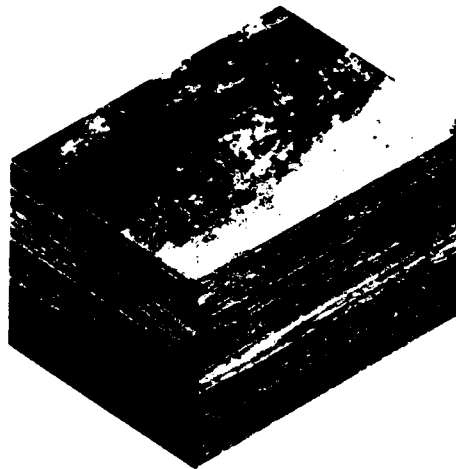
8090 T6



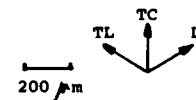
Cliché N° 58273



2091 T7X



Cliché N° 58311



CARACTERISTIQUES MECANQUES STATIQUES
MOYENNES

Parametre	Seas	2091 T7X	8090 T6	7175 T73
R _{0,2} (MPa)	L TL	345 370	355 370	- 420
R _m (MPa)	L TL	435 460	450 445	- 495
A%	L TL	8,9 7	5,6 5,2	- 10,5
E (GPa)	L TL	77,8 78,7	79,3 79,2	- 72

COMPORTEMENT EN CORROSION

		2091 T7X	8090 T6	7175 T73
Corrosion Inter cristalline Profondeur d'attaque		135 µ	190 µ	50 µ
CORROSION SOUS CONTRAINTES Flexion Plisse sur Eprouvettes Lisses	Contrainte (MPa)	280	270	300
	Ruptures / Essais	0 / 3	0 / 3	0 / 3
	Durée (jours)	> 36	> 48	> 48

INVESTIGATION ON SHEET MATERIAL OF 8090 AND 2091
ALUMINIUM-LITHIUM ALLOY

BY

W. ZINK, J. WEILKE, L. SCHWARMANN AND
K. H. RENDIGS

MESSerschmitt-Bölkow-Blohm GmbH
TRANSPORT AIRCRAFT GROUP
HÜNEFELDSTRASSE 1-5
2800 BREMEN 1
GERMANY

SUMMARY

The new aluminium-lithium alloys offer an attractive alternative of reducing structural weight for civil aircraft components.

For fuselage application the damage tolerant version of Aluminium-Lithium as substitution of 2024 T3 material is of greatest interest. Due to the responsibility of MBB/UT for fuselage structures within the Airbus production sharing investigations on damage tolerant 8090 and 2091 sheet material has been carried out a few years ago.

The Al-Li alloys 2091 and 8090, developed by Pechiney, Alcoa and Alcan for 2024 T3 substitution will be presented in view of mechanical properties and damage tolerant behaviour with special emphasis placed on the comparison with conventional alloys.

Fracture toughness data from R-Curves carried out on CCT-specimens as well as crack propagation behaviour and fatigue results will be discussed.

Finally a summary will be given on the different corrosion behaviours.

1. INTRODUCTION

The new aluminium-lithium alloys offer the aircraft manufacturers considerable weight gain potential without extensive conversions of their manufacturing facilities.

The fact that material manufacturers fix price increase factors between 2 and 5 for these alloys because of the costly alloying element lithium and the increased cost for melting and the manufacture of semi-finished product in comparison with conventional alloys in running series production, compels the final user to make economical use of these materials.

In civil aircraft manufacture, it seems that semi-finished products such as plates and die-formed parts with machining grades up to 95 % will be suitable for series production of very few selected components only.

However, the situation is quite different for sheet material and extrusions where fly-to-buy ratios are generally rather advantageous.

Intensive investigations carried out at MBB-UT have shown that the extra effort aimed at reducing weight by using aluminium-lithium sheet material and extrusions and caused by the higher price of the semi-finished products and the necessary adaptations within the production cycle, can be kept within reasonable limits.

Within the scope of the Airbus project, MBB is, above all, responsible for main parts of the fuselage structure. At present, the main material used here is the conventional alloy 2024 T3 which is perfectly suited to fulfill the requirements of these components because of its excellent damage tolerant properties.

This explains why, among the aluminium-lithium alloys available today, we are mainly interested in the variant which has been developed as a replacement for this range of applications.

This covers alloy 8090-C which has been developed and produced by ALCAN and alloy 2091 developed by the french company PECHINEY and now produced also by ALCOA under a licensing agreement.

This paper deals with test results obtained on semi-finished sheet material products coming from the three manufacturers ALCAN, PECHINEY and ALCOA. These semi-finished products were proposed as qualification material.

The reference material used for the comparison of all test results was alloy 2024T3 since the possible introduction of aluminium-lithium alloys is entirely based on the substitution principle, i.e. geometrical changes of components as a consequence of different mechanical and technological properties are not acceptable.

2. SCOPE OF INVESTIGATIONS

Throughout these investigations, the main emphasis was put on the characterization of ALCAN alloy 8090-C. This is explained by the existence of cooperation agreements with the french Airbus partner AEROSPATIALE who is primarily interested in PECHINEY alloy 2091.

In view of the future qualification of "ONE" aluminium-lithium alloy as a substitute material for 2024 T3, a whole series of alloy variants produced by the three potential manufacturers have been investigated in the course of the last few years.

The so-called screening programs were aimed at determining essential properties which would be relevant for a future application as substitute for 2024 T3. In many cases, test were abandoned prematurely when, upon characterization of the material, properties were found which could not be considered for application on real aircraft structures from the view points of material engineering or structural mechanics.

This explains why the extent of the investigation programs differs for the various alloy variants.

2.1 Alloys under Investigation

Fig. 1 shows the alloys available for investigation. ALCAN and PECHINEY variants are further developments which became necessary because the decisive criteria of the alloys did not meet MBB-UT requirements.

The relevant heat treatment data for the investigated alloys are given in Fig.2.

3. INVESTIGATIONS PERFORMED

The full scope of investigations performed on the respective alloy variants is represented in Fig. 3 which shows the different scopes of inspection for the different variants. Some reasons for breaking off investigations will be described in the following.

3.1 Tensile Properties

3.1.1 Tensile Tests for Determination of R_{p0.2}, R_m and A₅

The tensile tests were performed on flat specimens as per DIN 50114 and DIN 50125. The data used for comparison purposes were taken from the drafts of MBB material data sheets (MBBN-4800 and MBBN-4801) prepared for the aluminium-lithium alloys and represent requirements for a future series application.

Fig. 4 shows results achieved for ALCAN variants of 8090-C. It can be seen clearly that the alloy of the last development stage fulfills the specified requirements. The reasons for the different development stages are listed in the following:

The extension of the artificial ageing period (T8X to T8X*) was chosen in order to increase the fracture toughness. It is evident that the optimum combination was not reached in this case since the rupture strengths are slightly below the target values. Any further optimization efforts were discontinued in view of the development of the next variant with improved crack propagation behaviour.

Figs. 5 and 6 show the relevant data for alloy 2091 produced by ALCOA and PECHINEY.

The 2091 sheets supplied by ALCOA almost meet requirements regarding mechanical properties.

The PECHINEY sheets in condition T8X are in satisfactory agreement with the required values as per MBB specification. However, this is a condition which cannot be taken into consideration for the envisaged area of applications because of its poor SCC qualities. As a result, PECHINEY proposed modified conditions CPH in an effort to meet three main criteria. In principle, both CHP variants offer a good SCC resistance. The target set for CPH R is a damage tolerant alloy offering high strength values and satisfactory properties with regard to fracture mechanics. Fig. 6 shows that, as far as strength is concerned, the results obtained are quite good. In condition CPHK, the alloy was optimized to achieve an extremely good fracture toughness - at the expense of strength, so that 60° values do not fulfill the requirements of MBB-N.

3.1.2 Compression and Bearing Strength

Several tests were performed in order to determine compression and bearing strength. Figs. 7 and 8 shows the results obtained. As far as the bearing yield stress limits are concerned, it was shown that both alloys - 8090-C T8X and 2091 CPHR - can be compared with 2024 T3. 2091 CPHK values are slightly inferior.

The bearing tensile strength values of alloy 2024 T3 were reached by none of the variants under test. The best values are obtained with alloy 8090-C.

Fig. 8 shows a series of compression strength values. None of the tested materials were worse than the reference material 2024 T3.

3.2 Fatigue Behaviour

Fatigue strength properties were examined on specimens with different KT factors and on lap joint specimens representing a typical Airbus connection.

3.2.1 Fatigue on Specimens with different KT Values

Fig. 9 shows the different geometries of the specimens used. KT values were 1.0, 2.5 and 3.6. Tests were carried out at a frequency of 20 Hz and an R ratio of 0.1 at RT.

Figs. 10 and 11 show the comparison between the 8090-C alloys and 2024 T3 as reference to the requirements. It is obvious that the fatigue behaviour of alloy 8090-C is equal to or better than that of alloy 2024 T3. This applies to all conditions and KT factors tested.

3.2.2 Fatigue on Lap Joints

These tests were performed on alloys 2024 T3 and 8090-C T8X. The test bars represented single-shear three-row longitudinal lap joint sections complete with riveted stringer (Fig. 12). The test bars had been prepared with solid aluminium rivets 7050 T73 and were subjected to load-controlled tests until rupture at a frequency of 20 Hz at an R ratio of 0.1.

Fig. 13 shows the service life curves obtained. Service life characteristics are definitely better for alloy 8090-C T8X than for 2024 T3. Crack patterns as shown in Fig. 14 are similar for both materials.

3.3 Crack Growth Behaviour

Tests concerning crack growth behaviour are conducted on CCT specimens of 160 mm width (Fig. 15). Initial crack length was 4 mm; final crack length was approximately one third of specimen width.

3.3.1 Crack Growth Life

Fig. 16 shows results concerning crack growth life of 8090-C variants. All results were evaluated in comparison with 2024 T3.

For all three variants of alloy 8090 crack growth behaviour is definitely better than for 2024 and depends heavily on orientation. Crack deviation as shown in Fig. 17 was not acceptable and led to the optimized variant of alloy 8090-C T8X** which represents the definite stage.

Fig. 18 shows results obtained with PECHINEY alloys 2091 T8X, 2091 T8X CPHR and T8X CPHK.

It turns out that variant T8X is approximately equivalent to 2024 and variant CPHK slightly inferior. Variant CPHR shows a significantly inferior crack growth behaviour because of the heavy dependency of orientation.

3.3.2 Crack Propagation Rate

Fig. 19 shows the crack propagation rate for certain points of ΔK for variant 8090-C T8X**.

For T-L orientation, alloy 8090 shows a better behaviour over the entire ΔK range than 2024 T3. This is not true of L-T orientation. 8090-C is better up to values $\Delta K = 13 \text{ MPa } \sqrt{\text{m}}$ but is inferior to 2024 at higher ΔK values.

Fig. 20 shows the results of the comparison between 2091 T8X CPHK and 2024 T3. At low ΔK values 2091 is slightly worse, while at higher ΔK ($> 20 \text{ MPa } \sqrt{\text{m}}$) 2091 is slightly better than 2024. But the deviations, which have been found are within acceptable limits.

3.4 Fracture Toughness

For the assessment of damage tolerance performances of aircraft structures, the residual strength (for a given crack length) and/or critical crack length (for a given stress) have to be determined very carefully.

Provided fracture toughness data are known, determination of these values presents no difficulties at all. The required data can be obtained on the basis of the crack resistance curve (R-curve).

All tests were performed on CCT specimens of 400 mm width as specified in ASTM E 561. Comparative tests were carried out for conventional alloy 2024 T3. MBB did not perform tests on alloys 2091 CPHK and R but used relevant test results obtained by AEROSPATIALE. As far as the apparent fracture toughness is concerned, the values found are such that they are away from meeting MBB design requirements.

The same is true for 8090 alloys, but they are quite better than these of 2091. (Fig. 21, 22).

3.5 Corrosion Behaviour

Within the scope of these investigations, the alloys were subjected to a series of intergranular corrosion, exfoliation and SCC tests. The high sensitivity of 2091 alloys to stress corrosion cracking became apparent at an early stage. One of the consequences was the development of condition CPH by PECHINEY and another the discontinuation of MBB tests on ALCOA alloy 2091.

3.5.1 SCC Behaviour

A test performed on riveted sheet metal strips as developed by AEROSPATIALE has proved to be an excellent method for the determination of SCC sensitivity of thin sheet material. For this purpose, specimens are prepared as shown in Fig. 23 and are then subjected to an alternate immersion test as per MIL-STD-1312. Duration of test is 10, 20 and 30 days. At the end of the specified period, a sample is taken from each test lot and checked with regard to cracks.

Fig. 24 shows a specimen made of alloy 2091 (ALCOA). The cracks made visible by dye penetration test can be clearly seen. This test did not reveal any sensitivity to SCC for 8090-C variants or the two 2091 CPH versions.

3.5.2 Exfoliation and Intergranular Corrosion Behaviour

Tests aimed at finding out about intergranular corrosion behaviour were performed in accordance with MIL 6088 and those concerned with exfoliation were carried out on the basis of ASTM-M-34-79.

Fig. 25 shows intergranular corrosion attacks on 8090 C T8X. The attack depth of approx. 90 μm leads to results which are comparable to those of 2024.

The same is true for the exfoliation behaviour represented in Fig. 26 where an Exco-grade of EA has been found.

4. CONCLUSION

As preparation for the material qualification of a suitable aluminium-lithium alloy as a replacement for the conventional damage tolerant alloy 2024 T3, several alloy variants coming from the three potential aluminium-lithium manufacturers ALCAN, PECHINEY and ALCOA were subjected to a series of tests. As far as mechanical properties are concerned, all alloys are in satisfactory agreement with the required data.

As far as fatigue behaviour is concerned, alloy 8090-C tested on specimens with different KT values and on Airbus lap joint specimens offers service life values which are either indential to or even better than those of alloy 2024.

Crack growth life behaviour of alloy 8090-C T8X is better than that of 2024; however, the crack growth rate at higher ΔK values has proved to be slightly inferior.

As far as alloy 2091 CPHK is concerned crack growth life and crack growth rate for low ΔK are slightly worse than 2024 T3, while the crack growth rate for high ΔK is slightly better.

The apparent fracture toughness properties of PECHINEY alloy 2091 are away from fulfilling the requirement even in the special version CPHK, developed for this purpose.

Whether the slightly inferior behaviour of 8090-C T8X is acceptable, has to be checked very precisely in the near future. The decision of MBB to incorporate 8090-C in the major fatigue test specimen of the A330/A340 is a way to solve this item and is also necessary for testing these new alloys on real aircraft structures.

Alloys 2091 (ALCOA) and 2091 T8X (PECHINEY) are extremely prone to SCC. In the case of alloys 8090 CT8X** and 2091 CPH, resistance to SCC as well as to intergranular corrosion and exfoliation attacks can be described as good.

ALCAN	PECHINEY	ALCOA
8090CT8X	2091T8X	2091T8X CLAD
8090CT8X *	2091T8X CPHK	
8090CT8X **	2091T8X CPHR	

* AGING MODIFIED

** CHEMISTRY AND PRODUCTION SEQUENCES MODIFIED

Fig.1 Alloys under Investigation (1.6 mm Sheet)

ALLOY/SUPPLIER	TEMPERATURE	TIME
ALCAN		
8090CT8X	150 °C	12 HOURS
8090CT8X *	150 °C	24 HOURS
8090CT8X **	150 °C	24 HOURS
PECHINEY		
2091T8x	135 °C	12 HOURS
2091T8x CPHK	135 °C	12 HOURS
2091T8x CPHR	135 °C	12 HOURS
ALCOA		
2091T8x	121 °C	24 HOURS

Fig.2 Aging Practice

TEST	ALLOY PRODUCERS	2091T8x Pechiney	2091T8x CPHK Pechiney	2091T8x CPHR Pechiney	2091T8 CLAD Alcoa	8090-CT8x 12 150 °C Alcan	8090-CT8X* 24 150 °C Alcan	8090-CT8X** Modifi. Alcan
SRK		X	-	-	X	-	-	X
Tensile		X	X	X	X	X	X	X
Compression		-	X	X	-	X	-	X
Bearing		-	X	X	-	X	-	-
Fatigue		-	-	-	-	X	X	-
Lap Joint		-	-	-	-	X	-	-
Crack propagation		X	X	X	-	X	-	X
Crack propagation NaCl		-	-	-	-	X	-	-
Fracture toughness		-	X	-	X	X	-	X
Corrosion		-	-	-	-	X	X	X

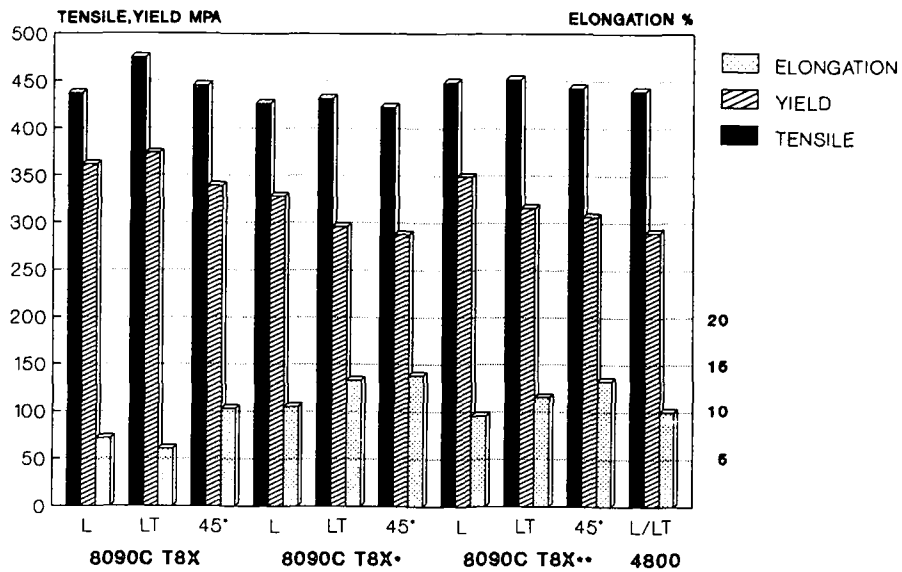


Fig.4 Mechanical Properties of 8090-C Sheet

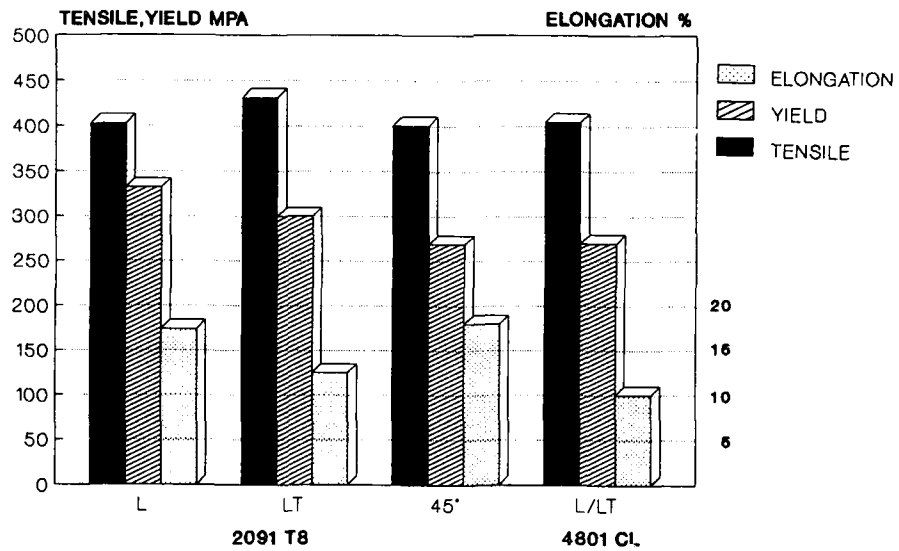


Fig.5 Mechanical Properties of 2091 Sheet (ALCOA)

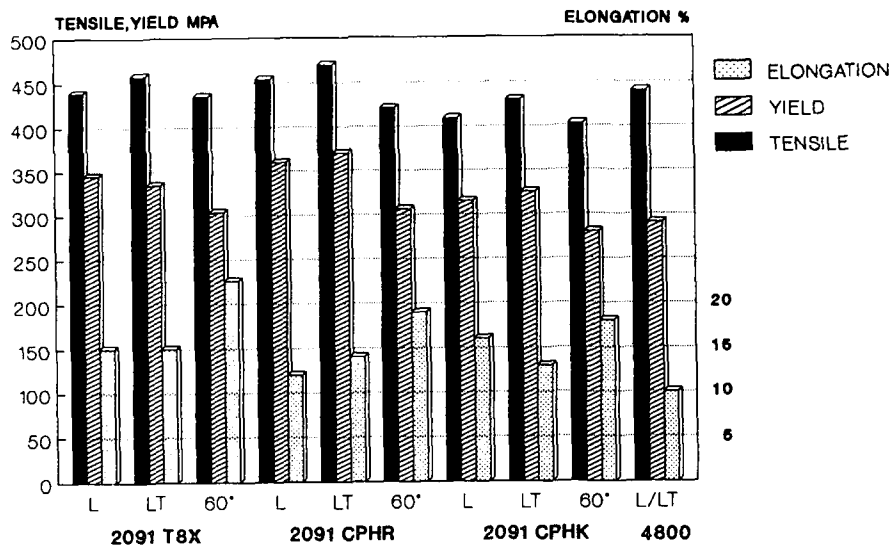


Fig.6 Mechanical Properties of 2091 Sheet (PECHINEY)

		SPEC.			TEST RESULTS						
		2024T3		2034T3		8090C-T8X		2091 T8X CPHR		2091 T8X CPHK	
		L1LT	L	LT	L	LT	L	LT	L	LT	
TENSILE	MPA	680	689	690	657	633	628	620	625	633	
YIELD	MPA	480	481	488	501	502	482	483	462	465	

Fig.7 Bearing Strength (e/D=1,5)

		SPEC		TEST RESULTS									
		2024T3		2024T3		8090C T8X		8090C T8X**		2091T8X CPHR		2091T8X CPHK	
		L	LT	L	LT	L	LT	L	LT	L	LT	L	LT
YIELD	MPA	260	300	299	336	317	344	300	334	367	400	320	341
E-MODULUS	MPA	73800		73700	73400	81200	86500	80600	81600	79700	80100	79700	80300

Fig.8 Compression Properties

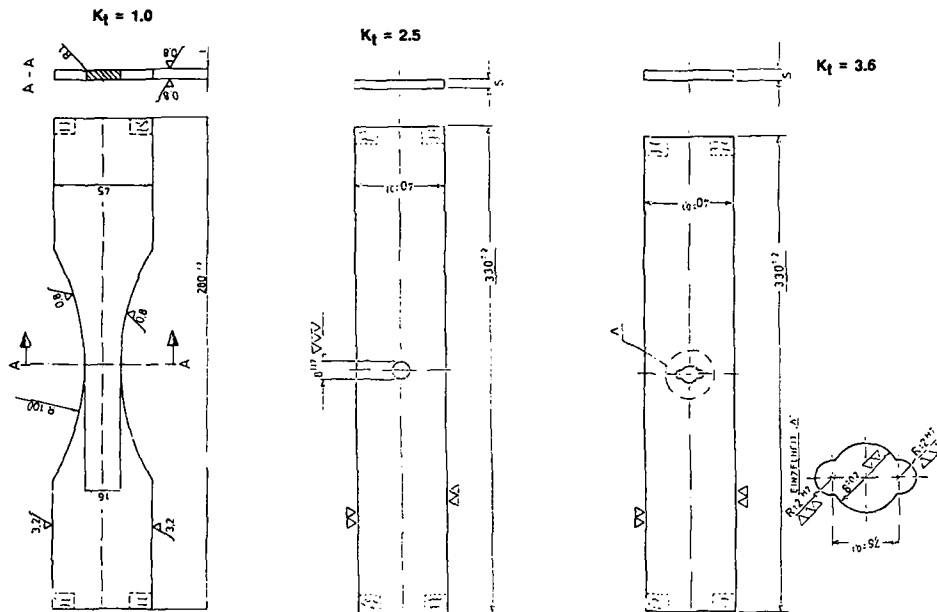


Fig. 9 Fatigue Test Specimen

COUPON-TESTS: CONSTANT-AMPLITUDE-LOADING, MAX. ALLOWABLE STRESS AMPLITUDE IN MPA (MEAN VALUES)

	K _t = 1.0		K _t = 2.5		K _t = 3.6	
	2024 T3	8090 T8X	2024 T3	8090 T8X	2024 T3	8090 T8X
N						
5 x 10 ⁴	162	160	91	92	70	72
1 x 10 ⁵	145	145	75	80	55	65
2 x 10 ⁵	120	135	67	72	45	59
5 x 10 ⁵	90	120	47	68	35	55
1 x 10 ⁶	72	105	38	65	32	52

Fig. 10 Fatigue Strength 8090-C T8X

COUPON-TESTS: CONSTANT-AMPLITUDE-LOADING, MAX. ALLOWABLE STRESS AMPLITUDE IN MPA (MEAN VALUES)

	K _t = 1.0		K _t = 2.5		K _t = 3.6	
	2024 T3	8090 T8X*	2024 T3	8090 T8X*	2024 T3	8090 T8X*
N						
5 x 10 ⁴	162	160	91	91	70	73
1 x 10 ⁵	145	152	75	80	55	62
2 x 10 ⁵	120	135	67	75	45	62
5 x 10 ⁵	90	122	47	66	35	56
1 x 10 ⁶	72	114	38	61	32	54

Fig. 11 Fatigue Strength 8090-C T8X*

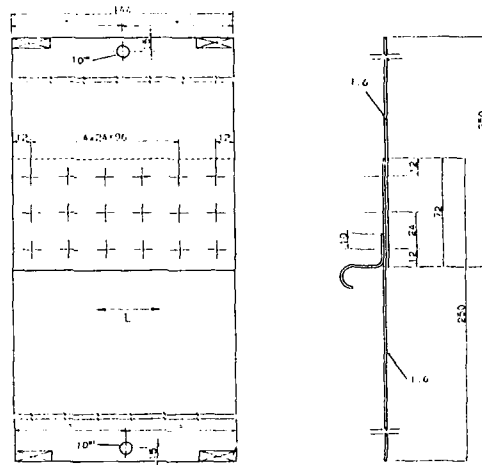


Fig. 12 Fatigue Strength, Lap Joint Specimen

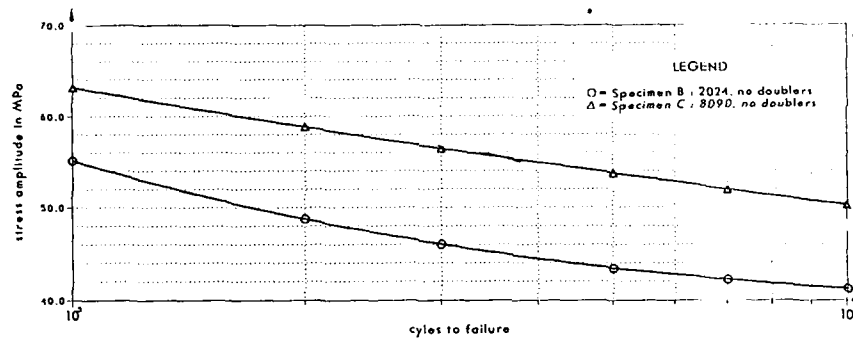


Fig. 13 Fatigue Strength of Lap Joints, R=0,1

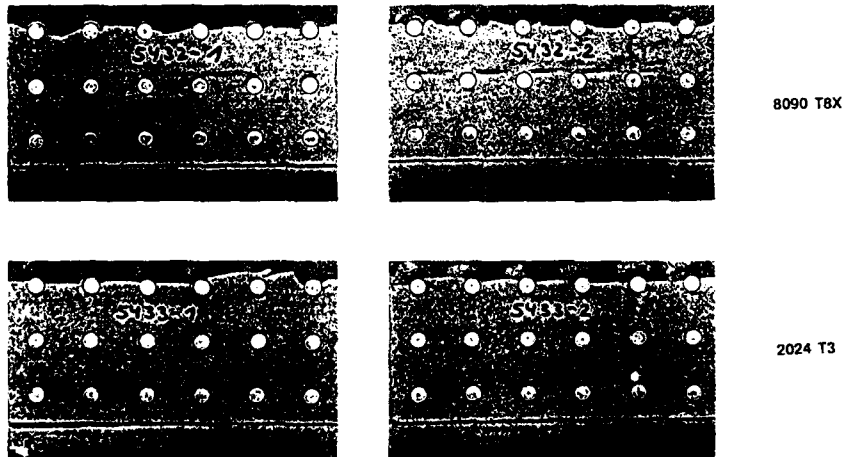


Fig. 14 Crack Shape of Lap Joint Specimen

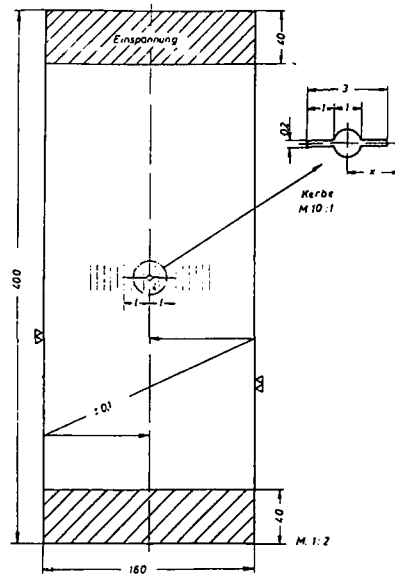


Fig.15 Crack Propagation Specimen

COUPON-TEST : CCT - SPECIMEN , WIDTH $W = 160$ MM , THICKNESS = 1.6 MM
 MEAN STRESS = 90 MPA , STRESS AMPLITUDE = + 40 MPA
 INITIAL CRACK LENGTH $2a_i = 4$ MM
 FINAL CRACK LENGTH $2a_f = W / 3$

MATERIAL	ORIENTATION	N (CYCLES)
2024 T3	L-T / T-L	1 0 1 5 0 0
8090 T8X	L-T	1 3 2 0 0 0
	T-L	4 3 0 0 0 0
8090 T8X*	L-T	1 1 5 0 0 0
	60°	4 7 5 0 0 0 !!
	T-L	2 8 0 0 0 0 !!
8090 T8X**	L-T	1 9 5 0 0 0
	T-L	2 8 5 0 0 0

!! CRACK TURN AT A CRACK LENGTH OF $a = 12$ MM

Fig.16 Crack Growth Life 8090-C Material

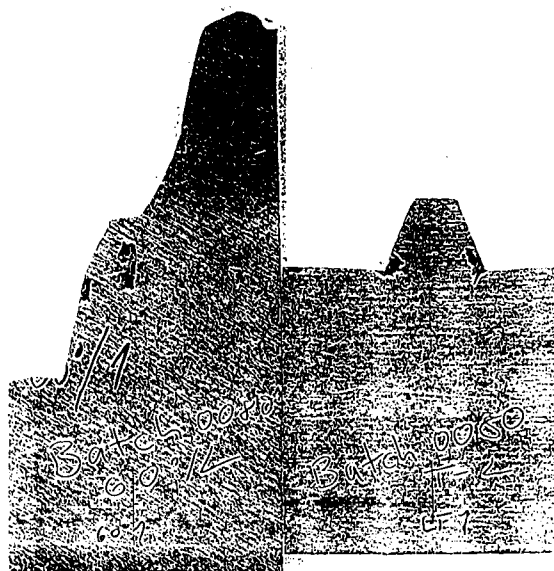


Fig.17 Crack Deviation of 8090-C T8X*

COUPON-TEST : CCT - SPECIMEN , WIDTH $W = 160$ MM , THICKNESS = 1.6 MM
 MEAN STRESS = 90 MPA , STRESS AMPLITUDE $\approx + 40$ MPA
 INITIAL CRACK LENGTH $2a_i = 4$ MM
 FINAL CRACK LENGTH $2a_f = W / 3$

MATERIAL	ORIENTATION	N (CYCLES)
2024 T3	L-T / T-L	1 0 1 5 0 0
2091 T8X	L-T	1 0 0 0 0 0
	T-L	1 1 5 0 0 0
2091 T8X CPHK	L-T	8 6 0 0 0
	60°	8 5 0 0 0
	T-L	9 7 5 0 0
2091 T8X CPHR	L-T	7 1 0 0 0
	60°	5 8 0 0 0
	T-L	8 8 0 0 0

Fig.18 Crack Growth Life 2091 Material

Coupon—tests: CCT—specimen, width $w = 160$ mm, thickness = 1.6 mm
 Mean stress = 90 MPa, stress amplitude = ± 40 MPa

crack propagation rate da/dn ($\times 10^{-5}$ /cycle)

ΔK MPa \sqrt{m}	2024 T3	8090C T8	
	L-T/T-L	L-T	T-L
5	1.3	0.5	0.4
10	10.5	8.3	2.6
15	36.9	45.1	8.5
20	96.9	166.3	21.0
25	223.8	517.5	55.0

Fig.19 Crack Propagation Rate 8090-C T8X

Coupon—tests: CCT—specimen, width $w = 160$ mm, thickness = 1.6 mm
 Mean stress = 90 MPa, stress amplitude = ± 40 MPa

ΔK MPa \sqrt{m}	da/dn ($\times 10^{-5}$ mm/cycle)			
	2024 T3 unclad/clad	L-T	2091 CPHK unclad	T-L
5	1.3	2.4	2.6	1.9
10	10.5	12.8	13.4	11.3
15	36.9	38.0	38.3	34.9
20	96.9	89.9	89.3	85.1
25	223.8	196.5	195.7	189.1

Fig.20 Crack Propagation Rate 2091 T8X CPHK

The apparent fracture toughness K_{c0} is determined from the R—curve using the tangent—approach. K_{c0} is defined as:

$$K_{c0} = \sigma_c \sqrt{\pi a_0 / \cos(\pi a_0 / w)}$$

σ_c = uniform remote gross—sectional failure stress
 a_0 = half crack length at the beginning of the loading
 w = width of the CCT—specimen

w mm	$2a_0/w$ —	a_0 mm	K_{c0} (MPa \sqrt{m})		
			2024 T3	8090C T8	8090 C T8**
400	0.333	67	96.5	86.9	89.6
2000	0.275	275	136.5	119.0	119.5

Fig.21 Apparent Fracture Toughness 8090-C

The fracture toughness is determined from the R-curve on unstiffened, flat, centre-cracked panels.

a) Width $w = 400$ mm			
$2a_0/w$	a_0	K_{c0} (MPa \sqrt{m})	
	mm	2024 T3	2091 CPHK
0.33	67	96.5	85.4

b) Width $w = 2000$ mm			
$2a_0/w$	a_0	K_{c0} (MPa \sqrt{m})	
	mm	2024 T3	2091 CPHK
0.275	275	137.5	98.6

Fig.22 Apparent Fracture Toughness 2091

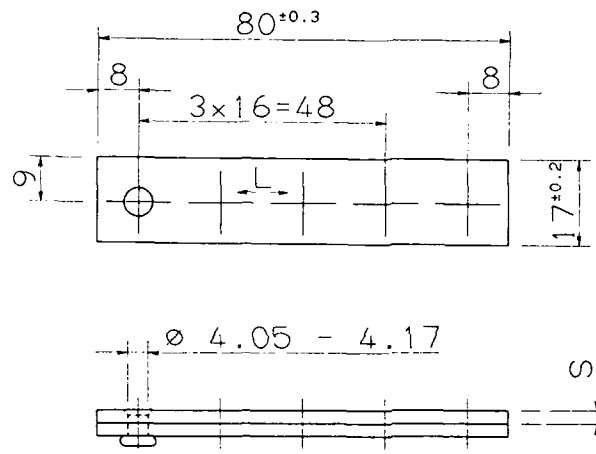


Fig.23 SCC Test Specimen

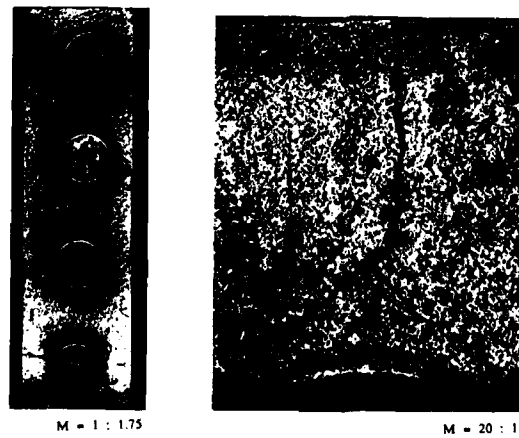
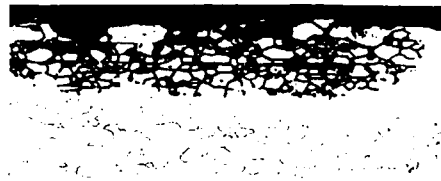


Fig.24 SCC Test Results 2091 (ALCOA)



M = 200 : 1

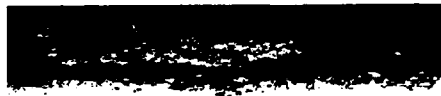


M = 200 : 1

Fig.25 Intergranular Corrosion Attack 8090-C T8X



M = 50 : 1



M = 50 : 1

Fig.26 Exfoliation Attack 8090-C T8X

ALUMINUM LITHIUM ALLOYS FOR NAVY AIRCRAFT

E. W. Lee and J. Waldman

Naval Air Development Center

Warminster, PA 18974

ABSTRACT

Ingot metallurgy alloys of aluminum with lithium additions offer large gains in structural efficiency due to reduced density together with increased strength and elastic modulus. Several alloys are now commercially available. The Navy has been sponsoring R&D activities in these alloys since the mid-seventies. Current efforts include ongoing multi-laboratory evaluations of aluminum-lithium alloys to replace 7075-T6 and 7075-T73. The Navy is also conducting R&D on thermal mechanical processing and superplastic forming on these alloys. Additional testing is being conducted to determine their corrosion resistance in an aircraft carrier environment.

Introduction

The first commercially available aluminum-lithium (Al-Li) alloy, 2020 was developed in the 1950's. The use of lithium bearing aluminum alloys for aircraft structure began in 1958 with the use of alloy 2020 on the Navy RA-5C Vigilante. Production problems and concerns about low fracture toughness led to the termination of further production in 1969. However an increasing need for more efficient aircraft rekindled strong research activities in Al-Li alloys among aluminum producers in conjunction with support from the U.S. Navy. As a result, several commercially available Al-Li alloys have been introduced by the major aluminum producers.

The U.S. Navy has been sponsoring and conducting R&D on Al-Li alloys since the mid-seventies. The Navy sponsored multi-laboratory evaluation of 2090 alloy has shown that the mechanical properties of 2090 alloy equal or exceed those of 7075-T6. The Navy has also been conducting research in such areas as the development of thick Al-Li plate, forging of powder metallurgy (PM) and ingot metallurgy Al-Li alloys, superplastic forming, conventional forming, corrosion, and quench sensitivity. As a result of this work and the extensive research and development efforts by producers, universities, and other government agencies, Al-Li alloys have become an important advanced structural materials for aerospace application.

This paper describes the mechanical and physical properties of 2090 Al-Li alloy. These mechanical and physical characteristics of 2090 alloy were explained in terms of microstructure variation. Also the corrosion behavior of Al-Li alloys was discussed.

Advantages

Al-Li alloys can reduce the weight by 7-15% and increase the modulus by 10-20% compared with currently used high strength aluminum alloys. In addition, Al-Li alloys provide other advantages over other conventional aluminum alloys. Fatigue crack propagation rates and spectrum fatigue resistance of Al-Li alloys are better than those of 7xxx alloys. Another benefit of using Al-Li alloys is their high temperature capability compared to 7xxx alloys. This is due to stable precipitates of Al-Li alloys at high temperatures. It has been reported that Al-Li alloys exhibit an 80°F advantage over 7xxx alloys in the same heat-treated condition. It was also found that Al-Li alloys exhibit excellent ductility and strength at liquid nitrogen temperature. The yield strength, UTS and ductility of 2090 at 77K are 90 Ksi, 108 Ksi and 12% respectively. While the higher temperature capability of Al-Li alloys is an important benefit for the high performance aircraft application, the excellent mechanical properties at low temperature make these alloys very valuable for rocket applications.

Al-Li Alloy Development

Different goals depending on the application were established for the development of Al-Li alloys by the Navy. Goal A alloy is a damage tolerant alloy which will replace 2024-T3. Goal B alloy is a high strength alloy which

will replace 7075-T6. Goal C alloy is a minimum density alloy. Goal D alloy is a thick section stress corrosion resistant alloy which will replace 7075-T73. Goal B alloy was first developed and designated as 2090 T8E41

Fig 1 shows the transition path for the development of 2090 alloy by the U.S. Navy. Note it began with basic studies and ending with system application. As it can be seen in Fig 1, the Navy has been sponsoring and conducting R&D since mid-seventies in the areas of phase relationships, precipitate kinetics. Li/Cu ratio, role of alloying elements, microstructure-mechanical properties relationships, corrosion and aging studies. At this point in time both the Navy and Air Force are sponsoring various activities for the production and evaluation of aircraft components.

Round-Robin Test Program

The Navy has been sponsoring a round-robin program to develop and exploit goal B and goal D Al-Li alloys. The specific objective of the Goal B program is to establish user experience which provide a basis for guiding future research as well as assessing a data base for the implementation of this alloy into various aircraft applications. Table I shows the participating organizations in the goal B program. Seven government agencies and 23 aerospace companies are participating.

Table II shows the base-line mechanical tests and supplementary tests. The base-line mechanical tests were performed by all participants. The supplementary tests were carried out by ALCOA and some participating organizations. In addition to these tests, the Naval Air Development Center (NADC) is conducting an aircraft carrier exposure testing program. This program will give corrosion results which will show how the actual environment that Navy aircraft are exposed to effect the Al-Li that will be used on Navy aircraft. These tests will also make it possible to determine which accelerated corrosion test, EXCO or MASTHAASIS best simulate the actual environment for these alloys.

Table III shows the product forms for goal B round-robin testing. The 0.5 inch plate, extrusion and 0.063 inch sheet have been delivered and the evaluation has been completed. The delivery of 1.5 inch thick plate was completed recently and the tests are now in progress.

Table IV shows the results of the Naval Air Development Center's work on tensile properties of the 0.5 inch thick 2090 T8E41 Al-Li plate compared with those of 7075-T651 plate. The tensile strength of this alloy equals or exceeds the goal properties. However, the ductility and compressive yield strength in the longitudinal direction are lower than those of 7075-T651 plate. The fracture toughness value of this alloy as shown in Table V exceeds the goal properties.

Fig. 2 shows the fatigue crack growth rate of 7075 T651 and 2090 T8E41 0.5 inch plate. Alloy 2090 exhibits superior fatigue crack growth resistance that is about two orders of magnitude slower than that of 7075 T651. In this work a compact tension specimen was used with a R-ratio 0.33 and 25 Hertz. A higher fatigue crack growth resistance was observed in the LT direction than in the TL direction. The superior fatigue crack growth resistance of this alloy can be explained by its microstructure and related deformation behavior. An unrecrystallized microstructure, strong texture and shearable precipitates promote long slip. Since long slip increases slip reversibility, less damage is accumulated at the tip of the crack thereby lowering fatigue crack growth rate. Long slip also promotes a tortuous crack path. Thus the actual crack length is much longer than the projected length. Also the tortuous crack path decreases the effective stress intensity range by increasing the roughness induced crack closure and increasing the offset angle of the crack propagation direction from 90° of loading direction. Therefore, low fatigue crack growth rates are observed.

Table VI shows the initial results of the mechanical properties of 1.5 inch thick 2090 T8E41 plate. The longitudinal and transverse direction tensile properties and fracture toughness values are equal or exceed the target properties. However, the short transverse ductility and fracture toughness values are below the goal properties. This is also associated with the microstructure of 2090 alloy. The large elongated pancake shape grain structure in conjunction with the presence of large grain boundary phases promote the grain boundary separation. Icosahedral, large elongated T_1 and equilibrium delta phases form at the grain boundaries. The size and distribution of these precipitates are related to quench sensitivity of this alloy.

Anisotropy in Mechanical Properties

While several distinctive benefits can be attained by using Al-Li alloys, there are disadvantages that are delaying the implementation and preventing

the wide spread use of these alloys for aircraft. Anisotropy in mechanical properties is one of the problems for sheet application. Fig. 3 shows tensile properties of 0.063 inch 2090 T8E41 Al-Li sheet as a function of angle between the tensile axis and the rolling direction. The tensile strength drops 15-20% when this angle is 45-60° compared to that of the longitudinal direction. The yield strength shows the same trend as the ultimate tensile strength. The ductility increases with decreasing tensile strength. Fig 4 shows the deformation structures of the fractured tensile specimens tested at three different directions (0°, 45°, 60°). When the tensile axis is 0° with respect to the rolling direction, both a uniform elongation in a microscopic view and a uniform distribution of dislocation in a TEM micrograph are observed. When the tensile axis is with 45° or 60° to the rolling direction non-uniform elongation and localized slip are observed. The localized deformation is probably due to the rolling texture and the precipitate morphology.

Effect of Stretching

Al-Li alloys containing copper (2090, 8091) need to be stretched prior to aging in order to obtain optimal strength and fracture toughness. The requirement for stretching has been an obstacle to the use of these alloys as superplastic forming, conventional forming and forging materials. The basic mechanisms of the T8 temper have been studied by NADC.

Fig. 5 shows the tensile strength of 2090 Al-Li alloy as a function of amount of stretch prior to aging. The yield strength and ultimate tensile strength increase with increasing amount of stretch. Although there are large strength differences between the samples aged at 160°C and 190°C observed in the unstretched condition, the tensile strengths of the 10% stretched materials are nearly the same. The introduction of dislocations during stretching provides heterogeneous nucleation sites for the T₁ precipitates. Consequently, stretching increases the number of precipitates and the homogeneity of their distribution.

The TEM dark field micrographs in Fig 6 show the typical size and morphology of T₁ precipitates at several conditions; (a) 0% stretch aged at 160°C, (b) 2% stretch, aged at 160°C, (c) 10% stretch, aged at 160°C, (d) 0% stretch, aged at 190°C, (e) 2% stretch, aged at 190°C, (f) 10% stretch aged at 190°C. The size of the T₁ phase decreases and the homogeneity of its distribution improves with increasing amount of stretch. When the alloy is aged at 190°C, the effect of stretch is associated with the refinement of the T₁ precipitates. However, when the alloy is aged at 160°C, the effect of stretch is associated with both the refinement and the formation of new T₁ precipitates.

Corrosion

The Naval Air Development Center is evaluating the corrosion resistance of 2090 alloy. Both accelerated laboratory test and atmospheric exposure tests were employed for the corrosion resistance evaluation. EXCO and salt spray plus sulfide oxide tests were conducted as an accelerated test. Shipboard exposure was utilized as an atmospheric exposure test. The alloy has been exposed on the deck of Navy aircraft carrier during a 6 month period. It is well known that EXCO test result is in good agreement with real time corrosion result for 7xxx alloys. However, the EXCO test has led to conflicting results for Al-Li alloys. EXCO tests on Al-Li result in a very poor rating for the alloy. Metallographic examination indicates that an intergranular dissolution mechanism is responsible for the severe rating. However, the shipboard results as shown in Fig 7 indicate that the corrosion resistance of Al-Li alloys is superior to that of similarly exposed 7075-T651. The surface appearance and the subsequent rating of the 2090 T8E41 after the 6 months shipboard exposure is almost the same as that of 7075-T73 alloy. This means that the alloy 2090 T8E41 exhibits an excellent resistance to exfoliation corrosion.

TABLE I. Participating organizations in the Goal B program.

1.	Aero Research Associates of Princeton
2.	Air Force, Wright Aeronautical Laboratories
3.	Alcoa Laboratories
4.	Army Mechanics and Materials Research Center
5.	AVCO Laboratories
6.	Boil Helicopter
7.	Boeing Commercial Airplane Company
8.	Douglas Aircraft Company, Long Beach
9.	Fairchild Republic Company
10.	General Dynamics - Convair
11.	General Dynamics - Fort Worth
12.	Grunman Aerospace Corporation
13.	Hughes Helicopters, Inc.
14.	Lockheed California Company
15.	Lockheed Georgia Company
16.	LTV Aerospace and Defense Company
17.	Martin Marietta Aerospace - New Orleans
18.	McDonnell Aircraft Company - St. Louis
19.	NASA Langley Research Center
20.	NASA Marshall Spaceflight Center
21.	Naval Air Development Center
22.	Naval Ocean Systems Center
23.	Naval Research Laboratory
24.	Naval Surface Weapons Center
25.	Northrop - Advanced Systems Division - Pico Rivera
26.	Northrop - Aircraft Division - Hawthorne
27.	Rockwell - MAAO - Los Angeles
28.	Rockwell - Space Transportation Systems - Downey
29.	Sikorsky Aircraft
30.	Teledyne Ryan Aeronautical

TABLE II. Base-line mechanical tests and supplementary tests for Goal B. program.

- Base Mechanical Tests — All Participants:
 - Tensile
 - Compressive
 - Shear
 - Bearing
 - Modulus (Tensile and Compressive)
 - Fracture Toughness
 - Fatigue Crack Growth — Constant Amplitude
- Supplementary Characterization — Alcoa:
 - Density
 - Composition
 - Microstructure — Optical Metallography
 - Residual Stress
 - Elevated Temperature (300-500°F) Tensile
 - Low Temperature (-60°F) Tensile and Fracture Toughness
 - OH-Axis Tensile, Compression, Shear and Fracture Toughness
 - Fatigue:
 - Axial S-N, Smooth and Notch (Kt = 3), Ambient Air and Aqueous Salt
 - Cyclic Strain Fatigue, Ambient Air
 - Crack Growth, Dry and Salt Spray
 - Spectrum Fatigue (FALSTAFF)
 - Erosion:
 - EXCO
 - MASTMAASIS
 - Seacoast
 - Stress Corrosion
 - Smooth Tensile Bars and C-Rings (3.5% NaCl By Alternate Immersion)
 - KISCC-Type (3.5% NaCl Dropwise)
 - Solution Potentials and Cyclic Polarization Curves
 - Fractography/Failure Analysis
- Supplementary Characterization — Other Laboratories:

TABLE III. Product forms for Goal B. program.

<u>2090 ALLOY PRODUCTS</u>	<u>STATUS</u>
0.063 in. THICK SHEET	TESTING COMPLETED
0.5 in. THICK PLATE	TESTING COMPLETED
1.5 in. THICK PLATE	TESTING IN PROGRESS
"T" SHAPED EXTRUSION	TESTING COMPLETED

TABLE IV. Tensile properties of the 0.5 inch thick 2090 T8E41 Al-Li plate and 7075-T651 plate.

	UTS Ksi	TYS Ksi	Elong. %	E(T) Msi	CYS Ksi	E(C) Msi
2090(L)	85	75	7.6	11.5	72	12.0
7075(L)	83	78	12	10.3	76	10.6
2090(LT)	85	80	6.2	11.6	81	12.1
7075(LT)	84	75	12	10.3	80	10.6

TABLE V. Fracture toughness values of the 0.5 inch thick 2090 T8E41 Al-Li plate and 7075-T651 plate.

Alloy	Fracture Toughness K_{Ic} (Ksi-In ^{1/2})
2090(L-T)	29
7075(L-T)	26
2090(T-L)	28
7075(T-L)	23

TABLE VI. Mechanical properties of 1.5 inch thick 2090 T8E41 plate

TEST DIR.	YS (KSI)	UTS (KSI)	ELONGATION (%)
L	81	85	6.8
T	79	84	4.5
S	64	70	1.1
45°	68	76	4.5

FRACTURE TOUGHNESS

TEST DIR.	K_{Ic} (KSI in)
L-T	34
T-L	27
S-L	7
S-T	8

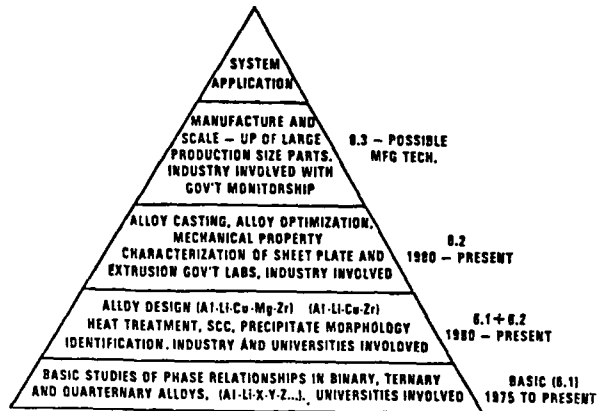


Fig. 1. Transition path for the development of 2090 alloy by the U.S. Navy. Note the progression of the alloy development program from 6.1 through 6.2 and 6.3 to eventual incorporation into fleet aircraft.

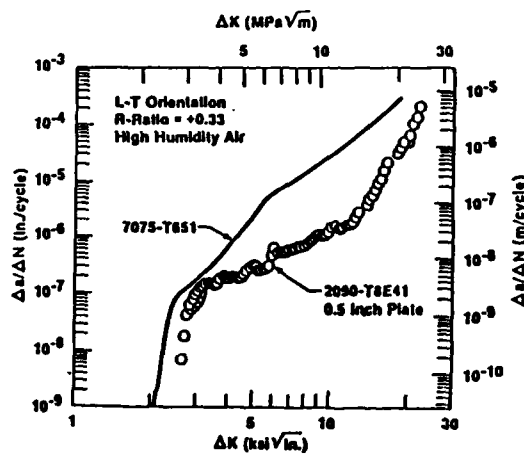


Fig. 2. Fatigue crack growth rate of 7075 T651 and 2090 T8E41 0.5 inch plate. Alloy 2090 exhibits superior fatigue crack growth resistance that is about two orders of magnitude lower than that of 7075 T651 at the stress intensity range of 10 Ksi $\sqrt{in.}$

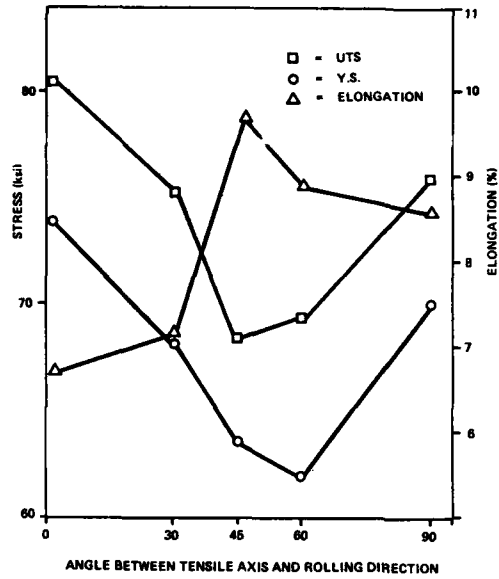


Fig. 3. Tensile properties of 0.063 inch 2090 T8E41 Al-Li sheet as a function of angle between the tensile axis and the rolling direction.

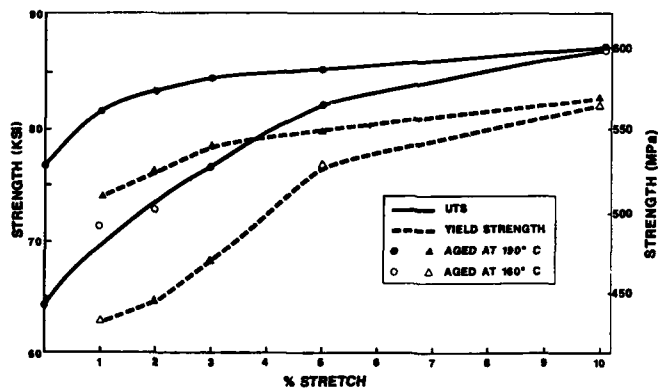


Fig. 5. Tensile strength of 2090 Al-Li alloy as a function of amount of stretch prior to aging.

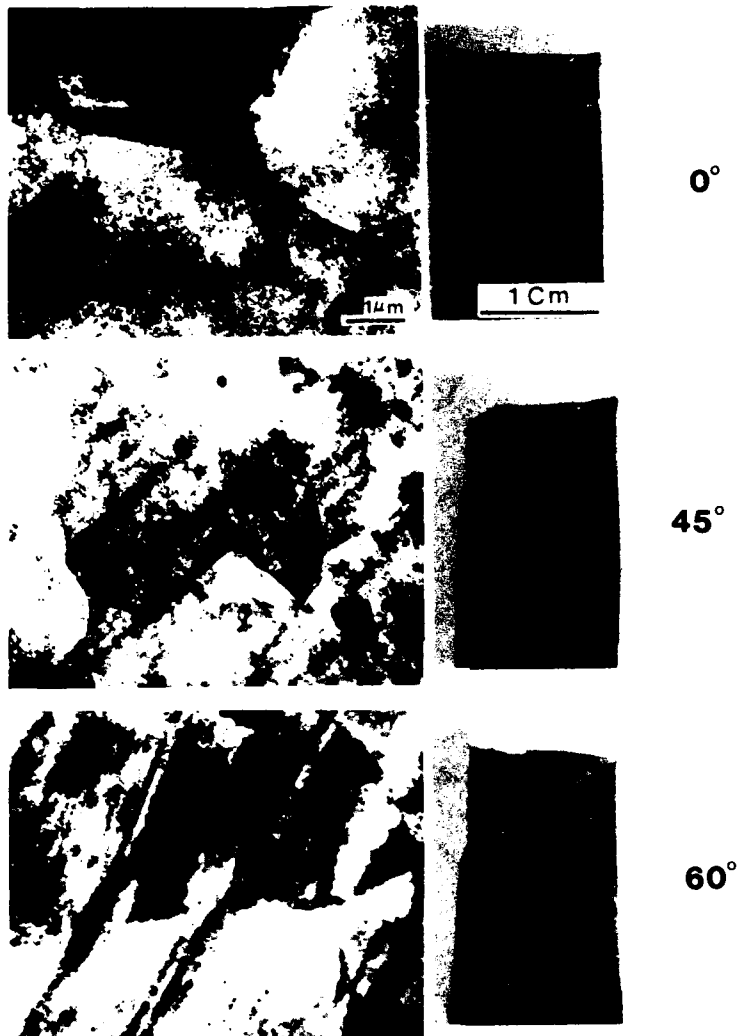


Fig. 4. Deformation structures of the fractured specimens tested at three different directions (0° , 45° , 60°).

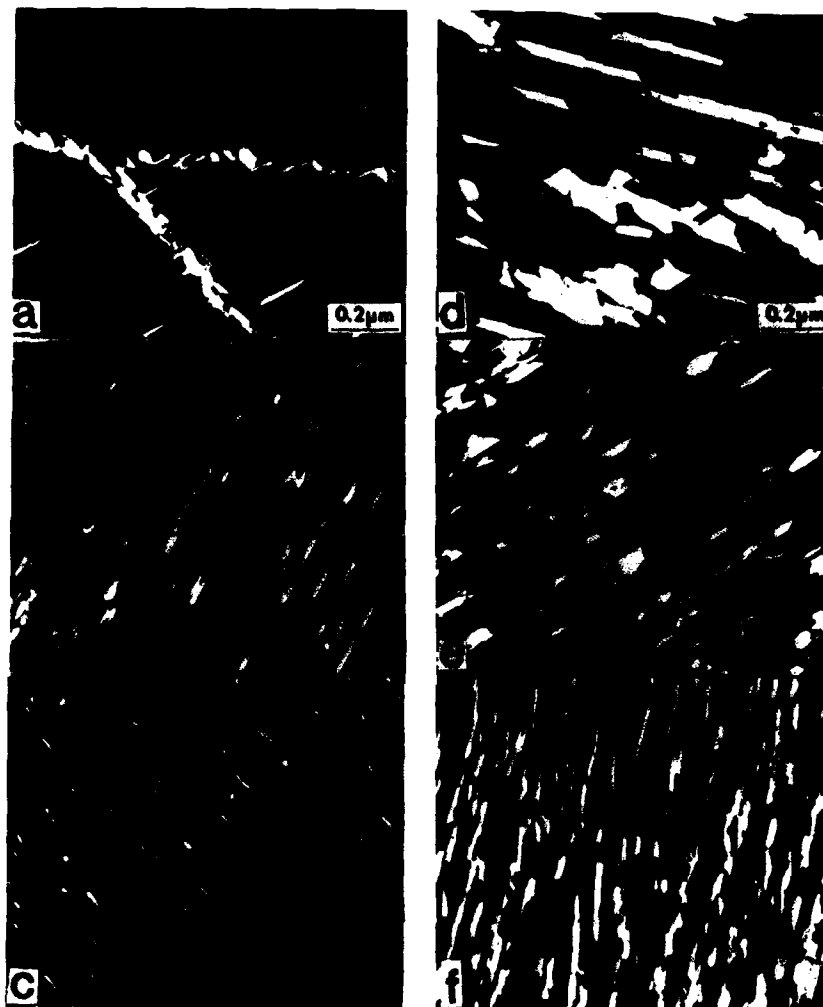


Fig. 6. TEM dark field micrographs showing the size and morphology of T_1 precipitates at several conditions; (a) 0% stretch, aged at 160°C , (b) 2% stretch, aged at 160°C , (c) 10% stretch, aged at 160°C , (d) 0% stretch, aged at 190°C , (e) 2% stretch, aged at 190°C , (f) 10% stretch, aged at 190°C .

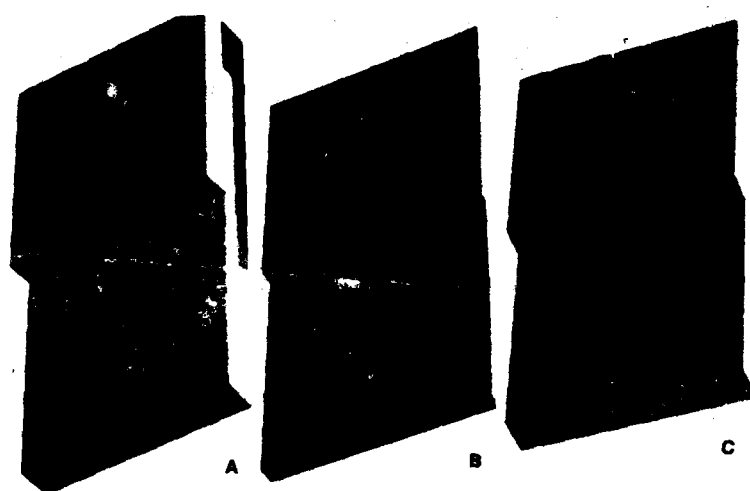


Fig. 7: Surface appearances of (a) 7075 T651, (b) 2090 T8E41, (c) 7075, T7351 after 6 months shipboard exposure.

FATIGUE, FRACTURE MECHANICS AND CORROSION PROPERTIES
OF SOME ALUMINIUM-LITHIUM ALLOYS*

G. Cavallini, L. Lazzeri
Department of Aerospace Engineering, University of Pisa
Via Diotisalvi, 2 - 56100 Pisa (Italy)

M. Scolaris, F. Boschetti
Aeritalia, Gruppo Velivoli da Combattimento
Corso Marche, 41 - 10146 Torino (Italy)

A. Solina, M. De Sanctis
Department of Chemical Engineering, University of Pisa
Via Diotisalvi, 2 - 56100 Pisa (Italy)

G. Zennaro
Divisione Aerea Studi Ricerche e Sperimentazioni
00040 Pratica di Mare (RM), (Italy)

ABSTRACT

A research programme for the evaluation of the main characteristics of the newly developed Al-Li alloys has been undertaken under the sponsorship of the Italian National Research Council (C.N.R.). Many Italian aeronautical Industries and Research Institutes take part in this programme, which comprises a large variety of experimental activities: static tests, fatigue tests, crack propagation tests, fracture toughness, corrosion susceptibility, formability, workability and other tests.

Different producers (British Alcan, Cegedur Pechiney and Alcoa) provided the alloys tested in this programme; 2091, 8090 and 2090 alloys have been object of investigation.

The paper describes some of the results obtained so far in the C.N.R. programme and some results obtained by Aeritalia in its own programs. The results are relevant to fatigue tests carried out both on notched and unnotched specimens, under Constant Amplitude loading ($R=0.1$). Fatigue tests, together with structural (TEM) and fractographic (SEM) studies, have been carried out also for assessing the influence of different ageing on both mechanical properties and failure modes of materials.

Crack propagation tests were carried out under both C.A. loading and FALSTAFF sequence and are here presented, together with results from fracture toughness tests.

Corrosion properties have been assessed by measuring the free corrosion potential according to ASTM G 69 standard method and also in neutral salt solution of Na_2SO_4 (0.1 M). Preliminary results obtained show that Li-containing materials exhibit an intermediate behaviour between traditional 2024 and 7075 alloys and that the presence of Li does not influence appreciably the corrosion mechanism.

1. INTRODUCTION

The introduction of advanced composite materials in aircraft construction represents a milestone in material selection. Predictions about their use in modern aircraft, designed for the '90s and beyond, are of more than 50% of total structural weight for tactical military airplanes, /1/, and at least 25% for commercial aircraft, /2/. The increasing use of advanced composite materials has fostered the natural development of new advanced aluminium alloys by the metallurgy industry.

In this general situation, the so-called new Al-Li alloys occupy an important position; they differ from the traditional Al-Cu or Al-Zn alloys because of the presence of Lithium, in quantities of about 2-3% in weight, as the first or second alloying element. This produces a density reduction of about 8-10%. Moreover, the utilization of Al-Li alloys does not require new special equipments or tooling investment (as composite materials do) and classical design and manufacturing techniques, as well as established aircraft maintenance (and repair) practices, can be preserved.

Therefore, the new Al-Li alloys developed in the last decade by the main industries have been looked upon with great interest by the aircraft manufacturing industry. Some of them, such as 2090, 2091 and 8090 alloy, have reached an advanced stage of development and are almost ready for commercialization. Each of them has a different

* This work was partly financed by the Italian National Research Council.

target alloy which it is intended to substitute:

- a) 2090 is a high-strength alloy, mainly developed to replace 7075-T6; however, many different tempers have been developed in order to obtain particular specific properties.
- b) 2091 was developed to obtain medium strength and good toughness properties; it seems likely to replace 2024-T3 in the proper temper conditions.
- c) the target of 8090 is quite similar to that of 2091, but with higher static properties. According to the heat treatment, it is likely to replace either 2024-T3 or 2014-T6.

Evaluation programs are currently being carried out by many aircraft manufacturing Industries and Research Institutes. This paper contains the results of research aimed at assessing the fatigue and damage-tolerance properties of certain Al-Li alloys, carried out by Aeritalia-UVIC (Gruppo Velivoli da Combattimento) and by the Departments of Aerospace Engineering and Chemical Engineering of the University of Pisa. Corrosion potentials have been assessed by D.A.S.R.S., Pratica di Mare. Some of the results were obtained within the framework of an on-going research programme, financed by the Italian National Research Council (C.N.R.), which coordinates research carried out by both Industries and Research Institutes. Other results are the property of Aeritalia, to whom the Authors are grateful for allowing publication.

2. EXPERIMENTAL PROGRAM

Batches of 2090, 2091 and 8090 alloys were supplied by Alcoa, British Alcan and Cegedur Pechiney. The as-received materials were available in different thicknesses and, in certain cases, also in different heat treatments or in overaged conditions. This paper only contains the results of fatigue tests performed on notched and unnotched specimens and of Fracture Mechanics tests, besides preliminary assessment of corrosion susceptibility. No discussion will be found here of all the other kinds of experimental activities included both in the Aeritalia and in the C.N.R. assessment programs (static, stress corrosion cracking, riveted joints, formability, workability, etc).

Fatigue tests were carried out on plain specimens, whose geometry is shown in fig. 1 ($K_t = 1.07$, $/3/$); the same geometry was used for the notched specimens, when a hole, 5 mm in diameter, was simply drilled at the center ($K_t = 3.1$ referred to gross area, $/3/$). Whenever sufficient material was provided, fatigue tests specimens were prepared both in the L and LT direction. Due to the preliminary nature of the investigation, fatigue tests were carried out under Constant Amplitude (CA) axial loading, with a stress ratio $R (=S_{min}/S_{max})$ equal to 0.1.

Crack propagation tests were carried out mainly under CA loading, characterized by different stress ratios, but preliminary tests under FALSTAFF spectrum loading, $/4/$, were also performed.

The Department of Chemical Engineering of the University of Pisa cooperated in the program by carrying out sample fractography by using a JEOL T300 SEM and structural characterization of materials by means of Transmission Electron Microscopy.

D.A.S.R.S. carried out an assessment of corrosion properties by measuring corrosion potential according to ASTM G 69 standard method and also in neutral salt solution of Na_2SO_4 (0.1 M).

3. FATIGUE TEST RESULTS

The fatigue test results will be presented in the following separately for each material. Certain observations can be made which hold good for all the tested materials. The presence of Lithium, a highly reactive element, causes quick oxidation of the fracture surfaces; therefore timely dismounting of the failed specimen from the fatigue machine and gold coating are necessary, in order to ensure surface readability in subsequent metallographic analysis.

Fatigue test results have been compared with data from MIL-HDBK-5D, but personal experience is that quite often the actual fatigue behaviour of a material is somewhat lower than expected according to MIL-HDBK-5D data, which refers to electropolished specimens.

2091 Alloy

The typical chemical composition is shown in table I; the average density is 2.57 gr/cc. Three thicknesses were available: 1.6 mm and 3.0 mm sheets and 12.0 mm plate. The three materials, all from the same manufacturer, were also in different heat treatments: $t=1.6$ mm: T6; $t=3.0$ mm: T8; $t=12.0$ mm: T651.

The three heat treatments produced different properties in the material. Nevertheless, fatigue test results obtained from the different batches will be compared in the following, without showing conspicuous differences.

Fig. 2 contains the results from unnotched specimens. The data is almost uniformly distributed and no particular influence can be ascribed to thickness or to the principal rolling direction. Comparison with the reference material, 2024-T3, from MIL-HDBK-5D,

shows poor fatigue behaviour: for equal life, the reduction in stress is about 20%.

It is difficult to draw definite conclusions from the examination of the data in fig. 2, due to the existence of contradictory tendencies in the results and the differences in the batches (heat treatment, thickness, grain orientation), which can interfere with each other. A rather wide scatter is also observed.

Another batch of material, 2091-T8X, 1.6 mm thick, was made available by another manufacturer. Only L specimens were made and tested; fig. 3 contains a comparison between the two manufacturers, for the same thickness and grain orientation, but slightly different heat treatment. The material of the second producer proved to possess better characteristics: compared to the traditional alloy, the reduction in stress for equal life is only 10% in the low number of cycles while the fatigue limit seems to be very similar.

Fatigue tests were carried out also on overaged material obtained by imposing the 3.0 mm thick sheet, originally in the T8 condition, to different holding times at high temperatures. As the structure of the material was underaged in the as-received state, it was decided to perform some fatigue tests on small lots of specimens which had undergone the following overaging treatments:

(B) 100 hours at 135°C; (C) 200 hours at 135°C; (D) 100 hours at 190°C.

Fig. 4 shows the fatigue test results and it can be observed that the overaging treatment (B) induces an improvement in the material fatigue strength, whilst longer holding times at 135 °C (heat treatment (C)) do not seem to give better results with respect to those obtained on the as-received material (T8 condition). On the contrary, following the overaging heat treatment (D), a strong modification in the material behaviour is induced and this point will be returned to later.

Fig. 5 shows the results of fatigue tests carried out on notched specimens, made from 1.6 mm sheet material and from plate 12.0 mm thick. The material is the same as that used for the unnotched specimens in fig. 2. Stresses are referred to gross area. The results are well grouped, independently of thickness and the principal grain direction. Comparison with data in the literature concerning the 2024-T3 alloy ($K_t=3.4$, gross area) shows lower fatigue strength, even for notched specimens; in this case, too, the reduction in stress for equal life is about 20%.

8090 Alloy

The average chemical composition of this alloy is given in Table I. Lithium is the first alloying element with a weight percentage of about 2.3-2.6%, thus resulting in an average density of about 2.54 gr/cc. Only one manufacturer supplied batches of material; two thicknesses were available: 1.6 mm and 3.0 mm. The heat treatment was T6, but for 1.6 mm sheet a small quantity of the T651 condition was also available, from which only unnotched L specimens were obtained. The results are shown in fig. 6. A certain amount of contradictory behaviour is observed: smaller gauge did not show higher fatigue strength, as on the contrary it is expected, as well as L specimens did. The behaviour of the T651 sheet specimens was consistent with the T6 material, but the points fall mainly in the lower part of the scatter band.

Anyway, for this material, too, the comparison with the handbook properties of traditional alloys is unfavourable, to the usual extent of about 20% in stress.

Notched specimens were not prepared due to the small quantity of material available.

2090 Alloy

This is a rather different alloy from the previous ones: it is aimed at achieving high strength characteristics. The tested material was in the T8E41 condition, which is the temper that most closely approximates the overall properties of 7075-T6. Three thicknesses were available: 1.6 mm, 3.3 mm and 12 mm, from a single manufacturer. Plain specimens were built with this alloy, in the L and LT directions, with the exception of the LT direction for the 1.6 mm material. The results are shown in fig. 7, compared with 7075-T6. In this case, too, the fatigue strength of the Al-Li alloy is lower than that of the traditional alloy, but to a considerably lesser extent than the other alloys. Taking into account the fact that the effective stress concentration factor of plain specimens is 1.07, it may be stated that the aim of obtaining the same fatigue properties as in the case of 7075-T6 has been achieved. It should be noted that the results look homogeneous, irrespective of the lamination direction and of the thickness. The only observation that needs to be made concerns the particularly poor fatigue strength of the L specimens 3.3 mm thick which, however, may be ascribed to surface defects, in the form of small pitting.

Fatigue tests were carried out also on overaged material, from the plate and the sheet, subjected to different treatments (10 hours and 100 hours at 125°C). The results, presented in /5/, do not show a particular change in fatigue behaviour.

Notched specimens were prepared from the plate and from 1.6 mm sheet. Comparison with data in the literature concerning 7075-T6, available for $K_t=3.4$, shows a quite similar fatigue strength, fig. 8. Curiously enough, the LT direction produced better results than the L direction. Anyway, it can be concluded that the fatigue properties of 2090-

T8E41 do not seem to be inferior to those of the alloy to be substituted (7075-T6).

4. FRACTURE MECHANICS TESTS RESULTS

Determination of fatigue crack propagation behaviour and fracture toughness is very important for the evaluation of a new material for aircraft constructions, because these are fundamental properties for the design of damage-tolerant structures. Therefore, fatigue crack propagation tests were planned, both under CA loading and under flight-by-flight spectrum, using the FALSTAFF standard sequence. Center cracked tension (CCT) specimens were used for these tests. According to the material available, two kinds of specimen geometries were used: the first one was 120 mm wide and the second one 400 mm. This last specimen was used for the fracture toughness tests. The notch at the center of the specimen was made by means of a jeweller's saw and, after precracking, the initial crack length was, on the average, 6 mm. No particular attention was paid, due to the preliminary character of the test program, to the investigation of small fatigue crack behaviour and threshold. The test results were analysed by means of standard programs developed by the Department of Aerospace Engineering and based on the use of spline functions for the numerical determination of the crack growth rate.

4.1 - Crack propagation results

2091 Alloy

CA tests were carried out on 2091-T8 material, available from one manufacturer in two thicknesses: 3.0 mm and 1.6 mm.

The first material was evaluated, using 120 mm wide CCT specimens. Ten specimens were tested by applying the load in the L direction, at different stress ratios (S_{min}/S_{max}), ($R = -0.2, 0., .2$ and $.5$) and six specimens were tested in the LT direction ($R = -0.2, 0.$ and 0.4). Some of the results of the L specimens are summarized in a da/dN - ΔK plot in fig. 9 and those of the LT specimens in Fig. 10. In both figures, a comparison with some typical results of 2024-T3 Alclad, from /6/, is also shown; these last results are relevant to a thinner material (1.00 mm). The comparison shows that crack propagation properties of 2091 are comparable to those of the best aeronautical alloys, at least in the range of high ΔK values. Besides, the characteristics in the LT direction seem even slightly better than in the L direction.

Only three specimens of 2091-T8, supplied by the same manufacturer, were available for the 1.6 mm thickness; they were 400 mm wide and all in the L direction. They were tested under CA loading, with R values of 0.1 and -0.2 (fig. 11). Comparison with the same nominal material, 3.0 mm thick, shows much better behaviour, specially at intermediate ΔK values.

The same batch of material used for a lot of unnotched specimens, (i.e. 2091-T8X, 1.6mm, see fig. 3) was utilized for preparing 400 mm wide CCT specimens, which were tested under CA loading, in the L direction. The results are plotted in fig. 12, which shows substantial improvements in performance, specially at positive stress ratios.

Sometimes, engineering materials exhibit a crack propagation resistance under spectrum loading which is completely different from the CA case; therefore, crack propagation tests were also carried out using the FALSTAFF sequence. The tests were carried out on specimens of 2091-T8, 3 mm thick and 120 mm wide (same batch as the one of CA tests, figs. 9-10); two values of maximum stress in the spectrum were used: 196 MPa and 235 MPa. The test results, which are partly shown in fig. 13, were analysed in terms of da/df versus K_{max} . Comparison with results obtained on 2024-T3 Alclad in research carried out at the Pisa Department of Aerospace Engineering, /7/, shows quite similar behaviour, i.e. it confirms the conclusions that had been drawn on the basis of CA tests. In both cases, L specimens were used.

8090 Alloy

This alloy was supplied by the manufacturer in two thicknesses, 1.6 mm and 3.0 mm; they were both in the T6 condition. Crack propagation tests under CA loading were carried out on 400 mm wide CCT specimens, in the L direction. Due to the limited amount of material available, only three tests were performed. The data obtained are relevant to the intermediate-high ΔK range and are shown in fig. 14. A slight influence of thickness on the crack propagation rate, consistent with the expected trend, can be noted. Bearing in mind that heat treatment T6 is not specifically designed for damage tolerance, the results show interesting characteristics of 8090-T6, in no way inferior to those of the traditional 2024-T3.

2090 Alloy

This material was supplied by the manufacturer in the T8E41 condition. Seven specimens, 1.6 mm thick and 400 mm wide, were tested under CA loading with the load applied in the L direction and four in the LT direction. The results of the first group of specimens are shown in fig. 15, together with reference data obtained at the Pisa

Department of Aerospace Engineering on 7075-T6 Alclad, 1.0 mm thick, $R=0.06$, /8/. A considerable improvement in crack resistance can be noted. The results relevant to LT specimens are shown in fig. 16, compared with similar data obtained from 7075-T6 Alclad, 1.27 mm thick, $R=0.06$, /8/.

4.2 - Fracture toughness

For those materials, for which sufficiently wide specimens (i.e. 400 mm) were available, fracture toughness was evaluated at the end of fatigue crack propagation. The following average values of K_{IC} were obtained:

2091-T8, L, $t=1.6$ mm:	---> $K_{IC} = 103 \text{ MPa}\sqrt{\text{m}}$
2091-T8X, L, $t=1.6$ mm:	---> $K_{IC} = 106$ "
8090-T6, L, $t=1.6$, 3 mm:	---> $K_{IC} = 70$ "
2090-T8E41, L, $t=1.6$ mm:	---> $K_{IC} = 43$ "
2090-T8E41, LT, $t=1.6$ mm:	---> $K_{IC} = 40$ "

These results are quite interesting, compared with the following values, obtained in tests carried out at the Pisa Department of Aerospace Engineering, /9/, on traditional alloys:

2024-T3 Alclad, L, $t=1.27$ mm:	---> $K_{IC} = 98 \text{ MPa}\sqrt{\text{m}}$
7075-T6 Alclad, L, $t=1.27$ mm:	---> $K_{IC} = 71$ "
7075-T6 Alclad, LT, $t=1.27$ mm:	---> $K_{IC} = 60$ "

The damage-tolerant alloy 2091 shows a high toughness, i.e. considerable capability to carry loads in the presence of defects. The value obtained, specially for the T8X condition, must be considered as a lower limit of the actual characteristics, because the width of 400 mm of the panels proved to be inadequate for this material, according to the Feddersen theory, /10/.

On the contrary, the value obtained for 2090-T8E41 is very low and anyway much less than the comparison material, 7075-T6.

5. OPTICAL AND ELECTRON MICROSCOPY

Microstructural observations were carried out on most materials here presented, by using both optical and electron (SEM, TEM) microscopy. In the following, a brief description of the main results, obtained by electron microscopy, is summarized.

2091 Alloy

The 2091-T8 alloy exhibited an essentially recrystallized structure, although a band of unrecrystallized grains was observed at the central region of the sheet, fig. 17. The only age-hardening product detected by TEM was the δ' cubic phase (ordered, cubic orientation with respect to the matrix) with spherical precipitates of reduced dimensions, as shown in fig. 18. Moreover, the grain boundaries were practically free of precipitates, whilst many Fe-containing intermetallics were present within grains, as a probable consequence of recrystallization, fig. 17. Finally, a high density of helical and loop dislocations (these last mainly around δ' -particles) was evident as well as the presence of many unit dislocation pairs, fig. 19. These observations confirm the structural underaging related to the processing conditions (stretching followed by artificial ageing, 12 hours at 135°C).

Some preliminary studies were carried out on TEM samples extracted from regions very close to the tips of fatigue-propagated cracks, where large plastic deformations presumably took place. Fig. 20 shows the typical dislocation arrangement inside the matrix and it is worth noting that the plastic deformation is uniformly distributed within the grain with no evidence of localized slip bands.

Some overaging heat treatments were imposed to the as-received 2091-T8 alloy and extensive fractographic studies (SEM) were carried out on fatigue failed samples. The following denomination will be used to indicate different material conditions:

A: T8; B: T8 + 100 hrs at 135°C; C: T8 + 200 hrs at 135°C; D: T8 + 100 hrs at 190°C.

Fatigue failed regions exhibited some general features which were common to all investigated samples. In fact, in all samples this region consisted of areas with typical fatigue growth lines (fig. 21) mixed with plane areas characterized by the presence of marked slip lines, fig. 22. Many secondary cracks were frequently observed in this region of the samples. Moreover, ductile dimples formed in correspondence to intermetallic inclusions and X-ray microanalysis measurements (WDX) revealed that most of them were Fe-rich, although they were frequently coupled with Cu-containing particles. However, some differentiations were observed as far as fatigue striations are concerned, since their morphology changed from a ductile to a brittle appearance going from type A to type D samples and for this last set of specimens many intergranular fractures were in addition observed, fig. 23.

On the contrary, different heat treatment conditions induced marked differentiations

on the mechanism of static fracture of samples. In fact, type A samples exhibited an essentially transgranular static fracture with a high density of microdimples (fig. 24) and only rare presence of flat fracture facets. Moreover, in type A samples, serrated slip lines have been observed laying on many slip systems. The fracture mechanism in type B samples (following 100 hours at 135°C) was essentially the same, although with deeper microdimples (fig. 25) and sharper slip lines (fig. 26). Following 200 hours at 135 °C (type C samples), the static fracture mechanism becomes gradually intergranular with a high density of fracture flat facets (fig. 27), although many slip lines are still present, fig. 28. The static fracture becomes completely intergranular in type D samples, fig. 29. It is interesting to point out that the high density of gb precipitates was not associated, at least on the planes perpendicular to the load, with microdimples formation, fig. 30.

The strong variation in the observed static fracture was also evident by means of optical examinations: the fracture surface of type D samples was macroscopically perpendicular to the load direction, whilst in all the other ageing conditions the fracture surface was inclined about 45° vs. the load direction.

Similar fractographic observations have been made also on samples of 2091-T8X alloy of the same batch of material whose fatigue test results are shown in fig. 3. The fatigue failed region was characterized by a transgranular fracture with presence of ductile fatigue striations and formation of dimples originated by intermetallic inclusions (see fig. 31). The static fracture was transgranular and similar to that one previously described for 2091-T8 alloy, although an enhanced ductility can be associated with a greater density of tearing dimples and serrated slip lines, fig. 32.

2090 Alloy

Structural (TEM) and fractographic (SEM) observations for 2090-T8E41 alloy have been already reported in /5/ and only a brief summary will be reported here. The age-hardening precipitates consisted of spherical δ' (Al_2Li) and plate-like T_2' (θ'), T_1 (Al_2CuLi). Moreover, gb precipitates of reduced dimensions were observed with a practical absence of pfz formation at grain boundaries. The fractographic analysis of fatigue failed regions showed areas with ductile striations mixed with areas of rapid crack propagation. The region of static fracture consisted of surfaces exposed along both the orthogonal and parallel directions with respect to the load. Along these directions, the fracture was transgranular or intergranular (in this last case with a high density of ductile microdimples), respectively.

6. CORROSION PROPERTIES

D.A.S.R.S. cooperated in the research programme coordinated by the Italian C.N.R., studying the corrosion behaviour of Al-Li alloys. The whole programme, planned by D.A.S.R.S., has been articulated in four phases:

- (a) evaluation of the influence of surface finishing on the electrochemical behaviour of materials;
- (b) evaluation of the materials behaviour in relation to pH, O_2 , Cl^- ;
- (c) resistance of materials against particular corrosion kinds (SCC, galvanic, EXCO);
- (d) exposure of Al-Li alloys to standard corrosive environments.

The program is still in progress; only the results of the first phase will be presented. The following Al-Li alloys have been investigated: 2091-T8, 2091-T8X, 2090-T8E41 and 8090-T651, and, for comparison, also 2024-T3 and 7075-T6 reference alloys. The thickness was 1.6 mm for all the materials, which belonged to the same batches whose fatigue test results have been discussed in paragraph 3.

The different kinds of surface finishing assessed in this research are:

- surface roughness (emery papers or abrasive pastes with different average dimension of particles were used for polishing the samples);
- passivation condition in air (different time periods elapsed from final polishing to exposure to test solution).

These different surface finishing did not have a strong influence on the value of free corrosion potential, measured according to ASTM G 69 method. Table II summarizes the average results obtained and the examination of these data suggests the following corrosion rating:

2024-T3 < 2091-T8X < 2091-T8 < 2090-T8E41 < 7075-T6 < 8090-T651.

Potential measurements have been carried out not only on the sample external surface but also on internal planes which were obtained by repeated grinding of layers of 0.1 mm in thickness. In the case of 2091-T8 alloy, the free corrosion potentials shown in table III were obtained. All the other alloys did not show such variation through the thickness. A possible explanation of the behaviour of 2091-T8 can be ascribed to the different kinds and concentration of precipitates between surface and core of the material; this hypothesis has not yet been verified in this research program.

The Li weight percent content of the samples has been measured and correlated with average corrosion potential, as shown in table IV. Fig. 33 shows a plot of the data in the table and suggests the existence of an almost linear relationship between Li percent weight content and E_{corr} .

Some measurements have been carried out also in Na_2SO_4 0.1 M solution (O_2 or N_2 saturated) which, compared with the ASTM G 69 method, provides results that are more sensitive to the sample surface condition. The results obtained are affected by a large scatter but show that roughness has a stronger influence in the alloy behaviour than the presence of O_2 in the solution. A better surface finishing is, as expected, associated with an easier passivation. It is interesting to point out that 2090 and 8090 alloys show a larger scatter than the other Al-Li alloys, which can be explained by their higher reactivity shown before.

Some tests of phase (c) of the D.A.S.R.S. research programme have already been carried out, namely EXCO test (ASTM G 34-79). The preliminary evaluation of the results obtained so far shows a good agreement with the corrosion rating previously presented.

7. CONCLUSIONS

Many results concerning fatigue and Fracture Mechanics characterization of available Al-Li alloys have been presented and discussed; they must still be considered as preliminary, because these materials are still in the final stage of development. Besides, it must be pointed out the presence of intermetallic inclusions which appear in appreciable quantity, mainly in 2091, though inferior to what is commonly found in commercially available 2024. 2090 alloy is the nearest to being commercially available on an industrial basis. From these results, the following conclusions can be drawn:

- (a) fatigue behaviour does not yet seem to be adequate, compared with data from MIL-HDBK-5D. Anyway, 2090 substantially equals the fatigue performance of the substitution alloy, while for 2091 and 8090 lower stresses are required for equal life.
- (b) the crack-propagation characteristics seem excellent: all three alloys prove to be a substantial improvement on the traditional alloys.
- (c) fracture toughness is adequate for the 2091 alloy while further work is necessary for 8090 and even more for 2090.
- (d) SEM fractography shows that 2091-T8 exhibits adequate characteristics of ductile behaviour, which are not negatively affected by further permanence at 135°C for 100 hours; this treatment, on the contrary, brings to some improvements in fatigue and static strength.
- (e) preliminary assessment of corrosion behaviour shows intermediate properties between 2024 and 7075.

Al-Li alloys possess also other mechanical properties which make them very attractive for aerospace applications: the static strength is comparable to that of traditional alloys while the elastic modulus is about 8-10% higher. Besides, traditional anti-corrosion surface finishes can be applied with satisfactory results, /11/. An example of application of the data obtained so far in the research programme has been carried out in /5/, by means of compliance with simplified durability and damage tolerance requirements. The results show that, for appropriate structures, whose dimensions depend on compliance with damage-tolerance requirements, lighter solutions can be obtained.

All these features seem to lead to the conclusion that application of Al-Li alloys in aeronautical programs will soon take place, but some open questions still exist. From one side, military aircraft industry is much more interested in large thickness components, typically forgings, while, at the current level of development, only small gauge materials, i.e. sheets, show satisfactory characteristics. On the other side, commercial aircraft industry claim that the current high cost of Al-Li alloys (about three times the price of conventional alloys) together with a low fuel price drastically reduces their cost effectiveness, because Direct Operative Costs, the appropriate parameter for assessing a material with a view to application in commercial aircraft structures, do not reduce appreciably. Besides, production costs will rise due to the necessity of scraps segregation and separate processing. Therefore, it is very difficult to make predictions for the future, but the general feeling is that Al-Li alloys will find wide application, even if not in short term programs.

ACKNOWLEDGEMENT

The authors wish to thank Mr. S. Giaconi, post-graduate student, for assistance in the experimental activity and in the analysis of the results and Mr. R. Valleggi, graduating student, for assistance in fractographic observations.

REFERENCES

- /1/ - Hadcock R., Huber J.: 'Specific examples of aerospace applications of composites', paper in AGARD-LS-124, 'Practical considerations of design, fabrication and tests for composites materials', September 1982.
- /2/ - Wilson R.D.: 'Advanced composite development for large transport aircraft', paper presented at the 16th ICAS Congress, Jerusalem, August 1988.
- /3/ - Peterson R.E.: 'Stress concentration design factors', J. Wiley and Sons, N.Y., 1953.
- /4/ - Anon.: 'Description of a fighter aircraft loading standard for fatigue evaluation, FALSTAFF', joint report of F+W (CH), LBF (GER), NLR (NL) and IABG (GER), March 1976.
- /5/ - Cavallini G., Lazzeri L., Boschetti F., Solina A., De Sanctis M.: 'Fracture Mechanics and fatigue characterization of Aluminium-Litium alloys', paper presented at the 16th ICAS Congress, Jerusalem, August 1988.
- /6/ - Lanciotti A., Lazzeri L.: 'Problematiche di fatica in campo aeronautico: alcune attività svolte presso il Dipartimento di ingegneria Aerospaziale dell'Università di Pisa', presented at the 2nd Meeting 'New Technologies for Vertical Flight', Lugo di Romagna, May 1988.
- /7/ - Salvetti A., Cavallini G., Lazzeri L.: 'Fatigue crack growth under variable amplitude loading in built-up structures', Final technical report, European Research Office, United States Army, London, April 1982.
- /8/ - Lazzeri L.: 'Risultati delle prove di propagazione della fessura su pannelli piani non irrigiditi di cui alla AEPE n. 52062005 emessa dalla Soc. Aeritalia di Napoli', Pisa Dept. Aerospace Engineering, DDIA 83-8, Sept. 1983.
- /9/ - Frediani A.: 'Risultati delle prove di resistenza statica residua su pannelli piani non irrigiditi di cui alla AEPE n. 52062003 emessa dalla Soc. Aeritalia di Napoli', Pisa Department of Aerospace Engineering, DDIA 83-3, July 1983.
- /10/ - Peddersen C.E.: 'Evaluation and prediction of the residual strength of center cracked tension panels', ASTM STP 486, 1971, pp. 50-78.
- /11/ - Leonard R.W.: 'New developments in aluminium alloys and aluminium structures', Douglas paper 8073, May 1988.

Alloy	Li	Cu	Mg	Zr	Zn	Ti	Mn	Cr	Fe	Si	Al
2091	1.7-2.3	1.8-2.5	1.1-1.9	.04-.16	.25	.10	.10	.10	.30	.20	rem.
8090	2.3-2.6	1.0-1.4	.5-0.9	.10-.14	.25	.10	.10	.10	.30	.20	rem.
2090	1.9-2.6	2.4-3.0	.25	.08-.16	.10	.15	.05	.05	.12	.08	rem.

Table I - Nominal chemical composition of the Al-Li alloys evaluated in the program.

Al alloy	Ecorr (average)
2091-T8	-749.0 \pm 4.0 mV/SCE
2091-T8X	-738.0 \pm 1.5 mV/SCE
2090-T8E41	-798.0 \pm 8.6 mV/SCE
8090-T651	-817.7 \pm 4.4 mV/SCE
2024-T3	-675.2 \pm 14.3 mV/SCE
7075-T6	-799.0 \pm 20.0 mV/SCE

Table I - Average free corrosion potential measurements.

sample thickness	Ecorr
1.6 mm (*)	-743 mV/SCE
1.5 mm	-745 mV/SCE
1.4 mm	-755 mV/SCE
1.3 mm	-770 mV/SCE
1.2 mm	-790 mV/SCE

(*) as-received sample

Table III - Through the thickness variation of free corrosion potential in 2091-T8.

Alloy	2091-T8	2091-T8X	2090-T8E41	8090-T651
% Li	1.68	1.77	1.89	2.23
Ecorr (mV/SCE)	-738.0	-749.0	-798.0	-817.7

Table IV - Measured Li content and free corrosion potential.

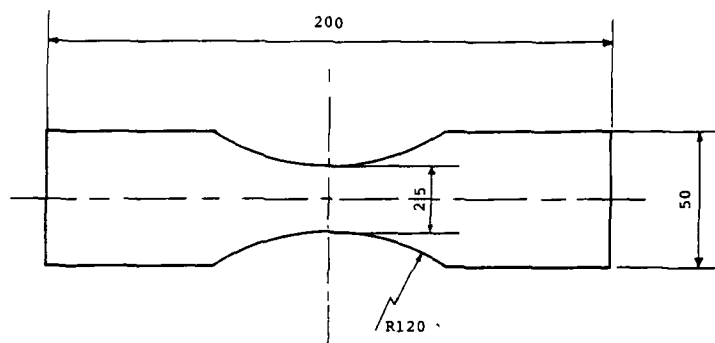


Fig. 1 - Unnotched specimen geometry.

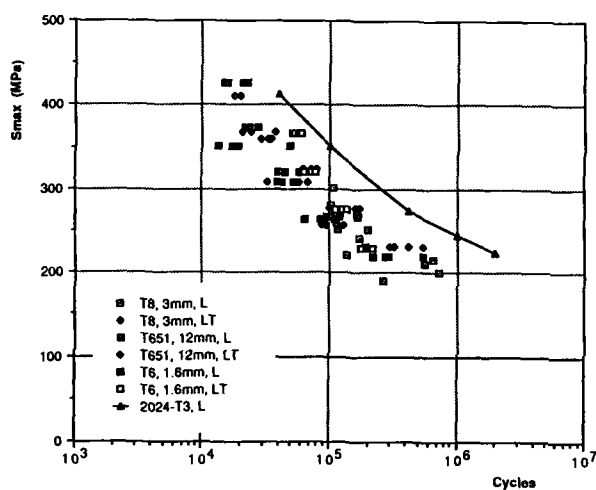
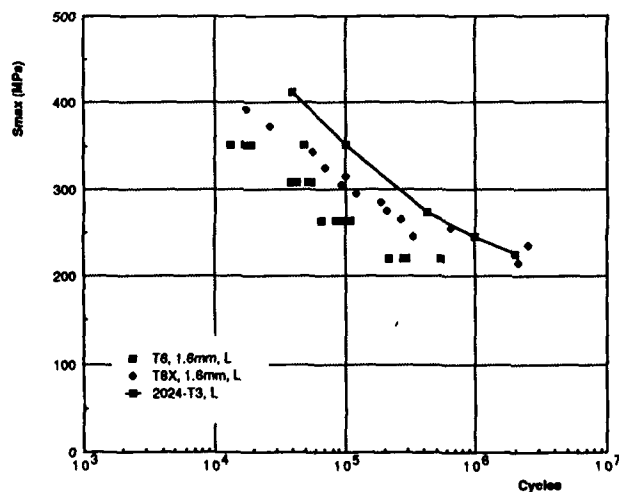


Fig. 2 - Fatigue test results of unnotched specimens made of 2091 alloy.

Fig. 3 - Fatigue test results of unnotched specimens made of 2091 alloy: comparison of two different producers.



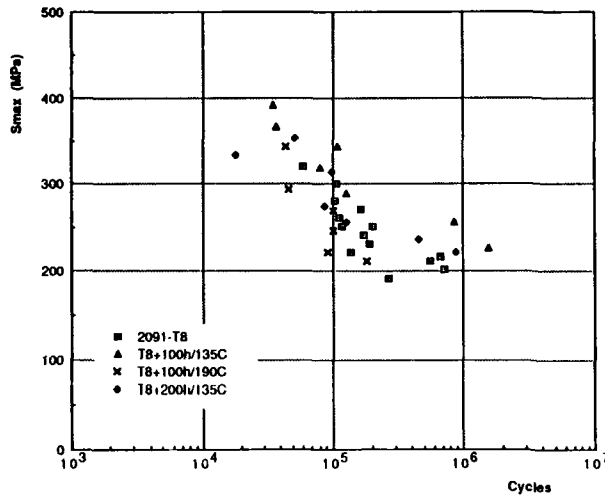


Fig. 4 - Influence of over-aging treatments on the fatigue strength of unnotched specimens made of 2091-T8, L, t=3.0 mm.

Fig. 5 - Fatigue test results of notched specimens made of 2091 alloy, (Kt=3.125).

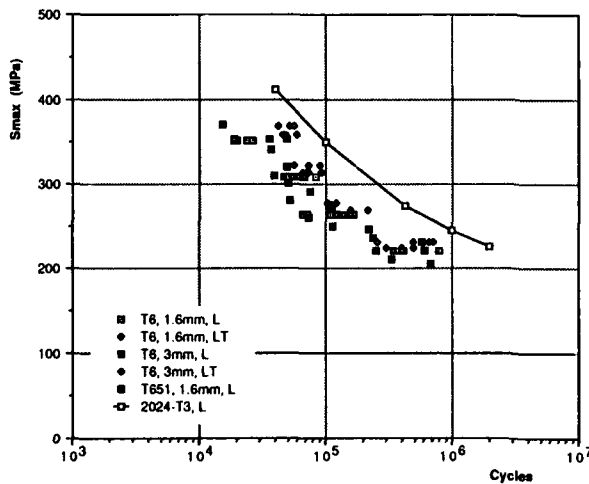
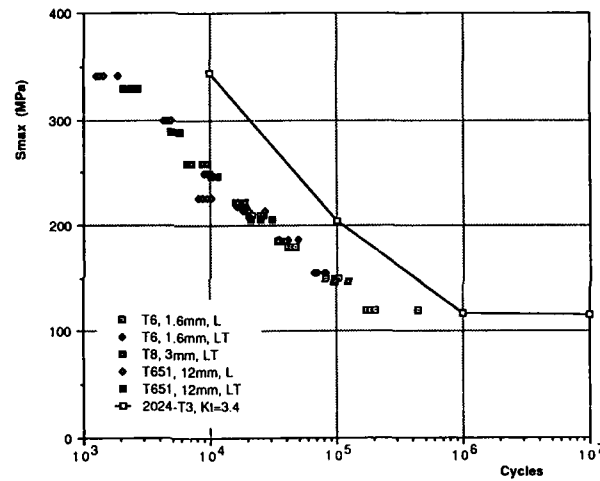


Fig. 6 - Fatigue test results of unnotched specimens made of 8090 alloy.

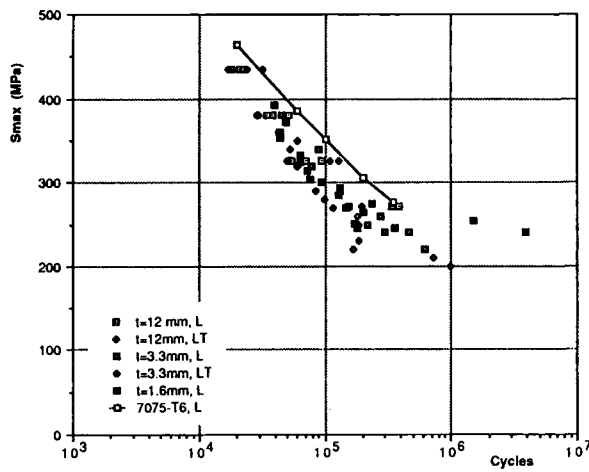


Fig. 7 - Fatigue test results of unnotched specimens made of 2090-T8E41 alloy.

Fig. 8 - Fatigue test results of notched specimens made of 2090-T8E41 alloy, ($K_t=3.125$).

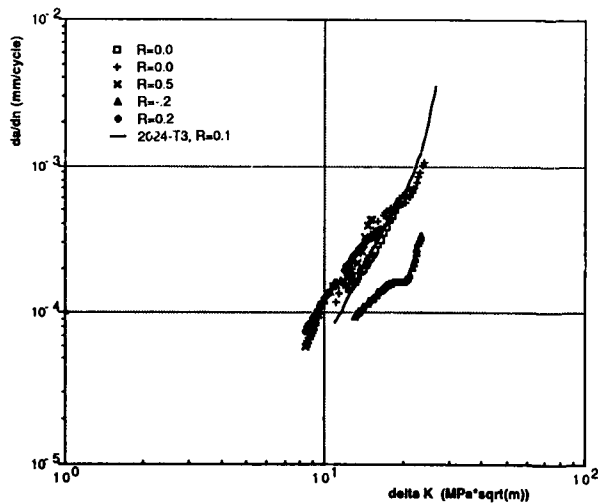
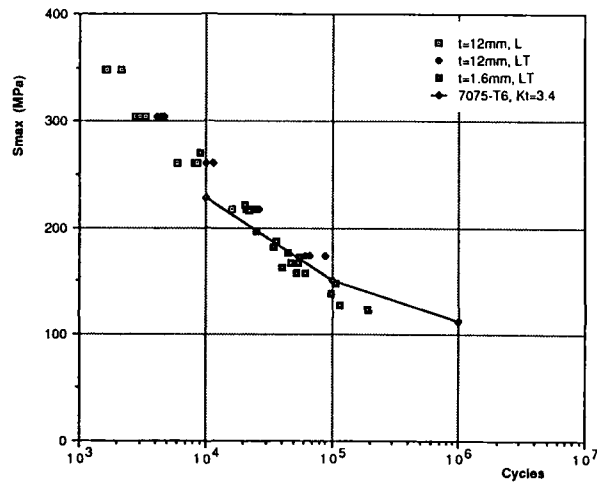


Fig. 9 - Fatigue crack propagation results, 2091-T8, L/T, $t=3.0$ mm.

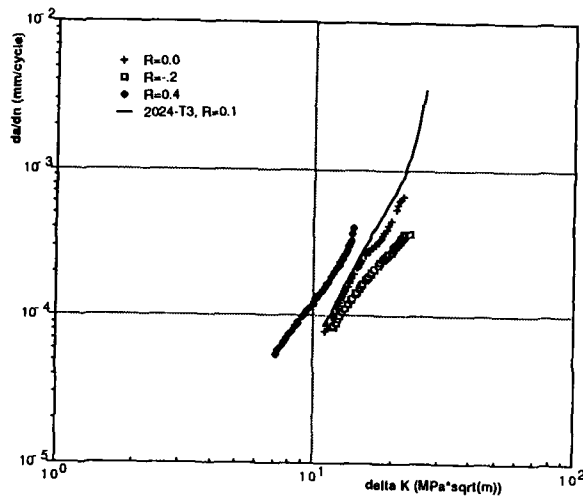


Fig. 10 - Constant amplitude fatigue crack propagation results, 2091-T8, T/L, $t=3.0$ mm.

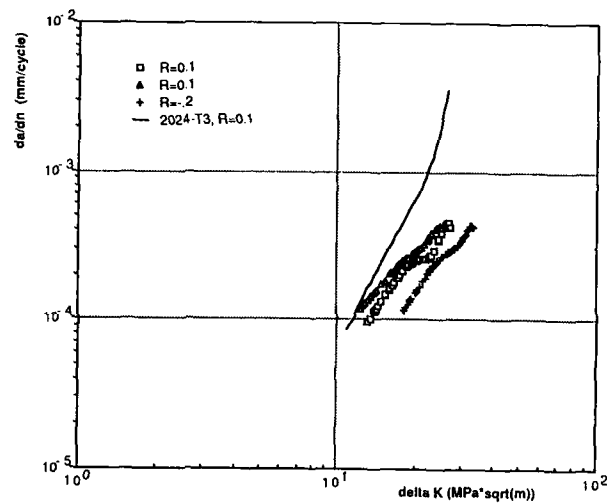


Fig. 11 - Constant amplitude fatigue crack propagation results, 2091-T8, L/T, $t=1.6$ mm.

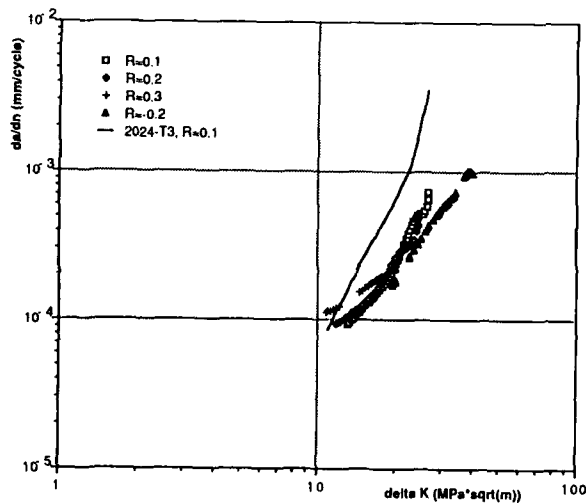


Fig. 12 - Constant amplitude fatigue crack propagation results, 2091-T8X (second producer), L/T, $t=1.6$ mm.

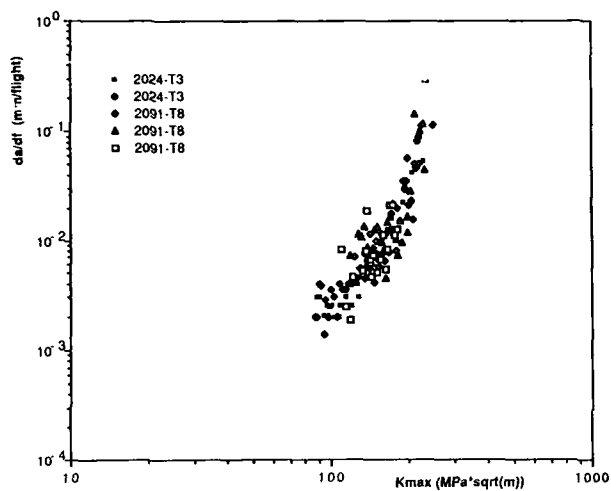


Fig. 13 - Results of crack propagation tests under FALSTAFF sequence ($S_{max}=235$ MPa), 2091-T8, L/T, $t=3.0$ mm.

Fig. 14 - Constant amplitude crack propagation results, 8090-T6, L/T, $R=0.1$

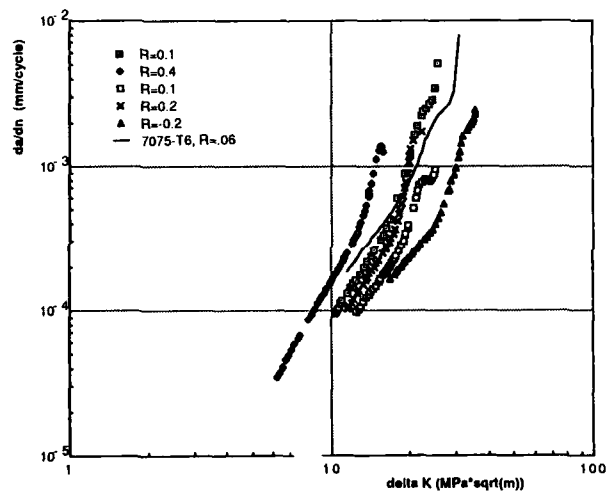
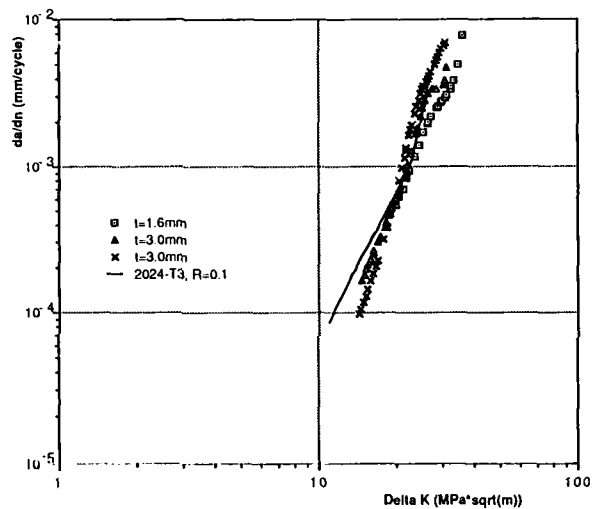


Fig. 15 - Constant amplitude crack propagation results, 2090-T8E41, L/T, $t=1.6$ mm.

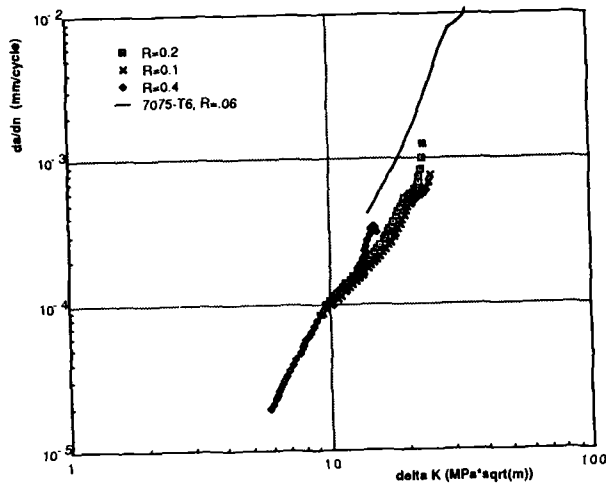


Fig. 16 - Constant amplitude crack propagation results, 2090-T8E41, T/L, $t=1.6$ mm.

Fig. 17 - Transmission electron micrograph of 2091-T8 alloy from the central region of the sheet.

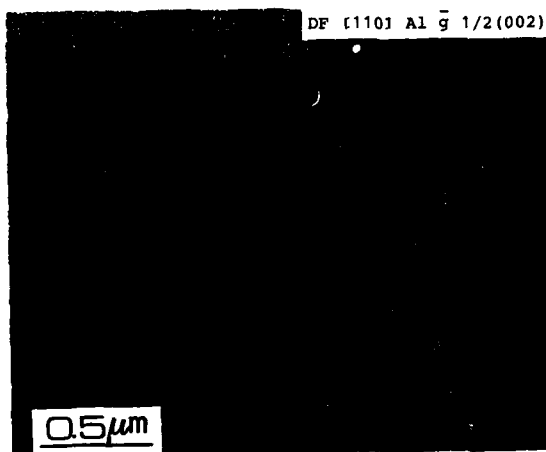
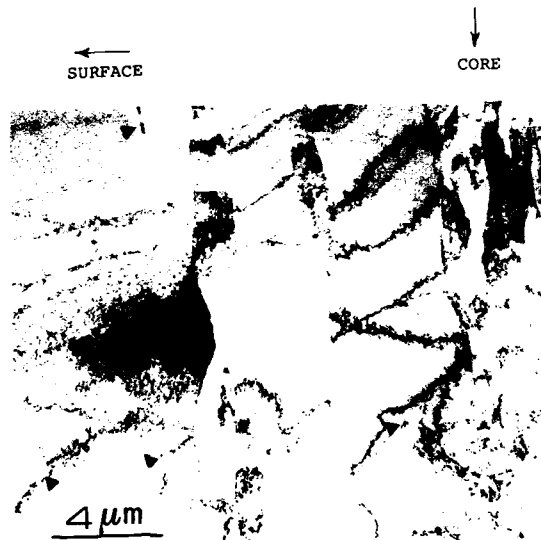


Fig. 18 - Electron micrograph (DF) showing the precipitation of spherical δ' particles.



Fig. 19 - Electron micrograph showing the dislocation arrangement in as-received 2091-T8 alloy (B close to [110]Al)

Fig. 20 - 2091-T8, region near a crack tip: high density of dislocations, homogeneously distributed

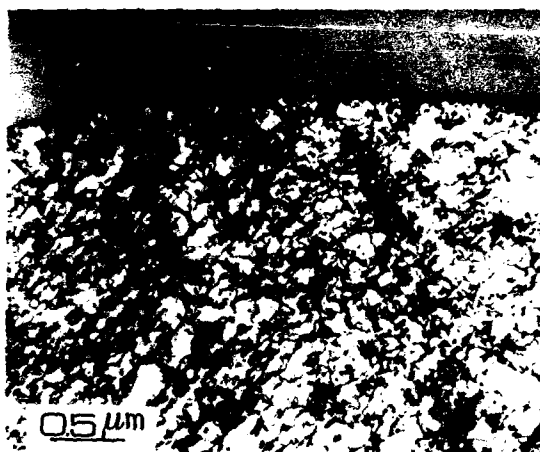


Fig. 21 - Type A sample. Particular of fatigue growth lines. Fatigue crack propagation is from left to right.



Fig. 22 - Type A sample. Representative view at intermediate magnification of fatigue failed region. Massive presence of slip lines with examples of secondary cracks

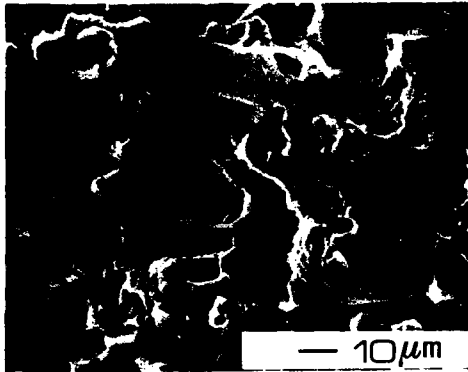


Fig. 23 - Type D sample. Fatigue failed region: intergranular fracture facets with secondary cracks.

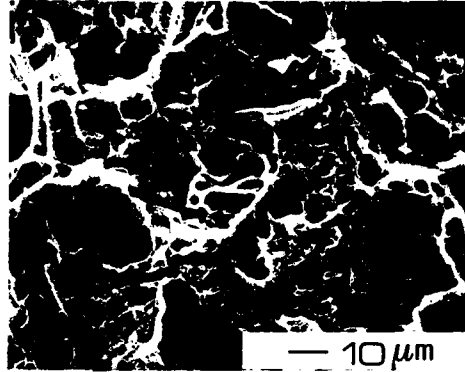


Fig. 24 - Type A sample. Static propagation region: transgranular fracture mode with a marked presence of microdimples.

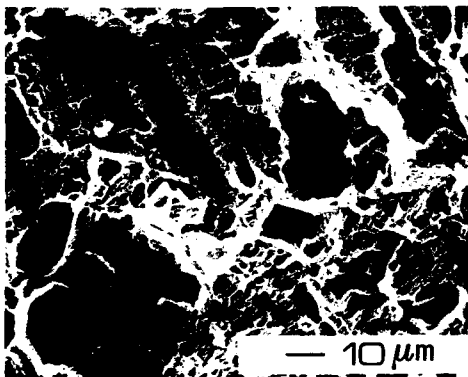


Fig. 25 - Type B sample in static propagation region. Fracture mechanism is similar to type A sample; more marked microdimples.

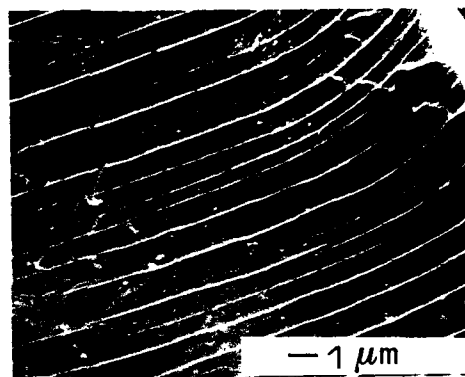


Fig. 26 - Sharp slip lines in static propagation region of type B sample.

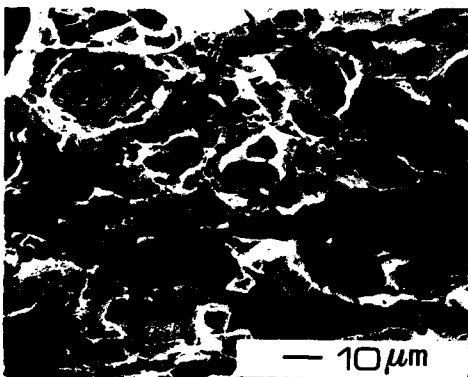


Fig. 27 - Type C sample. Fracture mechanism becomes gradually intergranular. Microdimples are still present on fractured facets.

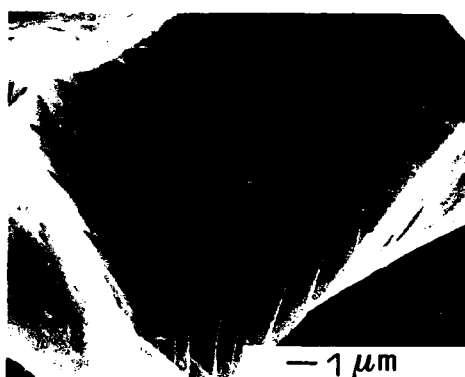


Fig. 28 - Type C sample. Slip lines on a grain boundary.

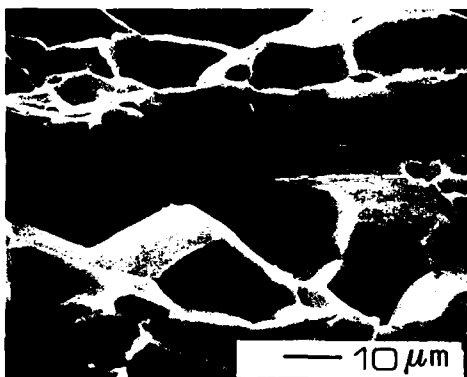


Fig. 29 - Type D sample. Static fracture becomes completely intergranular.

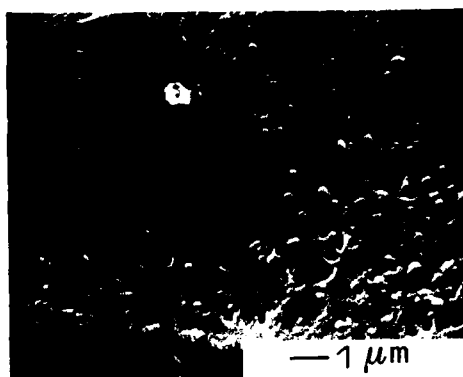


Fig. 30 - Type D sample. High magnification of a gb perpendicular to load application. High density of precipitates and absence of local ductile deformation are observed.



Fig. 31 - 2091-T8X sample. Fatigue failed region: transgranular fracture with ductile fatigue striation and dimples.

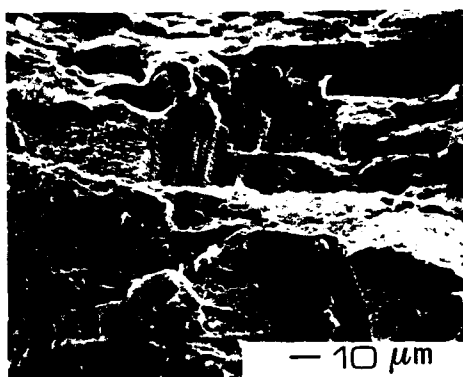


Fig. 32 - 2091-T8X sample in static fracture region: transgranular fracture similar to A, B and C samples. Serrated slip lines and tearing dimples.

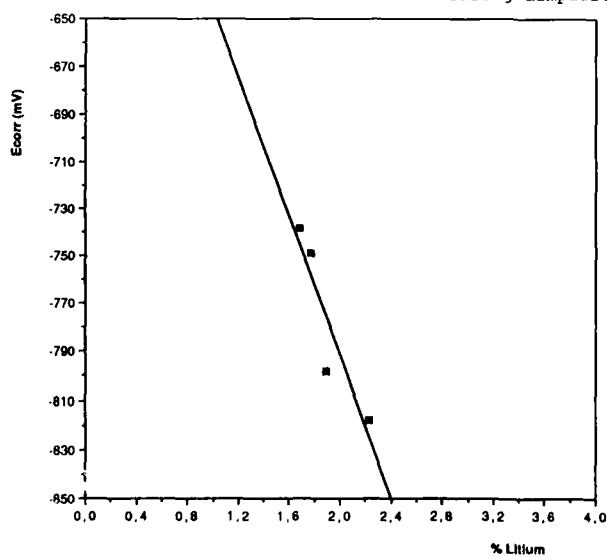


Fig. 33 - Free corrosion potential vs. percentage weight Li content.

FATIGUE AND FRACTURE BEHAVIOUR OF A PM AL-LI ALLOY

by

Rainer Schäfer
IABG
Einsteinstraße 20
D - 8012 Ottobrunn

and

Brigitte Weiss
Universität Wien
Währinger Straße 42
A - 1090 Wien

SUMMARY

The fatigue life, fatigue crack growth behaviour and fracture toughness properties of the experimental mechanically alloyed Al-Mg-Li alloy Al 905 XL were investigated. This material has been developed, above all, for being fabricated into structural components by forging.

HCF as well as LCF data were determined at room temperature and elevated temperature (180°C). Crack growth rates have been measured including near threshold behaviour.

The mean values of fatigue life at room temperature have been found to be slightly better than the values of conventional high strength aluminium alloys. Internal defects, however, like inclusions or pores, may reduce fatigue life considerably. At 180°C fatigue strength decreased to approximately 60% of room temperature values. Crack propagation was noticeably faster in Al 905 XL than in conventional ingot alloy 7075, for example. Fracture toughness tests finally resulted in rather low K_{IC} -values compared to conventional Al alloys.

1 INTRODUCTION

Basic problems in aluminium-lithium production techniques are up to now to achieve sufficient ductility and fracture toughness as well as to realize a fairly good homogeneity of structure and mechanical properties. Powder metallurgy and, in particular, mechanical alloying is expected to represent a promising technique for solving a part of these problems. The mechanical alloying technique supplies an extremely fine grained homogeneous structure with a large fraction of dispersoids which in combination results in good strength and may improve ductility /1,2/.

One attractive alloy system is Al-Mg-Li with additional content of carbon and oxygen. The material investigated here is an experimental alloy named Al 905 XL. The alloy contains 1.5% lithium which low level is chosen to avoid or minimize embrittling precipitates which may form during age hardening /3/.

The alloy needs not to be heat-treated, which means, that problems of component distortion and residual stresses due to heat treatment are avoided. As a further advantage the material shows uniform properties even throughout thick sections. A superior resistance to general corrosion results from the compositional uniformity in combination with the fine-grain structure /3,4,5/. In spite of the low lithium content the alloy offers a density advantage of 8% and a modulus advantage of 10% compared to conventional aluminium alloys.

The aim of the investigations described in the following was to evaluate some essential mechanical properties of Al 905 XL, in particular, to describe fatigue and fracture mechanics properties.

2 MATERIAL

The alloy Al 905 XL represents a mechanically alloyed PM aluminium alloy with 4% magnesium and 1.5% lithium. The chemical composition is given in Table 1.

The first sample used for taking specimens was an extruded rod, 175 mm long, with a diameter of 100 mm. As the material needs no additional heat treatment for developing properties the sample was used as delivered.

Another sample was a sector of a profile rolled ring produced during a forging trial programme. The ring was manufactured in the following steps: hydraulic press upsetting, hammer forging in dies, press upsetting and further hydraulic press upsetting into a die followed by ring rolling /4/. Shape and dimensions of the rolled ring and the extruded rod as well are shown in Figure 1, some basic mechanical and physical properties are compiled in Table 2.

The microstructure of the alloy in the as-extruded condition was characterized by light microscope (LM), transmission electron microscope (TEM) and scanning electron microscope (SEM) techniques /4,6/. The microstructure consists of predominantly uniform fine grains (grain size about 0.3 μm) but also some clusters of larger grains (up to 2 μm) have been detected. The microstructure is orientated in longitudinal direction, following the extrusion direction, see Figure 2. A large number of fine dispersoids (less than 400 nm) could be revealed, located primarily at grain boundaries resembling the former particle surfaces /4/.

Occasionally small clusters of sm_2 particles could be observed within individual grains. Some fine particles could be identified by electron diffraction techniques as Al_4C_3 , some larger inclusions (about 0.5 μm) as alpha or gamma Al_2O_3 . But also larger inclusions with dimensions up to 30 μm could be detected, Figures 3 and 4, mostly in the inner areas of the rod, with spherical or angular shape. By microanalysis some of these inclusions could be identified to contain Mg and Si, above all, probably in form of oxides

or carbides.

3 EXPERIMENTAL INVESTIGATIONS

3.1 SAMPLING

The extruded rod and the section of profile rolled ring were cut up and specimens for fatigue and fracture mechanics tests were machined.

For constant amplitude high cycle fatigue (HCF) and low cycle fatigue (LCF) tests unnotched round specimens were chosen. The specimens from the extruded rod had a 15 mm long gauge section with 4 mm diameter, the specimens from the profile rolled ring were hour-glass formed with 2.5 mm diameter. Most of the specimens were taken in longitudinal direction (L) corresponding to the extrusion direction and to the axis of the rolled ring respectively. The gauge sections of all fatigue specimens were mechanically polished in the longitudinal direction before testing.

For evaluating fracture toughness CT specimens according to ASTM-Standard E-399 were employed (16 mm thick from the extruded rod, 12 mm thick from the rolled ring). For fatigue crack growth measurements CT specimens according to ASTM E-647, 4 mm thick and 32 mm wide, were prepared, for measurements near threshold plate shaped specimens with a cross-section of 6 mm x 16 mm were used. Each specimen was mechanically polished in the mid-section. Subsequently a lance-shaped surface notch (2 mm long, 0.5 mm deep) was introduced by EDM to initiate growth of a semi-elliptical fatigue crack.

3.2 EXPERIMENTAL PROCEDURES

The load controlled HCF tests were carried out in an electromagnetic resonance testing machine with a test frequency of about 120 Hz at stress ratios of $R = -1$ and $R = 0$ at room temperature (R.T.) and 180°C as well. For additional tests with numbers of load cycles up to 10^9 an ultra-high frequency resonance testing system, operated at 20 kHz, was employed. Failure criterion was complete fracture of the specimens.

The strain controlled LCF tests were carried out in a mechanically loaded testing machine with a testing frequency of about 0.1 to 0.2 Hz (strain rate 3%/per second) at a strain ratio of $R = -1$ at room temperature and 180°C as well. Failure criterion was crack initiation announced by the beginning of the decrease of tension load and the beginning of buckling of the stress-strain hysteresis loop.

Fracture toughness tests have been carried out according to ASTM E-399 at room temperature.

For the determination of fatigue crack growth behaviour a servohydraulic testing machine, operated at test frequencies between 10 and 50 Hz, was used. Tests were carried out in laboratory air at room temperature with stress ratios of $R = 0.1$ and $R = 0.5$.

Fatigue crack growth data and threshold data (corresponding to $da/dN < 10^{-12}$ m/cycle) were obtained according to the pertinent ASTM recommendations in ASTM E-647 and E-740 respectively. Crack nucleation and fatigue crack growth were observed under stroboscopic illumination with the aid of a long focal-length microscope with a resolution of approximately 50 μ m. Crack growth in region II (Paris region) was measured by a PD (potential drop) method with special crack gauges. All specimens were L-T orientated.

Crack closure effects were determined by a strain gauge method [7] in which a miniature gauge (0.6 mm x 0.6 mm active area) is centered over the tip of the fatigue crack in the unloaded specimen (the penetration of adhesive into the crack can be prevented by vapor-depositing a narrow strip of carbon along the surface trace of the crack). Monotonic load-displacement curves were recorded under increasing tensile loading after completion of the threshold measurements. The closure stress (defined here as the stress of first contact between mating areas of the fracture surface) is revealed by the point of deviation from linearity of the elastic unloading compliance curve.

The stress intensity of semi-elliptical surface cracks were computed according to Raju and Newman [8]. To determine the shape factor of the semi-elliptical surface crack (required for this computation) all specimens were ruptured in tension after the measurements; the shape of the fatigue fracture surface was measured on fractographs. The effective threshold stress intensity value was computed according to

$$\Delta K_{th\ eff} = K_{max} - K_{op} \quad \text{for } K_{op} > K_{min} \quad \text{and } K_{op} = K_{cl}$$

3.3 RESULTS AND DISCUSSION

3.3.1 FATIGUE LIFE

The results of HCF-tests up to 10^7 cycles are shown in Figures 5 and 6, Figure 5 representing the results for $R = -1$ and Figure 6 those for $R = 0$.

There is a considerable effect from both the test temperature and the stress ratio on fatigue life. The fatigue limit at 10^7 cycles at 180°C is only approximately 60% of that at room temperature.

Comparing the results of tests on specimens from the extruded rod with those from the rolled ring, no significant difference can be recognized. It is, according to this, possible to forge the alloy without changing fatigue properties. The results from some spot checks with transverse specimens from the rolled ring agree with the results from longitudinal specimens as well, in consequence of the homogeneity of the material.

The fatigue life up to 10^9 cycles at $R = -1$ and 20 kHz is presented in Figure 7. A combination of 120 Hz and 20 kHz data in Figure 8 shows reasonable agreement, revealing, however, that fatigue limit

continues to decrease even beyond 10^7 cycles.

Figure 9 demonstrates that Al 905 XL provides rather good fatigue properties at R.T., compared to Al 7075 T6, for example, especially at high numbers of cycles. It has to be considered, however, that the results from Al 905 XL are based only on a small number of tests, for which reason the scatter cannot be estimated. But it is supposed that a special effect might determine the "lower boundary" of the scatter band: As mentioned above, the material contained several inclusions, see Figures 3 and 4, which, if situated in the fatigue stressed area, may have the effect of a sharp notch and consequently will reduce fatigue life.

This statement is supported by some individual test results marked by "I" in Figures 6, 7 and 9. These results represent relative low fatigue lives. Fractographic analysis of the fracture surfaces of these specimens revealed inclusions at the crack origin, see example in Figure 10, obviously accelerating crack initiation. In the fracture surfaces of some specimens the fatigue crack even was observed to start from inclusions situated far away from the specimen surface /6/.

The results of LCF tests are given in Figure 11 in the form of a diagram where the total strain amplitudes are plotted versus the number of cycles to crack initiation. These results show, just like the results of HCF tests, the detrimental influence of elevated temperature on the fatigue life of Al 905 XL. Another mechanically alloyed PM aluminium alloy, Al 9021 (without lithium), tested for comparison, is less sensitive to elevated temperature, see Figure 11. Similarly here, specimen orientation has no significant effect. Any runaways like those on HCF tests due to inclusions have not been found.

The monotonic and cyclic stress-strain curves in Figure 12 confirm the decrease of sustainable stress due to elevated temperature, but also present a nearly neutral stress strain behaviour, that means there is nearly no strain softening or hardening during LCF test. In addition, the LCF tests at 180°C revealed a special characteristic property of the material: increasing strain rate at 180°C increases alloy yield strength and, probably, also ultimate strength. To demonstrate this effect, the stress-strain curve from tensile tests with a strain rate of 10^{-4} /s is compared in Figure 12 to the monotonic and cyclic stress-strain curves from LCF tests with a strain rate of $3 \cdot 10^{-3}$ /s. Due to lack of test material this strain rate effect could not be studied more extensively. Similar observations, however, have been made with tests at 400°C in /3/.

3.3.2 FRACTURE TOUGHNESS AND CRACK PROPAGATION BEHAVIOUR

Fracture toughness tests on three specimens in L-T orientation and one specimen in C-R orientation from the extruded rod resulted in K_{IC} -values of 13 to 14 MPa \sqrt{m} , tests on two specimens from the rolled ring resulted in 11.5 MPa \sqrt{m} (L-T orientation) and 16 MPa \sqrt{m} (T-L orientation).

There is obviously no significant influence of specimen orientation in the extruded rod. The difference in the results from the rolled ring must also be regarded as not significant, since only one specimen each could be tested, due to lack of material.

The fracture toughness represented by the above values has to be regarded as rather low, compared to Al 9021 or to conventional ingot material Al 7075, see Figure 13. The fracture surfaces of the CT specimens from Al 905 XL consequently appear extremely brittle without any shear lips.

Higher K_{IC} -values, reported in /9/ from tests on other batches of Al 905 XL may point to problems of maintaining constant material properties in this actual state of development.

The results of crack propagation measurements at stress ratios of $R = 0.1$ and 0.5 at R.T. are presented in Figure 14, where crack propagation rates are plotted versus stress intensity ranges.

The influence of stress ratio on crack propagation rate is evident, becoming even more distinctive following increasing stress intensity range.

In Figure 15 the crack propagation rates evaluated for Al 905 XL are compared to those for two other mechanically alloyed PM aluminium alloys and for conventional ingot alloy Al 7075, showing that crack propagation is noticeably faster in Al 905 XL.

Threshold values of 905 XL were found to be virtually independent of the stress ratio R , see Figure 16. Since measuring the crack closure behaviour revealed no closure effect, the ΔK_{th} -value may be considered as to be equal to $\Delta K_{I,eff}$, which consequently remains also independent of R .

The absence of a closure contribution may be understood on the basis of SEM fractographs of the fatigue fracture surfaces in the near-threshold region: the fracture surfaces appear extremely flat, only a negligible increase in roughness may be discerned in specimens tested at $R > 0$. It may only be speculated that this small increase in roughness is the result of some plastic deformation ahead of the crack tip, causing the slight increase in ΔK_{th} at positive R -values.

The combined evaluation of the experimentally determined fatigue limit and effective threshold value in form of a Kitagawa-type diagramme /10,11/ resulted in a critical defect size for surface cracks about 80 μm crack depth, as shown in Figure 17. Following this, semi-elliptical surface cracks of smaller depth appear not to affect the plain bar fatigue limit. This value is, in the order of magnitude, in reasonable agreement with observations on the size of defects (pores or inclusions) which acted as nuclei for fatigue cracks.

4 CONCLUSIONS

The mechanically alloyed experimental PM Al-Li alloy Al 905 XL provides good tensile strength and fatigue life at room temperature, but only moderate values at elevated temperature. The material, however, can be fabricated into components by forging without loss of strength. Ductility and fracture toughness of the batches investigated here, are rather low, crack propagation rather fast compared to conventional ingot high strength Al alloys or to other mechanically alloyed PM aluminium alloys. There are, however, some signs that these properties could be improved in other batches of the alloy, pointing possibly to temporary problems of maintaining constant quality in this actual state of material and processing development.

Fatigue life appears to be governed by the size of defects and inclusions. A further increase of fatigue strength will be feasible if such defects can be avoided by improving processing methods.

ACKNOWLEDGEMENTS

The investigation work was supported by grants of the German BMFT and of the Austrian BMWF.

REFERENCES

- / 1 / Gilman, P.S.: The physical metallurgy of mechanically alloyed, dispersion-strengthened Al-Li-Mg and Al-Li-Cu alloys, in: Aluminium-Lithium Alloys II, TMS-AIME, Warrendale, PA, 1984, p. 485
- / 2 / Donachie, S.J. and P.S. Gilman: The microstructure and properties of Al-Mg-Li alloys prepared by mechanical alloying, in: Aluminium-Lithium Alloys II, TMS-AIME, Warrendale, PA, 1984, p. 507
- / 3 / Gilman, P.S., J.W. Brooks and P.J. Bridges: High temperature tensile properties of mechanically alloyed Al-Mg-Li alloys, in: Aluminium-Lithium Alloys III, The Institute of Metals, London, 1986, p. 112
- / 4 / Angus, H.C. and J.W. Brook: Microstructure and preliminary forging trials with mechanically alloyed aluminium alloy. Unpublished results from running investigations within COST 503 action
- / 5 / Schwellinger, P.: Corrosion of Al 4.5Mg1.5Li (Al 905 XL). Unpublished results from running investigations within COST 503 action
- / 6 / Kemper, H., B. Weiss, R. Stickler and R. Schäfer: Fatigue and fracture behaviour of a powder metallurgical Al-Li alloy, in: Proceedings of the 8th International Light Metals Congress, Leoben - Wien, 1987
- / 7 / Kemper, H., B. Weiss and R. Stickler: Effect of compressive portion of loading cycles on the near threshold fatigue closure behaviour in: Proceedings Fatigue -87, 1987
- / 8 / Raju, I.S. and J.C. Newman: Stress-intensity factors for a wide range of semi-elliptical surface cracks in finite-thickness plates. Eng. Fract. Mech. 11, No. 4, 1979, pp. 817-829
- / 9 / Bridges, P.J.: Summary of properties of mechanically alloyed aluminium-base alloys. INCO Alloy Prod. Ltd., Birmingham
- / 10 / Kitagawa, H. and S. Takahashi: Applicability of fracture mechanics to very small cracks or the cracks in the early stages. Proc. ICM-2, ASM, 1976, p. 627
- / 11 / Blom, A.F., A. Hedlund, W. Zhao, A. Fathulla, B. Weiss and R. Stickler: Short fatigue crack growth behaviour in Al 2024 and Al 7475, in: The Behaviour of Short Fatigue Cracks, EGF Pub. 1, 1986, Mechanical Engineering Publications, London, pp. 37-66
- / 12 / Military Standardization Handbook 5E. Department of Defense, USA, 1987
- / 13 / Schäfer, R. and W. Schütz: Mechanical properties and microstructure of high temperature PM aluminium alloys. IABG report TF-2320, 1988
- / 14 / E WL 3.4364 Teil 100, Mai 1988. Werkstoffhandbuch der Deutschen Luftfahrt Teil 1: Metallische Werkstoffe. Beuth Verlag, Berlin, Köln
- / 15 / Damage Tolerance Design Handbook. Metals and Ceramics Information Center Batelle, Columbus Laboratories, Columbus, Ohio, 1983

Table 1: Chemical composition of Al 905 XL

Element	Mg	Li	C	O ₂	Al
Nom. content, in weight %	4,0	1,5	1,1	0,8	Bal.

Table 2: Basic mechanical and physical properties of Al 905 XL

Product		extruded rod		rolled ring
Specimen orientation ²⁾		L	T	C
0,2 % yield strength $R_{p0,2}$ in MPa	R.T. 180 °C	480 220 ¹⁾	420	465
Tensile strength R_m in MPa	R.T. 180 °C	545 235 ¹⁾	515	555
Elongation A_5 in %	R.T. 180 °C	5 50 ¹⁾	5	6
Modulus E in GPa	R.T. 180 °C	78 65	77	81
Density ρ in g/cm ³		2,57		

¹⁾ Strain rate 10^{-4} /s. Values depend on strain rate.
For example, $R_{p0,2}$ increases to 275 MPa at $3 \cdot 10^{-3}$ /s.

²⁾ L: longitudinal, T: transverse, C: circumferential

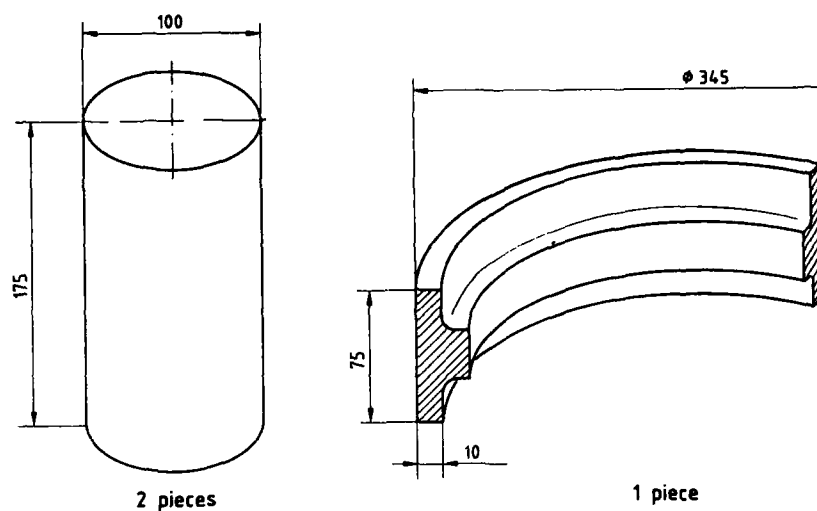


Figure 1: Extruded rod and sector of a profile rolled ring from Al 905 XL

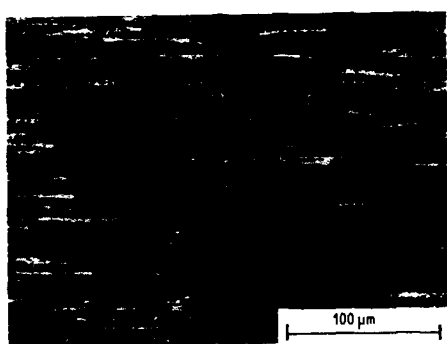


Figure 2: Microstructure of Al 905 XL, extruded rod, longitudinal direction

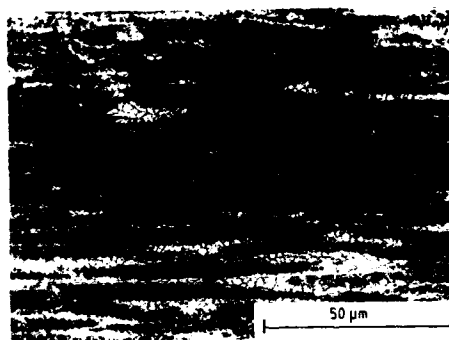


Figure 3: Microstructure of Al 905 XL, extruded rod, showing inclusions

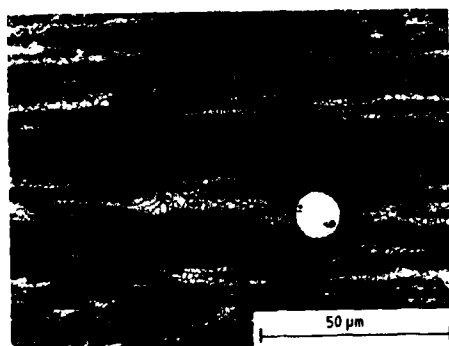


Figure 4 a

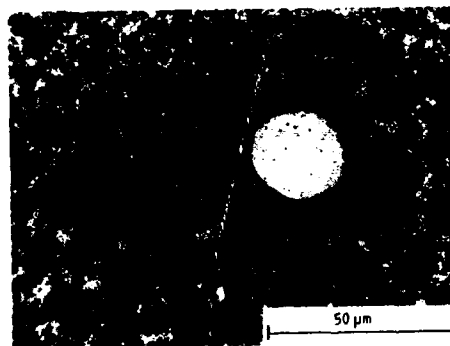


Figure 4 b

Figure 4 a and b: Microstructure of Al 905 XL, extruded rod, showing inclusions

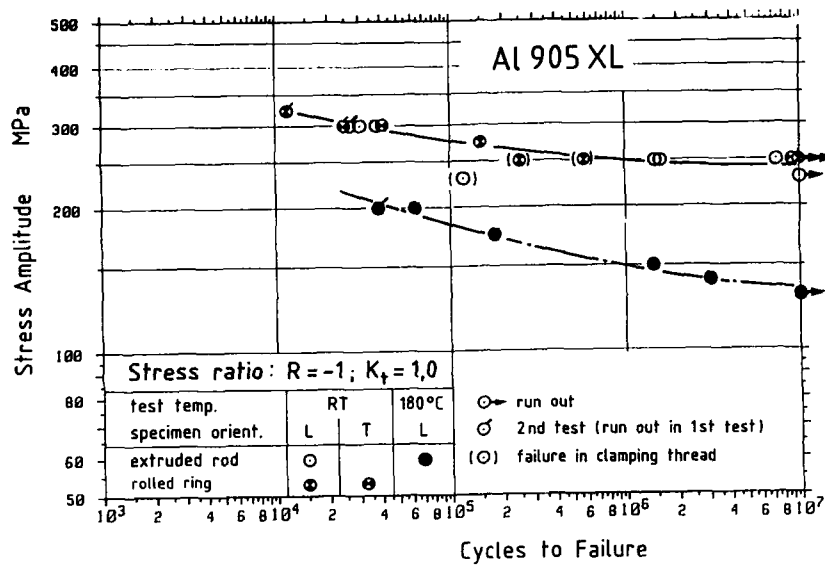


Figure 5: Results of HCF tests on Al 905 XL. Stress ratio $R = -1$, test frequency 120 Hz

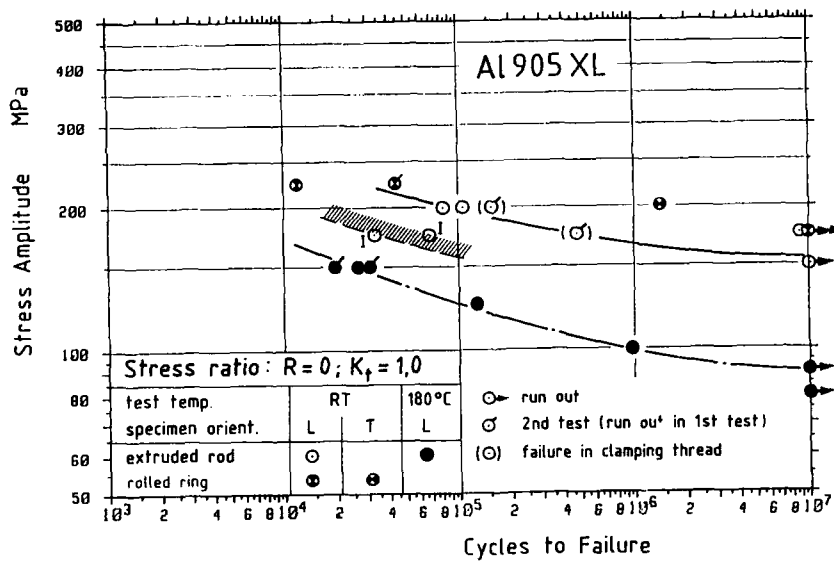


Figure 6: Results of HCF tests on Al 905 XL. Stress ratio $R = 0$, test frequency 120 Hz.

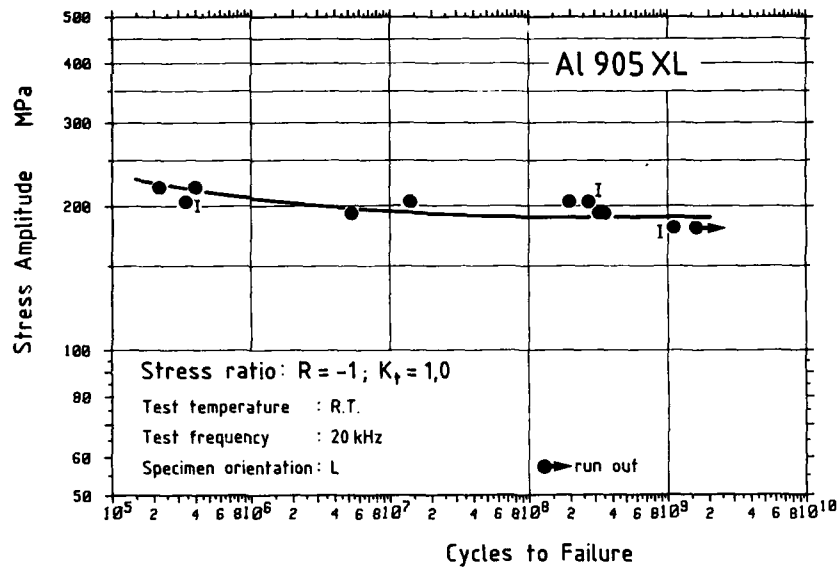


Figure 7: Results of HCF tests on Al 905 XL. Stress ratio $R = -1$, test frequency 20 kHz. Specimens from extruded rod

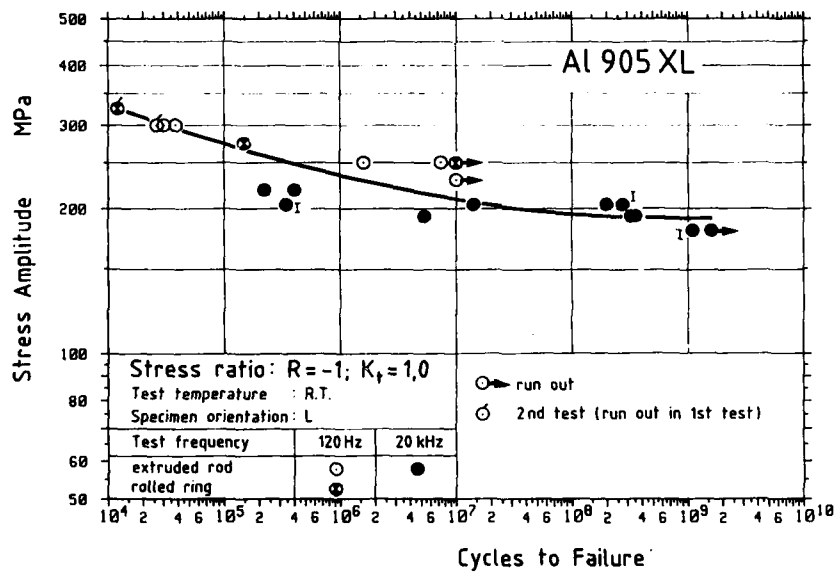


Figure 8: Combined results of HCF tests at 120 Hz and 20 kHz, cf Figures 5 and 7

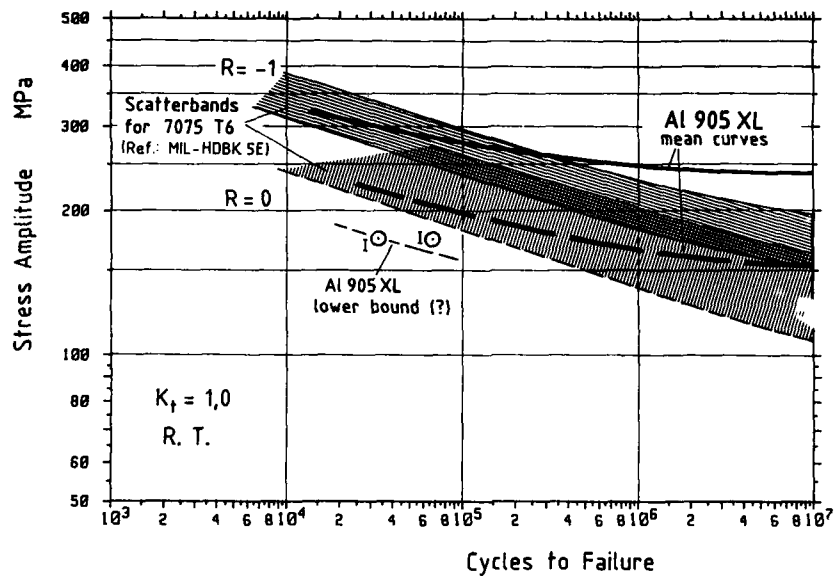


Figure 9: Fatigue life of Al 905 XL compared to Al 7075 T6 (values for 7075 T6 from / 12 /)

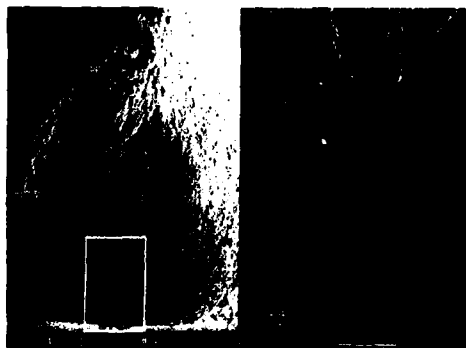


Figure 10: SEM fractograph from a fracture surface with an inclusion at the crack origin

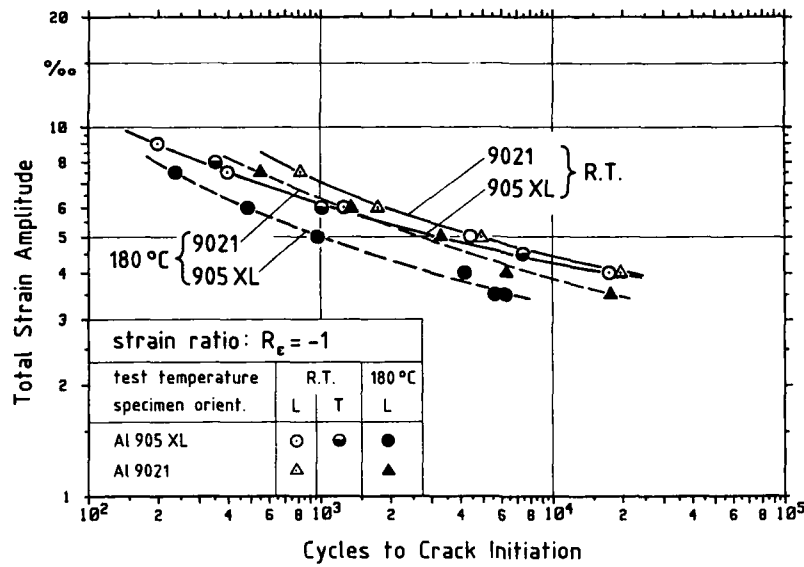


Figure 11: Results of strain-controlled LCF tests on specimens from extruded rod of Al 905 XL compared to Al 9021 (from / 13 /)

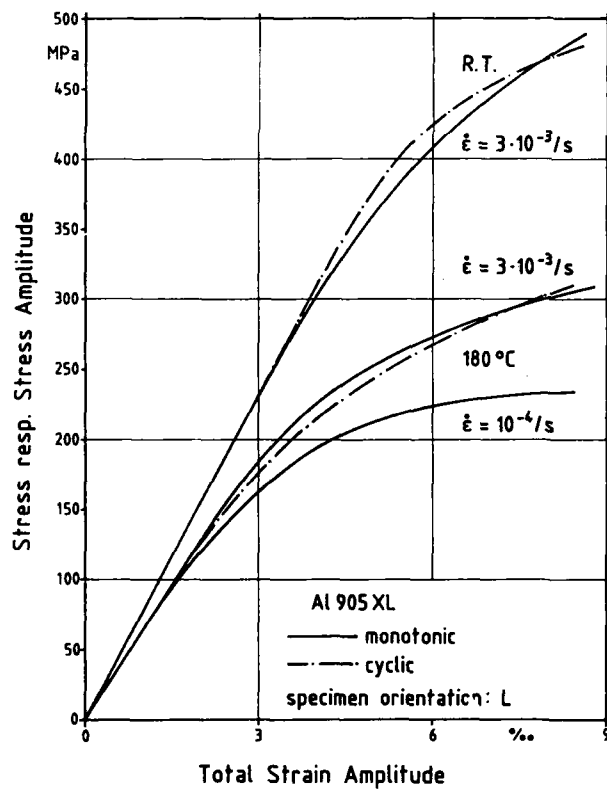


Figure 12: Monotonic and cyclic stress-strain curves

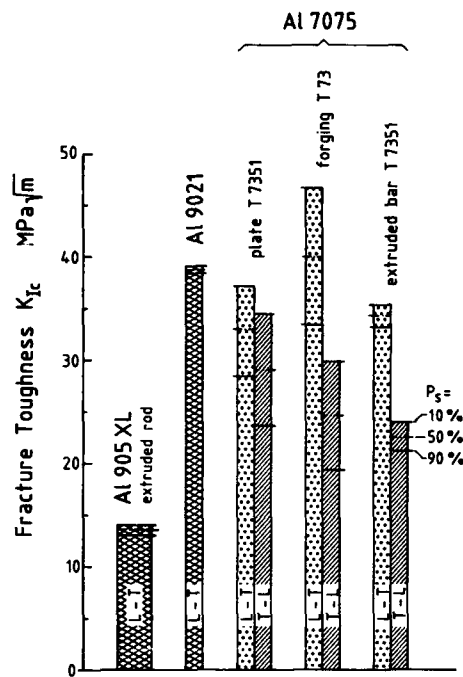


Figure 13: Fracture toughness of Al 905 XL compared to PM aluminium alloy Al 9021 (from / 13 /) and to conventional ingot alloy Al 7075 (from / 14 /)

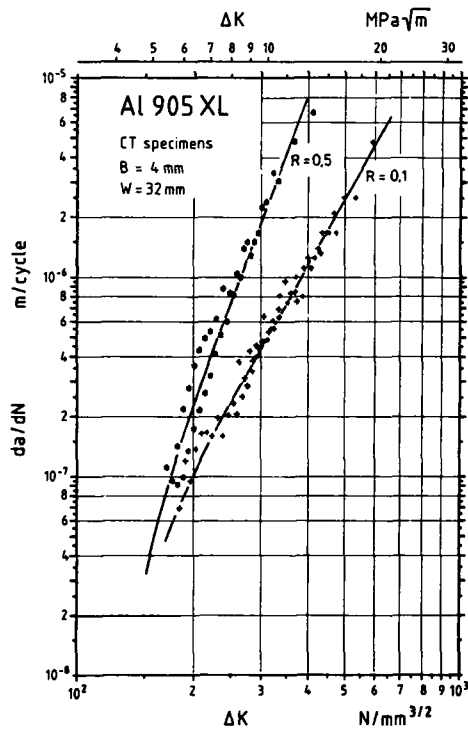


Figure 14: Fatigue crack propagation behaviour of Al 905 XL. Specimens from extruded rod

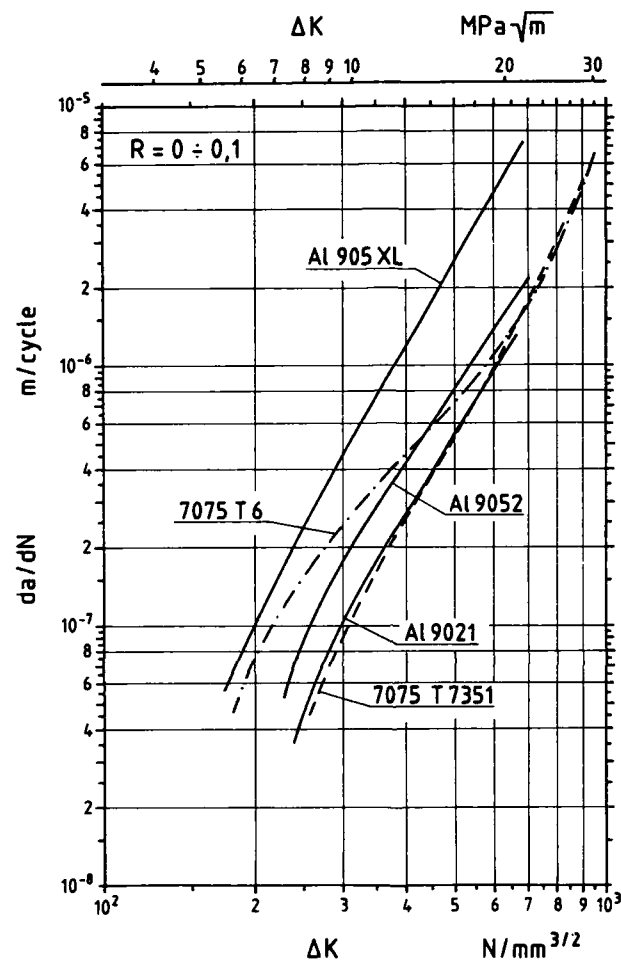


Figure 15: Fatigue crack propagation behaviour of Al 905 XL compared to PM aluminium alloys Al 9021 and Al 9052 (from / 13 /) and to conventional ingot alloy Al 7075 (from / 12 / and / 15 /). Stress ratio $R = 0 \dots 0,1$

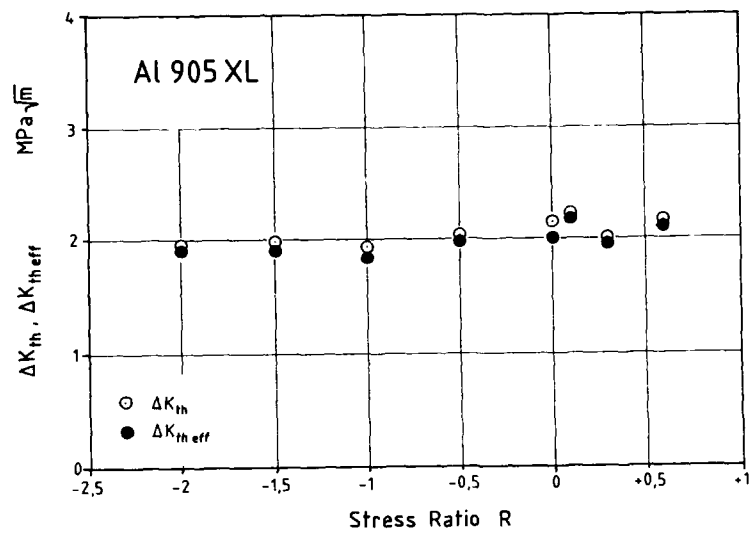


Figure 16: Threshold values of Al 905 XL as function of stress ratio

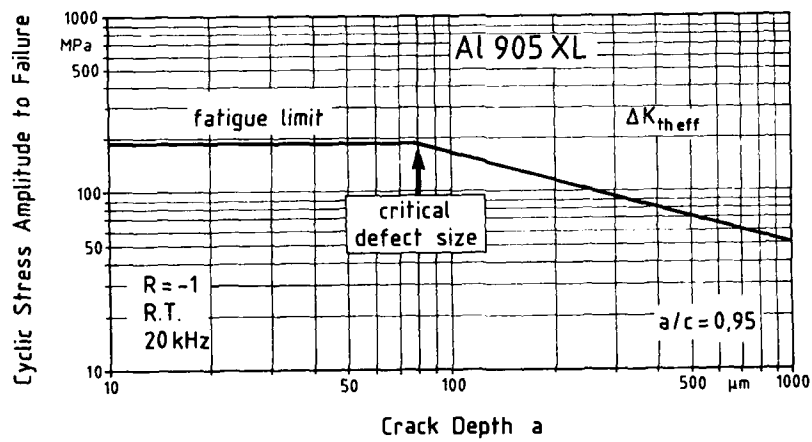


Figure 17: Estimation of critical defect size from a Kitagawa type diagram

FABRICATION OF TEST-ARTICLES FROM Al-Li 2091 FOR FOKKER 100

by

Dr. G.J.H. Vaessen, C. van Tilborgh and Dr. H.W. van Rooijen
 FOKKER AIRCRAFT B.V.
 Engineering Laboratories
 Material and Fabrication Technology
 P.O. Box 7600
 1117 ZJ Schiphol-Netherlands

SUMMARY

The technical requirements for introduction of Aluminium-Lithium-alloys in secondary structures of aircraft are formulated. The general corrosion behaviour, stress-corrosion properties and mechanical properties of the alloy 2091-T3 from Cegedur-Pechiney meet these requirements.

The successful fabrication of access doors in the underwing fairing of the Fokker 100 is described. The same manufacturing techniques as for 2024 can be used for 2091, i.e. machining, blanking, bending, chemical milling, surface pretreatments, adhesive bonding, solution heat treatment and drop hammer forming, stretch forming, painting and rivetting. Operational in-service trial on Fokker 100 and F28 operated by major airlines as Swissair and Garuda has started.

An estimate of the cost-effectiveness of the access doors out of 2091 is given.

1. INTRODUCTION

Aluminium-Lithium alloys have reached the near production stage. Since 1986 Cegedur-Pechiney offers the Al-Li alloy 2091 commercially for aerospace applications as a replacement for 2024 in the T3/T4 temper. A comprehensive research program has been conducted in close harmony between several research centres, aircraft manufacturers and material suppliers for establishing the ins and outs of a wide range of Al-Li alloys. The 2091-alloy promises a good combination of strength, ductility and formability [1], although an overall good compromise of properties equivalent to 2024-T3 has not yet been optimized.

As part of an Aircraft Technology Program, Fokker has decided to introduce the 2091-alloy on experimental base for secondary structural applications. As a consequence of this approach only the advantage of the 8% lower density is used and the profit of the 8% increased stiffness compared to the conventional alloys could be incorporated in a later stage. Fokker has selected access doors in the underwing fairing of the Fokker 100 to be manufactured out of 2091-sheet, figure 1, to gain experience in fabrication techniques in a production environment and to study the operational in-service behaviour of these panels. This paper describes the technical requirements for sheet used for secondary structures and the test results for 2091-T3. The used fabrication techniques are dealt with and an estimate of the cost-effectiveness of the access doors out of 2091 is given.

2. TECHNICAL REQUIREMENTS FOR SECONDARY STRUCTURES

For secondary structures, where strength, fatigue and damage-tolerance play no important role, still some technical requirements exist for unclad Al-Li sheets:

1. the alloy should possess good general corrosion behaviour, i.e. good exfoliation and intergranular corrosion resistance
2. stress-corrosion properties should be sufficient, because residual stresses can be introduced during forming operations (e.g. bending) in the final T3-condition or during rivetting.

If these properties are insufficient, this could mean that parts would have to be exchanged too often. These requirements also hold partially for clad Al-Li, because some parts are chemically milled to achieve their final form. Some strength of the alloy would be nice. May be the most important requirement is, that the fabrication processes used for conventional Al-alloys apply to Al-Li alloys and in turn manufacturing parts out of Al-Li does not negatively influence the production of conventional Al-alloys. E.g. surface pretreatment of Al-Li should be possible in the same solutions and baths as used for 2024 and 7075 and vice versa.

Table 1: Range of chemical composition in wt-% of delivered 2091-sheets with several thicknesses

Cu	Li	Mg	Zr	Si	Fe	Ti
1.95-2.1	1.8-2.1	1.5-1.6	0.07-0.09	0.02-0.04	0.03-0.04	0.02-0.07

3. MATERIAL AND PROPERTIES

The Al-Li alloy 2091-T3 was supplied as sheets with thicknesses of 1.2, 1.6, 2.0 and 3.0 mm and dimensions 2000 x 1000 mm² by Cegedur Pechiney in January 1987. The range of the chemical composition of the delivered sheets is given in table 1. (Mill-test certificate). Microstructural investigation shows a fully recrystallized microstructure for the 1.2 mm thick sheets with an equal grain size in rolling and transverse direction of 40 μ m, figure 2. The core of the 2.0 and 3.0 mm thick sheets show a somewhat elongated grain structure compared to the 1.2 mm thick sheet.

Micro-hardness measurements performed on a polished cross-section of the 1.2 mm thick sheet reveal a zone of about 100 μ m with lower hardness than the bulk, figure 3. 100 μ m beneath the surface the bulk hardness of HV120 is reached. The lower hardness can be attributed to a Li- and Mg-depletion in this zone, which occurs e.g. after solution heat treatment [2, 3].

The aging kinetics of 2091 material has been studied at ambient temperatures for establishing the forming requirements. Since time delays are experienced between the quenching and actual forming operations, there exists a need to examine the "time window" beyond which the alloy begins to increase in strength and decrease in ductility and the material's formability is reduced. Therefore, 2091 specimen, having a T3 delivery condition, were solutionized at 525°C for 20 minutes and quenched subsequently in cold running tap water within 7 seconds. The effect of the time window on 2091 was studied for a period more than 1 year. Figure 4 shows the natural aging data presented as ultimate tensile strength, yield tensile strength and elongation after fracture vs. aging time. Values in figure 4 are averages of 3 specimen tested according to ASTM E8-85a in rolling direction. It can be seen that the amount of additional hardening upto natural aging times of 4 days is neglectable, which in turn suggests that the formability would not be affected significantly in this period. The conventional alloy 2024 is usually being formed within 2h after quenching. From an aging time of 3 weeks onwards the effect of aging time on the ultimate and/or yield strength is relatively small and 2091 is stable. For 2024-T3/T42 the aged properties are achieved after 4 days exposure at ambient temperature. 2091-T4 reaches a strength level equivalent to 2024-T42 alclad. Tensile test specimen were cut under different directions to the rolling direction to investigate the mechanical anisotropy of the sheet. 2091 was tested in the T3-condition and in a naturally aged condition 1100 h after solution heat treatment and quenching as described above. Results given in figures 5 and 6 are averages of 3 observations. 2091-T3 shows a remarkable isotropy. The results of 2091-T4 show that the T3-condition does not contain much cold deformation.

The susceptibility of 2091-T3 to exfoliation corrosion was tested according to ASTM G34-79. Both specimen with the original surface, including a Li-depleted zone of approximately 100 μ m and specimen, after removal of a surface layer of 0.2 mm on both sides by mechanically grinding, were immersed for 48 and 96 h. Results in table 2 show a rating of N-P comparable with the ratings for 2024. There is no difference between the ratings for the surface and core of the material and immersion times of 48 and 96 h. Our experience with EXCO-testing of 2091 shows that exfoliation ratings of EA-ED occur after artificial aging in the temperature range 150°C to 200°C.

Table 2: Exfoliation corrosion of 1.2 mm sheet out of 2091-T3, according to ASTM G34-79

	2091-T3		2024-T3
	SURFACE	CORE	
EXCO 48H	N - P	N - P	N
EXCO 96H	N - P	P	N

The results of the intergranular corrosion test according to MIL-H-6088 are given in table 3. Again specimen including and excluding a Li-depleted zone were tested. The maximum depth of the intergranular attack and the percentage surface attack are for the specimen with the original surface comparable to those of 2024-T3 and for specimen without the Li-depleted zone lower than those of 2024-T3.

Table 3: Intergranular corrosion of 1.2 mm sheet out of 2091-T3, according to MIL-H-6088

	2091-T3		2024-T3
	SURFACE	CORE	
MAX. DEPTH (μ m)	145	63	150
% SURFACE ATTACK	20	2	36

The resistance to stress corrosion cracking of 2091-T3 was tested by NLR [4] using bent-beam strips loaded in the long transverse direction, which were alternately immersed in synthetic seawater. Specimen did not fail after 42 days at stress levels of 200 and 300 MPa. This behaviour is comparable to that of 2024-T3. The same results have been reported by [5] after alternate immersion testing in a 3.5% NaCl solution.

From the above mentioned properties it can be concluded, that 2091-T3 meets the technical requirements for secondary structures and an artificial aging to a T8X-condition is not necessary.

4. MANUFACTURING OF ACCESS DOORS

The manufacturing of 8 access doors can be divided into the following operations: machining, chemical treatments, forming and joining.

Machining:

All sheets were cut to the starting size by guillotine shearing. Drilling, milling, deburring and blanking can be carried out using the same techniques as for conventional Al-alloys. Chips from Al-Li which were generated during machining were separated from conventional chips. Fine turnings which fell on the ground were collected together with the normal garbage. Scrap separation is in a production environment indeed a problem, because cleaning the milling machines every time a part out of Al-Li has been machined takes too much time. Depending upon the amount of parts out of Al-Li, compared to the amount of parts out of conventional alloys the production logistic has to be changed.

Chemical treatments

The thicknesses of the sheets out of 2024-T3, which are up till now used for the two types of access doors are: 0.6, 0.8, 1.0, 1.2, 2.0 and 2.5 mm. Two-side chemical milling in a solution of NaOH with a concentration of 135 g/l at a temperature of 80°C has been used to reduce the original thickness of 2091-T3 from 1.2 mm to 0.6, 0.8 and 1.0 mm and from 3.0 mm to 2.5 mm. Chemical milling from two sides has been used, whenever possible, to remove the Li-depleted zone, so that an eventual recrystallization in this soft zone can not occur after a re-solution heat treatment. After chemical milling the surface roughness of 2091 is in the same range as for 2024. Sometimes deficiencies from the original surface were visible on the chemically milled surfaces.

The surface-pretreatment for adhesive bonding and painting consisted of [6]: CrO_3 - H_2SO_4 pickling for 20 min. and CrO_3 -anodizing (40/50V) according to DEF STAN 03/24. The thickness of the anodic layer is 3.5 μm and is equal to the layer formed on 2024-T3 clad. Also the pore-diameter of the oxide is in the range observed for 2024-T3 clad, i.e. 25 nm. Good adhesive bond strength have been achieved using the adhesive Redux 775 L/P. The quality of the adhesive bond of the parts has been tested using the Fokker-bondtester.

For painting standard techniques were used, which gave satisfactory quality of the painted products.

Forming operations

The minimum bend radii at a given sheet-thickness (R/t) have been calculated for several tempers and angles to the rolling direction [7] according to the formula [8]:

$$R = \frac{1}{t} \frac{1}{\epsilon - 1}$$

where $\epsilon = \ln L_0/L$ means the natural elongation, figure 7.

In figure 7 also the minimum R/t ratios for 2024-T3 and 2024-AQ/W according to Fokker specifications are indicated. The formability of 2091 increases (i.e. lower R/t values) in the order of tempers T8 (48h 150°C), T3, T42 (1100h naturally aged) and AQ/W. In all cases some anisotropy of R/t values is present. The R/t ratio for 2091-T3 is comparable to the ratio for 2024-T3. An example of the use of calculated R/t values in predicting the ability to form a simple shape in 1.6 mm 2091-T8 sheet, is shown in figure 8. In the L-direction of 2091-T8 sheet the elongation after fracture reaches a value of 12.7% and in LT-direction a value of 10.6%. This leads to different R/t ratios. A bending test was carried out using a radius of 6 mm (R/t=3.75). One part cracked due to the low elongation in LT-direction (R/t=4.5). Bending of some profiles for the access doors was performed in the T3-condition where R/t values of 3.3 and 4.2 were used, figures 9 and 10.

Stretching, pressing and drop hammer forming was performed in the AQ/W condition and here the advantage of the long AQ/W-time was pleasant. The drop hammer formed parts out of 2024 are fabricated starting from an O-condition and then before applying the last forming step solution heat treated to reach the strength of a T4 condition. The parts out of 2091 can be completely formed in the AQ/W condition without any problems.

Rivetting was carried out in standard practice using 2017 rivets.

Figures 9 and 10 show the parts from which 4 access doors of each type have been assembled. Figure 11 shows one set of complete access doors. The weight saving of the access doors out of Al-Li 2091 compared to the same products out of 2024 clad is 100-130 grams, meaning 8%. The access doors have been installed on Fokker 100 and Fokker F28 aircraft operated by Swissair and Garuda to gain experience with the in-service behaviour of Al-Li 2091 in different climatic environments. The doors are mounted on the right-hand side of the underwing fairing (figures 12 and 13), while similar panels on the left side are made out of 2024. In this way a realistic comparison can be made of the behaviour of both materials. Over the next five years the panels will be regularly inspected in order to establish the durability, i.e. bonding, painting, corrosion of 2091.

5. COST-EFFECTIVENESS

One of the major requirements for introduction of Al-Li alloys in Fokker aircraft is cost-effectiveness. Material utilization is a critical consideration in the cost effectiveness analysis, since the scrap on the shop floor does not reduce the weight of the airplane [9]. The cost-effectiveness of the two access doors out of Al-Li 2091 was analyzed using the following equation [9]:

$$\frac{\Delta C}{\Delta W} = \frac{F_r C_p - (1-F_r) C_o + (V_{so} - F_r V_{sn})(1-U)}{(1-F_r)U}$$

where ΔC = Change in material cost per unit weight of original purchased material (\$/kg)

ΔW = Weight reduction per unit weight of original purchased material (kg)

F_r = Density ratio = $\frac{\text{Density Al-Li}}{\text{Density conventional Al}}$

C_p = Material cost premium per unit weight = $C_n - C_o$

C = Material cost per unit weight (\$/kg)

V_s = Value of scrap per unit weight (\$/kg)

U = Material utilization factor = 1-scrap ratio

Subscript o = Original material

n = New material

In the analysis only material cost differences were taken into account, because the fabrication costs and nonrecurring costs (e.g. new tooling) are roughly identical for access doors out of 2091 and 2024. It is further assumed that the value of Al-Li scrap is the same as for 2024 and for the calculation of material utilization of the access doors out of 2091, that the same sheet thicknesses out of 2091 are available as for 2024. Figure 14 shows the results for two price-levels of 2091, i.e. 2.5 and 3.5 times the price of conventional 2024. The costs of 1 kg weight saved, which the aircraft manufacturer is willing to pay, is unique to each company and depends on many factors. In figure 14 two values of \$200 and \$400 per kg weight saved are indicated. Cost-effectiveness is the case for those parts of the curves below the horizontal lines of \$200 or \$400. The material utilization for the two access doors is in the range from 30% to 100%, which means that the access doors can only be introduced in a cost-effective way, if the price of Al-Li is 2.5 times the price of conventional Al and at a cost of \$350 per kg weight saved. At a price of Al-Li which is 3.5 times the price of conventional Al, a cost-effective introduction is difficult to achieve.

6. CONCLUSIONS

- The Al-Li alloy 2091-T3 in the product form sheet meets the technical requirements formulated for secondary structures. This means: adequate general corrosion resistance and stress-corrosion properties and mechanical properties, which are in the same range as those of 2024-T42 clad.
- Eight access doors in the fuselage lower fairing of Fokker 100 and Fokker F28 have been successfully manufactured out of 2091-T3, starting with sheet-thicknesses of 1.2, 2.0 and 3.0 mm.
- The manufacturing techniques used for the access doors out of 2024-T3 can be used with minor modifications for 2091-T3: cutting, deburring, drilling, milling, rolling, blanking, bending, chemical milling, surface pretreatment including chromic acid anodizing and adhesive bonding, drophammer forming and stretching in as-quenched conditions, painting, rivetting.
- In-service trial of access doors on Fokker 100 and Fokker F28 operated by major airlines as Swissair and Garuda has started.
- Cost-efficiency analysis for the access doors shows, that cost-effective introduction is possible if the price of the 2091 alloy would be 2.5 times the price of conventional 2024 and the costs to save 1 kg \$350.

7. REFERENCES

1. G. le Roy, Ph. Meyer and D. Constant
General review of Al-Li development at Pechiney
Al-Li symposium; March 22-24, 1988; Los Angeles, CA
2. C.J. Peel, B. Evans, C.A. Baker, D.A. Bennett, P.J. Gregson and H.M. Flower
The development and application of improved Aluminium-Lithium alloys.
"Aluminum-Lithium Alloys II", Proc. Second Intl. Conf., Monterey, CA, T.H. Sanders
and E.A. Starke, eds., TMS-AIME, Warrendale, PA, 1984, pp 363-392.
3. S. Fox, H.M. Flower and D.S. McDermid
Formation of solute depleted surfaces in Al-Li-Cu-Mg-Zr alloys and their influence
on mechanical properties.
"Aluminium-Lithium Alloys III", Proc. Third Intl. Conf., Oxford, U.K., C. Baker,
P.J. Gregson, S.J. Harris and C.J. Peel eds, Institute of Metals, London, U.K, 1986,
pp. 263-272.
4. L. Schra and J.A.M. Boogers
Corrosion properties of Al-Li-Cu-Mg-Zr sheet materials
National Aerospace Laboratory NLR, The Netherlands, Report no. NLR TR88047L.
5. F.S. Lin, Y. Moji, W.E. Quist and D.V. Badger
Corrosion resistance of Aluminium-Lithium alloys
"4th International Aluminium Lithium Conference", G. Champier, B. Dubost,
D. Miannay, L. Sabetay eds., Journal de Physique, 1987, pp. C3 904-911.
6. R. Exalto and J. Koning
Adhesive Bonding of Al-Cu-Li Alloy 2091-T8
Fokker report no. R-3541, 1986
7. C. van Tilborgh and J. Koning
Formability of Al-Li CP274-2091 material
Fokker report no. R-3505, 1988
8. W.W. Wood et al
Theoretical Formability, Volumes I and II
Vought Aeronautics, Texas, August 1961.
9. P.W. Scott
The cost effectiveness of weight reduction by advanced material substitution.
SAWE Journal Fall/Winter 1986 Paper no. 1693, pp 55-71

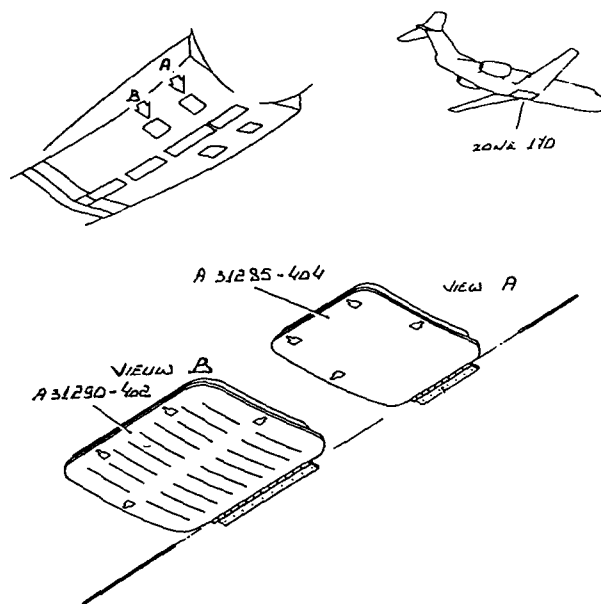
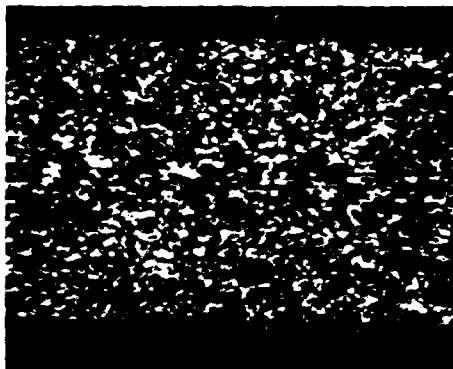
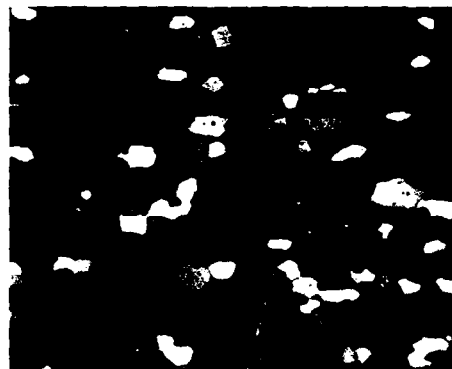


Fig. 1: View of the access doors and location in the underwing fairing of Fokker 100



Magn.: 50x



Magn.: 200x

Fig. 2: Microstructure (L-ST-plane) of 1.2 mm thick sheet out of 2091-T3

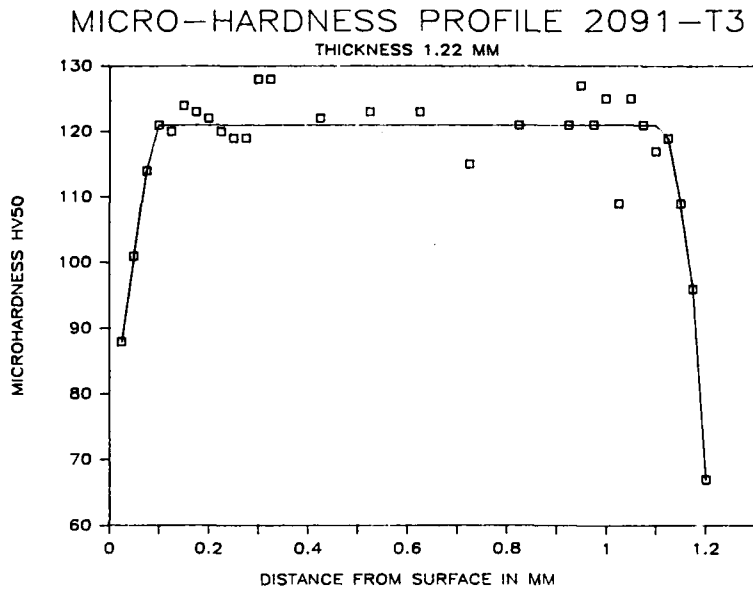


Fig. 3: Micro-hardness profile (50 gf) across thickness of 2091-T3 sheet

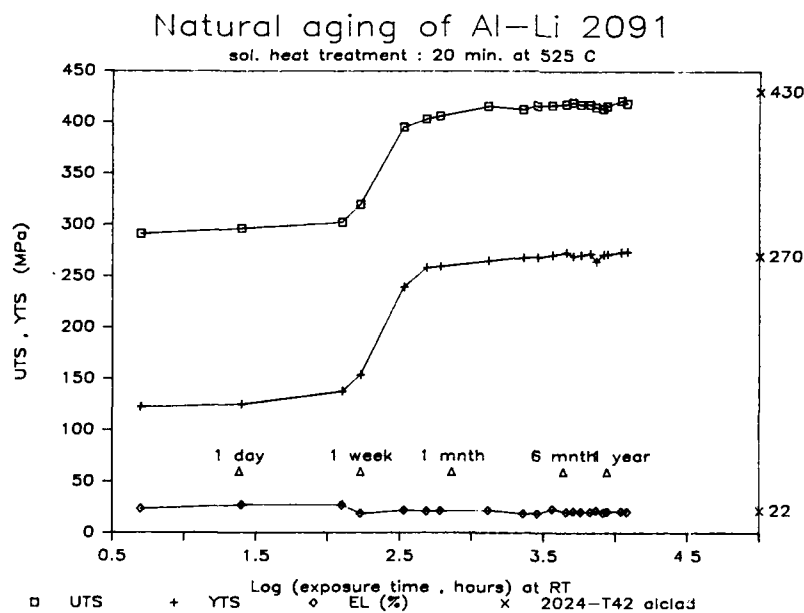


Fig. 4: Natural aging response of Al-Li 2091

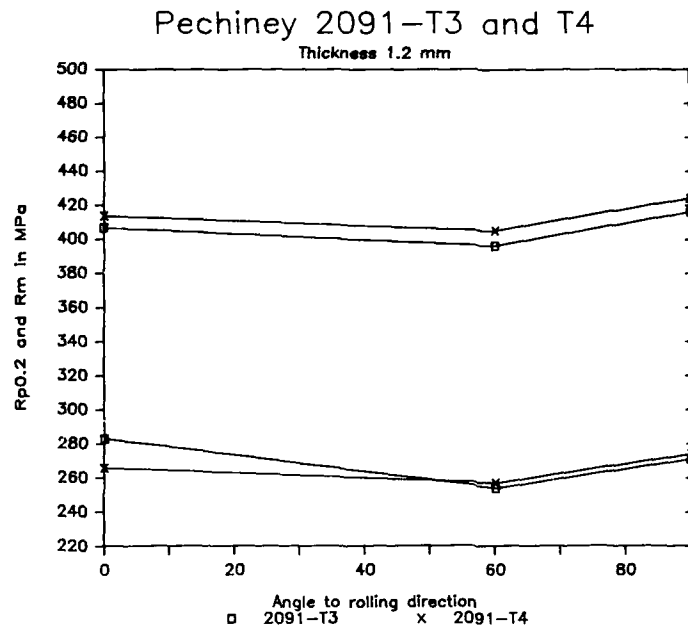


Fig. 5: Mechanical anisotropy of 2091-T3 and T4

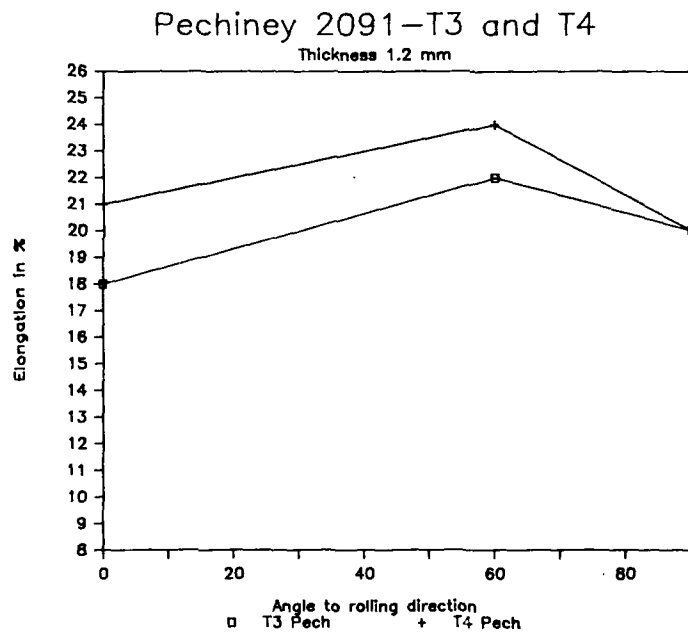


Fig. 6: Anisotropy of elongation after fracture of 2091-T3 and T4

MINIMUM BENDING RADIUS / SHEET GAUGE

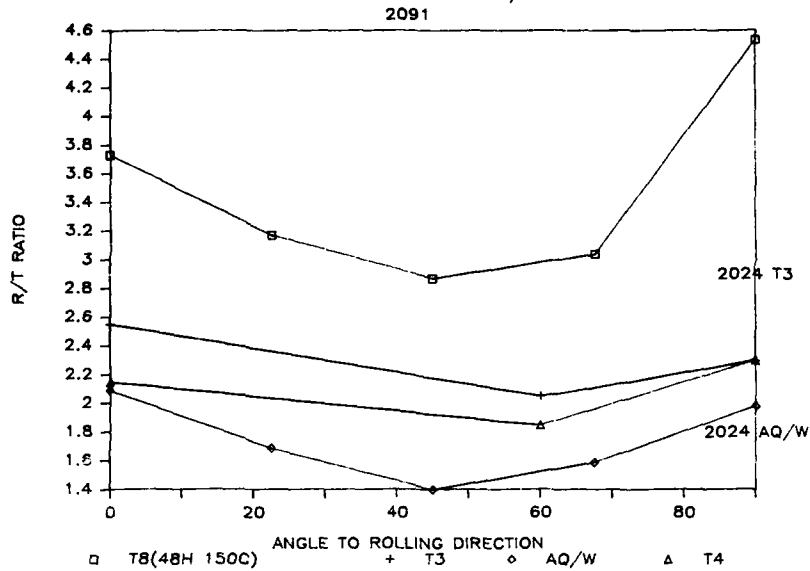


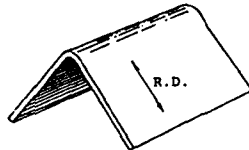
Fig. 7: Calculated minimum bending radii at a given sheet thickness as a function of the angle to the rolling direction and temper of 2091

BENDING OF 2091-T8 (48H 150°C)

L-DIRECTION

AS0 = 12.7 %

R/T = 3.7



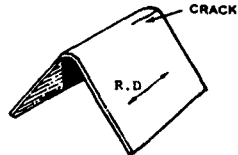
RADIUS 6 MM

BENDANGLE 100°

LT-DIRECTION

AS0 = 10.6 %

R/T = 4.5



RADIUS 6 MM

BENDANGLE 47°

TEST-RATIO

$R/T = (6/1.6) = 3.75$

Fig. 8: Experimental verification of calculated R/t-ratios

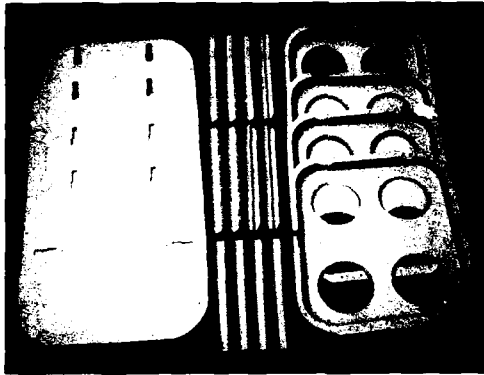


Fig. 9: Parts out of 2091 before assembling access doors, type A 31285-404

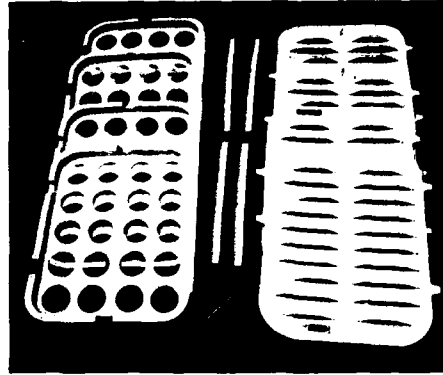


Fig. 10: Parts out of 2091 before assembling access doors, type A 31290-402

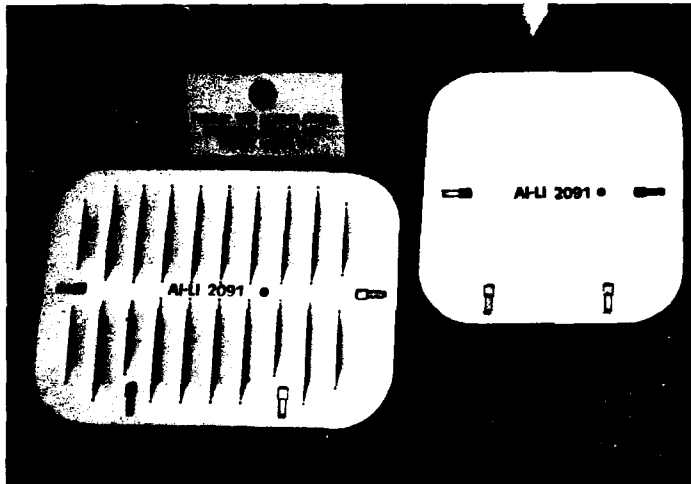
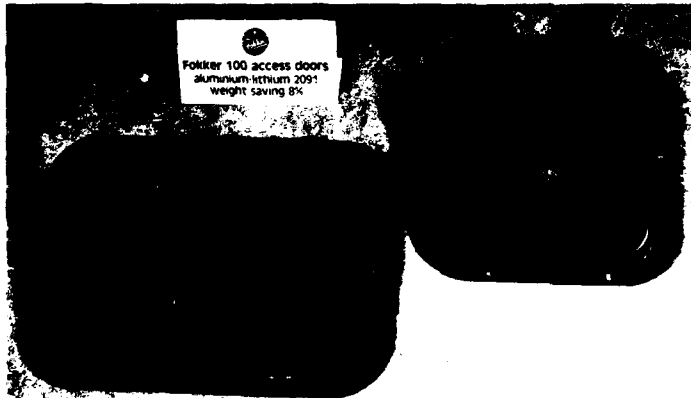


Fig. 11: Two types of access doors out of Al-Li 2091



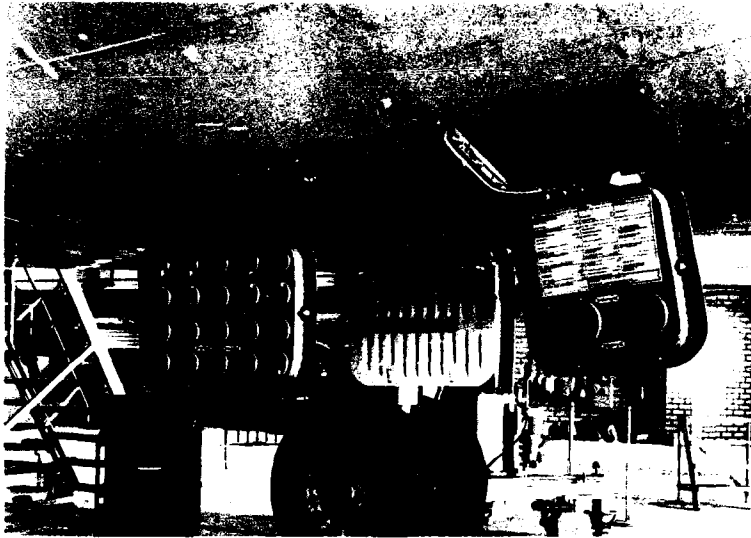


Fig. 12: Access doors out of Al-Li 2091 installed on a Fokker 100 for Swissair

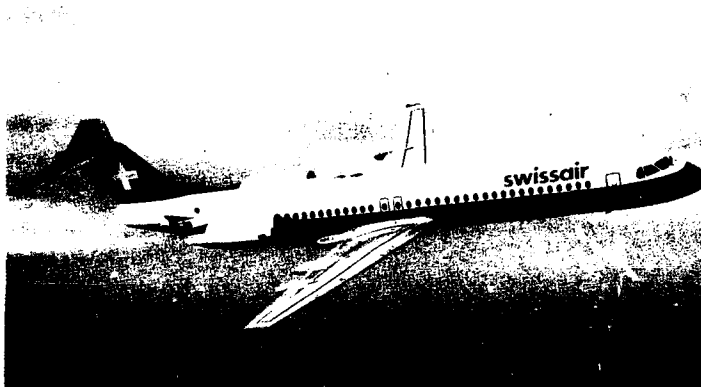


Fig. 13: In-service trial of access doors out of Al-Li 2091 on Fokker 100 for Swissair and on Fokker F28 from Garuda has started

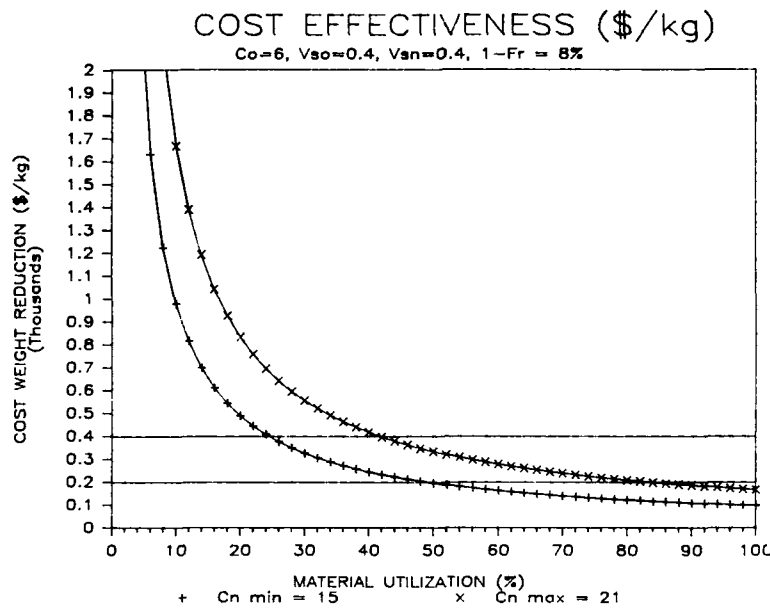


Fig. 14. Cost-effectiveness analysis of access doors out of .091, calculated for two price levels C_n of 2091, which are 2.5 and 3.5 times the price of conventional 2024 (C_0). Two values for the costs of 1 kg weight saved are indicated.

MISE EN OEUVRE DE L'ALLIAGE 2091

par J. BEVALOT
 AVIONS MARCEL DASSAULT-BREGUET AVIATION
 78 Quai Marcel Dassault
 92214 SAINT-CLOUD

Dans l'objectif de remplacer sur avion le 2024 T3 en produits minces par l'alliage aluminium-lithium 2091, des essais de fabrication ont été effectués et ont abouti à la production d'ensembles structuraux amenant ainsi une première expérience industrielle. A partir de gammes existantes pour le 2024 ont été déterminées et optimisées des gammes applicables au 2091. De cette étude les principales conclusions suivantes ont été tirées. Le 2091 a une plus grande capacité de déformation donnant la possibilité de former des panneaux en 1 passe sur trempe fraîche au lieu de 2 passes pour le 2024. Le temps de travail sur trempe fraîche est très important pour le 2091 : de l'ordre de 3 jours. Par ailleurs, on a enregistré une très bonne soudabilité par point, une bonne usinabilité chimique et une bonne transposabilité des gammes de protection actuelles utilisées sur le 2024.

Etant donné l'intérêt du remplacement du 2024-T3 par l'Al-Li 2091 T8X (gain en module de 7 % avec un gain de densité de 8 %) nous nous sommes attachés à définir les domaines de mise en oeuvre de cet alliage en produits minces par des essais technologiques.

PECHINEY nous avait au préalable fourni un certain nombre d'informations sur la maturation de l'alliage ou sur la valeur de l'écrouissage critique commençant au voisinage de 6 %.

Ainsi, afin d'obtenir une expérience industrielle nous avons injecté dans des circuits de production de série d'ensembles structuraux d'avions à la place du 2024, les mêmes demi-produits en 2091.

Plusieurs ensembles ont ainsi été produits en utilisant les technologies usuelles.

L'analyse des résultats des essais technologiques et des informations recueillies pendant les fabrications permet de mieux statuer sur les possibilités d'utilisation du 2091.

Les essais technologiques se sont décomposés en :

- 1/ Formage par tendage
- 2/ Cambrage.

Ensuite ont eu lieu les essais et examens métallurgiques.

Dans une 3ème partie nous parlerons des réalisations.

ESSAIS TECHNOLOGIQUES

1 - Formage par tendage

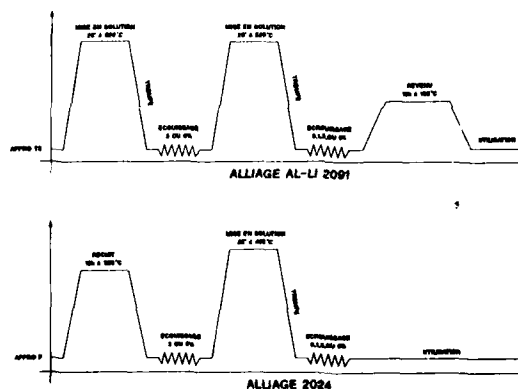
1.1 Gammes de formage et caractéristiques statiques

Des simulations de gammes de formage ont été comparativement réalisées sur des tôles minces.

C'est un formage par tendage en deux passes aboutissant à un maximum de déformation de 12 % (deux fois 6 % pour être juste en deçà de l'écrouissage critique). Sur le 2024, la gamme usuelle se décompose en un formage sur recuit suivi d'un formage final sur trempe fraîche. La planche n° 1 schématise ces gammes

GAMME COMPARATIVE DE FORMAGE DE PANNEAUX

Planche 1



La gamme sur 2091, conseillée par PECHINEY s'effectue sur 2 trempes successives, le recuit étant déconseillé par manque de ductilité sur cet état.

De ces essais nous avons d'ores et déjà pu déduire (que ce soit sur le 2091 ou sur le 2024) que les caractéristiques mécaniques finales ne sont pas influencées d'une manière décelable par le degré d'écroutissage de la première passe de formage (3 à 6 %), le traitement de trempe ultérieur effaçant tout ce qui est effectué avant.

Les planches n° 2, 3 et 4 montrent les divers résultats obtenus en sens long, travers long et à 60° du sens long, direction de faiblesse dans les alliages aluminium-lithium.

Planche n° 2

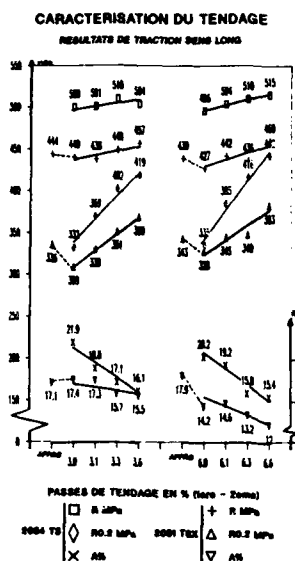


Planche n° 3

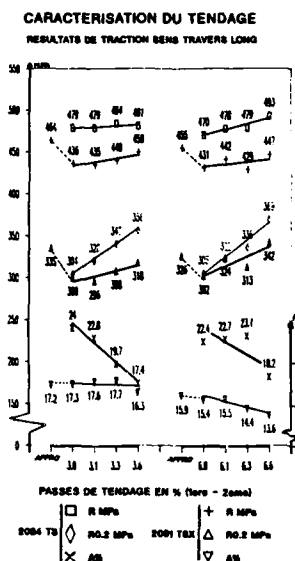
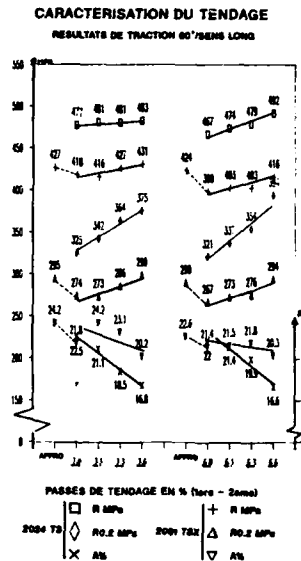


Planche n° 4



Par contre la 2ème passe provoque en relation avec un écroutissage passant de 0 à 6 % une croissance de la limite élastique, plus faible sur le 2091 que sur le 2024, alors que la charge de rupture varie d'une façon plus modérée.

L'allongement à rupture A % du 2024 chute d'une façon plus importante que celui du 2091 mais reste toujours supérieur à ce dernier.

On voit donc que si dans le sens long les caractéristiques en final sur une pièce en 2091 T8X sont légèrement supérieures pour un fort écroutissage (3 % et 6 % respectivement pour chacune des passes) dans tous les autres cas les caractéristiques sont inférieures ou au plus égales aux valeurs de départ (y compris sur travers long et à 60° du sens long).

1.2 - Essais de pliage

En complément à ces formages, ont été étudiées les possibilités de rayons de pliage à 180°. Il faut augmenter le rayon de pliage au fur et à mesure de l'écroutissage, mais on remarque que la capacité de pliage selon les matériaux et leurs traitements thermiques peut être notée de la façon suivante :

$$2091 T3 > 2091 T8X > 2024 T3$$

Tableau n° 5

			ECROUISSAGE		
			3%	à	6%
2024	T3	TL	2	→	3,5
		L	2	→	3
2024	W	TL	0,5	→	1
2091		TL	1,3	→	1,6
2091	T3	L	1,5	→	1,6
		TL	1,6	→	2

EVOLUTION DU RAYON DE PLIAGE r/e MINI

Le tableau n° 5 donne l'évolution des rayons r/e mini déterminée juste avant l'apparition de légères gerçures.

Après ces essais technologiques nous avons entrepris de chiffrer les diverses caractéristiques.

1.3 - Vitesse de propagation des criques de fatigue et courbes R

Toutes les fissurations ont été effectuées dans le sens long c'est-à-dire que les éprouvettes ont été prélevées dans le sens travers long. Les résultats ne présentent pas de particularités notables.

On peut seulement dire que :

Si consécutivement à la première passe de formage un grossissement de grain a eu lieu (6 % d'écroissage) l'écroissage final semble augmenter très légèrement la vitesse de propagation.

D'une façon générale les vitesses de propagation relevées sur le 2091 restent inférieures ou égales à celles du 2024.

Pour le 2091, on enregistre une vitesse de propagation de $\frac{da}{dn} \approx 10^{-4}$ mm/cycle pour une valeur de ΔK de 10 MPa \sqrt{m} .

Sur le 2024, la vitesse de propagation pour le même ΔK est double.

L'essai de ténacité "Courbe R" mené sur éprouvettes IRWIN de 100 x 300 prélevées dans le sens long et dans le sens travers long de la tôle a montré que dans tous les cas l'ouverture de la fissure initiale a_0 se produit pour un même facteur d'intensité de contrainte, indépendamment de l'écroissage, de 40 MPa \sqrt{m} .

2 - Formage par cambrage

Le cambrage a été réalisé sur une presse hydrafluide. Des pliages sur parties droites ont d'abord été réalisés avec diverses valeurs de rayons pour déterminer les valeurs minimales admissibles sans apparition de gerçures superficielles. Ces essais ont permis de tracer le tableau n° 6.

Tableau n° 6

ETUDE DES RAYONS DE PLIAGE EN CAMBRAGE

MATIERE	CAMBRAGE SUR ETOU	r/e mini à 90°			
		$e = 1,6$ mm		$e = 2,5$ mini	
		TL	L	TL	L
2091	W	<1,1	<1,1	1,5	1,5
2024		<1,1	<1,1	1,5	1,5
2091	T3	1,5	1,7	1,8	1,8
2024		1,8	1,8	2	2,4
2024	O + W	<0,7	<0,7	<1,1	<1,1



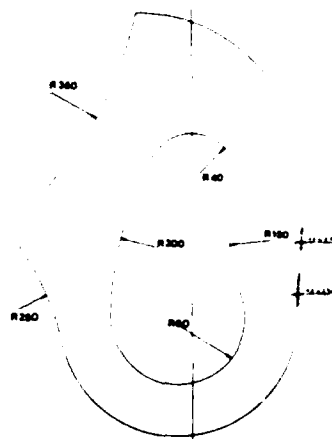
Sur état W l'aptitude au cambrage du 2091 est équivalente à celle du 2024 tandis que sur état T3 le 2091 est meilleur.

Le retour élastique du 2091 à l'état W est voisin de celui du 2024 au même état quoiqu'un peu plus élevé. Mais à l'état T3 ils sont différents, ce qui entraîne des modifications de l'outillage pour passer de l'un à l'autre.

Les essais ont ensuite été poursuivis sur outillages à rayons de courbure évolutifs selon le dessin n° 7 avec bord tombé de 12 mm à l'intérieur et de 20 mm à l'extérieur. Cet outillage rassemble à peu près toutes les difficultés rencontrées sur des pièces avion, en effet un rayon de courbure est influencé par les conditions de ses extrémités (localisation privilégiée des ruptures). Les valeurs de rayon de pliage en essais étant de 2e et de 2,5e.

Dessin n° 7

OUTIL EN COUMACON



Les résultats du 2091 formé à l'état W sont meilleurs que ceux du 2024 dans le même état. Ainsi ont été validés les rayons mini de pliage de 2e et de 2,5e pour des tôles d'épaisseur de 1,0 mm et de 2,5 mm à l'état W.

B - ESSAIS ET EXAMENS METALLURGIQUES

1 - Essais préliminaires

Au préalable nous avons vérifié qu'il n'y avait pas d'influence notable du temps d'attente entre trempe et revenu (sur les caractéristiques statiques, les propriétés en fatigue, la corrosion) laissant ainsi toute latitude pour l'opération de revenu final.

2 - Essai de corrosion

Les premiers essais menés ont concerné la corrosion. Les tôles utilisées en 2091 TSX étaient recristallisées sans gamme CPH. Leur tenue à la C.S.T. à 30 jours est donnée pour un niveau de 75 à 100 MPa.

Des plaquettes assemblées soit avec des rivets Titane MGPL diamètre 4 (montés avec une interférence de 32 μ m) soit avec des rivets 2017A diamètre 3,2 montés selon les standards AMD-BA n'ont révélé aucune anomalie de C.S.T. hormis quelques attaques galvaniques dues au couple Titane-Aluminium (planche n° 8). Cependant nous avons appris que la société AEROSPATIALE avait observé des fissures après 20 jours d'immersion-émersion alternée sur des assemblages rivés avec rivets en 7050. Ces résultats sont sans doute dus à des poses plus sévères car des essais croisés (AMD-BA/AEROSPATIALE) réalisés sur une même tôle Al-Li 2091 TSX de 2 mm avec des rivets en 7050 posés aux AMD-BA n'ont révélé aucune anomalie après 30 jours d'I.E.A.

2091 TSX (12 heures à 135°C)

Assemblage avec rivets Titane MGPL ϕ 4 (sertage 32 μ m)

Planche n° 8

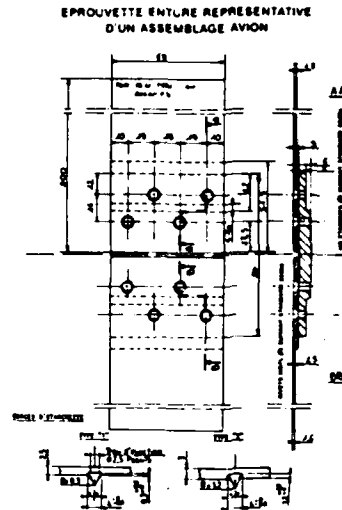


Après 30 jours en Immersion Émersion alternée en solution A3
(petites fissures intergranulaires sur corrosion galvanique)

3 - ESSAIS DE FATIGUE

Des éprouvettes d'assemblage représentatives d'une liaison de revêtements de fuselage sur une semelle de cadre de fuselage ont été réalisées. Cette éprouvette complexe est montrée sur la planche 9. Le cadre est en 2214 T6 et habituellement le revêtement est en 2024 T3. Ce dernier est remplacé par du 2091 T8X. Cette éprouvette, comme un ensemble de cellules d'avion, a subi l'usinage chimique (sur état revenu T8X), les gammes de protection et d'assemblage avion : rivets MGPL diamètre 5 ou vis étanches diamètre 5. La solution en 2091 T8X a été testée comparativement en traction ondulée P-O,1P sous une contrainte de 85 MPa en pleine tôle. La présence du 2091 n'a pas été préjudiciable à la tenue de l'assemblage qui s'est comporté identiquement dans les 2 solutions, ayant une durée de vie d'environ 110.000 cycles.

Planche n° 9



A propos d'assemblages, signalons en passant que le 2091 se soude très bien par point. Les macrographies des points soudés sont très bonnes. On ne décèle pas de défauts de compacité et les diamètres des points sont corrects.

Aux essais de déboutonnage, ces points ont des tenues mécaniques supérieures à ceux réalisés en équivalence sur du 2024.

C - REALISATIONS

L'ensemble de ces résultats nous ayant conforté dans l'emploi du 2091, nous avons donc lancé en fabrication des sous-ensembles avion actuellement réalisés en série en 2024 T3.

Les photos n° 10, 11 et 12 montrent ces réalisations.

Photo n° 10

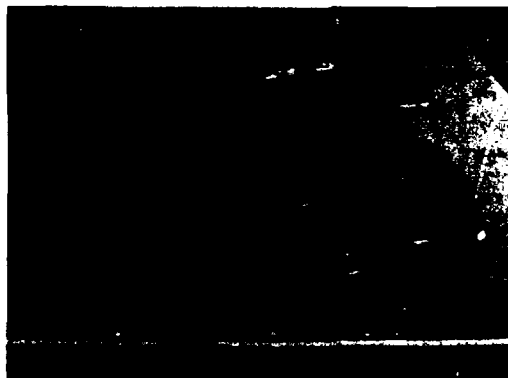
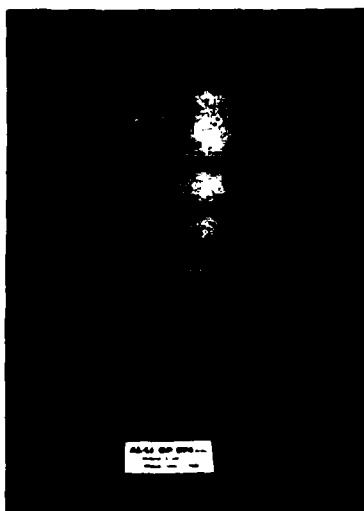


Photo 11



Photo 12



Observations sur ces réalisations

Quelques essais ont été réalisés sur des éprouvettes prélevées dans des panneaux

- choc
- caractéristiques statiques
- fatigue.

a. Essais à l'impact

Cet essai est mené sur un mouton pendule muni d'un embout sphérique de diamètre 6 mm.

A partir de 11 joules une peau d'orange apparaît du côté opposé à l'impact.

A 12 joules il y a apparition de fissures.

Comparativement ce seuil de fissuration est de 15 joules sur l'éprouvette en 2024.

b. Caractéristiques statiques

On a noté que l'écroutissage final avant revenu a une influence primordiale sur les caractéristiques mécaniques finales.

Le tableau n° 13 montre qu'il y a intérêt à avoir l'écroutissage maximal admissible avant revenu. En particulier si c'est possible, de former en une seule passe.

Tableau n° 13

CARACTERISTIQUES MECANQUES SUR PIECES
FORMEES EN 2021
(VALEURS MOYENNES SUR 3 ESSAIS)

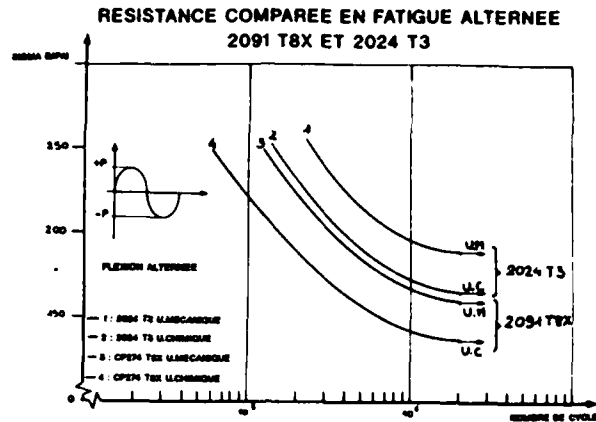
			R		A%
			80Pa	80Pa	
FORMATION EN 1 PASSES	L	17%	446	374	15,6
	TL	3%	467	366	13,4
	90°/L		441	314	10,8
FORMATION EN 2 PASSES	L	6%	438	333	10,1
	TL	1%	449	317	10,7
	90°/L		413	277	20,5
QUAL. PROMOUEE	L		434	348	14,5
	TL		456	339	17
	90°/L		427	304	23,8

c/ Essais de fatigue

Des éprouvettes de flexion plane ont été prélevées dans les pièces dans des zones surfacées mécaniquement ($\sim 2/10e$) sur chaque face, ou dans des zones usinées chimiquement sur une face (l'autre face ayant été seulement décapée pour l'adhérence du masque).

L'ensemble des résultats de fatigue donné par la planche n° 14 montre que : l'usinage chimique (sans compression de surface ultérieure) fait perdre 25 MPa sur la contrainte admissible à $2 \cdot 10^7$ cycles vis à vis de l'usinage mécanique.

Planche n° 14

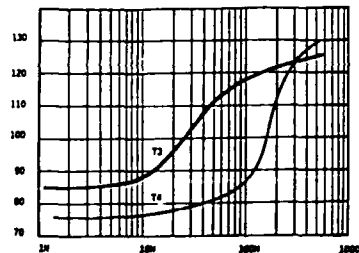


Cette influence est comparable à celle décelée sur le 2024 quoique ce dernier donne des résultats légèrement plus élevés.

Planche n° 15

TEMPS DE MATURATION DU 2091 T3 ET T4

Hv (10 kg) Dureté Vickers



Source : CRV PECHINEY

CONCLUSIONS

Le 2091 vis à vis du 2024 a une capacité de déformation plus grande. le travail sur trempe fraîche est le plus favorable et il est souhaitable d'avoir le maximum de déformation avant le revenu. D'où l'optique de réaliser le formage en 1 seule passe sur trempe fraîche. Rappelons que les possibilités de travail sur trempe fraîche sont importantes : au moins 3 jours. C'est ce que montrent les courbes CRV Pechiney de la planche 15.

Signalons toutefois que l'alliage semble susceptible à la piqûre à cet état et que des précautions doivent donc être prises.

Toutes les opérations habituellement réalisées sur 2024 sont transférables sur le 2091.

Malgré tout il y a quand même l'inconvénient d'être obligé d'effectuer un traitement thermique de revenu en fin de gamme alors que le 2024 en est dispensé.

Pour finir tout en signalant que si quelques petits problèmes annexes sont aussi à prendre en considération tels que celui de la conduite des bains d'usinage chimique (régénération et élimination des boues) ou le problème de la ségrégation des chutes et des copeaux d'Al-Li pour les recyclages on peut dire que la maîtrise de la mise en oeuvre des alliages Al-Li est acquise et ne pose donc pratiquement pas de problèmes d'utilisation industrielle.

FABRICATION CHARACTERISTICS OF 8090 ALLOY

BY

V.H.Mould, C.Eng., F.I. Prod. E.,
Head of Production Development & Methods
British Aerospace Public Limited Company
Filton House, Bristol, Avon, BS99 7AR

UK

Summary

This paper collates some of the experience gained so far, by a user, during a production process evaluation of 8090 medium strength Al-Li. alloy.

It examines the four primary production processes, Machining, Forming, Joining, and Construction, in this sense Finishing, Treatments, Painting, Plating and so forth are classed as secondary processes. Sufficient work has been completed to give the author confidence in the ability of this material to respond to these four basic processes, and produce a quality article.

No fundamental changes will be required of Machine tools, Cutting tools, Plant or equipment. Some techniques will change from the conventional alloy requirements, particularly with Forming, where further work is required, as 8090 does not form well in the cold condition. Superplastic forming characteristics are noted, extensive work is being done, but the subject is outside the scope of this paper.

The author concludes with the view that 8090 medium strength Al-Li. alloy is becoming available in sufficient quantity and quality to enable design engineers to specify the material for applications that can exploit the proven weight and strength advantages. The final responsibility resting with the manufacturing engineers to ensure that Al-Li. can be utilised as an economic proposition.

PREFACE

By the year 1982 sufficient materials and properties work had been completed to give the aircraft industry sufficient confidence, bearing in mind the X2020 alloys of the early sixties, that the newer developed versions of Lithium bearing aluminium alloys were becoming a feasible proposition for use on current aircraft, both Civil and Military.

British Aerospace therefore embarked upon a specific production evaluation programme designed to establish whether, or not, the material could be processed, and if so, under what constraints and conditions. This early programme, starting about April 1982, set out to examine one of the family of Aluminium Lithium Alloys and its behaviour when subjected to the four basic and primary production disciplines, namely:-

- a) Machining
- b) Forming
- c) Joining
- d) Construction

These four disciplines are, in fact, common to most manufactured products comprising an assembly, such as aircraft, motor vehicles, washing machines, and for that matter electric kettles. Thus it may be accepted that if any material can be successfully manipulated through these processes, an article can be made.

The material selected for this first programme was a Medium Strength Alloy, in Sheet form known as DTD 000A (DTD XXKA after solutionising), in the Plate form as DTD YYYA solution treated and stretched, and in the extruded (Bar) form, as DTD ZZZA solution treated. The material required needed to be of sufficient dimension and quality to be able to be worked and produce results, and provided aircraft properties were met, no other constraints were put on the supplier. The programme, undertaken between 1983 and 1984 used material produced from small ingots and rolled in the supplier's laboratory. The quantity processed was six pieces 1200 mm x 300 mm x 38 mm thick plate, about 32 square metres of sheet ranging from 1,0 mm to 1,6 mm thickness, and some 2 metres of 50 mm dia extruded bar.

The current Production Evaluation programme, unlike the earlier programmes (for which laboratory produced material was used), is using production manufactured material, namely 8090 'A' specification medium strength, in both the plate and sheet form fully released to aircraft standards, further work will extend to the 'B' high strength and the 'C' damage tolerant versions. Thus by processing through the normal production manufacturing routes aircraft demonstrator components can be made for both design and properties assessment. Having established the competence of the traditional production methods to produce components to the required quality standards further work is proposed to ascertain the optimum economic production procedures. In addition, work will be extended into the secondary manufacturing processes, treatments, anodising, painting, and so forth.

1. PRODUCTION EVALUATION

a) Machining

The majority, (over 95%), of traditional aluminium alloy aircraft components produced from plate are machined in the fully heat treated condition. However, in order to fully understand the machinability of this DTD YYYA material two simple specimens were processed, both in the as received solutionised and stretched condition, and in the fully heat treated (FHT) condition. Extracted from 1200 mm x 38 mm thick plate both specimens were machined on a conventional manually operated milling machine. The first, a small forked item designed to check for distortion and 'closing-in' of the flanges, typical of that type of component, and the second, designed to check the behaviour of slot drills in an enclosed pocket, fig 1. Similar specimens were produced at the same time in L93 in the FHT condition.

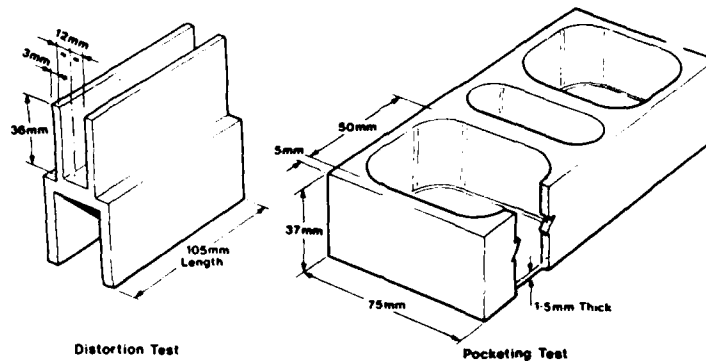


fig 1 MACHINING TEST

The tools used were standard aerospace M42 high speed steel two tooth and four tooth milling cutters, but a commercial face mill in K20 carbide was used to clean up the material. These preliminary cuts showed the Al-Li. medium strength alloy in the solutionised condition to have a dull and inferior surface texture in comparison to the L93 in the FHT condition, furthermore cutter 'pick-up' and smearing of material was evident along the primary rake angle of the cutter, fig 2. The Al-Li alloy seemed to behave in a manner normally associated with pure aluminium, but in the heat treated condition the alloy cut cleanly with a marked improvement in surface texture.

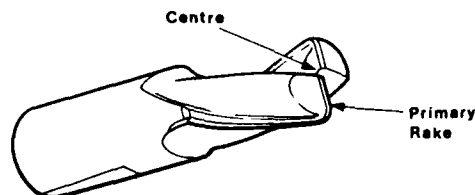


fig 2 CUTTER FORM (TWO TEETH)

The forked item was checked for distortion. This did not exceed normal expectations, there being less than 120μ closing-in over 105 mm length, at the tip of the 3 mm thick prongs 36 mm deep. Some N.C. routered test pieces seemed to confirm these initial findings.

The programme continued using material in the FHT condition. This treatment was carried out at British Aerospace.

The specimen, fig 3 was machined on an N.C. router from FHT DTD YYYA plate 300 x 1140 x 38 mm thick plate. Pocketed to typical airframe configuration it was designed to enable assessments to be made of distortion characteristics, surface texture and high flanges, the reaction of tungsten carbide cutting tools at established routing metal removal rates, and so forth. A similar specimen in L93 alloy was machined under the same conditions for comparative purposes.

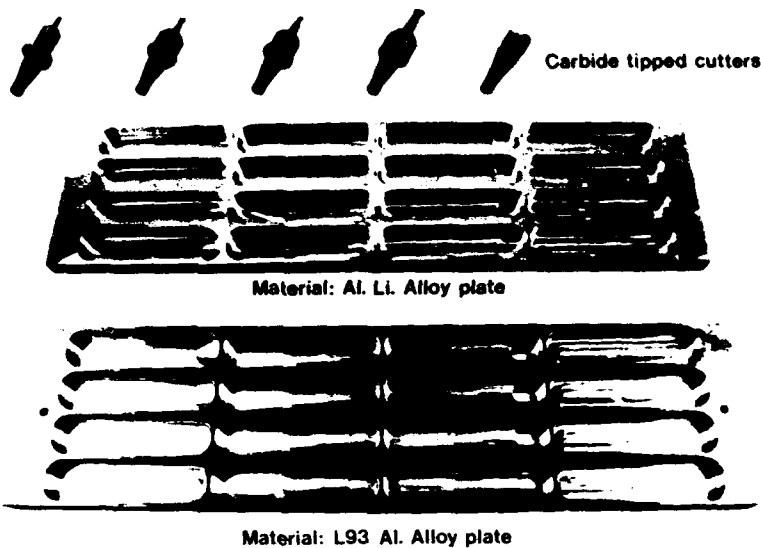


fig 3 N.C. ROUTING SPECIMENS

The cutting tools were the British Aerospace range of tungsten carbide tools for light alloy routing, similar in geometry to the currently proposed I.S.O. standards. The coolant was a mist spray of a conventional water soluble mineral oil at 40:1 mix.

Since the material was received in the solutionised condition normal test pieces were taken for Aerospace heat treatment requirements. Proof, Tensile, and Elongation results were within the specified limits.

To avoid the complication of inducing machining stresses into the material, feeds and speeds, were in accordance with normal procedures kept to the recommended low rate for delicate parts, that is, Roughing at approximately 1200 mm/minute feed rate, producing a tooth load of 0,12 mm at 6000 r.p.m. and finishing at an average of 500 mm/minute feed rate producing approximately 0,05 mm tooth load at 6000 r.p.m.

Fig 4 shows a simple bracket used on the BAe 146 aircraft, N.C. machined, twin spindle, for comparative purposes machining Al-Li. FHT under one spindle, and L93, the currently used material under the other. In both cases running on existing proven production tapes a normal machined finish was obtained, and both specimens were dimensionally correct to the drawing. Subsequently anodised and painted to aircraft standards the weight of the L93 part was 387g and the AL.Li part 340g, representing approximately, a 12% weight saving.

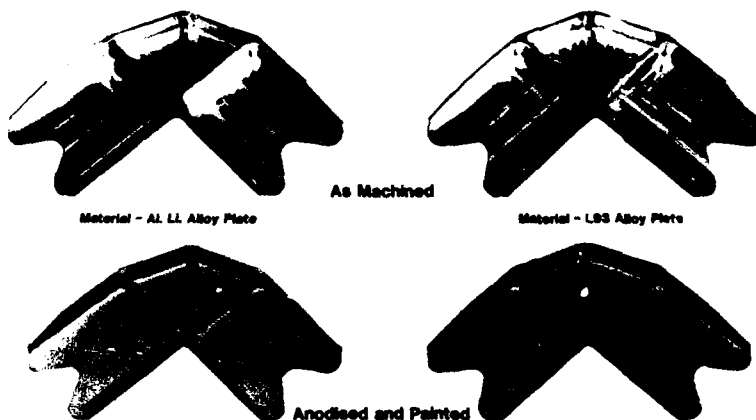


fig 4 AIRCRAFT CORNER BRACKETS

Two further aircraft rib components were produced in a similar manner. Being slender delicate items, the machinist was looking, in particular for distortion and cutter burn due to material overheating. Both of these items were completed correct to drawing requirements and later successfully anodised.

A turned specimen was produced from the 50 mm dia extruded bar in the F.H.T condition. Conventional turning enables a machinist to get a 'feel' for a material. The specimen approximately 170 mm long was drilled and tapped each end and finely ground on the major outside diameters. During this processing the material behaved in a manner similar to conventional aluminium alloys.

Most aircraft sheetmetal parts are produced initially from a flat profile routed shape - production economics demand this, primarily because of the short (can be 1, average batch quantity, say 35) batch quantities involved, the cost of a continuous batch quantity compound press tool installation could not be justified. Furthermore aircraft designers can be concerned about sheared edges that emanate from the punching process. The routing process, using a rotating cutting tool produces a less crack sensitive edge surface.

At the moment Al-Li. alloys are more costly than their traditional counterparts. The responsibility to ensure that the aircraft designer has the new materials available at a competitive price rests not only with the manufacturer, but with the user, that is, the production engineer. Hence, these current trials, accepting, that, from the results of the early work, components can be made, are designed to establish:-

- The most economic use of raw material
- Maximum metal removal rate
- Optimum processing conditions available from advancing technology

Fig 5 shows the cutting head of a sheet routing machine, DNC driven, developed for the purpose of producing at a high rate (feeds up to 10 m/minute) parts in a nested array, which in itself effects a saving of over 30% in the amount of material used per batch of components.

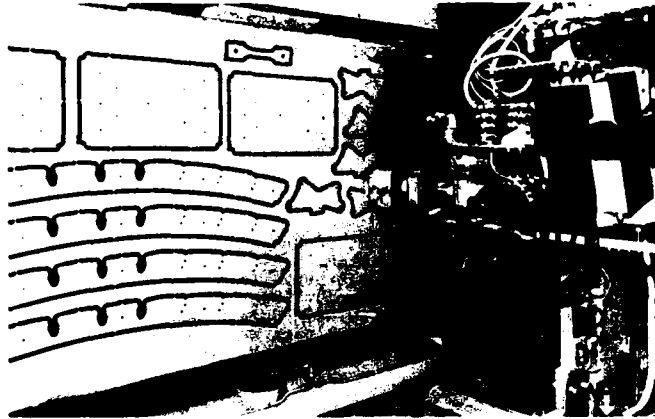


fig 5 SHEET ROUTED NESTED PARTS

The specimen, fig 6 has been produced from 8090 production released plate in order to assess optimum machining conditions. Using an existing production N.C. machine, routing cutters of various carbide types were run at the maximum 9000 r.p.m. through various feed rates ranging from 0,5 to 0,2 mm tooth load. The cutting tools were, in some instances, plunged directly into the material, and in others were ramped in at the established 15° at varying feed rates up to 1500 mm/min. Abusive conditions were intentionally set-up using:-

- Feed/surface speed ratios excessive to normal practice
- Tool materials and geometries known to burn L93.
- Worn tools

The shapes produced were in the form of standard Tensile Test Specimens 2,0 mm thick and were subsequently passed over to the laboratories for extensive evaluation.

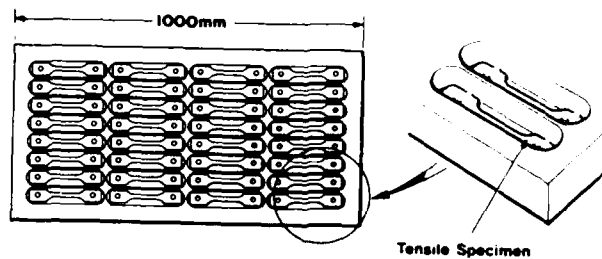


fig 6 8090 PANEL

Summary conclusion from experience to date

- 8090 Al-Li. alloy machines better in the FHT condition
- 8090 Al-Li. alloy will demand no change to existing H.S.S. or tungsten carbide cutting tools.
- 8090 Al. Li alloy will demand no change to the design of existing metal removal machine tools

Should it be necessary to machine in the solutionised condition polished flute high rake cutters can be used.

b) Forming

Trials conducted with the "laboratory" materials were in solutionised condition sheet. Spinning tests, at room temperature on 115 mm dia cup shaped aircraft components fig 7a revealed, prior to complete forming, severe cracking in the walls. It was noted that these cracks are transverse to the grain direction, unlike traditional aluminium alloys which would crack with the grain direction, fig 7b. A comparable test in L164, in the annealed condition was completed with no forming problems, and no wall cracking.

It is a characteristic of Al-Li. alloys that they cannot be annealed. For this reason further tests were conducted at elevated temperatures. Cracks were evident up to a temperature of 200°C. Successful spinning was accomplished at 250°C.

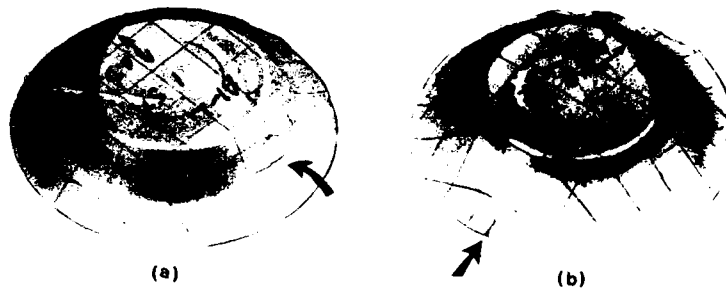


fig 7 SPINNING (ROOM TEMP) a) Al-Li. b) L164

Drop hammer pressings at room temperature produced cracks around a tight form, a right angled half-section 75 mm bore flanged pipe, and a less severe section, 100 mm bore with no flanges was successfully pressed.

The shear angle, fig 8 of 8090 sheet 1.0 mm thick, seen in the flat form with the nested parts fig 5 was subjected to joggle forming and flange forming on a standard production rubber press, using existing form tools. Prior to forming the flange holes were edge polished and the material solutionised at 530°. It is quite clear from the various amounts of edge cracking seen on these specimens that a fine edge condition (surface texture) is extremely important, and we would recommend a finish of less than 1.6 µm.

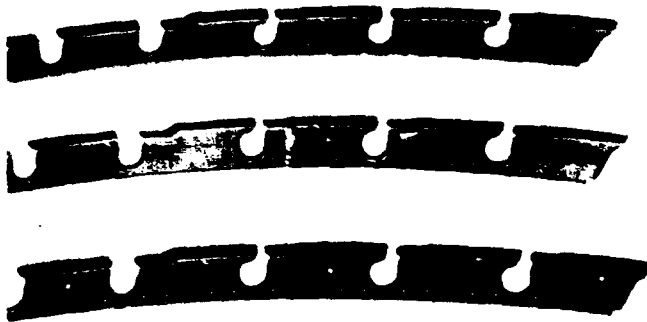


fig 8 FORMED SHEAR ANGLE

Bend tests are indicating a lower material spring back than is associated with conventional alloys. Fig 9 summarises some of the results emerging from extended tests. For comparison, these materials in the 'as-received' condition were subjected to a bend of 90° approaching at 0°, 45° and 90° to the rolling direction, the two lithium alloys averaging a lower value. Tests on 8090 going down to 2 T bend radius successfully without damage. Further tests in the solutionised condition are indicating that spring back is averaging 2° lower than a traditional L164. Whereas L164 shows a relatively constant springback through the directional range, the lithium alloys show a marked increase after 45°.

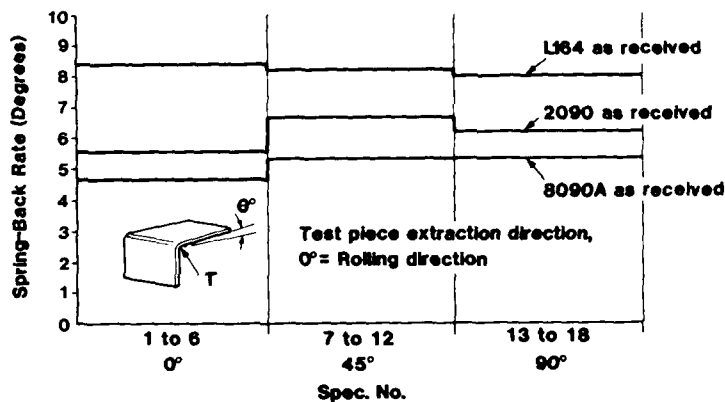
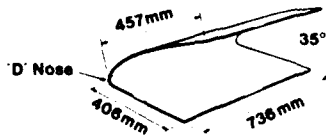


fig 9 AVERAGE SPRING BACK

Stretch forming, a process by which sheet is wrapped around a forming block and then control stretched to form sections, in particular aerofoil, has been carried out with sufficient success to give a degree of confidence to the process as a means of producing typical aircraft forms. Table 1 relates to a Wing 'D' nose skin being successfully formed in 1,6 mm Al-Li. sheet on a comparative basis with L164.



	THICKNESS	CONDITION	WRAP FORCE TONNES	STRETCH FORCE TONNES
8090	1.6 mm	SOLUTIONISED 530°C WATER QUENCH	18	34 (1%)
L164	2.0 MM	SOLUTIONISED 505°C	20	40 (2%)

TABLE 1 FORMING PRESSURES

Summary

- 8090 forms better in the solutionised condition
- Spinning may require elevated temperatures, say, 250°C
- 2T bends seem to be a practical proposition
- Spring-back values for bending may be less than for conventional alloys
- Flanged holes require a fine edge finish

c) Joining

It is a requirement within the Aircraft Industry that, prior to any production run involving spot welding test specimens are taken to the requirements of controlling documentation. A series of 14 Spot Weld shear specimens were taken from 1,00 mm and 1,2 mm DTD XXXA sheet with satisfactory results. This process is little used particularly on civil aircraft, no work has been done within BAE on the 8090 alloy.

Referring back to fig 3 Taper-Lok fasteners can be seen successfully installed in the Al-Li. specimen. These fasteners require a close tolerance taper reamed hole to a fine surface texture (under 0.2µm) with a 60% minimum bearing contact.

Riveting work, so far completed shows a good hole fill with no distortion of the sheet surfaces, nor any evidence of cracking around the hole, using normal aircraft standard 3,2 mm and 4,0 mm L37 countersunk full head rivets. Various combinations of sheet thickness were riveted from 1,0 mm down to 0.5 mm. Other rivet systems were evaluated including the Type 7i wire drawn Monel Cherry rivet for thick sheet, and the type 80 aluminium Bulbed Cherry rivet for thin sheet.

"Spacematic" drilling and countersinking into 9,5 mm plate shows that finish and dimensional accuracy can be maintained, as in traditional alloys.

Summary

- Aluminium Lithium (Medium Strength) reacts to the installation and removal of interference fasteners in the same manner as other aluminium alloys.
- Initial rivet specimens show an acceptable level of hole fill and clench.
- A degree of confidence exists to suggest that spot welding will be successful.

d) Construction

A specimen assembly, fig 10 has been produced of a Tornado Laser Module, situated in the front fuselage area of this military aircraft, forming part of the outer, or skin profile. The assembly requires a variety of forming and fitting techniques to complete. Items that normally require annealing in traditional alloys were, in Al-Li., because of its peculiar nature, subjected to solution treatment; after which any flattening and straightening was carried out by the traditional method between rollers.

A total of 71 parts were formed - as soon as possible after heat treatment, namely:-

- 45 Hand bench formed
- 18 Rubber Press formed
- 8 Stretch formed

also, 7 flat non-formed items were produced. All of these were subjected to normal finishing and inspection procedures, including a 'pickle' in 'Aluclean 915' de-oxidiser, and a percentage, 25% approximately, were subjected to crack detect.

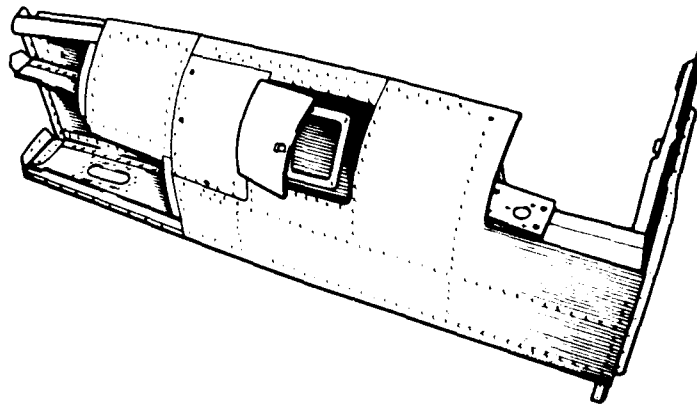


fig 10 LASER MODULE ASSEMBLY

Crack detection tests revealed no fundamental faults. Shrinkage was noted in certain components mainly because tooling holes, accurately positioned, were not lining up with the precision production jigs. This shrinkage was attributed to the first solution treatment, the material having been received in the 'as rolled' condition. Subsequent solution treatment did not escalate shrinkage. Work hardening during some of the severe hand forming operations, was noted to be more than is generally associated with conventional aluminium alloys.

A favourable reaction was received from the workshops during the manufacturing processes of nibbling, routing, drilling, and piercing, and the assembly proceeded with no significant problems.

Summary

- No fundamental problems emerged during assembly operations.
- Precision assembly tool designers must develop a full understanding of shrinkage factors.

2.0 Comments

- 2.1 Families of materials tend to behave, and to react to production processes in a similar way. Techniques, particularly with metal removal processes can be readily adapted to accommodate a variation of chemical composition and/or properties. Hence, so far as Al-Li. is concerned the criteria established for the 8090 medium strength can be used as a basis from which to work with the damage tolerant and higher strength materials. Limited production evaluation work so far confirms this assumption.
- 2.2 Manufacturers are demonstrating their ability to produce lithium bearing alloys that meet the requirements of aircraft design and aircraft properties engineers. Production produced materials are now emerging in a stable and predictable quality to be of interest to the production and manufacturing engineers.
- Sufficient work has now been completed to give the author confidence in the ability to process 8090 medium strength Al-Li. alloy through the four primary manufacturing processes, Machining, Forming, Joining and Construction. As a general rule if a material can be machined and formed, then it is possible to manufacture components from that material. The medium strength alloy can certainly be machined using existing tools and equipment.
- It can certainly be formed with existing tools and equipment, although techniques may need modifying, but, even then, not beyond the realms of established knowledge and practices. Superplastic Forming is not within the scope of this paper, except to say that the material exhibits superplastic properties and extensive programmes are in hand aimed at evaluating the benefits that can be gained from the use of these properties.
- In conclusion it is the author's view that designers should now specify the use of this material, to design for applications that exploit and capitalise on the compounded advantages of added strength and reduced weight. The responsibility of both the manufacturer and the user (Production Engineer) must be to respond by utilising the most cost effective methods to ensure that these alloys can be introduced as an economic and cost-justifiable proposition.

ACKNOWLEDGEMENTS

Acknowledgements are due to:-

British Alcan, Banbury for material development and assistance in the evaluation programme.

British Aerospace participating factories
 Chadderton site the early forming trials
 Brough site the initial riveting investigations
 Warton site constructing the laser module
 and colleagues at Filton for the machining assessments and others including those involved in photographic and artwork.

SUPERPLASTIC PERFORMANCE AND PROPERTIES
OF THE LITAL ALLOYS

R.G. Butler and B.J. Dunwoody
Superform Metals Ltd
P.O. Box 150
Worcester
WR3 8TR
England

S U M M A R Y

The requirements in a superplastic sheet material are either to possess a fine uniform grain size or to be capable of developing such a grain structure during the course of superplastic deformation. The Lital Alloys processed by the optimum route to produce superplastic grade sheet fall into the latter category. This paper is devoted to describing the evolution, superplastic performance and properties of 8090 SPF produced by a commercial production route. The sheet produced by this processing route has good isotropic superplastic properties, the ability to be formed at the solution heat treatment temperature and low quench sensitivity. Properties determined on components formed with hydrostatic confining pressure are presented. The low flow stress of the material enables cavitation to be controlled during forming by this process.

Introduction

Superform Metals Ltd has been producing superplastically formed aluminium alloy components for the aerospace industry since 1973. With facilities in Worcester and California Superform has developed into the world's largest producer of superplastic aluminium components. The company remains the only specialist in the field and is still leading the way with new materials and techniques to make this route for the manufacture of complex components more attractive.

Supral 100 and 150 are widely used in many non-structural applications from internal furnishings on civil aircraft to components for weapons delivery systems.

There is now an increasing demand for structural parts. These must be of high integrity and thus demand back pressure forming to minimise cavitation. The most suitable alloys are 7475 and Aluminium-Lithium. Alcan Lital 8090 SPF is 10% lighter and 10% stiffer than conventional alloys. These attributes are important since a high proportion of structural sheet components are stiffness critical.

This paper describes the evolution, performance and properties primarily of 8090 SPF with reference to 8091 SPF where applicable.

Alloy Selection

In 1985 it was reported (1) that a wide range of aluminium alloys containing lithium could be rendered superplastic. The alloys considered are given in Table 1. The alloying additions range from 1.9 to 3.3% Lithium, 0 to 4.0% Copper, 0 to 2.8% Magnesium and 0 to 0.5% Zirconium. It was therefore considered appropriate to make the alloy choice on the basis of the chemistry that produces the required service properties, rather than that which confer superplasticity. The principal contenders for aerospace applications were believed to be Alcoa Alithalite B (2090), Pechiney CP 276, CP 274 (2091) Alcan Lital A (8090) and Lital B (8091). There is no doubt that all of these alloys can be rendered superplastic if processed correctly.

The factors considered to assess the relative merits of these alloys for superplastic applications were:-

Manufacturing route

Service properties

Superplastic behaviour above solution treatment temperature

Flow stress for cavitation control

Isotropic superplastic performance over a range of strain rates and temperatures

Quench sensitivity

Of the main contenders for general applications, 8090 SPF was believed to be closest to satisfying these requirements. The manufacturing route is commensurate with British Alcan plant capability. The alloy has reasonable strength and can be produced in peak aged or damage tolerant tempers. It has a low copper level to impart reasonable corrosion behaviour. It is superplastic through a wide temperature range, including that required for solution treatment.

The material processed through the 'superplastic route' offers a low flow stress and isotropic superplastic deformation. Finally 8090 has a low quench sensitivity imparting benefits described later.

Processing Route

The alloy options considered demanded either a powder or ingot metallurgy route. Given that the ingot route was capable of producing the properties required, it was decided to ignore powder production as uneconomic.

The thermo-mechanical processing must be capable of producing sheet which possesses either a fine stable grain structure, or sheet which is capable of achieving a stable fine grain structure during superplastic deformation. The former can be provided by the Rockwell 7475 type route and the latter by dynamic recrystallisation as seen in the Supral alloys. Experience has indicated that dynamically recrystallising materials offer the easier manufacturing route.

A range of hot and cold rolling schedules together with a variety of thermal treatments were explored. The starting point for this work was the production route established for the conventional sheet product.

The experimental 8090 SPF materials were subjected to evaluation by uniaxial tensile tests and the superplastic forming of property boxes. Some of this work has been reported elsewhere (3).

The ingot used for 8090 SPF is cast at British Alcan's purpose built Al-Li facility at Alcan Plate, Birmingham. Rolling and thermal treatments are conducted by British Alcan's speciality rolling mill, the Aluminium Corporation Ltd, Dolgarrog.

Microstructural Evolution

8090 superplastic sheet transforms from a worked structure to one of fine stable grains during plastic/superplastic deformation. It has been reported (3) that an equiaxed grain size of $4\text{-}5\mu\text{m}$ is produced after a strain of 0.4 during tensile testing. Increasing strain results in a very gradual coarsening of the structure. Undeformed test pieces exhibit a worked structure of elongated grains, after 15 minutes. This structure also coarsens slowly, but exhibits only modest change after a period of 1 hour.

The ability of the material to produce a similar structure throughout a superplastically formed component, regardless of strain is important for uniform service properties.

Flow Stress/Cavitation

The flow stress of 8090 SPF has been found⁽³⁾ to reach 5.3 - 4.8 Mpa during tensile tests deformed at an initial strain rate of 2×10^{-3} /sec at 525-530°C under a superimposed hydrostatic pressure of 4.5Mpa. Under similar conditions the flow stress for 8091 SPF was 3.9-4.4 MPa.

The low flow stress values obtained enabled the cavitation of 8090 SPF to be virtually eliminated after a log thickness strain of 1.6 under 4.5MPa hydrostatic pressure. At a lower hydrostatic pressure of 2.1MPa the cavitation was less than 1%.

Similar results were obtained for 8091.

Further cavitation determinations have been reported (4) for the highly strained run-off regions of back pressure formed components. Figure 1 indicates the effect of various pressures on cavitation level.

Quench Sensitivity

8090 has a very low quench sensitivity as demonstrated in Fig.2. Close to full cold water quench properties are obtained by forced air quenching from the solution treatment temperature.

This ability is extremely important for superplastically formed components, as it avoids the distortion problems associated with the liquid quenching of shaped sheet structures. The absence of a separate solution treatment reduces costs and the opportunity for lithium loss from the surface.

Properties

Production quality superplastic 8090 and 8091 sheet has been available since the beginning of 1988. The material has been subjected to full release testing. The T62 figures for UTS and 0.2% proof stress are indicated by the histograms presented as Figs.3 and 4. The values obtained from the non-deformed samples are somewhat lower than those produced by actual parts. Table 2 gives examples of the mechanical properties obtained from components formed at 515°C under a superimposed hydrostatic stress of 2.75 MPa. The parts were forced air cooled and subsequently aged at 175°C for 20 hours. Further components were given a post forming solution treatment of 15 minutes at 525°C and a similar precipitation treatment. The properties obtained were near peak, although this may not be the fully optimised heat treatment.

The superplastic elongations measured for release test purposes are given in Fig.5. The test pieces were deformed with a constant cross head velocity of 1mm min⁻¹ (initial strain rate 1.3×10^{-3} sec⁻¹) at 525°C under atmospheric pressure. The test conditions chosen were for release purposes and do not represent the maximum elongation obtainable from the material. Fig 5 demonstrates good isotropic superplastic performance with some notably high elongations. When tested under optimised conditions under superimposed hydrostatic stress, all of the production batches will exceed 1000% elongation.

Conclusions

By optimisation of the thermal mechanical processing 8090 SPF sheet is now being produced commercially with good isotropic superplastic capabilities together with the ability to be simultaneously formed and heat solution treated.

It has been shown that 8090 SPF has low quench sensitivity, enabling parts to be aged to near peak properties after air cooling from the forming operation.

Cavitation in highly strained areas of formed components can be reduced to below 0.5% by the use of hydrostatic confining pressure up to 2.8MPa, during forming.

Further Work

A programme of work is currently being carried out by Superform to determine the service properties of 8090 SPF components. The components are being formed with varying hydrostatic confining pressures and different amounts of strain.

The following properties are being determined:

Tensile strength; fracture toughness; fatigue;
stress corrosion and intergranular corrosion susceptibility.

The results will be published in a forthcoming paper.

Acknowledgements

The authors wish to thank R. Grimes, J. Jones and A.J. Barnes for their assistance in the preparation of this paper.

References

1. R. Grimes AGARD lecture series N°154
- Superplasticity
2. R. Grimes International Conference on Superplasticity
- Grenoble Sept. 16-19 1985
3. W.S. Miller and J. White
TMS AIME annual meeting
Phoenix Arizona USA 25-28 January 1988
4. A.J. Barnes R.G. Butler R. Grimes
Proceedings of International Conference on Superplasticity and
Superplastic Forming
Blaine Washington USA August 1-4 1988

TABLE 1

ALUMINUM LITHIUM BASED ALLOYS EXHIBITING SUPERPLASTICITY

Composition (wt %)				Elongation (%)
Li	Cu	Mg	Zr	
2.0	-	-	-	320
3.3	-	-	0.15	340
3.0	-	-	0.5	1035
2.7	-	2.8	0.15	680
2.5	1.2	0.5	0.10	875
3.0	4.0	-	0.5	825
1.9	2.9	1.0	0.15	798
1.9	2.8	0.9	0.2	654
2.0	4.0	-	0.2	700
2.5	1.8	0.7	0.12	1200

TABLE 2

TENSILE PROPERTIES FOR 8090 SPF COMPONENT FORMED WITH
2.8 MPa ARGON ATMOSPHERE CONFINING PRESSURE

	HEAT TREATMENT SCHEDULE	0.2PS MPa	UTS MPa	E1 %
8090 Flange (0% thickness strain)	1	362	449	6
	2	371	445	6
SP Formed 8090 (50% thickness strain)	1	372	442	3
	2	372	445	3

Heat Treatment schedule 1 - Air cool from forming temperature of 515°C and artificially age at 175°C for 20 hours.

Heat Treatment schedule 2 - Solution treat at 525°C for 15 minutes then rapid quench 20% glycol water solution and age as 1.

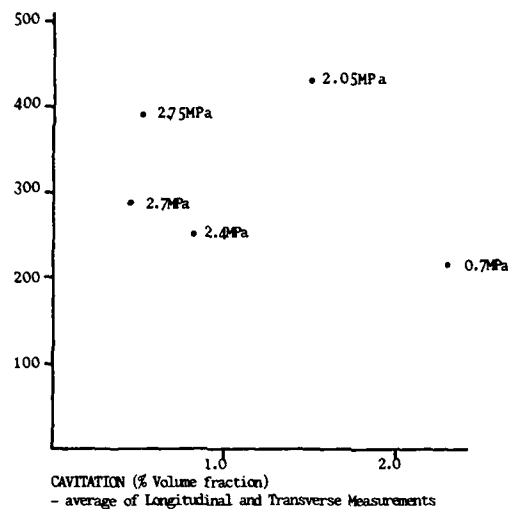


FIGURE 1 INFLUENCE OF STRAIN LEVEL AND CONFINING PRESSURE ON CAVITATION OF 8090 FORMINGS

$$\text{Equivalent strain \%} = \left(\frac{\text{Starting thickness}}{\text{Final thickness}} - 1 \right) \times 100$$

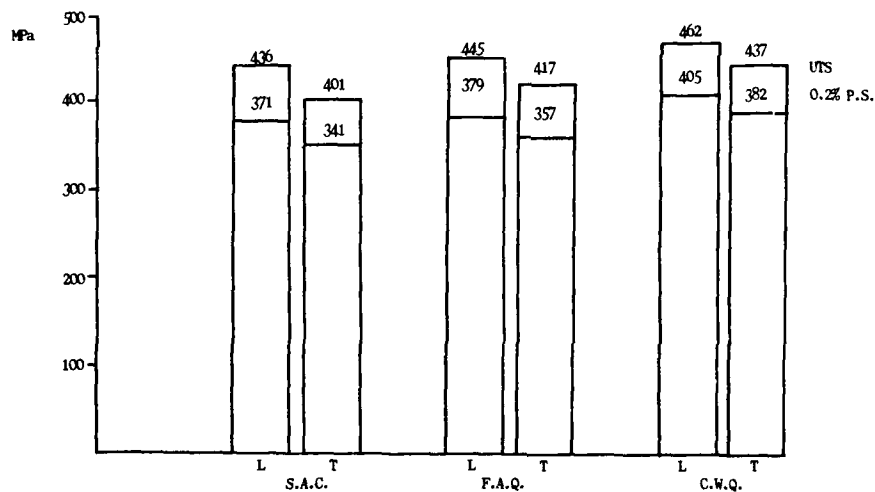


FIGURE 2 HEAT TREATMENT RESPONSE OF 8090 FOR VARIOUS QUENCH RATES

(Solution treat at 530°C,
Precipitation treatment at 170°C for 32 hours)

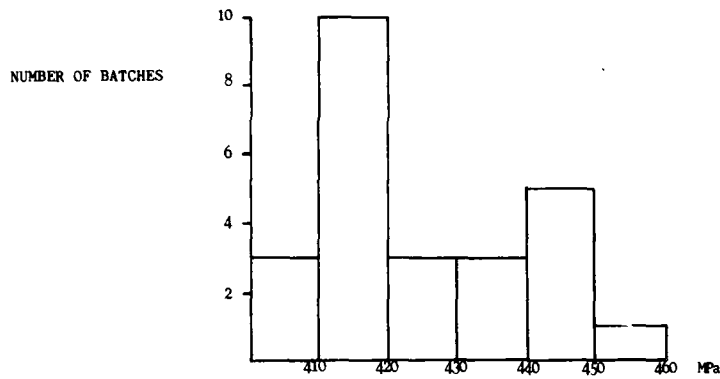


FIGURE 3 HISTOGRAM OF RELEASE ULTIMATE TENSILE STRENGTH RESULTS FOR PRODUCTION 8090 SPF BATCHES

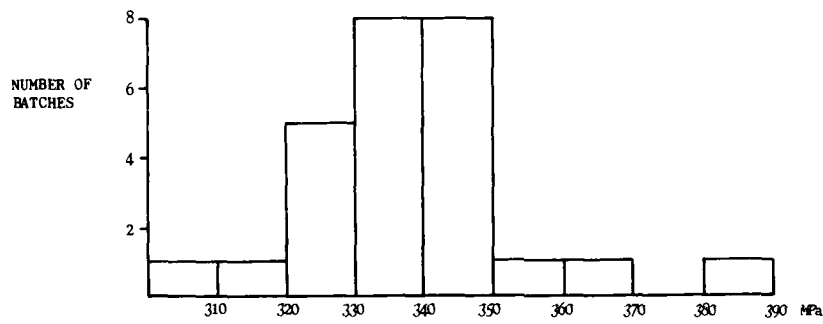


FIGURE 4 HISTOGRAM OF RELEASE 0.2% PROOF STRENGTH RESULTS FOR PRODUCTION 8090 SPF BATCHES

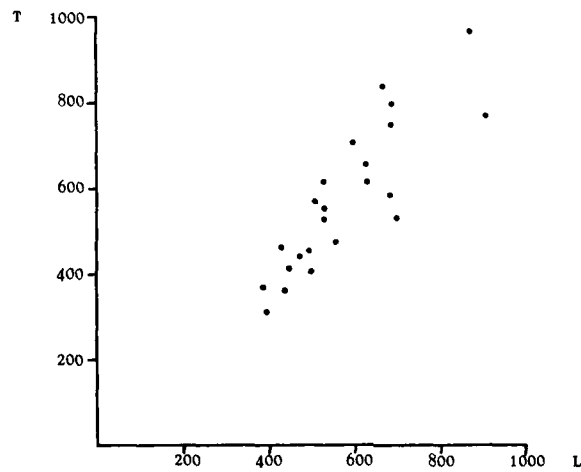


FIGURE 5 ISOTROPY OF PRODUCTION 8090 SPF RELEASE SUPERPLASTIC ELONGATIONS

POINT OF VIEW OF A CIVIL AIRCRAFT MANUFACTURER ON AL-LI ALLOY

by

Johannes KOSHORST
 Manager, Advanced Structures and Materials
 AIRBUS INDUSTRIE
 (Technology and New Product Development Directorate)
 1, Rond Point Maurice Bellonte
 31707 BLAGNAC Cedex
 France

SUMMARY

The process of evaluating a new material for use in a civil transport aircraft is rather complex and long.

The introduction of Al-Li appears as being a particular difficult item. Initially developed for application in combat aircraft aiming for high strength properties, a civil transport airplane however requires Al-Li in a damage tolerant version.

Equivalence to existing alloys is requested (equal or better) but Al-Li demands a compromise between major properties as strength, damage tolerance and corrosion resistance.

Progress in achieving acceptable and harmonized material quality is very slow and time constraints have prevented introduction in a planned way in a number of programs.

The question is raised whether a cost effective use of Al-Li can be envisaged over the next years.

INTRODUCTION

At the occasion of the 4th Al-Li Conference in Paris, June 1987, J.P. ROEDER Sr. Vice President Technology and New Product Development at Airbus Industrie in his Key Note Lecture had to a large extent outlined the fundamental requirements of the civil airplane manufacturers as regards the introduction of Al-Li in airliners.

I have to recall the major statements J.P. Roeder made in his lecture; not only for consistency but also because the situation has not significantly changed.

DISCUSSION OF THE SUBJECT

The title of this presentation already suggests that the basic environment in which we, as a civil aircraft manufacturer, have to operate, is somehow different to that encountered for military developments.

What our airline customer rightly expect from us is a product that is :

- technically sound
- well timed to meet market demands
- cost effective or commercially viable

These are in a way constraining factors which put limits to our freedom of action. They are logically fully applicable to the ingredients, contributing to the construction of our airplanes, and materials, in this particular context Al-Li, have a major importance. These more general statements obviously apply also to military airplanes but compliance requires different approaches.

When we review Al-Li as an advanced technology light alloy, the first question to be asked is technical.

The design of metallic aircraft structure has been, in the past, based on static analysis, with consideration of lower, repeated loads and their effect on the initiation of cracks within the structure based on fatigue ("safe-life") analysis.

However, a recent change in design criteria for civil transport airplanes requires additional consideration of structural integrity, assuming certain damages to exist in the structure. These can be the result of fatigue, environmental effects (corrosion, for example) or accidents, of material processing or manufacturing procedures. This new criteria is generally referred to as "damage tolerance", which means that the structure, though damaged to a limited extent, is capable of sustaining a pre-defined load until the damage can be detected and repaired.

This is the essential difference in the design requirements between a civil and a military aircraft.

For ease of understanding a rough comparison of the major design requirements is given below :

REQUIREMENT	COMBAT-TYPE AIRCRAFT	CIVIL TRANSPORT AIRCRAFT
Major material properties	- static strength predominant - fatigue consideration - corrosion	- fatigue strength predominant - damage tolerance - stress corrosion
Total life	~ 7 000 FH	~ 50 000 FH
Inspection threshold	~ 2 400 FH	~ 18 - 20 000 FH
Repeated Inspection	~ 600 FH	~ 4 500 FH

Above picture might give an idea of the different constraints under which a new material has to be evaluated and qualified, depending on its specific application.

The introduction of Al-Li with a 8-10% density reduction, while maintaining the other main characteristics of either the damage tolerant 2024 alloy or the high strength 7075 alloy, seemed to offer, for both applications, significant improvements in terms of aircraft structural efficiency without the need for changing classical design and manufacturing techniques as well as established maintenance practices.

Of particular interest also, appeared the possibility of introducing the material by substitution into currently existing products. The minimum requirement obviously is then that the major characteristics of this new material be at least equal to the material to be replaced.

Initially developed for application in combat airplanes aiming for high strength properties, Al-Li apparently complies with these requirements in its high strength version. Manufacturers as Dassault and Lockheed for example are about to introduce it or have already, Al-Li in their products in significant quantities.

A civil transport airplane manufacturer however needs Al-Li in a "damage tolerant" version. Unfortunately this fundamental requirement was only understood by the material suppliers at a rather late stage, more precisely, when first discussions took place between suppliers and aircraft design experts.

This inspite the fact, that major application for Al-Li must be seen within the civil transport market. An example might be the weight gains anticipated by our favourite competitor and ourselves in 1983 for the product lines, as then assumed; production deliveries being considered from 1988/1989 onward. (Fig. 1)

Al-Li weight reduction potential (preliminary estimates 1983)

figure 1

• B737-300	1 500 lb
• B 7-7	1 900 lb
• A320	2 500 lb
• B757	3 100 lb
• B767	4 700 lb
• A310	5 700 lb
• A300-300	6 500 lb
• A340 (TA11)	8 500 lb
• B747SP	9 300 lb
• B747-200	11 500 lb

41/103754

As a consequence of what appeared to be an encouraging situation Airbus Industrie undertook with its partners a combined approach to :

- define a joint material specification,
- speed-up the evaluation process for an early introduction into the design of new or derivative airplane types,
- encourage suppliers to minimize the number of alloy variants by standardization.

A work-sharing was agreed, covering the whole range of Al-Li products from all potential suppliers, with the aim of obtaining first results at the end of 1984 and complete component testing in the following years.

Throughout 1984 and 1985 difficulties were however reported with procurement of test materials, and the quality of those supplied remained unsatisfactory. In early 1986 we had reached results which appeared from a technical viewpoint to justify application to structural components of secondary importance only.

Application to primary structural components as fuselage sections and wing skins could not be considered, as damage tolerant properties like crack propagation behaviour and stress corrosion resistance remained very unsatisfactory until very recently. Progress to produce consistent quality material with at least acceptable properties has now been reported by the suppliers and we would assume today, that at least thin products of the desired technical quality can be obtained.

The necessary technical progress is made now, just in time to allow at least a decision making for eventual application of Al-Li to the full scale fatigue test specimen of our A330/A340 airplane.

The following scenario could then apply.(Fig. 2)

Using Al-Li on major components of the fatigue test specimen presents still a certain risk. If some cracks generate at an early stage of testing on these parts, the reasons have to be clearly identified whether it is a material or a design deficiency. This can take much time and eventually delay certification. Extensive application of Al-Li to the full scale fatigue test specimen will not mean that the decision for application on production airplanes is taken but it is a necessary technical back up for a management decision on application based subsequently on industrial and economical risk consideration.

There can be no doubt, that the price of a material is an essential factor in this respect. If a worthwhile return in terms of performance and/or economics cannot be shown by the aircraft to which it is applied, we can forget it. This is fundamental.

Extensive application of Al-Li to the first A330/A340 production airplanes in any way cannot be expected.

A340 full scale fatigue test

Evaluation of AL-LI material

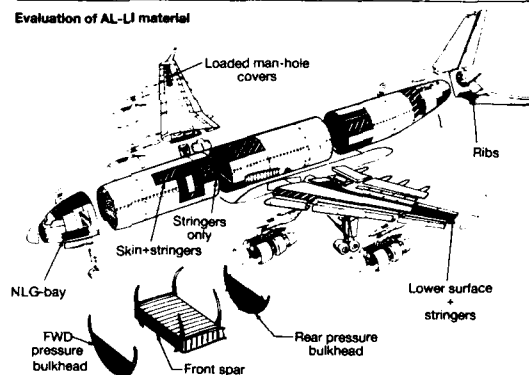


figure 2

A330 / A340 introduction of aluminium-lithium

Development + production milestones

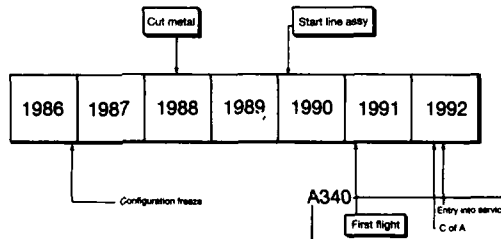


figure 3

Looking at the development and production milestones of the A340 programme we see that time has run out.(Fig. 3)

To allow a minimum of pre-qualification of the materials to be used and in order to establish a data basis for design and be sure about the decision to proceed with Al-Li, the material for qualification testing should have been in our laboratories before the end of 1986, which did not happen.

At about the same time new price indications began to reach us : instead of being twice that of current alloys as initially announced, factors of three and more were now quoted by the suppliers. This increased the doubts about the cost efficiency of the whole exercise.

Given the uncertainties which surrounded the new material, as to reliability of prediction, validation and cost, we had to revise our project studies and plans for its introduction, and necessary design changes could not be decided.

When looking at current design practice for airplane structures a change in design provisions would have been necessary for a cost efficient utilization of Al-Li.

Within the range of semi-finished al-alloy products (Fig. 4) the use of plate material today keeps a major share with a large amount of machining, which then results in an extremely high buy-to-fly ratio, leading to values of 10 and more for some components.

A cost effective design of structural components would therefore tend to reduce the demand for thick plate material in order to keep the buy-to-fly coefficient low and to increase the utilization of extruded parts and sheet material.

Structural design of the A330/A340 is frozen, and Al-Li can now be introduced only by substitution, which then is limited by economic considerations.

An example of what the economic efforts might be when trying to save weight through the introduction of Al-Li is shown for a typical fuselage section. (Fig. 5)

The various sub-parts as stringers, frames, sheets and window forgings are evaluated in terms of \$ per kg weight saved according to the type of semifinished material used, its purchase price and the corresponding buy-to-fly ratio (the total cost of a kg of material in flight is the material cost/kg multiplied by the buy-to-fly ratio).

Frame profiles from sheet material with a ratio of 1.85 show the most efficient material utilization whereas secondary parts with a ratio of 4.66 are less attractive.

The overall price with 497 \$/kg weight saved reflects a buy-to-fly ratio of about 3.1 .

The significance of Al-Li price factors has been shown and there can be no doubt that a massive reduction in Al-Li costs is a major target towards which the resources and energy of the aluminium industry must be directed.

Al-Li has only limited chances to be extensively used, when buy-to-fly ratios are greater than 3.

Limiting substitution to sheet and thin extrusions would ensure a minimum in waste of material, but impact on cost efficiency for many aircraft types would equally be limited. It would moreover drastically reduce the amount of Al-Li required and due to reduced production volume would push even further downstream the point at which the suppliers break even. Thick products, such as plate, must therefore eventually become a vital element in suppliers efforts.

In this respect only weight saving potentials based on the lower density of the material can be taken into consideration. In none of the cases can weight savings due to improved stiffness of Al-Li be accounted for, since this effect has shown to be small. Also, improved crack propagation properties of the material would scarcely be visible in this type of diagram, though they would be helpful in airline service.

Utilisation of semi-finished al-alloy products on current design

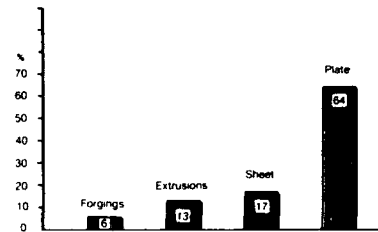
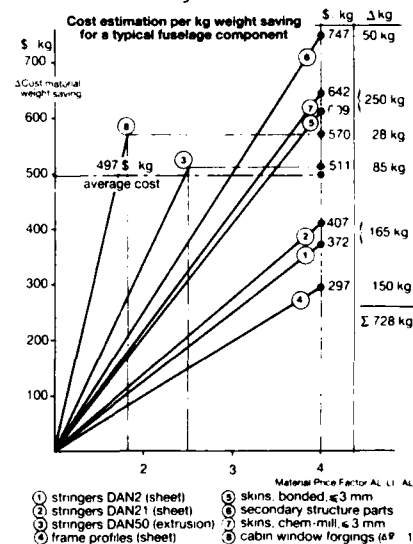


figure 4

Introduction of AL-Lithium

figure 5



CONCLUSION

Today, the decision for introducing Al-Li is still heavily risk loaded, due to lack of knowledge of the material and the timing aspects.

There is a continuous evolution of the Al-Li scenario, but this evolution is not constant and is still subject to too many up's and down's.

The economic situation forces us to do just the absolutely necessary to save weight through the utilization of the new material.

To catch the important substitution market remains fundamental for the aluminium industry in order to build up production. Strong emphasis on the damage tolerant alloy is essential in this context.

It must however also make every conceivable effort to get out of an extremely marginal situation through improving cost efficiency by all means. This is a very serious issue, which will not go away, until the present economical environment will fundamentally change and the designer might say "Al-Li is a material I like to work with".

REFERENCES

- J.P. ROEDER, Airbus Industrie
Key-Note Lecture To The Fourth Al-Li Conference
Journal de Physique, Colloque C3, Tome 48, Sept 1987
- J. KOSHORST, Airbus Industrie
Aspects of advanced structures and materials development in the A330/A340 project
19th EACMT Meeting, Madrid, Oct 22, 1986
- Internal documents - Airbus Industrie, MBB, AS, BAe

USES AND PROPERTIES OF AL-LI ON THE NEW EH101 HELICOPTER

by

A F Smith
Westland Helicopters Ltd
Yeovil, Somerset, BA20 2YB
England

SUMMARY

The EH101 is a long range, large capacity helicopter developed and built jointly by Westland Helicopters of the UK and Agusta of Italy to meet the needs of civil, naval and utility operations and in which many new aerodynamic, electronic and structural design concepts are successfully combined. In order to effect significant structural weight reductions, extensive use will be made of aluminium-lithium based alloys which are now becoming commercially available. The results of a weight-saving cost analysis favour the use of aluminium-lithium sheet, extruded profiles and forgings on the EH101, while corresponding plate and extruded bar will not be used due to the combined effects of low utilisation rate and the inherently higher material cost of aluminium-lithium. Accordingly, greater emphasis is being placed upon the use of die forgings, particularly for the manufacture of components hitherto machined from non-lithium containing aluminium plate. Extensive evaluation programmes are currently in progress covering AA 8090 and AA 2091 sheet, together with specific EH101 extruded profiles and forgings also in AA 8090 but with additional studies in alloy AA 8091; comparisons will be made with alloys AA 2014, 2024, 7075 and 7010 where appropriate. Notwithstanding the lower ductilities and anisotropic effects characteristic of aluminium-lithium, the results to date show that direct substitution of current aluminium alloys may be realistically pursued, particularly as superior fatigue properties are indicated in the new materials. This paper reviews the use of aluminium-lithium based alloys on the EH101 and reports on the findings of the current studies.

THE EH101 HELICOPTER

The EH101 helicopter, figure 1, was born as a collaborative project in 1979 when the British and Italian governments signed a Memorandum of Understanding to develop a naval helicopter. The following year, these countries' respective helicopter manufacturers, Westland and Agusta, formed EMI (European Helicopter Industries) to manage the design, development, manufacture, marketing and support of the EH101. Following government approval, project definition commenced in June 1981. A study established that helicopter variants sharing the same basic airframe and dynamics could meet not only naval and commercial requirements, but also those of the utility/air mobility support roles. A single integrated programme with a common core of design, development and test activity was therefore initiated to cover all primary variants.



Figure 1. The WESTLAND-AGUSTA EH101 HELICOPTER

Full programme go-ahead was announced in January 1984 and culminated in the first flight of the Westland constructed prototype, designated PP1, at Yeovil on 9th October 1987 while the first flight of PP2, built by Agusta, took place at Cascina Costa on 26th November 1987. The integrated nature of the project gives rise to an unusually extensive flight development phase utilising nine aircraft produced in both countries. These are pre-production helicopters rather than hand built prototypes in order to facilitate early introduction into service. Prototypes PP1 and PP2 are allocated to basic development, with the former concentrating on performance and handling while the latter contributes primarily to flight development of the dynamics. The first four flying aircraft will all contribute to a basic EH101 qualification programme aimed at developing the 'highest common helicopter'. In addition, PP3 will develop commercial version features while PP4 will concentrate on common naval avionics. Aircraft PP5 and PP6 are assigned to the specific mission requirements of the Royal Navy and Italian Navy. PP7 and PP9 are allocated to Agusta for development of the utility variant while Westland will undertake civil certification with PP8, assisted by PP3.

The design criteria for the EH101 helicopter emerged from worldwide market studies which identified a growing requirement for a multi-turbine helicopter capable of lifting large payloads over long distances cost effectively and which would meet the needs of maritime, utility and civil operations. Thus, the size of the EH101 has been determined by role requirements and not by adapting an existing air frame to try to meet tactical needs. Leading particulars of the aircraft are shown in Table 1.

Configuration	5 blade main rotor 4 blade tail rotor 3 engines	
Dimensions	Length, rotors turning Length, folded Main rotor diameter Tail rotor diameter Cabin length Cabin width (at floor level) Cabin height (on centre line)	22.90 m 15.85 m 18.59 m 4.00 m 6.50 m 2.39 m 1.82 m
Weights	Approx. basic weight Approx. max. take-off weight	7280 kg 13530 kg
Max speed		295 km/h
Range		1850 km ferry
Crew + pax		2/3 + 30

Table 1. Leading particulars of the EH101 helicopter

For maritime helicopter operations, the primary role of the EH101 may be summarised as below:-

- Anti-submarine warfare
- Anti-ship surveillance and tracking
- Anti-surface vessel
- Amphibious Operations
- Search and Rescue
- Airborne Early Warning
- Vertical Replenishment
- Electronic Countermeasures

Alternatively, when constructed to meet civil operational requirements in which up to 30 passengers can be accommodated, it is believed that the EH101 will, for the first time in a helicopter, approach the stringent safety and performance standards previously only associated with fixed-wing aircraft. Wherever proven and cost effective, 'state-of-the-art' technology has been incorporated within the basic EH101 airframe. For example, the EH101 will possess the most advanced health and usage monitoring system yet employed in any rotary wing aircraft and will provide a continuous analysis of dynamic components during flight. Further, the automatic flight control system will include a highly advanced failure-survivable system offering both coupled and uncoupled modes, way point steering, automatic transition to hover, etc.

Finally, the utility variant incorporates an alternative rear fuselage module with a rear loading ramp. Typical roles for this version of the EH101 are:-

- Offshore oil support
- Civil Defence
- Vehicle/troop transportation
- Air ambulance
- Exploration
- Logging
- SAR

WEIGHT SAVING ON THE EH101

Vehicle weight is arguably of greater importance in helicopters than in fixed wing aircraft and the EH101 is no exception. As with all new aircraft, strenuous efforts are being made to reduce the overall weight, and this may be achieved in two ways. Firstly, use of stronger material can offer the possibility of reduced section size on a given component and this approach has been adopted where possible on the EH101. However, in general, minimum section sizes are already used and there is clearly a limit to which these may be reduced. Secondly, and more importantly, the use of inherently lighter materials may offer considerably greater weight savings and it is in this category that the new

aluminium-lithium alloys fall, together with organic matrix fibre composites. Cost of both material and manufacture also enters the equation and while the extensive use of the latter would reduce weight by a significantly greater extent than the use of aluminium-lithium based alloys, the greater versatility and relatively easy formability of the metal frequently represents the least expensive route to component manufacture. Furthermore, the relatively poor impact resistance and the degradation of compressive strength when exposed to hot/wet conditions frequently exhibited by current organic matrix composite systems clearly precludes their use from some specific applications, although it would be naive to think that these problems and the manufacturing costs are not being addressed by the material manufacturers. For the time being, therefore, and certainly in the case of the EH101, valuable weight savings are envisaged by direct substitution of non-lithium-containing, so-called 'conventional' aluminium alloys with those in which lithium is a major alloying element.

It is an indication of the industry-wide desire to reduce structural weight, whilst supporting the continued use of aluminium-alloys, when it is realized that at least one aluminium-lithium alloy has taken considerably less than a decade to progress from small scale laboratory to full scale commercial production (ignoring the now-obsolete 2020 alloy composition of the late 1950's/early 1960's) and which is attracting the intense interest of the airframe constructor which the latter alloy never enjoyed. Because of the urgency to incorporate these new alloys into airframes, the scope and depth to which they have been studied and assessed must surely surpass that of any previous aluminium alloy. This is certainly the case at Westland Helicopters Ltd (WHL) where experience and confidence gained from studies during the past five years has led to the current commitment to incorporate aluminium-lithium alloys in the EH101 airframe where it is technically acceptable and cost effective.

An analysis of the EH101 airframe has led to a target minimum weight saving, solely from the use of aluminium-lithium alloys in the forward and centre fuselages of approximately 55 kg; complete replacement of all 'conventional' aluminium alloys in these regions (excluding sheet [0.8 mm]) would yield a weight saving of approximately 82 kg. Because of the intrinsically higher material cost of aluminium-lithium alloys of approximately three to five times that of 'conventional' aluminium alloys, depending upon product form, cost considerations must enter into the decisions to use the material. It is assumed that if a component is manufactured in aluminium-lithium by the same method as the component it replaces, then no additional manufacturing costs are incurred. When the manufacturing route is different, for example in the case of aluminium-lithium forgings as replacements for components machined from 'conventional' aluminium alloy plate, then die costs will occur. In the WHL analysis, however, these are excluded since it is assumed that these will be largely offset by an estimated 10-15% cost saving associated with machining forgings compared to machining components from plate, when amortised over 100 aircraft. The cost controlling criterion in the weight saving analysis is then given by the following relationship:-

$$\frac{\text{Additional material cost of aluminium-lithium}}{\text{Weight saved} \times \text{material utilisation rate}}$$

This yields a figure which represents the costs over and above those associated with the manufacture of components in conventional aluminium alloys. It can be shown that the cost of weight saving for various product forms can be ranked in order of their material utilisation rates, shown in Table 2. Thus, extrusions (90% utilisation rate) represent the cheapest weight saving while plate (7% utilisation rate) is the most expensive. A break-even cost of weight saving for the EH101 has been calculated and using

Material form	Material Utilization
Forging	20%
Extrusion	90%
Plate	7%
Sheet	50%

Table 2. Utilisation rates of various wrought aluminium alloy product forms

the above relationship, it is concluded that it is cost effective to consider (a) extruded profiles, (b) sheet and (c) forgings in aluminium-lithium alloys. Because of significantly higher weight-save costs associated with components machined from extruded bar and plate product forms, together with a relatively low identified weight save, a change to aluminium-lithium alloys on the EH101 cannot be justified for these product forms on current costs. Included in the target minimum weight saving figure of 55 kg is the assumption that structural members of the cabin main lift frame will be manufactured from aluminium-lithium forgings, as this has been shown to be below the 'break even' cost of weight saving, while machining from plate in this alloy would incur an unacceptable cost. Similarly, further weight savings may be possible from areas other than the cabin structure through the use of aluminium forgings instead of machining from 'conventional' aluminium alloy plate.

Within the aforementioned product forms, specific components identified for manufacture in aluminium-lithium alloys include only those from which a significant weight saving can be realistically achieved. In the case of extruded profiles, for example, only those sections which use in excess of 0.7 metres per aircraft or show a potential weight saving greater than 0.02 kg per aircraft have been considered. Similarly, small cleats, brackets and fittings in other categories where weight savings are minimal are excluded. With regard to sheet, only those components manufactured from thicknesses greater than 0.8 mm have been included in this analysis, as thinner gauges are not currently available commercially.

On the basis of the above analyses and together with past and present metallurgical studies, decisions have been taken as to the choice of alloy for manufacture of specific EH101 components in aluminium-lithium alloys and are summarized in Table 3. Test programmes currently in progress cover the evaluation of production grade sheet, a number of EH101 extruded profiles and a main lift frame structural member in the form of a die forging as a substitute for plate in 'conventional' aluminium alloy. Figure 2 shows schematically the location of these extrusions and forgings within the main cabin. The measured properties of the above three product forms are discussed in detail below.

Product form	Alloy	Condition	Substitute for:
Extruded sections	AA8090	Unrecrystallised 'Medium strength'	AA7075-T7411 (BS L160)
Forgings	AA8090	Unrecrystallised 'Medium strength'	AA7010-T7452 (forgings) AA7010-T736 (forgings) AA7010-T7451 (plate)
Sheet	AA8090	Unrecrystallised 'Medium strength'	AA2014-T6 (BS L157, BS L159, BS L165)
	AA2091/AA8090*	Recrystallised 'Medium strength'	
Sheet	AA8090 AA2091	Recrystallised 'Damage Tolerant'	AA2024-T3 (BS L109)

* Final decision yet to be taken as testing still in progress.

Table 3. Aluminium-lithium alloy variants to be used on the EH101.

Extrusions

Forty three different EH101 extruded sections have been identified which will be produced in AA8090 instead of alloy 7075-T7411 (L160) in which they were originally designed. To date, four different profiles have been made in commercial grade AA8090 via direct extrusion and consist of a C-channel, I-beam, right angle and seat track, these having been selected specifically to represent the general 1.6-4.5 mm range of extruded section thicknesses, fig. 3. Prototype aircraft sets of 7 m lengths have been delivered, excess material being utilized for property and microstructural evaluations incorporating comparisons with identical sections in alloy L160. Figure 4 presents the mean tensile properties of the material studied to date and shows that minimum L160 specified strength values are generally achieved although lower AA8090 ductilities are frequently measured.

Two shipments of the C-channels have been received, processing conditions of the first comprising of a nominal 2% stretch after solution heat treatment, followed by ageing for 12h at 190°C. The second batch of extrusions were subjected to a nominal 3% stretch prior to ageing for 42h at 170°C. Figure 5 shows statistically higher properties in the second material batch and are attributable to the concomitant effects of increased cold working and use of the lower ageing temperature. The resultant effect upon microstructure is illustrated in the Transmission Electron Micrographs in figure 6 in which the 2% stretch has resulted in a fairly widespread distribution of heterogeneously nucleated S'-Al₂CuMg phase, fig. 6a, although numerous, relatively S'-free regions are readily apparent. In contrast, the greater uniformity of S'-precipitation in the second material batch, fig. 6b, is primarily attributable to the associated increased degree of stretch to 3% and accounts for the enhanced properties; no significant differences in Al₃Li precipitation were detected between the material batches, fig. 6c. In view of these results, the I-beam and seat track extrusions were similarly subjected to a 3% stretch followed by ageing at 170° for 42h, as will be all subsequent extrusions.

Although the majority of extrusions will be used in straight lengths, certain configurations and applications may occasionally dictate some degree of forming. Samples from C-channels in alloys AA8090 and AA8091 (extrusions in this latter alloy were manufactured purely for research purposes) in the as-received fully aged condition were subjected to a typical re-solution treatment which may be entailed. Figure 7 shows that although T.S. and elongation levels are only slightly affected, there is a significant decrease in 0.2% PS values. This is attributable primarily to the relatively sparse S'-Al₂CuMg precipitation due to the lack of stretch-induced dislocations necessary for heterogeneous nucleation, (1-3) figure 8. The 8091 samples exhibit correspondingly higher strengths, commensurate with the higher lithium, copper and magnesium levels of this composition. Figure 7 also demonstrates some enhancement of strength in both alloys by use of a lower ageing temperature. In view of the effects of re-solution heat treatment, an alternative approach is to order in the T3511 temper those extrusions which are subject to forming during aircraft build, manufacturing trials having shown that AA8090 alloy can be manipulated in this condition: final ageing may be subsequently carried out in-house.

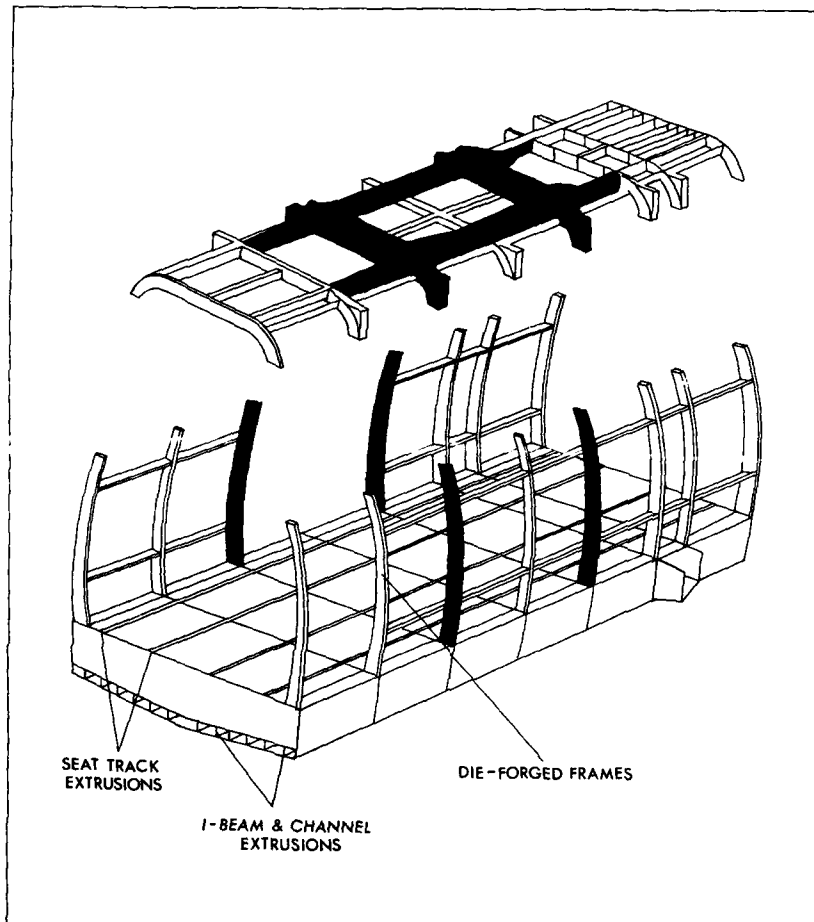


Figure 2. EH101 Main Cabin Structure. Shaded areas will remain in AA7010 plate, all other frames will change to Al Li die forgings.

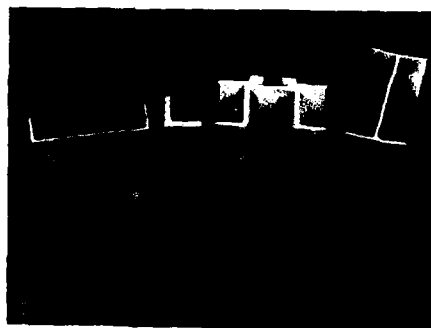


Figure 3. A selection of EH101 extrusions in alloy AA8090

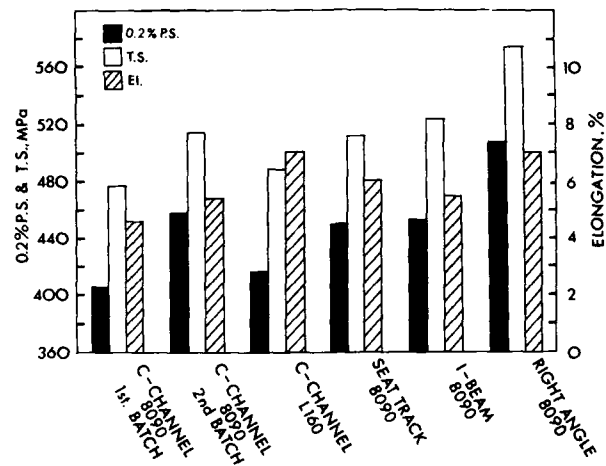
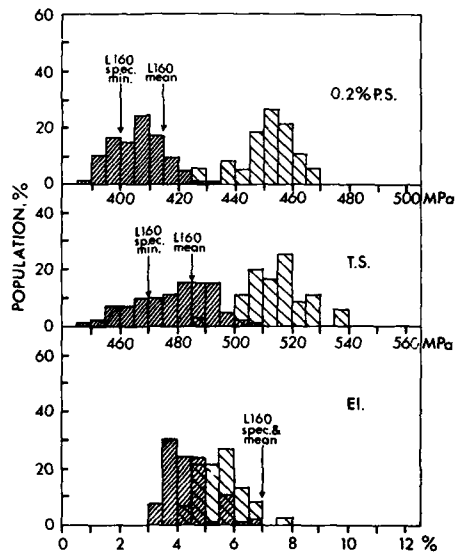


Figure 4. Mean longitudinal tensile properties of selected EH101 extrusions.



■ Initial extrusion batch, 2% stretch + 12h at 190°C
 ▨ Current extrusions, 3% stretch + 42h at 170°C

Figure 5. Longitudinal tensile properties of channel extrusions in alloy AA8090-T6511 with mean measured L160 and specified minimum values.



Figure 6. Transmission Electron Micrographs of channel extrusions in AA8090-T6511.

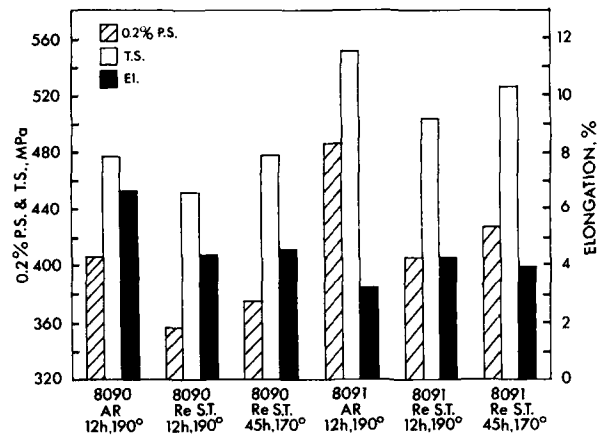


Figure 7. Mean longitudinal tensile properties of EH101 channel extrusions after various heat treatments (AR = S.T. + 2% stretch).

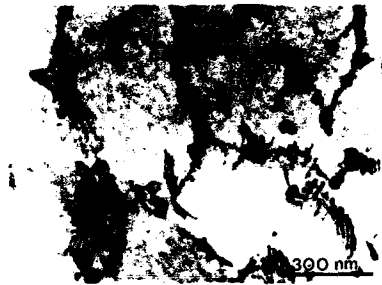


Figure 8. Sparse S' - Al_2CuMg precipitation in re-solution treated AA8090 channel extrusions aged 12h at 190°C.

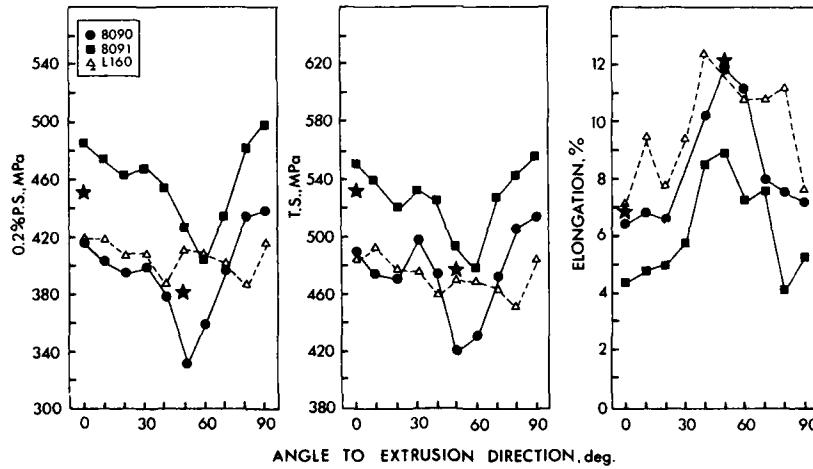


Figure 9. Mechanical property anisotropy in initial channel extrusions (2% stretch + 12h at 190°C). ★ denotes properties in corresponding extrusions but given 3% stretch + 42h at 170°C.

Due to texture effects arising from the zirconium-induced unrecrystallised grain structure of these extrusions, mechanical properties show some degree of anisotropy. Figure 9 indicates a noticeable decrease in AA8090 & AA8091 strength properties of the C-channels at an angle of $\sim 50^\circ$ to the longitudinal direction, with a corresponding increase in ductility. It should be noted however that this data was generated from material from the first batch of extrusions and reference to figure 4 indicates that an $\sim 10\%$ increase in 0.2%PS and TS may be anticipated upon adoption of the 3% stretch/42h at 170°C processing schedule. Tests to confirm this have been carried out, and although full 'round-the-clock' properties have not been measured, those at 0° and 45° to the extrusion directions are noticeably higher, as indicated in figure 9. Further, the prescribed relationship between limit and ultimate design loads leads to the stipulation that the 0.2% PS:TS ratio should be at least 0.75 and 0.67 respectively for UK-constructed military and civil aircraft (4). A 10% increase in the AA8090 TS at 50° to the longitudinal direction gives a value of ~ 460 MPa which is only marginally below the L160 specified minimum and the corresponding minimum 0.2% PS levels using the above stipulated ratios would be 345 MPa for military and 308 MPa for civil aircraft, these values being achieved in the second batch of material. Additionally, it should be noted that the channel sections, I-beams and seat track extrusions under discussion were manufactured from billet which, to date, has invariably contained magnesium levels at the bottom end of the AA8090 specification range and have been typically 0.6 w/o. A number of studies have shown that, within limits, mechanical properties are a function of magnesium content (5,6) and this is consistent with the enhanced strengths of the right angle sections, these having been extruded from AA8090 billet which contained a significantly higher magnesium level of ~ 1.3 w/o. It is understood from the metal manufacturers that all future AA8090 billet will contain higher magnesium contents of at least 1 w/o which would be expected to produce further mechanical property increases, including those at intermediate angles between L and LT directions. In summary, therefore, although low mechanical properties at 50° to the longitudinal direction have been measured on the first batch of C-channels, modifications to alloy composition and processing parameters are likely to substantially elevate strengths in similar extrusions for production aircraft construction.

The fatigue behaviour of the C-channels has been investigated and figure 10 shows a similar response from plain test specimens from AA8090 (first batch) and L160 extrusions. In order to simulate actual production procedures, further testing compared the fatigue properties of riveted lap shear specimens which were anodised and epoxy primed prior to wet assembly with Polycast. As illustrated in figure 11, again, samples from the AA8090 (first batch) and L160 extrusions behaved similarly. Although both alloys failed by multi-origin fatigue adjacent to the fixing holes, the fatigue fractures of the AA8090 samples displayed a distinctive 60° angle to the extrusion direction, figure 12. This is consistent with the tensile data referred to above and presented in figure 8 and indicates that the fatigue crack follows the path of least resistance which, due to texture effects, lies at 50 - 60° to the extrusion direction.

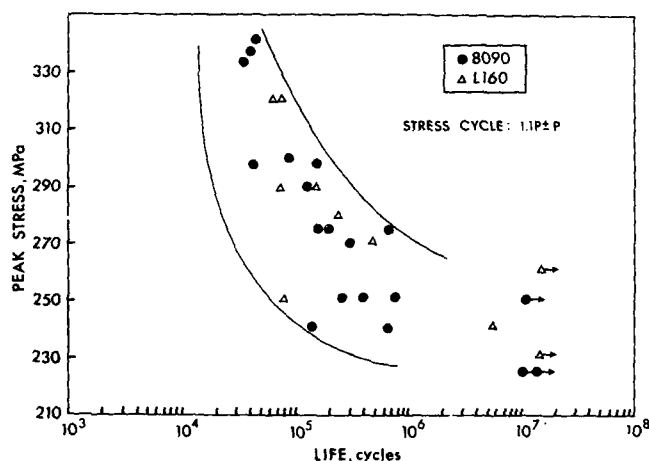


Figure 10. Plain section axial fatigue properties of channel extrusions in AA8090 - T6511 (initial batch) and 7075-T7411 (L160) alloys.

As has been observed by other workers in aluminium lithium alloys (7-9), exposure of the AA8090 extrusions to elevated temperatures results in surface depletion of lithium and magnesium. This has been minimised by use of a salt bath solution heat treatment. Nevertheless, the effect persists and as shown in figure 13, the micro-hardness gradient adjacent of the extruded metal surface indicates that the depleted layer extends beyond the limit of the band of peripheral coarse grain, the latter also being clearly evident on the L160 extrusions. Since lithium and magnesium both contribute to the strength of the metal via precipitation of Al_3Li and $\text{S-Al}_2\text{CuMg}$, the existence of a depleted surface layer may be partly likened to a clad material, thus exhibiting reduced measured mechanical properties compared to the 'unclad' material. Although pickling and anodizing will remove a layer of this surface feature, the depleted layer will still occupy a significant proportion of the 1.6 mm cross-section of the C-channels and I-beams with attendant reduction in measured mechanical strength. Clearly, such reductions will progressively diminish (for a given depleted depth) as section size increases.

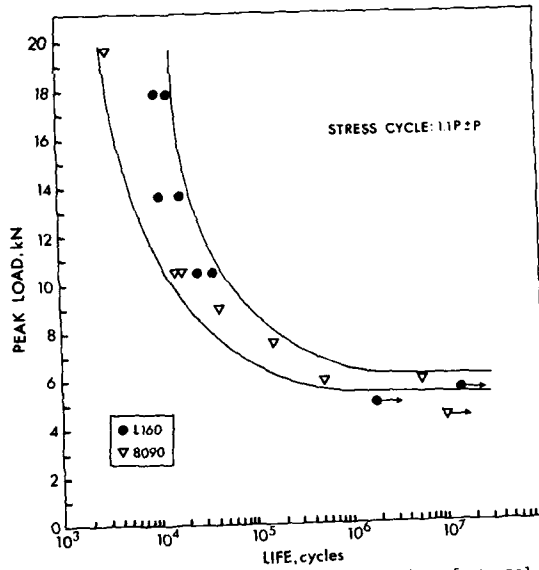


Figure 11. Lap shear axial fatigue properties of channel extrusions in AA8090-T6511 (initial batch) and 7075-T7411 (L160) alloys

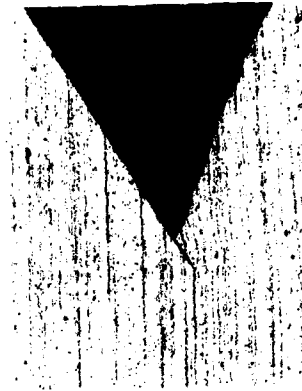
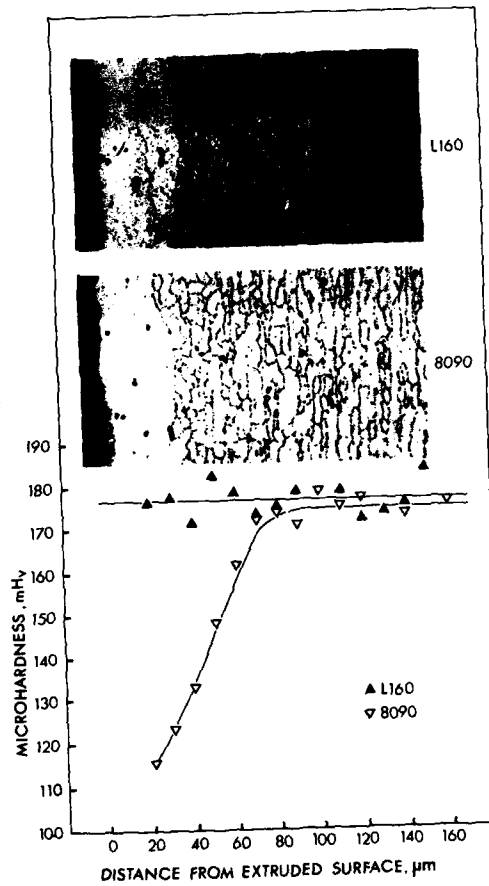


Figure 12. Typical axial fatigue failure in AA8090 channel extrusions

Figure 13. Location of Li-Mg depleted surface layer w.r.t. peripheral coarse grain band in channel extrusions.



Sheet

The minimum gauge of aluminium-lithium sheet currently produced commercially is 1.0 mm (Alcan) and 1.2 mm (Pechiney), whereas AA2014-T6 sheet thicknesses of as low as 0.4 mm are required for the EH101. Accordingly, until the metal manufacturers situation changes, only partial substitution with aluminium-lithium in this product form will be possible. However, for areas on the aircraft where sheet thickness greater than 1 mm or 1.6 mm are specified, it is envisaged that both AA8090 and AA2091 alloys will be used in the following ways:-

a) 'Medium strength' clad and unclad AA2014-T6 sheet (BS L165 and BS L157 respectively) will be replaced by unclad, unrecrystallised AA8090-T8 or unclad, recrystallised AA2091-T8.

b) 'Damage tolerant' clad 2024-T3 sheet (BS L109) will be replaced by unclad, recrystallised AA8090-T81 or unclad recrystallised AA2091-T81.

Although there is a general effort within WHL to reduce the number of permitted materials on the aircraft, the above intended use of two alloys for the same requirement is, at present, unavoidable. This arises from the fact that dual sourcing of a single alloy which could meet both 'medium strength' and 'damage tolerant' properties is not possible, since AA8090 sheet is available only from Alcan while AA2091 sheet is currently produced only by Pechiney. Projects currently in progress at WHL aim to verify that the proposed alternative use of the two alloys, as outlined above, is acceptable as far as properties are concerned. It should be noted that both unrecrystallised and recrystallised AA8090 is available from Alcan, whereas for thin sheet (<3 mm), it is believed that Pechiney will only supply recrystallised material primarily for underaging to satisfy 'damage tolerant' requirements. The behaviour of AA 2091 aged to this latter category is being studied, the T81 temper being achieved by ageing solution heat treated and stretched 1.6 mm sheet at 130°C for 12h. Figure 14 shows that strength properties exceeding the minimum specified values of BS L109 can be achieved and generally match the measured levels in that alloy. Both alloys exhibit some degree of anisotropy. However, characteristically lower ductilities are evident in the aluminium-lithium alloy.

It is anticipated that the majority of components will be formable in the as-received T3 temper and trials in AA2091 are planned to confirm this. In the event that re-solution heat treatment is necessitated, tests have shown this to have no measurable effect upon strength after ageing at 135°C for 12h and is consistent with the fact that, unlike the 'medium strength' unrecrystallised AA8090 extrusions discussed previously, recrystallised AA8090 and AA2091 sheet for 'damage tolerant' applications is significantly underaged. This is of a degree insufficient to form the S-Al₂CuMg phase whose presence is not necessary to meet the relevant strength requirements, and hence elimination of the stretch during re-solution heat treatment of material in the T3 temper would appear to be of little consequence. The corresponding Transmission Electron Micrographs in figure 15 show that the only noticeable effect upon the sub-microstructure of AA2091 alloy is a modification of dislocation characteristics in material re-solution heat treated prior to ageing: S-Al₂CuMg was not detected in either sample. In addition to static property tests, fatigue behaviour of 'damage tolerant' AA2091 sheet has also been studied (10).

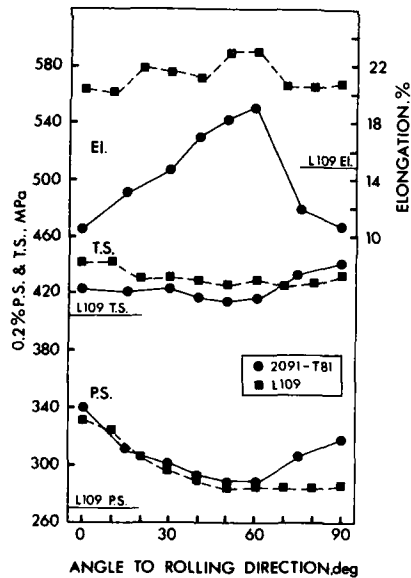


Figure 14. Static mechanical properties of 'damage tolerant' AA2091-T81 alloy sheet compared with BS L109.

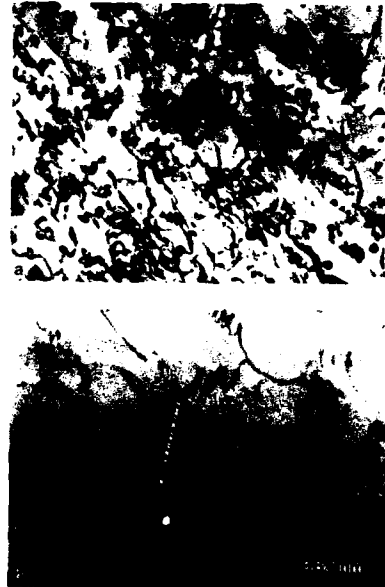


Figure 15. Recrystallised AA2091 sheet (a) T3 + 12h at 135°C and (b) re-solution treated + 12h at 135°C.

The S-N curves in figure 16 correlate with the above findings and show no noticeable difference in properties of material re-solution heat treatment prior to ageing. Further, at equivalent peak stress levels of ~250 MPa and below, AA2091-T81 specimens exhibit noticeably longer fatigue lives compared to L109 and which accord with the lower fatigue crack propagation rates generally claimed for aluminium-lithium based alloys (11,12). Studies of recrystallised 'damage tolerant' AA8090 sheet are about to commence.

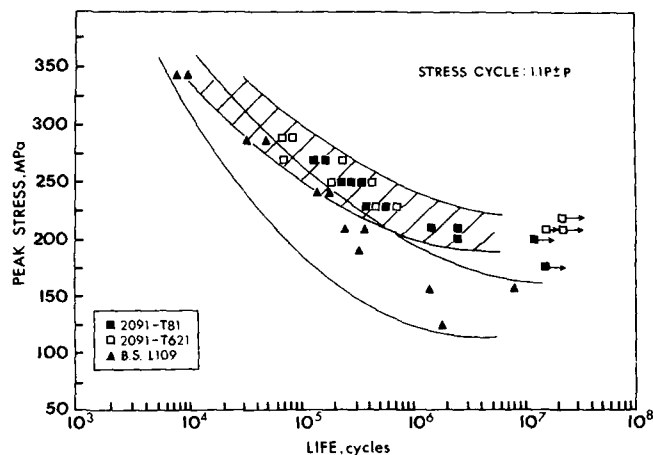


Figure 16. Comparison of fatigue behaviour of (i) stretched and (ii) re-solution treated recrystallised AA2091 sheet aged 12h at 135°C, with AA2024-T3 sheet (BS L109).

Work to assess 'medium strength' properties of recrystallised AA2091 and unrecrystallised AA8090 alloys in sheet form is also in progress. Figure 17 compares static properties obtained by ageing T3 temper sheet for 20h at 185°C with those from samples of alloy BS L157 (unclad AA2014A-T6). Alloy AA8090-T8 exhibits marked anisotropy, with strength levels producing a minimum at 55° to the rolling direction and which, between angles 40°-70°, fail to achieve corresponding BS L157 specified values. However, the majority of sheet originally designated for use on the EH101 is of the clad version (i.e. BS L165), minimum specified strength levels of which are met by AA8090-T8 at all orientations. In contrast, properties in alloy AA2091-T8 are noticeably less anisotropic, with minimum BS L157 specified strengths being achieved at all test angles. As found for 'damage tolerant' sheet, most aluminium-lithium ductilities are significantly lower than measured values from corresponding 'conventional' aluminium alloy. With the exception of elongation, the results demonstrate that 'medium strength' static properties can be achieved in alloy AA2091 and also clearly differentiate between recrystallised and unrecrystallised grain structures, the diminished retention of rolling texture in this material and in BS L157 leading to greater isotropy of properties.

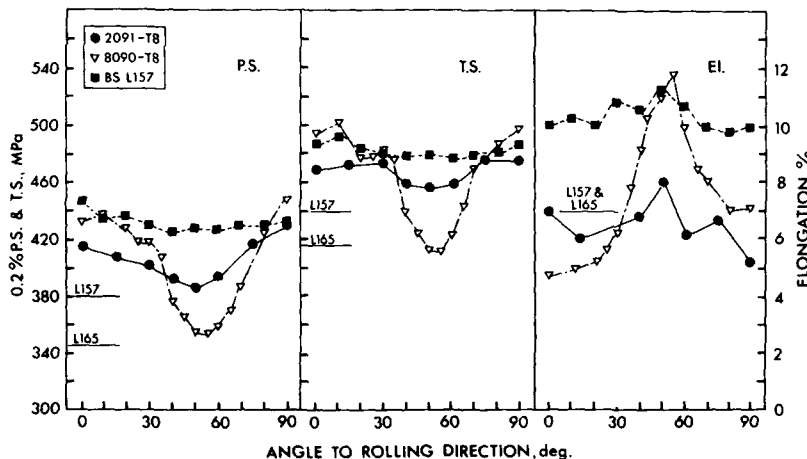


Figure 17. Mechanical property anisotropy in 'medium strength' recrystallised AA2091-T8 and unrecrystallised AA8090-T8 alloy sheet compared with BS L157.

WHL studies have been made of the effect of ageing parameters upon the degree of anisotropy in unrecrystallised AA8090-T8 sheet. The results are summarised schematically in figure 18, indicating that the anisotropy, measured as a percentage reduction in 0.2% PS at 55° to the rolling direction compared to the corresponding longitudinal value, decreases as the degree of ageing increases and has been attributed to the resultant greater S-phase precipitation (13,14). However, there are limits to which an alloy can be practically overaged and as shown by the 12h at 210°C schedule in figure 18, heavy overaging can result in an unacceptable reduction of strength. Further, a number of workers have indicated that fracture toughness decreases with increased degree of ageing, optimum values being demonstrated in relatively underaged tempers (14, 15, 16). In this respect the previously mentioned work on AA2091 sheet may be an indication of the direction which future events may follow, wherein ageing of recrystallised sheet to 'medium strength' levels will become the norm, the reduction in strength at the 55° orientation being considerably less than that achievable by any degree of overaging of unrecrystallised material and without the associated deleterious effects upon other properties. Further studies to this effect are in progress at WHL, together with parallel investigation on producing 'medium strength' properties in recrystallised AA8090 sheet.

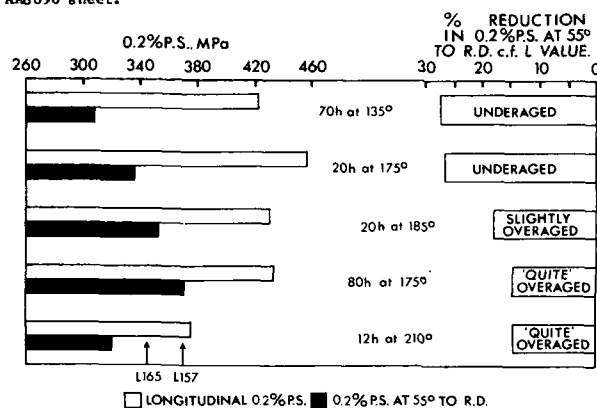


Figure 18. Effect of different ageing treatments upon anisotropy in unrecrystallised AA8090-T8 sheet.

As with AA2091 subsequently aged to the 'damage tolerant' temper, it is the intention to cold form unrecrystallised AA8090 sheet in the T3 temper in order to retain the post-solution heat treatment stretch. Forming trials on this alloy have been carried out and the material has behaved satisfactorily. However, it should be noted that the metal in question had been manufactured approximately one year prior to testing and although it is not expected that longer term natural ageing would have any effect, this cannot be confirmed at the moment. Sheet from the aforementioned batch has been isolated and further forming trials will be carried out in a few years time. In the event that re-solution heat treatment is necessitated, trials have been carried out to assess the effect upon properties. Figure 19 illustrates typical results and show a significant drop in 0.2% PS values upon re-solution treatment values of TS are less affected and are similar for both alloys while AA2091 exhibits significantly higher ductilities. Figure 20 shows Transmission Electron Micrographs of AA2091 sheet and confirm that removal of the stretch-induced dislocation network inhibits widespread fine S-phase precipitation, coarser particles of which form predominantly upon helical dislocations formed during quenching; similar features were exhibited by the AA8090 sheet.

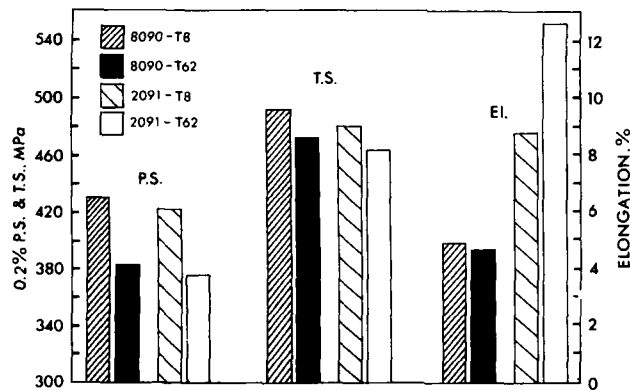


Figure 19. Longitudinal mechanical properties of stretched and re-solution treated AA2091 and AA8090 sheet prior to ageing 24h at 185°C (T8 and T62 respectively).



Figure 20. Transmission Electron Micrographs showing differing S-Al₂CuMg precipitation in AA2091 sheet (a) stretched and aged 24h at 185°C to achieve T8 temper, (b) re-solution heat treated and aged 24h at 185°C to achieve T62 temper

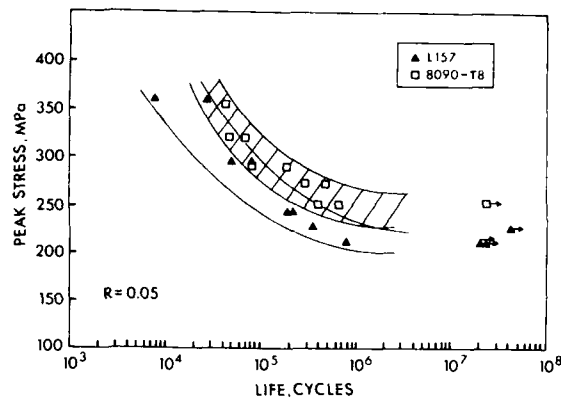


Figure 21. Comparison of long transverse fatigue behaviour of BS L157 and AA8090-T8 sheet.

Fatigue testing of unrecrystallised AA8090 sheet is in progress and some of the data generated so far is shown in figure 21. Compared to BS L157, the aluminium lithium alloy appears superior, particularly at the lower applied stress levels, and again substantiates claims of lower fatigue crack growth rates in these alloys. Further work will investigate fatigue behaviour in AA2091 sheet aged to the 'medium strength' category from both the T3 temper and after re-solution heat treatment. The effect of the latter upon unrecrystallised AA8090 sheet properties will also be studied, as will test pieces cut at an angle of 55° to the rolling direction.

Forgings

As mentioned earlier in this paper, there is considerable scope for the incorporation of aluminium-lithium forgings in the EH101 airframe. During the past few years, WHL have evaluated a number of sample components to give an indication of the feasibility of using this product form, in addition to gaining an insight into the processing parameters necessary to obtain optimum mechanical properties. Figure 2 shows the location of components within the cabin structure which will be changed from AA7010-T7451 plate (DTD 5130A) to aluminium-lithium die forgings. Figure 22 shows as-forged and machined samples of the latter which is a structural side member recently manufactured for WHL in alloys AA8090, AA8091 and AA7010. The forging stock consisted of round billet machined from a cast ingot. After solution treatment the forgings were cold water quenched and cold compressed nominally 3% prior to ageing for 20h and 30h at 175°C for AA8091 and AA8090 respectively.



Figure 22. Aluminium-lithium EH101 main cabin lift frame die forgings before and after machining to finished dimensions.

An extensive evaluation programme is currently in progress and is comprised primarily of tests to assess static tensile, fatigue, stress corrosion, I.C. corrosion, fracture toughness and fatigue crack growth rate behaviour: these will be complemented by full metallographic and analytical studies. The adopted approach to the programme has been to cut each forging into five sections of approximately equal size. The extent of subsequent testing is indicated by examples of the corresponding sectioning diagrams, shown in figure 23. Extensive tensile testing has been carried out to fully assess the variability in properties to be expected from a forging of this configuration and size.

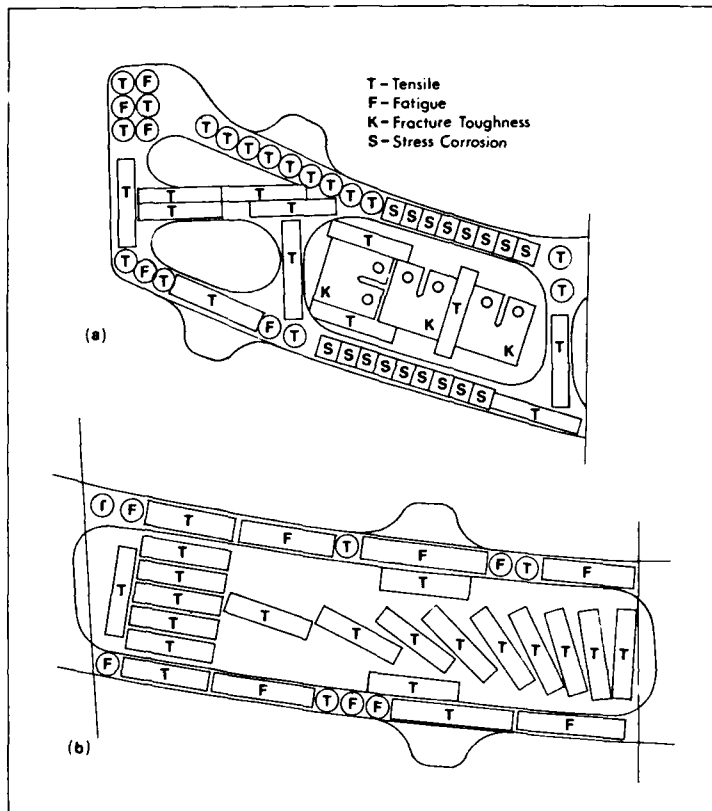


Figure 23. Typical sectioning diagrams for EH101 main cabin lift frame die forgings.

Comparisons have been carried out from identical locations within the three alloys, with additional tests on AA7010-T7451 plate where appropriate. Space does not permit consideration of results from each specific location, but instead, the general trend of properties is presented below.

Reference to figure 23b indicates that tensile tests were taken from the central plane of the forging in order to assess any anisotropy effects which may be present: the results are shown in figure 24. With the exception of a noticeably higher longitudinal 0.2% PS in AA 8091, there is little difference in static tensile properties between the two aluminium-lithium alloys. Both show significant anisotropy particularly in 0.2% PS values, with minimum levels occurring at 20-30° to the longitudinal direction. The geometrical longitudinal direction was generally coincident with that with respect to grain structure. This is in contrast to the corresponding 55° angle at which minimum properties generally occur in other aluminium-lithium product forms and it is interesting to note that a 55° angle measured from the long transverse direction is coincident with a 25° angle measured from the longitudinal direction. Although confirmatory tests have yet to be carried out, it may be that metal flow in the long transverse direction during forging is analogous to that occurring in the longitudinal direction during manufacture of rolled products and extrusions. If this is the case, then similar texture effects would be expected to arise, thereby giving strength minima at the angle observed.

Strength values in the AA7010 forging appear to follow a similar trend as above but to a much lesser extent and although the 0.2% PS of the aluminium lithium alloys is significantly lower, they nevertheless generally achieve the minimum allowable EH101 main lift frame requirements (S-values) as determined by WHL Stress office for longitudinal, long transverse and short transverse directions. As with the extrusions discussed earlier, the anticipated use of higher magnesium levels within the AA8090 specification range would be expected to elevate the entire 0.2% PS curve in figure 24 to higher property levels.

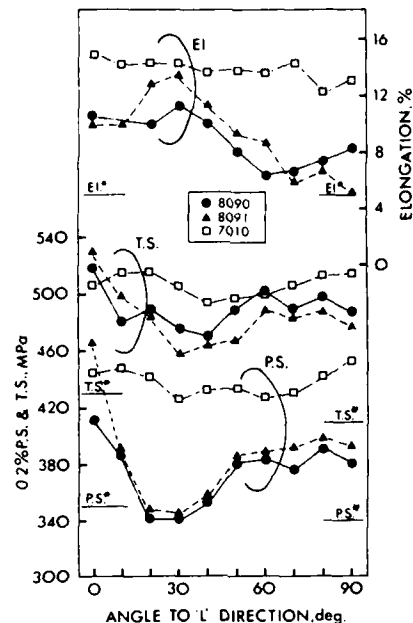


Figure 24. Mechanical property anisotropy in AA8090, AA8091 and AA7010 EH101 die forgings (* - WHL stress office minimum requirements).

Tensile properties in longitudinal, long transverse and short transverse directions have been measured from numerous locations within the components. Analysis of the results so far has shown noticeable property variations throughout each forging but which do not appear to be associated with any particular location. These may be due to local and random modifications to S-Al₂CuMg precipitation characteristics associated with differing degrees of post-solution treatment cold-compression: this has yet to be confirmed and is the subject of current work. Figure 25 shows graphically the range of 0.2% PS and TS levels measured as a function of ductility in relation to the aforementioned minimum specified property levels for the EH101 main cabin frame. The following conclusions may be drawn from the work to date:-

- 1) The considerable degree of overlap in AA8090 and AA8091 0.2% PS, TS and elongation properties is consistent with the corresponding similarities shown in figure 24.
- 2) For a given location, AA7010 ductilities are consistently higher than corresponding aluminium-lithium levels.
- 3) In the longitudinal and long transverse directions, 0.2% PS and TS values of the AA7010 component overlap with those at the upper end of the AA8090 and AA8091 ranges. In the short transverse direction, AA7010 values, in most cases, clearly exceed those of aluminium-lithium.
- 4) Minimum specified 0.2% PS and TS values are exceeded by AA8090 and AA8091 in nearly every case, although corresponding specified ductility values are not always achieved in the longitudinal and long transverse directions. However, these lower values may be acceptable, since it has been shown that, unlike 'conventional' aluminium alloys, low ductilities in aluminium-lithium do not necessarily correspond to low fracture toughness properties and in fact, superior values have been measured in the new alloys (12). Tests are in hand to confirm this on the present forgings. Further, enhanced ductility would be expected from the aforementioned planned higher magnesium levels for AA8090 billet.
- 5) Comparison of AA8090 and AA8091 property ranges in figures 25 b/c with those in figures 25 e/f indicate that T.S. values exceed the minimum specified requirements by a noticeably greater degree than corresponding 0.2% PS properties. The implication here is that a higher minimum TS values may be specified, particularly in the ST direction.

Although other property measurements as outlined previously have yet to be completed, on the basis of the tensile data it is almost certain that (a) substitution of an aluminium-lithium alloy into the EH101 main cabin lift frame will take place and (b) of the two aluminium-lithium alloys studied, AA8090 will be selected for use on production aircraft. This is fortuitous, as this alloy is the most advanced in terms of commercial and production aspects and, metallurgically, is less likely to exhibit some of the less desirable features associated primarily with the higher copper content of AA8091, such as greater quench sensitivity and increased susceptibility to corrosion/stress corrosion.

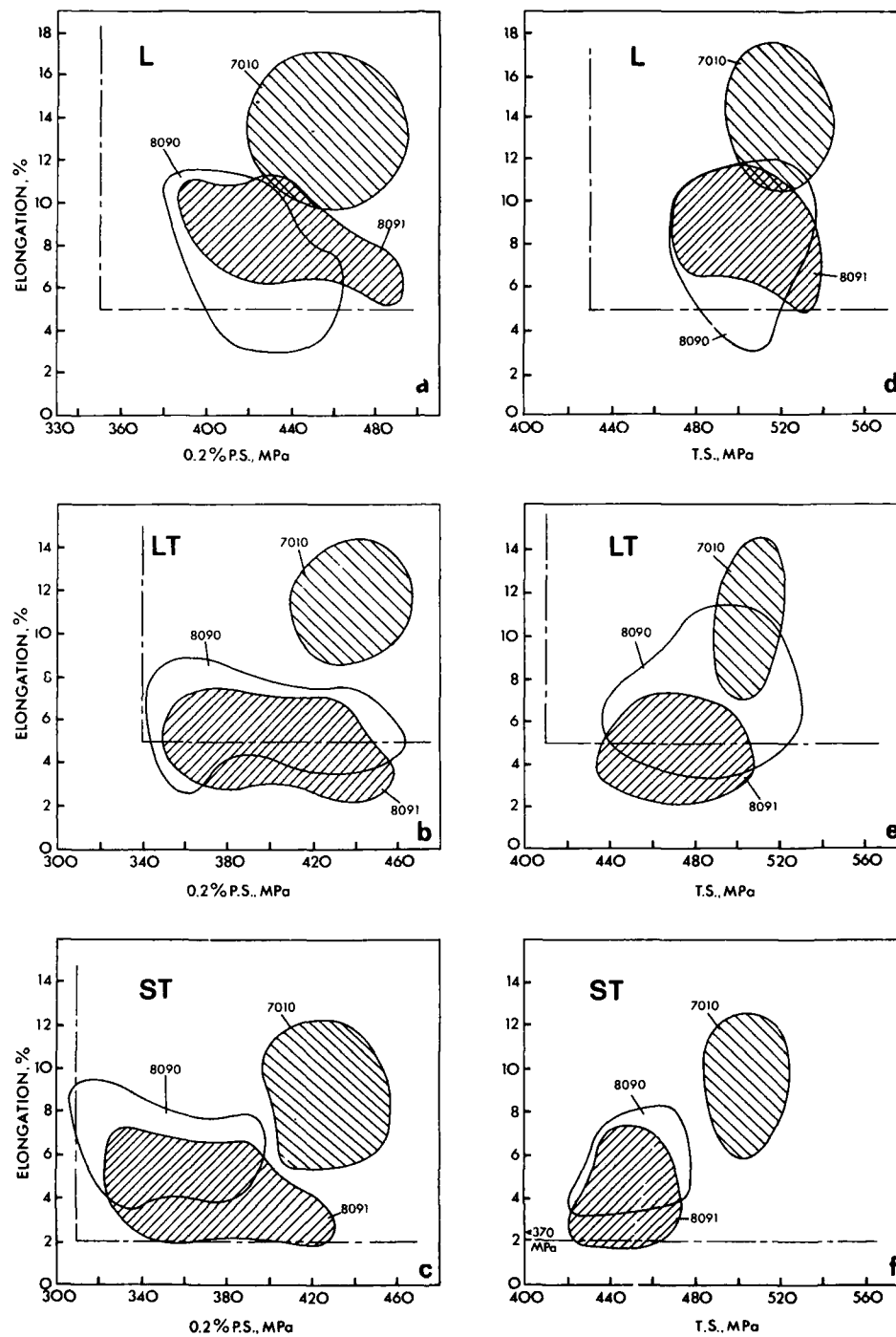


Figure 25. Summary of mechanical properties measured on AA8090, AA8091 and AA7010 EH101 main lift frame die forgings showing VBL stress office minimum requirements.

Preliminary metallographic and fractographic studies have commenced upon tested tensile specimens. Noticeable differences are apparent between the two aluminium-lithium alloys, AA8090 containing a relatively uniform distribution of unrecrystallised grains of a flattened but cylindrical appearance as shown in figures 26 a,b, and which exhibit a tensile failure mode predominantly of intergranular fracture lengthwise along the grains and across the grain ends as illustrated in figures 27a and 27b respectively. Significant ductility at the grain boundaries is indicated by the dimpled appearance of the intergranular facets in figure 27c and is consistent with the good ST elongation values measured in this alloy. In contrast, the AA8091 forging contained a duplex grain structure comprised of relatively coarse, unrecrystallised grains but surrounded by colonies of significantly smaller grains which also appeared to be unrecrystallised, figure 26, c,d. Corresponding tensile failure took place by intergranular fracture primarily through the latter to produce fracture surfaces similar to those from AA8090 but which exhibited noticeably less dimpling on the intergranular facets, possibly accounting for the lower overall ST ductility of AA8091 as shown in figure 25f. Transmission Electron Microscopy is about to commence to relate this feature to the submicrostructure.

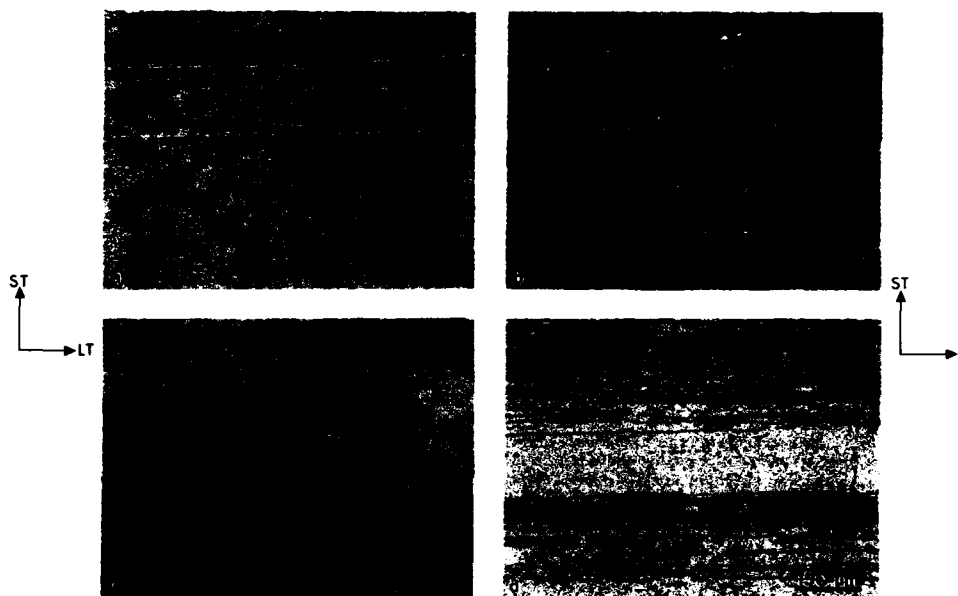


Figure 26. Grain structures in aluminium-lithium die forgings.
(a) and (b) AA8090 and (c) and (d) AA8091.

Fatigue testing has commenced and although relatively few results have been generated so far, initial indications are that 8090 and 7010 properties are essentially the same at high stress levels, but those of the aluminium-lithium alloy are marginally superior at low applied stress. This, again, is in accordance with the claimed lower fatigue crack growth rates of aluminium-lithium. Some degree of scatter has been found as would be expected in attempting to generate an S-N curve using specimens from various locations within a forging. Additionally, in order to derive a direct comparison between the three alloys, specimens will be tested such that those from any one specific location will be subjected to a common applied stress, thereby reducing any effects of differing grain structure, cold compression, rates of quench, etc. Construction of an eventual S-N curve will be attempted using only data points from locations which, after post failure examination of corresponding test pieces, appear similar in microstructure. By following this approach, it is hoped that the degree of scatter may be minimised.

CONCLUSIONS

A weight saving cost analysis of the potential incorporation of aluminium-lithium alloys on the EH101 helicopter at WHL has rejected the use of plate and extruded bar as uneconomical, but has shown sheet, extruded profiles and die forgings to be cost effective. As a result, a number of the larger components, originally intended to be machined items, will now be produced as aluminium-lithium forgings. Specific EH101 components in alloys AA8090 and AA2091 have demonstrated satisfactory and sometimes superior properties to those of the 'conventional' aluminium alloys AA2014, AA2024, AA7075 and AA7010 currently employed. Accordingly, extensive use will be made of the new materials to effect significant weight savings and which will lead to the emergence of the EH101 as the world's first 'aluminium-lithium' helicopter.

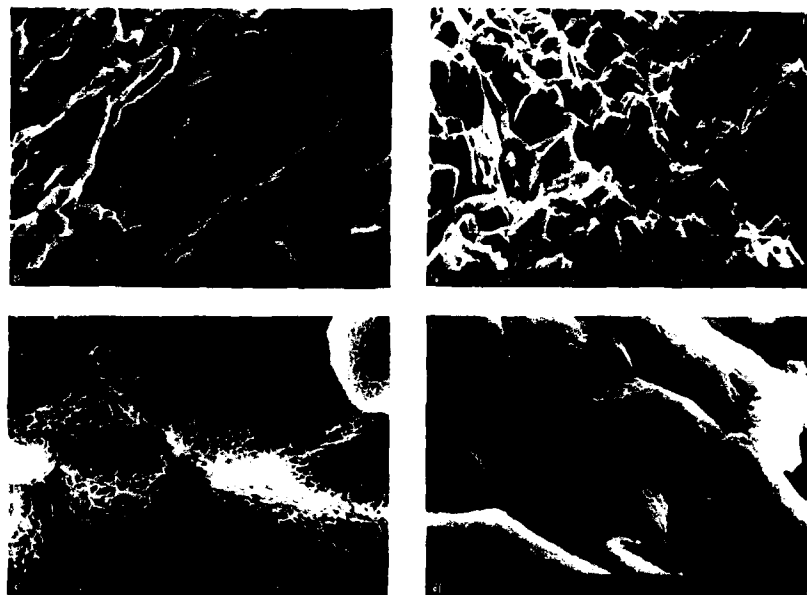


Figure 27. Intergranular fracture from aluminium lithium die forgings (a) AA8090 ST-fracture surface (b) AA8090 L-fracture surface (c) Dimpled intergranular facets on AA8090 ST fracture surface and (d) slightly dimpled AA8091 ST fracture surface.

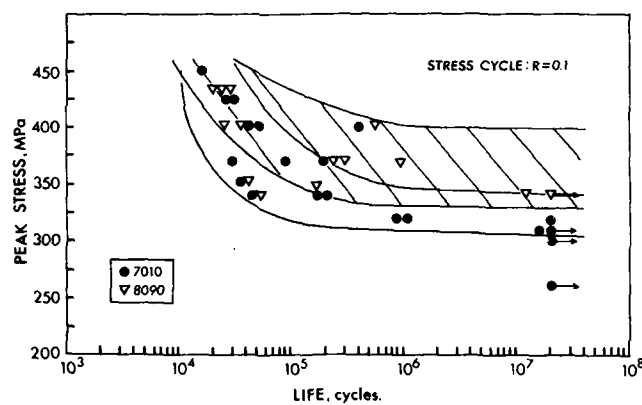


Figure 28. S-N curves for AA8090 and AA7010 die forgings.

REFERENCES

1. P J Gregson and H M Flower, Acta Met., 1985: 33, 527
2. C J Peel, B Evans, C A Baker, D A Bennett, P J Gregson and H M Flower, Proc - 2nd Int. Conf. on Al-Li alloys, 1983, TMS-AIME, New York, 363.
3. J White, W S Miller, I G Palmer and T S Saini, Proc. 3rd Int. Conf on Al-Li alloys, 1986, Institute of Metals, London, 26.
4. C J Peel, B Evans and D S McDermid, Ibid ref. 3.
5. P J Gregson, C J Peel and B Evans. Ibid ref. 3, 516
6. S J Harris, B Noble and K Dinsdale, Proc. 4th Int. Conf on Al-Li alloys, 1987. Societe Francaise de Metallurgie, 48, C3-643.
7. S Fox, H M Flower and D S McDermid, Scripta Met, 1986, 20, (1), 71
8. S Fox, H M Flower and D S McDermid, Ibid ref 3,
9. A F Smith, Metals and Materials, 1987, 8, 438
10. A F Smith, Paper submitted to Materials Science and Technology, 1988
11. P Meyer and B Dubost, Ibid ref. 3, 37
12. R Grimes, T Davis, H J Saxty and J E Fearon, Ibid ref 6, C3-11
13. P J Gregson and H M Flower, Acta Meta, 1985, 33, 3, 527
14. M A Reynolds, A Gray, E Creed, R M Jordan and A P Titchener. Ibid ref. 3, 57.
15. W S Miller, J White, M A Reynolds, D S McDermid and G M Starr. Ibid ref. 6, C3-151.
16. K Wilgemann, H Buhl, R Braun and M Peters. Ibid ref. 6, C3-677.

ACKNOWLEDGEMENTS

The author is indebted to EH Industries for permission to publish this paper. Thanks are due to colleagues at Westland Helicopters Ltd whose efforts contributed to the work described in the paper, and in particular to Mr B Bagwell for his invaluable assistance with the experimental work and to Mr W S Clifford for carrying out the weight saving cost analysis. Finally, Mr B C Gittos, Mr N L Bottrell and Mr R Sanders are thanked for their support and proof reading of the manuscript.

Aluminum-Lithium: Application of Plate and Sheet to Fighter Aircraft

Byron A. Davis
Branch Chief
Materials and Process Development
McDonnell Aircraft Company
P.O. Box 516
St. Louis, Missouri 63166
U. S. A.

SUMMARY

The potential for weight savings resulting from the low density and high stiffness of aluminum-lithium (Al-Li) alloys led McDonnell Aircraft Company to consider Al-Li alloys for use on both new and existing aircraft. The successful fabrication, and flight testing, of several demonstration parts on both the F-15 and F/A-18 increased interest in these alloys. In support of these and other applications of Al-Li plate and sheet, the mechanical properties, conventional formability and superplastic formability of 2090 and 8090 were evaluated. With a few notable exceptions, such as the anisotropy in sheet, these Al-Li alloys were comparable to conventional aluminum alloys. Chemical processing and corrosion resistance of 2090 and 8090 were also investigated and again were found comparable to conventional aluminum.

INTRODUCTION

A study [1] at McDonnell Aircraft Company (MCAIR) in 1978 showed that an advanced aluminum alloy with 10 percent lower density would give a larger weight savings per aircraft than a 10% increase in strength and modulus combined (Figure 1). With the introduction of the current generation of aluminum-lithium (Al-Li) alloys, which are 8 to 10 percent less dense than conventional aluminum alloys, this large weight savings is now within reach. Al-Li alloys are superplastic [2-4], and further cost and weight reductions are possible through designs that reduce the number of detail parts and fasteners. MCAIR has thus been evaluating the Al-Li alloys 2090, 8090 and 8091 for potential applications on existing and future aircraft. These three alloys can be considered production ready, although not all mill product forms are available for all of the alloys.

Our first attempt to use Al-Li alloys was in 1985 when these alloys were considered for the three upper and two lower wing skins of the F-15E. Use of alloy 8090 for these wing skins would have potentially reduced the weight of each aircraft by 83 lbs. (369 N). However, 8090 could not be incorporated into the F-15E design because production lots of plate were not available in time.

Subsequently, the 2124-T851 upper aft inboard wing skins on the F-15 Short Takeoff and Landing Maneuvering Technology Demonstrator (S/MTD) were replaced with wing skins made from 1.8 inch (45.7 mm) 8090-T851 plate. The 8090 wing skins, shown in Figure 2, were manufactured using the same sequence of operations as the 2124 wing skins. The 8090 plate was machined at Cleveland Pneumatic Corporation, Tullahoma, TN; peen formed to the moldline configuration at Metals Improvement Company, Pacoima, CA; fluorescent penetrant inspected at CED-TEK Corporation, Los Angeles, CA; and finally, sulfuric acid anodized/dichromate sealed at Anadite Corporation, Los Angeles, CA. The 8090 wing skins were then drilled, painted, and installed on the S/MTD aircraft. The wing skins were successfully flight tested in September 1986 (Figure 3).

The fabrication of the 8090 wing skins for the F-15 S/MTD revealed no notable differences in the response of this alloy to machining, peen forming, inspection and finishing operations normally performed on 2124 plate. In a parallel machining study, face milling and peripheral milling of 1.8 inch (45.7 mm) 8090-T851 plate was compared with 7075-T7351 plate. The force, horsepower and tool wear during these operations were monitored and the values for 8090 were equal to or less than those for 7075-T7351. No special tooling or setup requirements were identified.

Next, eighteen ALR 45/Detector Access Covers for the F/A-18 (Figure 4), normally roll formed from 7075-T6 clad sheet, were fabricated without difficulty from 0.10 inch (2.54 mm) 2090-T83 clad sheet. The 2090-T83 covers were roll formed and then chemically milled to reduce the sheet thickness and produce the required pocket. The chemical milling was accomplished using a proprietary MCAIR solution developed for 2090. Fabrication was completed by drilling and countersinking holes, and applying an exterior moldline finish (Figure 5). Plans are to install the covers on carrier based F/A-18 aircraft and evaluate their in-service performance.

In light of these successes, Al-Li alloys are being considered for use on the next generation F/A-18, the Hornet 2000. Direct substitution of Al-Li alloys for conventional aluminum without redesign is being considered for all aluminum structure on the aircraft. Figure 6 shows applications for which Al-Li alloys are considered to be currently ready and those for which it is believed that Al-Li alloys will be ready by 1990. This breakdown shows that the applications for Al-Li alloys having the largest potential weight savings, sheet applications in primary structure and hand and die forgings, will not be realized until the 1990's.

In support of this program and other advanced programs, MCAIR has been investigating the mechanical properties, formability and secondary processing of alloys 2090, 8090 and 8091.

MECHANICAL PROPERTIES

It has been reported in the literature [5] that the experimental Al-Li alloys had anisotropic tensile properties in sheet products because of the large amount of texture in sheet coupled with the ease of planar slip in Al-Li alloys. Minimum values of yield and ultimate strengths were reported at approximately 55° from the longitudinal direction. The maximum tensile elongations were also reported to be at 55° from the longitudinal direction. Proprietary processing and aging treatments [5] which make the tensile properties of Al-Li sheet isotropic have been developed by British Alcan Aluminum Ltd.

Tensile tests were conducted to evaluate the amount of anisotropy in available 2090 sheet. MCAIR has only recently been able to obtain 8090 sheet for evaluation. Measurements of tensile properties of 0.063 in. (1.6 mm) and 0.100 in. (2.5 mm) ALCLAD sheet 2090-T83 sheet at 0°, 30°, 45°, 60° and 90° to the rolling direction have shown that the minimum properties occur between 45° and 60° off the rolling axis. The minimum properties differ by about 15 ksi (103.4 MPa) from the maximum properties. This difference is considerably more than in conventional aluminum alloys as is shown in Figure 7. Unless orientation of a part with respect to the rolling direction is considered when a part is fabricated, the minimum properties of 2090 sheet must be used as design allowables. If minimum properties are used, substitution of 2090-T83 for 7075-T76 will be difficult.

Current MCAIR designs are developed using the minimum properties, which occur at 90° to the rolling direction in conventional aluminum alloys, without requiring special orientation of the part. Sheet utilization is then maximized in production by using a computer generated nesting plan. Specifying orientation in the sheet for each part as part of the design would not be cost effective at MCAIR. Hence, we feel that 2090 can be directly substituted for 2024-T81 but not for 7075-T76.

Anisotropy was also evaluated in Al-Li plate and was found not to be a problem. Figure 8 shows that the anisotropy in the ultimate strength of 8090-T8771 is less than 5 ksi (34 MPa). The minimum tensile strength of 8090-T8771 plate is only 5 ksi (34 MPa) less than the minimum tensile strength of 7050-T7451. Potential substitution of 8090-T8771 for 7050-T7451 by 1990 seems realistic. Currently the properties of 8090-T8771 exceed those of 7075-T7351 and direct substitution of 8090 for 7075 plate is considered viable today.

The existence of a lithium-depleted layer of approximately 0.01 in. (0.25 mm) depth on the surface of Al-Li alloys following exposure to various environments at temperatures of 930°F (500°C) has been reported in the literature [6-8]. The effect of this layer on tensile and fatigue properties was investigated. Specimens were fabricated from 0.063 in. (1.6 mm) 2090-T83 sheet. Half the specimens were chemical milled before testing to remove 0.007 in. ± 0.001 in. (0.18 mm ± 0.03 mm) per side and half were tested as received. The averages of the three tensile tests in each condition are shown in Figure 9. No differences were found in the tensile properties. The fatigue specimens were cycled under load control with R=0.02. The results of these tests are shown in Figure 10. Again the presence of the lithium-depleted layer had no detrimental effect on the material.

FORMABILITY OF SHEET

The formability of 2090 sheet was evaluated in both the AQ and T3 tempers. 2090-AQ gives maximum formability and 2090-T6 properties after aging. 2090-T3 gives maximum strength after aging to the T8 temper.

The minimum bend radii for 2090-AQ achieved in brake forming were smaller than for 2024-AQ or 7075-AQ as is shown in Figure 11. The results for brake forming of 2090-T3, -T6 and -T8 are also shown in Figure 11. Again 2090 performed at least as well as 2024 and 7075 in the same tempers. Tight bend radii help minimize weight on an aircraft by minimizing the amount of material in a bend. Al-Li alloys give equal, if not tighter, bend radii than conventional aluminum alloys, so there will be no weight penalty in bends when using Al-Li.

Several production parts, normally stretch formed from 2024-T3 sheet, were stretch formed from 2090-T3 sheet. Parts were formed from 2024-T3 at the same time in order to provide a comparison. The 2090-T3 was judged to stretch form better than 2024-T3. 2024-T3 failed before the part was completely formed more than once under conditions where 2090-T3 formed completely without failure. Less displacement of the tool was required to achieve complete forming detail for

the 2090-T3, and there was less springback with the 2090-T3 than 2024-T3. Stretching in both the longitudinal and transverse directions was performed. The best results were obtained when the stretching was done in the longitudinal direction. The post-formed T8 properties of both alloys were measured after aging. The lowest 2090-T8 properties were slightly higher than the lowest 2024-T8 properties as shown in Figure 12.

Hydroforming of stretch and shrink flanges was investigated using the form block and blanks in Figure 13. 2090-T3 and -AQ were compared to 2024-T3 and -AQ. The blanks for 2090 were oriented in the longitudinal (L), transverse (T), and 45° directions as shown in Figure 13. Cracks were observed in the stretch flange where the joggle joined the radius R_1 in all the 2090-T3 L-blanks. These cracks were not present when the blanks were removed from the press, but seemed to occur as the formed pieces rearranged themselves after forming and were carried around the shop. The material was apparently stretched to its limit in this location. This result agrees with measurements of maximum tensile elongations for the different directions in 2090-T3. The L direction has a tensile elongation of only 10% which is comparable to 7075-O, whereas the T and 45° directions have tensile elongations of about 15% which is comparable to the tensile elongation of 2024-T3. The strain at the intersection of the joggle and the radius R_1 was estimated to be 8%.

Hydroformed shrink flanges in 2090-T3 and AQ had slightly less wrinkling than similar shrink flanges in 2024-T3 and AQ, respectively. This result was expected since the elastic modulus of 2090 is about 10% greater than the modulus for 2024 and wrinkling of the flanges is the result of buckling.

The form block for the hydroform trials had 90° angles over which the flanges were bent. Springback of the flanges was measured as the amount by which the flange angle deviated from 90°. The results of these measurements are shown in Figure 14. The springback in the 2090 blanks was not affected by the blank orientation; the L, T and 45° blanks had the same amount of springback in each temper. There was less springback in 2090-AQ than in 2090-T3. 2090-T3 had less springback than 2024-T3, while 2090-AQ and 2024-AQ had the same amount of springback.

SUPERPLASTIC FORMING

A particularly attractive feature of Al-Li alloys is that they are superplastic [2-4]. Combining the lower density of Al-Li alloys with the possibility of reducing the number of detail parts and fasteners through superplastic forming (SPF) will result in substantial weight savings. For this reason, MCAIR is extremely interested in superplastic applications of Al-Li alloys.

The superplasticity of 2090, 8090 and 8091 was characterized by forming cones approximately 2.5 inches (62.5 mm) tall and 2.5 inches (62.5 mm) in diameter at the base as shown in Figure 15. The flow stresses in Figure 16 for a particular strain rate were similar for all the materials and were comparable to the flow stresses for superplastic 7475 obtained from [9]. The post-SPF tensile strengths of 2090 and 8090 SPF'd to an equivalent thickness strain, %EQS = $(t_i/t_f - 1) \times 100\%$ where t_i is the initial thickness and t_f is the final thickness, of about 55% and aged to the T6 temper are shown in Figure 17. These properties are less than the post-SPF T6 tensile strengths of 7475-T6.

Aluminum alloys cavitate during SPF and Al-Li alloys are no exception [10]. Two cones each of 2090 and 8090 were formed with a 400 psi (2.76 MPa) back pressure to suppress cavitation: one at a constant strain rate of 5×10^{-4} /sec and one at a constant strain rate of 10^{-3} /sec. These cones were sectioned and the density of the material was measured as a function of %EQS. The densities were then converted to volume percent cavitation using the rule of mixtures and assuming that all the cavities were filled with air during the density measurements. This data is shown in Figure 18. The 400 psi (2.76 MPa) back pressure was very effective at suppressing the formation of cavities in all the alloys up to very high strains.

One of the difficulties with SPF Al-Li which must be overcome is the quench distortion of the thin SPF parts. This is especially true for some of the large parts which may be SPF'd. 8090 holds some advantages over the other Al-Li alloys in this regard. 8090 is SPF'd at the solution heat treat temperature. 8090 is also not as quench sensitive as the other Al-Li alloys. A water quench after solution heat treatment is not needed in order to obtain acceptable tensile properties. Acceptable properties can be obtained with an air cool and normal age. The tensile properties for 8090 in Figure 17 are from specimens which were air cooled then aged.

The potential of SPF 8090 will be demonstrated when the F-15 Air Refueling Receptacle (ARR) Fairing is formed and flight tested later this year (Figure 19). The ARR Fairing is a classic example of the SPF technology in that three separate parts, an aluminum casting and two stretch formed aluminum parts, will be formed as a single SPF part.

CHEMICAL PROCESSING

Secondary manufacturing operations such as cleaning, anodizing, painting and chemical milling were investigated. The cleaning, anodizing and painting procedures used on conventional aluminum alloys were found to be acceptable for Al-Li alloys. An acceptable surface finish of 55 RHR was achieved for chemical milling of 8090 in the standard sodium hydroxide etchant with

triethanolamine and sodium sulfide, however, the etch rate was 20% faster for 8090 than for conventional alloys. It may not be possible to mix 8090 with conventional aluminum alloys during processing because of its faster etch rate.

Chemical milling of 2090 in the standard etchant resulted in an unacceptable surface finish of about 200 RHR. A non-standard etchant was developed for 2090 which resulted in a surface finish between 30 and 90 RHR on 2090 sheet and extrusion (Figure 20) including the F/A-18 access covers mentioned earlier. The modified process uses the same chemical tank operating temperature and life as the standard process and does not require extreme process control. The modified chemical milling solution is not satisfactory for conventional aluminum alloys. Consequently, a dedicated tank will be required to chemical mill 2090 on a production basis.

CORROSION RESISTANCE

The corrosion resistance of Al-Li alloys has not been characterized thoroughly. Limited studies at MCAIR have shown that the corrosion resistance of these alloys is comparable to that of conventional aluminum alloys. Limited testing at MCAIR on pre-production alloys has shown that Al-Li alloys are more resistant to corrosion than conventional aluminum alloys in finish system tests.

The resistance of 8090-T851 and 2090-T8E41 to pitting corrosion was compared to that of 7075-T76 sheet and 2124-T851 plate in SO₂ salt fog exposure for 32 days (Figure 21). Both conversion coated and sulfuric acid anodized/dichromate sealed surfaces were tested. The results in Figure 22 show that the Al-Li alloys had a smaller number of pits per square inch than conventional aluminum alloys and those pits were not as deep as those on the conventional aluminum alloys.

Stress corrosion cracking (SCC) around interference fit fasteners in Al-Li alloys was demonstrated to be no more of a problem than in conventional aluminum alloys. Various fasteners, representative of the types of fasteners used at MCAIR, were used to fasten a 2 in. X 2 in. (50 mm X 50 mm) piece of 7075 plate, 8090 plate, 2024 sheet or 2090 sheet to a similarly sized piece of 2090 extrusion. Again the parts of these specimens were sulfuric acid anodized/dichromate sealed before they were joined together. The specimens were subjected to 30 days of alternate immersion in salt water. This test also demonstrated that there would be no corrosion problems when Al-Li parts are joined to other aircraft structure made from conventional aluminum.

Accelerated laboratory test such as the EXCO (ASTM G34) and MASTMASSIS (ASTM G85, A2) tests were developed to determine the susceptibility to exfoliation corrosion of conventional 2000- and 7000-series alloys. However, the results of these accelerated tests for Al-Li alloys have not correlated well with those of atmospheric exposure tests in sea coast, industrial and carrier environments [11-12]. The evaluation of the in-service performance of the F/A-18 access covers mentioned earlier in a carrier environment will provide further information on the extent of correlation between the accelerated and field service tests.

FUTURE WORK

The evaluation of Al-Li alloys at MCAIR to date has been very limited. While these initial studies indicate that Al-Li plate and sheet are very similar to that conventional aluminum plate and sheet, there were enough differences observed that in order to put Al-Li alloys into production on a large scale more thorough investigations are needed in specific areas. For instance, all of the laboratory corrosion studies reported here were performed on material which had not undergone any forming operation such as hydroforming or stretch forming. The effect of the cold work which the material receives during a forming operation upon the corrosion resistance is unknown. Before SPF Al-Li sheet is used extensively in production, the minimum radii which can be superplastically formed in 2090, 8090 and 8091 must be investigated.

Very little work has been done on Al-Li extrusions or forgings. These are two important applications which must be addressed, especially since the weight savings potential of forgings on the Hornet 2000 (Figure 6) is second only to primary sheet structure. As a result, MCAIR in cooperation with Alcan and Weber Metals, Inc., will investigate the potential of 8090 hand and die forgings during the coming year.

CONCLUSION

Al-Li alloys have the potential for greatly reducing the weight of fighter aircraft. This weight savings is primarily the result of the 8 to 10 percent lower density of Al-Li alloys in comparison to conventional aluminum.

No particular manufacturing problems exist for Al-Li alloys. Al-Li alloys are as formable in conventional forming operations as 2000- and 7000-series aluminum alloys and can be cleaned, anodized, and painted just like conventional aluminum alloys, though for some operations Al-Li can not be mixed with conventional aluminum. The superplasticity of Al-Li alloys is a significant advantage. A wide range of applications with potentially high structural efficiency are open to Al-Li alloys because of their superplasticity.

Anisotropy in current Al-Li sheet has limited the application of sheet to secondary structure only because the minimum properties, which occur between 45° and 60° off the rolling axis, must be used in the design of Al-Li structure. This anisotropy may also show up in other product forms such as extrusions and forgings where large amounts of cold-work may result in a highly textured microstructure. As these Al-Li alloys mature, perhaps this anisotropy can be eliminated with special mill practices such as the one developed by Alcan.

Studies on the Hornet 2000 for direct substitution of Al-Li alloys for conventional aluminum have shown that the applications with the highest potential weight savings are forgings and primary structure applications for sheet. Current Al-Li alloys have not been developed sufficiently to make direct substitution in these areas possible. These two applications are where MCAIR would like to see the aluminum suppliers direct their efforts.

REFERENCES

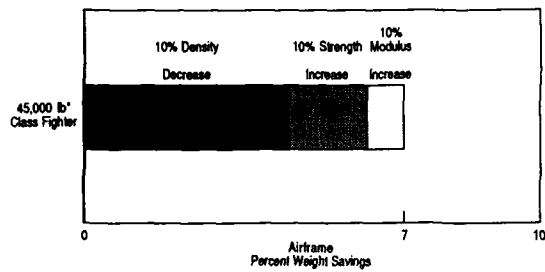
1. Dresser, C., AIR-TO-SURFACE (ATS) TECHNOLOGY EVALUATION AND INTEGRATION STUDY, McDonnell-Douglas Report MDC A49941, AFWAL-FD Contract No. F33615-76-C-3101, Jan. 1978.
2. Wadsworth, J., Palmer, I.G., Crooks, D.D., and Lewis, R.E., "Superplastic behavior of aluminum-lithium alloys", ALUMINUM-LITHIUM II, 12-14 April 1982, Monterey, CA, pp.111-135.
3. Lederich, R.J. and Sastry, S.M.L., "Superplastic deformation of P/M and I/M aluminum-lithium based alloys", ALUMINUM-LITHIUM II, 12-14 April 1982, Monterey, CA, pp.137-151.
4. Grimes, R. and Miller, W.S., "Superplasticity in lithium containing aluminum alloys", ALUMINUM-LITHIUM II, 12-14 April 1982, Monterey, CA, pp.153-167.
5. Peel, C.J., Evans, B., Baker, C.A., Bennett, D.A., Gregson, P.J., and Flower, H.M., "The development and application of improved aluminum-lithium alloys", ALUMINUM-LITHIUM II, 12-14 April 1982, Monterey, CA, pp. 363-392.
6. Fox, S., Flower, H.M. and McDermid, D.S., "Formation of solute-depleted surfaces in Al-Li-Cu-Mg-Zr alloys and their influence on mechanical properties", ALUMINUM-LITHIUM ALLOYS III, 8-11 July 1985, University of Oxford, pp. 263-272.
7. Papazian, J.M., Schulte, R.L. and Adler, P.N., "Lithium depletion during heat treatment of aluminum-lithium alloys", MET. TRANS. A, Vol. 17A, April 1986, pp. 635-643.
8. Papazian, J.M., Wagner, J.P.W. and Rooney, W.D., "Porosity development during heat treatment of aluminum-lithium alloys", J. DE PHYSIQUE, C3:9, Tome 48, Sept. 1987, pp. 513-519.
9. Ghosh, A.K., and Hamilton, C.H., "Influences of material parameters and microstructure on superplastic forming", MET. TRANS. A, Vol. 13A, May 1982, pp. 733-743.
10. Ridley, N., "Cavitation and superplasticity", SUPERPLASTICITY, AGARD-LS-154, Aug. 1987, Paper No. 4.
11. Lane, P.L., Gray, J.A., and Smith, C.J.E., "Comparison of corrosion behavior of lithium-containing aluminum alloys and conventional aerospace alloys", ALUMINUM-LITHIUM ALLOYS III, 8-11 July 1985, University of Oxford, pp. 273-281.
12. Scutti, J.J., Bresnahan, K.M., Bohlen, J.W., and Fetchko, P.A., "Stress corrosion and exfoliation corrosion resistance of near-commercial aluminum-lithium alloys", TMS-AIME Fall Meeting, Orlando, FL, Oct.1986.

ACKNOWLEDGEMENTS

The author wishes to express his gratitude to V. M. Vasey-Glendon and Drs. K. K. Sankaran and E. J. Tuegel for their help in putting this paper together. The work reported in this paper was performed under the MCAIR Independent Research and Development Project 7-220.

20-6

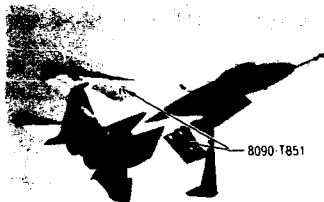
20-6



* All metal baseline; 50% Conventional Aluminum Direct Substitution for all Aluminum product forms

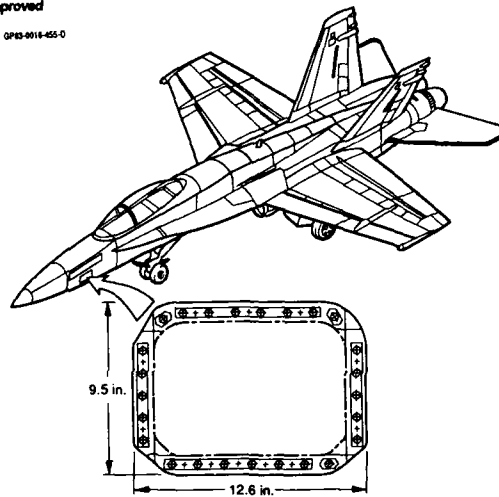
Figure 1. Percent Weight Reduction on an Airframe From Improved Aluminum Properties

GPB-0016-455-0



GPB-0016-161

Figure 3. First Flight of Aluminum-Lithium Wing Skins on the F-15 S/MTD Aircraft



GP73-0168-14-A

Figure 4. F/A-18 ALR 45/Detector Access Cover



GPB-0168-7-C

Figure 5. 2090-T83 Air 45/Detector Access Cover

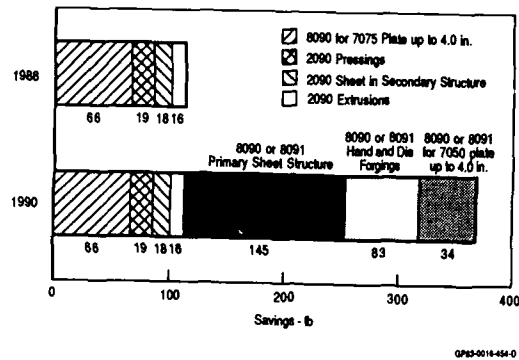


Figure 6. Potential Weight Savings From Al-Li Substitution for Hornet 2000

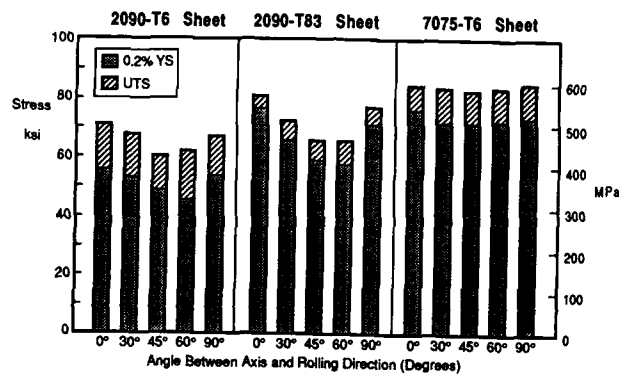


Figure 7. Comparison of Typical 2090 and 7075 Sheet Tensile Strengths

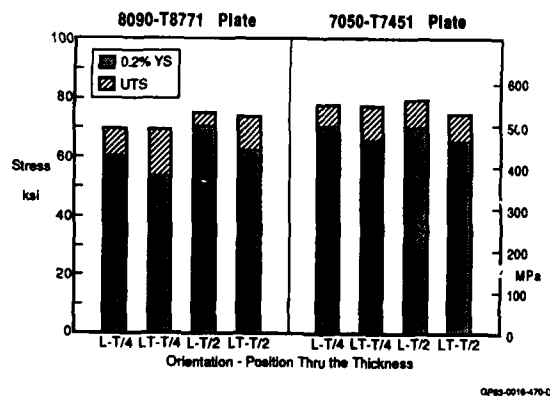


Figure 8. Comparison of Typical 8090 and 7050 Plate Tensile Strengths

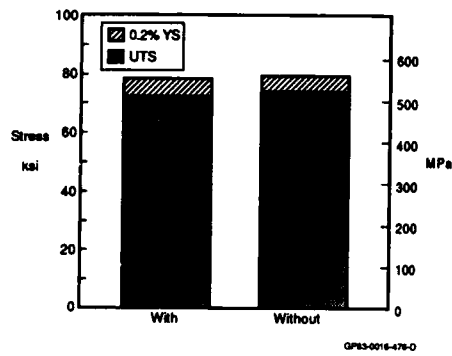


Figure 9. Tensile Strengths of 2090-T83 Sheet With and Without a Lithium-Depleted Layer

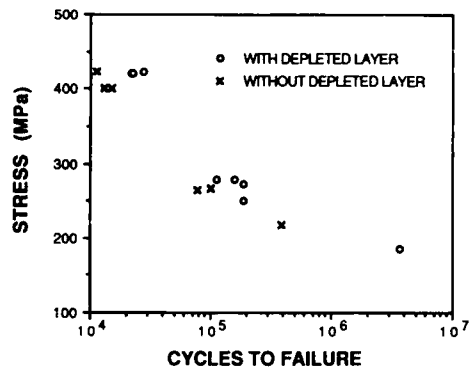


Figure 10. Fatigue data (R=0.02) for 2090-T83 with and without lithium depleted layer

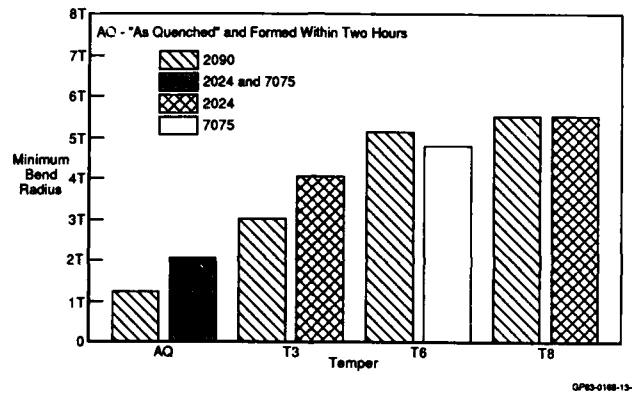


Figure 11. Minimum Bend Radii as a Function of Temper for 2090, 2024 and 7075

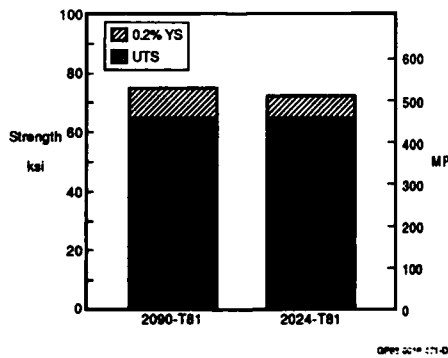


Figure 12. Minimum bend radii as a Function of Temper for 2090, 2024 and 7075

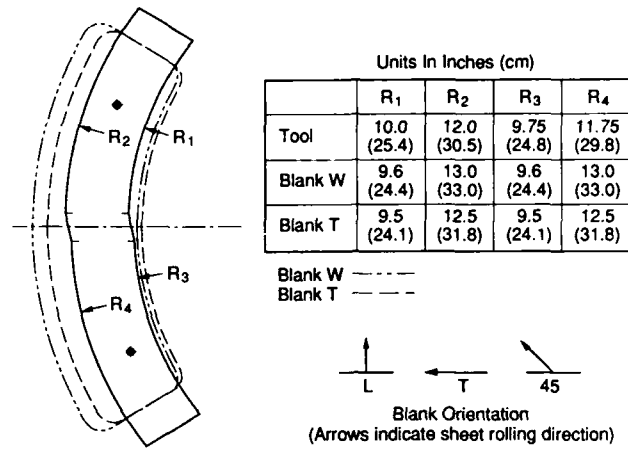


Figure 13. Tool and Blanks for Hydroforming of Stretch and Shrink Flanges

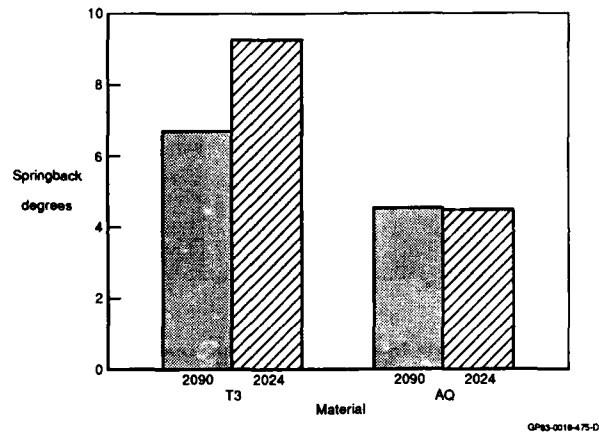


Figure 14. Springback Measured on a Hydroformed 90° Bend

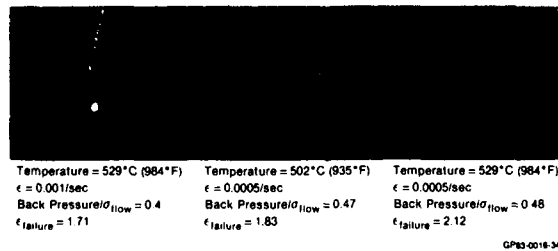


Figure 15. Superplastically Formed Cones of Alcan 8090 Formed Under 400 psi (2.75 MPa) Back Pressure

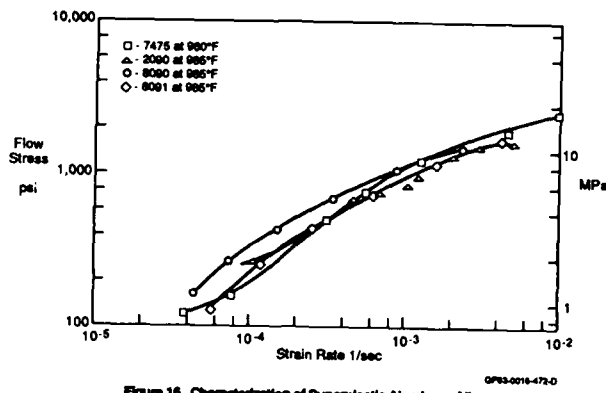


Figure 16. Characterization of Superplastic Aluminum Alloys

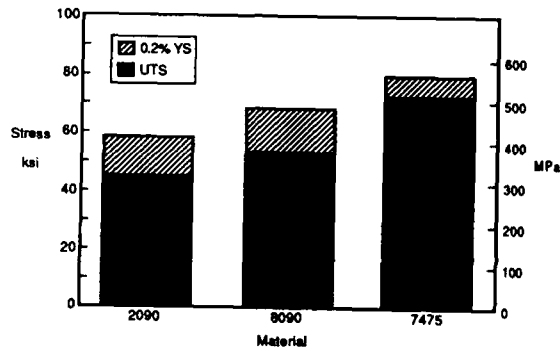


Figure 17. Typical Post-Formed -T6 Tensile Properties of Superplastic Aluminum Alloys

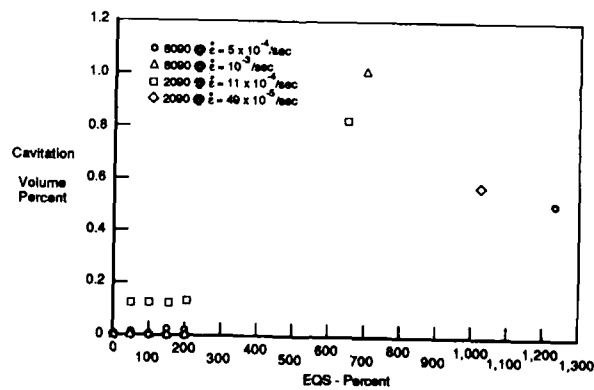
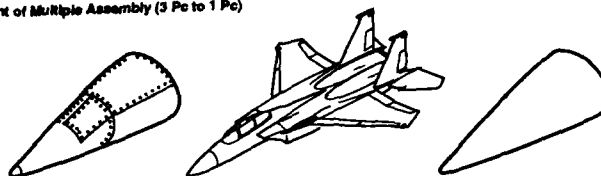


Figure 18. Cavitation of Al-Li Alloys Superplastically Formed at 985°F (529°C) Under 400 psi (2.75 MPa) Back Pressure

Replacement of Multiple Assembly (3 Pc to 1 Pc)



Conventional Structure:

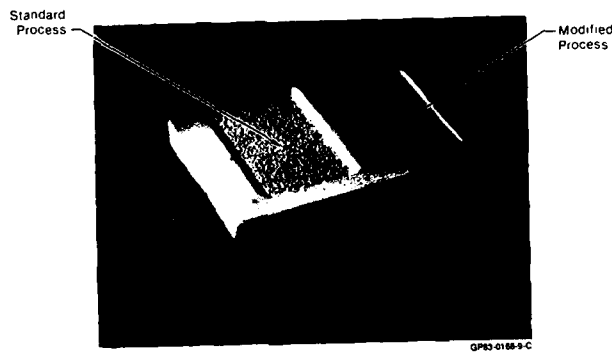
- A356 Investment Casting
- 2024-T62 Stretch Form Skin Panel
- 2024-T72 Stretch Form Skin Panel
- Weight Total - 8.85 lb

SPF Structure:

- Aluminum Lithium 8090 Superplastic Grade
- Weight Total - 7.79 lb (Projected Production)

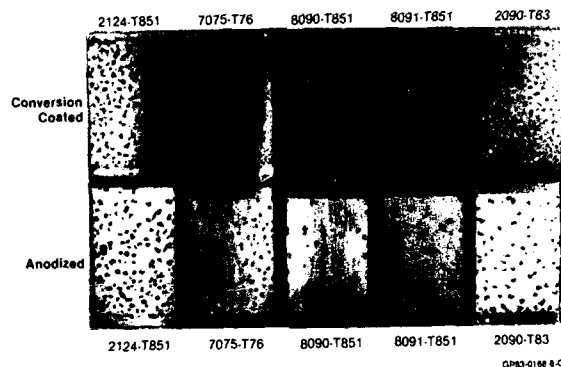
Figure 19. F-15 Air Refueling Receptacle Fairing, Potential Superplastically Formed 8090 Structure

QP83-0216-420-A

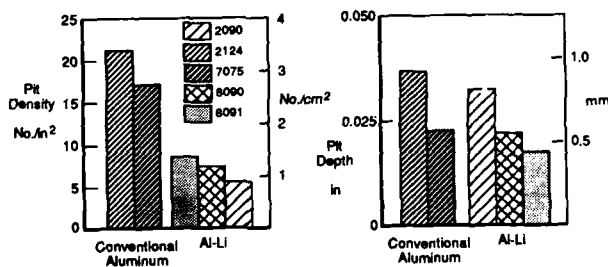


QP83-0188-9-C

Figure 20. Comparison of 2090 Chemical Milled With the Standard Process and the MCAIR modified Process



QP83-0188-9-C

Figure 21. Al-Li and Aluminum Specimens Exposed to SO₂-salt Fog for 32 DaysFigure 22. Pit Density and Pit Depth on Al-Li and Aluminum Specimens Exposed to SO₂-salt Fog for 32 Days

QP83-0216-474-D

CURRENT STATUS OF THE APPLICATION OF CONVENTIONAL ALUMINIUM-LITHIUM ALLOYS
AND THE POTENTIAL FOR FUTURE DEVELOPMENTS

by
C J Peel
Materials and Structures Department
Royal Aerospace Establishment
Farnborough
Hampshire GU14 6TD UK

SUMMARY

Commercial aluminium-lithium alloys are now entering service use and, whilst it cannot be claimed that they are yet fully achieving their maximum potential, it is now appropriate to consider the limitations to their further development and the possibilities for the development of other systems and composites based on light alloys, especially suited for aerospace structures.

All the commercial aluminium-lithium alloys presently offered have been designed to present a reduction in density and an increase in elastic modulus as their main benefits to the designers contemplating their application. The other important metallurgical properties of the alloys, such as strength and fracture toughness, have been matched to the performance of existing 2000 and 7000 series alloys.

This paper considers the possibilities for further density reductions and increases in mechanical properties, comparing the potential improvements with those offered by non-metallic composites. Three types of structure are considered generically namely damage tolerant structure, typified by a pressurised fuselage skin, structure limited by inadequate material stiffness in either the case of aeroelastic performance or resistance to buckling and structure limited by currently obtainable strength levels at both ambient and elevated temperatures.

It transpires from the following brief analysis that future developments may well have to be optimised against the special requirements of the three simple categories outlined above and that the simple principle underlying the development of the conventional aluminium-lithium alloys cannot be extended greatly.

1 INTRODUCTION

Table 1 lists some of the types of applications now being considered for aluminium-lithium alloys. Currently, structural parts have been built for airworthiness qualification and in a few examples components have already been approved for use. The types of alloy and temper known to the author to have progressed to this state are listed, undoubtedly more examples are available. It can be seen in Table 1 that the applications have been broken down into the three chosen design categories. Obviously these categories are not necessarily mutually exclusive in the sense that some structure may prove to be critical in both strength and damage tolerance for example and again significant quantities of structure can prove to be limited by minimum gauge considerations.

The present performance and potential for improvement is now considered for each of the design categories necessarily extracting real data for some aluminium-lithium alloys however it is not the purpose of this paper to contrast the relative performances of these commercial variants but to take a forward look beyond the cautious emergence of aluminium-lithium as a major structural material.

The properties of the current aluminium-lithium alloys are assessed and, where appropriate, comparison is made with conventional carbon fibre reinforced composite. The potential improvements offered by aluminium alloy based composite materials, including those based on aluminium-lithium alloys, are assessed in the light of those now being signalled for the non-metallic composites and the possible role of magnesium based materials is discussed.

2 DAMAGE TOLERANT MATERIALS

Damage tolerance requirements for metallic materials comprise a balanced mixture of strength, fracture toughness, resistance to fatigue crack growth and possibly to crack initiation. Throughout the considerations on the performance of metallic materials the possibility of degradation by corrosive environments has to be considered. Two contenders for employment as damage tolerant aluminium-lithium alloys have emerged to date, these being 2091 and 8090 in appropriate tempers and product forms such as sheet and thin plate. The microstructures and tempers of both alloys have been adjusted to attempt to achieve the balance in strength and fracture toughness offered by the well tried conventional 2024 alloy on the basis that, although 2024 may not itself be the optimum damage tolerant material, as the incumbent most of the design rules and considerations for aircraft structure have been based on the perceived performance of 2024 in a naturally aged condition.

High fracture toughness is required of a damage tolerant aluminium alloy to resist the catastrophic failure at limit load of a structure containing a large crack, perhaps as large as the spacing of ribs in a pressure cabin. At the same time the alloy must be strong enough to prevent plastic deformation at limit load or tensile failure before ultimate design load. The natural relationship between the yield and ultimate tensile strengths of naturally aged 2024 alloy is approximately 2:3 and to achieve the required balance in yield and ultimate strength of the aluminium-lithium alloys has required careful adjustments, in particular the yield strength (more correctly 0.2% proof stress) must be kept low to maximise fracture toughness whilst maintaining a high ultimate tensile strength. The comparative

performance of the two contending aluminium-lithium alloys and 2024 is included (Fig 1). It can be seen that at least at present whilst the aluminium-lithium alloys compete with 2024 reasonably at the low strength levels, remembering that they have the advantage of an 8%-10% density reduction, they fall short of the performance of the 2XXX series alloys as the strength level is increased. This finding suggests that to further reduce the weight of damage tolerant structure by an increase in working stress levels beyond those for 2024-T3 will find the aluminium-lithium alloys inadequate in fracture toughness. Alternatively, attempts could be made to further increase the levels of addition of lithium or magnesium to the aluminium-lithium alloys thereby achieving a further density reduction. Most efficient of these would be an increase in lithium beyond the 2.0%-2.5% presently employed in alloys such as 2090, 2091 and 8090. However, a brief inspection of the literature¹ reveals that further additions of lithium especially in the presence of other alloying elements such as copper or magnesium will reduce fracture toughness rapidly (Fig 2). This suggests that to achieve weight savings reconsideration of the nature of damage tolerance requirements will be needed.

Resistance to the growth of fatigue cracks is also an important contribution to damage tolerance and here once again aluminium-lithium alloys have improvements to offer beyond those of density reduction. That is it is becoming clear that the new alloys do possess a naturally high resistance to fatigue crack growth stemming in part from their high elastic modulus and in part from the tortuous fatigue cracks that are produced in their refined microstructures (Fig 3). Because the reduction in fatigue crack growth rates stems in part from the propensity to planar slip found in the aluminium-lithium alloys there would appear to be little room for further improvements beyond those already offered by 2091 or 8090 other than perhaps a slight further reduction in density or increase in strength and in these two aspects it has already been stated that the current alloys appear to be optimised.

The aluminium-lithium alloys appear to differ from 2024 in the particular respect of a reduced sensitivity to load interaction effects and the pronounced crack retardation found with 2024 is seemingly not so pronounced with aluminium-lithium alloys. This may prove a further advantage, not yet quantified, when the effects of gust alleviation techniques are realised in terms of the reduction in the magnitudes of infrequent major tensile gust loads. It may be that there will prove to be some opportunity to optimise the resistance of aluminium-lithium alloys to fatigue crack growth under truncated spectra. However, for major further improvements in the weight of damage tolerant structure, a significant change in the construction techniques and in the qualification requirements may well be necessary. For example the use of laminated or locally reinforced metallic skins may well provide a major step forward. For example the improvements in resistance to fatigue crack growth provided by material such as Arall^{2,3} tend to suggest that increased working stresses could be accommodated in fatigue critical structure. Fig 3 includes a crack growth curve produced in RAE⁴ for a laminate produced using aluminium-lithium skins reinforced with aramid fibres. Clearly the high crack growth resistance of the aluminium-lithium is further improved by the fibre reinforcement, at least when stressed longitudinally and the density of the laminate is significantly reduced. It may be that future damage tolerant structure will require a combination of conventional alloy skins based on an aluminium-lithium alloy coupled to local strap reinforcements or crack stoppers made from adhesively bonded fibre reinforced aluminium-lithium laminates.

3 MATERIALS WITH ENHANCED STIFFNESS

Large proportions of aircraft, weapon and space structures are stiffness critical whether in terms of resistance to bending or buckling and it is in this regime that the aluminium alloys encounter the most challenge from the non-metallic composite materials such as carbon fibre reinforced plastic. Aluminium-lithium alloys improve the attractiveness of the conventional aluminium alloys quite significantly in this respect, but there is some scope for yet more dramatic improvements. Comparison with the fibre reinforced composites [CFRP] is made difficult by the need to optimise fibre lay-ups to suit selected pieces of structure. In this analysis therefore, isotropic aluminium alloys and variants of them are compared with quasi-isotropic lay-ups with selected proportions of their fibres lying in the stressing direction. A constant loading of 60% volume fraction has been chosen for the CFRP using two fibre types, the existing XAS fibre and a notional improved intermediate modulus fibre with relative stiffnesses of 230 GPa and 280 GPa respectively.

Comparison (Fig 4) of the specific stiffnesses $[E/\rho]$ of the conventional aluminium alloys with the XAS type CFRP reveals that approximately 30% of the fibres need to be loaded in the direction examined to match the conventional alloy stiffness. The improvements achieved with conventional aluminium-lithium alloys, here exemplified by 8090, require slightly more than 35% of the fibre to be aligned in the test direction. Since a quasi-isotropic lay-up of fibre may well require 25% of the fibres in each of four directions 0° , $\pm 25^\circ$, 90° , it can be seen that conventional aluminium alloys compete quite well in isotropic situations. The emergence of intermediate modulus fibres has improved the competitive position of the CFRP to some extent such that 8090 now only competes up to a level of approximately 30% loading. To further improve the competitiveness of the conventional alloys it may be possible to maximise the specific stiffness by choosing a rich alloy of the Al-Li-Mg type for example Al-3%Li-2%Mg, originally tested in RAE, but this rich light alloy still produced a specific stiffness of no more than 33.5 GPa. It would seem more attractive to combine the merits of the aluminium-lithium alloys with those of the isotropic particle reinforced metal matrix composites [MMC]. To this end samples of 8090 alloy reinforced with particulate SiC have been produced in RAE and elsewhere and tested. Although by no means optimised it is clear that this type of material is capable of producing specific stiffnesses of the order of 45 GPa requiring nearly 55% of the fibre in XAS-CFRP to be aligned in the examined direction or 42% of the IM fibre type. Clearly an attractive option if the other properties of this new type of material can be satisfactorily balanced.

There remains the possibility that use could be made of aligned fibre reinforcement in an aluminium alloy matrix to produce extremely high specific stiffness at least in the aligned direction. However, although such a material would be competitive with fully aligned CFRP, like the CFRP it would be brittle and limited to totally elastic design concepts. This may be most effective for compressively loaded struts but likely to attract punitive safety factors

in structure heavily loaded in tension. It would be necessary to demonstrate that the superior matrix properties claimed for the metal matrix composites do in fact produce a better transverse performance and greater resistance to delamination than found with organic matrices so that punitive safety factors could be avoided at least in the compressive design case.

The effects of improved stiffness on the resistance to elastic buckling can be studied by comparing the specific values of the third root of the elastic modulus. It is at once apparent that the low density of the CFRP produces values that cannot be met by the conventional aluminium alloy or the improved reinforced alloy systems (Fig 5). However, it would be expected that the metallic systems could be used in a post buckled condition to some extent as long as plastic deformation was avoided. This makes an accurate comparison even more difficult. It is evident that a reduction in the density of the matrix material would be most beneficial in this particular category and in any situation where minimum gauge requirements may dominate. In this respect the attractiveness of magnesium alloys as a matrix becomes self evident because of the further density reduction to 1.74 g/cc.

4 HIGH STRENGTH MATERIALS

Frequently in the design of aerospace structures high strength, whether in tension, compression or shear, is required to achieve low parasitic mass. Increasingly, consideration is given to obtaining high performance at elevated temperatures to accommodate the increasing speed of the vehicles. The competitive position of the aluminium alloys in terms of specific strength is set out in a similar manner to that for specific stiffness (Figs 6 and 7) except that high strength titanium alloys are now added to the picture because of their relatively good performance in this category. Similarly, the high strength 7000 conventional aluminium alloys and the high strength 8091 and 2090 aluminium-lithium alloys are chosen as the natural contenders in this category. It would seem to be important to develop an ultra-high strength aluminium-lithium alloy probably only in the form of thin plate to maximise the weight saving potential in upper wing skins where a mixture of strength and stiffness is required. This is illustrated by the 8091 and 2090 high strength variants in comparison with the conventional high strength 7150 alloy in terms of both specific strength (Fig 7) and specific stiffness (Fig 4). Fibre reinforced plastic materials are not used to their ultimate strength because, being sensitive to notches and environmental degradation, significant safety factors have to be employed. In this comparison a limiting strain of 0.5% has been applied for the tension case and a more severe level of 0.4% for structure loaded in compression where the poor resistance to delamination can also be exploited. Design allowable values for strength are quoted for the metals.

It can be seen (Figs 6 and 7) that the conventional aluminium alloys, including those containing lithium compete favourably with the CFRP especially when loaded in compression. The addition of SiC particulate to the conventional alloys has only a slight benefit to the specific strength levels obtainable essentially because of a limitation to ductility imposed by the presence of the brittle ceramic phase. The potential improvements achievable with fibre reinforced metal matrix composites are very significant provided aligned composites can be exploited. When produced as a quasi-isotropic material they show no real benefit at all (Fig 8).

High temperature requirements are hard to define because material choices are made in distinct steps. That is aluminium alloys are deemed to be limited in application much beyond 150°C except for extremely short high temperature exposures and the next common selection would be of a titanium based alloy capable of operating to perhaps 450°C. Similar quantised steps are beginning to emerge for the non-metallic matrices. Fig 9 indicates that the high temperature performance of the conventional aluminium lithium alloys will not differ greatly from that of conventional alloys but that metal matrix composites of both the particulate reinforced and fibre reinforced types could show some distinct improvements with the possibility of extending the working range of the aluminium based alloys up towards that for the titanium alloys. The fracture performance of these metal matrix composites would have to be improved very considerably to compete with the high levels of strength and fracture toughness achieved by the conventional titanium alloys, but very significant increases in specific stiffness would be naturally obtained.

5 DISCUSSION

The arguments developed in this paper are based on real data currently available and, whilst it is more than possible that material improvements may change the balance of attractive properties, some of the conclusions would seem inescapable. It would seem that the newly emerging metal matrix composites will have little to offer in terms of a material for damage tolerance applications, because of a deterioration in fracture toughness. In this special category the best possible light-weight combination of materials may well be offered by an aluminium-lithium skin and stringer combination possibly with crack stoppers exploiting the advantages of aligned fibre. The extent to which reliance could be placed upon fibre reinforcement techniques being very dependent on the design of the structure in question.

To continue to compete in the structural category dependent upon high specific stiffness will require very significant improvements from the metallic matrix materials because of the developing performance of carbon fibre reinforced plastic. To the author, the most attractive option would seem to be to extend the high specific stiffness of the aluminium-lithium alloys by the addition of particulate ceramic reinforcement. It being judged most important to maintain an isotropic mechanical performance. Particular attention needs to be focussed on the fracture toughness of such materials which has been found to be lower than that for conventional alloys of similar strength. It may be argued that the use of CFRP would be a more cost effective route to comparable weight savings than the use of metal matrix composites of high initial price. It would seem that the cost of manufacture of the two types of composite will be the crucial issue. It would be a major benefit if conventional metallic practices could be established for the metal matrix composites.

In terms of materials with high specific strengths, the advent of metal matrix composites would appear to be of dubious value especially when a required balance of strength and fracture toughness is

considered. It would seem that ultra-high strength aluminium alloys of the 7000 and possibly the aluminium-lithium types will remain the dominant choice for some considerable time. However, this consideration changes when higher operating temperatures are in demand in which case the use of ceramic reinforcement of both fibrous and particulate forms would appear to have much to offer.

6 CONCLUSIONS

- i It is concluded that the concept of a general increase in performance of aluminium alloys beyond the level presently offered by the emerging aluminium-lithium alloys will be difficult to achieve and rather that new light alloy systems will need to be designed for restricted selected purposes.
- ii Possible trends for future development in damage tolerant material would appear to include fibre reinforced laminates based on aluminium-lithium skins to maximise weight savings in crack stoppers and fatigue critical structure.
- iii There would appear to be considerable scope to increase the specific stiffness of the metallic matrices to compete more favourably with fibre reinforced non-metallic composites. The use of particulate reinforcement in an aluminium-lithium matrix or a magnesium alloy matrix would seem most attractive.
- iv Whilst ultra high strength applications of aluminium alloys will continue to require the application of the 7000 series alloys and possibly the emerging high strength variants of aluminium-lithium, it may be possible to exploit the significant improvements offered by ceramic reinforcement of light alloy matrices to increase operating temperatures significantly above present light alloy limits.

7 ACKNOWLEDGEMENTS

The author is grateful for the information supplied by Dr D S McDermid and Dr R Moreton of RAE Materials and Structures Department.

8 REFERENCES

- 1 S Suresh, A K Vasudevan, Proc. 3rd Int. Conf Aluminium-Lithium alloys, Oxford (1985), p.595. The Institute of Metals, London (1986).
- 2 J W Gunnink, L B Voeglesang, J Schijve, Proc. 13th Int. Congress on Aeronautical Science (1982), 2.6.1 p.990. ICAS (1982).
- 3 L N Mueller, J L Prohaska, J W Davis, Proc. AIAA Aerospace Engineering Conf., Los Angeles (1985), AIAA (1985).
- 4 R Moreton, C J Peel, Unpublished RAE data.

TABLE.1
POTENTIAL APPLICATIONS FOR ALUMINIUM-LITHIUM ALLOYS
IN. SELECTED TEMPER AND PRODUCT FORMS

POTENTIAL APPLICATIONS	PRODUCT FORMS	ALLOYS
FUSELAGE SKIN AND WING SKIN FOR TRANSPORT AIRCRAFT AND HELICOPTERS	DAMAGE TOLERANT STRUCTURE	
	THIN PLATE AND	2091-T81
	RECRYSTALLISED SHEET	8090-T81 8090-T8151
DETAILED FORMED PARTS AND SPF PARTS. SKINS FOR FLYING CONTROL SURFACES. STRINGERS FOR AIRCRAFT AND HELICOPTERS. WING SKINS FOR CIVIL AIRCRAFT AND SPACE STRUCTURE SKINNING	STIFFNESS CRITICAL STRUCTURE	
	RECRYSTALLISED AND	**2090-T8E50
	UNRECRYSTALLISED	2091-T8X/T8
	SHEET IN MEDIUM AND	8090-T6/T8
	HIGH STRENGTHS	2091-T81
FRAMES, RIBS, SPARS UNDERCARRIAGE PARTS FLOOR BEAMS	EXTRUSIONS, PLATE	8090-T651 8090-T8771
	STRENGTH CRITICAL STRUCTURE	
	STRETCHED PLATE	** 2090-T8E41
	FORGINGS	8090-T8771
	EXTRUSIONS	8090-T652
	STRETCHED SHEET	8091-T6 2091-T81 8090-T651

** Several tempers available

FIG.1 PLANE STRESS FRACTURE TOUGHNESS OF DAMAGE TOLERANT SHEET
2091 AND 8090 ALLOYS COMPARED WITH 2024 AND 2014 ALLOYS

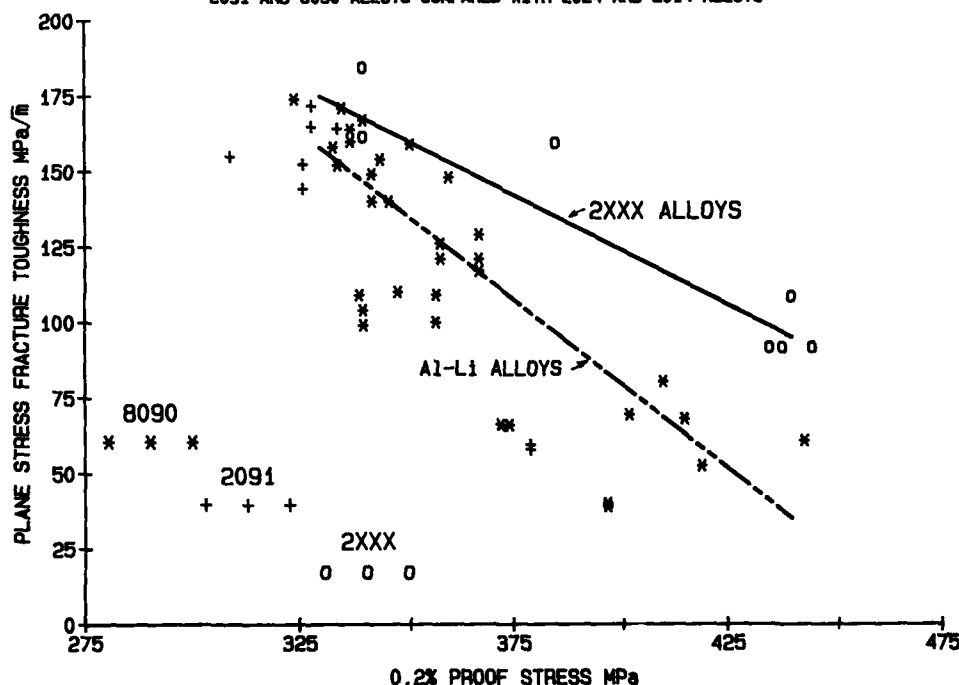


FIG.2 THE EFFECT OF LITHIUM CONTENT ON FRACTURE TOUGHNESS
8090 CONTAINING 2.4%Li COMPARED TO ALLOYS CONTAINING 2.8%Li

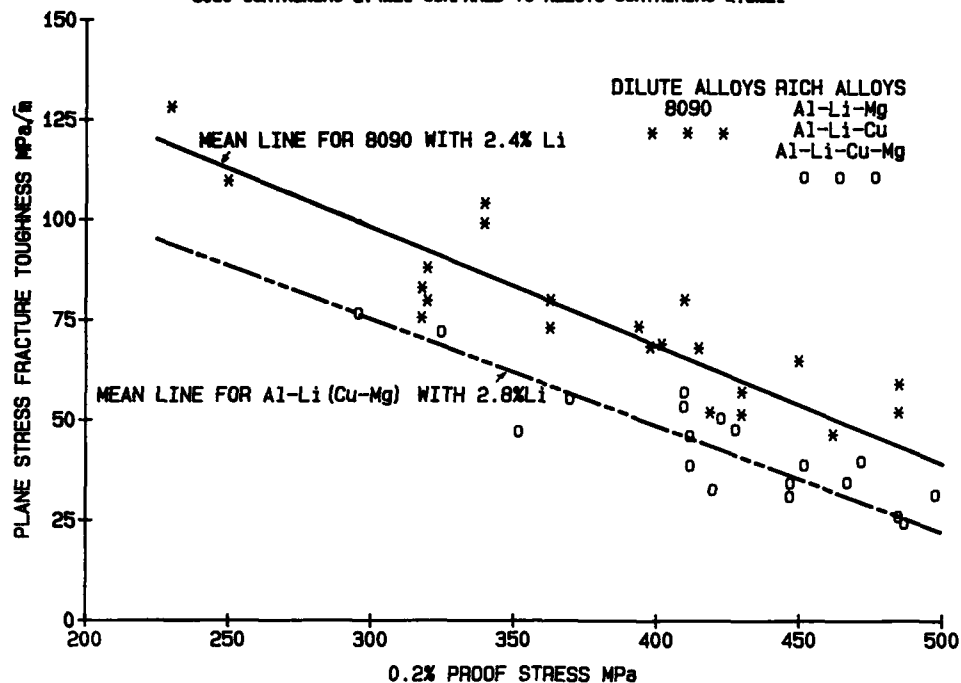


FIG.3 FATIGUE CRACK GROWTH RATES FOR DAMAGE TOLERANT SHEET
2091 AND 8090 ALLOYS COMPARED WITH 2024 AND LAMINATED 8090
L-T TEST DIRECTION R=0.4

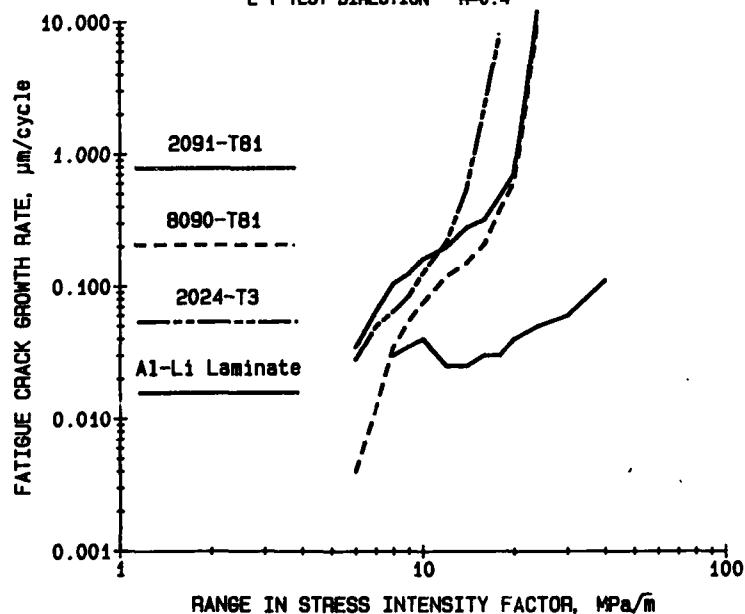


FIG.4 SPECIFIC STIFFNESSES FOR ALLOYS AND COMPOSITES
Typical Values for the Longitudinal Testing Direction

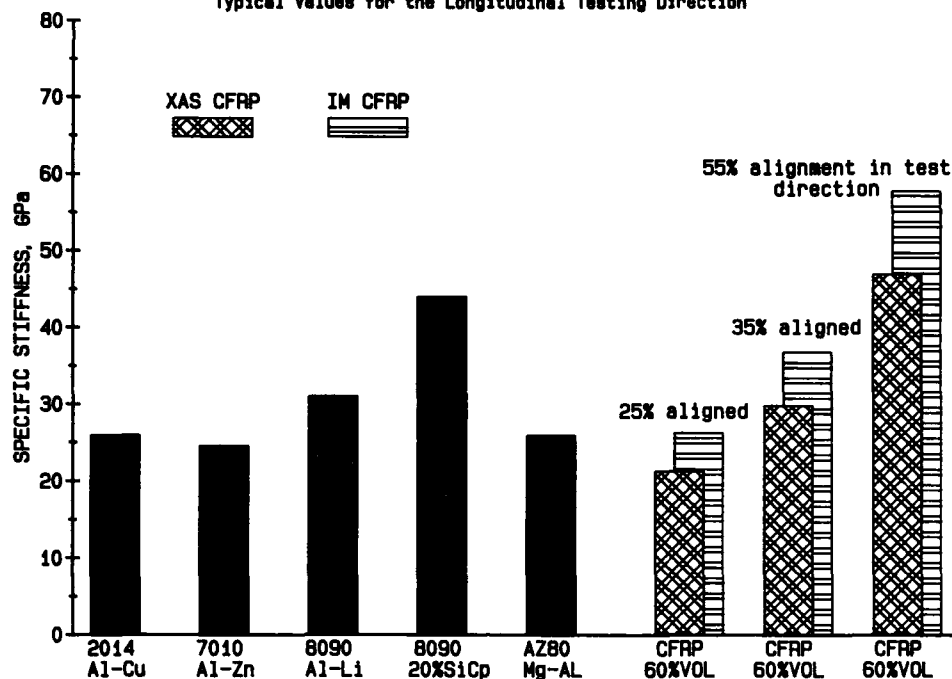


FIG.5 SPECIFIC ELASTIC BUCKLING RESISTANCE
Typical Values for the Longitudinal Testing Direction

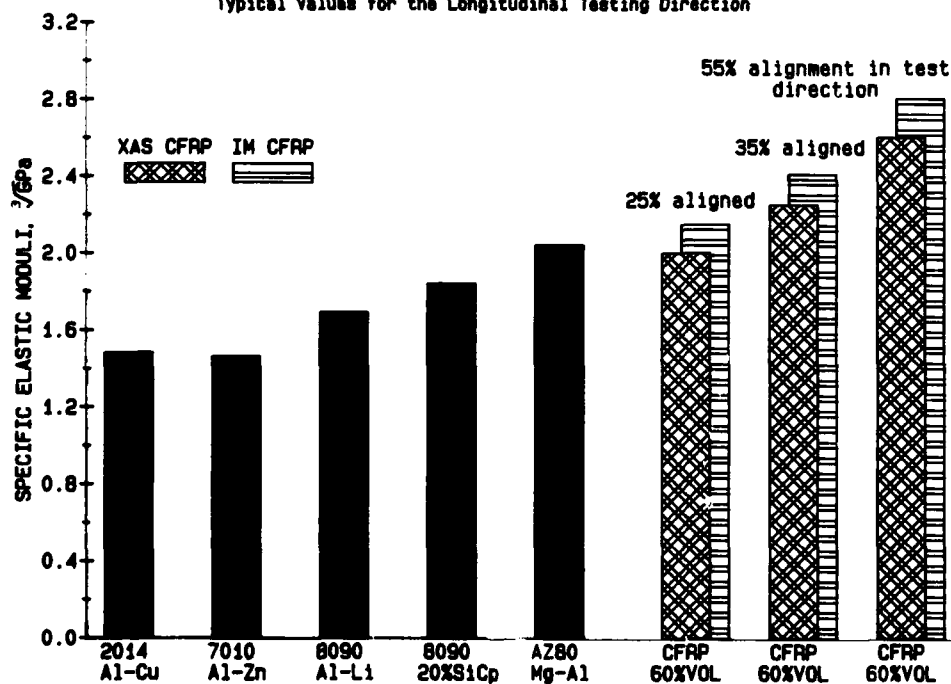


FIG.6 SPECIFIC TENSILE DESIGN ALLOWABLE STRENGTHS
Longitudinal Specific Strengths Allowed at Limit Load

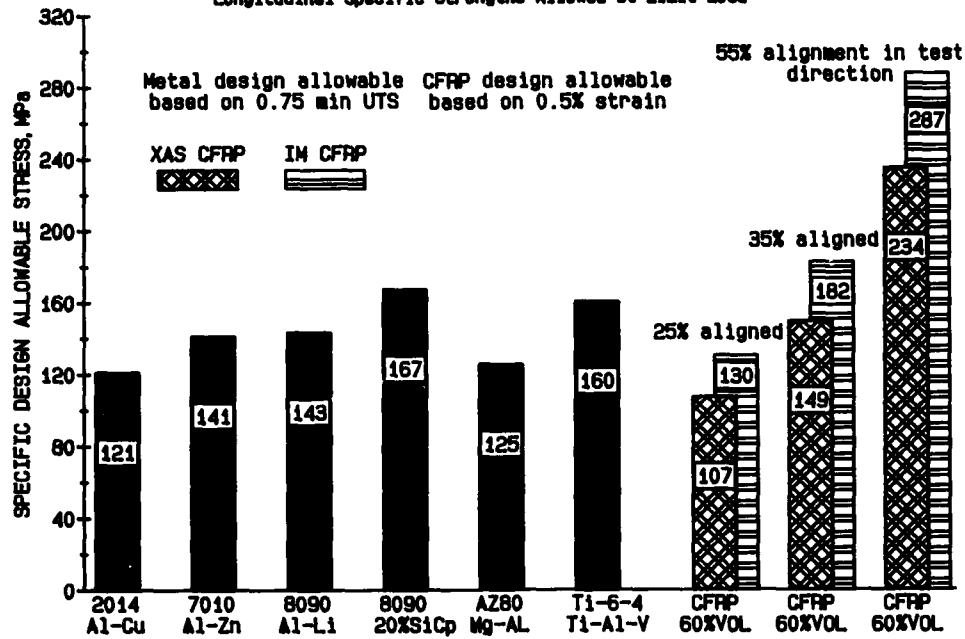


FIG.7 SPECIFIC COMPRESSIVE DESIGN ALLOWABLE STRENGTHS
Longitudinal Specific Strengths Allowed at Limit Load

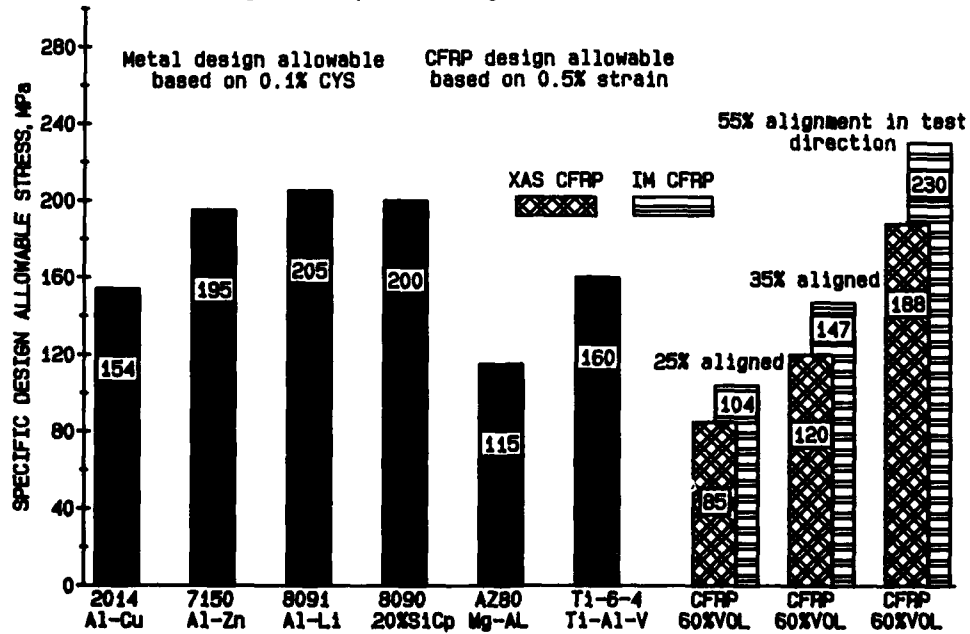


FIG.8 SPECIFIC TENSILE DESIGN ALLOWABLE STRENGTHS
Longitudinal Specific Strengths Allowed at Limit Load

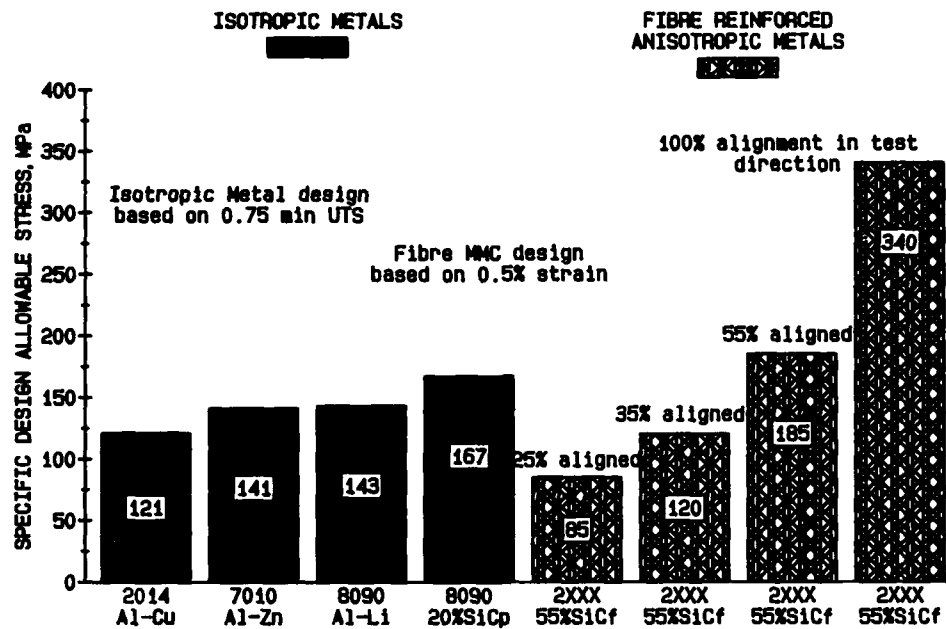
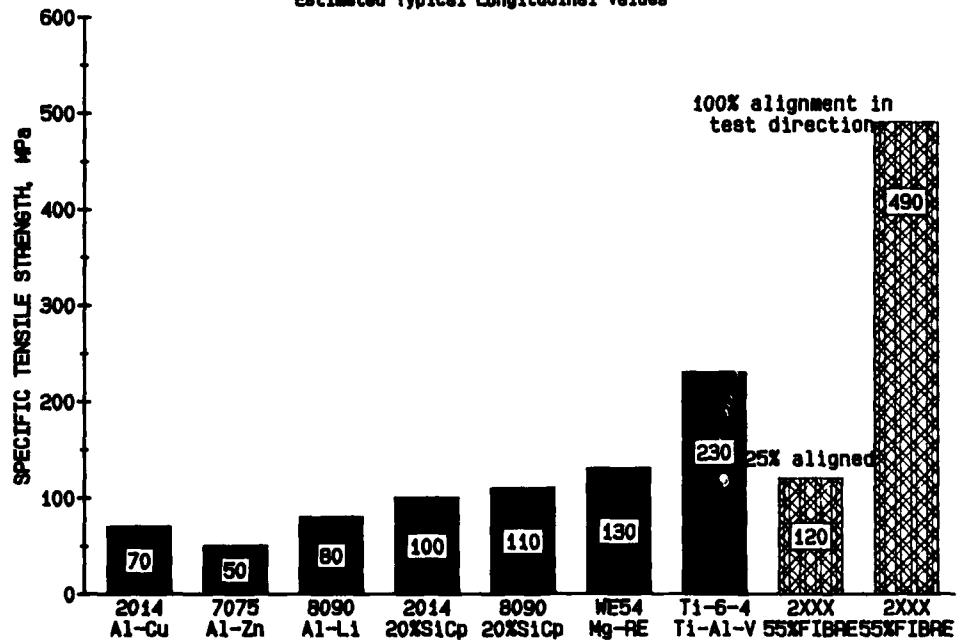


FIG.9 SPECIFIC TENSILE STRENGTHS AT 250C
Estimated Typical Longitudinal Values



HIGH PERFORMANCE POWDER METALLURGY ALUMINUM ALLOYS - AN OVERVIEW

by

M.J. Koczak and M.K. Premkumar
Department of Materials Engineering
Drexel University
Philadelphia, PA 19104

ABSTRACT

The historic development of aluminum powder metallurgy dates back to the early 1900's with initial flake powder production and has matured to the present day production of viable aerospace alloys. Primary powder production and processing techniques, such as atomization and mechanical alloying are reviewed. Processing-microstructure-property relationships in four classes of high performance powder metallurgy (P/M) aluminum alloys are considered. These are (i) high strength alloys (Al-Zn-Mg-Cu-Co); (ii) high specific modulus alloys (Al-Li-Cu); (iii) high temperature alloys (Al-Fe-Co, Al-Fe-Ni); (iv) mechanically alloyed material (Al-Mg) and composite alloys. Direct property comparisons with counterpart ingot metallurgy alloys are presented where ever appropriate. Aluminum powder metallurgy alloy development is now at a mature stage of growth where commercial and aerospace application are being sought and developed in competition with traditional aluminum ingot metallurgy, titanium and composite structures. The future growth and development of these alloy systems is vested in reliable economic processing.

1. INTRODUCTION

1.1 Historic Perspective of Aluminum Powder Metallurgy Alloys

One hundred years ago, Hall and Heroult independently discovered a process to produce aluminum by electrolysis. This refining technology opened the door for economical production of the light metal and initiated a search for new applications. Use of aluminum as powders began when flake-type aluminum powder was manufactured in the early 1900's by milling or attriting thin sheets into tiny flakes which were used as a pigment in paint formulations. Introduction of the atomization process in the 1920's provided for a more efficient production process and marked a new era in aluminum powder production. This process, coupled with the beginning of World War II and the development of aluminized high explosives, created a major market for atomized aluminum powder. Subsequently, atomized aluminum powder has found commercial applications in diverse areas of technology. A partial listing includes: pigments for paints and roofing, commercial blasting materials, reducing agents for the manufacture of metals and alloys, pharmaceuticals, cellular concrete, pyrotechnics, chemicals and rocket propellants. Furthermore, the commercial viability of low cost pressed and sintered aluminum powder metallurgy parts emerged in the 1960's, resulting in a further expansion of the powder metal market into near-net shape components. The historic development of precipitation and dispersion alloys are shown in Tables 1 and 2, respectively. The dispersion alloys can be categorized into five classes: high temperature alloys, low density alloys, high modulus alloys, mechanically alloyed materials and metal matrix composites. In contrast, the precipitation alloy systems are more conveniently categorized by alloy chemistry or alloy codes e.g. 2000, 7000 series, etc. Several referenced review articles summarize the development of powder aluminum alloys.

Fully dense dispersion alloys are reviewed [Towner 1961] where aluminum powders were first utilized for wrought components. Sintered aluminum products (SAP) utilized Al_2O_3 dispersions to improve the high-temperature strength of parts consolidated from milled aluminum powder. During this period, experimental work on atomized aluminum powders containing high solute contents was initiated which provided the genesis of research on current aluminum P/M alloys. These alloys utilized the benefits derived from rapid solidification which include alloying flexibility, increased solid solubility limits, fine-scale microstructures, and compositional homogeneity. From the embryonic research efforts emerged several types of alloy systems. The alloy systems created can be classified into dispersion strengthened alloys, precipitation systems or hybrid systems e.g. mechanically alloyed or composite reinforced systems. The dispersion-strengthened aluminum P/M alloys contain fine dispersions of relatively insoluble intermetallic phases. These alloys have good elevated temperature strength, thermal stability, wear resistance and exhibit a high elastic modulus. An example of this type of alloy system is the Al-Fe-X alloys where X represents a variety of elements which form a high volume fraction (e.g. 5 to 40 percent) of intermetallic aluminide phases in a low solute aluminum matrix.

A major class of alloy developed along the lines of traditional heat-treatable 2XXX, e.g. Al-Cu and 7XXX, e.g. Al-Zn-Mg ingot metallurgy compositions. In this case, rapid solidification resulted in the ability to produce a fine grain size and refined microstructure and resulted in an alloy with combinations of strength, fracture toughness and corrosion resistance that exceeds ingot alloys. As these alloy systems are being developed for commercial applications, alloys including Al-Li for lower density and metal matrix composites for greater stiffness are currently being explored. In many cases, the alloy chemistry corresponded to traditional alloys. However, alloy design efforts are seeking modifications based upon the benefits of rapid solidification. Previously, the application of highly alloyed systems via conventional solidification approaches has been hindered by the limited ductility and strength as a result of coarse second phase constituent intermetallics. Given the attributes of the powder processing approach, an opportunity exists to develop novel and high performance alloy chemistries for improved strength and reliability. The benefits derived from aluminum powder metallurgy, Figure 1, are appropriate to the aerospace industry.

Apart from the considerations of alloy chemistry, emphasis has been directed to processing of the powders i.e. powder degassing, consolidation, and secondary operations, e.g. extrusion and heat treatments. In addition to development of alloys for high performance structural applications, rapidly solidified particulate, in the form of powder, ribbon, or attrited flake must be consolidated to full density. In order to maximize mechanical properties, retention of the benefits from rapid solidification during subsequent densification and thermomechanical processing of the wrought product is an important consideration. Therefore, procedures must be carefully designed in order to maintain the refined structure and its inherent benefits. During the last ten years advances in powder processing, i.e. hot isostatic pressing, extrusion and mechanical alloying has aided the progress of aluminum powder metallurgy processing. To this end, development of alloys for high performance structural applications rapidly solidified particulate, in the form of powder, ribbon, or attrited flake have been consolidated to full density with excellent mechanical properties.

1.2 Powder Production Techniques

The development of aluminum powder metallurgy was aimed at producing high quality powders coupled with improved processing. The factors which influence powder production include solidification rate, melt chemistry, atomizing gas content and pressure. In an effort to produce high specific strength and high specific modulus alloys, alloy chemistries can be modified to provide higher solute contents to reduce density and increase modulus, Figures 2 and 3. Density reductions can be achieved with lithium, magnesium, boron, beryllium and silicon, while elements which significantly contribute to modulus are lithium, manganese and cobalt.

Duweez (1963) and Duwez and Willens (1967) initially developed techniques to produce rapid solidified structures with solidification rates in excess of 10^3 K/s. Solidification rates in excess of 10^4 - 10^5 K/s have been produced via atomization through a number of approaches. The benefits involve:

- finer grain size, dendrite arm and eutectic spacing
- extension of terminal solid solutions
- morphological changes of microstructure
- metastable phase formation
- vacancy supersaturation

The available solidification/atomization techniques range in dendrite arm spacing and cooling rates as indicated in Table 3. In addition to the effect of solidification rate on dendrite arm spacing, Figure 4, the extension in solid solubility was pioneered and shown for several binary aluminum alloys by Jones (1978), Table 4. The developed atomization techniques for aluminum alloys have included gas atomization, centrifugal atomization, rotating cup, rotating electrode process, single and double roll quenching, ultrasonic gas atomization, the Osprey process and solubility gas process. Following production of alloy powders, secondary processes, i.e. mechanical alloying combining carbide reinforcement provide opportunities for high temperature strength and modulus improvements. The refinement of microstructure via rapid solidification, Table 3 and the extension of solid solubility Table 4 are important physical features of the process. The resulting benefits, i.e. the mechanical property improvement versus weight saving demonstrate the utility of aluminum powder metallurgy alloys in aerospace applications, Figure 1. Commercial techniques for aluminum powder production and processing are depicted in Figures 5 and 6. A comparison of the relative sizes of microstructural features for P/M 7000 series aluminum alloys is shown in Table 5.

The atomization process can be considered in three stages (i) molten metal processing, (ii) atomization and (iii) powder handling, and each stage is subject to powder contamination. In the molten liquid, the liquid temperature and thermal gradients prior to atomization must be controlled in order to minimize the size of primary intermetallic phases. During atomization, high purity, moisture free gases combined with high gas pressure inhibit formation of coarse primary phases and undesirable oxides and carbides. The final stage of powder handling should prevent contamination from organics, moisture and foreign particles. Following powder atomization, the processing sequence can take a variety of routes to include cold compaction, canning of the powder preform, vacuum degassing, hot processing or extrusion of mill products of forging preform.

The goal of the atomization process is to reduce the particle size, reduce segregation and dendrite arm spacing. The aluminum powder particle must be consistent with clean surfaces and free from contamination. The variation of dendrite arm spacing with aluminum powder size is depicted in Figure 7 for ultrasonic gas atomization (USGA). Powder size fraction of fifty microns have typical dendrite arm spacings of two microns. The particle size of aluminum powders can vary with melt superheat and atomization pressure. As atomization pressure and melt superheat are reduced, particles sizes are significantly increased, Figure 8, e.g. 6.3 MPa (900 psi) and 720°C yields 250 microns at 50% retained versus 8.75 MPa (1250 psi) and 720°C which yields 110 microns at 50% retained versus 8.4 MPa (1200 psi) and 820°C which yields 25 microns.

Powders for press and sinter powder metallurgy application were initially developed for low strength structural components. The powders typically were mixed elemental blend with admixed lubricants added to facilitate compaction. Often, the sintering operation involved a liquid phase which assisted in breaking the tenacious particle oxide film. Close control of the sintering atmosphere, dew point and temperature were essential for process and property optimization. The next evolution of aluminum powder metallurgy involved prealloy powders which were processed into full density billets and subsequently hot-worked in order to improve properties. The primary purpose of the atomization process was to generate an extremely fine dendrite arm spacing. The fine structure with secondary dendrite arm spacings of one micron promotes rapid homogenization and short billet soaking times. A three millimeter diameter chill cast rod with a ten micron secondary dendrite arm spacing can be homogenized in ten minutes. In comparison, a 227 Kg direct chill cast ingot with a secondary dendrite arm spacing of fifty to one hundred microns requires over six hundred hours to homogenize. In summary, the refinement of the microstructure was directly related to the cooling rates from the melt. In addition, the fine dispersion of intermetallics promotes strength and corrosion resistance for high performance structural application.

2. PROCESSING, MICROSTRUCTURES AND PROPERTIES OF P/M ALUMINUM ALLOYS

2.1. Processing of P/M Aluminum Alloys:

The particulates produced by the various RSP techniques ultimately have to be consolidated into useful forms. The final product may be a complex P/M shape or a wrought P/M shape such as a sheet, rod or plate. In either event it is necessary to consolidate the particulate to full density. The initial definitive work in this area was concerned with consolidation of 7XXX Series aluminum alloys [Cebulak et al. 1976, Lyle and Cebulak 1975]. Subsequently these consolidation fundamentals have been applied to the other class of aluminum alloys.

Basic steps involved in aluminum alloy particulate consolidation are [Cebulak et al. 1976]:

- Cold compaction
- Vacuum preheating and degassing
- Hot consolidation
- Hot working
- Heat treatment, if required.

Common processes for consolidating Al alloy powders are shown schematically in Figure 5. Sufficient degassing is essential in order to have a fully dense consolidated product. If insufficiently degassed, when this material is exposed to a sufficiently high temperature either during heat treatment or during application, the moisture and hydrogen released can cause blistering in the product and the pores will reduce the ductility and toughness of the material as they are a source of fracture initiation. In the case of heat treatable alloys, vacuum degassing is usually performed slightly above the solution heat treatment temperature. On the other hand, too high a degassing temperature cannot be employed for risk of deteriorating the very fine microstructure produced by rapid solidification (RS); e.g. dispersion strengthened high temperature aluminum alloys; too high a temperature would coarsen the intermetallics decreasing the alloy's strength. The process of degassing and hot extrusion has resulted in considerable coarsening of the microstructure as compared to the original powder microstructure. Hence there is need to optimize the degassing and extrusion temperature for the alloy system under consideration.

Important parameters in terms of integrity of the consolidated material are amount of reduction and the hot working temperature. Due to the presence of the oxide film on powder particle surfaces, sufficient reduction must be employed in order to break up the film and establish good metal to metal bonding. The hot working temperature is critical from the point of view of ease of deformation and undue coarsening of the microstructure. Most commonly employed hot working operations for aluminum alloys are forging and extrusion.

A more recent development in the processing of aluminum alloys is the process of mechanical alloying. This involves charging the atomized aluminum powder into a high energy grinding mill where it is subjected to a ball milling operation. The constant fracturing and welding of the composite powder particles results in a more uniform final product. The mechanically alloyed powder is consolidated in the manner described earlier in this section. Benjamin and Bomford (1977) compared mechanically alloyed aluminum with conventionally produced SAP and found that mechanically alloyed aluminum containing about 2.75% to 5.4% by volume of dispersoid had strength levels equal to or better than SAP containing 11.5% by volume of dispersoid. The elevated temperature properties of the mechanically alloyed aluminum was also superior to that of SAP. The improved ambient and elevated temperature properties of the mechanically alloyed products are explained by the very fine, evenly distributed, equiaxed Al_2O_3 dispersoid as opposed to the flaky and inhomogeneously distributed dispersoid of conventional SAP. Intermediate P/M billet shapes are inherently more expensive to consolidate than the cost of continuously casting an analogous ingot. Hence, wrought Al alloy P/M parts suffer a cost disadvantage when compared to their I/M counterparts. In an effort to reduce this premium, a number of innovative "In situ consolidation" processes (e.g. spray forming, liquid dynamic compaction, plasma deposition, etc.) are being developed. These processes would retain the RS structure/property advantages but bypass the usual loose powder state because of its many complications [Ronald et al. 1984].

2.2 High-Strength Aluminum Alloys

P/M aluminum alloys for aerospace applications have been based on the I/M 7XXX series alloys. Due to their high strength, toughness and good corrosion resistance, these alloys have been used extensively in aircraft structural components since World War II. The 7XXX series alloys contain Zn, Mg and Cu as the principal alloying elements with minor alloying elements such as Cr, Zr, Mn and Ti which may be present in amounts of ~0.1% to 0.4%. Impurities such as Fe and Si form detrimental insoluble second phase particles and result in anisotropy of ductility. An example of a commercial 7XXX series alloy is the alloy 7075 which is the workhorse of the high strength aluminum industry.

Efforts to improve the toughness of the I/M 7XXX series alloys were undertaken in the late 1960's and early 1970's [Pickens 1981] and resulted in the development of commercial alloys with lower Fe and Si contents, e.g. high purity alloys, 7050 and 7475. Simultaneously, various thermal mechanical treatments were developed to upgrade these alloys through microstructural control. The resulting microstructure is an equiaxed recrystallized structure, compared to greatly elongated grains that produce anisotropic behavior for conventional processing.

P/M technology has been used to process alloys of conventional composition with an improvement in mechanical properties. For example, Voss (1978, 1979) investigated alloys 2024 and 7075 made both by P/M and I/M. He found that P/M reduced the grain size by an order of magnitude and the constituent particle size was decreased. P/M 7075 also had improved resistance to recrystallization and increased strength-isotropy. In general, it was also found that corrosion and fatigue crack initiation resistance are improved by P/M technology. Although the conventional compositions produced by rapid solidification are superior, by no means do they represent optimum P/M alloys. Even greater gains can be realized by modifying alloy composition to take advantage of the full potential of P/M technology.

The first generation P/M alloys are typified by the alloys X7090 and X7091 [Ronald et al. 1984]. These alloys were developed by Alcoa and were basically modifications of the I/M 7XXX alloys. Cobalt, an insoluble element results in a fine uniform dispersion of Co_2Al_9 , which produces a more favorable grain morphology giving rise to superior combinations of strength, toughness and stress corrosion cracking resistance compared to I/M 7075 and 7050. Alloy 7090 is similar to 7091 but is more highly alloyed in Co and Zn. The increased Co content results in a higher volume fraction of the Co_2Al_9 dispersoids which together with the higher Zn content gives the alloy a 10% strength improvement over 7891, although fracture toughness is reduced. Nominal chemical compositions of some high strength P/M aluminum alloys are listed in Table 6 along with the composition of I/M 7075 and 7050 for comparison purposes.

Kaiser Aluminum concurrently developed the alloys PM61 and PM64 vis a vis 7090 and 7091 alloys. Basically, the Kaiser alloys are similar in composition but in addition they contain 0.2% Zr. The Zr is added for additional grain refinement or stabilization. PM61 and PM64 are melt atomized alloys processed by powder metallurgy techniques. INCO P/M aluminum alloys, IN-9052 and IN-9021 illustrate the high strength P/M alloys developed by Novamet using the mechanical alloying process. IN-9052 is a non-heat-treatable alloy which derives its strength from Mg solid solution hardening and dispersion strengthening due to a fine oxide/carbide distribution. In addition, ultrafine grain size and substructure provide strengthening. Since precipitation hardening is not necessary, the alloy has excellent general corrosion strength. Precipitation strengthening adds to the above strengthening mechanisms in the Al-Cu-Mg alloy IN-9021. The fracture toughness and fatigue resistance of IN-9021 are similar to IN-9052 but it possesses higher strength. Some properties of high strength wrought aluminum P/M alloys are compared in Table 10 with I/M XXXX alloys.

Continued development of XXXX P/M alloys has led to the second generation alloy designated by Alcoa as CW67 [Hildeman et al. 1986]. This alloy is much more heavily alloyed in Zn (Table 6) and notable improvements include twice the fracture toughness as 7090 with equivalent strength. CW67 is expected to play a major role in the continued commercialization of 7000 series P/M alloys for high strength aerospace applications. Typical property levels for the Alcoa CW67 are listed in Table 10 and compared with existing alloys. Figure 10 compares the yield strength versus fracture toughness of CW67 and 7090 and 7091. While alloy and process development efforts continue, applications are being actively pursued.

2.3 High Specific Modulus Alloys

Addition of Li to Al reduces density and increases modulus. A 1 wt% Li addition increases modulus by 6% while decreasing density by 3%. As Figures 2 and 3 show, Li has the most beneficial effect on aluminum. These combined property improvements make Al-Li alloys extremely valuable to the aerospace community. Al-Li alloys have been investigated for the past several decades and were commercially used in the early 1960's [Ronald et al. 1984, Pickens 1981, Tietz and Palmer 1981]. An example is Alcoa's Al-Li-Cu alloy 2020. Due to its lower fracture toughness and its ductility, future was limited. Strengthening in these alloys is achieved by the precipitation of metastable, coherent and ordered δ' (Al_3Li) phase. However, upon plastic deformation, these precipitates are sheared by dislocations resulting in strain localization and hence lower fracture toughness. Impurity elements such as hydrogen, sodium, potassium and calcium also affect fracture toughness by virtue of forming harmful phases and grain boundary segregation.

In addition to problems associated with low fracture toughness, powder metallurgy Al-Li alloys have not attained commercial acceptability due to problems associated with melting, casting and processing of Li containing alloys. Currently, research and development of Al-Li alloys is being pursued using both the I/M and P/M approaches. Rapid solidification techniques such as P/M with its inherent advantage of finer grain size and dispersoid size has been shown to promote homogeneous slip and improved mechanical properties.

Alloying elements that are currently added to Al-Li alloys are Cu, Mg, Be and Zr. Mechanically alloyed Al-Li and Al-Mg-Li alloys containing oxides and carbides have also been developed and have good mechanical properties. An attractive feature of this class of alloys is their superplastic behavior which makes them even more interesting. Table 8 lists the most promising Al-Li based alloys along with their mechanical properties. A potential future alloy is Al-Li-Be based alloys. Be also improves modulus of aluminum while decreasing density. However, there are handling and toxicity problems associated with Be which have to be overcome.

2.4 High Temperature Alloys:

2.4.1 Early Developments:

The concept of using aluminum alloys for elevated temperature applications dates back to about 1950 when oxide dispersion strengthened aluminum was developed. At that time in Switzerland, Irmann [Irmann 1949, Bloch 1961] discovered that sintered aluminum had mechanical properties similar to those of aluminum alloys; he attributed this enhancement in strength to the presence of oxide films surrounding the individual powder particles in the sintered material. On subsequent cold compaction and hot working, the oxide was broken up and distributed as small dispersoids thereby giving rise to strengthening of the aluminum matrix. These materials are known as the SAP materials, i.e. sintered aluminum products. Subsequently in the USA, Alcoa developed a range of oxide dispersion strengthened aluminum materials similar to SAP. The first detailed study of these SAP type materials in the United States was conducted by Lyle (1952). It was found that these materials had high room temperature strength, of the order of some aluminum alloys. They also had the ability to retain strength after prolonged exposure at temperatures as high as 482°C. Moreover, strength decreased with increasing temperature at a lower rate than conventional aluminum alloys with comparable room temperature strength. These products were designated APM. Typical room and elevated temperature tensile properties of these oxide strengthened aluminum alloys are listed in Table 9. The materials designated SAP are the ones developed by Aluminum-Industrie-Aktier-Gesellschaft (AIA) of Switzerland while the M series are the APM products of Alcoa.

The previous work on SAP and SAP type alloys lead to the development of other types of dispersion strengthened aluminum alloys in which intermetallic compounds constituted the dispersed phase. These alloys may be expected to have good elevated temperature properties. These phases are difficult to add directly as compounds because of poor wettability between the intermetallic and the liquid or solid aluminum matrix. These dispersoids can however, be formed in-situ during atomization of the alloy melt. Such particulates are termed prealloyed powders and these are subsequently compacted and hot consolidated. The resulting aluminum alloy differs from SAP and SAP type materials since they contain deliberate levels of alloying elements but only incidental, and to a large extent detrimental, oxides at a level of about 0.5 wt %.

Towner (1958) studied several alloys in which the dispersoid was an intermetallic. The rationale for selecting the alloying elements was to achieve a fine dispersion of an insoluble constituent in the solid alloy. Hence alloying elements such as Fe, Cr and other transition elements were chosen which had low solubilities and low diffusion rates in solid aluminum. The transition elements form thermally stable intermetallic compounds of relatively low density, so that appreciable amounts of alloying elements may be added without a prohibitive increase in the density of the final alloy. An alloy of Al-4.5% Fe-7.0% Ni had the best room temperature strength (537 MPa).

From the developmental work of Towner (1958), binary Al-Fe alloys containing 7.5 wt%, 10 wt% and 12.8 wt% Fe gave the highest tensile strengths at 315°C and 427°C. More complex alloys of composition 7.89 wt% Fe and 0.2 wt% each of Cr, Ti, V, Zr and a quaternary alloy of aluminum with 2.5 wt% Fe, 0.4 wt% Cr and 3.4 wt% V also gave excellent high temperature strength up to temperatures of 427°C. Consistent with strength retention, these alloys all exhibited microstructural stability above ambient. The complex alloy of aluminum containing 7.8 wt% Fe and 0.2 wt% each of Cr, Ti, V and Zr had the best stress-rupture properties at 315°C. In the 1960's attention was directed towards the development of 1M 2XXX series aluminum alloys for use at intermediate temperatures i.e. up to approximately 200°C [Doyle 1969]. In contrast to SAP and SAP type alloys strength is derived via precipitation hardening. Additional strengthening can be provided by intermetallics based on Fe and Ni. The best commercial alloy (X2219) has a composition Al-2.2 w/o Cu - 1.4 w/o Mg - 0.2 w/o Si - 0.9 w/o Fe - 1.0 w/o Ni and achieves a strength level of 361.8 MPa [60]. At 200°C there is a 38% drop in strength.

Table 10 compares the properties of Towner's intermetallic strengthened alloys with an oxide strengthened alloy and an 1M 2XXX series alloy. The precipitation hardened alloys (2XXX series) have a severe limitation in that the precipitates coarsen rapidly above ~200°C with attendant loss of strength.

2.4.2. New Class of Alloys:

The most recent development in the area of elevated temperature P/M aluminum alloys pertain to dispersion strengthening via intermetallics [Pickens 1981, Milan 1983]. The intermetallics based on transition and rare earth elements (Fe, Ni, Co, Cr, Ce, etc.) are thermodynamically stable and resistant to coarsening. This is a consequence of the extremely low equilibrium solid solubilities and small diffusion rates of the alloying elements in the aluminum matrix.

To achieve sufficient strength at ambient and elevated temperatures, it is necessary to have a high volume fraction of the dispersoids on a fine scale uniformly distributed throughout the matrix. This can only be achieved by resorting to rapid solidification via P/M processing. It is impossible to produce these alloys by conventional ingot solidification since attendant slower cooling rates result in considerable macrosegregation, with coarse primary intermetallics.

Structural transitions in rapidly solidified binary alloys of Al with Fe, Ni, Cr, Mn, Co, Ti and V were studied by Jones (1969). It was observed that metallographically two distinct zones were present namely A zones and B zones. Zone A consisted of a very fine dendritic or cellular α -aluminum structure and was optically featureless. The microhardness of this zone was approximately twice that of zone B and did not change significantly with annealing up to temperatures of 200°C after which it decreased. Zone B consisted of a much coarser structure. The transition from the zone A to the zone B structure was explained in terms of the cooling rates experienced by the two regions. The region of the splat in contact with the metal substrate experienced a higher cooling rate and this resulted in the finer zone A type structure. Upon consolidation, the microstructure in these new class of aluminum alloys consists of a matrix subgrain structure with essentially equiaxed intermetallics. The hot extrusion results in dynamic recovery of the aluminum matrix and the high volume fraction of dispersoids prevents any recrystallization.

Stability of strengthening dispersoids is a very important criterion in selection of this new class of aluminum alloys for high temperature applications. Pontikakos and Jones (1982) studied the coarsening behavior of intermetallics in several Al-transition metal alloys produced by rapid solidification. Al-Fe, Al-Ni and Al-Cr alloys were heat treated at 500°C - 625°C for time periods up to 1000 hrs and the size and distribution of the corresponding dispersoids were analyzed with respect to current particle coarsening theories. At lower temperatures, coarsening was enhanced due to residence of the dispersoids on the grain boundaries. The observed increases in the average particle size of FeAl₃ were found to be in good agreement with predictions based on grain boundary diffusion control at 500°C, and lattice diffusion control at 600°C. The highest resistance to coarsening was exhibited by CrAl₇ at 500°C while FeAl₃ was more resistant than NiAl₃ for all conditions. In the Al-Fe-Ni system [Premkumar 1985], the coarsening kinetics of the FeNiAl₉ intermetallic was studied at 450°C and 550°C. The kinetics were found to be in good agreement with the grain boundary diffusion model. In general, the microstructural stability was excellent up to 400°C.

A number of aluminum alloy development programs sponsored by the U.S. Air Force were initiated in the early 1970's with the objective of developing alloys for service in the temperature range 230-340°C. These programs developed several rapidly solidified alloys utilizing the P/M technology with significant property improvements over the best high temperature 1M alloys. Alcoa [Griffith et al., 1982] carried out a systematic program for alloy development for P/M aluminum alloys. Initially, six binary and fifteen ternary compositions were investigated and the most promising alloys were found to be Al-Mn-Co, Al-Fe-Co, Al-Mn-Ni, Al-Fe-Ce and Al-Fe-Cr. Subsequently, 5 compositions were selected for further evaluation. These included one Al-Fe-Co composition, two Al-Fe-Ni alloys, one Al-Fe-Ce alloy and one Al-Fe-Misch alloy. In the Al-Fe-Ni, Ni is substituted for the more expensive Co, and in the Al-Fe-Misch, the Misch metal is substituted for the more expensive Ce. The Al-Fe-Ce alloys was found to have the best combinations of strength and ductility and was chosen for a complete engineering property evaluation. Improvements in processing methods increased the ductility of the Al-Fe-Ce alloy from the earlier level of 0.7% to 7%. The alloy was also found to exhibit excellent creep and stress corrosion cracking resistance.

Pratt and Whitney conducted a research program to develop an aluminum alloy for fan blade applications [Adam et al. 1981]. Alloys containing Fe, Mn, Cr, Si, Ti, Nb, Zr, Hf, V, Mo and W were investigated and the most promising composition reported was Al-8Fe-2Mo.

Ternary Al-Fe-V and Al-Fe-Zr and quaternary Al-Fe-V-Zr systems were examined by Skinner et al. at Allied Corporation [Skinner et al. 1984] for Fe contents in the range of 8-12 wt%. An Al-13.9 w/o Fe - 2.2 w/o V alloy containing predominantly a zone A type microstructure was found to have a room temperature UTS of greater than 600 MPa with a ductility of 5%. These values decreased by 50% at 327°C with a 50% increase in ductility. The quaternary Al-Fe-Zr-V system was found to exhibit excellent strength and ductility at high volume fraction levels compared to the ternary alloys in which high volume fractions of dispersoids resulted in reduced ductility.

Simultaneously, there has been a research effort directed towards understanding some of these alloys at a more fundamental level. These studies are important in order to further improve the alloys and optimize the compositions. Recently, the Al-Fe-Ni alloy system [Premkumar 1985] was examined with a view to understanding the strengthening mechanisms and microstructural stability. One of the findings of this study was that above 250°C, the yield strength of the alloys was independent of the volume fraction of the FeNiAl₉ dispersoid, Figure 11. The results were explained on the basis of a dislocation climb mechanism which appeared to be insensitive to dispersoid volume fraction at the high levels ($V_f 0.19 - V_f 0.32$) present in these alloys.

In summary, the most promising high temperature aluminum alloys to date are Alcoa's Al-8.0Fe-3.4 Ce, Pratt and Whitney's Al-8Fe-2Mo and Allied's Al-10.1Fe-3.2Zr-2.3V. The tensile properties of these alloys are shown in Table 11 along with those of an 1M 2XXX series high temperature alloy for comparison. Also included in the table are data for an experimental Al-6Cr-1Fe alloy produced by vapor deposition developed by Alcan.

2.5 Mechanical Alloying

Since the development of sintered aluminum powders, e.g. SAP alloys, dispersion aluminum alloys have provided oxide reinforced systems which have good combinations of strength and thermal conductivity. The enhanced properties are a result of a fine grain equiaxed structure with a uniform dispersion of oxide via a vis dispersion alloys. Typically, the mechanical alloying technique utilizes a ball milling or attrition process which involves the deformation, fracture and welding of fine mixed elemental or prealloyed powders. The surface oxide film on the aluminum powders is broken and dispersed within the powder particles. Several authors, e.g. Townner (1961), Grant and Preston (1957), Benjamin and Bomford (1977) Gilman et al. (1986), Schelling and Donachie (1977), have investigated dispersion strengthened aluminum alloys. Inco has actively developed several mechanically alloyed systems, e.g. Al-4Mg (IN9052), Al-4Cu-1.5Mg (IN9021) and Al-4Mg-1.5Li (IN 905X1). In general, the strengths, creep response and corrosion resistance are enhanced with a reduction in elongation and toughness. In addition, the mechanical alloying process can be utilized to incorporate a fine reinforcing particulate or whisker, e.g. SiC, Al₂O₃. A comparison of the mechanical properties of IN9021 and IN9052 versus an ingot metallurgy 7075 alloy is provided in Table 12. In a comparison of the physical properties, mechanically alloyed products achieve longitudinal and transverse properties from 550-650 MPa, for ultimate tensile strengths with reasonable elongation levels from 2.5 to 14% depending on orientation.

Efforts have been undertaken to improve the elevated-temperature properties of RS aluminum alloys by combining RS and mechanical alloying in high strength, corrosion resistant and high-temperature aluminum alloy systems, e.g. Al-Zn-Mg, Al-Cu, Al-Mg, Al-Fe-Ni, Al-Fe-Ce, and Al-Ti. By superimposing the dispersion strengthening provided by the fine, stable oxides and carbides introduced by mechanical alloying with the intermetallic dispersoids in the RS powder, improved ambient temperature strength and elevated-temperature strength are achieved. Furthermore, mechanical alloying alters the texture by inducing the formation of stabilized low-angle boundaries and grain boundaries pinned by oxides. Static recrystallization, grain growth, and intermetallic coarsening are therefore inhibited.

The processing of mechanically alloyed products is critical for good combinations of strength and ductility. As a result, the processing is a critical step and the microstructure of a mechanically alloyed powder is depicted in Figure 12. As the mechanical alloying process proceeds, the powder thickness decreases and the hardness of the powders, i.e. the degree of cold working increases. The process provides shorter diffusion distances and studies by Ovecogulu and Nix (1982) and Frazier and Koczak (1986) have monitored the interdiffusion process and microstructural development. The x-ray characterization of the annealed mechanically alloyed Al-Ti system Figure 13 shows the development of Al₃Ti as a function of temperature. In a comparison of mechanically alloyed aluminum alloys versus non-mechanically alloyed systems, Al-Fe-Ni alloys, Ezz et al. (1986) have demonstrated improved microstructural stability and strength over a temperature range from ambient to 500°C. The mechanically alloyed high temperature alloys demonstrate increased strength, however limited ductility. Important achievements and limitations include: (i) a significant increase in microstructural stability at elevated temperature, compared to non-mechanically alloyed material, (ii) a large improvement in strength at all temperatures and enhancement in creep resistance compared to nonmechanically alloyed material, (iii) a limited failure strain, 2 - 5% at ambient temperature for the strongest material. In Al-Fe-Ni, yield strength increases of 77% at 25°C and 35% at 400°C were achieved by mechanical alloying. The hardness remained unchanged after 1-h exposure at up to 500°C. At temperatures over 500°C, the sharp drop in hardness indicated considerable coarsening of (FeNi)Al₉. A key question is the mechanism by which these fine dispersions inhibit coarsening.

In an excellent comparison of mechanically alloyed versus prealloyed powder alloys, Gilman et al. (1986) examined the high temperature response in Al-4Mg-1.5Li alloys. In addition, SiC and CeO₂ additions were incorporated in order to understand the effects of the variations of strength versus the Al₂O₃ and Al₄C₃ in conventionally mechanical alloyed systems. As depicted in Figure 14, the hardness retention following exposure at 400°C is excellent. The strength of the SiC modified alloy is higher than the CeO₂ and oxide/carbide dispersion Mg-Li systems, however, the ductility is limited, Figure 15. The additional benefit of the SiC addition is an enhanced creep resistance, Figure 16. Gilman et al., has demonstrated that the mechanical alloying process combined with CeO₂ and SiC provides good ambient and elevated temperature properties. An important issue is the balance of properties or trade-offs which can be achieved by combining the prealloyed aluminum powders, a fine oxide dispersion generated by the attrition process and the incorporation of high-modulus/high-strength particulates or whiskers. The key issues to address within the mechanical alloying process are the microstructural development e.g. oxide distribution, and the concurrent effect on mechanical and physical properties. For instance, with increased oxide level, improvements are apparent in microstructural stability, yield strength and ultimate tensile strength. Simultaneously, reductions in ductility, toughness, electrical conductivity are apparent with increased levels of oxide dispersions. As a result, a processing balance must be achieved in the initial prealloyed powder processing as well as the attrition, consolidation and secondary forming operations. In the development of powder alloys, the mechanical alloying process adds a facet where improved strength and microstructural stability are possible not only for aluminum base powder alloys, but also for copper and nickel based systems.

An important issue to resolve is the processing and mechanical property reliability, economy of scale of the product forms coupled with the ability to produce complex structure shape via extrusion, superplastic forming or forging approaches. Issues which also pose challenges to these high temperature structural alloy systems are fatigue crack initiation and propagation response coupled with the stress corrosion performance.

ACKNOWLEDGEMENT: The authors gratefully acknowledge research program support in aluminum powder metallurgy from the Naval Air Development Center and the Air Force Office of Scientific Research

REFERENCES

- Adam, C.M., R.G. Bourdeau, J.W. Broch and A.R. Cose, 1981, Final Report, AFWAL Contract No. F33615-76-C-5136.
- Ansell, G.S., 1966, in: *Oxide Dispersion Strengthening*, eds. G.S. Ansell, T.C. Cooper and F.V. Lenel (AIME), p. 61.
- Ansell, G.S. and J. Weertman, 1959, *AIME Trans.*, 215, 838.
- Ardell, A.J., 1972 a, *Acta. Met.*, 20, 61.
- Ardell, A.J., 1972 b, *Acta. Met.*, 20, 601.
- Ardell, A.J. and R.B. Nicholson, 1966, *J. Phys. Chem. Solids*, 27, 1793.
- Benjamin, J.S. and M.J. Bamford, 1977, *Met. Trans.*, 8A, 1301.
- Bloch, E.A., 1961, *Met. Rev.*, 6, #22, 193.
- Brailsford, A.D. and P. Wynblatt, 1979, *Acta. Met.*, 27, 489.
- Bridenbaugh, P.R., W.S. Cebulak, F.R. Billman and G.J. Hildeman, 1985, *Processing and Properties of Advanced High Temperature Alloys Symposium*, MIT, Cambridge, MA.
- Cebulak, W.S., E.W. Johnson and H. Markins, 1976, *Met. Engg. Quart.*, p. 37.
- Chellman, D.J. and A.J. Ardell, 1974, *Acta. Met.*, 22, 577.
- Coble, R.L., 1963, *J. of Appl. Phys.*, 34, 1679.
- Courtney, T.H., 1982, in: *Solid-Solid Phase Transformations*, eds. H.I. Aaronson, D.E. Laughlin, R.F. Sekerka and C.M. Wayman (The Metallurgical Society of AIME, Warrendale, PA), p. 1057.
- Decker, R.F., 1973, *Met. Trans.*, 4, 2495.
- Davies, G.K.L., P. Nash and R.N. Stevens, 1980, *Acta. Met.*, 28, 179.
- Doyle, W.M., 1969, *Aircraft Engineering*, 41, #11, 11.
- Duwez, P. and Willens, 1963, *TMS-AIME*, 227, 362.
- Duwez, P., 1967, *Trans. ASM*, 60, 607.
- Ezz, S., M.J. Koczak, A. Lawley and M.K. Premkumar, 1986, in *High Strength Powder Metallurgy Aluminum Alloys - II*, eds., G.J. Hildeman and M.J. Koczak (The Metallurgical Society of AIME, Warrendale, PA), p. 287.
- Froes, F.H. and J.R. Pickens, 1984, *J. of Metals*, 36, #1, p. 14.
- Frazier, W.F. and M.J. Koczak, 1986, in *High Strength Powder Metallurgy Aluminum Alloys - II*, eds., G.J. Hildeman and M.J. Koczak (The Metallurgical Society of AIME, Warrendale, PA), p. 353.
- Gemmell, G.D. and N.J. Grant, 1957, *J. of Metals*, p. 417.
- Gibbs, G.B., 1967, *Mater. Sci. Engg.*, 2, 269.
- Gilman, P.S., J.W. Brooks and P.J. Bridges, 1985, in *Third International Conference on Aluminum-Lithium*, Oxford, England.
- Grant, N.J. and O. Preston, 1957, *Trans. AIME*, 209, 349.
- Grant, N.J., 1982, in: *High Strength Powder Metallurgy Aluminum Alloys*, eds., M.J. Koczak and G.J. Hildeman (The Metallurgical Society of AIME, Warrendale, PA), p. 3.
- Greenwood, G.W., 1956, *Acta. Met.*, 4, 234.
- Griffith, W.M., R.E. Sanders, Jr. and G.J. Hildman, 1982, in: *High Strength Powder Metallurgy Aluminum Alloys - II*, eds., G.J. Hildeman and M.J. Koczak (The Metallurgical Society of AIME, Warrendale, PA), p. 209.
- Herring, C., 1950, *J. of Appl. Phys.*, 21, 437.

- Hildeman, G.J., L.C. Labarre, A. Hafeez and L.M. Angers, 1986, in: *High Strength Powder Metallurgy Aluminum Alloys - II*, eds., G.J. Hildeman and M.J. Koczak (The Metallurgical Society of AIME, Warrendale, PA), p. 25.
- Hirehner, H.O.K., 1971, *Met. Trans.*, 2, 2861.
- Humphreys, F.J., 1983, in: *Deformation of Multi-Phase and Particle Containing Materials*, Proceedings of 4th RISO International Symposium on Metallurgy and Materials Science, p. 41.
- Irmann, R., 1949, *Techn. Rundschau*, 41, #36, 19.
- Jones, H., 1969, *Mater. Sci. Eng.*, 5, 1.
- Jones, H., 1978, *Aluminum*, 54, 274.
- Lagneborg, R., 1972, *Int. Met. Rev.*, 17, 130.
- Lifshitz, I.M. and V.V. Sylozov, 1961, *J. Phys. Chem. Solids*, 19, 35.
- Lyle, J.P., Jr., 1952, *Metal Progress*, 62, #6, 109.
- Lyle, J.P., Jr. and W.S. Cebulak, 1975, *Met Trans.*, 6A, 685.
- Lund, R.W. and W.D. Nix, 1976, *Acta. Met.*, 24, 469.
- Martin, J.W. and R.D. Doherty, 1976, in: *Stability of Microstructure in Metallic Systems*, Cambridge University Press.
- Martin, J.W., 1980, in: *Micromechanisms in Particle Hardened Alloys*, Cambridge University Press.
- McLean, D., 1962, *Met. Rev.*, 7, #28, 481.
- Milan, P.P., Jr., 1983, *J. of Metals*, 35, 76.
- Morgan, J.T., H.L. Gegel, S.M. Doraivelu, L.E. Matson, I.A. Martorell and J.F. Thomas, Jr., 1982, in: *High Strength Powder Metallurgy Aluminum Alloys*, eds., M.J. Koczak and G.J. Hildeman (The Metallurgical Society of AIME, Warrendale, PA), p. 193.
- Mukharjee, A K., 1975, in *Treatise on Materials Science and Technology*, Vol. 6, Ed. R.J. Arsenault, p. 164.
- Mullendore, A. W. and N.J. Grant, 1984, *J. of Metals*, p. 973.
- Murthy, K.L., F.A. Mohamed and J.E. Dorn, 1972, *Acta Met.*, 20, 1009.
- Nabaro, F.R.N., 1948, *Proceedings of the Conference on the Strenth of Solids*, Bristol, Physical Society, London, p. 75.
- Oriani, R.A., 1964, *Acta. Met.*, 12, 1399.
- Ostwald, W., 1900, *Z. Phys. Chem.*, 34, 495.
- Ovecogulu, M.L. and W.D. Nix, 1982, in: *High Strength Powder Metallurgy Aluminum Alloys*, eds., M.J. Koczak and G.J. Hildeman (The Metallurgical Society of AIME, Warrendale, PA), p.
- Pickens, J.R., 1981, *J. Mater. Sci.*, 16, 1437.
- Perepezko, J.H., S.E. LeBeau, B.A. Mueller and G.J. Hildeman, 1986, in *ASTM-STP 890, Rapidly Solidified Powder Aluminum Alloys*, p. 118.
- Pontikakas, I. and H. Jones, 1982, *Metal Science*, 16, 27.
- Premkumar, M.K., 1985, Ph.D. Dissertation, Drexel University, Philadelphia, PA.
- Scamans, G.M. and A.S. Rehal, 1979, *J. of Mater. Sci.*, 14, 2459.
- Schelling, R.D. and S. Donachie, 1983, *Metal Powder Report*, 38, 575.
- Sellars, C.M. and R.A. Petkovic-Luton, 1980, *Mater. Sci., Eng.*, 46, 75.
- Skinner, D.J., R. Ker, M.J. Koczak and A. Lawley, 1981, in: *Modern Developments in Powder Metallurgy*, eds. H.H. Hausner, F. W. Antes and G.D. Smith (MPIF, Princeton, NJ), Vol. 13, 483.
- Skinner, D.J., K. Okazaki and C.M. Adam, 1984, in: *ASTM Symposium on Rapidly Solidified Powder Aluminum Alloys*, Philadelphia, PA.
- Staley, J.T., May 1976, *Mat. Eng. Quart.*, p. 52.
- Starke, E.A., Jr., 1977, *Mater. Sci. Eng.*, 29, 99.
- Starke, E.A., Jr. and J.A. Wert, 1986, in: *High Strength Powder Metallurgy Aluminum Alloys - II*, eds., G.J. Hildeman and M.J. Koczak (The Metallurgical Society of AIME, Warrendale, PA), p. 3.

Tietz, T.E. and I.G. Palmer, 1981, in: *Advances in Powder Technology*, Louisville, Kentucky, ed.: G.Y. Chin (ASM, Metals Park, OH).

Towner, R.J., 1958, *Metal Progress*, 73, #5, p. 70.

Towner, R.J., 1961, *Met. Eng. Quart.*, 1, #1, p. 24.

Voss, D.P., 1978, Air Force Office of Scientific Research, 77-3440.

Voss, D.P., 1979, Air Force Office of Scientific Research, 77-3440.

Wagner, C., 1961, *Z. Elektrochem*, 65, 581.

Weertman, J., 1955, *J. of Appl. Phys.*, 21, 1213.

Wilcox, B.A. and A.H. Clauer, 1966, *Trans. AIME*, 236, 570.

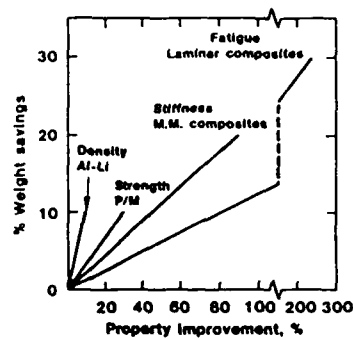


Figure 1: The physical and mechanical property benefits derived from aluminum powder metallurgy-relationship between mechanical property improvements and weight savings. (Hildeman, 1986)

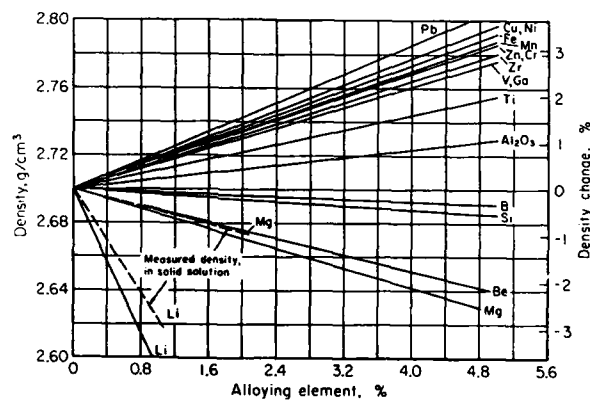


Figure 2: Effect of alloying elements on the density of aluminum alloys. (Hatch, 1983)

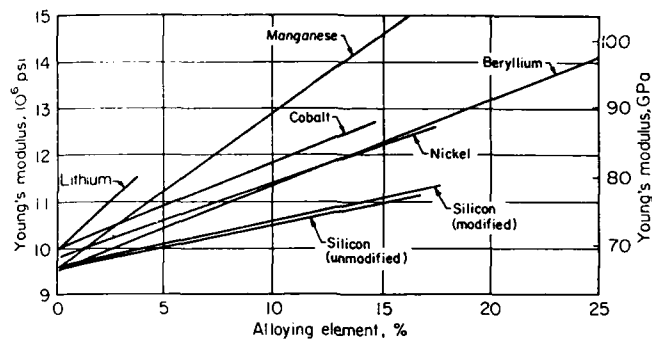


Figure 3: Effect of alloying elements on the modulus of aluminum alloys. (Hatch, 1983)

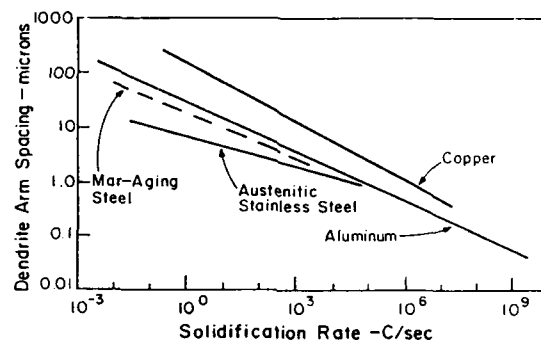


Figure 4: Variation of dendrite arm spacing with solidification rate. (Grant, 1982)

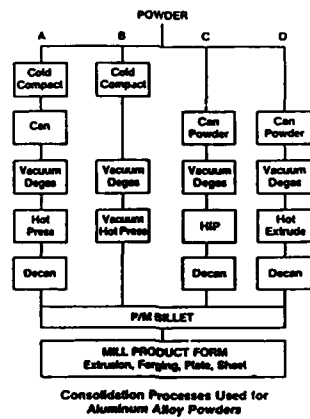


Figure 5: Processing scheme for aluminum powders. (Bridenbaugh et al., 1985)

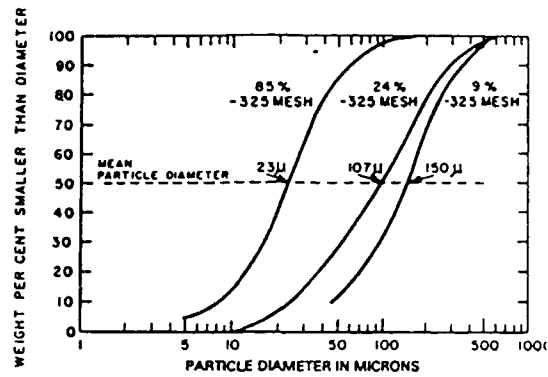


Figure 9: Particle size distribution for air atomized aluminum powders. (Grant, 1982)

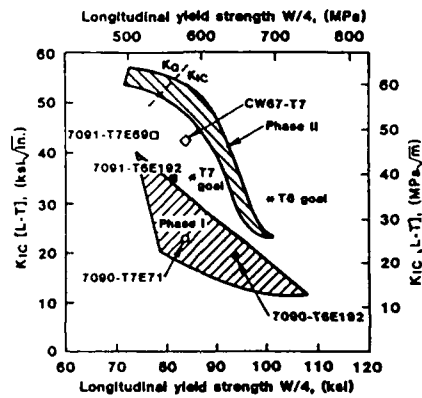


Figure 10: Yield strength - fracture toughness relationships of CW67, 7090 and 7012 extrusions. Phase I and phase II alloys represent exploratory alloys. (Hildeman et al., 1986)

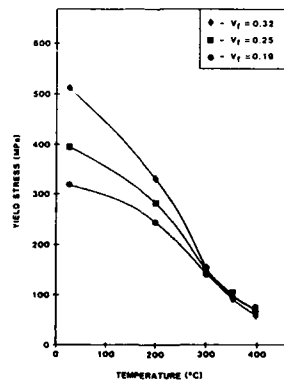


Figure 11: Effect of volume fraction (V_f) on the elevated temperature yield strength response of P/M Al-Fe-Ni extrusions.

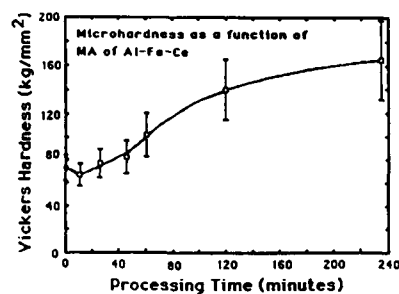


Figure 12: Hardness values of mechanically alloyed powders as a function of processing time (Ovecoglu and Nix, 1986)

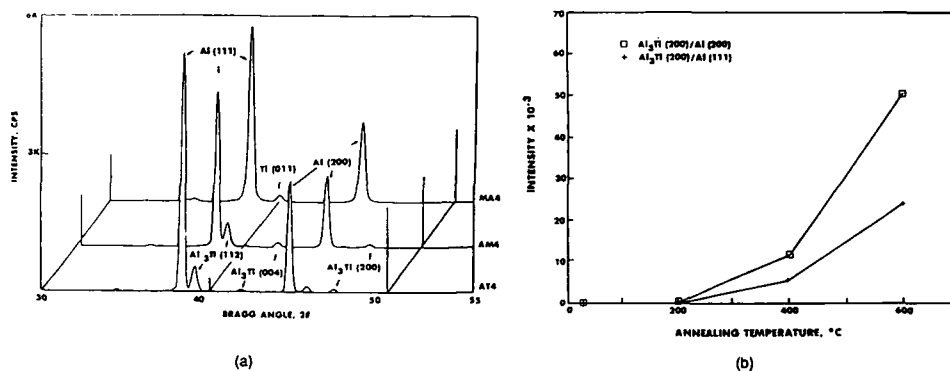


Figure 13: (a) X-ray spectra of atomized Al-4 w/o Ti (AT4) and mechanically alloyed Al-4 w/o Ti alloys (MA4 and AM4) showing Al, Ti and intermetallic lines. (b) increase of intermetallic line intensity with annealing at various temperatures (Frazier and Koczek 1986).

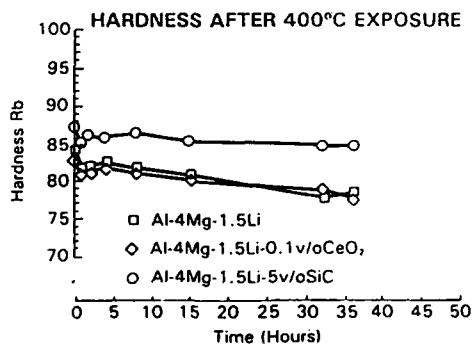


Figure 14: Hardness of various Al-Mg alloys following exposures at 400°C (Gilman et al. 1986).

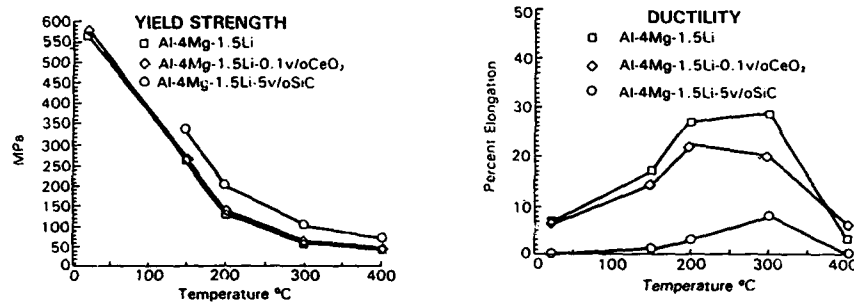


Figure 15: Yield strength and ductility response versus test temperature for various mechanically alloyed Al-Mg alloys (Gilman et al. 1986).

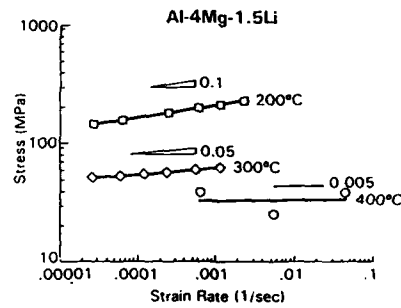
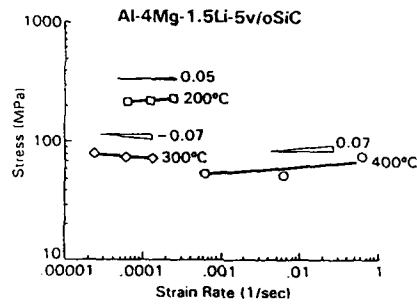


Figure 16: Creep response at various temperatures for SiC reinforced and unreinforced mechanically alloyed Al-Mg-Li alloys (Gilman et al. 1986).

TABLE 1.

HISTORIC DEVELOPMENT
OF
PRECIPITATION HARDENED
ALUMINUM POWDER METALLURGY ALLOYS

TIME PERIOD		
1940-1960	1960 - 1980	1980 - 1986 +
2000 SERIES Al - Cu Alloys		
(Mixed Elemental - Press and Sinter) (Prealloyed Compositions)	Al - Cu - Li Modified Alloys	Less Development Activity
5000 SERIES Al - Mg Alloys		
(Prealloyed Compositions)	Al - Mg Modified Alloys	IN 9051, IN 9052
	Mechanically Alloyed	Corrosion Resistant Applications
6000 SERIES Al - Mg - Si Alloys		
(Mixed Elemental - Press and Sinter) (Prealloyed Compositions)	Al - Mg - Si Modified Alloys	Less Activity
7000 SERIES Al - Zn - Mg Alloys		
(Prealloyed Compositions)	Al - Zn - Mg Modified Alloys	
7075	MA 87, MR61, MR64, X7090/7091	X7064, CW 67
	Metal Matrix Composites - SiC Dispersion & Superplastic Forming of 7000 Series	

TABLE 2

HISTORIC DEVELOPMENT
OF
DISPERSION STRENGTHENED
ALUMINUM POWDER METALLURGY ALLOYS

TIME PERIOD			
1940-1960		1960 - 1980	1980 - 1986 +
<u>HIGH TEMPERATURE ALLOYS</u>			
SAP ALLOYS			
Al - Fe , Al - X Alloys		Al-Fe-Ni, Al-Fe-Co, Al-Fe-Ce, Al-Fe-Mo-V Al-Zr-Cr, Al-Fe-Mo	Development of CU78 (Al-Fe-Ce)
<u>LOW DENSITY ALLOYS</u>			
		Al-Li, Al-Li-Be, Al-Mg-Li	Developmental Alloys
<u>HIGH MODULUS ALLOYS</u>			
		Al-Mn, Al-Mn-Cr, Al-Fe-Ni-Co	
<u>MECHANICALLY ALLOYED SYSTEMS</u>			
	Al-Mg, Al-Mg-Li,	IN9051, IN9052, IN9021	
	Metal Matrix Composites (e.g. SiC, Al ₂ O ₃ , C) via Mechanical Alloying		
<u>METAL MATRIX COMPOSITES</u>			
2000, 6000, 7000 series with SiC, C reinforced P/M Alloys			

TABLE 3: Variation of Cooling Rate with Solidification Mode

Solidification Mode	Dendrite Arm Spacing (Microns)	Cooling Rate K/s
Ingots	100	10 ⁻²
Gas Atomization	1-100	10-10 ³
Water Atomization	1-10	20-10 ⁴
Roller Quenching	0.5	10 ³ -10 ⁶
Splat Techniques	0.1	10 ⁶ -10 ⁸

TABLE 4: Extension of Solid Solubility for Binary Aluminum Alloys (Jones, 1978,

Elements	at % Equilibrium	at % Reported Maximum
Cr	0.44	5-6
Cu	2.5	17-18
Fe	0.025	4-6
Mg	18.9	37-40
Mn	0.7	6-9
Ni	0.023	1.2-7.7
Si	1.59	10-6
Zn	66.5	38

TABLE 5: Relative Sizes of Typical Microstructural Features in 7XXX Alloy Wrought Products

Feature	I/M Product	P/M Product
Constituent Particles (Fe, Si Types)	2-100 Microns	0.5 Micron
Nonmetallic Inclusions (Common Limits of Melt Filtration Technology)	< 10	10
Dispersoid Particles	0.01-0.5 (Zr, Cr, Mn Types)	0.01-0.5 (Zr, Cr, Mn, Fe, Ni, Co Types)
Age Hardening Precipitates	0.002-0.008	0.002-0.008
Oxide Film Thickness on Powder Particle	-	~0.01
Individual Oxide Particle After Hot Deformation	-	~0.01
Random Oxide Clusters After Hot Deformation	-	~0.05

TABLE 6 Chemical Compositions (wt%) of High Strength Aluminum P/M and I/M Alloys [Tietz and Palmer, 1981]

Alloy	Zn	Mg	Cu	Si	Fe	Ni	C	O	Mn	Cr	Ti	Zr	Co	Al
P/M Alloys														
X7090	7.7	2.5	1.0	<0.12	<0.15	-	-	0.35	-	-	-	-	1.5	bal.
X7091	6.3	2.5	1.5	<0.12	<0.15	-	-	0.35	-	-	-	-	0.4	bal.
PM 61	8.9	2.5	1.5	<0.10	<0.20	-	-	<0.50	-	-	-	0.2	0.6	bal.
PM 64	7.0	2.3	2.0	-	-	-	-	-	-	0.10	-	0.2	0.2	bal.
IN 9052	-	4.0	-	<0.10	<0.10	-	1.1	0.80	-	-	-	-	-	bal.
IN 9021	-	1.5	4.0	<0.10	<0.10	-	1.1	0.80	-	-	-	-	-	bal.
CW67	9.0	2.5	1.5	-	-	0.1	-	0.35	-	-	-	0.14	-	bal.
I/M Alloys														
7075	5.6	2.5	1.6	0.40	0.50	-	-	-	0.30	0.23	0.20	-	-	bal.
7050	6.2	2.3	2.3	0.12	0.15	-	-	-	0.10	0.04	0.06	0.12	-	bal.

TABLE 7: Typical Mechanical Properties of High Strength Aluminum P/M and I/M Wrought Products

Alloy	0.2% Yield Strength (MPa)	Tensile Strength (MPa)	Elongation (%)	Elastic Modulus (GPa)	Density (g/cc)	Fracture Toughness (MPa√m)
P/M Alloys						
7090-T7E71	579	621	9	73.8	2.85	30.8
7091-T7E69	545	593	11	72.4	2.82	46.2
PM61-T76510	641	669	12	72.4	2.82	-
PM64-T76510	627	655	13	72.4	2.82	31.9
IN 9052	379	448	13	72.0	2.66	44.0
IN 9021	469	538	13	74.4	2.80	39.6
CW 67	579	614	12	-	-	47.0
I/M Alloys						
7075-T6	505	570	11	71.7	2.80	30.8

TABLE 8: Mechanical Properties of High Specific Modulus Alloy [Tietz and Palmer, 1981]

Alloy	0.2% Yield Strength (MPa)	Tensile Strength (MPa)	Elongation (%)	Elastic Modulus (MPa)	Density (g/cc)
<i>P/M Alloys</i>					
Al-2.3Li-1.4Cu-1.0Mg-0.1Zr	412	490	7.4	-	2.54
Al-2.5Li-3.1Cu-1.7Mg-0.6Mn	373	483	10.0	83.5	2.59
Al-1.8Li-3.0Cu-0.8Mg-0.2Zr	387	510	15.3	76.9	2.64
Al-1.0Li-4.6Cu-0.4Mn-0.1Cd	565	606	5.8	77.9	2.68
<i>I/M Alloys</i>					
Al-2.8Li-0.14Zr	433	474	4	80.5	2.49
Al-3.0Li-2.0Mg-0.2Zr	395	500	3	84.0	-
Al-2.2Li-2.7Cu-0.12Zr	537	586	10	76.5	2.58
2020	531	579	7	76.0	2.71

* Compositions in wt%

TABLE 9: Tensile Properties of Oxide Dispersion Strengthened Aluminum [Bloch, 1961]

Alloy	Oxide Content (wt %)	Test Temperature (°C)	0.2% Yield Strength (MPa)	Tensile Strength (MPa)	Elongation %
M255	0.5-1.0	20	101.6	151.6	28
		316	50.8	56.8	22.5
M257	5.0-8.0	20	162.2	250.1	17
		204	121.3	142.5	16
		371	87.9	95.5	8
SAP 930	6.0-8.0	20	129.6	231.2	22
		200	120.5	151.6	21
		400	75.0	76.5	8.5
SAP 895	9.0-11.0	20	197.1	318.3	10
		200	159.2	204.6	6
		400	96.3	105.3	5
SAP 865	12.0-14.0	20	216.8	341.8	7.5
		200	182.7	231.2	5.5
		400	109.9	125.1	4.3
M276	15.0-17.0	20	230.4	360.8	7
		204	181.9	216.8	6
		371	121.3	128.8	4

TABLE 10 Mechanical Properties of Dispersion Strengthened P/M Aluminum Alloys. [Towner, 1958]

Alloy (Composition in wt%)	Test Temperature (°C)	0.2% Yield Strength (MPa)	Tensile Strength (MPa)	Elongation (%)	Creep Stress for 1% Strain in 100 hours
Al-7.6 Fe	20	216.3	313.5	16	-
	316	122.6	150.9	19	58.9
	427	53.7	69.6	28	-
Al-4.5Fe-7.0Ni	20	416.8	473.3	3.5	-
	316	99.9	144.0	15	-
	427	33.6	49.6	34	-
Al-2.5Fe-0.4Cr-3.4V	20	216.3	301.8	14	-
	316	115.1	141.2	18	65.5
	427	59.9	77.9	18	-
Al-7.8Fe-0.2Cr-0.2V-0.2Ti-0.2Zr	20	234.9	332.8	15	-
	316	143.3	167.4	16	89.6
	427	74.4	96.5	23	-
M257-0DS Aluminum (8 wt% Al ₂ O ₃)	20	165.4	254.9	17	-
	316	103.4	117.1	13	75.8
	427	75.8	82.7	5	-

TABLE 11 Mechanical Properties of High Temperature P/M Aluminum Alloys [Tietz and Palmer, 1981]

Alloy (Composition in wt %)	Test Temperature (°C)	Hold Time at Test Temperature Prior to Testing (hrs)	0.2% Yield Strength (MPa)	Tensile Strength (MPa)	Elongation (%)
Al-8Fe	20	-	504	572	5.0
	232	100	260	280	9.6
	343	100	148	172	12.3
Al-8Fe-4Ce	20	-	445	550	9.0
	232	1000	367	395	6.0
	343	1000	152	176	7.0
Al-8Fe-2Mo	20	-	472	492	6.7
	204	1000	427	452	7.0
	343	100	200	222	10.0
Al-10.1Fe-3.2Zr-2.3V	20	-	632	645	8.7
	232	-	414	420	7.3
	343	-	240	252	10.2
Al-6Cr-1Fe	20	-	-	664	6.0
	200	-	-	572	6.0
	300	-	-	432	10.0
2219-T851 (LM)	20	-	345	455	12.0
	232	1000	186	221	20.5
	343	1000	54	65	65.0

TABLE 12 Tensile Properties of Mechanically Alloyed Forgings

Alloy	Orientation	Ultimate Tensile Strength		Yield Strength		Elongation %
		MPa	ksi	MPa	ksi	
9052	Longitudinal	595	86.3	560	81.2	6
	Short Transverse	568	82.4	550	79.7	2.5
9021 T4	Longitudinal	625	90.7	597	86.6	14
	Short Transverse	597	86.6	585	84.8	11
LM 7075 T7	Longitudinal	483	70	407	59	8
	Short Transverse	448	65	372	54	4

MICROSTRUCTURE/MECHANICAL PROPERTY RELATIONS IN A MECHANICALLY ALLOYED ALUMINUM

by

W.J.D. Shaw

Department of Mechanical Engineering
University of Calgary, Calgary, Alberta, T2N 1N4, Canada

SUMMARY

Mechanically alloyed aluminum has not lived up to its initial expectations and very little progress has been made in understanding, controlling and improving this material over the last decade. The complexities of the reactions that occur in this material are presented in terms of our present state of knowledge. This current understanding is linked to the mechanical properties of the material. It is necessary that an understanding of the mechanisms regarding the role of oxygen and carbon or hydrocarbon in the material be obtained before further development is undertaken. Once an understanding of the inherent reactions taking place in these materials is determined, then major advances in research and development will occur resulting in an unlimited potential of engineered materials.

1. INTRODUCTION

The process of mechanical alloying, MA, has been around for a number of years (1,2) and was first brought to general attention by Benjamin (3-6). However an understanding of these materials has not progressed significantly over the last ten years. It is known that the process works but it is not completely understood how or why. This understanding is required if improvements and control of the mechanical properties are to be obtained.

The processing involved in making these materials is so fundamentally different from other alloy processing, and the inherent properties of the processed material are similarly fundamentally different from any other class of materials that it is suggested that these materials be placed in a category of their own. Nowadays most people group these materials as powder metallurgy, P/M, materials for lack of understanding the fundamental differences of the material. Mechanical alloys are made by a continuous controlled fracture and cold welding process. On an extremely fine scale the material is ground with high inputs of energy that cause integral mixing of the various chemical constituents. This fine fracture/cold weld process results in a mechanical mixing of the elements within a grain of powder. Once a stable powder size of approximately 40 μm has been achieved, the powder is then collected, and consolidated using conventional P/M techniques.

After consolidation the material is usually exposed to some type of thermal mechanical processing prior to its final use. What makes this material so unique and sets it apart from other materials, are the bonding reactions that occur throughout the powder particles. The end result is a material that normally has an ultra fine grain size and a very homogenous distribution of the various chemical elements throughout the grain. MA processing results in a metastable material. However, this metastable condition is extremely stable in many respects up to temperatures in the range of the melting point of the material. Therefore one of the major applications of materials processed in this manner has been for use in creep resistant structures.

The strength of MA aluminum is usually thought to occur from a number of mechanisms. The primary mechanisms being oxide dispersion strengthening, ODS, and carbide dispersion strengthening, CDS. The secondary strengthening mechanisms are thought to be solid solution strengthening due to the presence of magnesium, precipitation strengthening due to precipitates of copper/aluminum and finally grain size strengthening due to the ultra fine grain size and based on the Hall-Petch relationship. It is also believed that the dispersoids act to increase the elastic modulus of the material.

The material, AL 9021, is chemically analogous to the ingot metallurgy 2024 aluminum alloy except for the additions of oxygen and carbon or hydrocarbon. The overall chemical composition of the material using standard methods for element analysis is shown in Table 1.

In the nickel-based mechanical alloy, yttrium oxide is added directly as one of the constituents to be mixed with the base metal. This means that the processing utilizes both ceramic and metallic materials and the oxide is finely dispersed throughout the grain structure of the material during processing. This then results in an ODS material. Most people accept that the same process occurs when dealing with aluminum alloys. However in the case of aluminum alloys, the processing conditions are somewhat different as the oxygen is introduced into the material from the exposure of the aluminum to the atmosphere. During initial processing of MA aluminum oxygen was

introduced accidentally into the material. It is usually taken for granted that this oxygen combines with the aluminum to form aluminum oxide and hence this material is labelled an ODS material. This reaction does not take place as has been shown by direct evidence indicating the bonding strength between the oxygen and the aluminum (7). The details of this will be discussed later. Another difference in the MA processing of aluminum alloys is the use of a control agent to balance the amount of cold weld and fracture. The control agent used for processing aluminum alloys is stearic acid. It has been assumed that stearic acid breaks down during the high energy attrition milling to form the pure element carbon, which then combines with the aluminum to form aluminum carbide. Therefore the MA aluminum is taken as being a CDS material in addition to the ODS mechanism. Originally the control agent started out as a long chain hydrocarbon and it is unreasonable to expect that after processing it ends up as pure carbon. A more rational expectation would be that the hydrocarbon would end up broken into shorter chained molecules and in fact may combine in some manner with the metallic elements during the deformation processing. Indirect evidence of this has been obtained and will be discussed later. Therefore, it should be noted that the mechanisms occurring in MA nickel are not necessarily the same mechanisms that are occurring in the MA aluminum.

Originally when the first aluminum alloys were processed using the mechanical alloying technique, the resulting properties were better than anything previously obtained for aluminum alloys. Strengths in the order of 600 MPa with ductilities of around 15% were found for the aluminum alloy AL 9021 (8). Thus MA aluminum properties were found to give a combined value of both strength and ductility in excess of what could be achieved using either ingot metallurgy or other P/M techniques. This combined high strength and high ductility suggested that these aluminum alloys were on the way to achieving even higher strengths and ductilities when improvements were made to the MA processing technique. This expectation has not materialized. However some other amazing properties have resulted, these will be presented and discussed.

Initially, a large market was seen for AL 9021 material due to its high strength to weight ratio and other beneficial mechanical properties. However, this market has not materialized and the commercial output of the material has been rolled back and nearly discontinued. Some reasons for this are discussed in this paper.

The paper also summarizes the current state of knowledge pertaining to mechanically alloyed aluminum and gives reasons for the lack of understanding regarding these materials and points out the potentials inherent in the future development of this type of material.

2. MICROSTRUCTURE

Our understanding of a material arises primarily from the study and analysis of its microstructure. Considerable difficulty occurs when studying AL 9021 and other mechanically alloyed aluminum. The difficulty arises as a result of size and type of reactions occurring. The size of the microstructure is ultra fine and in many cases, regular techniques do not yield any useful information. As an example, normal x-ray diffraction, XRD, studies on a bulk quantity of material yields almost identical information to that obtained from the analysis of 2024 aluminum alloy. From all practical purposes, the diffraction peaks and intensities are identical between the AL 9021 material and the 2024 material. Thus one would expect that the copper is combined in the material in the same manner for the two materials. However, as will be shown this is not the case and therefore, general XRD analysis does not yield any useful information about this specially processed material. If the material is slowly dissolved in nitric acid and the sludge remaining is analyzed using XRD analysis, it is found that there is no difference between the 2024 material and the AL 9021 material.

Other XRD analysis conducted on material that has been solution treated at a temperature of 600°C, then air cooled indicates that a large increase in CuAl₂ precipitate has occurred. If the material is then heated back up to 600°C and water quenched, XRD analysis indicates that the material has reverted back to its original state as compared to the as-received material. However, it is known that subtle changes occurred due to oxygen reactions in the material; therefore this indication cannot be totally correct. Overall it would appear that whatever mechanisms occur generally in the material, these mechanisms are reversible providing that the melting point temperature of the material has not been reached.

This example indicates that precautions should be taken in interpreting the results when using standard techniques which are usually applied to conventional ingot metallurgy materials. These results do not necessarily lend themselves to conventional interpretation when applied to MA materials.

When investigating materials, the first place to start is usually with optical microscopy. The microstructure of this material as shown by optical microscopy is seen in Figure 1. This figure utilizes a high range of magnification, near the upper limit available. This figure indicates that the grain size is still too small to be determined, although it would appear that the material contains some type of stringer inclusion. Figure 2 shows a more detailed analysis of these apparent inclusions using the scanning electron microscope, SEM, with the material polished and sputter coated with gold. This analysis shows that these areas are in fact small cracks within the material (9).

The determination of grain size in this material is not at all straight forward and a representative value of grain size is somewhat difficult to determine unless special techniques are used. The most common approach used is that of thin foils in conjunction with the transmission electron microscope, TEM. A major disadvantage of this technique is that it requires considerable preparation in making a thin foil and then is later restricted in terms of the amount of thinned area available for viewing. Additionally it has been found that dissolution of this material does not occur evenly but rather the small grain regions are attacked preferentially before the larger grain areas. Thus, there is no guarantee that representative grain size determination can be made from thin foil analysis. Rather the technique that should be utilized is a modified technique of optical metallographic preparation and used in conjunction with the SEM. The modification requires very light etching of the polished surface and sputter coating with gold prior to viewing. A representative value of grain size can then be determined. Figure 3 shows a representative micrograph of grain size and subgrain size for the AL 9021 material. If over etching occurs, the grain size that is measured will be considerably larger than that shown in Figure 3. Measurements from this figure indicate that the grain size is approximately 0.18 μm with subgrains in the order of 0.02 μm . In time with further study it may in fact turn out that what we now call subgrains are the true grain size of the material and the larger clusters being an artifact. In any event this material is one of the finest grain size materials created to date.

It can therefore be appreciated that in order to study this material, extremely high magnifications must be employed in conjunction with the development of new techniques. In order to study any form of precipitation or element combination, either dispersed throughout the material or along the grain boundaries, extremely high magnifications are required.

As the material is aged, a coarsening effect occurs along with the growth of some second phase particles. The coarsening progresses as a function of both time and temperature. Once sufficient coarsening has taken place the microstructure can be studied using the optical microscope. An example of this is shown in Figure 4. The material was exposed to a temperature of 400°C for a period of 1484 hours. Analysis of these coarsened particles using energy dispersive x-ray analysis, EDXA, were found to consist of approximately 50% Cu and 50% Al with traces of Zn and Fe along with a high content of Carbon or hydrocarbon. Thus it is expected that these second phase particles are a type of organometallic compound. What appears to be dark particles are in fact, voids caused by gas evolution out of the matrix. This can only be confirmed by using SEM analysis.

Once the material reaches a temperature of 595°C, fiber formation takes place throughout the material. EDXA analysis indicates that these fibers are comprised of approximately 30% copper, 15% iron, 55% Al with a medium amount of carbon or hydrocarbon. Figure 5 illustrates the presence of this fiber formation using SEM microscopy. This figure also shows the coarse second phase particles and a few small voids. The fiber and coarse second phase particle formations are reversible and microstructure indicates that if the material is heated back up to a temperature range of 600°C and water quenched, the resulting structure appears identical to the as-received condition, with the exception of damage being done in the formation of voids and microcracking due to the gas evolution out of the matrix. It should be noted that these types of structures do not form in 2024 aluminum alloy which has the same weight composition of copper and magnesium as the AL 9021 material. Therefore it can be concluded that the presence of both the oxygen and the carbon or hydrocarbon have drastically modified these second phase particle formations in the mechanically alloyed material. This difference is not found from a comparison of the XRD analysis between the two materials.

The method of determining the carbon or hydrocarbon content was very qualitative and used the rate of count buildup of secondary electrons from the gold coating previously sputtered on the surface. This method gave a relative indication of the amount of carbon or hydrocarbon present in the area being analyzed.

Other microstructural studies that have been done on this material have been confined to TEM analysis. Much of this TEM analysis has measured and identified aluminum oxide particles within the material using electron diffraction (10-12). The interpretation of the electron diffraction analysis is either erroneous or not representative of the role of oxygen within this material since it has recently been shown that aluminum oxide is not present (?) at least in any significant amount.

3. HEAT TREATMENT AND MATERIAL MICROHARDNESS

The heat treatment condition that the as-received AL 9021 material was subjected to was that of a -T452 condition. The material is normally solution treated at 495°C, water quenched and naturally aged at room temperature and compression stress relieved. As the material is heated and exposed to temperatures above room temperature, an over aging effect occurs which results in the coarsening mechanism taking place in the material. However, at about 380°C, a distinct change in mechanisms occur and the material suddenly hardens. As the temperature is continually increased beyond this point, the material begins to soften. This behaviour is apparent in Figure 6 which shows the Vickers hardness of the material as a function of exposure to various temperatures for a period of 1 hr followed by furnace cooling at a rate of 120°C/hr.

Additionally some other information regarding solution treating and water quenching is also presented in this figure. The return of hardness after water quenching and aging further confirms the general reversibility of the material. At the 380°C position, the only distinct change that can be identified from a microstructural point is that of gas evolution and microcracking. This process is shown by the formation of small voids within the material due to the linking of microcracks as indicated in Figure 7. Thus some detrimental damage is occurring in the material, even at temperatures considerably lower than that used for solution treating in the initial processing of the -T452 condition.

4. DILATOMETRY

Some initial dilatometric studies have been conducted on the material, both on the as-received material, as well as on the normalized condition using a solution treatment temperature of 600°C. These studies indicate that a major change occurs in the material in terms of a contraction over the temperature range of 420 to 480°C. This change is identical in terms of either heating or cooling. A minor change seems to occur at 340°C in terms of expansion within the material. This portion is not reversible and only occurs during the heating cycle. The cyclic effects indicate that the material, although being metastable, is for most practical purposes an extremely stable material with nearly complete reversibility taking place. Subsequent cycling confirms that reversible reactions are occurring. A typical dilatometric curve for the as-received material is shown in Figure 8. The temperature of 340°C is fairly close to that of 380°C temperature found from the microhardness tests that were correlated to gas evolution out of the material in the form of microcracks. The gas evolution is consistent with the expansion measured at this temperature. From microhardness the temperature of 450°C appears to indicate the presence of a second type of softening reaction and correlates well with the dilatometry results.

5. GAS EVOLUTION

A preliminary investigation into the welding characteristics of AL 9021 and the microstructural formation in the heat affected areas, pointed out that a tremendous amount of gas evolution out of this material was occurring (13). Additionally, it was found that some free carbon was rejected out of the material when welded under tungsten inert gas conditions. This initial study resulted in a more extensive investigation regarding the gas evolution of the material. From this extensive study, it was found that by using carefully controlled conditions and gas chromatograph techniques, that oxygen was the primary cause of the void formation and microcracking in the material (7). A typical gas analysis is shown in Figure 9. This figure indicates that oxygen accounts for more than 90% of the gas evolution out of the material. In order to conduct this analysis, charges of material were placed in a glass crucible, sealed within a glass envelope and evacuated to a low vacuum condition. The material was then heated using an induction coil furnace, such that time at the high temperature was kept to a minimum and that the gas evolution occurred quickly. This helped to limit the reaction of the gas with the metal at the high temperature. If heating takes place slowly such as in conventional furnaces, then the gas that is evolved has time to react with the metal at the high temperature. Conventional furnace heating results in the true formation of aluminum oxide but is a consequence of the test procedure. Thus, even with the precautions taken, using induction heating, the amount of oxygen evolved out of the material, will be underestimated, as not all of it will remain as a gas, but some of it will react with the metal at the high temperature and other portions will remain trapped in void pockets within the material. In any event, it can be seen that oxygen is the major constituent that is causing the cracking and void formation within the material.

Thus, it becomes apparent that a true form of aluminum oxide cannot be present within the material, since at relatively low temperatures of 600°C, true aluminum oxide is completely stable. If aluminum oxide were present, no oxygen gas evolution would occur, rather these tests have indicated that the bonding between oxygen and aluminum is not in the form that takes place in aluminum oxide as we know it. Therefore, if the electron diffraction analysis as has been conducted in the past on this material is to be believed to be representative of the oxygen within the material, then a mechanical proximity reaction must occur (7). This means that on a 3-dimensional arrangement basis, the oxygen is located in the proper positions with respect to the aluminum and therefore satisfies the geometric locations that would reflect back the x-ray diffraction patterns but the bond strength has not taken place, such that the formation of a full chemical reaction of aluminum oxide has not occurred. This interpretation has lead to a definition of a mechanical proximity reaction rather than a pure chemical reaction.

These findings raise a number of questions regarding both the role of oxygen and carbon or hydrocarbon within the material. The type of reactions that are occurring within the material due to this unique combination of elements, appears to be at present beyond our total understanding. The fine distribution of these elements throughout the material makes it extremely difficult to obtain any degree of meaningful analysis.

As can be appreciated the absence of aluminum oxide formation in these aluminum alloys, make these materials wrongly labelled when they are described as ODS materials. However, it is felt that the role of oxygen does contribute, on the basis of the mechanical proximity reaction, to the strength of the material.

In addition to measuring the oxygen evolution out of the material, it was also determined that methane was given off from the material starting at relatively low temperatures being in the order of 150°C. The measurement of this methane gas was also confirmed by retaining the services of an independent chemical analysis laboratory. The results showing an evolution of hydrocarbon out of the material, suggests that the carbon within the material is in the form of a hydrocarbon. This indirect evidence suggesting that stearic acid has not broken down completely to carbon but rather to a shorter chained molecule. Work is currently under way to substantiate or disprove this by obtaining direct evidence.

An indication of the type of void formation that occurs during the oxygen evolution out of the material is shown in Figures 10 - 12. Figure 10 is a small block material soaked at 600°C for a few minutes, air cooled and then cut in half. It shows the overall damage that can occur in this material due to oxygen evolution at high temperatures. On the other end of the scale, Figure 7 shows the small detrimental effect that occurs due to microcrack formation which develops at relatively low temperatures due to oxygen pressure. Other types of material defects are in the form of microsuperplastic voids such as shown in Figure 11 and globular melting and void formation as shown in Figure 12. Both the temperature and time relationship of heating the material determines the type of void formation within the material.

6. UNIQUE AND SPECIAL PROPERTIES OF AL 9021

There are a number of unique fracture mechanisms that occur in this material that do not normally occur in other materials. One of these features is known as shear ridges (13) and is illustrated by an arrow on Figure 13. This fractograph is that of a fracture toughness specimen near the start of crack extension. This mechanism is a result of internal cracking along planes of weakness or microcracking due to oxygen evolution from within the material. The cracked region forms either during processing or during loading due to planes of weakness within the material. This cracked region then acts as a free surface forming an interior shear lip. Thus the material can be evaluated with regards to planes of weakness and inherent cracks within the material by studying the density of the shear ridge features on the fractured surface caused by either tearing, fatigue or tensile overload. It can be appreciated that the processing of the material due to the solution treatment conditions, as well as any forging operations will have a direct influence on this parameter. Since this defect is tied up with the behaviour of oxygen within the material, it is imperative that this role be understood in order to be able to control and prevent this mechanism from occurring.

Another mechanism that when first found was almost unbelievable, was that of microsuperplasticity (14-16). This mechanism is one that occurs during high temperature deformation and is the result of a combined effect of both intergranular and superplastic transgranular behaviour on a microscopic scale. An example this mechanism is shown in Figure 14. Thus during creep crack growth within the material, a balanced condition occurs between a brittle failure mechanism of intergranular fracture and a superplastic failure mechanism. The areas of superplasticity form as islands with localized flowing of the material resulting in the formation of fibers on the fracture surface. These totally opposed mechanisms work together in some type of balanced arrangement. Since this mechanism was originally identified in the AL 9021 material, it has subsequently been found to occur in rapidly solidified and processed aluminum alloy (17). This microsuperplastic phenomena has been found to occur at a temperature as low as 200°C for the AL 9021 material. In addition to the formation of the mechanism, the material property relationships are such that an improvement of creep strength with respect to 2024 material of approximately 300% is found. Again an understanding of this mechanism is tied to an understanding of the roles of both the oxygen and the carbon within the material.

A third mechanism that is totally unique to the AL 9021 material is that of the formation of stress striations (18). This mechanism occurs due to the oxygen evolution out of the material and takes place when a high shear stress results as a consequence of the gas evolution process. Striations are formed in the fracturing of a void within the material and are essentially initial stages of microsuperplastic formation. An indication of these striations are shown Figure 15. It can be seen in this figure that gas bubble formation has occurred on some of the striation surfaces. Thus, it can be appreciated that an understanding of the microstructure and fractography that occurs in these materials is tied up in a direct understanding of the mechanisms in which the oxygen and carbon or hydrocarbon are bonded within the material.

It is apparent that the unique type of processing for producing mechanically alloyed aluminum results in the unexpected property relationships and unusual defects found in this material. Therefore, in order to improve and fully utilize mechanical property relationships that can be obtained from mechanical alloying, it is necessary to appreciate the complexities involved and to stop thinking of the material as an ODS and CDS strengthened alloy.

7. TENSILE MECHANICAL PROPERTIES

Initially when this material was first developed as an experimental alloy, it was reported to have a tensile strength and ductility combination far in excess of the best 7075 aluminum alloys of that time. However, after the material went to

commercialization, it was found that the ductility portion of the material did not measure up to the amount of ductility initially reported.

Table 2 shows the mechanical properties tested for a billet of commercial material that was received and tested in 1982 and reported later (19). Also compared in this table are the initial values reported in 1982 at the very onset of commercialization (8). Other values measured and reported are also listed (20,21) as well as values for 2024 and 7075 for comparison. Examination of this table shows a very drastic loss in ductility has occurred between the initial development of this alloy and its subsequent commercialization. In fact, the ductility has dropped down to almost half the value that was initially reported. Therefore it can be seen that very little advantage occurs with regard to choosing the AL 9021 material over the 7075-T6 material based on mechanical properties, although a premium in price for the MA material is enormous. Whereas the original experimental material had strengths far in excess of 7075 and ductility comparable to 2024.

The tensile behaviour of AL 9021 has a very distinct upper and lower yield point, with an average difference between these two levels of 20 MPa. This is in contrast to the gradual yielding and nonlinear behaviour that is exhibited by both the 2024-T4 and 7075-T6 materials. The 0.2% offset method is needed to define yield stress in these two common materials. The other difference in the stress/strain curve for AL 9021 as compared to the other two alloys occurs in the strain hardening region. Here strain hardening takes place in a somewhat serrated fashion rather than a gradual and smooth manner as occurs in the 2024 and 7075 alloys.

As can be appreciated the property relationships of a material are a combination of strength and ductility together rather than each one individually. Thus, it would appear that a good deal of the demise of the commercialization of this material is due to the fact that the processing parameters as they affect the microstructure and mechanical property relationships of the material were not understood nor controlled in a manner that allowed the initial high combination of strength and ductility. When considering the high premium that is paid due to the special processing techniques to produce mechanically alloyed material, it is not surprising that potential customers would demand mechanical property combinations that were not obtainable by utilizing other less expensive means. The high strength of the AL 9021 commercial alloy, in conjunction with its low ductility, means that it is directly competing with other processed materials such as rapid solidification, P/M materials and ingot metallurgy materials without any mechanical property advantage. Therefore, the early demise of this material is primarily due to premature commercialization of a new technology that is only in its infancy and not yet understood enough to be able to apply it in a completely controlled manner.

8. FRACTURE TOUGHNESS PROPERTIES

The fracture toughness behaviour of AL 9021 is shown in Table 3 (22). Also compared in this table are other fracture toughness values that have been obtained from different sources (8,23,24) along with measured values of 2024 and 7075 materials. It can be seen that the initial or early measurements are relatively consistent and considerably higher than the later measurement from the commercial material. It is very likely that the loss of ductility in the commercially produced material resulted in a much lower fracture toughness value than that measured during the experimental processing of this material. In comparison the 2024 material is slightly inferior to the fracture toughness values measured for the experimentally produced AL 9021. However, the commercially available material is not nearly as good as the 2024 material. It can also be seen that the 7075 material is not much different from the commercially available AL 9021 material. Therefore on the basis of using the commercial MA material rather than the 7075 material, there is not any distinct advantage. Thus, it can be appreciated that the loss of ductility during the commercialization of this material has resulted in its demise to a major degree when based on fracture toughness.

9. FATIGUE PROPERTIES

The fatigue property relationships of AL 9021 are shown in Figure 16 and as a comparison various reference information (8,21,25,26) are indicated on this figure. In addition the fatigue behaviour of 7075-T6 is shown for comparison. It can be seen that the fatigue behaviour of the experimental AL 9021 was better than that of 7075 material. However, other studies using the commercially available form of the material have shown that the 7075 material is somewhat better than the commercially produced material. Thus again the performance advantage has been lost once commercialization was established. Fatigue characteristics of a material are closely related to the combined overall strength and ductility relationships. Therefore it can be appreciated that a loss of ductility will directly affect the fatigue life of a material when operating in the crack propagation regime. Again it is found that the commercially available material has no advantage over using other conventional materials with respect to its fatigue properties.

10. CONCLUSIONS

As can be seen this mechanically alloyed aluminum started out with a number of material properties that were better than anything that was available by whatever means of other processing used. The initial material was developed such that it had higher

strength/ductility combinations and higher fracture toughness values and better fatigue crack growth relationships than any other material available. However, during the application of extending the material to commercialization, a loss of control was experienced in maintaining the initial property relationships. Much of this loss of control is due to the difficulty in understanding the inherent relationships between the oxygen and carbon or hydrocarbon within the material. This difficulty in appreciating the complexity of the material is primarily due to the ultrafine grain size within the material, but also is a result of totally different reactions occurring within the material that we are not knowledgeable of at the present time.

This very complex but unique type of reaction as presently designated as a mechanical proximity reaction holds enormous promise for the development of super materials in the future. It would appear that specially designed materials can be fabricated in a manner that would include a harmonious relationship between metal, ceramic and polymer co-existing simultaneously within the material on an extremely fine intermixed scale. Therefore it is much too early to write off the aluminum mechanically alloyed materials as not living up to their initial expectations as it would appear that the commercialization aspect got too far ahead of the research and understanding aspect for these materials.

From what has been determined to date with regards to the unique property relationships and the phenomena that occurs in these materials, it would appear that this is an extremely fruitful area to project future research and development. It is most likely that the future of tomorrow will use an engineered material processed by mechanical alloying.

REFERENCES

1. Alexander et al, U.S. Patent No. 2,972,529, Feb 21, 1961.
2. Anders, F.J., Jr., U.S. Patent No. 3,159,908, Dec 8, 1964.
3. Benjamin, J.S., "Dispersion Strengthened Superalloys by Mechanical Alloying", Met. Trans., V1, 1970, pp. 2943-2951.
4. Benjamin J.S., and Volin T.E., "The Mechanism of Mechanical Alloying", Met. Trans., V5, 1974, pp. 1929-1934.
5. Benjamin J.S., "Mechanical Alloying", Scientific American, V234, 1976, pp. 40-48.
6. Gilman P.S. and Benjamin J.S., "Mechanical Alloying", Ann. Rev. of Mater. Sci., 1983, V13, pp. 279-300.
7. Shaw W.J.D., "Gas Evolution and Analysis from Mechanically Alloyed IN-9021", Materials Letters, V6, 1987, pp. 75-79.
8. Erich D.L. and Donachie S.J., "Benefits of Mechanically Alloyed Aluminum", Metal Progress, V121, 1982, pp. 22-25.
9. Shaw W.J.D., "Microstructural Analysis of IN-9021 Aluminum Alloy", Micron and Microscopica Acta, V16, 1985, pp. 179-182.
10. Singer R.F., Oliver W.C., and Nix, W.D., "Identification of Dispersoid Phases Created in Aluminum During Mechanical Alloying", Met. Trans., V11A, 1980, pp. 1895-1901.
11. Kang S.K., "The Microstructure of Mechanically Alloyed Aluminum Alloys", ASM Publication 8305-051, 1983, pp. 1-10.
12. Froes F.H. and Pickens, J.R., "Powder Metallurgy of Light Metal Alloys for Demanding Applications", Journal of Metals, V36, 1984, pp. 14-28.
13. Shaw W.J.D., "Fracture Toughness of IN-9021 Aluminum Alloy", Metallography, V18, 1985, pp. 405-412.
14. Shaw W.J.D., "Microsuperplastic Behavior", Materials Letters, V4, 1985, pp. 1-4.
15. Shaw W.J.D., "Superplastic Behaviour of Creep in IN-9021 Aluminum Alloy", Micron and Microscopica Acta, V16, 1985, pp. 281-284.
16. Shaw W.J.D., "Creep Crack Growth Fracture Morphology of IN-9021 Aluminum Alloy", Metallography, V19, 1986, pp. 335-343.
17. Claeys S.F., Jones J.W. and Allison J.E., TMS Poster, Materials Week, Cincinnati, Ohio, 1987.
18. Shaw W.J.D., and Rowell, R.E., "Microstructure and Kinetically Induced Changes in a Mechanical Alloy", Microstructural Science, V16, 1988, pp. 349-360.

19. Shaw W.J.D., "Surface Corrosion Comparisons of Some Aluminum Alloys in 3.5% NaCl Solution", Microstructural Science, V12, 1985, pp. 243-262.
20. Bridges P.J., "Mechanically Alloyed Aluminum Base Alloys", The Metallurgy of Light Alloys, Proceedings Institution of Metallurgists, Loughborough Univ. (England) Mar 24-26, 1983, pp. 101-104.
21. Minakawa K., Levan G., and McEvily A.J., "The Influence of Load Ratio on Fatigue Crack Growth in 7090-T6 and IN9021-T4 P/M Aluminum Alloys", Met. Trans., V17A, 1986, pp. 1787-1795.
22. Shaw W.J.D., "Aspects of Accelerated SCC Tests on Aluminum Alloys in 3.5% NaCl Solution", Microstructural Science, V13, 1985, pp. 565-581.
23. Schelleng R.A. and Donachie S.J., "Mechanically Alloyed Aluminum", Metal Powder Report, V38, 1983, pp. 575-576.
24. Donachie S.J., Round Robin AFWAL Test Program Memo, 1982.
25. Shaw W.J.D., "Fatigue Evaluation of a Mechanically Alloyed Aluminum", New Materials and Fatigue Resistant Aircraft Design, Ed. D. Simpson, 1988, EMAS, pp. 215-226.
26. Shaw W.J.D., "Fatigue Morphology of IN-9021 Aluminum Alloy", Metallography, V19, 1986, pp. 235-242.

ACKNOWLEDGEMENTS

The author is grateful to the Natural Sciences and Engineering Research Council of Canada for financial support of this work. Thanks is given to Bob Konzuk, Department of Mining, Metallurgy and Petroleum Engineering at the University of Alberta for running the dilatometry tests. Thanks is also given to the Department of Civil Engineering at the University of Calgary for the extensive use of their XRD equipment.

Table 1. Chemical Composition of Al 9021

	Cu	Mg	C	O	Si	Fe	Mn	Cr	Zn	Al
Wt %	4.0	1.5	1.1	0.8	0.05	0.02	0.01	0.01	0.01	Balance

Table 2. TENSILE MECHANICAL PROPERTIES

Property	AL 9021-T452				2024-T4	7075-T6
	Later Commercial Mtl		Early Experimental Mtl			
	Ref(19)	Ref(21)	Ref(8)	Ref(20)		
<u>Longitudinal</u>						
yield stress, MPa	528	535	579	560	335	490
ultimate stress, MPa	590	600	616	600	442	537
elongation, %	9.8	7.2	15	12	13.4	9.2
<u>Transverse</u>						
yield stress, MPa	547	523	591	-	-	-
ultimate stress, MPa	609	587	612	-	-	-
elongation, %	8.1	8.3	14	-	-	-

Table 3. FRACTURE TOUGHNESS

Property	AL 9021-T452				2024-T4	7075-T6
	Later Commercial Mtl		Early Experimental Mtl			
	Ref(22)	Ref(8)	Ref(23)	Ref(24)	Ref(22)	Ref(22)
K _{IC} , MPa/m	28.5	37.5	39.5	38.4	36.9	26.5
K _C , MPa/m	37.7	-	-	-	54.3	29.2

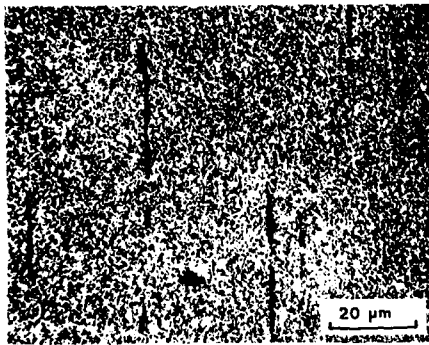


Figure 1. Optical microscopy, AL 9021 material, etchant Keller's reagent.

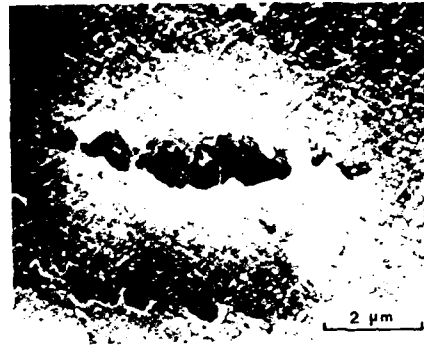


Figure 2. SEM microscopy, cracks in material.

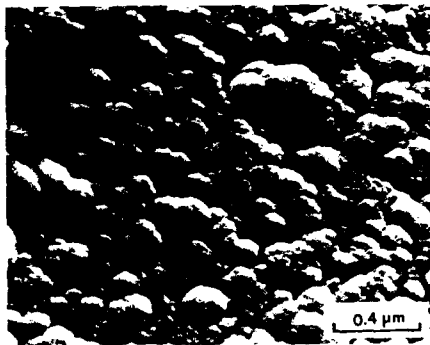


Figure 3. SEM microscopy, grain size.

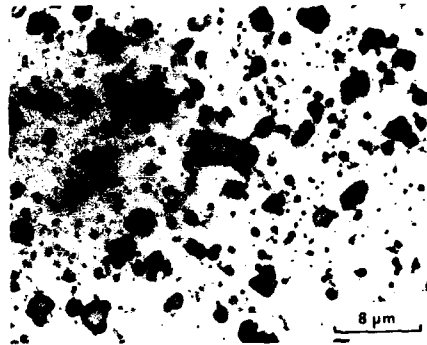


Figure 4. Optical microscopy, 1484 hr creep specimen, exposure 400 °C.



Figure 5. SEM microscopy, fibers and globular precipitates formed at 595 °C.

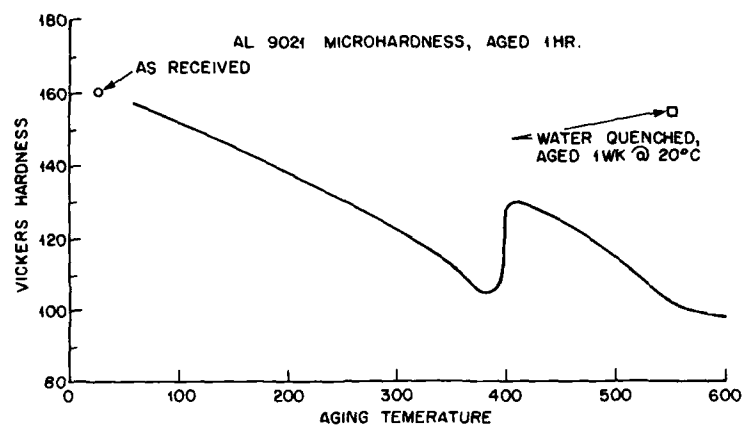


Figure 6. Microhardness of aged AL 9021 material.

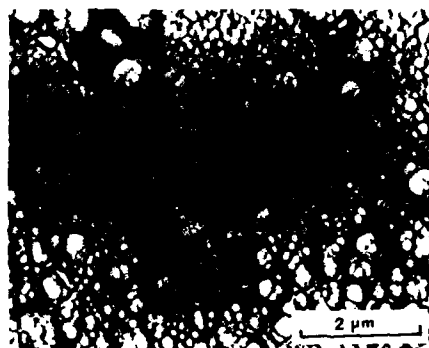


Figure 7. SEM microscopy, microcracking and void formation.

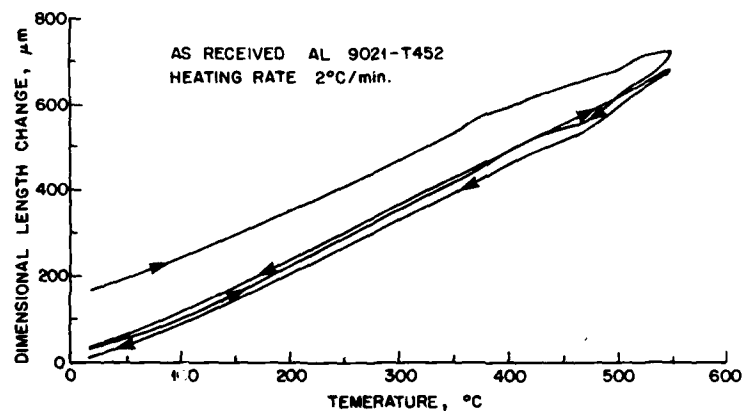


Figure 8. Dilatometric behaviour of as-received AL 9021.

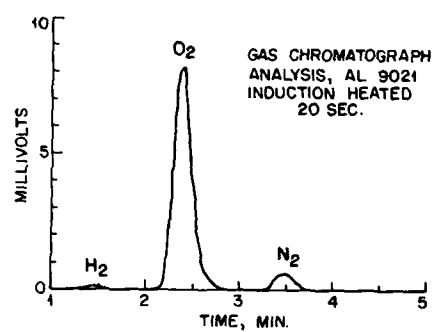


Figure 9. Chromatograph analysis of evolved gas out of AL 9021.

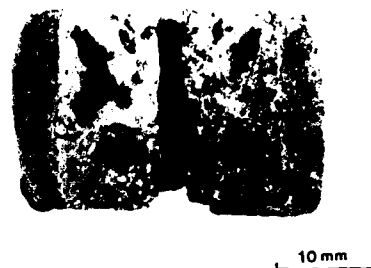


Figure 10. Extensive gas porosity in material.

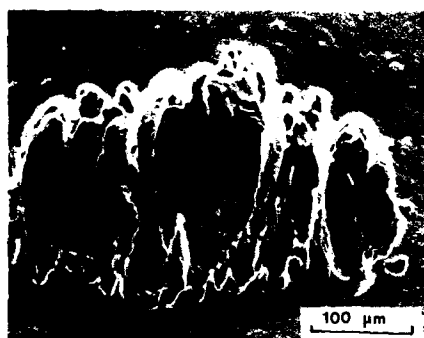


Figure 11. SEM microscopy, microsuperplastic behaviour in gas void formation.

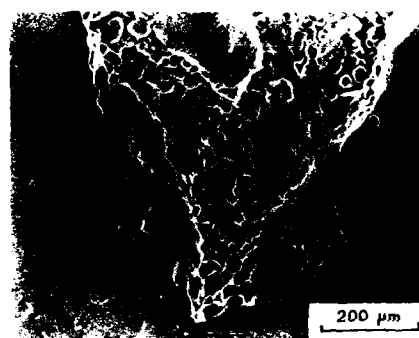


Figure 12. SEM microscopy, melted globular behaviour in gas void formation.

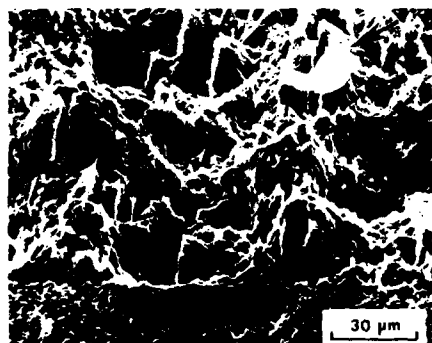


Figure 13. SEM microscopy, shear ridges.

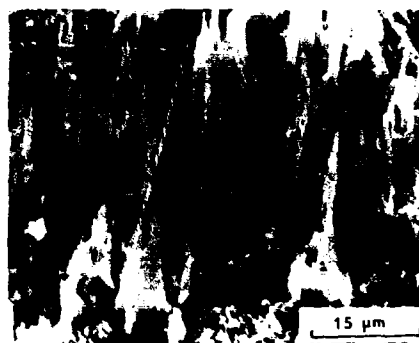


Figure 14. SEM microscopy, microsuperplasticity



Figure 15. SEM microscopy, stress striations.

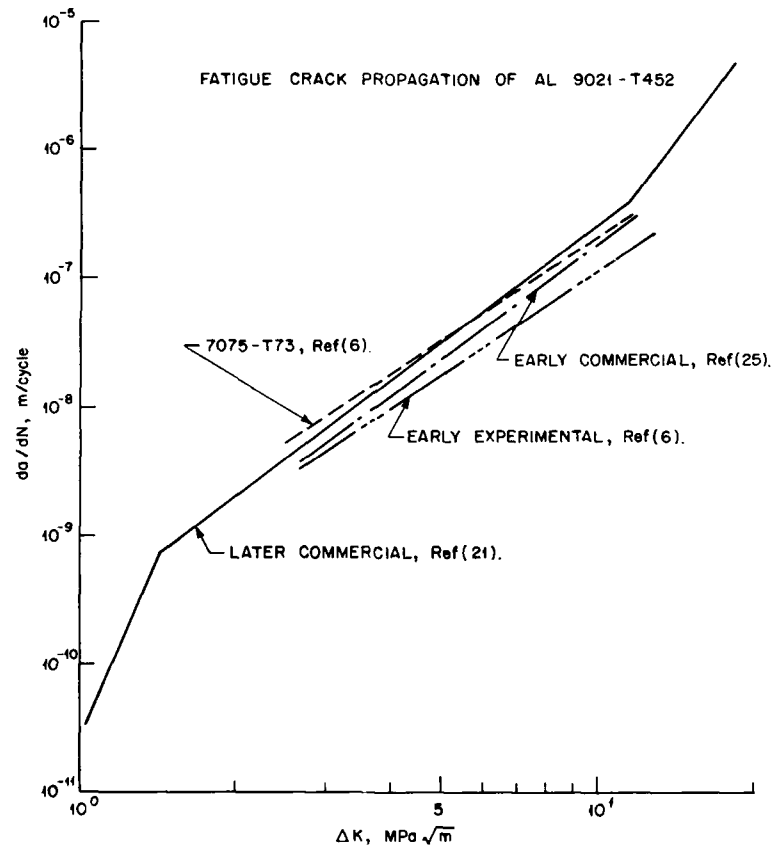


Figure 16. Fatigue crack growth behaviour of AL 9021.

COMPOSITES A MATRICE METALLIQUE ET A FIBRES LONGUES INORGANIQUES

par

P.F.Gobin
G.E.M.P.P.M - U.A. CNRS 341
I.N.S.A. Lyon - Bât.502
69621 Villeurbanne Cedex
France

RESUME

Les matériaux composites à fibres sont constitués d'un renfort fibreux qui peut être complexe et qui leur confère éventuellement une anisotropie, et d'une matrice qui occupe le reste du volume.

Les fibres de renforcement sont le plus souvent minérales : carbone, bore, oxydes, carbures, nitrures.

Dans les matrices organiques et métalliques on recherche un renforcement de la matrice avec dans le cas des fibres longues une exploitation maximale des propriétés des fibres. Pour les composites à matrice organique la température d'utilisation est limitée et pour aller vers des températures d'utilisation plus élevées les composites à matrice métallique sont une voie intéressante.

Bien que certaines caractéristiques et utilisations des C.M.M. à fibres longues soient encore couvertes par le secret, il existe dans la littérature ouverte des études qui permettent de cerner les paramètres d'élaboration et le comportement microscopique et macroscopique de tels matériaux et donc de mieux prévoir les applications possibles.

Dans ce papier, après un bref rappel des problèmes généraux posés par les C.M.M., nous citons une série d'études récentes menées en France dans ce domaine et qui concernent les principaux aspects où des recherches sont encore nécessaires pour maîtriser technologiquement ces matériaux.

1 - INTRODUCTION

Les matériaux composites à fibres longues et à matrice organique associent résistance et rigidité, à une faible masse volumique et à un bon comportement sous sollicitations cycliques ; ils ont donc connu un développement important dans les applications où le gain de poids est essentiel, c'est à dire les industries des matériels de transport au sens large et le domaine du sport.

Malgré des performances remarquables ces matériaux présentent cependant quelques points faibles : une tenue limitée en température, en dépit de gains récents significatifs mais coûteux, une résistance à l'environnement limitée en particulier vis à vis des atmosphères humides et des rayonnements U.V., une conductivité thermique et électrique faible.

L'extension de la notion de composite à des matrices minérales peut permettre de surmonter ces difficultés. Les métaux - et plus particulièrement les alliages légers - sont des matrices possibles :

- leur tenue en température est largement supérieure à celle des matrices organiques.
- leur allongement à la rupture est dans tous les cas supérieur à celui des fibres ce qui permet d'en tirer le meilleur parti.
- leur caractéristiques mécaniques propres conduisent à de meilleures propriétés de résistance perpendiculairement aux fibres (caractéristiques transverses)
 - ils sont bons conducteurs de la chaleur et de l'électricité.
 - ils présentent - sous certaines réserves une bonne stabilité vis à vis de l'environnement.

Bien entendu, la présence de fibres légères à haute résistance, à fort module, permet en outre d'obtenir des caractéristiques étonnantes (tableau I), améliorant à la fois à la température ambiante et à chaud la contrainte à rupture, le module d'Young et la tenue en fatigue. Il est également possible de jouer sur le coefficient de dilatation (en le diminuant).

Il faut noter cependant que ces gains de caractéristiques sont acquis aux dépens de l'allongement à la rupture, de la stabilité dimensionnelle sous cyclage thermique et des possibilités de mise en oeuvre et d'assemblage.

Le choix de matrices performantes et de fibres de renforcement de qualité est sans doute nécessaire pour atteindre les meilleures propriétés possibles, mais la disposition des fibres par rapport à la direction de sollicitation ne l'est pas moins.

En effet, la résistance à rupture du composite 6061/P100 du tableau I (1) peut tomber de 745 à 125 MPa si l'axe de traction est à 15° de la direction des fibres. Ce résultat illustre la nécessité de l'emploi de fibres longues dont on maîtrise l'orientation pour tirer le meilleur parti de l'assemblage fibre-matrice. Enfin, certaines techniques d'élaboration des composites à fibres longues permettent d'utiliser une fraction volumique élevée de matériau de renforcement.

II - LES MATRICES METALLIQUES

Les métaux et alliages les plus utilisés sont évidemment les alliages légers et semi-légers à base d'aluminium et de titane qui offrent après renforcement un module et une résistance spécifique qui peuvent les placer favorablement par rapport aux composites à matrice organique ...

L'aluminium et ses alliages constituent la classe de matériaux la plus utilisée et le tableau (IIa) rassemble les propriétés physiques et mécaniques essentielles des alliages disponibles à l'état de demi-produit et utilisés le plus fréquemment comme base de matrice.

Il faut ajouter à cette liste les alliages de fonderie où le silicium est l'élément d'alliage principal (série 4000). Dans ce cas, les matrices les plus employées pour les procédés d'élaboration par voie liquide contiennent entre 5 et 13 % de Si.

Enfin, quelques alliages à haute résistance du type Al-Zn - Mg - Cu (série 7000) ont été également essayés.

Les qualités qui font de l'aluminium une bonne matrice potentielle : basse densité, bas module, faible résistivité, bonne conductivité thermique, se retrouvent à des degrés divers dans le cas du magnésium et de ses alliages (tableau (II b)).

La densité du magnésium (1,74) le rend tout à fait comparable aux matrices organiques et aux fibres de carbone (de 1,7 à 2). De plus, son très bas module et sa résistance à la rupture modeste en font un excellent candidat à la rigidification et au renforcement par des fibres.

L'intérêt du Titane et de ses alliages malgré leur densité déjà élevée (4,51 à l'état pur) se situe dans le fait qu'ils présentent avec un bas module une résistance mécanique voisine de celles des aciers et un comportement à chaud qui permet d'extrapoler largement les possibilités des alliages de magnésium et d'aluminium.

Comme le procédé d'élaboration nécessite des feuillards minces (environ 15 μ m) seules les alliages de type α - β et parmi eux le TA6V, ou β métastables peuvent être retenus.

D'autres matrices à bases d'éléments plus denses (superalliages, Ni, Co, Cu, Pb) ont fait aussi l'objet d'essais soit pour des matériaux modèles, soit pour des applications spécifiques. Nous ne les évoquerons pas ici.

III - LES FIBRES DE RENFORCEMENT

IIIa - Nature et propriétés des fibres

Les fibres de renforcement doivent posséder à la fois :

- une résistance à la rupture élevée et un haut module d'élasticité stables dans le domaine d'usage avec la matrice métallique.
- une faible densité
- une grande stabilité chimique et une compatibilité chimique et physique avec la matrice (mouillabilité, réaction chimique à l'interface, et coefficient de dilatation)

Il est clair que les solides légers covalents carbone, silicium, bore et leurs combinaisons, auxquelles il faut ajouter l'alumine permettront de remplir les deux premières conditions.

Les tableaux III rassemblent les principales caractéristiques de quelques fibres (filament multibrins ou fibres CVD) qui ont parfois été conçus spécialement pour le renforcement des matrices métalliques. Ces fibres sont également réfractaires, (SiC se décompose à 2700°C, l'alumine fond à 2050°C, le carbone se sublime vers 3500°C) et certaines possèdent une bonne inertie chimique qui justifie leur emploi avec les métaux. Par contre leur coefficient de dilatation est toujours inférieur à celui des matrices (env. 3 à 5 10^{-6} K⁻¹)

Les fibres multibrins à base de carbone, de carbure de silicium, et d'alumine, sont obtenus par filage d'un précurseur liquide suivi d'une pyrolyse et éventuellement d'un traitement de graphitisation à haute température.

Dans le cas des fibres de carbone qui se présentent sous forme de mèches comportant plusieurs milliers de filament élémentaires de faible diamètre (7 à 10 μ m), le traitement de graphitisation permet d'augmenter le module d'Young et la conductivité électrique, tout en diminuant la réactivité chimique, mais cette évolution se fait aux dépens de la résistance à la rupture et de la densité. Ces fibres sont fortement anisotropes ; le module peut varier d'un ordre de grandeur entre la direction de l'axe de la fibre et la direction perpendiculaire de même que le coefficient de dilatation avec une valeur éventuellement négative parallèlement à l'axe (- 0,5 10^{-6} K⁻¹ pour la fibre T300 ; - 1,6 10^{-6} K⁻¹ pour la fibre P100).

Cette propriété associée à une conductibilité thermique et électrique élevée est à l'origine de l'emploi de la fibre P100 pour les composites "sans dilatation".

La fibre multibrins commercialisée par NIPPON CARBON sous la marque NICALON est obtenue à partir d'un précurseur de polycarbosilane et n'est pas constituée de SiC pur mais contient de l'oxygène combiné et du carbone libre (SiC 64 C 15 SiO₂ 21) avec une certaine variabilité.

Des recherches actives sont actuellement menées et en particulier en France pour développer de nouvelles fibres multibrins à base de SiC (ou Si₃N₄).

Les fibres multibrins à base d'alumine sont soit constituées d'alumine pure α (fibre FP de DUPONT) ou d'alumines de transition (SAFFIL de ICI) ou d'alumines vitreuses (SUMITOMO et 3M). Sauf dans le cas de la fibre FP, les fibres à base d'alumine contiennent de la silice qui favorise le fibrage permettant d'obtenir des diamètres plus petits et élève la résistance à la rupture, tout en diminuant le module d'Young (Tableau III.b).

Dans le cas des filaments le dépôt chimique en phase vapeur au contact d'un fil chaud n'a conduit à des produits disponibles que dans le cas du bore et du carbure de silicium.

Les filaments de bore pour lesquels les premiers travaux remontent aux années 1960 (SNPE) se présentent sous forme d'un filament à âme de carbone de 100 à 150 μ m de diamètre présentant simultanément une résistance spécifique et un module spécifique.

Mais le bore réagit très fortement avec la plupart des métaux et il faut le recouvrir d'une barrière de diffusion. Le filament B/B₄C développé par la SNPE et fabriqué par AVCO est sans doute le plus performant actuellement (tableau III B)

Les filaments de SiC sont obtenus par CVD au contact d'une âme de carbone défilant à environ 1300°C dans une atmosphère contenant un chlorosilane. On peut moduler la nature et la composition du dépôt pendant l'élaboration et la société AVCO dispose de filaments de SiC à structure relativement complexe spécialement conçus pour le renforcement des matrices métalliques. La nuance SCS2 recouverte d'un film de pyrocarbone de l'ordre de 1,5 µm dopé en silicium très près de la surface est destinée aux matrices d'aluminium et de magnésium, la nuance SCS6 aux matrices de titane (2) (Tableau IIIb)

Bien d'autres fibres inorganiques ont été envisagées pour le renforcement des matrices métalliques : métaux (W, Mo, Cr, Aciers, oxydes etc.) mais elles ne correspondent plus au critère de faible densité que nous nous sommes fixés

III b L'interaction fibre-matrice - compatibilité avec les matrices métalliques

Les métaux liquides et en particulier l'aluminium et le magnésium, ne mouillent pas spontanément le carbone à leur température de fusion. Dans ces conditions le liquide ne s'étalant pas à la surface des fibres, ne pénètre pas spontanément par capillarité au sein d'une mèche ou d'une préforme. Ce phénomène paraît lié à la présence d'une fine pellicule d'alumine à la surface de l'aluminium liquide.

Il faut donc, soit améliorer la mouillabilité en ajoutant à la matrice certains éléments d'alliage (Li, Ca, Mg) ou en modifiant les propriétés de surface des fibres, soit faire appel à des techniques d'imprégnation sous pression élevée (forgeage liquide).

Par ailleurs le carbone réagit avec les métaux pour donner dans la zone d'interaction des carbures fragiles dont la fissuration entraîne par concentration de contrainte locale une rupture prématurée des fibres.

Il faut également noter que les carbures formés sont sensibles à l'action de l'eau et les interfaces fibre-matrice peuvent devenir des chemins privilégiés de corrosion.

Enfin, la réactivité des fibres de carbone dépend de leur microstructure et elle est plus faible dans le cas des fibres les plus graphitées du type P100 ou les plans graphitiques sont sensiblement parallèles à la surface de la fibre [4] [5].

L'amélioration du mouillage par traitement superficiel des fibres peut se faire grâce à trois types de traitement (6) :

- le revêtement de la fibre par un métal déposé grâce à une gamme très large de procédés physiques ou physico-chimiques et même par voie électrolytique puisque la fibre est conductrice.

- le traitement par un métal alcalin (Na, K ou alliage Na-K) qui la rend spontanément mouillable par l'aluminium et le magnésium ou par des fluorures (K₂ZrF₆ pour les matrices aluminium (7)).

- le revêtement par un film de céramique (TiB, SiO₂, SiC, ...).

Dans le cas des fibres à base d'alumine, c'est l'addition de lithium à l'aluminium qui s'est montrée la plus efficace pour améliorer le mouillage. Par ailleurs, les procédés de dépôt sur fibres par voie physique sont également applicables. La situation est meilleure dans le cas du magnésium puisque les fibres d'alumine sont spontanément mouillées par le magnésium et ses alliages. Par ailleurs, la compatibilité du magnésium avec l'alumine doit être bonne du fait de la grande stabilité de cet oxyde.

Comme le carbone, le carbure de silicium n'est pas mouillé par l'aluminium liquide à 650°C et la transition mouillage - non mouillage se fait vers 950°C sous air. Par ailleurs, l'établissement d'un diagramme Si-C Al(8) a permis de montrer que le carbure de silicium est en équilibre avec l'alliage liquide à base d'aluminium si celui-ci contient suffisamment de silicium.

Dans le cas des filaments à base de SiC, la structure de la fibre est conçue pour que le produit de la réaction chimique superficielle inévitable ne soit pas nocif ; une couche de pyrocarbone (homogène ou une séquence pyrocarbone-SiC) sert à la fois de couche sacrificielle et d'obstacle à l'extension dans la fibre des microfissures initiées dans la couche de carbure, soit pendant l'élaboration, soit pendant le fonctionnement du composite.

IV - PROCÉDES D'ÉLABORATION

On peut classer les procédés d'élaboration des C.M.M. à fibres longues en deux grandes catégories (6) :

- les procédés par voie solide et semi liquide à partir de pré-imprégnés ou de nappes alternées de fibres et de feuillets.
- les procédés d'imprégnation de préformes par voie liquide.

Le pré-imprégné par analogie avec le "pré-preg" des composites à matrice organique est déjà un demi produit où le renfort et la matrice coexistent dans la proportion juste nécessaire à la réalisation du composite.

L'élaboration des pré-imprégnés s'effectue en continu sur des mèches étalées soit par imprégnation directe, soit par le passage dans un bain liquide précédé ou non d'un prétraitement de la fibre suivant la mouillabilité du renfort par le métal.

Les méthodes directes : dépôt chimique en phase vapeur, évaporation sous vide, placage ionique, éventuellement dépôt électrolytique..., permettent difficilement d'ajuster la composition de la matrice et l'étalement des mèches est délicat. Dans le cas des filaments on peut réaliser les pré-imprégnés en plaquant une nappe de filaments contre un feuillet d'alliage et on solidarise par exemple l'ensemble par une projection plasma du même alliage.

L'imprégnation par voie liquide s'effectue par un trempé (réalisé ou non sous pression) suivi d'une opération de pultrusion. La composition de l'alliage peut évidemment être ajustée - éventuellement pour assurer le mouillage de la fibre qui peut également être traitée au préalable dans le même but.

A partir de ces pré-imprégnés il est possible d'obtenir par pressage à chaud des plaques ou des formes minces. Sauf dans le cas où le pressage s'effectue en phase semi-liquide, le comportement plastique de la matrice et la diffusion en phase solide contrôlent la mise en oeuvre de ce procédé. On peut également empiler des couches alternées de fibres maintenues en place par des résines éliminées dans les premières phases du chauffage et des feuillets de l'alliage constituant la matrice.

Le pressage à chaud a été employé pour les trois types de matrices métalliques évoquées plus haut.

Dans l'imprégnation par coulée on dispose de peu d'informations techniques en dehors des cas simples unidirectionnels. Pourtant dans l'élaboration des C.M.M. par moulage, la réalisation de la préforme fibreuse est une étape essentielle qui nécessite pour l'orientation des fibres, des tissus ou des filaments une parfaite connaissance du système des contraintes dans la pièce finie.

L'imprégnation de formes complexes se heurte aux difficultés déjà rencontrées dans la réalisation de pré-imprégnés par trempé : manque de mouillabilité des fibres et réaction chimique inévitable entre fibre et matrice. Ces deux conditions qui conduisent à des conclusions contradictoires sur la durée et la température de l'interaction fibre matrice sont d'autant plus difficiles à concilier que l'écoulement du métal liquide à travers la préforme peut être difficile.

Ce paramètre supplémentaire a conduit au développement de techniques de coulée sous forte pression.

Il n'y a pas de discontinuité réelle entre les procédés de coulée par simple gravité et le forgeage liquide, le domaine des pressions intermédiaires (jusqu'à quelques MPa) est donc utilisé dans divers procédés en fonction de l'alliage utilisé ou des traitements préalables des renforts. Dans le forgeage liquide, les fortes pressions utilisées (env. 50 à 100 MPa) permettent d'assurer l'imprégnation même dans l'hypothèse d'une mouillabilité médiocre, et d'accroître les propriétés mécaniques en fermant les porosités.

Bien entendu, toute amélioration de la mouillabilité (§ III) permet de diminuer à la fois la pression nécessaire - ce qui peut éviter l'endommagement des fibres dans les préformes rigides - et la durée d'application ce qui limite l'interaction fibre matrice.

V - MAITRISE SCIENTIFIQUE ET TECHNIQUE DES COMPOSITES A MATRICE METALLIQUE

L'ensemble des propriétés d'usage a pratiquement été testé (souvent à l'ambiante et à chaud) pour toutes les combinaisons fibres-matrices que nous avons envisagées.

- module, limite élastique, charge de rupture, allongement à rupture, comportement en fatigue, amortissement, résilience, cyclage thermique, dilatation, conduction thermique et électrique, résistance à l'usure, à l'érosion, à la corrosion, assemblage, ... mais il paraît raisonnable de dire que, sauf dans certains cas particulier, les connaissances actuellement disponibles ne permettent pas encore un véritable développement technologique.

En effet, bien que la somme des résultats concernant les caractéristiques des C.M.M. soit devenue considérable au fil des ans, les valeurs numériques ne sont pas toujours convergentes. Dans les paragraphes précédents, nous avons brièvement évoqué les divers paramètres intervenant dans l'élaboration et il est clair que les dispersions cumulées (et pas toujours maîtrisées) à la fois au plan des matériaux de base et des procédés (technique choisie, séquence thermique et mécanique...) entraînent l'existence d'une très large fourchette de valeurs pour presque toutes les propriétés. En outre, les techniques de mesure pour l'instant calquées sur celles des matériaux isotropes ne sont pas toujours adaptées et peuvent entraîner des dispersions supplémentaires.

Nous nous bornerons donc dans ce très vaste ensemble possible à proposer quelques axes d'intérêt à propos des propriétés de résistance. Cependant, il faut distinguer entre les résultats obtenus pour le module d'élasticité où la convergence est bonne, et les valeurs expérimentales proches de celles données par la règle des mélanges, et ceux observés pour la limite élastique et la résistance à la rupture qui sont parmi les plus dispersés, car sensibles au détail de la microstructure et tout particulièrement de l'interface fibre-matrice.

Dans une approche simple de ce problème on peut postuler que le composé d'interface d'épaisseur "e" est fragile et que sa fragmentation constitue pour la fibre une amorce de rupture. La charge de rupture de la fibre (compte tenu de son propre comportement fragile modélisé par une loi de Weibull) ne sera pas affectée tant que "e" demeurera inférieure à la dimension des défauts propres à la fibre ; au delà d'une épaisseur critique "e_c" la charge de rupture de la fibre doit décroître suivant une loi du type Griffith en $e^{-1/2}$. (2). La nature et l'épaisseur de cette zone d'interaction doit donc être maîtrisée bien qu'elle soit difficile à discerner dans certains composites Al(SiC) ou Al(Al₂O₃) élaborés par forgeage liquide. Il faut également poursuivre des actions fondamentales au niveau de la compréhension fine des mécanismes de réaction et de la structure des produits obtenus. Par exemple, il semble utile de bien connaître la stoechiométrie des carbures de titane puisqu'elle gouverne la diffusion des éléments de la fibre et de la matrice à travers cette "barrière de diffusion".

Il faut souligner à ce propos le modèle que constitue l'adaptation progressive des filaments de SiC (AVCO) aux matrices métalliques Al (éventuellement Mg) et Ti, basée semble-t-il sur une prise en compte à la fois de la physico-chimie et de la mécanique de la rupture.

Par ailleurs, et contrairement aux composites à matrice polymère, la matrice métallique contribue de façon significative aux propriétés mécaniques de l'ensemble. La réponse de la matrice à des conditions de coulée très particulières (infiltration des préformes) qui

favorisent la microségrégation (10)(11) ou des traitements thermiques en présence de contraintes internes et d'une grande densité de dislocations (12), introduit un facteur de dispersion supplémentaire et influe fortement sur les propriétés de résistance et tout particulièrement sur la contrainte d'écoulement. Cette contrainte d'écoulement $\sigma(\epsilon)$ s'écrit (pour une déformation imposée ϵ), (13)

$$\sigma(\epsilon) = \sigma_0 + \sigma_f + \sigma_m \quad (1)$$

où σ_0 est la contrainte d'écoulement de la matrice à l'état massif,

σ_f la contrainte de "frottement" associée au franchissement des fibres pour les dislocations par un mécanisme du type OROWAN

σ_m la contrainte moyenne dans la matrice

σ_m est localement la somme d'un terme provenant des contraintes internes qui prennent naissance pendant le refroidissement du matériau microscopiquement hétérogène, et d'un terme issu de l'interaction fibre-matrice en présence d'une déformation globale imposée ϵ . Dans le cas des composites à fibres longues σ_m est prépondérant (13) et il devient important pour maîtriser la limite élastique conventionnelle de développer non seulement les études systématiques de microstructures mais également des mesures de contraintes internes dans le matériau massif par diffraction neutronique (14). Le terme σ_0 par ailleurs sera modifié par la présence d'éventuels éléments d'alliage destinés soit à abaisser la température d'élaboration par voie solide (15) ou liquide (6) soit à promouvoir le mouillage.

Enfin la modélisation du comportement thermoélastique des matériaux microhétérogènes englobant les composites, a fait l'objet de nombreux travaux (Hill 1963, Halpin et Tsai 1967, Kröner, 1973,...) et le problème apparaît comme quasi résolu. Les travaux actuels portent sur l'amélioration des techniques de calcul et des méthodes d'homogénéisation (16), mais dans l'hypothèse d'un développement industriel, le passage des C.M.M. aux bureaux d'études rend nécessaire la prise en compte dans les modèles prévisionnels des phénomènes de plasticité et d'endommagement. Des études expérimentales parallèles sont alors nécessaires pour tester les hypothèses des modèles et valoriser les résultats.

VI - LES COMPOSITES A MATRICE METALLIQUE EN FRANCE

La France après avoir fait figure de pionnier dans les années 1960 pour certains C.M.M. (travaux de la SNPE, de la SNECMA,... sur les Bore/Al et les SiC/Al appuyés sur les recherches menées à l'Ecole des Mines de Paris et à l'ONERA...), a ensuite limité ses efforts sans doute en l'absence d'une motivation soutenue par des réalisations industrielles. La recherche sur les matériaux eux-mêmes s'est alors concentrée dans quelques laboratoires et tout spécialement au laboratoire de chimie du solide de l'Université de Bordeaux. Cependant, depuis quelques années, et dans l'hypothèse raisonnable d'applications à moyen terme un intérêt nouveau se manifeste.

C'est dans ce contexte qu'en 1986 le Ministère de la Recherche et de la Technologie a estimé utile d'encourager à la fois la recherche industrielle et des recherches de base en faisant travailler ensemble autour de projets à finalité technologique des chercheurs du secteur public et du secteur privé. Ce "groupement d'intérêt scientifique" (G.I.S.) rassemble des industriels élaborateurs (PECHINEY, UNIREC,...) des industriels utilisateurs (AEROSPATIALE, DASSAULT, SNECMA, TURBOMECA, d'une part, P.S.A. et Renault, d'autre part) et des équipes de recherche réparties dans près de 20 laboratoires.

Dans l'ensemble des recherches menées dans ce contexte d'intérêt renouvelé, il y a peu de travaux consacrés spécifiquement aux composites à fibres longues mais les études à caractère général sont aussi dans notre propos. Nous illustrerons donc quelques aspects jugés importants dans les paragraphes précédents à l'aide de travaux récents.

La figure (1) montre une pièce réalisée par le Groupe Pechiney en collaboration avec l'Aérospatiale. Les propriétés mécaniques ont été mesurées sur éprouvette et les figures (2) et (3) donnent les variations avec la température de la résistance en flexion et du module

dynamique. C'est une bonne illustration des possibilités d'usage à chaud des C.M.M. à matrice aluminium (17).

Le comportement en cyclage thermique est illustré par la fig. (14). Les auteurs soulignent que le coefficient de dilatation n'est plus une propriété intrinsèque du matériau puisque l'apparition d'une très forte non linéarité associée à la limite d'écoulement de la matrice dépend non seulement de la contrainte appliquée mais aussi des contraintes internes et donc de l'histoire thermique et mécanique du matériau (18).

La fragmentation d'un mono-filament fragile dans une matrice ductile est une technique d'accès à la mécanique de l'interface et donc à l'efficacité d'un traitement superficiel par la mesure du cisaillement critique τ_c qui règle le transfert de charge.

On montre ainsi (19) que τ_c est égal à 195 MPa dans un composite TA6V/SiC quand la fibre est nue et que cette valeur passe à 295 MPa s'il s'agit d'une fibre AVCO du type SCS6. Cependant, le modèle simple donnant accès à τ_c paraît insuffisant comme le montre la comparaison entre le nombre de ruptures estimé théoriquement dans ce cadre et les valeurs expérimentales (observées sur un composite mono filamentaire Al/SiC (fig. 5) (20)). Il faut sans doute pour expliquer cet écart encore mal compris tenir compte des contraintes internes, de la différence du coefficient de Poisson entre fibre et matrice, etc. Un modèle global tente une prise en compte de l'ensemble des effets (21).

La méthode de la goutte posée est l'approche expérimentale la plus commune pour étudier le mouillage d'une céramique par un métal liquide. La fig. (6) représente en traits continus la courbe obtenue classiquement ; l'angle de contact θ reste élevé jusqu'à 1150°K puis décroît brusquement au moment de la disparition de la couche d'alumine. Des expériences ont été conduites (22) sur les couples Al-Al₂O₃ et Al-SiC sous un vide poussé (10^{-5} Pa) qui provoque la désoxydation en quelques minutes vers 950 K.

Dans le cas Al/Al₂O₃ (traits discontinus (fig. 6)) la valeur d'équilibre de θ passe de 125° à 60° en un temps qui dépend de la température d'essai. Le processus de mouillage paraît contrôlé par le processus de dissolution de SiC dans l'aluminium et non par la formation du carbure Al₄C₃ (qui peut être évitée par la présence d'une quantité suffisante de silicium dans l'alliage Al-Si).

Cette méthode permet donc d'atteindre la valeur intrinsèque de l'angle de contact qui s'établit dès la rupture de la couche d'oxyde dans des procédés du type forgeage liquide par exemple.

Les fibres de carbone multibrins sont handicapées par leur faible aptitude au mouillage et leur forte réactivité chimique vis à vis des métaux et de l'oxygène. C'est pourquoi le revêtement des fibres de carbone par des carbures est très travaillé et les procédés se rangent en deux catégories : ceux où le métal et le carbone du revêtement sont apportés par les gaz réactifs et ceux où le carbone est fourni par la fibre elle-même (23). Dans les deux cas, des dépôts homogènes ont été obtenus malgré les difficultés d'imprégnation à cœur de la mèche et la figure (7) montre la tenue à l'oxydation à l'air d'une fibre C/SiC recouverte par le second procédé.

L'élaboration par squeeze casting est l'un des procédés qui peut, à terme, assurer une production en série et les essais d'un tel procédé se sont multipliés. Cependant le résultat final dépend d'un tel nombre de paramètres qu'il est utile de posséder un modèle pour ne pas multiplier les essais. La figure (8) montre les résultats d'une approche réalisée dans l'hypothèse de fibres longues disposées parallèlement ou perpendiculairement au flux métallique (imprégnation de fibre SiC (Nicalon) par de l'aluminium (24)). La longueur limite d'imprégnation décroît très vite avec la fraction volumique. L'intérêt de ce type de modèles est qu'il permet de dégager rapidement les paramètres importants sur lesquels il faut faire porter l'effort expérimental.

Cette liste n'est évidemment pas exhaustive ; bien d'autres résultats ont été obtenus récemment et des travaux divers sont en cours en France dans les laboratoires intéressés par les C.M.M.

VII - CONCLUSION

Les composites à matrice métallique à fibres longues répondent bien en principe aux besoins exprimés par l'industrie aéronautique de matériaux rigides, et possédant une meilleure tenue en température que les composites à matrice organique classique.

Un certain nombre de barrières technologiques ont été levées depuis les premiers travaux et des applications ont été trouvées dans des circonstances où l'aspect "performance" est primordial (charpente tubulaire de la navette spatiale - renforts structuraux d'avions de combats - matériaux sans dilatation pour optique spatiale,...). Les produits utilisés dans ce cas ont atteint une maturité technique certaine, mais les procédés utilisés ne peuvent conduire qu'à des matériaux élaborés en petite quantité sans grand espoir d'une véritable industrialisation.

Il paraît clair par contre que les procédés basés sur une imprégnation obtenue par coulée constituent une voie d'avenir par la possibilité d'accès à la série, il est cependant nécessaire dans ce cas d'approfondir nos connaissances sur l'interaction fibre-matrice (mouillabilité, réaction chimique et mécanique de la rupture...) pour améliorer en parallèle la technique même d'imprégnation qui en est la conséquence directe (compétition entre le forgeage liquide et le moulage basse et moyenne pression).

L'effort consenti sur la macro et la microstructure de la matrice (ségrégation, durcissement par précipitation,...) est actuellement insuffisant. Les études sur les renforcements hybrides qui permettent de gagner sur les deux derniers termes de l'expression (1) doivent être encouragées.

Par ailleurs, le prix des filaments CVD limite probablement leur emploi aux applications prestigieuses rappelées plus haut ; On peut par contre envisager un tassement du coût des fibres multibrins disponibles.

Le véritable démarrage industriel des C.M.M. à fibres longues en dépend pour l'essentiel.

REFERENCES

- (1) Analysis of the strength and fracture behaviour of unidirectional and angle-ply graphite aluminium composite -
V.C. NARDONE, J.R. STRIFE
J. of Mat. Sc., 22, 1987, p. 592-600.
- (2) Modern Boron and SiC CVD filaments - a comparative study
Y. LE PETITCORPS, R. PAILLER, M. CHAMBON and R. NASLAIN
Composites Science and Technology, 3 (1988) p. 31-55.
- (3) Introduction aux matériaux composites, Vol. (2) - Matrice métalliques et céramiques
Bordeaux (1985) Ed. R. NASLAIN - Edition CNRS et IMC
- (4) Reinforcement of light metals by carbon fibers
J. MAIRE, R. GREMION
III^e Conference on industrial carbon and graphite (1971) p. 491-496
- (5) Fiber wetting and coatings for composite fabrication
H. KATZMAN
Metal and ceramic Matrix composite procession conference - Columbus 13-15 Nov (1984) p. 1-8
- (6) Procédés d'élaboration des matériaux composites fibreux à matrice d'alliage base aluminium
J.P. ROCHER, F. GIROT, J.M. QUENISSET, R. PAILLET, R. NASLAIN
Mémoires Revue de Métallurgie, Fév. 1986, p. 69-85.

- (7) A new casting process for carbon or SiC based fibre aluminium matrix low cost composite materials
J.P. ROCHER, J.M. QUENISSET, R. NASLAIN
J of Mat. Sc. Letters 4, (1985) p. 1527-1529
- (8) Development in the Science and Technology of composites materials
J.C. VIALE, P. FORTIER, C. BERNARD, J. BOUIX
First European Conf. on Composites Materials 24-27 septembre 1985, Bordeaux
- (9) Kinetics of the reaction between SiC (SCS 6) filaments and TA6V matrix WHATLEY, W J
WAYNER, F.E.
J of materials Science, 4, (1984) p 173-175
- (10) Processing of metal and ceramic matrix composites
J.A. CORNIE, YET MING CHIANG, D.R. UHLMANN, A. MORTENSEN, J.M. COLLINS
Ceramics Bulletin, 65, 2, (1986) p 293-304
- (11) Composite structure of silicon carbide fiber reinforced metals by squeeze casting
HIDEHARU -FUKUNAGA KOICHI GODA
Bulletin of J. S.M.E., 28, 235, (1985) p 1-6.
- (12) Microstructural development in an aluminium alloy SiC Wisker composite
TCHRISTMAN and S. SURESH
Acta Met. 36, 7, (1988) p 1961-1704
- (13) The strength of metal matrix composites under mechanical and thermal loading
H. LILHOLT
LES ACTES DU COLLOQUE I.S.C.M.A. 8, Tampere (août 1988) p 61-79
- (14) Internal stresses measured by neutron diffraction in metal matrix composite exposed to thermal treatments
H. LILHOLT and JUUL - JENSEN
"Composites evaluation" Edité par J. Herriot. Butterworths, Sevenoaks (1987) p 156-161
- (15) The Effect alloying additions on superplastic properties of Ti-6 Al-4V
LEADER - NEAL - HAMMOND
Met transactions, Vol. 17A, n° 1, (1986) 93-106
- (16) Comportement thermomécanique des composites à matrice métallique
F. CORVASCE, P. LIPINSKI, M. BERVEILLER
à présenter aux 6èmes journées nationales sur les composites (JNC-6) Paris, Oct. 1988
- (17) Metal Matrix composites : properties and development outlook
S. DERMARKAR
présenté au Word Materials Congress 1988
Symposium on Advances in cast reinforced Metal composites, 25-30 septembre 1988, Chicago
- (18) Non linearity in thermal expansion of continuous fiber metal matrix composites
X. DUMONT, F. FERROT, G. RAGAZZONI
présenté au Word Materials Congress 1988
Symposium on Advances in cast reinforced Metal composites, 25-30 septembre 1988, Chicago
- (19) A method to evaluate the bonding between fibre and matrix in Ti-based composite
A. VASSEL, M.C. MERIDIENNE, F. PANTONNIER, L. MOLLIEUX, J.P. FAVRE
présenté au symposium Titane, Cannes, juillet 1988
- (20) Study of acoustic emission due to the multiple fibre fracture in a single SiC filament - aluminium matrix model composite
P. BONIFACE, P. FLEISHMANN, R. FOUGERES, P.F. GOBIN, D. ROUBY, F. LONCA-HUGOT, M. BOIVIN
présenté au Word Materials Congress 1988
Symposium on Advances in cast reinforced Metal composites, 25-30 septembre 1988, Chicago

(21) Modelisation statistique du processus de fragmentation dans les composites modelés a monofilament
à présenter aux 6ème Journées nationales sur les composites (JNC-6) Paris 1988

(22) The wetting kinetics of aluminium and its alloys on single crystal SiC
V LAURENT, D CHATAIN, X DUMANT, N EUSTATHOPOULOS
présenté au Word Materials Congress 1988
Symposium on Advances in cast reinforced Metal composites, 25-30 septembre 1988, Chicago

(23) Procédé et dispositif de revêtement des fibres de carbone par un carbure, et fibres de carbone ainsi revêtues
J BOUIX JC VIALA, H VINCENT C VINCENT JP PONTENIER J DAZORD
Brevet français n° 8617157 (4.12.1986)

(24) Effect of the squeeze casting conditions on the infiltration of ceramic preform
JM QUENISSET
présenté au Word Materials Congress 1988
Symposium on Advances in cast reinforced Metal composites, 25-30 septembre 1988, Chicago

TABLEAU I

Matrice	Al/6061	Al/6061	Mg	Ti/TA6V
Renfort	SiC/SCS2	Gr P100	Gr P55	SiC SCS6
Fraction volumique de renfort %	40	42	40	35
Contrainte de rupture en tension σ_r MPa	1467	745	827	1470
Allongement à rupture %	0,86	0,23		
Module longitudinal G Pa	200	332	172	240
Coefficient de dilatation 10^{-6}K^{-1} (0-100 °C)			0,3	
Masse volumique			1,88	

Ordre de grandeur des caractéristiques de quelques composites à fibres longues à la température ambiante

TABLEAUX II

Alliage	Masse Volumique g/cm^3	Module G Pa	Contrainte rupture MPa	Coefficient de dilatation 10^{-6}K^{-1}	Résistivité $\mu\Omega \text{cm}$	Conductivité therm. $\text{W/m}^\circ\text{C}$
Al 1050	2,71	69	80	23,6	2,8	231
2014(T6)	2,80	74	480	22,5	5,1	135
2024(T3)	2,77	73	465	22,9	5,7	120
5454(O)	2,69	70	250	23,7	5,1	136
6061(T6)	2,70	69	305	23,6	4,0	167

(O) état recuit - (T3) trempé écroui et mûri - (T6) trempé et revenu

Tableau IIa

Ordre de grandeur des propriétés physiques et mécaniques de quelques alliages d'aluminium disponibles à l'état de demi-produit et utilisables comme matrice

Alliage	Masse Volumique $20^\circ\text{C} \text{ g/cm}^3$	Module G Pa	Contrainte à rupture MPa	Coefficient de dilatation 10^{-6}K^{-1} 20 - 100°C	Résistivité $\mu\Omega \text{cm}$ 20°C	Conductivité therm. $\text{W/m}^\circ\text{C}$
Mg	1,74	45,5		21,1	4,46	154,8
GA3Z1	1,78	43	230/280	26,0	10,0	83,72
G Ag2(F)	1,83	44	170/220	27,0	14,1	72,35
GZ4Tr(F)	1,84	44	200/230	27,1	6,8	113,01

(F) Alliage de fonderie - (C) Alliage de corrosion

Tableau IIb

Ordre de grandeur des propriétés physiques et mécaniques de quelques alliages de magnésium utilisables comme matrice

TABLEAUX III

Nature de la fibre	diamètre μm	Masse Volumique g/cm^3	Module G Pa	Résistance à la rupture MPa	Allongement à la rupture %
Fibres de Carbones					
T 300		1,8	230	3,450	1,5
M 40		2	390	2450	1,2
GY 70	8,4	1,96	520	1860	0,4
P 100	10	2,05	700	2400	0,3
Autres Fibres					
SiC (Nicalon)	10-15	2,55	180/200	2500	
Al_2O_3 FP	19	3,95	390	2000	0,4
Al_2O_3 - SiO_2 (Nextel)	10-12	3,1	220	1750	0,8
Al_2O_3 - SiO_2	9	3,1	250	2600	

Tableau IIIa
Ordre de grandeur des caractéristiques de quelques fibres multibrins

Nature du Filament	Nature de l'âme	Diamètre μm	Résistance à la rupture MPa	Module G Pa	Densité g/cm^3	Module de Weibull
Bore	Carbone	100	3 280	365	2,22	
Bore/B ₄ C	W	140	4 075	405	2,46	30
SCS/2	Carbone	140	3 275	385	3,3	7
SCS/6	Carbure	140	4 675	390	3,3	14,5

Tableau IIIb
Ordre de grandeur des caractéristiques de quelques filaments obtenus par dépôt chimique en phase vapeur

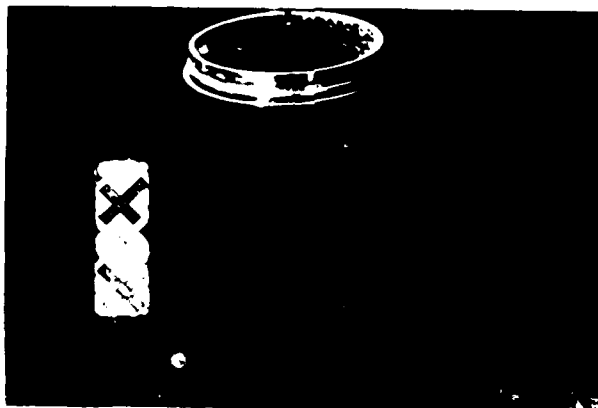


Figure 1. Composant creux obtenu par forgeage liquide (Réf. (17))

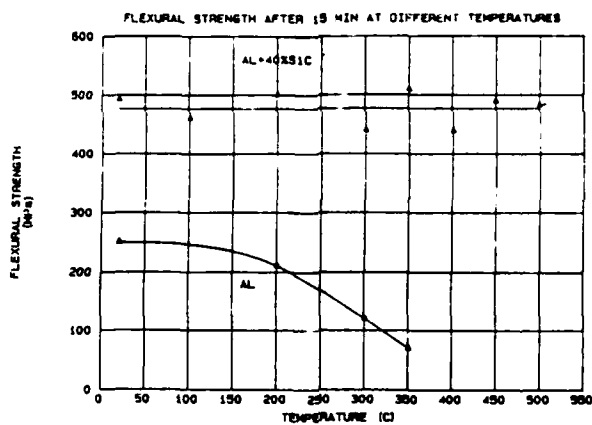


Figure 2. Résistance en flexion d'un C.M.M. Al-40 % SiC en fonction de la température (réf. (17))

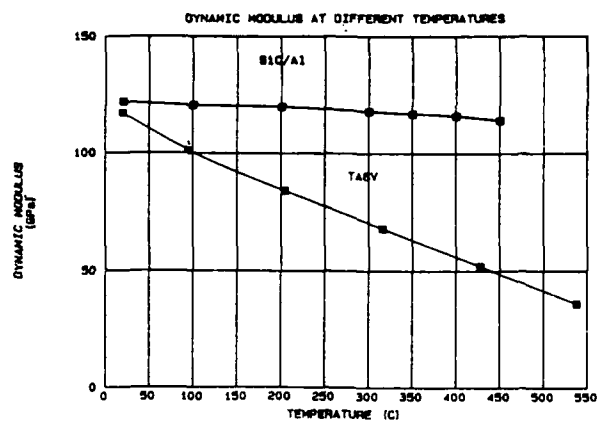


Figure 3 : Module dynamique d'un C.M.M. Al + 40 % SiC en fonction de la température (Réf. (17))

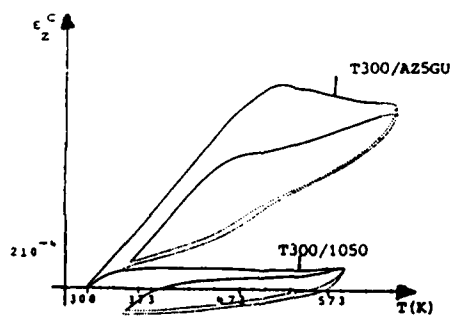


Figure (4) : Variation dimensionnelle pendant le cyclage thermique de deux composites unidirectionnels
Al 1050/T300 - AZ5GU (T6)/T 300 (Réf. (18))

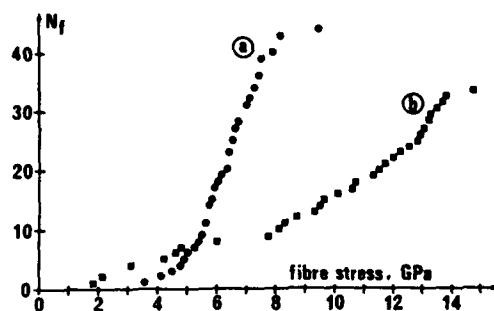


Figure (5) : Variation du nombre de ruptures d'un monofilament dans un composite modèle 6061 (T6)/SiC - a) résultats d'une simulation ; b) résultats expérimentaux (réf(20))

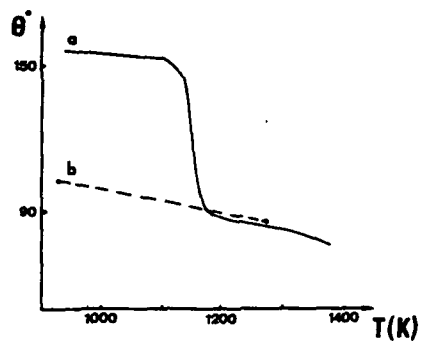


Figure (6) : Variation de l'angle de contact liquide - solide en fonction de la température dans le système Al/Al₂O₃

a) courbe classique ($P = 10^{-2}$ à 10^{-4} Pa)

b) Courbe obtenue sous vide élevé (P de l'ordre 10^{-5} Pa) réf (22)

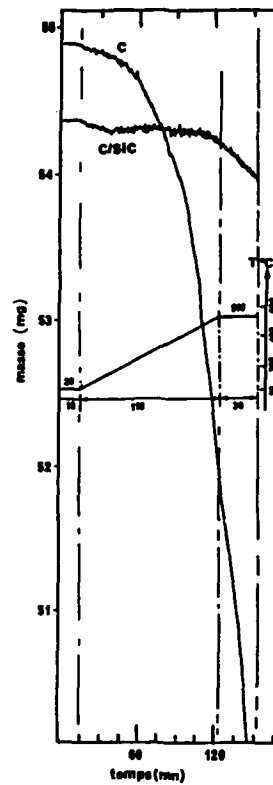


Figure (7) : Tenue à l'oxydation à l'air d'une fibre de carbone recouverte de SiC par le procédé de la référence (23) - Comparaison avec la fibre de carbone d'origine (c).

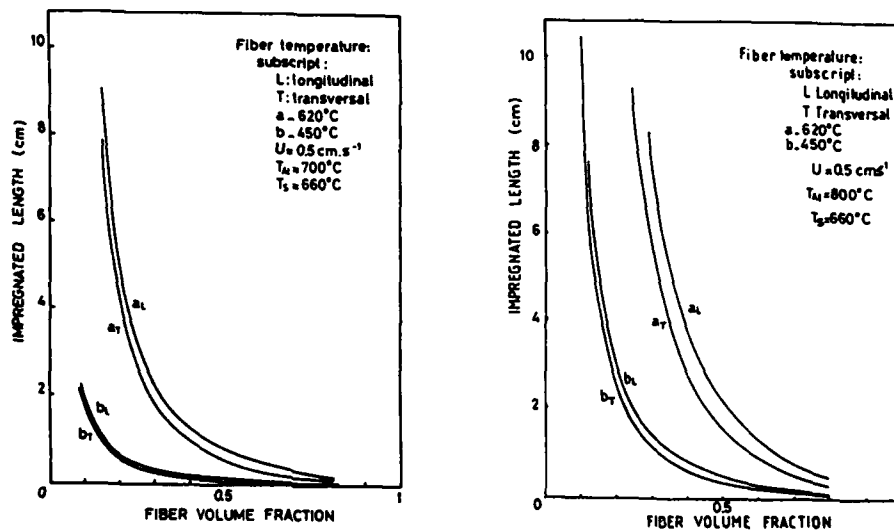


Figure (8) : Influence de la fraction volumique de fibres, de la direction d'infiltration et de la température de la préforme sur la longueur imprégnée pour deux températures du métal liquide. a) $T_{A1} = 700^{\circ}\text{C}$ - b) $T_{A1} = 800^{\circ}\text{C}$. (ref (24))

SHORT FIBRE AND PARTICULATE REINFORCED METAL MATRIX COMPOSITES

by

S.J. Harris

Department of Metallurgy & Materials Science,
University of Nottingham,
Nottingham NG7 2RD
UK

ABSTRACT

Short fibres, whiskers or particles of ceramic materials, e.g. silicon carbide and alumina, when dispersed in a more or less random manner in a metallic matrix can promote increases in stiffness and strength at ambient and elevated temperatures without imposing a weight penalty. The paper considers the available routes for the fabrication of such composites, e.g. by squeeze casting, spray forming, powder technologies and hot working etc. Influences of type and amount of reinforcement, matrix alloy selection and processing route on strength, creep and fatigue resistance are discussed. Comparisons are made with conventional metals and alloys, and polymers and metals reinforced with continuous fibres. Attention is drawn to the behaviour of these materials under compressive loading as well as to their thermal expansion and conductivity. The majority of the matrices considered are aluminium-based.

1. INTRODUCTION

In the design of a given component in those industries concerned with vehicle manufacture it is a major requirement that minimum weight of material be used in its subsequent production. This objective must be combined with the need to form and fabricate at reasonable cost and then the part should operate in service with minimum maintenance. Aerospace technology has consistently attempted to promote the concepts particularly since the rise in fuel costs of the 1970's. Such a philosophy has put traditional metallic materials under threat, e.g. aluminium alloys in airframe construction having to compete with low density carbon fibre reinforced plastics (CFRP) and in engine technology ceramics with the potential to operate at higher temperatures are undergoing active consideration as possible replacements for nickel base superalloys.

In modern military aircraft over one quarter of the airframe mass is fabricated in CFRP⁽¹⁾. Moves are being made to consider such organic matrix composites for further non-structural and structural parts of aircraft. To counter this challenge developments in light metals (Al, Mg and Ti) have taken place. In aluminium technology there has been a consistent effort to develop and promote lithium containing alloys and rapid solidification powder (RSP) materials. Alongside these developments continuous fibres, e.g. carbon, silicon carbide, alumina; whiskers, e.g. silicon carbide; short fibres, e.g. alumina, and particles, e.g. silicon carbide, have been introduced into light metal matrices in an attempt to improve specific properties. Metal matrix composites (MMC's) with discontinuous reinforcement (short fibres, whiskers and particles) have more isotropic properties⁽²⁻⁴⁾ than those fabricated with continuous unidirectionally aligned fibres and are potentially cheaper to manufacture. Significant levels of activity are being promoted in developing these MMC's in a number of international companies. This paper outlines the techniques which have been developed to produce such materials and then goes on to provide an insight into the mechanical and physical properties which have been achieved to date.

2. PRODUCTION OF DISCONTINUOUS METAL MATRIX COMPOSITES

The processes used to manufacture these materials attempt to produce an even distribution of short fibres or particles either completely throughout or in designated regions of the component. Fibre or particle volume fractions have been in the range 10% to 40%, although the majority of effort has concentrated in the lower end of the reinforcement range. Porosity in the composite should be minimised and conditions at the reinforcement-matrix interface should be controlled to optimise bond strength. Two major groups of manufacturing routes have been employed

- i) those using liquid metals to either infiltrate fibre bundles or preforms or to mix with particles, and
- ii) where solid state methods are employed, here metallic powders are mixed and blended with the reinforcement and then hot pressed. This is followed by secondary processing such as extrusion, forging or rolling to provide a product form.

Fig. 1 provides a more complete representation of possible production routes for composites with discontinuous reinforcement.

Use of Liquid Metal Technology

The simplest form of production for particle reinforced MMC's is the use of melt stirring. Here surface-treated particles, usually α -SiC ($\approx 10 \mu\text{m}$ in size), are stirred into the molten alloy. After achieving an even particle distribution the melt is then cast either to shape or to form an ingot for subsequent working. Surface treatment of the particles is necessary in order to achieve particle wetting and thereby even distribution in the melt. Excessive reaction between particle and melt has to be guarded against by controlling time and temperature in the molten state.

Rheocasting or Compocasting⁽⁵⁾ is related to melt stirring, the difference comes in the state of the metal, it is in the semi-solid or 'mushy' condition when mixed with the particles. During stirring thixotropic conditions occur provided control is maintained over the optimum volume fraction of solid

particles of appropriate size distribution. The method usually produces an ingot of MMC which is then subsequently worked.

A method of producing silicon carbide reinforced MMC's using a method based on the Osprey spray deposition process (see Fig 2) has been introduced by Alcan International, Banbury, Oxon(6,7). In this operation liquid aluminium alloys are atomised with nitrogen, and silicon carbide particles ($>5\mu\text{m}$ in size) are uniformly fed into the resultant liquid droplet stream. The liquid droplets freeze partially during flight and then finally on the collector surface. Control over the movement and the shape of the collector allows tube, forging stock, billets and ingots for extrusion and rolling to be produced. Densities approaching theoretical values, i.e. 95-98%, are achieved in the composites. Rates of MMC ingot production relate to those achieved in DC casting operations.

Squeeze casting has received significant attention(8,9) in the preparation of fibre reinforced MMC's. This process requires a preheated die, preform and ram which allows pressure to be applied to the superheated metal (see Fig 3). Pressures in the range 3-100 MPa are needed to overcome capillary effects and frictional forces experienced by the liquid flowing through the interfibre channels. There is a need to optimise mould and preform temperatures ($\approx 200^\circ\text{C}$ for aluminium alloys) as well as the melt superheat ($\approx 100\text{K}$ above liquidus temperature) and time for which pressure is applied. Otherwise, fibre distribution and degree of fibre-matrix interaction may be adversely affected. Squeeze casting usually produces net shaped parts.

Solid State Methods

These methods relate to particulate and whisker reinforced composites(2) although attempts have been made to incorporate short fibres(10). A typical processing route is shown in Fig.4. Techniques are based upon powder technology and involve the preparation of suitable pre-alloyed powders to which SiC whiskers or powders are added and blended. With aluminium alloys it is necessary to take precautions to minimise surface oxidation and contamination in these and subsequent operations. To assist in this, the blended powders are canned and vacuum degassed prior to consolidation. The consolidation process involves hot pressing or hot isostatic pressing (HIPping). Secondary processing such as extrusion, forging or rolling is necessary to break up remaining inter-particle oxide films. The processing can lead to net shaped parts and after hot working to produce sheet and sections.

A variant of the powder route involves the process which is called Mechanical Alloying(11); Pre-alloyed powders are not needed, and the pure metal powders, alloying ingredients with oxides and carbides, are subject to ball milling to break down and blend the constituents together. The resultant powder mixture is consolidated into composite shapes etc. by the powder metallurgy techniques described above.

3. MECHANICAL BEHAVIOUR UNDER AMBIENT CONDITIONS

Young's Modulus

Short fibres and whiskers all improve the stiffness of metal matrices. The fibres and whiskers aligned or randomly oriented all produce increases in modulus. Table I shows the improvements found in several different aluminium alloys produced by additions of Saffil 6-alumina fibres and α -silicon carbide particles. The modulus does not increase in a linear fashion with increasing volume fraction of reinforcement as is the case with uniaxially aligned continuous fibres in a metallic or polymer matrix, see Fig.5. This is influenced by the fibre-aspect ratio and the orientation of each fibre relative to the test direction.

The moduli achieved in all the aluminium matrix composites referred to in Table I exceed those of the recently developed aluminium-lithium alloys (8090 etc). Additions of silicon carbide and alumina particles or fibres to aluminium alloys usually produce a small increase in density. So that values of specific modulus calculated (see in brackets in Table I) for the reinforced composite alloys are not significantly above those achieved for the unreinforced version of the low density Al-Li alloy. Recently it has been demonstrated(7) that SiC particle reinforced 8090 alloys may be produced by the spray casting method. The combination of a low density alloy and a silicon carbide addition of 10 vol.% gives a density of 2600 kg/m^3 , a modulus close to 100 GPa and hence a specific modulus 18% greater than the unreinforced alloy.

Yield and Work Hardening Behaviour

Much of the data (see Table II) which has been reported upon discontinuous reinforced composites has included values of 0.2% proof stress. On occasions this has demonstrated strengthening improvements for the reinforced material over the unreinforced matrix; in other composite samples the proof stress has shown either little improvement or has been reduced by the addition of the reinforcement. These variations result from the influence of the reinforcement on the yield stress (as specified by the limit of proportionality) and the subsequent work hardening behaviour of the matrix. Additions of both particles and fibres has been shown to promote large increases in the work hardening of the matrix particularly at low levels of plastic strain. It is suggested that the following variables have a major influence over the yield and work hardening behaviour:

- the size and shape of the reinforcement,
- the volume fraction of the reinforcement,
- the type of alloy,
- the nature of the interface between reinforcement and matrix
- the processing route of the composite,
- the relative coefficients of expansion of reinforcement and matrix
- the heat treated state of the matrix alloy.

Composites have been produced chiefly with β -silicon carbide whiskers (diameter $< 1\mu\text{m}$ and aspect ratio

$\approx 50:1$), α -silicon carbide particles (size 5-20 μm irregular in shape with an aspect ratio $< 2:1$) and δ -alumina fibres (diameter 3 μm , aspect ratio $\approx 50:1$). In the case of the particles there is little evidence of a reduction in yield stress of the matrix alloy, the extent to which there is an increase in yield stress depends upon the matrix alloy and the way that the composite has been processed⁽⁴⁾. At the other extreme the presence of high aspect ratio δ - Al_2O_3 fibres tend in a number of alloy matrices to reduce the yield stress and only in special circumstances to increase it (see Fig.6). The volume fraction of fibres or particles has some influence on the yield behaviour e.g. at low volume fraction, i.e. < 5 volume per cent, the influence either positive or negative is relatively small, between 5 and 20% the effect grows, and beyond 25% changes are more marginal.

The type of matrix alloy can influence many factors, e.g. the alloy composition may promote fibre-matrix interaction promoting a strong bond between reinforcement and matrix. A matrix alloy may vary from a low strength, highly ductile, non-heat-treatable alloy which depends upon solute strengthening to an age hardening high strength alloy with reduced ductility. There are examples of situations where an interaction between fibre and matrix may remove or reduce the concentration of certain elements in the matrix and thus preventing precipitation taking place during ageing particularly adjacent to the fibre⁽¹²⁾.

The nature of the reinforcement-matrix interface besides influencing precipitation does affect the level of stress transfer between the two components of the composite. In continuous reinforced systems the precise nature of this interface is not always critical as there is sufficient fibre length over which transfer can take place. With the equiaxed particles, the ability to transfer load may be restricted particularly when the matrix begins to deform plastically. With the larger aspect ratio, fibres, e.g. δ - Al_2O_3 , load transfer may become significant when interfacial bond strengths are high.

Processing route can differ quite considerably between particulate, whisker and short fibre composites. Particulate reinforced composites can be hot or cold worked after prior formation by powder processing, stir casting or arc spray forming. Interactions between forming temperature, particle size and volume fraction, deformation rate, all influence the subsequent microstructure of the matrix^(13,14). The major influence often relates to processes of recovery and recrystallisation and the resultant grain sizes, substructures and textures which remain in the composite after processing. In general, the grain size reduces with particle diameter and with increasing volume fraction (see Fig.7). It is often possible to prevent recrystallisation at critical combinations of particle size and volume fraction (see Fig.7).

With small diameter whiskers then hot deformation still remains possible, but the larger whiskers will only remain intact at high working temperatures at slower deformation strain rates⁽¹⁴⁾. Particularly in extrusion conditions, some alignment of the whiskers is possible which tends to promote a degree of anisotropic in the yield behaviour of the composite⁽²⁾. Matrices containing short fibres of larger diameter and aspect ratio become difficult to deform⁽¹³⁾ and the majority of work which has been carried out relates to materials in the as cast and heat-treated condition^(4,10).

In both the silicon carbide-aluminium and alumina-aluminium systems there is a significant difference in the coefficient of thermal expansion, α , between fibre and matrix, e.g. δ - Al_2O_3 , $\alpha = 6 \times 10^{-6} \text{ K}^{-1}$ and Al, $\alpha = 23 \times 10^{-6} \text{ K}^{-1}$. Thus, after casting, hot working or heat treatment, the cool down to ambient promotes internal stresses in the composite. At temperatures in excess of 200°C these stresses in part are relaxed by matrix plastic deformation which can promote increased dislocation densities. Humphreys⁽¹⁴⁾ has demonstrated that in a SiC particulate reinforced aluminium composite a dislocation cell structure is formed during a fast cool or quench from 500°C. Under similar cooling conditions an Al-Cu-Mg (2014) alloy also reinforced with SiC particles was found to have dislocation loops and helices. Nardone and Prevorse⁽¹⁵⁾, Taya and Arsenault⁽¹⁶⁾ have demonstrated that such dislocations do form inhomogeneously in the matrix, i.e. close to the reinforcement. It is suggested by Humphreys⁽¹⁴⁾ that such a distribution is more likely in an alloy matrix where higher friction stresses would be found. The increase in dislocation density would promote increases in matrix yield strength and the work hardening rate.

Cooling below 200°C may promote further plastic deformation but now as the matrix yield stress rises with decreasing temperature the ability to retain elastic stresses increased. This leads to a situation where the reinforcement goes into compression and the matrix remains in tension. The residual misfit can be calculated in small particle volume fractions using Eshelby's theory. Many workers, Mori and Tanaka⁽¹⁷⁾, Taya and Arsenault⁽¹⁶⁾, have sought to apply this theory to larger volume fractions of particles and whiskers. Withers et al⁽¹⁸⁾ have demonstrated the existence of these stresses in short silicon carbide fibre reinforced aluminium composites using a neutron diffraction technique to measure lattice parameters of matrix and fibre during a heat and cooling cycle (see Fig.8). Differences may be expected between the mechanical behaviour of a whisker or short fibre composite at ambient and that of a composite containing more equiaxed particles. For equiaxed particles, the residual stress is hydrostatic whilst the pattern of such stresses in the whisker or short fibres composites has an anisotropic shear component. This results in short fibre reinforced materials, having yield stresses in compression which exceed those in tension particularly where there is some alignment of reinforcement, see fig. 9.

The use of heat treatable alloys is a prime requirement for obtaining reasonable levels of strength in discontinuously reinforced MMCs. The heat treatment procedure usually requires the alloy to be quenched after a solution treatment at temperatures close to 500°C. Such a quench will significantly increase the dislocation density of the matrix, and perhaps in an inhomogeneous fashion. Such dislocations may then influence the subsequent ageing treatment by altering the kinetics of precipitation or by changing the precipitation sequence. Christman and Suresh⁽¹⁹⁾ have demonstrated that the $\text{S}'(\text{Al}_2\text{CuMg})$ precipitates form on the increased number of helical dislocations in SiC whisker reinforced 2124 alloy. The incubation period and the time to peak hardening for the alloy are reduced by the introduction of the whisker reinforcement. Harris et al⁽²⁰⁾ have demonstrated that the introduction of δ - Al_2O_3 short fibres in an Al-4%Cu matrix alloy promotes the formation of $\theta'(\text{CuAl}_2)$ on the enhanced dislocation density at the expense of θ'' which is usually the age hardening precipitate at the peak hardening condition in the unreinforced matrix alloy. This can be confirmed by electron microscopy and by dilatometry where the formation of θ' is associated with a volume change (see Fig.10). A volume change begins to occur within 5h at 170°C with the composite material whereas it takes 75 h for the change to begin in the unreinforced

material. As in the case of the 2124 alloy the $\text{Si-Al}_2\text{O}_3$ fibres have been responsible for introducing dislocation loops and helices which act as suitable sites for the direction nucleation of θ' precipitation, it is worthwhile noting the improvement in proof stress values obtained on the $\text{Si-Al}_2\text{O}_3$ -Al-3.5%Cu matrix after the T6 treatment at 170°C above those achieved by natural ageing (T4). See Fig.1 (a and b). This improvement may be related to the volume increase which takes place during θ' precipitation, which is retained on returning to ambient and may in part offset the residual tensile stresses in the matrix (see Fig.12). It is noted that no significant volume change occurs during natural ageing, the ageing process at ambient is usually associated with the formation of GP zones.

The consequential effects of all the variables listed (a to g) previously, on the yield behaviour of the discontinuous MMC composites are complex. Certain factors which have been discussed almost certainly give positive increments to the yield stress others are negative. The positive factors may be listed as:

- (1) Fibre or whisker aspect ratio encouraging load transfer to the fibres provided the fibre-matrix bond strength is strong enough. This aspect is not very relevant to particulate reinforced composites.
- (2) High dislocation densities introduced during cooling. The magnitude of this effect is difficult to be confident about because of differences in dislocation type and distribution, nevertheless in most circumstances in aluminium alloys this contribution may be significant.
- (3) Small grain sizes and the presence of substructures are usually to be found in MMCs with particle or fibre volume fractions in excess of 10%. The Hall-Petch equation could indicate a significant level of strengthening, $> 50 \text{ MPa}$, to these composites.
- (4) Dislocations, substructures, grain boundaries influence precipitation processes in the matrix and in certain alloy systems, this might enhance yield stresses either by changing the precipitate, increasing its dispersion or providing helpful volume changes.

The negative factors as far as tensile yield behaviour is concerned are:

- (1) Residual elastic stresses in the matrix. Their influence on tensile yield are at the greatest level when the reinforcement has a large aspect ratio and when some alignment of the whiskers or short fibres has taken place in processing.
- (2) Strong fibre-matrix interfacial bond strengths which may prevent matrix relaxation and thus allow the retention of residual tensile stresses in the matrix.

Work hardening has been found to take place at very high rates in all particles, whiskers and short fibre reinforced MMCs immediately after yield. Contributions may arise from load transfer to the particles, short fibres or whiskers. The method of transfer may be via Orowan dislocation loops, Humphreys⁽¹⁴⁾ has calculated the work hardening rate for the particle case using the Brown and Stobbs⁽²¹⁾ equation

$$\tau = G' T V_f \epsilon \quad (1)$$

(where τ is the matrix mean stress, G' is the effective composite shear modulus, T is the Eshelby accommodation factor, V_f the particle volume fraction and ϵ the strain on the composite). This calculation indicates a work hardening rate value which is close to that measured at a stage immediately after yield. At higher strain where the work hardening rate in most composites begins to fall other mechanisms may become involved including the relaxation of Orowan loops and the generation of more dislocations.

Fracture

Fracture strain in discontinuous MMCs of all types varies between 0.7 and 8%. The lower values are encouraged by high volume fractions of reinforcement, reinforcement with a large aspect ratio, strong reinforcement-matrix interfacial bond strengths, strong matrix alloys and reinforcement with a small failure strain. Examination of fracture surfaces reveals evidence of ductile failure of matrix, failure at fibre-matrix interfaces and brittle fracture of the reinforcement. To highlight this variation in fracture behaviour it is useful to describe the fracture of aluminium alloy composites with $\text{Si-Al}_2\text{O}_3$ short fibre and $\alpha\text{-SiC}$ particle reinforcements.

A reinforced Al-Cu-Mg alloy (2618A) containing 20vol% Al_2O_3 fibres failed at low strain values in the T6 condition (see Table II) showing frequent fibre failure, particularly in those fibres aligned close to the tensile axis. Al_2O_3 fibre composites with 99.9%Al or Al-4%Cu matrices failed at higher strains and showed instances of fibre-matrix debonds, where the axis of the fibre was normal to the loading direction, and also of fibre pull-out where the fibre was aligned in this direction. This difference in behaviour appears to result in part from the varying bond strength between $\text{Si-Al}_2\text{O}_3$ fibres and the variety of alloy matrices. It is known that matrices which contain magnesium do promote strong bonding between Si -alumina fibres and the alloy⁽²³⁾. With the strong bond, stresses are more efficiently transferred from matrix to the fibres and opportunities increase for the fibre to reach its breaking stress. If this takes place at numerous positions in the cross-section, e.g. in a fibre-rich area, the composite is weakened and the cracks propagate from the fibres across the strongly bonded interface into the matrix. This can result in a lower failure stress of the composite than the tensile strength of the matrix. The more weakly bonded systems, i.e. unalloyed aluminium and Al-4%Cu, do not transfer load as effectively to the fibres and eventually with increasing stress the fibre-matrix bond breaks down at the ends of the fibres aligned in the loading direction or at other positions around the fibre periphery when they are transverse to that direction. Early yield in the composite also contributes to low failure strain particularly in the strongly bonded systems despite the high rate of work hardening which occurs in the presence of the Si -alumina fibres. These composites soon reach and exceed their failure strain (0.67%).

Silicon carbide particles were introduced into the matrix at lower volume fractions (10%) than the α -alumina (20%) and higher tensile strengths and elongations to failure have resulted, see Table II. The particles have a smaller aspect ratio and in this sense are not able to receive load as efficiently. Even so, McDanel's⁽²⁴⁾ has shown that increasing the volume fraction of particles above 10% does bring down the strain to failure. There is only a small amount of evidence of such particles fracturing and most fracture paths pass through the matrix or in some situations the fibre-matrix interface. Hunt et al⁽²⁵⁾ has suggested that fracture in these composites depends upon the nucleation of voids as a prerequisite for initiating ductile matrix failure. Such voids may nucleate at a number of sites including fibre-matrix interfaces. Argon et al⁽²⁶⁾ pointed out that high volume fractions of particles encourage local stresses to rise and thus help initiate failure at low strains, particularly in higher strength matrix alloys.

4. MECHANICAL BEHAVIOUR AT ELEVATED TEMPERATURES

It has been demonstrated that MMC's containing particles, whiskers and short fibres do show improvements in modulus and strength at elevated temperature over unreinforced alloys^(10,24). In the case of aluminium alloy matrices, composite strengths in excess of 200 MPa can be achieved at 300°C during short periods of exposure at this temperature, see Fig. 13. Comparative data for continuous fibre reinforced systems is also given on Fig. 13. Investigations have been made on more extended times at temperature and during thermal cycling and this has revealed certain dimensional instabilities. As the temperature rises the internal stresses within the composites begin to relax. At temperatures above 250°C processes of recovery take place more quickly and have been shown up by techniques such as neutron diffraction analysis⁽¹⁸⁾.

Humphreys⁽¹⁴⁾ has suggested that a transition in mechanical behaviour takes place in the discontinuous composites when tested at temperatures in the range 200-300°C. Below the transition, high work hardening rates, high flow stresses and low ductilities are found. Above the transition, the work hardening rate reduces and increased ductilities become apparent. Thermally controlled diffusional relaxation of stresses around particles have been put forward as the reason for this transition. Dislocations associated with the particles begin to climb at the elevated temperature, so that they do not accumulate around the particles as deformation takes place.

Silicon carbide whisker ($V_f = 20\%$) reinforced 2024 alloys have been stress rupture tested at 200°C and 300°C. At the higher temperatures these materials show that they can carry the same applied stress for a hundred times longer than the unreinforced 2024 alloy⁽²⁷⁾. Creep tests were also carried out on a similar type of composite material with the exception that the matrix alloy was 6061. The creep curves determined on specimens held at temperatures in the range 232-371°C had short primary, long steady state and negligible tertiary stages⁽²⁸⁾. The steady state creep rate with the composite is significantly lower than that found in the unreinforced alloy and the activation energy obtained from the data is three times greater than the activation energy for diffusion of aluminium. Lilholt and Taya⁽²⁹⁾ have confirmed that the stress sensitivity of such composites are larger than those associated with the matrix. Creep failure occurs in a ductile manner with no evidence of fibre failure.

At temperatures in excess of 500°C particulate composites begin to show evidence of grain boundary sliding. Under certain conditions, i.e. composites with small particles, 5 μ m in size and a fine matrix grain size 410 μ m, superplastic deformation of MMCs becomes possible⁽³⁰⁾. In the presence of large particles, coarse grains and higher strain rates, lower ductilities can result.

5. FATIGUE

It has been shown^(2,31,32) that improvements can take place in the fatigue properties of some particle whisker and discontinuous fibre reinforced composites. Stress amplitude versus number of cycle plots (S-N plots) obtained on samples tested under zero-tension cycling conditions revealed a pattern of behaviour similar to that found in monotonic tensile testing. If the reinforcements provide additional strengthening, i.e. enhancing the tensile strength beyond the values obtained upon the matrix alloy, then improvement particularly in low cycle fatigue strength results⁽³³⁾, see Fig. 14. Where strengthening of the matrix does not take place, then fatigue performance is below that of the matrix under low cycle conditions, but begins to approach it at high cycle lives.

From observations made on fracture surfaces and on surface cracking on samples subjected to cyclic loading in a four point bend test rig, it appears that in weakly bonded short fibre systems, multiple cracks initiate from fibre-matrix interfaces. The cracks grow into the matrix and then coalesce as the number of cycles increases. In the more strongly bonded composites, larger ceramic impurity particles or shot included on a random basis from the fibre production route can influence the fatigue behaviour. Evidence has been found of such particles cracking and initiating fatigue cracks in the matrix at relatively low cyclic plastic strains⁽³²⁾. The cracks then continue to grow through fibre and matrix at crack growth rates which exceed those determined on the unreinforced matrix at all values of ΔK .

In the case of silicon carbide particle reinforced alloys the influence of the particles and their interfaces is not entirely clear. Fatigue cracks often propagate through the matrix regions without apparently involving the particles⁽³³⁾. Where particles become involved then it is usually the interface which breaks down although some evidence of particle cracking has been observed in short life specimens. Recently Shang and Ritchie⁽³⁴⁾ have demonstrated in some work on fatigue crack growth rates that at higher growth rates a crack bridging phenomenon occurred in an alloy reinforced with 15% silicon carbide particles. It appears that particles crack ahead of the main crack but not necessarily in a position which lines up with the main crack. This introduces crack ligaments which then need to be linked and thus promote slower crack growth rates at a given ΔK . It remains to be seen whether there is some optimum particle size or volume fraction which promotes maximum crack bridging influences on crack growth behaviour.

6. THERMAL PROPERTIES

With the majority of ceramic fibre or particle reinforced materials there is a significant difference in thermal expansion coefficient between reinforcement and aluminium alloys. It has already been indicated in Section 3 that SiC short fibres have one quarter of the expansion coefficient of aluminium whilst the difference is greater in the case of $\alpha\text{-SiC}$ ($3.8 \times 10^{-6}/\text{K}$) and aluminium ($23 \times 10^{-6}/\text{K}$). The resultant coefficient for the composite depends upon the volume fraction of the reinforcement and in the case of short fibres or whiskers any alignment patterns will also influence the values. Fig. 12 demonstrates the change in the value of the coefficient in the temperature range 0-170°C which has taken place by the addition of 20% SiC short fibres to an Al-4%Cu alloy. The fibres here are arranged randomly in the plane and measurements were made parallel to that plane. Dinwoodie et al⁽¹⁰⁾ has demonstrated in a similar system that the value of the coefficient begins to change in a linear manner with increasing fibre volume fraction but as V_f increases above 12% the change occurs at a slower rate. It is also to be noted that processes such as precipitation of a second phase, recovery or other stress relieving processes in the matrix may influence the expansion characteristics of the composite. Several workers^(35,36) have noted a large enhanced creep deformation during thermal cycling SiC particulate and whisker reinforced aluminium under load. This cycle behaviour occurs without early void nucleation and fracture and also without changing the dislocation substructure from cycle to cycle. It is concluded by Pickard and Derby⁽³⁶⁾ that a mechanism must exist which allows recovery of the dislocation generation during the large strains which occur.

The introduction of discontinuous ceramic reinforcement into metal matrix reduced its thermal conductivity. The amount of the reduction depends on the volume fraction, shape and distribution of the reinforcement. Taya⁽³⁷⁾ has attempted to model this and other physical properties associated with short fibres with some success. The model is based upon Eshelby's model for elastic behaviour.

CONCLUSIONS

- (1) Metal Matrix Composites with discontinuous fibres and particles are lower cost materials than those containing continuous fibres.
- (2) Liquid metal technologies involving spray forming and squeeze casting, together with powder technologies with appropriate powder blending techniques, provide possible routes for the preparation of a range of useful MMCs.
- (3) The addition of ceramic particles, whiskers or short fibres at volume fractions in the range 10% to 30% can produce at least a 30% improvement in elastic modulus values of aluminium alloys. Using aluminium-lithium alloys as a matrix can also reduce density and promote further increases in elastic modulus.
- (4) Strength properties at 20°C can be improved in certain alloy systems. Improvements are usually found in intermediate strength alloys and then the fibre-matrix bond strength is not too great. Particles with low aspect ratio may allow greater bond strength to persist without causing significant levels of particle failure.
- (5) Improvements in yield strength of the composites are brought about by the introduction of increased dislocation densities during cooling after processing, and by the maintenance of fine grained structures. Residual tensile stresses in the matrix appear to reduce the yield stress in short fibre reinforced systems.
- (6) Short fibre and particulate composites have attractive mechanical properties at elevated temperatures, possibly up to 375°C in aluminium alloy matrices.
- (7) Two transitions at $\approx 250^\circ\text{C}$ and $\approx 500^\circ\text{C}$ take place in particle reinforced composites which influences composite ductility. At the lower temperature transition dislocation climb permits stress relief and thereby reduces the opportunity for void nucleation and fracture. At 500°C grain boundary sliding begins to occur which can allow superplastic deformation of the composite.
- (8) The introduction of short fibres or particles does not appear to significantly worsen the fatigue properties of the matrix alloy. In some cases where composites have weaker matrix-fibre bond strengths, intermediate strength alloy matrices and optimum particle volume fractions, they may be expected to show some improvements in fatigue loading under high stress (shorter life) conditions.

ACKNOWLEDGEMENTS

The author is indebted to his colleagues Dr. B. Noble, Mr. K. Dinsdale, Dr. T. Wilks and Mr. Y. Gao for their help in providing data for this paper. He would also like to thank Dr. J. Johnson of Rolls-Royce plc, Derby, Dr. J. Dinwoodie of ICI plc, Runcorn, Mr. J. Barlow, GRN Technology Ltd., Wolverhampton, and Dr. J. White, Alcan International Ltd., Banbury, for provision of materials and general support.

REFERENCES

1. C.A. Stubbington, "Materials trends in military airframes", *Metals and Materials*, **4**, 1988, pp. 424-431.
2. S.V. Nair, J.K. Tien and R.C. Bates, "SiC reinforced aluminium metal matrix composites", *Int. Met. Rev.*, **30**, 1985, pp. 275-290.
3. F.A. Girot, J.M. Quinisset and R. Naslain, "Discontinuous-reinforced aluminium matrix composites", *Composites Science and Technology*, **30**, 1987, pp. 155-184.

4. S.J. Harris, "Cast Metal Matrix Composites", *Materials Science and Technology*, **4**, 1988, pp. 231-239.
5. G.G. Levi, G.J. Abbashchian and R. Mehrabian, in *Proc. Workshop on 'Rheocasting'*, 1978, Battelle, Columbus, OH, pp. 41-54.
6. T.C. Willis, J. White, R.M. Jordan and I.R. Hughes in *3rd Int. Solidification Processing Conference*, 1987, University of Sheffield, pp. 21-24.
7. T.C. Willis, "Spray deposition process for metal matrix composites manufacture", *Metals and Materials*, **4**, 1988, pp. 485-488.
8. Y. Abe, S. Horikiri, K. Fujimura and E. Ichiki, in *Proc. Fourth Int. Conf. on 'Composite Materials'*, ICCMIV (ed. T. Hayashi et al), 1982, Japanese Society for Composite Materials, Tokyo, pp. 1315-1322.
9. T.W. Clyne and M.G. Bader, in *Proc. Fifth Int. Conf. on 'Composite Materials'*, ICCMV (ed. W.C. Harrigan Jr. et al), 1985, AIME, Philadelphia, PA, pp. 755-771.
10. J. Dinwoodie, E. Moore, C.A.J. Langman and W.R. Symes in *Proc. Fifth Int. Conf. on 'Composite Materials'*, ICCMV (ed. W.C. Harrigan et al), 1985, AIME, Philadelphia, PA, pp. 671-685.
11. P.J. Bridges, J.W. Brooks and P.S. Gilman, *Proc. Conf. on Advanced Materials Research and Development for Transport*, 1985, Strasbourg, p. 85.
12. P.J. Doorbar: personal communication, Rolls-Royce plc, Derby, 1986.
13. C.A. Stanford-Beale and T.W. Clyne, "Deformation of fibrous metal matrix composites at temperatures close to the matrix solidus", in *9th Riso Int. Symposium on Metallic and Ceramic Composites* (ed. S.I. Andersen et al), 1988, Riso National Laboratory, pp. 479-484.
14. F.J. Humphreys, "Deformation and annealing mechanisms in discontinuously reinforced metal matrix composites", *ibid*, pp. 51-74.
15. V.C. Nardone and K.M. Prew, "On the strength of discontinuously reinforced aluminium composites", *Scripta Met.*, **20**, 1986, pp. 43-48.
16. M. Taya and R.J. Arsenault, "Comparison between shear lag model and Eshelby model in predicting mechanical properties of short fibre composites", *Scripta Met.*, **21**, 1987, pp. 349-354.
17. T. Mori and K. Tanaka, "Average stresses in matrix and elastic energy of materials with misfitting inclusions", *Acta Met.*, **21**, 1973, pp. 571-574.
18. P.J. Withers, D. Juul Jensen, H. Lilholt and W.M. Stobbs, "Evaluation of internal stress in short fibre reinforced MMC by neutron diffraction", in *Proc. Sixth Int. Conf. on 'Composite Materials'*, ICCMVI (ed. by F.L. Matthews et al), vol. 2, 1987, Elsevier, London, pp. 255-263.
19. T. Christman and S. Suresh, "Microstructural development in an aluminium alloy-SiC whisker composite", *Acta Met.*, **36**, 1988, 1691-1704.
20. S.J. Harris, S.F. Moustafa and T.E. Wilks, presented at *Conf. on 'Metal Matrix Composites: Structures and Property Assessment'*, 1987, Institute of Metals, London.
21. L.M. Brown and W.M. Stobbs, "The work hardening of copper-silica, parts I and II", *Phil. Mag.*, **23**, 1971, pp. 1187-1199 and 1201-1233.
22. G.R. Cappleman, J.F. Watts and T.W. Clyne, "The interface region in squeeze infiltrated composites containing α -alumina fibre in an aluminium matrix", *J. Mater. Sci.*, **20**, 1985, pp. 2159-2168.
23. D.L. McDaniels, "Mechanical behaviour of aluminium matrix composites containing SiC reinforcement", *Metall. Trans. A*, **16**, 1985, pp. 1105-1115.
24. W.H. Runt, O. Richmond and R.D. Young, "Fracture in particle hardened materials with high volume fractions", in *Proc. Sixth Int. Conf. on 'Composite Materials'*, ICCMVI (ed. F.L. Matthews et al), vol. 2, 1987, Elsevier, London, pp. 209-233.
25. A.S. Argon, J. Im and R. Safoglu, "Cavity formation from inclusions in ductile fracture", *Met. Trans.*, **16A**, 1975, pp. 825-837.
26. H.J. Rack, T.R. Baruch and J.L. Cook, in *Proc. Fourth Int. Conf. on 'Composite Materials'*, ICCMIV (ed. T. Hayashi et al), 1982, Japanese Society for Composite Materials, Tokyo, pp. 1465-1471.
27. T.G. Nieh, "Creep rupture of a silicon carbide reinforced aluminium composite", *Met. Trans.*, **15A**, 1984, pp. 139-146.
28. H. Lilholt and M. Taya, "Creep behaviour of the metal matrix composite Al2124 with SiC fibres, in *Proc. Sixth Int. Conf. on Composite Materials*, ICCMVI (ed. F.L. Matthews et al), vol. 2, 1987, Elsevier, London, pp. 234-244.
29. M.W. Mahoney and A.K. Ghosh, "Superplasticity in high strength powder alloys with and without SiC reinforcement", *Met. Trans* **18A**, 1987, pp. 653-661.
30. S.J. Harris and T.E. Wilks, "Tensile and fatigue behaviour of alumina reinforced Al alloys at ambient and elevated temperatures", in *Fibre Reinforced Composites*, 1986, Institute of Mechanical Engineers,

London, pp. 19-28.

31. S.J. Harris and T.E. Wilks, "Fatigue crack growth in discontinuous fibre reinforced aluminium alloys", in Proc. Sixth Int. Conf. on Composite Materials, ICCMVI, vol. 2, Elsevier, London, pp. 113-126.
32. S.J. Harris, K. Dinsdale, Y. Gao and B. Noble, "Influence of heat treatment on the monotonic and fatigue properties of aluminium alloy composites", in 9th Riso Int. Symposium on Metallic and Ceramic Composites (ed. S.I. Andersen et al), 1988, Riso National Laboratory, pp. 373-382.
33. J.K. Shang and R.O. Ritchie, "Crack bridging by uncracked ligaments during fatigue-crack growth in SiC-reinforced Al-alloy composites", to be published in Met. Trans. A.
34. M.Y. Wu and O.D. Sherby, "Superplasticity in a silicon carbide whisker reinforced aluminium alloy", Scripta Met., 18, 1984, pp. 773-776.
35. S.M. Pickard and B. Derby, "Thermal cycle creep of Al/SiC particulate composite", in 9th Riso Int. Symposium on Metallic and Ceramic Composites (ed. S.I. Andersen et al), 1988, Riso National Laboratory, pp. 447-452.
36. M. Taya, "Modelling of physical properties of metallic and ceramic composites: generalised Eshelby model", ibid, pp. 201-231.

TABLE I

Values of Young's Modulus for Various Discontinuous Composites

Matrix	Fibre or particle volume fraction				
	0	0.1	0.15	0.20	0.25
Al-Si-Mg (LM25)	71.4 [26.6]*	...	84.1(a) [†] [30.4]	...	98.2(a) [34.6]
Al-4Cu	69.5	86(a)	...
Al-Cu-Mg (2014)	73.8 [26.3]	93.8(b) [‡] [33.0]
Al-Si-Mg (6061)	69.0 [25.6]	91.9(b) [33.4]
Al-Li-Mg-Cu (8090)	80.0 [31.5]	96.5(b) [37.2]

*Values given in brackets are for specific modulus, i.e. Young's modulus GPa divided by density (Mg m^{-3}).

[†] a = Al_2O_3 fibres

[‡] b = SiC particles

TABLE II

Proof Stress (PS) and Values of Ultimate Tensile Strength (UTS) for Discontinuous Composites

Material	0.2% PS MPa	0.5% PS MPa	UTS MPa	Elongation %
99.5%Al (LM0)	28	29	40	37.0
99.5%Al + Al_2O_3 ($V_f = 0.2$) as cast	75	116	142	1.1
Al-Cu-Mg 2618A (T6)	388	416	431	2.5
Al-Cu-Mg + Al_2O_3 ($V_f = 0.2$) (T6)	317	...	383	0.8
Al-4Cu (T6)	174	203	261	14.0
Al-4Cu + Al_2O_3 ($V_f = 0.2$) (T6)	264	335	384	2.2
Al-Cu-Mg 2014 (T6)	432	442	482	10.2
Al-Cu-Mg + SiC ($V_f = 0.1$) (T6)	437	461	484	6.9
Al-Si-Mg 6061 (T6)	240	-	264	12.3
Al-Si-Mg + SiC ($V_f = 0.1$) (T6)	321	-	343	3.8

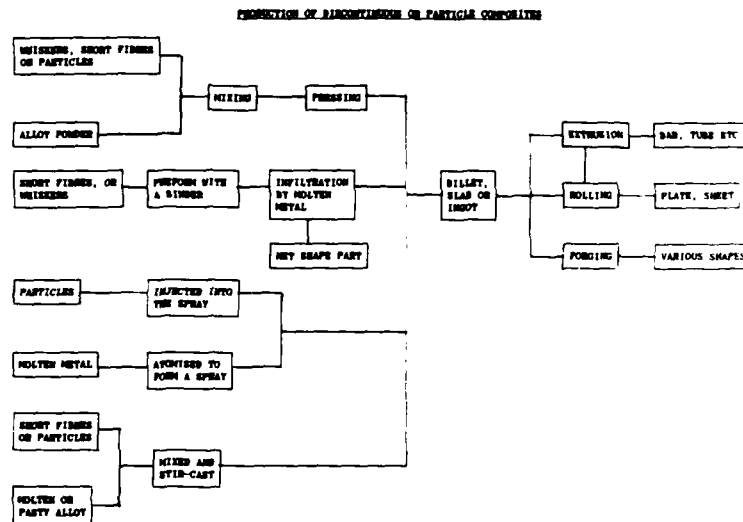


Fig. 1. Process routes for production of discontinuous fibre or particle composites (after Ref. 4).

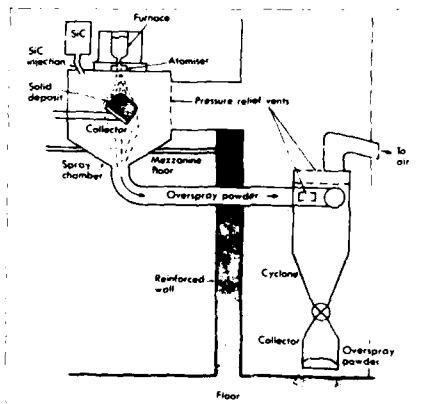


Fig. 2. Spray forming of metal matrix composites (after Ref. 7).

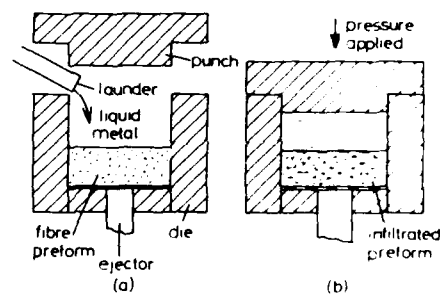


Fig. 3. Squeeze casting of composite materials using fibre preforms: (a) before casting, (b) after casting and while applying pressure (after Ref. 4).

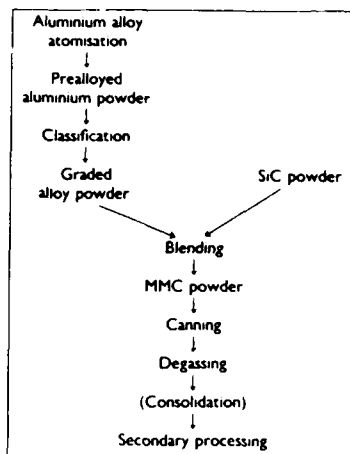


Fig. 4. Processing route for metal matrix composites using powder metallurgy technology (after Ref. 23).

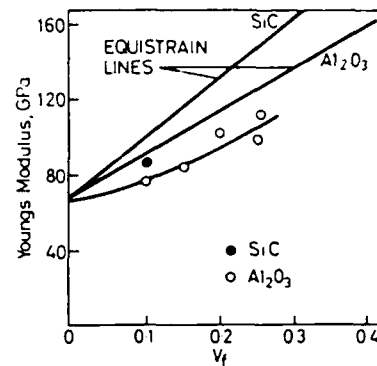


Fig. 5. Young's modulus values, E , determined on aluminium alloys reinforced with Al_2O_3 and SiC particles; comparisons are made with plots obtained from the Rule of Mixture equation which assumes equal strain in matrix and reinforcement (after Ref. 4).

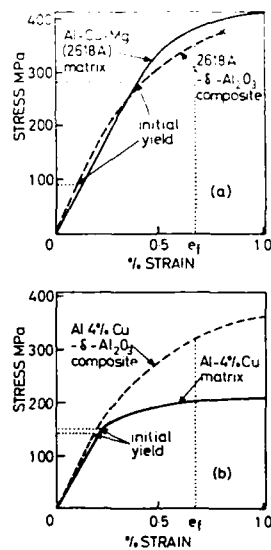


Fig. 6. Stress-strain plots for two composites and their respective unreinforced matrices, showing differences in stresses and strains where matrix starts to yield; e_f is the fibre fracture strain (after Ref. 4).

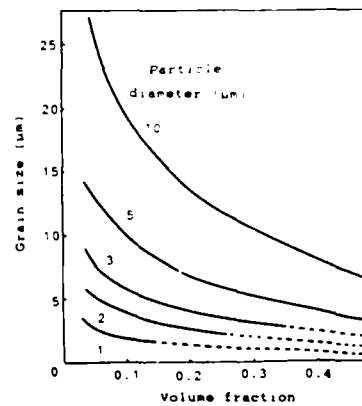


Fig. 7. Predicted recrystallised grain size as a function of particle size and volume fraction. Recrystallisation will probably not occur in the dotted regions (after Ref. 14).

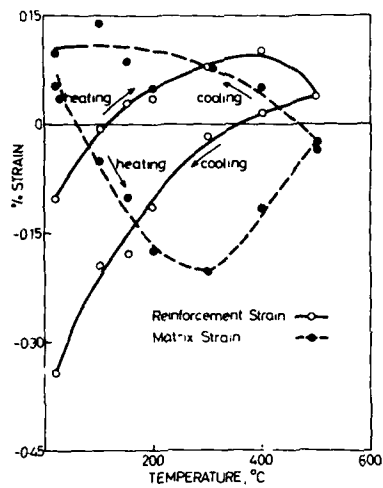


Fig. 8. Mean longitudinal strain values obtained on (a) aluminium matrix and (b) the silicon carbide whisker reinforcement during a heating and cooling cycle.

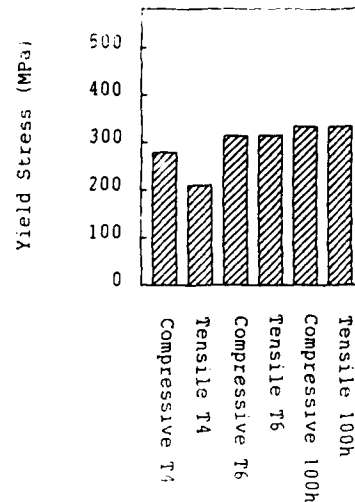


Fig. 9. Compressive and tensile yield stress in an δ - Al_2O_3 reinforced Al-4%Cu alloy after natural (T4) and artificial ageing (T6).

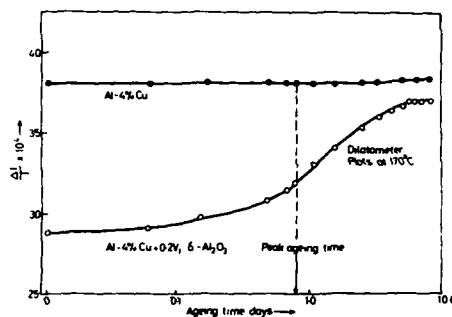


Fig. 10. Change in volume which takes place in an Al-4%Cu alloy with and without δ - Al_2O_3 short fibre reinforcement during isothermal ageing at 170°C.

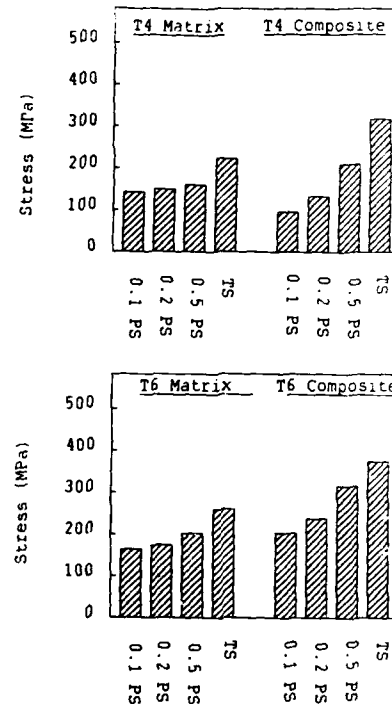


Fig. 11. Proof Stress (PS) and Tensile Strength (TS) values obtained on Al-4%Cu alloy matrix with and without δ - Al_2O_3 short fibre reinforcement after (a) Natural ageing (T4) and (b) artificial ageing at 170°C (T6).

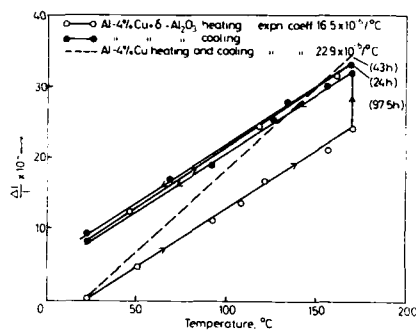


Fig. 12. Volume changes which take place in an Al-4%Cu alloy with and without δ -Al₂O₃ short fibre reinforcement. The alloy and composite have been heated to 170°C allowed to age for 100h and then cooled.

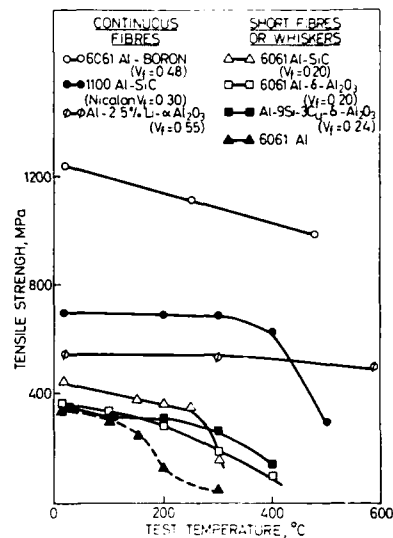


Fig. 13. Tensile strength values for continuous fibre, whisker and discontinuous alloys plotted against test temperature.

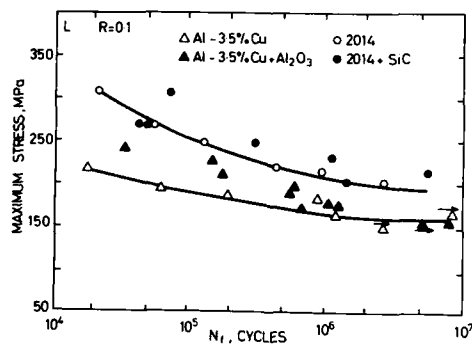


Fig. 14. S-N plots for Al-3.5%Cu alloy with and without δ -Al₂O₃ fibres and 2014 alloy with and without α -SiC particles. The alloys are in the T6 condition with the exception of reinforced 2014 where a T8 treatment was applied.

Metal Matrix Composites - A Promising Alternative to Conventional Alloys ?

K. Schulte, W. Bunk

DFVLR, Institute of Material Science

5000 Köln 90, W.-Germany

Summary

Conventional metallic materials have been tailored in the past close to their ultimate properties. New technological requirements ask for further improved materials. Metal-matrix composites (MMC) promise to reach this goal.

MMC can be described as materials whose microstructure comprise a continuous metallic phase (the matrix) into which a second phase has been artificially introduced during processing, as reinforcement. Presently the interest in MMC is primarily focused on light alloys reinforced with fibrous or particulate phases to achieve major jumps in selected mechanical properties or thermal stability. This new interest is mainly related to the fact that ceramic based reinforcement constituents became recently available, which are comparatively inexpensive. Al_2O_3 - or SiC-based fibres, whiskers and particles, but also carbon fibres are used to reinforce aluminium, magnesium or titanium matrix alloys.

1. Introduction

Metals and alloys are usefull and versatile materials which have been developed during a long time of the history of mankind to nearly perfection in their properties which are strength, toughness, deformability, thermal stability, fatigue and creep.

Various methods and mechanisms have been developed to improve metals and alloys e.g.

- solid solution strengthening
- precipitation hardening
- dispersion strengthening.

However, it seems that metals have now been developed in their major properties close to the ultimate so that a further improvement seems to remain rather limited. But still some properties gain further improvement.

In the past, mainly in the late sixties and early seventies, metal-matrix composites already attracted people and some major developments were performed. As a result, the boron fibre used as a reinforcement of aluminium was applied into the structure of the space shuttle. However, the cost of this composite was and remained extremely high. Therefore, nearly no further application is known.

In the last 10 to 15 years advances in the development of fibres, capable to withstand very high temperatures, offer the possibility of reinforcing metals. Most of the fibres presently available are based on silicon carbide and aluminiumoxide, although other variations are being studied. It is this, together with the comparatively low price, which is exiting so much interest for the reinforcement of metals.

2. Why composites with metal-matrix ?

In many technical areas extreme material properties are needed. High strength and stiffness should be combined with high temperature retention and low specific gravity. MMC can fulfill these needs. In Fig. 1 the specific strength of metals, various fibre reinforced plastics and of fibre reinforced metals is plotted vs. the specific modulus. With fibre reinforcement improved stiffness and strength can be achieved when compared to metals. If additionally a higher temperature retention is needed, then fibre reinforced plastics reach their limit at about 200°C. However, fibre reinforced metals can further be used. Their application temperature is mainly dependent on the matrix material used. Only beyond 1000°C MMC reach the maximum of their application. Higher temperatures can only be achieved if a ceramic matrix is used. In Fig. 2 is shown a comparison of the temperature up to which polymere matrix, metal matrix and ceramic matrix composites can be used [1]. In general, fibre reinforced metals can be taken into consideration for structural design [2,3] because:

- They have an improved temperature retention, when compared to the neat matrix metal.
- The high ductility and strength of the metal matrix improves the mechanical properties when compared to fibre reinforced polymers, as the interlaminar shear strength or the transverse tensile strength, as well as the fracture toughness.
- The high elastic modulus of the fibres increases the stiffness of the composite. Compared to fibre reinforced polymers the higher elastic modulus of the metal matrix leads at load levels under the matrix yield strength to a further increase in the MMC-stiffness.
- The superior physical properties as electrical and thermal conductivity or the magnetic properties are advantageous for many technical applications.
- Because of the low thermal expansion coefficient of the matrix MMC remain demension stable under temperature variations.
- They can resist environmental attack as ultra violet radiation, moisture or many chemicals. Besides, they are nearly undiffusiable for gases and liquids.

In the case of particulate reinforced composites in general no reinforcement, but an increase in fracture toughness and related properties can be achieved. The influence to improve the high temperature properties or the compressive strength seems to be rather limited. A substantial improvement is observed for the elastic modulus and the thermal expansion coefficient. However, the influence is less as in the case of fibre reinforcement and does not at all reach the values predicted with the rule of mixtures [4,5].

Positively to be mentioned is the relatively small anisotropy in the case of particulate reinforcement and the comparably uncomplicated fabrication based on casting or powder metallurgy techniques. Both, the fabrication technique and the particulates are relatively cheap, therefore the costs for a part can remain within acceptable margins. Machining of this type of composites seems to be relatively uncomplicated [6].

Besides all of these advantages MMC have some drawbacks:

Even light metals as Al, Mg or Ti - the most often used matrix materials - have a higher specific gravity as the polymers and the fabrication processes for MMC are in general more complicated and cost effective as for polymer matrix composites.

In general, the properties of MMC are dependent on the type and distribution of fibres (whiskers, short or continuous fibres) or particulates, the fibre or particle content, the orientation of fibres and the matrix alloy. The fibre/matrix bonding, what means the cohesion, wettability and chemical interaction is of further importance.

3. The composite constituents

One aim of fibre reinforcement is to increase strength. However, the theoretical strength of a metal is far higher as achieved in reality. Griffith [7] had already shown that the defect density in a compact body is the main reason why the theoretical strength values can not be achieved. From the observation, that a fibrous material has an extensively higher strength as if the same material is in a compact body - the strength is higher the thinner the fibre - he concluded that the number of defects decreases with decreasing diameter. Ibe [8] showed that in a compact body, i.e. a cube (Fig. 3a), at a given defect density the average defect free distance is essentially lower as in the case of a fibrous body of the same volume and identical defect density. The fibre diameter of 10 μm was chosen to be much smaller as the length of the cube axis of 10 mm. In the cube the distance between two defects was found to equal 1 mm, while in the fibre a defect free length of 12,73 m is calculated. This shows the relevance of fibre reinforcement.

3.1 The reinforcement fibres

The principal fibres which are currently available and of potential interest for use in MMC are listed in Table 1. The mechanical and physical properties are plotted together with the temperature stability up to which they can be used.

In the sixties boron fibres were used to reinforce aluminium alloys. The extreme high goals with respect to the mechanical properties could be reached. However, their extremely high costs reduced the applicability such, that they were only used in space-crafts. The high diameter of the boron fibres of 140 μm allows to use them only in relatively plane parts.

The high variability in the mechanical properties of carbon fibres, along with their high thermal stability, makes them to the ideal reinforcement for metals. However, the reactivity of carbon fibres with the metallic matrix very often reduces the superior fibre properties in the composite. Carbon fibres therefore generally need a protective coating, which increases fibre costs.

The ceramic non oxide SiC-fibres have, because of their low reactivity to the metal matrix, a high potential for technical application. The oxide fibres, mainly the Al_2O_3 based fibres, are already used in technical parts because they are relatively cheap, have suitable mechanical properties and their reactivity to the molten metal is low.

Three major groups of fibres can be distinguished:

1. Fibres with a diameter of about 100 to 140 μm produced by chemical vapour deposition (CVD). The most prominent of these is the extremely expensive boron-fibre. The SiC-fibres are presently successfully used to reinforced titanium alloys. These fibres carry a 20 μm core of tungsten or carbon around which boron or SiC was deposited by CVD. The fibres are stiff, difficult to handle and mainly be used as unidirectional reinforcement.
2. Fibres with a diameter of 10 - 15 μm , notably carbon and SiC, which were produced by first preparing a precursor fibre of a suitable polymer and burning this under carefully controlled conditions (pyrolyses). Similar techniques are used to produce aluminium oxide fibres from a precursor fibre consisting of a suspension of salts or oxide particles in a suitable liquid binder. It are exactly these types of fibres which found the interest of scientist for the reinforcement of metals as they are easy to handle and the fibre matrix compatibility is in most cases sufficient.

3. Whisker, fibrous single crystals with a diameter between 0,1 and 0,5 μm at a length of approximately 100 μm . They seem to be an ideal reinforcement material, as they exhibit excellent mechanical properties and can easily be processed. However, as a result of their geometry (small diameter) they are toxic with the risk of lung cancer. Therefore it is questionable if they can really be taken as an alternative reinforcement material.

From the ceramic oxide fibres the Al_2O_3 -fibres have focussed the greatest attention, while the ZrO_2 - and SiO_2 -fibres have not found the same interest. The mechanical properties of the Al_2O_3 -fibres do not reach the same values as the aforementioned, but their thermal stability and their low reactivity against the matrix materials and especially their low price have made the Al_2O_3 -fibre to the favourite reinforcement fibre for light metals.

3.2 The matrix

The main matrix materials which found attention are the light metals magnesium, aluminium and titanium. For high temperature application also nickel and cobalt as well as tungsten, molybdenum, niob or tantalum are considered (compare Table 2). At present the scientific work is mostly concentrated on aluminium and magnesium as matrix material. For the aircraft turbines also fibre reinforced titanium is of interest, to be used for compression blades. The main aim in science and technology is to increase the temperature retention of the matrix metal and being able to load it as close to the material solidus temperature (about 0,8 T_s) as possible.

The idea of MMC is to strengthen the matrix by adding a second phase, the fibres or particulates. Strengthening of the matrix can easily be achieved if continuous long fibres are used. The mechanical properties follow the rule of mixtures. However, in the case of discontinuous or particulate fibre composites the basic strengthening mechanisms which can be considered are [9]:

- High dislocation densities due to dislocation generation as a result of differences in coefficients of thermal expansion.
- Small subgrain sizes as a result of the generation of a high dislocation density.
- Residual elastic stresses.
- Differences in texture.
- Classical composites strengthening (load transfer).
- Dispersion strengthening.

The possibility of the matrix strengthening is indeed an advantage of metal matrix composites, however, it has the drawback that intensive internal stresses are build up, which have to be considered in design.

3.3 Fibre matrix compatibility

Fibre/matrix combinations are seldom in state of equilibrium; thus in most systems fibre and matrix will tend to interact usually with detrimental effects on the composite properties. The main interaction phenomena are [10]:

- Fibre dissolution in the matrix.
- Fibre dissolution and reprecipitation (coarsening processes).
- Chemical reaction between fibre and matrix.
- Segregation and/or precipitation of matrix constituents at the interface.
- Poisoning of fibres by matrix atoms.
- Thermal expansion mismatch.

Apart from the last the above phenomena are diffusion-dependent and therefore increase in importance with increasing temperature and time of exposure. Thus for most composite systems production methods are sought with as low temperatures and times as possible. Provide they survive manufacture, composites with potentially incompatible constituents can be used to certain temperature limits. To achieve a strong fibre reinforcement the fibres must be reserved to prevent extensive chemical reactions between fibre and matrix. This can mainly be achieved by coating the fibre surface. The main techniques to be used are chemical vapour deposition (CVD) and physical vapour deposition (PVD).

To achieve a strong and tough fibre reinforced material the interface also has to seek to detrimental requirements which are [11]:

- A weak interface, to achieve longitudinal strength and toughness by fibre debonding.
- Strong interface for good transverse properties.
- Further, ease of fabrication, including good wetting of the fibres if the matrix is combined in the liquid state, depends critically on interface chemistry for most economical processing methods.

The criteria to be satisfied will vary depending on the fibre, the matrix and application of the composite. There is, therefore, no given set of rules dictating chemical engineering of the interface of optimized properties. Contradictory demands have to be fulfilled what shows that interface chemistry has to be further studied.

4. Processing of metal matrix composites

4.1 Processing by liquid infiltration

The most sufficient processing techniques of metal matrix composites are various casting techniques. In general, a preform is infiltrated by the molten metal. The processing occurs at high temperatures with the risk of chemical reactions. In Table 3 the chemical compatibility of various metal matrices to SiC-fibres is shown dependent on temperature [1]. To avoid for example the reaction of aluminium with carbon fibres it is necessary to put a protective coating around the carbon fibre, as the melting temperature of the aluminium is above the reaction temperature of the carbon fibre with aluminium. Using SiC-fibres as reinforcement the reaction to aluminium can be expected above the melting temperature (T_s). From that point of view a coating seems not to be necessary. However, it could become necessary because of improving the wetting conditions. If no coating is performed to increase the wettability then a high defect density within the reaction zone can drastically reduce the composite strength. It is extremely disadvantageous when between opposing fibres brittle reactive products are present, so matrix material can not float into the vacancy to fully surround the fibres. Crack propagation would preferably occur in such areas. It is also possible, that an increasing amount of matrix precipitates conglomerates at the fibre/matrix boundary, which locally leads to an embrittlement. Also the dissolution of fibres in the matrix or the diffusion of matrix atoms into the fibre can become a problem and reduce the composite properties. Furtheron, and not less important is the existence of internal thermal stresses, after cooling down from the melt which are produced because of differences in the thermal expansion coefficients of the matrix metal and the fibres.

To produce composites in the liquid matrix state various methods are used:

- continuous infiltration
- vacuum infiltration
- various casting techniques, from which squeeze casting is the most prominent. It is schematically shown in Fig. 4.

Figure 5 shows a SiC/Al-composite where the SiC-whisker and -particulate coated Tyranno fibre is used to achieve a good wettability and an appropriate distance between the fibres.

4.2 Processing by diffusion bonding

To avoid chemical reactions between the fibre and the matrix low temperatures are needed for processing. This can occur only by diffusion bonding in the solid state of the matrix material. This technique is schematically shown in Fig. 6 [12]. The matrix metal being present in the form of foils or powder is compacted together with the reinforcement fibres under high pressure and at a temperature which is below the solidus temperature of the matrix. But even at the low temperatures of this processing technique reactions in the fibre matrix boundary can occur. Therefore, it is suitable to coat the reinforcement fibres, especially if the combination carbon fibre to aluminium or magnesium matrix is used. Figure 7 is a transmission electron micrograph of a composite with SiC-fibre (AVCO)/Ti6Al4V-matrix, where the fibre has a protective coating, to avoid chemical fibre/matrix reactions [13]. Different diffusion bonding techniques are the foil plating by coldrolling, explosion welding, hotpressing and hotisostatic pressing (HIP). In all these cases the matrix material is used in the form of foils. Figure 8 is a light micrograph of a SiC/Ti-composite which has been produced by hotisostatic pressing [14].

It is also possible that the composite material is available in the form of prepregs. Prepregs are the reinforcement fibres which are parallel orientated and already have a sufficient coating of the matrix material. The consolidation has not yet taken place, but occurs in a following hotpressing or hotisostatic pressing process. The prepregs are produced by four different routes, where the spreaded fibre strands are coated either by CVD or PVD processes, plasma spraying or continuous liquid infiltration. The prepregs presently available are produced by CVD (carbon fibre/aluminium) and plasma spraying (SiC/aluminium). Using prepregs has the advantage, that similar as with fibre reinforced polymers, plies of fibres, each in a different direction, can be stacked up to form a laminate. The laminate stacking sequence can be chosen due to the expected loading.

It is further possible that the matrix material is available in form of a powder. The preparation of metal matrix composites using the PM-techniques offers several advantages. Some of these are [15]:

1. Lower temperatures can be used during preparation of a PM-based composite compared to preparation of a fusion metallurgy-based composite. The result is less interaction between the matrix and the reinforcement.
2. The preparation of particulate or whisker reinforced composites is, generally speaking easier using PM blending techniques than it is, using casting techniques.
3. PM-based metal matrix composites are mainly reinforced by particulates or whiskers. The main processing techniques are either hotisostatic pressing or extrusion. They can be produced close to the final shape.

4.3 In-situ-processing, directionally solidified eutectic alloys

The formation of a composite material by directional solidification of an alloy allows to produce simultaneously the fibre and the matrix from liquid state of the metal. The two phases can only be formed separately if an equilibrium state in the melt exists.

Then a linked growth of those phases can occur. This can be made with eutectic alloys. A typical phase diagram is shown in Fig. 9. The simultaneous solidification of both phases allows to produce a material which has a regular distribution of both phases. Figure 10a schematically shows an equipment to produce a directionally solidified material. Figure 10b shows a scanning electron micrograph of an eutectic nickel based superalloy with TaC-fibres [16]. Directionally solidification gives a structure a higher temperature retention. Problems with wetting, chemical and physical reactions between the fibre and matrix, which can occur if the previous techniques are used, are of no immediate importance. However, the formulation of the alloy and the fibre volume content can not freely be chosen. The superior fatigue properties, especially at high temperatures (compare Fig. 11 [17]), is accompanied by an only moderate thermal fatigue behaviour. In general, the properties are strongly dependent on the test conditions. Three different aspects were observed for the 73C-alloy investigated:

- Transformation of a carbide $\text{Cr}_7\text{C}_3 \rightarrow \text{Cr}_{23}\text{C}_6$,
- spheroidizing of fibre ends
- a remaining constant strain (ratcheting).

The last effect has always to be expected in the case of two phases having different thermal coefficients of extension, where one of the two phases plastically extends more within a temperature cycle than the other. F.D. Lemkey et.al [18] rated the potential of directionally solidified eutectic alloys positive when compared to single crystals. The main reason why directionally solidified eutectic superalloys have not yet been used in series production, i.e. for turbine blades, the relatively low solidification rates. Because of its promising properties this class of "natural" alloys remains of further interest in materials science.

4.4 A general statement

The production costs of metal matrix composites seem to remain relatively high, especially if techniques with continuous fibres as reinforcement are used. Only in the case of short fibre reinforcements, whiskers or particulates an economical production might be possible. The casting techniques seem to be most promising.

5. Properties

The superior specific properties of metal matrix composites can then fully be utilized, if the conventional alloys come close to their ultimate. In the late sixties and early seventies it was expected that boron fibre reinforced aluminium would be used for light weight structures, because it has a high strength and stiffness in combination with a comparatively low weight. With the development of carbon fibre reinforced polymers a material is now available which has a higher specific strength combined with a high specific stiffness but at less costs. However, if polymer matrix composites are used the temperature retention is relatively low. Therefore, the main application of metal matrix composites will lie in those areas where high temperature retention is necessary. In Fig. 12 [19] the specific strength is plotted vs. the temperature for a high strength aluminium alloy used in aircraft structures together with a conventional titanium alloy. The development targets in Japan for the high temperature application of fibre reinforced metals and fibre reinforced plastics are additionally shown. Besides these aims the diagram shows, that fibre reinforced metals are superior to fibre reinforced plastics at temperatures above 200°C. The advantage of a fibre reinforcement compared to a non reinforcement can additionally be seen.

For a comparison the mechanical properties of some matrix alloys are shown in Table 4. In Table 5 the mechanical properties of fibre reinforced metals are summarized. In general the mechanical properties vary because of:

- different types of fibres
- different processing techniques
- differences in fibre volume content
- fibre orientation
- fibre length (whisker or continuous fibres)
- various matrix alloys
- test temperature.

It is difficult to give a full overview about the mechanical properties. In Table 5 are therefore summarized some data of unidirectionally reinforced metals which are loaded in fibre direction and transverse to the fibre direction. Fibre reinforcement increases the tensile strength and the elastic modulus. If loaded in fibre direction the properties are dominated by the fibres. However, in the transverse direction the properties are dominated by the matrix alloy. The influence of the fibre orientation to the tensile strength is shown in Fig. 13a [20]. The results show that fibre reinforcement leads to a unisotropy in the mechanical properties. Also the fatigue properties are improved by fibre reinforcement. Fig. 13b [21] demonstrates that the reinforcement with long fibres improves the fatigue properties. However, this improvement is not maintained into the high cycle regime, because of fibre-matrix debonding. Fig. 13b also shows, that the reinforcement with particulates does not necessarily improve the fatigue properties. One important property of fibre reinforced metals is their high wear resistance. Fig. 13c [22] shows the strong reduction of the wear rate when compared to conventional alloys if SiC-whisker reinforced aluminium is used. However, this extremely good wear behaviour can not always fully be utilized in a composite structure, because the wear counterpart has carefully to be chosen as the composite is strongly abrasive. The superior temperature retention of MMC is shown in Fig. 13d [23]. While reinforced aluminium shows with increasing temperature a pronounced decrease in tensile strength, in the continuous fibre reinforced aluminium only a minor reduction in tensile strength is observed.

For the mechanical properties of metal matrix composites the following conclusion can be drawn:

The Young's modulus of the matrix alloy increases significantly by the addition of fibres, whiskers or particulates. Both fibres and particulates promote changes in the precipitation kinetics. The yield stress and tensile strength of the composite are increased significantly above those of the matrix. However, the elongation to failure is reduced by the reinforcement. Fatigue and wear properties can be improved in MMC.

5. Conclusion

The reinforcement of metallic alloys with fibres particulates or whiskers broadens the useability of metallic alloys. It is especially interesting in those cases where extreme properties are needed, i.e. light weight, high temperature retention, high demension stability and good wear properties. MMC are advantageous for all this purposes. They will therefore find the application where their superior properties are needed, regardless their high costs. We can therefore now ask the question: are metal matrix composites a promising alternative to conventional alloys? We get an improvement in some material properties, however, the fracture toughness decreases dramatically and also the ductility is reduced when compared to the pure matrix metal. This means that in most applications fibre reinforced metals can not be an alternative to conventional alloys. They will only be used there, where the conventional metals have reached their

ultimate and further improvement is needed. Processing of metal matrix composites seems in the next future not to be as cheap as processing of unreinforced metals. Therefore, also this problem has to be solved.

One of the superior properties of metal matrix composites is their high temperature retention. In a first view, when only compared to the pure metal MMC seems to be a good solution for future development and application. However, one has to take into account, that polymers are currently under development with a temperature stability up to 400°C. That means, that fibre reinforced polymers will compete for the substitution of metals.

The chemical reaction between fibre and matrix during processing or high temperature application has yet not being solved in all cases. Furtheron, the wetting conditions of the fibres especially during cast processing, and the not finally answered question, do we need a strong or a weak bond, needs further work on the boundary and fibre surface coating problems. It therefore seems, that the final conclusion about the future of metal matrix composites can only be:

1. Metal matrix composites have a future for potential application.
2. They can substitute the conventional alloys only in those cases, where there specific properties are superior to conventional metals.
3. Metal matrix composites are in general too high in cost. This means, that cheaper processing techniques have to be developed. The availability of cheaper reinforcement fibres seems also to be necessary.
4. Fibre reinforced metals have a great potential and variability in their properties. However, to realize the properties in a part or a structure further development work has to be done. Fibre reinforced metals are therefore extremely interesting for scientific work. Their economic success still lies in the future.

6. Acknowledgements

The authors give their gratitude to the colleagues Dr. Dudek and Dr. Fritscher for helping preparing the manuskript.

7. Literature

- [1] Majidi, A.P.: Processing and properties of metal matrix composites. Workshop: Application of composite materials to industrial products, Center of Composite Materials, University of Delaware, USA, April 30, 1987.
- [2] Chou, T.W., Kelly, A., Okura, A.: Fiber-reinforced metal-matrix composites. Composites 16 (1985), pp.187-195.
- [3] Stöckel, D.: Faserverbundwerkstoffe, in: Metallische Verbundwerkstoffe, Festschrift zum 100jährigen Bestehen der Firma G. Rau, Pforzheim, 1977, pp.132-187.
- [4] McElman, J.A., Mittnick, M.A.: Continuous silicon carbide metal matrix composites. Proceedings: Advancing with composites, Int. Conf. on Comp. Mat., May 10-12, 1988, Milan, Italy, pp.177-229.

- [5] Bayoumi, M.A., Suéry, M.: Structure and mechanical properties of SiC-particle reinforced aluminium alloy composites. Proceedings: ICCM-VI and ECCM-2, Vol.2, 20-24 July, 1987, London, England, pp.2.481-2.490.
- [6] DURAL-MMC, Druckschrift der Firma Dural Aluminium Composites Corporation, San Diego, Ca., USA, 1987.
- [7] Griffith, A.A.: The phenomena of rupture and flow in solids. Phil. Trans. Roy. Soc. London A221 (1921), pp.163-198.
- [8] Ibe, G., Penkava, J.: Entwicklung faserverstärkter Aluminiumwerkstoffe. Metall 41 (1987), pp.590-600.
- [9] Arsenault, R.J.: The strengthening mechanisms in discontinuous SiC/Al composites. In: Mechanical and Physical Behaviour of Metallic and Ceramic Composites. Proceedings 9th Riso International Symposium on Metallurgy and Materials Science, 5.-9. Sept. 1988, pp.279-284.
- [10] Warren, R.: Metal Matrix Composites for High Temperature Structural Application: In: Mechanical and Physical Behaviour of Metallic and Ceramic Composites. Proceedings 9th Riso International Symposium on Metallurgy and Materials Science, 5.-9. Sept. 1988, pp.233-255.
- [11] Mortensen, A.: Interface chemistry of inorganic composite materials. In: Mechanical and Physical Behaviour of Metallic and Ceramic Composites. Proceedings 9th Riso International Symposium on Metallurgy and Materials Science, 5.-9. Sept. 1988, pp.141-155.
- [12] Lewis, C.F.: The exciting promise of metal-matrix composites. Materials Engineering (1986), pp.33-37.
- [13] Dudek, H.J.: Interface analysis in metal matrix composites. Fresenius' Z. Analytische Chemie, in press.
- [14] Leucht, R., Dudek, H.J., Ziegler, G.: SiC-faserverstärkte Titanlegierung Ti6Al4V. Z. Werkstofftechnik 18 (1987), pp.27-37.
- [15] Erich, D.L.: Metal Matrix Composites: Problems, Applications and Potential in the PM Industry, MPR 1988, pp.418-423.
- [16] Staniek, G.: Gefügestabilität von gerichtet erstarrten Eutektika. In: Verbundwerkstoffe mit Metallmatrix, Deutsche Gesellschaft für Metallkunde, Oberursel (1979), pp.54-74.
- [17] Sahm, P.R., Hildebrandt, U.W.: Gerichtet erstarrte eutektische Superlegierungen für stationäre Gasturbinen. BMFT-NTS 37, May 1978.
- [18] Lemkey, F.D., Thompson, E.R.: COST 50/501 Conference, 6.-9. Oct. 1986, Liege, Belgium.
- [19] Hayashi, T.: Recent research and development, future problems and trends in advanced composite materials in Japan. Sadhana 11 (1987), pp.299-325.
- [20] Shetty, H.R., Chou, T.W.: Mechanical properties and fibre characteristics of FP/Aluminum and W/Aluminum composites. Metallurgical Transactions 16A (1985), pp.853-864.

- [21] Harris, S.J., Dinsdale K., Gao Y., Noble B.: Influence of heat treatment of the monotonic and fatigue properties of aluminium alloy composites. In: Mechanical and Physical Behaviour of Metallic and Ceramic Composites. Proceedings 9th Riss International Symposium on Metallurgy and Materials Science, 5.-9. Sept. 1988, pp.373-382.
- [22] Ohira, K., Watanabe, H., Takeuchi, Y.: Silicon carbide whisker reinforced aluminium composites - fabrication and properties, Mat. Science and Technology 3 (1987), pp.57-60.
- [23] G. Wirth: Einführung in die Herstellungstechnologie, die Eigenschaften und die Einsatzmöglichkeiten von Verbundwerkstoffen mit Metallmatrix. In: Verbundwerkstoffe mit Metallmatrix, Deutsche Gesellschaft für Metallkunde, Oberursel (1979), pp.2-33.

Tables:

Table 1: Mechanical properties of various types of fibres.

Fibre-type	Trade	Supplier	Density [g/cm ³]	Diameter [μm]	Tensile strength [N/mm ²]	Elastic Modulus [N/mm ²]	Specific Strength [km]	Specific Modulus [km]	Strain to failure [%]	α * (10 ⁻⁶ K ⁻¹)	Maximum use of Temperature [°C]
Bor	Avco-Boron	AVCO	2,27	140	3500	400	148	16900	1		2000
C-Fibre	T300	Toray	1,75	7	3430	230	200	13000	1,5	-1,5	500 ⁺
	T800	Toray	1,8	5,5	5500	294	305	16300	1,9	-1,5	600 ⁺
	P100	Union Carbide	2,05	10	2200	724	102	33600	0,31	-1,6	600 ⁺
SiC	SCS-6	AVCO	3,05	140	3400	400	110	1160	1	1,5	600
	SIGMA	Berghof	3,5	100	3600	420	103	1200	1	4,5	600
	NICALON	Nippon-Carbon	2,55	15	2800	180	110	7200	1,5	3,1	1100
	Tyranno	Ube	2,4	10	2800	200	120	8000	1,5	3,1	1200
SiC Whisker	Tokamax	Tokai-Carbon	3,17	~ 0,5	3000-14000	400-700				0,4 - 4,0	
α -Al ₂ O ₃	FP	Du Pont	3,9	20	1500	380	38,5	9740		6,4	1000
δ -Al ₂ O ₃	Saffil	ICI	3,3	3	2000	300	60,6	9090		8	1000

* α = coefficient thermal extension

⁺ in oxide Atmosphere

Table 2: Matrix metals for MMC.

	Density [g/cm ³]	Melting point [°C]
- Low Density Metals		
Aluminium	2,7	660
Magnesium	1,8	650
Titan	4,6	1660
- High Melting Point Metals		
Nickel	8,9	1453
Superalloys	~ 8	~ 1400

Table 3: Chemical compatibility between SiC-fibres and various matrix metals, after A.P. Majidi [1].

	Sintering temperature (°C)											
	450	530	620	650	750	800	830	900	950	1000	1100	1200
Al	○	○	○									
Ag				○	○	○	○	○				
Cu					○	○	○	○	○	○		
Ni					○	○	○	○		○	×	×
Co					○	○	○	○		△	△	×
Fe					○	○	○	○		○	○	△
Ti					△			△		△	△	△
Cr								○		○	△	△
Mo						○		○		○	○	○

○: No reaction, △: Reaction layer and/or edge roughening.
 ×: Filament vanished. Observed with optical microscope (×1000).

Table 4: Mechanical properties of various matrix metals.

Alloy	Density [g/cm ³]	Tensile strength [N/mm ²]	Elastic-Modulus [GPa]	Fracture strain [%]
AL				
1100	2,71	90	69	45
2024	2,77	340	73	20
6061	2,71	310	69	16
7075	2,8	450	72	8
Mg				
AZ 63A	1,82	230	45	5
Ti				
Ti6Al4V	4,6	990	119	26

Table 5: Mechanical properties of some selected metal matrix composites at RT:

- a) unidirectional strength, in fibre direction,
 b) transverse tensile strength, normal to fibre direction.

a) Unidirectional, in fibre direction

	MMC	Density [g/cm ³]	Fibre volume content	Tensile strength [N/mm ²]	Elastic-Modulus [GPa]	Fracture strain [%]
0°	B/Al	2,5	48	1220	247	0,5
	B/Ti	3,5	50	962	210	
	C+Al	2,1	70	1250	250	0,5
	C/Mg	1,7	70	1350	150	0,9
	C/Cu	5,2	52	1100	140	0,8
	FP/Al	3,2	50	570	200	
	FP/Mg	2,8	50	520	200	0,3

b) Unidirectional, transverse fibre direction

90°	B/Al	2,5	48	150		
	B/Ti	3,5	50	408	195	
	FP/Al	3,2	50	140	150	
	FP/Mg	2,8	50	70	100	0,24

Figures:

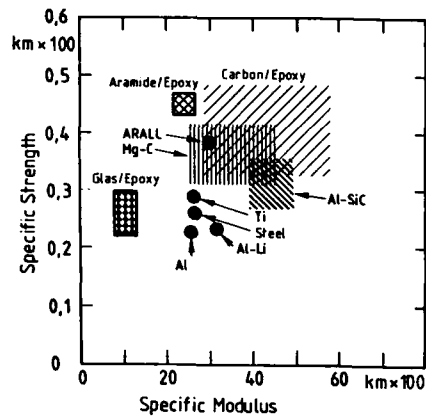


Fig. 1: Specific properties of various quasi isotropic fibre reinforced composites compared to selected metallic materials.

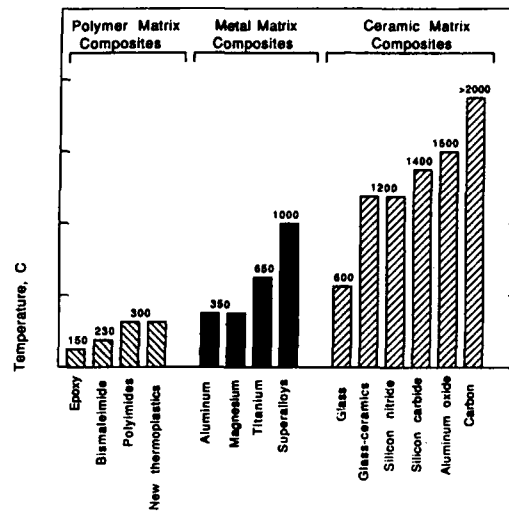


Fig. 2: Maximum service temperatures of various polymer-, metal- and ceramic-matrix composites (after A.P. Majidi [1]).

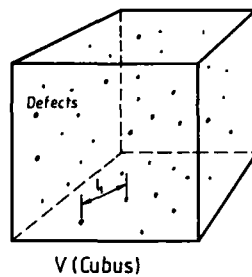


Fig. 3a: Distance and distribution of defects in a bulk volume (cube) at a given defect density (schematically, after G. Ibe et al. [8]).

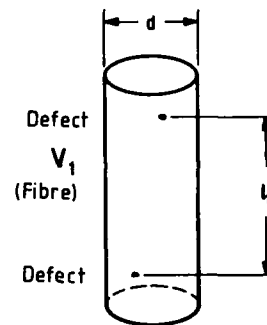


Fig. 3b: Defect distance in a fibrous volume at the same defect density as in Fig. 3a (schematically, after G. Ibe et al. [8]).

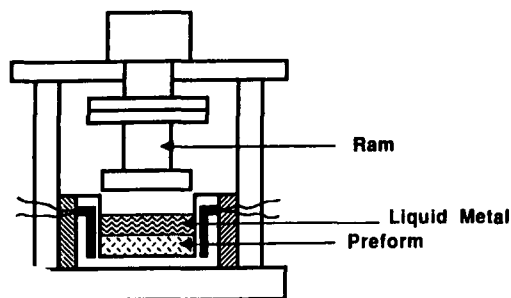


Fig. 4: Squeeze casting (schematically, after A.P. Majidi [1]).

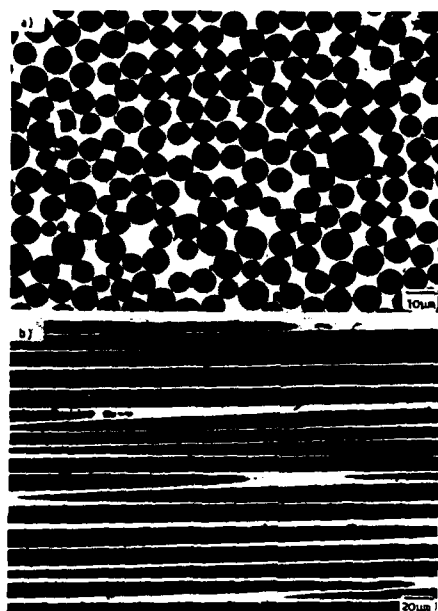


Fig. 5: Lightmicroscopy. Microstructure of a SiC-fibre (Tyranno)/aluminium composite;
a) Transverse to fibre direction,
b) normal to fibre direction.

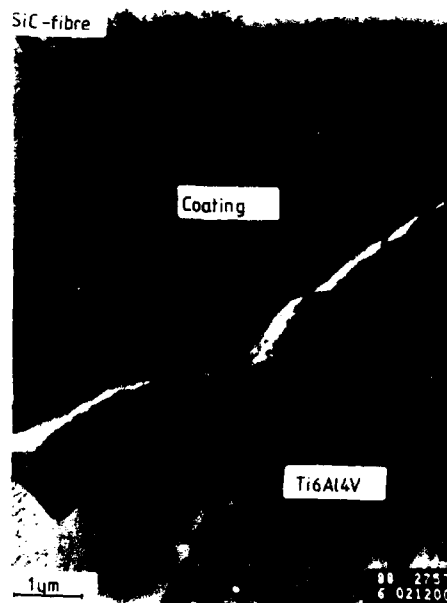


Fig. 7: Transmission electron micrograph of a fibre/matrix boundary. Fibre coating by CVD [13].

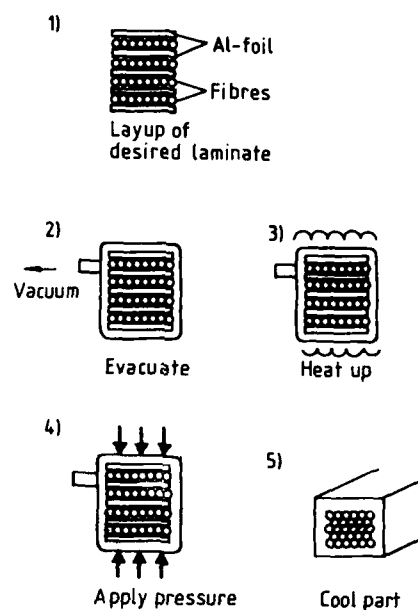


Fig. 6: Processing of boron-fibre/aluminium by hot pressing and diffusion bonding (schematically, after C.F. Lewis [12]).



Fig. 8: Scanning electron micrograph of a hot isostatically pressed SiC/Ti-composite [14].

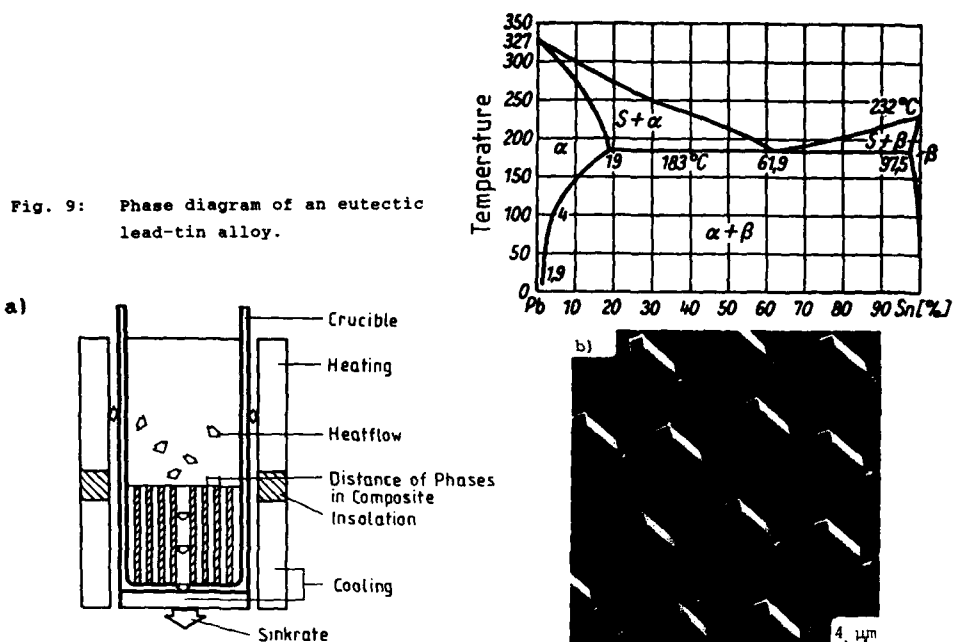


Fig. 10a: Equipment for a directionally solidified eutectic alloy (schematically after D. Stöckel [3]).

Fig. 10b: Directionally solidified eutectic Ni-alloy with TaC-fibres (scanning electron micrograph after chemical etching of the matrix [16]).

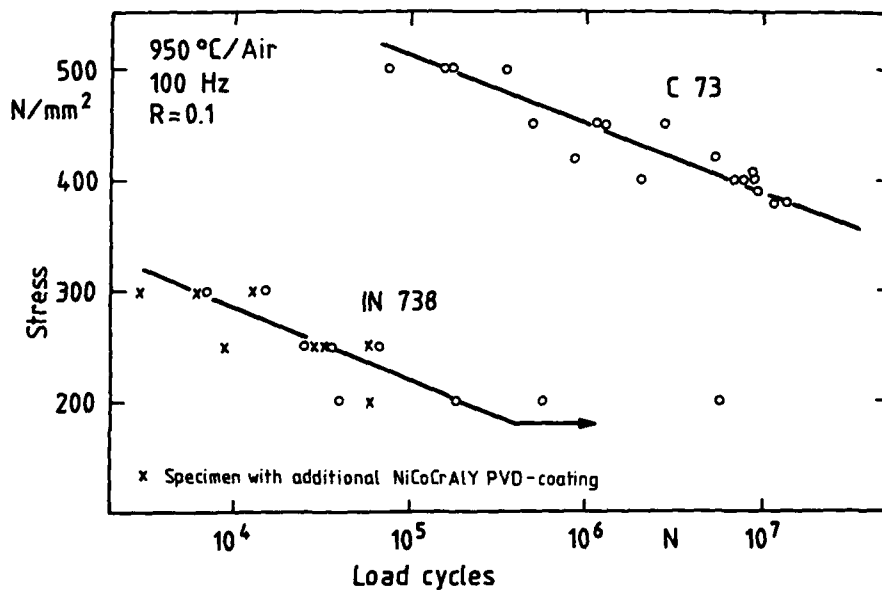


Fig. 11: Fatigue behaviour of the directionally solidified eutectic alloy 73C (Co-39Cr-2Al-2.2C in wt.%) and single crystalline super alloy IN 738 LC, after P.R. Sahm [17].

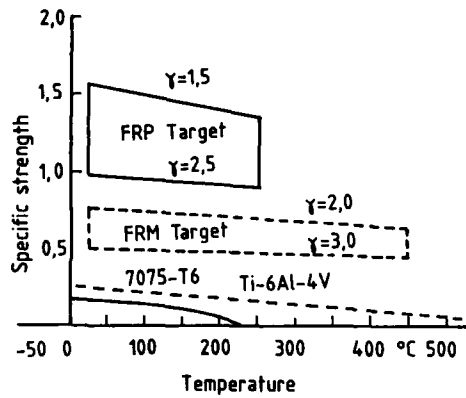


Fig. 12: Specific tensile strength versus temperature for various fibre reinforced composites, after T. Hayashi [19].

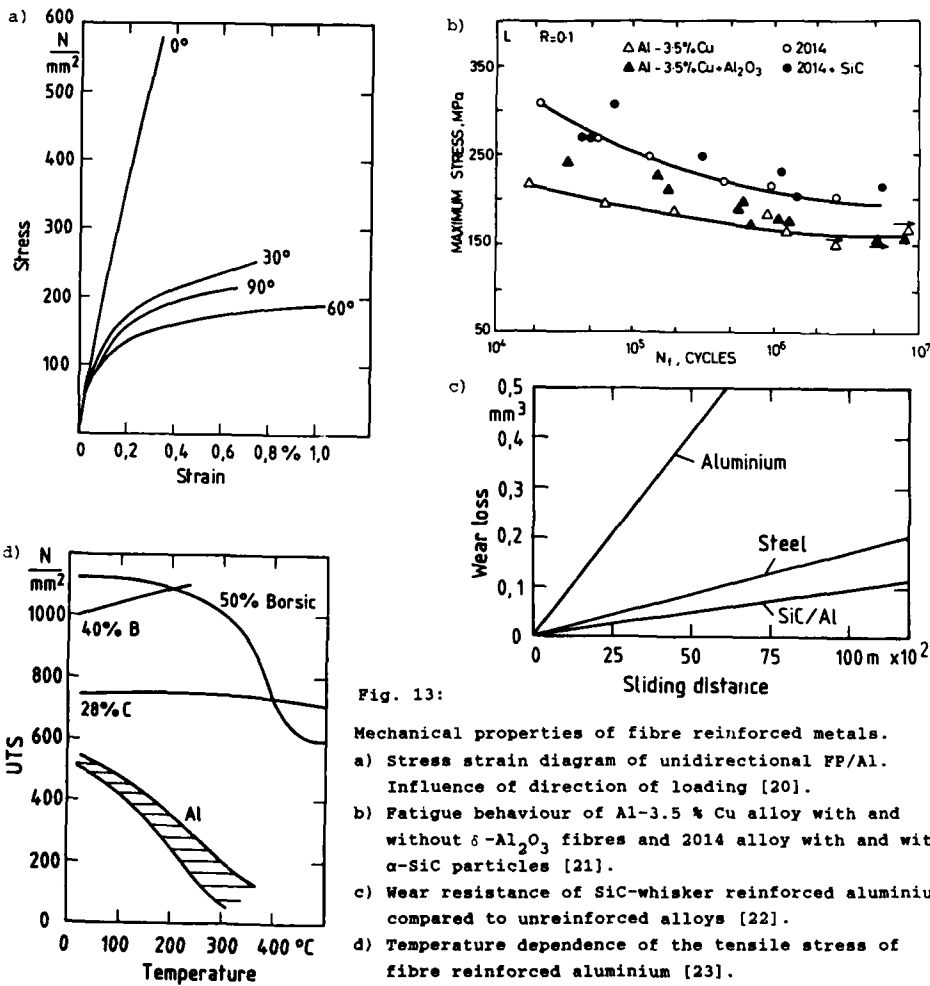


Fig. 13:

Mechanical properties of fibre reinforced metals.

- Stress strain diagram of unidirectional FP/Al. Influence of direction of loading [20].
- Fatigue behaviour of Al-3.5 % Cu alloy with and without δ - Al_2O_3 fibres and 2014 alloy with and without α -SiC particles [21].
- Wear resistance of SiC-whisker reinforced aluminium compared to unreinforced alloys [22].
- Temperature dependence of the tensile stress of fibre reinforced aluminium [23].

MAGNESIUM ALLOY TECHNOLOGY FOR AEROSPACE APPLICATIONS

by
D J Bray
Materials and Structures Department
Royal Aerospace Establishment
Farnborough
Hampshire GU14 6TD UK

SUMMARY

Recent developments in magnesium alloy technology for aerospace applications are reviewed. Most of the current requirements are met by cast alloys and two new alloys have been introduced; WE54 for high temperature applications up to 300°C, and high purity AZ91 with improved corrosion resistance. Improvements in casting technology permit the manufacture of more complex castings with wall thicknesses as low as 3.5 mm. A new polyimide coating has been developed for gearbox casings which resists attack by lubricating oils at temperatures over 200°C. Rapidly solidified magnesium alloys are at an early stage of development, but their potential is illustrated by the improvements in mechanical properties and corrosion resistance which have been obtained. The new rapidly solidified alloy EA55RS is reported to have a 0.2% proof stress of 435 MPa, a UTS of 472 MPa, 13% elongation and a corrosion rate in salt spray of 8 mils/year.

1 INTRODUCTION

The low density of magnesium alloys, about two thirds that of aluminium alloys, makes them attractive to the aerospace industry as weight saving materials. Most of the current applications for magnesium alloys in aerospace are in sand castings; typically in gearbox cases, cockpit canopy frames, under-carriage wheels and engine compressor housings¹. There are a few components which are forged, including some undercarriage wheels, but magnesium alloy sheet and extrusions are not used.

In the 1950s and 1960s the use of magnesium alloys in airframes and missiles was more widespread². For example, thin sheet was used for fuselage and wing skins, and extrusions were used in cabin floors and missile bodies. However, corrosion problems were often encountered and, although in some cases they could have been avoided if the correct precautions had been taken, the use of magnesium alloys in these applications was discontinued.

The specific strengths of wrought magnesium alloys are not as great as those of wrought aluminium alloys. Nevertheless, because of their low density, weight savings can still be made by using magnesium alloys in regions where minimum thickness is the design criteria or where buckling resistance is required at low to moderate loads³. In certain cases, magnesium alloys were chosen on technical grounds, but because of the fall in demand during the 1960s, small quantities could not be obtained economically and aluminium alloys had to be used instead³. More often, however, concern about their corrosion resistance has limited their wider use.

The inherent corrosion resistance of magnesium alloys is not as good as that of aluminium alloys⁴. A passivating film of magnesium hydroxide provides only partial protection and is rapidly attacked in acidic and salt water environments. Furthermore, the high negative electrode potential of magnesium alloys makes them susceptible to galvanic attack when they are in contact with more noble metals, and this has been the principal cause of corrosion of magnesium alloys in aircraft structures.

Therefore, it is essential that magnesium alloys are fully protected against corrosion^{5,6}. In the United Kingdom, the rules governing the protection of magnesium alloys in aircraft are set out in specification DTD 911C⁷. Briefly, the component is first cleaned by fluoride anodising, then chromate treated and finally the surface is sealed with resin. To prevent galvanic corrosion, wet assembly techniques are used with approved jointing compounds and joints are designed to avoid water entrapment. Even with these precautions, the current use of magnesium alloys is generally restricted to more massive components which can be inspected easily.

2 CASTING ALLOYS

The casting alloys currently used in aerospace applications fall into two groups^{8,9}. The main requirements are met by a range of alloys containing rare earth metals or thorium, which are grain refined with zirconium. These alloys have excellent casting properties and they can be welded easily. A low melting point eutectic at the grain boundaries suppresses microporosity during solidification and any porosity which does form is parallel to the surface, so that castings are pressure tight.

Alloys in this group include ZE41 and ZH62. These are medium strength alloys which retain their properties to about 150°C. ZE41 is the most common sand casting magnesium alloy, and is used in gearbox castings and cockpit canopy frames. EZ33 and HZ32 have lower room temperature strength but have good creep strength up to 250°C and 350°C respectively. The tensile properties of Mg-RE-Zr alloys are increased by the addition of silver; QE22 and QE21 are high strength magnesium alloys containing silver which are used in applications up to 200°C. The composition and tensile properties of these alloys are shown in Table 1.

A hydriding process can be used to increase the tensile properties of the Mg-Zn-RE-Zr alloys. The alloy is solution treated in a hydrogen atmosphere so that the rare earths in the eutectic phase are converted into rare earth hydrides and the zinc diffuses into the grains where it forms a strengthening precipitate on subsequent heat treatment. The alloys are easily cast and welded prior to hydriding. ZE63 has been used in thrust reversers, but its application is limited to castings with fairly thin sections.

because of the slow penetration rate of the hydrogen (6-10 mm in 24 h at 480°C and 1 atm). The time required can be approximately halved if a pressure of 2.5 atm is used⁹.

As the operating temperatures of engines become hotter, magnesium alloys with improved elevated temperature properties are needed. A new alloy, WE54, containing yttrium, has been developed by Magnesium Elektron Ltd to meet this requirement^{8,10}. The nominal composition is 5.25% Y, 3.5% rare earths and 0.4-0.5% Zr (all compositions are given in wt %). Pure yttrium is expensive and to reduce the cost, a mixture containing 75% Y and 25% rare earths is added. The alloy can be age hardened; the optimum properties being produced by solution treating for eight hours at 525°C, quenching and then aging for 16 hours at 250°C.

At room temperature, the 0.2% proof stress and the tensile stress of WE54 are reported to be slightly higher than those of QE22 (Figure 1), but WE54 is more stable for short times up to 300°C (Figure 2). Its tensile properties after 1000 hours at 250°C are also better than the silver containing alloys (Figure 3), as are its creep properties; the stress to reach 0.2% strain in 1000 hours at 250°C is reported to be typically 35 MPa, about double that of QE22⁸.

WE54 is weldable and it can be cast more easily than the silver containing alloys¹⁰. The addition of yttrium has also improved the corrosion resistance of WE54 in comparison with other magnesium alloys¹¹ (Figure 4), but the correct procedures must still be followed where it is in contact with other metals to prevent galvanic corrosion.

The second group of casting alloys used in aerospace are the Mg-Al-Zn alloys⁸; the most common being AZ91, which contains typically 9% Al and 0.5% Zn. These alloys are used in only a few applications. They are less expensive than the zirconium containing alloys, but they are more difficult to cast; microshrinkage occurs and, consequently, sand castings are not pressure tight. Their yield strengths are not as high as the zirconium containing alloys and they are only stable to about 120°C.

Recently, a high purity version of AZ91, designated AZ91E, has been developed by the Dow Chemical Co and AMAX Magnesium¹². The alloy contains very low levels of iron, nickel and copper, which are known to have an adverse effect on the corrosion rate of magnesium alloys¹³. These elements are insoluble in magnesium and they have more positive electrode potentials. Therefore they form particles which act as sites for cathodic reactions and so increase the general corrosion rate. In AZ91E, these sites have been removed and consequently the corrosion rate is reduced.

The tolerance limit of each element was defined¹⁴, resulting in the following specification: Fe 0.005% max, Ni 0.001% max and Cu 0.03% max. A minimum of 0.15% Mn is also added to control the tolerance level of iron. The corrosion rate of AZ91E is reported to be about a hundred times lower than that of standard AZ91C in salt water environments¹¹ (Figure 5). These improvements have been obtained in gravity and pressure die castings, but care must be taken to ensure that there is no iron pick-up from steel casting equipment, otherwise the benefits are lost¹⁵. Increasing the alloy purity has no effect on galvanic corrosion; a protective coating would still be needed for AZ91E in aircraft applications and the correct precautions would have to be taken to avoid galvanic corrosion.

3 DEVELOPMENTS IN CASTING TECHNIQUES

Fluxless melting has been used in die casting for some time, but its introduction to sand casting, where metal temperatures are higher, is more recent. Instead of using a flux, based on alkali and alkali earth halides, a protective atmosphere of air, argon or carbon dioxide containing 0.5-2% sulphur hexafluoride is used to inhibit the oxidation of magnesium up to about 800°C. Lower melting losses are incurred and in combination with filter systems, the use of fluxless melting has reduced the risk of inclusions becoming entrapped in the metal⁸.

Sand castings of increasingly complex shape are being produced with the use of cold setting, resin bonded sand for moulds and cores. The finish on the cast surface and dimensional accuracy are improved. Wall thicknesses of 3.5 mm and casting tolerances of ± 0.5 mm are achievable with consequent savings in weight. Passageways of at least 2 mm diameter, for lubricating oils or hydraulic fluid, can be incorporated into a casting and these are capable of withstanding 90 bar pressure^{8,16}.

Methods for sand casting magnesium under low pressure are being developed. The technique is already in use with permanent moulds, but can now be considered for sand casting because of the improvements in mould and core making. Under low pressure, the flow of metal into the mould can be controlled more easily than in gravity feeding so that castings are more reproducible and their microstructure and properties are more consistent across different sections. Running and gating systems can be made simpler so there is less turbulence and less metal is wasted. The technique is particularly suitable for producing thin wall castings¹⁶.

4 A NEW PROTECTIVE COATING FOR GEARBOXES

The use of magnesium alloys in aeroengine gearbox casings has been restricted to engines where the operating temperature of the lubricating oil is less than about 160°C. Above this temperature, chemical breakdown of the oil to a mixture of organic acids causes corrosive attack of the chromate based coating on magnesium alloys. A new coating system has been developed jointly by Rolls-Royce Ltd and Magnesium Elektron Ltd, under a contract sponsored by RAE Farnborough, which provides improved protection for magnesium alloys in systems where the oil temperature is greater than 200°C¹⁷.

Early investigations showed that a resin sealed Dow 17 coating was more resistant to high temperature oils than the resin sealed chromate pretreatment. The Dow 17¹⁸ pretreatment is a hard anodising process which forms a thick abrasion resistant, but porous coating, which must be sealed with resin. Therefore, different resins, epoxy, phenolic and polyimide, were applied to test-pieces which had been given a Dow 17 pretreatment and they were evaluated in static and flowing oil immersion tests to find which system gave the best protection. The alloy used in the tests was EZ33A.

The corrosion rate was monitored by measuring the magnesium content of the oil. After 300 hours at 170°C, the standard coating of a chromate pretreatment sealed with epoxy resin, had broken down. All the Dow 17 based systems were unaffected.

At 225°C, the Dow 17/polyimide coating showed no visible signs of break down, although there was a slight increase in the magnesium content of the oil after 300 hours (Figure 6). The Dow 17/epoxy coating was satisfactory up to 200 hours, but after 300 hours the coating was damaged at the edges of the test piece.

In the flowing oil impingement tests, the conventional chromate/epoxy coating blistered after 50 hours at 225°C, but the systems based on the Dow 17 pretreatment showed little change after 150 hours at this temperature. After 250 hours the phenolic resin system blistered, followed by the epoxy system after 300 hours. The polyimide system showed no visible signs of attack after 350 hours.

The polyimide sealed Dow 17 coating can thus be considered for future gearbox applications. The Dow 17 anodic pretreatment has excellent throwing power and therefore it should be possible to achieve satisfactory coatings in complex castings with internal passageways.

Good protection was also obtained in elevated temperature salt spray corrosion tests, indicating that the Dow 17/polyimide system is also suitable for protection in high temperature environments other than gearboxes.

5 RAPIDLY SOLIDIFIED MAGNESIUM ALLOYS

Further development of magnesium alloys by ingot metallurgy is limited by the structure of the phase diagram in many magnesium alloy systems. The strong electropositivity of magnesium favours compound formation rather than solid solutions and even when the size factor is favourable, the solid solubility of many elements in magnesium is less than 1%. To overcome these restrictions, and so widen the range of alloy development, attention is now turning to rapid solidification technology. The microstructural and constitutional changes which arise from rapid solidification can lead directly to improvements in the properties of magnesium alloys¹⁹⁻²¹.

Firstly, the mechanical properties can be improved. The specific strengths of magnesium alloys are not as high as those of aluminium alloys, partly because the response of magnesium alloys to age hardening is not as good. Using rapid solidification, precipitates can be distributed more finely and in greater volume fractions to increase strength. Also, the grain size can be made smaller and stabilised with intermetallics to improve strength and ductility.

The mechanical working of magnesium alloys is difficult because of the limited number of slip systems in the hexagonal lattice. At room temperature, only three slip systems are available, those on the basal plane in the $\langle 11\bar{2}0 \rangle$ directions, but twinning can also occur on the pyramidal $\{10\bar{1}2\}$ planes. Twinning only takes place when compressive stresses are parallel to the basal plane or when tensile stresses are perpendicular to it. Since extrusion and rolling of magnesium alloys at low temperature aligns the basal plane parallel to the extrusion and rolling directions respectively, then the compressive yield stress of magnesium alloys is usually lower than the tensile yield stress. The effect can be reduced by decreasing the grain size, and also, above about 225°C, additional slip systems begin to operate on the pyramidal $\{10\bar{1}1\}$ planes, thus making mechanical working easier. In rapidly solidified magnesium alloys, because the grain size can be made smaller, twinning is suppressed and the compressive yield stress is increased. Furthermore, if extended solid solutions are produced, containing elements which decrease the axial ratio of the hexagonal lattice, then prismatic slip becomes easier and mechanical working is improved²².

It was mentioned earlier that the corrosion resistance of magnesium alloys is poor because the naturally forming hydroxide film on the surface gives only partial protection. By using rapid solidification, it may be possible to produce extended solid solutions containing elements which cause a more protective film to form, thereby improving the corrosion resistance.

Most of the standard techniques of rapid solidification have been applied to magnesium alloys, including inert gas atomisation, the rotating electrode process, melt spinning and twin roller quenching¹⁹⁻²¹. Because of the reactivity of magnesium alloys, the use of a controlled atmosphere is essential to minimise oxidation of the powder particles. The volatility of magnesium also makes it difficult to obtain the required superheat when the liquidus temperature is high or if the dissolution rate of the alloying elements in magnesium is low. Consolidation is done by extrusion rather than sintering; the greater amount of shear in extrusion helps to break up the oxide layer around each particle and promote metal to metal bonding. The usual extrusion temperature for magnesium alloys is between 300 and 450°C, but rapidly solidified alloys are usually extruded at less than 250°C to retain the metastable microstructure.

The rapid solidification of magnesium alloys is at an earlier stage of development than that of aluminium alloys. Much of the work has concentrated on constitutional and microstructural changes, but in this section, discussion will be limited to developments where improvements in engineering properties have been reported.

Improvements were first obtained by rapidly solidifying alloys that were commercially available. For example, Isserow and Rizzitano²³ prepared powder of the commercially available ZK60 alloy using the rotating electrode process. The powder was cold compacted and extruded at room temperature, 65°C and 120°C, using an extrusion ratio of 10:1 in each case. Samples were then heat treated at 120°C and 150°C. The best combination of strength and ductility was obtained using an extrusion temperature of 65°C (0.2% proof stress 395 MPa, UTS 420 MPa and elongation 14%). The improvement in strength compared with a conventionally processed ZK60 alloy was explained by the smaller grain size, a finer dispersion of intermetallics and the combination of cold work and recrystallisation.

However, the fracture surfaces of tensile specimens were fibrous and showed delaminations, indicating that the transverse properties may have been poor. Flemings and Mortensen²⁴ prepared melt spun ribbon of

ZK60 alloy and showed that the amount of shear taking place with an extrusion ratio of 10:1 was insufficient to fully consolidate this alloy. Using an extrusion ratio of 30:1 and a temperature of 210°C, consolidation was improved and the fibrous fracture was replaced by a ductile one. The tensile properties were again better than conventionally processed ZK60 alloy; a yield stress of 365 MPa, a UTS of 388 MPa and an elongation of 19.6% were reported.

Meschter²⁵ examined the properties of Mg-10% Al and Mg-12.5% Al-1.5% Si alloys made by twin roller quenching and extrusion at 230°C-250°C. These alloys contained a greater percentage of aluminium than in conventional alloys. The grain size of the rapidly solidified Mg-10% Al alloy was 7 to 10 times smaller than in conventional alloys and that of the Mg-12.5% Al-1.5% Si alloys was further reduced by a factor of 4.6. The Mg-10% Al alloys were solution treated and aged at 100°C, 140°C and 180°C, and at 100°C and 140°C following a 2% stretch. The highest strengths were obtained in the stretched specimens; for example after stretching 2% and aging for 64 hours at 140°C, a yield stress of 351 MPa, a UTS of 430 MPa and an elongation of 3.8% were obtained. The smaller grain size encouraged discontinuous precipitation at grain boundaries rather than continuous precipitation within the grains but a 2% stretch increased the volume fraction of continuous precipitate and so improved the tensile properties. A higher yield stress was obtained in the silicon containing alloy, but the elongation was only 1.4%.

In the examples given above, specific strengths have been obtained which are comparable with high strength aluminium alloys. Alloys from the magnesium-lithium system are also attractive, not only because of their low density (1.35-1.56 gcm⁻³), but also because the addition of 1% Li changes the hexagonal structure of magnesium to a body centred cubic structure which can be cold worked. Although the Young's modulus of these alloys is only 44 GPa, their specific stiffness is very high. However, the conventional alloys such as LA141 and LA91 have low strength because of a large grain size and a lack of effective precipitation or dispersion hardening mechanisms. By rapidly solidifying a Mg-9% Li alloy containing 1% Si or 1% Ce, Meschter and O'Neal²⁶ introduced a fine dispersion of intermetallics into the microstructure which reduced the grain size by a factor of 10-30. The microstructure of as-cast flake coarsened at 300°C, but by using extrusion temperatures less than 200°C, the yield strength of a Mg-9% Li-1% Si alloy could be made 60% higher than that of a Mg-9% Li alloy made by ingot metallurgy²⁵.

There have been few attempts to improve the corrosion resistance of magnesium alloys using rapid solidification. Kruger et al.²⁷ made a systematic study of a number of binary magnesium alloys containing Al, Ca, Li, Si and Zn made by melt spinning. Only aluminium had a beneficial effect; the corrosion rate of a ribbon containing 40% Al was about a quarter that of the pure magnesium standard.

Akavipat et al.^{28,29} implanted iron and boron ions into the surface of magnesium alloys. Typically, the corrosion current for implanted samples was a factor 10 smaller than in unimplanted samples. Iron usually has a detrimental effect on the corrosion rate of magnesium alloys because it forms particles which are sites for cathodic reactions. This illustrates that when an element is forced to remain in solid solution, using rapid solidification, its effect on the corrosion rate of magnesium can be quite different.

If rapidly solidified magnesium alloys are to be accepted in aerospace applications then any improvements in mechanical properties must be accompanied by improvements in corrosion resistance. An attractive combination of these properties has been achieved in rapidly solidified Mg-Al-Zn-Rare Earth alloys, developed by Allied-Signal Inc. Initially, the effect of Ce, Pr, Y and Nd additions on the properties of rapidly solidified Mg-Al-Zn alloys was studied³⁰. Thin ribbon was prepared by planar flow casting or melt spinning and then comminuted to powder and extruded. The microstructures of the as cast ribbons containing Ce, Pr or Nd were cellular; grain size and cell size were typically 0.36-0.7 µm and 0.09-0.34 µm respectively.

Two compositions were selected by Allied-Signal Inc for further development; a Mg-5% Al-5% Zn-4.9% Nd alloy designated EA55RS, and a Mg-5% Al-5% Zn-5.9% Y alloy designated EA65RS³¹. Development of EA55RS is also being undertaken in the UK by Magnesium Elektron Ltd.

Preliminary test results have been reported^{31,32} (Table 2), which show that the yield stress and tensile stress of the alloys are greater than those of conventional magnesium alloys (Figure 7). EA65RS is the stronger of the two alloys, but EA55RS is more ductile. In the as-extruded condition the fracture toughness of both alloys is low, but it can be improved in EA55RS by a T4 heat treatment, with an accompanying reduction in strength³³. The low fracture toughness in the as-extruded condition is caused by brittle particles which dissolve during subsequent heat treatment. Unlike conventional alloys, the compressive yield strengths of these alloys are about the same as the tensile yield strengths because of the small grain size³¹.

The densities (ρ) of EA55RS and EA65RS are 1.94 and 1.92 gcm⁻³ respectively. Their specific strengths are thus higher than those of conventional aluminium alloys (Figure 8). The minimum weight criterion for buckling resistance is $E^{1/2}/\rho$, where E is the Young's modulus, and hence the values of $E^{1/2}/\rho$ for EA55RS and EA65RS are 10%-20% higher than for aluminium alloys.

EA55RS and EA65RS are also more corrosion resistant than conventional wrought magnesium alloys. Their performance in salt spray corrosion tests is comparable with the high purity version of AZ91; for example the corrosion rate of EA55RS-T4 is reported to be 8 mils/year³². The electrode potentials of the rare earth elements are close to that of magnesium so the intermetallic particles do not have a damaging galvanic effect. However, the alloys would still need a protective coating if used in aerospace, and wet assembly would be required to avoid galvanic attack at metal to metal joints.

6 CONCLUDING REMARKS

The use of cast magnesium alloys to save weight in aerospace applications is well established. The introduction of WE54 and AZ91E has increased the range of properties available from cast magnesium alloys; both have better corrosion resistance than other cast magnesium alloys and WE54 has improved room and elevated temperature tensile properties.

New casting methods, based on fluxless melting, resin bonded sand and low pressure, have led to improvements in the overall integrity of castings and enabled more complex shapes with thinner walls to be produced. By applying a polyimide/Dow 17 coating, magnesium alloys can still be considered for gearbox applications where the oil temperature exceeds 200°C. These developments will enable cast magnesium alloys to remain competitive in the future.

Magnesium alloy sheet and extrusions are not currently used in aircraft structures. Although their specific strengths are less than those of high strength aluminium alloys, there are applications where they could be used to save weight, but concern about their corrosion resistance has prevented this.

Improvements in the mechanical properties and corrosion resistance of magnesium alloys are being sought through the use of rapid solidification technology. The work is still in its early stages and very few alloy systems have been investigated, but already specific strengths greater than high strength aluminium alloys have been obtained and corrosion rates have been reduced. The low density of magnesium alloys in comparison with aluminium alloys gives them an advantageous starting point from which to develop alloys with good specific properties. Further developments in this area will be of considerable interest.

Magnesium based metal matrix composites are outside the scope of this paper, but they too are being considered for future aerospace applications. Before any advanced magnesium based alloy gains acceptance it will have to demonstrate that it can give satisfactory long term service. During the 1950s and 1960s magnesium alloys gained a reputation for corrosion problems, which in some cases could have been avoided if better precautions had been taken. If advanced magnesium based alloys are put into service, the correct measures must be taken to guard against corrosion, so that, in the long term, confidence in these alloys can be gained. Provided these precautions are taken, they have the potential to save weight in aerospace structures and the opportunities to exploit them should be fully explored.

REFERENCES

- 1 G B Evans, Applications of magnesium in aerospace. Magnesium Technology, Proceedings of London Conference, November (1986), The Institute of Metals, p.103-109.
- 2 E F Emley, Principles of magnesium technology. Pergamon Press, (1966), p.787-826.
- 3 G T Hudson, Designing with magnesium alloys, Reference 1, p.60-65.
- 4 H P Godard, The corrosion of light metals, Wiley, (1967), p.257-311.
- 5 G B Evans, Reflections and projections: thoughts on the use of magnesium alloys in airframes, Proceedings 43rd World Magnesium Conference, June (1986), Los Angeles, p.24-36.
- 6 MEL Ltd, Surface treatments for magnesium alloys in aerospace and defence, Magnesium Elektron Ltd, Regal House, London Road, Twickenham, TW1 3QA, UK.
- 7 Specification DTD 911C, Protection of magnesium rich alloys against corrosion.
- 8 A Stevenson, Mg casting alloys for the aerospace challenge, J. Metals, 39, p.16-19, (1987).
- 9 W Unsworth, Developments in magnesium alloys for casting applications, Met. and Mater., 4, p.83-86, (1988).
- 10 W Unsworth and J F King, New high performance casting alloy developed, Metallurgia, 53, p.199-200, (1986).
- 11 D S Tawil, Corrosion and surface protection developments, Reference 1, p.66-74.
- 12 D Magers, The potential for magnesium die castings in aerospace applications, Reference 5, p.58-65.
- 13 J D Hanawalt, C F Nelson and J A Peloubet, Corrosion studies on magnesium and its alloys, Trans. AIME, 174, p.273-299, (1942).
- 14 K N Reichert, K J Clark and J E Hillis, Controlling the salt water corrosion performance of magnesium AZ91 alloys, SAE Tech. Paper 850417.
- 15 K J Clark, AZ91E magnesium sand casting alloy: the standard for excellent corrosion resistance, Reference 5, p.37-41.
- 16 N Zeumer, H Fuchs and G Betz, New developments in casting of magnesium, Reference 1, p.18-24.
- 17 D Tawil and M Randu, Improved protection of magnesium alloys against synthetic aviation lubricants at elevated temperatures, Proc. SAE aerospace/airline plating and metal finishing Conference, Phoenix, USA, April (1988).
- 18 Specification MIL-M-45202, Anodic treatment of magnesium alloys.
- 19 F H Froes, Y W Kim and F Hehmann, Rapid solidification of Al, Mg and Ti, J. Metals, 39, p.14-21, (1987).
- 20 R E Lewis, A Joshi and H Jones, Rapidly solidified magnesium alloys for high performance structural applications: a review, Proc. Conf. Processing of structural metals by rapid solidification, Orlando, USA, October (1986), ASM International, p.367-378.

- 21 H Jones, A Joshi, R G Rowe and F H Froes, The current status of rapid solidification of magnesium-base and titanium-base alloys. *Internat. J. Powder Metall.*, 23, p.13-24, (1987).
- 22 F Hehmann and H Jones, Rapid solidification processing of magnesium, Reference 1, p.83-96.
- 23 S Isserow and F J Rizzitano, Microquenched magnesium ZK60A alloy. *Internat. J. Powder Metall. and Powder Tech.*, 10, p.217-227, (1974).
- 24 M C Flemings and A Mortensen, Rapid solidification processing of magnesium alloys, Massachusetts Inst. of Tech., September (1984), Report No AMMRC-TR-84-37, Government Accession No AD-A150270.
- 25 P J Meschter, Microstructures and properties of rapidly solidified Mg-10 Al and Mg-12.5 Al-1.5 Si alloys, *Metall. Trans. A*, 18A, p.347-350, (1987).
- 26 P J Meschter and J E O'Neal, Rapid solidification processing of magnesium-lithium alloys, *Metall. Trans. A*, 15A, p.237-240, (1984).
- 27 J Kruger, G G Long, D Tanaka, A Joshi and G L Hakar, A fundamental understanding of the effect of alloying elements on the corrosion resistance of rapidly solidified Mg alloys. John Hopkins Univ., Baltimore, USA, Acc. No AD-A189 385/8/WMS.
- 28 S Akavipat, E B Hale, C E Habermann and P L Hagans, Effect of iron implantation on the aqueous corrosion of magnesium. *Mater. Sci. and Eng.*, 69, p.311-316 (1985).
- 29 S Akavipat, C E Habermann, P L Hagans and E B Hale, Electrochemical and auger measurements on boron implanted magnesium, Fundamental aspects of corrosion protection by surface modification, Eds., E McCafferty, C R Clayton and J Oudar, *Electrochem. Soc.*, Pennington, New Jersey (1984), p.52-61.
- 30 C F Chang, S K Das, D Raybould and A Brown, Corrosion resistant high strength magnesium alloys by RSP, *Metal Powder Rep.*, 41, p.302-305 and 308, (1986).
- 31 F H Froes, W E Quist and S K Das, Advanced lightweight metals using rapid solidification, *Proc. Conf. PM Aerospace materials*, Luzern, 2-4 November, (1987), p.16.1-16.29.
- 32 MEL Ltd, Data sheet 900, Magnesium Elektron Ltd, Regal House, London Road, Twickenham, TW1 3QA.
- 33 C F Chang, S K Das and D Raybould, The effect of heat treatment on the properties of rapidly solidified Mg-Al-Zn-RE alloys, Reference 20, p.409-415.

ACKNOWLEDGEMENT

Discussion with Mr W Unsworth of Magnesium Elektron Ltd is gratefully acknowledged.

© Controller Her Majesty's Stationary Office London 1988

Alloy	Typical Composition (wt%)						Tensile Properties		
	Zn	RE	Th	Ag	Zr		0.2%PS (MPa)	UTS (MPa)	E%
ZE41	4.2	1.3	-	-	0.7		135	200	3
ZH62	5.5	-	1.8	-	0.7		155	255	5
EZ33	2.5	3.0	-	-	0.6		95	140	3
HZ32	2.2	-	3.0	-	0.7		85	185	5
QE22	-	2.0	-	2.5	0.6		175	240	2
EQ21	-	2.0	-	1.5	0.6		175	240	2

Table 1 Composition and tensile properties of cast magnesium alloys (RE = rare earths). Tensile properties are specification minima in precipitation treated condition (from MEL data sheet).

	0.2% Proof stress (MPa)	UTS (MPa)	Elongation %	Fracture toughness K _{IC} (MPa√m)	Youngs modulus (GPa)
EA65RS	460	515	5	-	47.5
EA55RS-F	435	472	13	10	45.5
EA55RS-T4	371	425	14	17	45.5

Table 2 Typical tensile properties for extruded bar of EA65RS³¹ and EA55RS³².

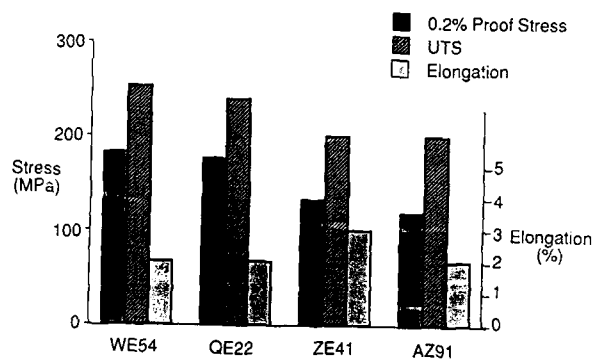


Fig 1 Minimum tensile properties of WE54 and other cast magnesium alloys in precipitation treated condition (from MEL data sheet).

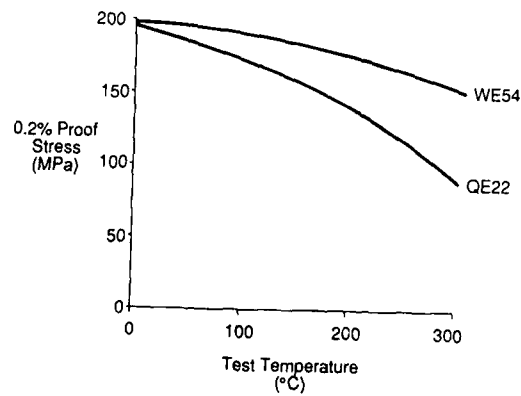


Fig 2 Effect of temperature on tensile properties of WE54 and QE22 (minimum values)⁶.

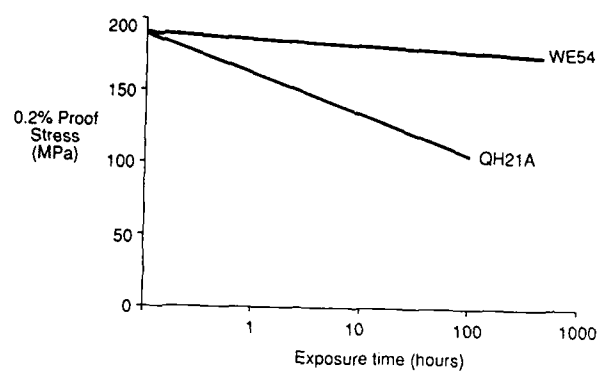


Fig 3 Effect of exposure at 250°C on the room temperature tensile properties of WE54 and QH21A (minimum values)⁸.

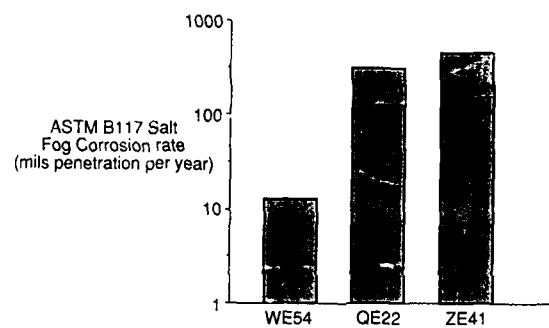


Fig 4 Typical corrosion rates of WE54 and other cast magnesium alloys¹¹.

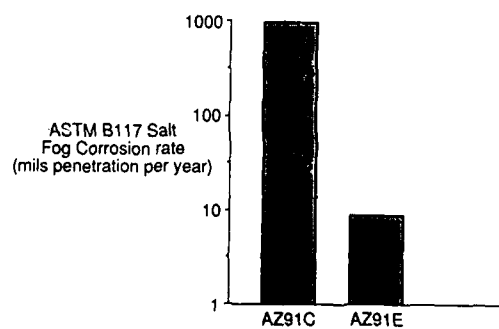


Fig 5 Typical corrosion rates of AZ91C and high purity AZ91E¹¹.

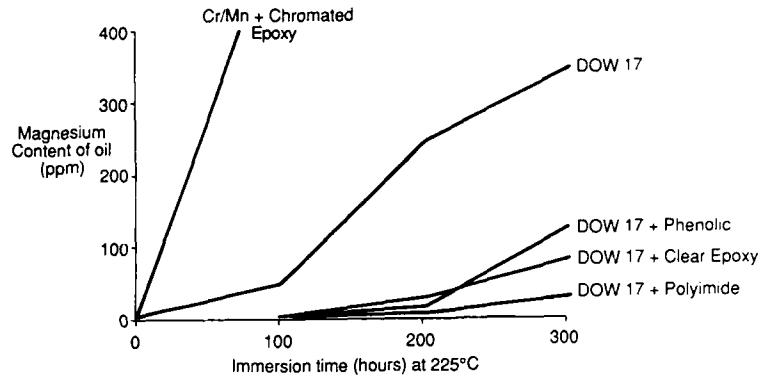


Fig 6 Comparative performance of different coatings in static lubricant immersion tests at 225°C (courtesy MEL Ltd).

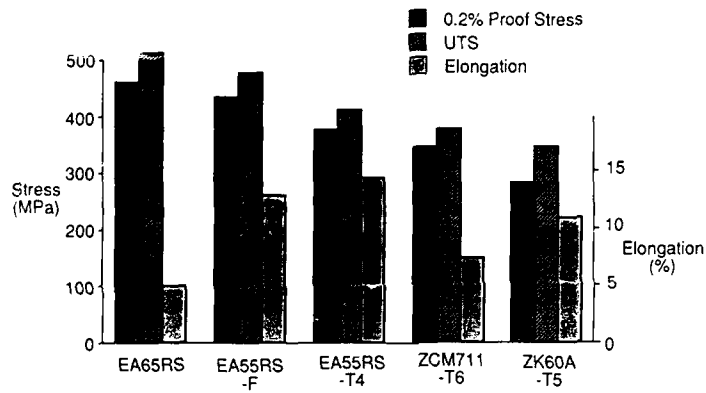


Fig 7 Typical tensile properties for extruded bar of rapidly solidified alloys EA65RS and EA55RS and other wrought magnesium alloys.

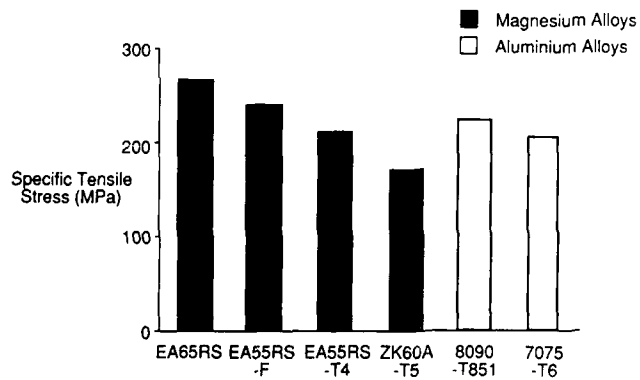


Fig 8 Specific tensile stress for extruded bar of EA65RS, EA55RS and other wrought alloys.

REPORT DOCUMENTATION PAGE

1. Recipient's Reference	2. Originator's Reference	3. Further Reference	4. Security Classification of Document						
	AGARD-CP-444	ISBN 92-835-0519-0	UNCLASSIFIED						
5. Originator	Advisory Group for Aerospace Research and Development North Atlantic Treaty Organization 7 rue Ancelle, 92200 Neuilly sur Seine, France								
6. Title	NEW LIGHT ALLOYS								
7. Presented at	the 67th Meeting of the Structures and Materials Panel of AGARD in Mierlo, Netherlands, 3—5 October 1988.								
8. Author(s)/Editor(s)	Various		9. Date August 1989						
10. Author's/Editor's Address	Various		11. Pages 356						
12. Distribution Statement	This document is distributed in accordance with AGARD policies and regulations, which are outlined on the Outside Back Covers of all AGARD publications.								
13. Keywords/Descriptors									
<table border="0"> <tr> <td>Aluminum alloys</td> <td>Powder alloys</td> </tr> <tr> <td>Lithium containing alloys</td> <td>Composite materials</td> </tr> <tr> <td>Magnesium alloys</td> <td>Airframes</td> </tr> </table>				Aluminum alloys	Powder alloys	Lithium containing alloys	Composite materials	Magnesium alloys	Airframes
Aluminum alloys	Powder alloys								
Lithium containing alloys	Composite materials								
Magnesium alloys	Airframes								
14. Abstract									
<p>The publication reports the proceedings of a Specialists' Meeting on New Light Alloys organised by the AGARD Structures and Materials Panel. The meeting reviewed the status of current developments in aluminium-lithium alloys, the characterization of commercially available products, and their likely applications in aircraft structures. The meeting also considered developments in other lightweight metallic materials such as magnesium alloys, aluminium powder metallurgy alloys and aluminium metal matrix composites.</p> <p>Papers presented at the 67th meeting of the Structures and Materials Panel in Mierlo, Netherlands on 2—7 October 1988.</p>									

<p>AGARD Conference Proceedings No.444 Advisory Group for Aerospace Research and Development, NATO NEW LIGHT ALLOYS Published August 1989 356 pages</p> <p>The publication reports the proceedings of a Specialists' Meeting on New Light Alloys organised by the AGARD Structures and Materials Panel. The meeting reviewed the status of current developments in aluminium-lithium alloys, the characterization of commercially available products, and their likely applications in aircraft structures. The meeting also considered developments in other lightweight metallic materials such as magnesium</p> <p>P.T.O.</p>	<p>AGARD-CP-444</p> <p>Aluminum alloys Lithium containing alloys Magnesium alloys Powder alloys Composite materials Airframes</p>	<p>AGARD Conference Proceedings No.444 Advisory Group for Aerospace Research and Development, NATO NEW LIGHT ALLOYS Published August 1989 356 pages</p> <p>The publication reports the proceedings of a Specialists' Meeting on New Light Alloys organised by the AGARD Structures and Materials Panel. The meeting reviewed the status of current developments in aluminium-lithium alloys, the characterization of commercially available products, and their likely applications in aircraft structures. The meeting also considered developments in other lightweight metallic materials such as magnesium</p> <p>P.T.O.</p>	<p>AGARD-CP-444</p> <p>Aluminum alloys Lithium containing alloys Magnesium alloys Powder alloys Composite materials Airframes</p>
<p>AGARD Conference Proceedings No.444 Advisory Group for Aerospace Research and Development, NATO NEW LIGHT ALLOYS Published August 1989 356 pages</p> <p>The publication reports the proceedings of a Specialists' Meeting on New Light Alloys organised by the AGARD Structures and Materials Panel. The meeting reviewed the status of current developments in aluminium-lithium alloys, the characterization of commercially available products, and their likely applications in aircraft structures. The meeting also considered developments in other lightweight metallic materials such as magnesium</p> <p>P.T.O.</p>	<p>AGARD-CP-444</p> <p>Aluminum alloys Lithium containing alloys Magnesium alloys Powder alloys Composite materials Airframes</p>	<p>AGARD Conference Proceedings No.444 Advisory Group for Aerospace Research and Development, NATO NEW LIGHT ALLOYS Published August 1989 356 pages</p> <p>The publication reports the proceedings of a Specialists' Meeting on New Light Alloys organised by the AGARD Structures and Materials Panel. The meeting reviewed the status of current developments in aluminium-lithium alloys, the characterization of commercially available products, and their likely applications in aircraft structures. The meeting also considered developments in other lightweight metallic materials such as magnesium</p> <p>P.T.O.</p>	<p>AGARD-CP-444</p> <p>Aluminum alloys Lithium containing alloys Magnesium alloys Powder alloys Composite materials Airframes</p>

<p>alloys, aluminium powder metallurgy alloys and aluminium metal matrix composites.</p> <p>Papers presented at the 67th meeting of the Structures and Materials Panel in Mierlo, Netherlands on 3—5 October 1988.</p> <p>ISBN 92-835-0519-0</p>	<p>alloys, aluminium powder metallurgy alloys and aluminium metal matrix composites.</p> <p>Papers presented at the 67th meeting of the Structures and Materials Panel in Mierlo, Netherlands on 3—5 October 1988.</p> <p>ISBN 92-835-0519-0</p>
<p>alloys, aluminium powder metallurgy alloys and aluminium metal matrix composites.</p> <p>Papers presented at the 67th meeting of the Structures and Materials Panel in Mierlo, Netherlands on 3—5 October 1988.</p> <p>ISBN 92-835-0519-0</p>	<p>alloys, aluminium powder metallurgy alloys and aluminium metal matrix composites.</p> <p>Papers presented at the 67th meeting of the Structures and Materials Panel in Mierlo, Netherlands on 3—5 October 1988.</p> <p>ISBN 92-835-0519-0</p>